

ADVERTIMENT. La consulta d'aquesta tesi queda condicionada a l'acceptació de les següents condicions d'ús: La difusió d'aquesta tesi per mitjà del servei TDX (www.tesisenxarxa.net) ha estat autoritzada pels titulars dels drets de propietat intel·lectual únicament per a usos privats emmarcats en activitats d'investigació i docència. No s'autoritza la seva reproducció amb finalitats de lucre ni la seva difusió i posada a disposició des d'un lloc aliè al servei TDX. No s'autoritza la presentació del seu contingut en una finestra o marc aliè a TDX (framing). Aquesta reserva de drets afecta tant al resum de presentació de la tesi com als seus continguts. En la utilització o cita de parts de la tesi és obligat indicar el nom de la persona autora.

ADVERTENCIA. La consulta de esta tesis queda condicionada a la aceptación de las siguientes condiciones de uso: La difusión de esta tesis por medio del servicio TDR (www.tesisenred.net) ha sido autorizada por los titulares de los derechos de propiedad intelectual únicamente para usos privados enmarcados en actividades de investigación y docencia. No se autoriza su reproducción con finalidades de lucro ni su difusión y puesta a disposición desde un sitio ajeno al servicio TDR. No se autoriza la presentación de su contenido en una ventana o marco ajeno a TDR (framing). Esta reserva de derechos afecta tanto al resumen de presentación de la tesis como a sus contenidos. En la utilización o cita de partes de la tesis es obligado indicar el nombre de la persona autora.

WARNING. On having consulted this thesis you're accepting the following use conditions: Spreading this thesis by the TDX (www.tesisenxarxa.net) service has been authorized by the titular of the intellectual property rights only for private uses placed in investigation and teaching activities. Reproduction with lucrative aims is not authorized neither its spreading and availability from a site foreign to the TDX service. Introducing its content in a window or frame foreign to the TDX service is not authorized (framing). This rights affect to the presentation summary of the thesis as well as to its contents. In the using or citation of parts of the thesis it's obliged to indicate the name of the author

Ground Plane Booster Antenna Technology for Wireless Handheld Devices

by

Aurora Andújar Linares

Director: Dr. Jaume Anguera Pros

Ph.D. Dissertation

Department of Signal Theory and Communications (TSC)

Universitat Politècnica de Catalunya (UPC)

Technology and Intellectual Property Rights Department (Fractus)

Barcelona, May 2013



UNIVERSITAT POLITÈCNICA
DE CATALUNYA
BARCELONATECH



fractus

Optimised Antennas
for Wireless Devices

A mis padres porque a ellos les debo todo lo que soy

ACKNOWLEDGEMENT

Como decía el gran filósofo Aristóteles, no se puede desatar un nudo sin saber cómo está hecho. Con el deseo de aprender me adentré en esta nueva etapa profesional, el doctorado, donde la curiosidad, la inquietud, las dudas, el conocimiento, la ignorancia, el esfuerzo, la voluntad, y la constancia son algunos de los conceptos que imperan. El camino ha sido intenso, largo, y en ocasiones tortuoso. No obstante, la carga ha sido considerablemente atenuada por los extraordinarios compañeros de viaje con los que he tenido la suerte de poder contar. A ellos les dedico este esfuerzo.

En primer lugar a mis padres, Ramón Ignacio Andújar Álvarez y Aurora Linares Nájjar, porque sin ellos nada de esto existiría. No encuentro palabras para agradecerles su infinita e incondicional generosidad. A ellos les debo todo lo que soy. Ellos son el principal motor de mi vida, de mi voluntad, mi mayor referente, y gracias a ellos esta tesis es hoy una realidad. Sólo espero saber devolveros todo ese amor con la misma intensidad.

A toda mi familia, a los presentes y a los que nos dan fuerza desde el cielo. A Núria, al pequeño Diego que estará con nosotros muy pronto, y muy especialmente, a mi hermano por regalarme cada día lo que tan sólo un hermano puede ofrecer.

A Fran, qué decirte, gracias por ser mi compañero de viaje no sólo en éste, sino en todos los que emprendo y emprenderé en la vida. Gracias por darle sentido. Recuerda siempre nuestro secreto.

A mis amigos por hacerme olvidar los pequeños problemas del día a día inundando mi vida de sonrisas. Gracias por todos los momentos compartidos y por compartir.

A mi director de tesis Dr. Jaume Anguera por confiar en mí, por orientarme, por no dejar que me rindiera, por apoyarme siempre, por sus tan valiosas enseñanzas, por sus consejos, por su entrega, por su dedicación, por su entusiasmo, en definitiva por estar siempre ahí. Jaume, ciertamente aquel ascenso a aquella montaña que proponías al inicio de esta aventura parecía imposible pero, miranos, finalmente hemos conseguido alcanzar la cima. Lograrlo no ha sido fácil ya que el camino no ha estado sólo lleno de alegrías y satisfacciones, sino también de obstáculos y preocupaciones. Gracias por haber estado ahí en todas y cada una de las etapas, por compartir esas alegrías y por atenuar esos obstáculos. Como acostumbras a decir es hora de mirar atrás para contemplar con satisfacción los frutos de nuestro esfuerzo. Como decía Gandhi, nuestra recompensa se encuentra en ese esfuerzo y no en el resultado, un esfuerzo total es una victoria completa.

Agradecer especialmente al Dr. Carles Puente su apoyo, sus enseñanzas, y sus consejos. Gracias Carles por brindarme la oportunidad de poder realizar esta tesis doctoral en Fractus. Gracias a Fractus por ofrecerme este reto y gracias a todos mis compañeros por hacerme más llevadero el día a día, en particular gracias a la Dra. Carmen Borja por su ayuda, apoyo y comprensión en todos los momentos.

Finalmente, me gustaría hacer una mención especial a todos los proyectistas que han colaborado de una manera u otra en el desarrollo de esta tesis. Gracias a Yolanda Cobo, José Luis Leiva, Víctor Díaz,

y Carlos García. Gracias por vuestra dedicación, por vuestras ganas de aprender, y por vuestro entusiasmo.

Hoy me encuentro al final de esta etapa y aunque es mucho lo aprendido, infinito lo que queda por aprender. Precisamente ahí es donde reside la magia, ya que la vida es eso, un continuo aprendizaje. Sólo espero estar preparada y que en ese camino me acompañen todas y cada una de las personas con las que he podido contar hasta ahora.

*We would like to thank the Spanish Ministry
of Industry, Energy, and Tourism
for its financial support*

ABSTRACT

This thesis is framed in the field of mobile communications and more particularly in handset antennas. The wireless industry is constantly growing, which entails challenging handset antenna specifications. Handset antennas not only have to be multi-band for satisfying the great number of communication services, but also sufficiently small as for fitting in the reduced space imposed by the handset platforms. The appearance of the MIMO (Multiple Input Multiple Output) technology, further exacerbates these challenges. In order to satisfy these requirements, this thesis proposes the use of the ground plane, inherently present in any handset platform, as the main radiator. Electrically small non-resonant elements, called along this thesis as ground plane boosters, are used to transfer energy to this ground plane. The solution removes the need of including a dedicated antenna featured by considerable dimensions, thus releasing space to integrate other antennas, as well as, other handset components, services and functionalities.

TABLE OF CONTENTS

CHAPTER 1 INTRODUCTION	1
1.1. Introduction	1
1.2. Hypothesis and Preliminary Results	6
1.3. Methodology.....	12
1.4. Objectives	15
1.5. State of the Art	17
1.6. Publications.....	23
1.6.1 Patents	23
1.6.2 Journals	23
1.6.3 International Conferences.....	25
1.6.4 National Conferences	27
1.7. References.....	28
CHAPTER 2 FUNDAMENTAL PRINCIPLES	33
2.1. Introduction	33
2.2. Characteristic Modes Theory.....	34
2.2.1 Characteristic Modes of Representative Handset Platforms.....	36
2.3. Ground Plane Contribution using Radar Cross Section Analysis (RCS).....	41
2.3.1 Radar Cross Section (RCS) Analysis	42
2.3.2 Practical Application.....	45
2.3.2.1. Ground Plane Size.....	45
2.3.2.2. Enlarging the Ground Plane through Conductive Strips	47
2.3.2.3. Enlarging the Ground Plane with Slots.....	50
2.4. Resonant Elements versus Non-Resonant Elements	52
2.4.1 On the Behavior of Several Geometries.....	53
2.4.1.1. Resonance of the Element (f_r) equal to 900MHz.....	54
2.4.1.2. Resonance of the Element (f_r) equal to the Resonance of the Ground Plane (f_{GP}).....	56
2.4.1.3. Resonance of the Element (f_r) above the Resonance of the Ground Plane (f_{GP})	58
2.5. Physical Approximation to an Asymmetric Dipole	60
2.6. Conclusions	62
2.7. References.....	65
CHAPTER 3 GROUND PLANE BOOSTER ANTENNA TECHNOLOGY	
.....	71
3.1. Introduction	71

3.2. Volumetric Ground Plane Boosters: Capacitive Elements	72
3.2.1 Theoretic Principles	74
3.2.2 Concept Definition	76
3.2.2.1. <i>Electrical Model of the Radiating Structure</i>	76
3.2.2.2. <i>Broadband Matching Network Design</i>	77
3.2.3 Multi-Band Design: Simulated Results	81
3.2.4 Multi-Band Design: Experimental Results	83
3.2.4.1. <i>Reflection Coefficient and Efficiency</i>	84
3.2.4.2. <i>Radiation Patterns</i>	85
3.2.4.3. <i>SAR Measurement</i>	86
3.3. Coplanar Ground Plane Boosters: Capacitive Elements	88
3.3.1 Hepta-Band Solution	89
3.3.1.1. <i>Simulated Results</i>	89
3.3.1.2. <i>Measured Results</i>	95
3.3.2 Nona-Band Solution	96
3.3.2.1. <i>Simulated Results</i>	97
3.3.2.2. <i>Measured Results</i>	101
3.4. Coplanar Ground Plane Boosters: Inductive Elements	102
3.4.1 Theoretical Background and Concept Definition	104
3.4.1.1. <i>On the location of Magnetic Boosters</i>	105
3.4.1.2. <i>Electrical Model and Matching Network Design</i>	107
3.4.2 Simulated Results	109
3.4.3 Experimental Results	112
3.5. On the Radiofrequency System	116
3.5.1 Physical Insight and Simulated Results	117
3.5.2 Measured Results	118
3.6. Conclusions	119
3.7. References	122
CHAPTER 4 HUMAN HEAD INTERACTION	129
4.1. Introduction	129
4.2. Description of the Radiating Systems	130
4.3. Functional Analysis	132
4.3.1 Reflection Coefficient: S_{11}	133
4.3.2 Absorption Ratios and Free-space Efficiency	134
4.3.3 Antenna Efficiency regarding Human Head	137
4.3.4 Radiation Patterns	138
4.4. Biological Compatibility	140
4.5. Evaluation Criteria	141

4.5.1 SAR versus Power Absorption and Antenna Efficiency	141
4.5.2 Figure of Merit.....	143
4.6. Conclusions	144
4.7. References.....	146

CHAPTER 5 DISTRIBUTED RADIATING SYSTEMS 151

5.1. Introduction	151
5.2. Distributed Antenna Technology based on Resonant Elements	152
5.2.1 Theoretical Analysis	153
5.2.2 Distributed Antenna System Design	156
5.2.3 Human Hand Effect.....	160
5.3. In-phase versus Out-of-phase Distributed Antenna Systems.....	164
5.3.1 Theoretical Analysis	165
5.3.1.1. <i>Out-of-phase Distributed Antenna Systems</i>	165
5.3.1.2. <i>In-phase Distributed Antenna Systems</i>	166
5.3.2 In-phase Distributed Antenna System Design	168
5.3.2.1. <i>Simulations</i>	168
5.3.2.2. <i>Measurements</i>	171
5.3.3 Human Hand Effect.....	173
5.4. Distributed System based on Ground Plane Boosters	176
5.4.1 Radiating Structure and Radiofrequency System	177
5.4.2 Multi-Band Design: Simulated Results.....	180
5.4.3 Multi-Band Design: Experimental Results.....	184
5.4.3.1. <i>Free-Space Measurements</i>	185
5.4.3.2. <i>Hand Loading</i>	186
5.5. Conclusions	189
5.6. References.....	192

CHAPTER 6 GROUND PLANE BOOSTERS IN MIMO SYSTEMS 199

6.1. Introduction	199
6.2. MIMO Concept and Relevant Parameters	201
6.3. State of the Art	205
6.4. MIMO Systems based on Resonant Antennas	207
6.4.1 Description of the Radiating Systems	208
6.4.2 MIMO Analysis.....	211
6.5. MIMO Systems combining Resonant Antennas with Boosters	219
6.5.1 Distance Effect	220
6.5.2 Slot in the Ground Plane as Isolation Technique	221
6.5.3 MIMO Solution: Coupled Monopoles and Ground Plane Boosters	222

6.5.3.1. <i>Simulated Results</i>	222
6.5.3.2. <i>Measured Results</i>	225
6.6. MIMO Systems based on Ground Plane Boosters	228
6.6.1 Description of the MIMO Solution	229
6.6.2 Simulated Results	230
6.6.3 Measured Results.....	234
6.7. Conclusions	238
6.8. References.....	241
CHAPTER 7 CONCLUSIONS	245

LIST OF FIGURES

- Fig. 1.1 Handset antenna evolution: a) Example of an external antenna and a handset including such external antenna; b) Example of two internal antennas and handsets including internal antennas. 1
- Fig. 1.2 Multiple mobile communication standards offering a great number of services and functionalities integrated in the new multifunctional wireless devices commonly known as smartphones 2
- Fig. 1.3 Handset components associated to the handset phone Blackberry 8703e: a) Image showing the keyboard; b) Image showing the speaker, the battery, and a handset antenna (top edge); c) Image showing the LCD display; d) Image showing several shieldings containing memory modules, microprocessors, communication circuits, multiplexors, etc., and another handset antenna (bottom edge). 3
- Fig. 1.4 a) Input impedance associated to the simulated geometry b) including a non-resonant capacitive ground plane booster on a ground plane having a size of 100 mm x 40 mm according to a typical bar-type phone (featuring capacitive input impedance) (triangular markers) and input impedance associated to the simulated geometry c) including a non-resonant inductive ground plane booster element (featuring inductive input impedance) (square markers). 6
- Fig. 1.5 Inherent bandwidth and quality factor versus frequency calculated regarding the radiating structures shown in Fig. 1.4 b) (left plot) and c) (right plot) through the corresponding input impedances according to equations (1.1) and (1.2). 7
- Fig. 1.6 a) Equivalent electrical circuit associated to the radiating structure of Fig. 1.4b after the addition of the reactance cancellation element (*RLC* series circuit) and the two stages broadband matching network; b) Conditions required to attain a broadband matching network capable of increasing the inherent bandwidth of a radiating structure featuring a *RLC* series input impedance in a factor around 2.45 for $S \leq 3$; c) Step by step input impedance sequence starting by the addition of the reactance cancellation element and concluding with the two stages matching network with the proper C_m and L_m values that allow inscribing the impedance loop in a circle of $S \leq 3$ 8
- Fig. 1.7 a) Radiating system designed for achieving a penta-band behavior consisting in a reactance cancellation element, a broadband matching network, and a notch filter for each frequency region [7]-[9]. Note that the first stage of the notch filter and the broadband matching network can be simplified using only two components. The two-port box is the simulated input impedance of the radiating structure shown in b); b) Detailed view of the radiating structure obtained from the simulated layout comprising two non-resonant ground plane boosters with dimensions 5 mm x 5 mm x 5mm each one in charge of the ground plane (100 mm x 40 mm) excitation for each frequency region (low frequency region comprising the communication standards (GS850 and GSM900) and high frequency region comprising the communication standards (GSM1800, GSM1900, and UMTS); c) Current distribution associated to the radiating structure at the central frequencies of both frequency regions ($f=0.89$ and $f=1.94$ GHz) that demonstrates the effectiveness of the boosters in exciting efficient radiation modes of the ground plane. 9
- Fig. 1.8 Penta-band prototype designed according to the schematic shown in a) including besides the reactance cancellation inductor and the broadband matching network, the notch filters required for providing isolation between both frequency regions. 9
- Fig. 1.9 Comparison between current internal antenna technologies and the technology proposed in this thesis. Note that the PCB space is considerable increased when the dedicated antenna (framed in dashed line (left)) is replaced by the non-resonant ground plane boosters (framed in dashed line (right)). 10
- Fig. 1.10 Left: Example of several handset platforms featuring different form factors and consequently dissimilar internal antennas especially customized for being integrated in such specific handset

platforms; Right: Ground plane booster elements as the promising standard solution that enables the integration in any handset platform without the need of a complex customization process.....	11
Fig. 1.11 Main aspects regarding human interaction considered along this thesis: biological and functional.....	11
Fig. 1.12 Tools used along the different phases that compose this thesis.	13
Fig. 1.13. Handset antenna evolution envisaged in this thesis.	14
Fig. 1.14 Thesis Objectives.	16
Fig. 1.15 Two representative examples of current internal antenna technologies: a) Current distribution associated to coupled monopoles representing ‘off-ground’ coplanar structures; b) Current distribution associated to PIFA antenna over a slotted ground plane illustrating ‘on-ground’ technology together with ground plane shaping techniques; c) Coupled monopoles prototype [12],[14]; d) PIFA antenna prototype[19]-[27]. These handset antenna designs are also being analyzed in this thesis for comparison purposes.	18
Fig. 1.16 Current distribution associated to existing antenna technologies intended for providing intelligence to the ground plane by electrically enlarging it through the addition of a conductive strip (left) [28]-[30] or by the insertion of slots (right) [19]-[27].....	19
Fig. 1.17 a) Image of the coupling elements given in [34] where an antenna structure consists of coupling elements and two resonant circuits to provide operation in two frequency regions separately; b) Image corresponding to [37] showing the two coupling elements with volumes 624mm^3 and 64mm^3 , presented for covering each frequency region respectively.	20
Fig. 1.18 a) Geometry and dimensions associated to the radiating structure, as a first solution of this thesis development comprising two non-resonant ground plane boosters, each one in charge of the ground plane excitation for each frequency region. Current distribution referred to the excited ground plane mode at $f=0.892\text{GHz}$; b) Prototype associated to the geometry shown in a).....	21
Fig. 2.1 Physical interpretation of the matrix J . The columns of the matrix correspond to each characteristic mode and they contain information about its current distribution. In this case, the conducting structure is a rectangular conducting body of dimensions $100\text{ mm} \times 40\text{ mm}$	36
Fig. 2.2 Modal significance associated to the characteristic modes J_1, J_2, J_3, J_4 of a bar type handset platform having dimensions of $100\text{ mm} \times 40\text{ mm}$	37
Fig. 2.3 Eigenvalues associated to the characteristic modes J_1, J_2, J_3, J_4 of a bar type handset platform having dimensions of $100\text{ mm} \times 40\text{ mm}$	38
Fig. 2.4 Current distribution regarding a bar type handset platform having dimensions of $100\text{ mm} \times 40\text{ mm}$ corresponding to a) Characteristic mode J_1 ; b) Characteristic mode J_2 ; c) Characteristic mode J_3 ; d) Characteristic mode J_4	38
Fig. 2.5 Modal significance associated to the characteristic modes J_1, J_2, J_3, J_4 of a bar type handset platform having dimensions of $120\text{ mm} \times 50\text{ mm}$	39
Fig. 2.6 Current distribution regarding a bar type handset platform having dimensions of $120\text{ mm} \times 50\text{ mm}$ corresponding to a) Characteristic mode J_1 ; b) Characteristic mode J_2 ; c) Characteristic mode J_3 ; d) Characteristic mode J_4	39
Fig. 2.7 Modal significance associated to the characteristic modes J_1, J_2, J_3, J_4 of a clamshell type handset platform having two PCBs being adapted to be folded together, each one comprising a ground plane with dimensions of $80\text{ mm} \times 40\text{ mm}$	40
Fig. 2.8 Current distributions regarding a clamshell type handset platform having two PCBs being adapted to be folded together, each one comprising a ground plane with dimensions of $80\text{ mm} \times 40\text{ mm}$. a) Characteristic mode J_1 ; b) Characteristic mode J_2 ; c) Characteristic mode J_3	40
Fig. 2.9 Polarization of the incident wave used to determine the fundamental mode of a metal plate with dimensions of a ground plane associated to a bar-type wireless handheld device.	42

Fig. 2.10 Comparison between normalized RCS and modal significance for a bar-type platform 100 mm x 40 mm.....	43
Fig. 2.11 Comparison between normalized RCS and modal significance for a smartphone platform 120 mm x 50 mm.....	44
Fig. 2.12 Comparison between normalized RCS and modal significance for a clamshell having two PCBs being adapted to be folded together, each one comprising a ground plane with dimensions of 80 mm x 40 mm.....	44
Fig. 2.13 Comparison between the resonance of the fundamental mode of a bar-type platform with dimensions 100 mm x 40 mm and the resonance of the fundamental mode of a smartphone platform (120 mm x 50 mm).	45
Fig. 2.14 Comparison of a PIFA and a ground plane booster both for GSM850 and GSM900 operation. The size of the PIFA is 40 mm x 15 mm x 6 mm whereas the size of the ground plane booster is just 5 mm x 5 mm x 5 mm.....	46
Fig. 2.15 Measured reflection coefficient for a non-resonant element of 5 mm x 5 mm x 5mm including a broadband matching network and regarding two ground planes of different size.....	46
Fig. 2.16 a) Ground plane of dimensions 100 mm x 40 mm; b) the same ground plane having a conductive strip of 40 mm x 33 mm x 3 mm. Both ground planes are supported by a thin dielectric slab of 1mm thick with $\epsilon_r=4.15$	47
Fig. 2.17 Comparison of the normalized RCS for a ground plane of 100 mm x 40 mm and the same ground plane with the conductive strip (Fig. 2.16).....	48
Fig. 2.18 Induced current (A/m) for a plane wave excitation according to Fig. 2.9 at a) $f=0.96\text{GHz}$; b) and $f=1.02\text{GHz}$. Same maximum and dynamic range is used for both illustrations.	49
Fig. 2.19 Simulated radiation efficiency for a PIFA on a ground plane 100 mm x 40 mm and the conductive strip 40 mm x 33 mm x 3mm.....	50
Fig. 2.20 Ground plane having dimensions of 100 mm x 40 mm and integrating an open slot with dimensions of 38 mm x 3 mm. The ground plane is etched on a thin dielectric slab of 1mm thick and $\epsilon_r=4.15$, $\tan\delta=0.013$	51
Fig. 2.21 Comparison of RCS for three different ground planes: 100 mm x 40 mm, 100 mm x 40 mm with a conductive strip as shown (Fig. 2.16), and a ground plane 100 mm x 40 mm with slot 38 mm long and 3mm width (Fig. 2.20). The plane wave impinges the ground plane according to Fig. 2.9. All ground planes are etched on a thin dielectric slab of 1mm thick and $\epsilon_r=4.15$, $\tan\delta=0.013$	51
Fig. 2.22 Geometry of the proposed structures (spiral, H2, H3, and pad) placed in a corner of a ground plane having dimensions of 90 mm x 40 mm etched in a 1mm FR4 substrate $\epsilon_r=4.15$ $\tan\delta=0.013$. For this case, spiral, H2, and H3 resonate at 900MHz whereas the pad element presents a higher resonant frequency around 1921MHz.	54
Fig. 2.23 BW_0 associated to the spiral, H2, and H3 when they are resonating at 900MHz, and to a pad resonating at 1920MHz. All the elements considered, are placed in a corner of a ground plane having dimensions of 90 mm x 40mm and being etched in a 1 mm FR4 substrate ($\epsilon_r=4.15$, $\tan\delta=0.013$).....	55
Fig. 2.24 Dipole configurations for the pad and spiral used to compute the Q of the element itself. A dipole arm corresponds to the element used in Fig. 2.22.	56
Fig. 2.25 BW_0 for the spiral, H2, H3, and pad when the resonant frequency of the antenna element becomes equal to the resonance of the ground plane mode ($f_r=f_{GP}=1170\text{MHz}$).	57
Fig. 2.26 Comparisons of the BW_0 attained by H3 when it is designed to resonate at 900MHz and at 1170MHz, which coincides with the ground plane resonance.	58

- Fig. 2.27 Comparison of the BW_0 attained by the four geometries under study when they are designed to resonate above the resonant frequency of a ground plane having dimensions of 90 mm x 40 mm and being etched over a 1 mm thick FR4 substrate ($\epsilon_r=4.15$, $\tan\delta=0.013$) ($f_{GP}=1170\text{MHz}$)...... 59
- Fig. 2.28 Comparison of the BW_0 attained by the four geometries under study when they are designed to resonate above the resonant frequency of a ground plane having dimensions of 120 mm x 50 mm and being etched over a 1 mm thick FR4 substrate ($\epsilon_r=4.15$, $\tan\delta=0.013$) ($f_{GP}=925\text{MHz}$). 59
- Fig. 2.29 Left: Modulus of the input impedance according to the feeding arrangement. The current distribution relates to the frequency of 825 MHz, which corresponds, approximately, to the center frequency of the frequency range (690-960MHz). The current maximum is fixed to 0.5A/m and the dynamic range is 30dBs; Right: Smith Chart representation of the input impedance..... 60
- Fig. 2.30 Left: BW_0 according to the feeding arrangement and the dipole arms width. The current distribution relates to the frequency of 825 MHz, which corresponds, approximately, to the center frequency of the frequency range (690-960MHz). The current maximum is fixed to 0.5A/m and the dynamic range is 30dBs; Right: Radiation efficiency and quantitative BW_0 61
- Fig. 3.1 Eigenvalues (λ) and modal significance versus frequency associated to the first and second predominant modes (λ_1 and λ_2) regarding a PCB with dimensions 100 mm x 40 mm. Current distribution (A/m) at the frequency of $f=892\text{MHz}$ provided by the first radiating mode J_1 75
- Fig. 3.2 Geometry and dimensions associated to the radiating structure comprising two non-resonant ground plane boosters located at a 2 mm distance from the ground plane edge, each one in charge of the ground plane excitation for each frequency region. Current distribution referred to the excited ground plane mode at $f=0.892\text{GHz}$ The ground plane is supported by a thin FR4 substrate layer of 1mm thick having $\epsilon_r=4.15$ and $\tan\delta=0.013$ 76
- Fig. 3.3 Q_a and related BW_0 versus frequency referred to the radiating structure of Fig. 3.2. 77
- Fig. 3.4 a) Equivalent circuit regarding the input impedance referred to the radiating structure, the reactance compensation (series inductor (L)) stage and the broadband matching network; b) Condition required for achieving a BW enhancement around one half of Fano's limit. 78
- Fig. 3.5 a) Equivalent circuit regarding the input impedance referred to the radiating structure, the reactance compensation (series inductor (L)) stage and the broadband matching network for the low frequency region; b) The same sequence but regarding the high frequency region. 80
- Fig. 3.6 a) Impedance associated to the radiating structure (triangular markers); Impedance after the addition of the series inductor as a reactance compensation element for the low frequency region (square markers); Impedance according to the schematic shown in (Fig. 3.5a) (rhombus marker); b) The same sequence but regarding the high frequency region (Fig. 3.5b)..... 80
- Fig. 3.7 Reflection coefficient associated to the radiating structure without any components (dashed line); Reflection coefficient associated to the schematic shown in (Fig. 3.5a) designed for covering the low frequency region (solid line with square markers); Reflection coefficient associated to the schematic shown in (Fig. 3.5b) designed for covering the high frequency region (solid line with triangular markers). 80
- Fig. 3.8 a) Radiating system designed for achieving a penta-band behavior consisting in a reactance cancellation element, a broadband matching network, and a notch filter for each frequency region. Note that the first stage of the notch filter and the broadband matching network can be simplified using only two components. The two-port box is the simulated input impedance of the radiating structure shown in Fig. 3.2; b) Detailed view of the radiating structure obtained from the simulated layout comprising two non-resonant ground plane boosters with dimensions 5 mm x 5 mm x 5mm, and a ground plane with dimension 100 mm x 40 mm. The ground plane boosters are located at a 2 mm distance from the edge of the ground plane. 81
- Fig. 3.9 Reflection coefficient associated to the schematic shown in Fig. 3.5a (dashed line with square markers) and in Fig. 3.5b (dashed line with triangular markers) for providing operability in both

frequency regions separately; Reflection coefficient to provide penta-band operation simultaneously achieved with the radiating system proposed in Fig. 3.8 (solid line).	82
Fig. 3.10 a) Radiation efficiency (η_r), and antenna efficiency (η_a); b-c) Current distribution associated to the radiating structure at the central frequencies of both frequency regions ($f=0.89$ and $f=1.94$ GHz), respectively. The antenna efficiency takes into account the mismatch losses since it is defined as $\eta_a=\eta_r\cdot(1- S_{11} ^2)$	82
Fig. 3.11 Reflection coefficient to provide penta-band operation simultaneously achieved with the radiating system proposed in Fig. 3.8 (solid line). Reflection coefficient associated to the same radiating structure (Fig. 3.8b) but with the difference that the size of the ground plane boosters (previously 5 mm x 5 mm x 5 mm) has been reduced to only 3 mm x 3 mm x 3 mm (dashed line). The topology of the radiofrequency system remains equal and corresponds to that illustrated in Fig. 3.8a, whereas the values of the reactive components have been adjusted.	83
Fig. 3.12 Prototype including the reactance cancellation inductor and the broadband matching network used for covering one frequency region The components of the matching circuit are SMD 0402 type.	84
Fig. 3.13 Penta-band prototype designed according to the schematic shown in Fig. 3.8 including besides the reactance cancellation inductor and the broadband matching network, the notch filters required for providing isolation between both frequency regions.	84
Fig. 3.14 Reflection coefficient related to the penta-band prototype (Fig. 3.13).	85
Fig. 3.15 Radiation efficiency (η_r) and antenna efficiency (η_a) related to the penta-band prototype (Fig. 3.13). The antenna efficiency takes into account the matching losses since $\eta_a=\eta_r\cdot(1- S_{11} ^2)$	85
Fig. 3.16 Set-up for radiation measurement in the Fractus' anechoic chamber Satimo Stargate-32 showing the coordinate system. The ground plane lies in the XY plane having the longest dimension aligned with the Y-axis.	86
Fig. 3.17 Main cuts ($\Phi=0^\circ$ and $\Phi=90^\circ$) of the radiation pattern provided by the penta-band prototype (Fig. 3.13) measured at the frequencies of $f=900$ MHz, $f=1800$ MHz, and $f=2000$ MHz.	86
Fig. 3.18 SAR measurements for the low frequency region at the specific frequencies of $f=835$ MHz and $f=900$ MHz regarding both positions: left ("Boosters Up") and right ("Boosters Down"). Right cheek position is tested.	87
Fig. 3.19 SAR measurements for the high frequency region at the specific frequencies of $f=1700$ MHz, $f=1800$ MHz, $f=1900$ MHz and $f=2000$ MHz regarding both positions: left ("Boosters Up") and right ("Boosters Down").	88
Fig. 3.20 Effect of the ground plane size over the first and the fourth radiating mode. Note that the second and the third radiating modes have not been illustrated due to the fact that they mainly contribute to store energy rather than to radiate it (see section 2.2.1). Note that the dielectric support is omitted in this calculus; its consideration would produce a further shifting to lower frequencies.	90
Fig. 3.21 Current distribution associated to the first and fourth radiating modes of a ground plane having dimensions of 100 mm x 40 mm and 120 mm x 50 mm.	91
Fig. 3.22 Detailed view of a radiating structure comprising two coplanar non-resonant ground plane boosters with dimensions 6 mm x 6 mm, and a ground plane with dimension 120 mm x 50 mm. The ground plane boosters are located at 1 mm distance from the shortest edge of the ground plane. The ground plane is supported by a thin FR4 substrate layer of 1mm thick having $\epsilon_r=4.15$ and $\tan\delta=0.013$	92
Fig. 3.23 Input impedance associated to the radiating structure shown in Fig. 3.22 regarding one ground plane booster.	92
Fig. 3.24 BW_0 associated to a handset platform featuring dimensions of 120 mm x 50 mm as a function of the booster size regarding the low frequency region. a) comparison for several square-shaped	

pads; b) comparison for two pads having the same area but different orientation. A smaller pad is included also as a reference.	93
Fig. 3.25 BW_0 associated to a handset platform featuring dimensions of 120 mm x 50 mm as a function of the booster size regarding the high frequency region. a) comparison for several square-shaped pads; b) comparison for two pads having the same area but different orientation. A smaller pad is included also as a reference.	93
Fig. 3.26 Radiofrequency system proposed including two broadband matching networks (LC resonators) each one intended respectively for the low and high frequency regions. The series C is used to allocate the impedance loop at the center of the Smith chart.	94
Fig. 3.27 a) Current distribution at $f=0.9\text{GHz}$ and b) at $f=2.2\text{GHz}$ when considering the proposed radiofrequency system depicted in Fig. 3.26.	94
Fig. 3.28 Simulated reflection coefficient (S_{11}) and input impedance after the addition of the proposed radiofrequency system depicted in Fig. 3.26.	95
Fig. 3.29 a) Front-view of a radiating system comprising two coplanar ground plane boosters; b) Detailed view of the radiating system depicting the integration of the radiofrequency system described in Fig. 3.26.	96
Fig. 3.30 Measured reflection coefficient (S_{11}) of the prototype depicted in Fig. 3.29.	96
Fig. 3.31 Measured radiation (η_r) and antenna efficiency ($\eta_a=\eta_r\cdot(1- S_{11} ^2)$) of the prototype depicted in Fig. 3.29.	96
Fig. 3.32 BW_0 for a pad of 12 mm x 6 mm and a pad of 6 mm x 6mm on a ground plane of 120 mm x 50mm (solid line). The dashed line represents the potential bandwidth enhancement (BW_p) due to the broadband matching network. The square represents the required bandwidth at a given frequency band (see Table 3.1).	98
Fig. 3.33 BW_0 for a pad of 6 mm x 6 mm in a ground plane of 120 mm x 50 mm (square markers). The line with circular markers represents the potential bandwidth enhancement (BW_p) due to the broadband matching network. The square represents the required bandwidth at a given frequency band (Table 3.1).	98
Fig. 3.34 Architecture of the proposed small, multi-band, and planar radiating structure, comprising four pads placed at the corners of a ground plane of 120 mm x 50 mm etched on a thin layer of FR4 having 1mm thick, $\epsilon_r=4.15$, $\tan\delta=0.013$. Pad 1 is designed for LTE700; pad 2 for GSM850 and GSM900; pad 3 for GPS; and pad 4 for GSM1800 up to LTE2500. The distance between the pad and the transversal edge of the ground plane is 1mm. The total area occupied by the pads is only 153mm ²	99
Fig. 3.35 Radiofrequency system selected for the radiating structure of Fig. 3.34. Port 1, 2, 3, and 4 correspond to LTE700, GSM850/GSM900, GPS, and GSM1800/GSM1900/UMTS/LTE2300/LTE2500, respectively. Port 1, 2 and 4 includes broadband matching networks whereas port 3 (GPS) include a single series component. The values shown are those selected for the built prototype.	99
Fig. 3.36 a) Simulated input impedance for all the ports showing the input impedance loops due to the addition of a broadband matching network (Fig. 3.35), except for the GPS pad, which only requires a single series reactive element; b) Simulated S-parameters for the proposed radiating system (Fig. 3.35).	100
Fig. 3.37 Computed surface current distributions at several frequencies. a) $f=750\text{MHz}$ port 1 excited; b) $f=950\text{MHz}$ port 2 excited; c) $f=1575\text{MHz}$ port 3 excited; d) $f=2200\text{MHz}$ port 4 excited. Each pad is connected to the matching network illustrated in Fig. 3.35.	100
Fig. 3.41 Geometry and dimensions associated to the radiating structure comprising a magnetic booster located at the center of the longitudinal edge of the ground plane. Current distribution referred to the excited ground plane radiating mode at $f=900\text{MHz}$ and $f=1940\text{MHz}$. The ground plane is etched over a 1mm thickness FR4 piece ($\epsilon_r=4.15$ and $\tan\delta=0.013$).	105

Fig. 3.42 Geometry and dimensions associated to the radiating structure comprising a magnetic booster located at the center of the transversal edge of the ground plane. Current distribution referred to the excited ground plane radiating mode at $f=900\text{MHz}$ and $f=1940\text{MHz}$. The ground plane is etched over a 1mm thickness FR4 piece ($\epsilon_r=4.15$ and $\tan\delta=0.013$).	106
Fig. 3.43 Effect of the size and the arrangement of the magnetic booster over the radiation efficiency (η_r) of the radiating structure.....	106
Fig. 3.44 Q and BW_0 versus frequency referred to the radiating structure comprising a magnetic booster with dimensions 5 mm x 18 mm as a function of their placement with respect to a ground plane with dimensions 100 mm x 40 mm.	107
Fig. 3.45 Q and BW_0 versus frequency referred to the radiating structure comprising a magnetic booster with dimensions 5 mm x 10 mm as a function of their placement with respect to a ground plane with dimensions 100 mm x 40 mm.	108
Fig. 3.46 Radiofrequency system including a reactance compensation and a broadband matching network for the low frequency region. The one-port box corresponds to the simulated impedance of the radiating structure comprising a magnetic booster of 5 mm x 18 mm placed in the center of the longest edge of the PCB (100mm x 40mm).	108
Fig. 3.47 Radiofrequency system including reactance compensation and broadband matching network for the high frequency region. The one-port box corresponds to the simulated impedance of the radiating structure comprising a magnetic booster of 5 mm x 10 mm placed in the center of the longest edge of the PCB (100mm x 40mm).	109
Fig. 3.48 Impedance associated to the radiating structure comprising a magnetic booster of 5 mm x 18 mm (triangular markers); Impedance after the addition of the series capacitor as a reactance compensation element for the low frequency region (square markers); Impedance attained through the radiofrequency system shown in Fig. 3.46 (rhombus markers).	110
Fig. 3.49 Reflection coefficient associated to the radiating structure (dashed line); Reflection coefficient regarding the addition of the reactance compensation element (solid line with square markers); Reflection coefficient associated to the radiofrequency system shown in Fig. 3.46 designed for covering the low frequency region (solid line with rhombus markers).....	110
Fig. 3.50 Impedance associated to the radiating structure (triangular markers); Impedance after the addition of the series capacitor as a reactance compensation element for the high frequency region (square markers); Impedance attained through the radiofrequency system shown in Fig. 3.47 (rhombus markers).....	111
Fig. 3.51 Reflection coefficient associated to the radiating structure (dashed line); Reflection coefficient regarding the addition of the reactance compensation element (solid line with square markers); Reflection coefficient associated to the radiofrequency system shown in Fig. 3.47 designed for covering the high frequency region (solid line with rhombus markers).....	111
Fig. 3.52 Radiation efficiency (η_r) associated to the proposed radiating structures and antenna efficiency (η_a) referred to the radiating systems presented in Fig. 3.46 and Fig. 3.47. The antenna efficiency takes into account the matching losses since it is defined as $\eta_a = \eta_r \cdot (1 - S_{11} ^2)$. The dashed area corresponds to the frequency ranges associated to the low frequency region (824-960MHz) and to the high frequency region (1710-2170MHz).	112
Fig. 3.53 a) Prototype intended for the low frequency region comprising a magnetic booster with dimensions of 5 mm x 18 mm and the radiofrequency system depicted in Fig. 3.46; b) Prototype intended for the high frequency region comprising a magnetic booster with dimensions of 5 mm x 10 mm and the radiofrequency system depicted in Fig. 3.47. Ground plane size is 100 mm x 40 mm. Both magnetic boosters are located at the center of the longest edge.	112
Fig. 3.54 Set-up measurement in the anechoic chamber Satimo Stargate-32.	113
Fig. 3.55 Measured reflection coefficient associated to the prototype depicted in Fig. 3.53a.	113
Fig. 3.56 Measured reflection coefficient associated to the prototype depicted in Fig. 3.53b.	114

Fig. 3.57 3D radiation patterns for approximately the central frequency of the low frequency region (900MHz) and the high frequency region (1900MHz).	114
Fig. 3.58 η_r and η_a referred to the radiating system presented in Fig. 3.53a. The dashed area corresponds to the frequency ranges associated to the low frequency region (824-960MHz).	115
Fig. 3.59 η_r and η_a associated to the radiating system presented in Fig. 3.53b. The dashed area corresponds to the frequency ranges associated to the high frequency region (1710-2170MHz).	115
Fig. 3.60 Matching network topology and input impedance response associated to the different stages that constitute the proposed radiofrequency system. a) reactive cancellation for the low frequency region; b) reactive cancellation for the high frequency region; c) combination into a single port; d) fine-tuning stage that place the impedance loops at the center of the Smith chart.	117
Fig. 3.61 Reflection coefficient and input impedance obtained from the proposed radiofrequency system depicted in Fig. 3.60d.	118
Fig. 3.62 Radiating structure comprising two ground plane boosters (5 mm x 5 mm x 5 mm) and a ground plane (120 mm x 50 mm) etched over a 1 mm thick FR4 piece (left); radiation properties are measured using anechoic chamber Satimo Stargate-32 (right).	119
Fig. 3.63 Measured reflection coefficient (S_{11}) associated to the prototype depicted in Fig. 3.62.	119
Fig. 3.64 Measured radiation (η_r) and antenna efficiency ($\eta_a = \eta_r (1 - S_{11} ^2)$) associated to the prototype depicted in Fig. 3.62.	119
Fig. 4.1 Geometry of the four radiating systems proposed. All prototypes are etched over a 1 mm thick FR4 piece ($\epsilon_r = 4.15$, $\tan\delta = 0.013$). Penta-band coupled monopoles set (left), penta-band compact radiating system (2 nd column), dual-band PIFA (top right), and hexa-band PIFA with a slotted ground plane (bottom right).....	131
Fig. 4.2 Set-up for radiation measurement in the anechoic chamber Satimo Stargate-32 showing the coordinate system regarding free-space and the human head presence for the “Antenna Down” position.	132
Fig. 4.3 S_{11} regarding free-space and head interaction. a) Dual-band PIFA; b) Hexa-band PIFA with a slotted ground plane; c) Coupled Monopoles; d) Compact radiating system.....	133
Fig. 4.4 Antenna efficiency measured by 3D integration pattern in the anechoic chamber Satimo Stargate-32 regarding the: dual-band PIFA (Fig. 4.1 (top right)), hexa-band PIFA (Fig. 4.1 (bottom right)), coupled monopoles (Fig. 4.1 (left)), and compact radiating system (Fig. 4.1 (2 nd column)) in free-space. The antenna efficiency takes into account the mismatch losses, since it is defined as $\eta_a = \eta_r (1 - S_{11} ^2)$	134
Fig. 4.5 Radiation efficiency associated to the dual-band PIFA (Fig. 4.1 (top right)), the hexa-band PIFA (Fig. 4.1 (bottom right)), the coupled monopoles (Fig. 4.1 (left)), and the compact radiating system (Fig. 4.1 (2 nd column)) regarding free-space.	135
Fig. 4.6 Measured radiation efficiency in the low and high frequency region for the dual-band PIFA (Fig. 4.1 (top right)), the hexa-band PIFA (Fig. 4.1 (bottom right)), the coupled monopoles (Fig. 4.1 (left)), and the compact radiating system (Fig. 4.1 (2 nd column)) regarding a)-b) “Antenna Up” position and c)-d) “Antenna Down” position.	136
Fig. 4.7 Average absorption ratios across the low frequency region (824-960 MHz) and the high frequency region (1710-2170MHz) regarding both positions “Antenna Up” and “Antenna Down”.	136
Fig. 4.8 Measured antenna efficiency in the low and high frequency region for the dual-band PIFA (Fig. 4.1 (top right)), the hexa-band PIFA (Fig. 4.1 (bottom right)), the coupled monopoles (Fig. 4.1 (left)), and the compact radiating system (Fig. 4.1 (2 nd column)) regarding a)-b) “Antenna Up” position and c)-d) “Antenna Down” position.	137

Fig. 4.9 Main cuts ($\Phi=0^\circ$ and $\Phi=90^\circ$) of the radiation patterns provided by the compact radiating system prototype (Fig. 4.1 (2 nd column)) measured at the frequency of 900MHz and 2000MHz regarding free-space and human head for both positions: “Boosters Up” and “Boosters Down”. See coordinate axis at Fig. 4.2.....	138
Fig. 4.10 Measured directivity in the low frequency region regarding the four prototypes in free-space and human head conditions.....	139
Fig. 4.11 Measured directivity in the high frequency region regarding the four prototypes in free-space and human head conditions.....	139
Fig. 4.12 Figure of Merit regarding “Antenna Up” position.....	143
Fig. 4.13 Figure of Merit regarding “Antenna Down” position.....	144
Fig. 5.1 Schematic example of a distributed antenna system consisting of a passive array of two monopole antennas placed at the corners of the ground plane of a handset device. A phase delay ϕ is used to optimize the bandwidth.....	153
Fig. 5.2 a) Electrical model for a distributed antenna system similar to that schematically depicted in Fig. 5.1. Z_1 and Z_2 correspond to the complex input impedances of monopoles 1 and 2, respectively, which are connected through a transmission line with characteristic impedance $Z_0=50 \Omega$ and electrical length ϕ ; b) Electrical model for a distributed antenna system comprising three monopoles.....	154
Fig. 5.3 Simulated impedance for the electrical circuit of Fig. 5.2a. a) Input impedance Z_1 of a monopole antenna (triangular markers); b) Z_2' which is the resulting input impedance Z_2 after the addition of a transmission line featuring 90° at f_0 (square markers); c) distributed system with $Z_1=Z_2$, $\phi=90^\circ$ at 900 MHz (rhombus markers).....	154
Fig. 5.4 Simulated impedance for the electrical circuit of Fig. 5.2b. a) Input impedance Z_1 of a monopole antenna (triangular markers); b) Z_2' which is the resulting input impedance Z_2 after the addition of a transmission line featuring 60° at f_0 (square markers); c) Z_3' which is the resulting input impedance Z_3 after the addition of a transmission line featuring 120° at f_0 (rhombus markers); d) distributed system with $Z_1=Z_2=Z_3$, $\phi_1=60^\circ$ and $\phi_2=120^\circ$ at 900MHz (double triangle markers).....	155
Fig. 5.5 Simulated reflection coefficient (S_{11}) associated to an impedance Z_1 corresponding to a series RLC circuit featuring $f_0=900\text{MHz}$, $R=20\Omega$, $Q=20$ (triangular markers); S_{11} regarding Z_2' (square markers); S_{11} regarding Z_1 connected to a generator having an internal impedance $Z_g=R$ (double triangle markers); S_{11} for the distributed antenna system of Fig. 5.2a (2 monopoles) connecting two equal impedances $Z_1=Z_2$ with a $\phi=90^\circ$ (900MHz) transmission line having a characteristic impedance $Z_0=50 \Omega$ (rhombus markers); and S_{11} for the distributed antenna system of Fig. 5.2b (3 monopoles) having $Z_1=Z_2=Z_3$ and $\phi_1=60^\circ$ and $\phi_2=120^\circ$ at 900MHz (circular markers).....	156
Fig. 5.6 Left) single monopole; middle) distributed antenna system comprising two monopoles; right) distributed antenna system of three monopoles. The ground plane in all cases presents dimensions of 90 mm x 40 mm and is printed on a FR4 substrate 1 mm thick. The footprint for the monopoles is 13 mm x 11 mm.....	157
Fig. 5.7 Measured reflection coefficient for the radiating systems of Fig. 5.6.....	158
Fig. 5.8 Measured antenna efficiency for the radiating systems shown in Fig. 5.6. The antenna efficiency takes into account both radiation efficiency and mismatch losses $\eta_a=\eta_r (1- S_{11} ^2)$	158
Fig. 5.9 Measured directivity for the single monopole and the distributed antenna systems of two and three monopoles. Measured 3D radiation pattern at 900MHz showing the typical $\lambda/2$ dipole-type pattern for the distributed system of three monopoles.....	159
Fig. 5.10 Simulated current distribution at $f=850\text{MHz}$ depicting the current aligned with the longitudinal edges of the ground plane, hence approximating that of a typical half-wavelength mode, null at the transversal edges and maximum at the center of the longitudinal edges.....	159

Fig. 5.11 Left: common holding position during a call; right: the phantom hand emulating the real situation illustrated in the figure on the left.....	160
Fig. 5.12 Detail of the phantom finger covering the upper right corner of the PCB for the three prototypes under consideration: a) single monopole; b) two monopoles; c) three monopoles.	161
Fig. 5.13 Measured antenna efficiency taking into account the phantom hand over the PCB and the finger in the right position.....	161
Fig. 5.14 Detail of the phantom finger covering the upper middle area of the PCB for the three prototypes under consideration: a) single monopole; b) two monopoles; c) three monopoles.	161
Fig. 5.15 Measured antenna efficiency taking into account the phantom hand over the PCB and the finger in the middle position.	162
Fig. 5.16 Detail of the phantom finger covering the upper left corner of the PCB for the three prototypes under consideration: a) single monopole; b) two monopoles; c) three monopoles.	162
Fig. 5.17 Measured antenna efficiency taking into account the phantom hand over the PCB and the finger in the left position.....	162
Fig. 5.18 Average antenna efficiency (824-960MHz) in free-space and regarding hand loading for the proposed antenna systems (Fig. 5.6) and regarding the three finger positions analyzed.	163
Fig. 5.19 Hand losses averaged in the 824-960MHz frequency range for the proposed antenna systems (Fig. 5.6) and regarding the three finger positions analyzed.	163
Fig. 5.20 Simulated impedance for the electrical circuit of Fig. 5.2a. Input impedance Z_1 of a monopole (triangular markers); Z_2' which is the resulting input impedance Z_2 after the addition of a transmission line featuring 90° at f_0 (square markers); distributed system with $Z_1=Z_2$, $\phi=90^\circ$ at 900 MHz (rhombus markers). Both RLC series circuits Z_1 and Z_2 are characterized by an input resistance $R=20\Omega$, quality factor $Q=20$, and resonant frequency $f_0=900\text{MHz}$	166
Fig. 5.21 Electrical model of a distributed antenna system comprising a passive array of two monopoles fed in-phase when $\phi_1=\phi_2$. Z_1 and Z_2 correspond to the complex input impedances of monopoles 1 and 2, respectively, which are connected through two transmission lines with characteristic impedances $Z_0=50\ \Omega$ and electrical length ϕ_1 and ϕ_2 , respectively	167
Fig. 5.22 Simulated impedance for the electrical circuit of Fig. 5.21. Input impedance Z_1' and Z_2' are respectively, the resulting input impedances Z_1 and Z_2 after the addition of two transmission lines, each one featuring 90° at f_0 (square and triangular markers); distributed system with $Z_1=Z_2$, $\phi_1=\phi_2=90^\circ$ at 900 MHz (rhombus markers). $Z_1=Z_2$ have $R=20\Omega$, $Q=20$, and $f_0=900\text{MHz}$	167
Fig. 5.23 Geometry associated to the proposed radiating system composed by two Hilbert monopoles having a footprint area of 12 mm x 14 mm. The Hilbert monopoles are arranged at the corners of the shorter edge of a ground plane having dimensions of 90 mm x 40 mm.	168
Fig. 5.24 Proposed radiofrequency systems. a) Broadband matching network and fine-tuning stage for a single Hilbert monopole; b) Out-of-phase distributed antenna system; c) In-phase distributed antenna system. Both, in-phase and out-of-phase schemes include a matching network after the combination of the response into a single input/output port. Note that the one-port box depicted in a) corresponds to the input impedance associated to a single Hilbert monopole while the two port-box shown in b) and c) corresponds to the distributed antenna system depicted in Fig. 5.23.	169
Fig. 5.25 Reflection coefficient corresponding to the radiating structures and the radiofrequency systems depicted in Fig. 5.23 and Fig. 5.24.	169
Fig. 5.26 Current distribution at frequencies 850 MHz (a-c) and 900 MHz (d-f); a) and d) single Hilbert monopole (Fig. 5.24a); b) and e) out-of-phase distributed antenna system (Fig. 5.24b); c) and f) in-phase distributed antenna system (Fig. 5.24c). Amplitude (in volts) and phase (in degrees) information for each port takes into account the radiofrequency systems of Fig. 5.24. The arrows represent schematically the sense of the current vectors.	170

Fig. 5.27 Simulated radiation efficiency (η_r) associated to the radiating systems under study taking into account the corresponding radiofrequency systems of Fig. 5.24.....	170
Fig. 5.28 a) Single Hilbert monopole connected to the radiofrequency system depicted in Fig. 5.24a; b) In-phase distributed antenna system comprising two identical Hilbert monopoles and connected to the radiofrequency system defined in Fig. 5.24c; The ground plane in all cases presents dimensions of 90 mm x 40 mm and is printed on a FR4 substrate 1mm thick. The footprint of the monopoles is 14 mm x 12 mm.....	171
Fig. 5.29 Measured reflection coefficient for the radiating systems of Fig. 5.28.....	172
Fig. 5.30 Measured antenna efficiency (η_a) for the radiating systems shown in Fig. 5.28. The antenna efficiency takes into account both ohmic losses and mismatch losses, $\eta_a = \eta_r \cdot (1 - (S_{11})^2)$. Shaded area ranges from 824 to 960MHz.....	173
Fig. 5.31 Measured directivity (dB) for the Hilbert monopole and the in-phase distributed antenna system. Measured 3D radiation pattern at 900MHz showing the typical $\lambda/2$ dipole-type pattern for the in-phase distributed antenna system.....	173
Fig. 5.32 Measured reflection coefficient and antenna efficiency taking into account the phantom hand over the PCB; Detail of the phantom finger covering the upper part of the single Hilbert monopole prototype for the three positions under study: a) Left; b) Middle; c) Right.	174
Fig. 5.33 Measured reflection coefficient and antenna efficiency taking into account the phantom hand over the PCB; Detail of the phantom finger covering the upper part of the distributed system prototype for the three positions under study: a) Left; b) Middle; c) Right.	175
Fig. 5.34 Measured average antenna efficiency (824-960MHz) for the single Hilbert monopole, the in-phase distributed system, and a coupled monopoles taking into account the phantom hand...	176
Fig. 5.35 Modal significance associated to the current modes J_1, J_2, J_3, J_4 supported by a ground plane having dimensions of 120 mm x 50 mm. The modal significance represents the normalized amplitude associated to the current modes and provides a physical insight into their radiation properties. As long as the curve approaches the maximum value of one, radiation efficiency increases. The current distributions for the modes J_1 and J_4 are shown.....	178
Fig. 5.36 Geometry and dimensions associated to the radiating structure comprising four non-resonant ground plane boosters located at the corners of the rectangular ground plane having typical dimensions of current smartphones 120 mm x 50 mm. Each ground plane booster is a square metallic cube comprising six faces of 5 mm length.	178
Fig. 5.37 a) Schematic example of a distributed antenna system; b) In-phase feeding scheme ($\phi_1 = \phi_2$); c) Out-of-phase feeding scheme (ϕ phase difference between Z_1 and Z_2). Z_1 and Z_2 correspond to the complex input impedances of the first and second non-resonant elements, respectively...	179
Fig. 5.38 a) In-phase feeding mechanism applied to the HFR; Out-of-phase feeding mechanism where b) the impedances are substantially complementary; c) the impedances are substantially conjugated. The two input impedances illustrated in each Smith chart correspond to the input impedance measured at the corresponding input port of the circuit schematics depicted below each Smith chart.	180
Fig. 5.39 Proposed radiofrequency system based on: a) in-phase feeding scheme for the LFR and HFR, and b) out-of-phase feeding scheme for the HFR and in-phase feeding scheme for the LFR. Ports LFR 1, LFR 2, HFR 1, and HFR 2 represent the ports of Fig. 5.36.....	181
Fig. 5.40 S-parameters resulting from the radiating system gathered in Fig. 5.39a. Solid line with bowtie markers corresponds to the S_{11} measured at the input/output port 2, whereas solid line with square markers refers to port 1. Transmission coefficient (S_{21}) between ports is represented by a solid line with rhombus markers.	182
Fig. 5.41 S-parameters resulting from the radiating system gathered in Fig. 5.39b. Solid line with bowtie markers corresponds to the S_{11} measured at the input/output port 4, whereas solid line with	

square markers refers to port 3. Transmission coefficient (S_{21}) between ports is represented by a solid line with rhombus markers.	182
Fig. 5.42 a)-c) Current distribution regarding an in-phase feeding scheme (Fig. 5.39a), an out-of-phase feeding scheme (Fig. 5.39b), and a single element with a broadband matching network, for the center frequency of the LFR (825MHz), respectively, and d)-f) for the center frequency of the HFR (2100MHz), respectively.	183
Fig. 5.43 Comparison between the impedance bandwidth attained by an in-phase feeding scheme (solid line with square markers), an out-of-phase feeding scheme based on conjugated input impedances (solid line with bowtie markers), and a single element solution (5 mm x 10 mm x 5 mm) with a broadband matching network (solid line with triangular markers).	184
Fig. 5.44 Prototyped solution including a) in-phase feeding scheme for both frequency regions; b) in-phase feeding scheme for the LFR (upper edge) and out-of-phase feeding scheme for the HFR (bottom edge); c) Single element 5 mm x 10 mm x 5 mm with a broadband matching network (note that for the single element case the component values of the matching network are adapted according to the frequency region of operation). The reactive elements used are SMD0402.	184
Fig. 5.45 S-parameters resulting from the radiating system gathered in Fig. 5.44a (solid lines) compared with those extracted from simulations (dashed lines) (Fig. 5.40). Solid line with bowtie markers corresponds to the reflection coefficient measured at the input/output port 2 (Fig. 5.39a), whereas solid line with square markers refers to port 1 (Fig. 5.39a). Transmission coefficient between ports (solid line with rhombus markers).	185
Fig. 5.46 S-parameters resulting from the radiating system gathered in Fig. 5.44b (solid lines) compared with those extracted from simulations (dashed lines) (Fig. 5.41). Solid line with bowtie markers corresponds to the reflection coefficient measured at the input/output port 4 (Fig. 5.39b), whereas solid line with square markers refers to port 3 (Fig. 5.39b). Transmission coefficient between ports (solid line with rhombus markers).	186
Fig. 5.47 Phantom hand holding the prototype. a) finger in the left; b) finger in the middle; c) finger in the right.	186
Fig. 5.48 Left: Measured S_{11} (up to down): In-phase and single element solutions regarding LFR and HFR, and out-of-phase scheme for the HFR; Right: Measured η_a in free-space and regarding hand loading.	187
Fig. 6.1 Schematic representation of a MIMO System with a MIMO order of two.	200
Fig. 6.2 Schematic illustration of a SIMO, MISO, and MIMO system, respectively.	202
Fig. 6.3 MIMO Technique: Spatial multiplexing.	203
Fig. 6.4 a) Geometry of the proposed dual-band PIFA etched over a plastic carrier of 1 mm thick ($\epsilon_r=2.55$, $\tan\delta=0.013$) and being placed over a ground plane etched over an FR4 piece of 1 mm thick ($\epsilon_r=4.15$, $\tan\delta=0.013$); b) Reflection coefficient.	208
Fig. 6.5 a) Geometry of the proposed hexa-band PIFA etched over a plastic carrier of 1 mm thick ($\epsilon_r=2.55$, $\tan\delta=0.013$) and being placed over a ground plane etched over an FR4 piece of 1 mm thick ($\epsilon_r=4.15$, $\tan\delta=0.013$). In this case, a matching network is used for providing the hexa-band operation; b) Reflection coefficient. The axis coincide with those illustrated in Fig. 6.4a.	209
Fig. 6.6 a) Geometry of the proposed coupled monopoles etched over an FR4 piece of 1 mm thick ($\epsilon_r=4.15$, $\tan\delta=0.013$) and being placed over a ground plane also etched over an FR4 piece of 1 mm thick ($\epsilon_r=4.15$, $\tan\delta=0.013$); b) Reflection coefficient. The axis coincide with those illustrated in Fig. 6.4a.	209
Fig. 6.7 Radiation efficiency and antenna efficiency corresponding to the proposed radiating systems.	210

- Fig. 6.8 a)-c) Current distribution at 900MHz regarding the dual-band PIFA, the hexa-band PIFA, and the coupled monopoles, respectively; d)-f) Current distribution at 1900MHz regarding the dual-band PIFA, the hexa-band PIFA, and the coupled monopoles, respectively. Max E-current is fixed to 8 A/m and the dynamic range is 30dBs. The axis coincide with those illustrated in Fig. 6.4a. 210
- Fig. 6.9 Left) Geometry of the proposed multi-band MIMO system comprising two dual-band PIFA antennas. In this case, the antennas are placed over a 1 mm thick FR4 piece ($\epsilon_r=4.15$, $\tan\delta=0.013$) and the ground plane is also etched over a 1 mm thick FR4 piece ($\epsilon_r=4.15$, $\tan\delta=0.013$); Right) S-parameters. The axis coincide with those illustrated in Fig. 6.4a..... 212
- Fig. 6.10 Left) Correlation coefficient computed regarding radiation patterns (6.9) and S-parameters (6.10); Right) Radiation and antenna efficiency for each one of the dual-band PIFAs. 212
- Fig. 6.11 E-total regarding the main cuts of the radiation patterns associated to the radiating systems of Fig. 6.9 at the frequency of 0.9GHz. a) $\phi=0^\circ$; b) $\phi=90^\circ$. Note that the null appearing at $\phi=90^\circ$, $\theta=90^\circ$ is due to infinite FR4 piece considered in the simulation. In practice, when finite dielectrics are regarded, the $\phi=90^\circ$ cut is omnidirectional..... 213
- Fig. 6.12 Left) Geometry of the proposed multi-band MIMO system comprising two hexa-band PIFA antennas. In this case, the antennas are placed over a 1 mm thick FR4 piece ($\epsilon_r=4.15$, $\tan\delta=0.013$) and the ground plane is also etched over a 1 mm thick FR4 piece ($\epsilon_r=4.15$, $\tan\delta=0.013$); Right) S-parameters. The axis coincide with those illustrated in Fig. 6.4a..... 213
- Fig. 6.13 Left) Correlation coefficient computed regarding radiation patterns (6.9) and S-parameters (6.10). The S-parameters computation considers the matching network scheme illustrated in Fig. 6.12 for both ports; Right) Radiation and antenna efficiency for each one of the hexa-band PIFAs. In this case, the matching network is properly considered at each antenna port..... 214
- Fig. 6.14 E-total regarding the main cuts of the radiation patterns associated to the radiating systems of Fig. 6.12 at the frequency of 0.9GHz. a) $\phi=0^\circ$; b) $\phi=90^\circ$. Note that the null appearing at $\phi=90^\circ$, $\theta=90^\circ$ is due to infinite FR4 piece considered in the simulation. In practice, when finite dielectrics are regarded, the $\phi=90^\circ$ cut is omnidirectional..... 214
- Fig. 6.15 Left) Geometry of the proposed multi-band MIMO system comprising two set of coupled monopoles. The coupled monopoles are etched over a 1 mm thick FR4 piece ($\epsilon_r=4.15$, $\tan\delta=0.013$) and the ground plane is also etched over a 1 mm thick FR4 piece ($\epsilon_r=4.15$, $\tan\delta=0.013$); Right) S-parameters. The axis coincide with those illustrated in Fig. 6.4a..... 215
- Fig. 6.16 Left) Correlation coefficient computed regarding radiation patterns (6.9) and S-parameters (6.10); Right) Radiation and antenna efficiency for each set of coupled monopoles..... 215
- Fig. 6.17 a)-b) E-total regarding the $\phi=0^\circ$ and $\phi=90^\circ$ cuts associated to the radiating systems of Fig. 6.15 at the frequency of 0.9GHz; c)-d) E-total regarding the $\phi=0^\circ$ and $\phi=90^\circ$ cuts associated to the radiating systems of Fig. 6.18e at the frequency of 0.9GHz. Note that the null appearing at $\phi=90^\circ$, $\theta=90^\circ$ is due to the infinite FR4 piece considered in the simulation. In practice, when finite dielectrics are regarded, the $\phi=90^\circ$ cut is omnidirectional. 216
- Fig. 6.18 a) Correlation coefficient computed regarding radiation patterns (6.9) when the antenna elements are fed at the same edge of the ground plane; b) Correlation coefficient computed regarding radiation patterns when the antenna elements are fed at opposite edges of the ground plane; Proposed feeding arrangement at opposite edges of the ground plane for c) dual-band PIFA, d) hexa-band PIFA, and e) coupled monopoles. The axis coincide with those illustrated in Fig. 6.4a..... 217
- Fig. 6.19 Left) Geometry of the proposed multi-band MIMO system comprising a set of coupled monopoles and an hexa-band PIFA; Right) S-parameters. In this case a matching network is required for the coupled monopoles not only due to the mutual coupling appearing between both structures but also due to the fact that in this case coupled monopoles are etched over a

finite piece of FR4 ($\epsilon_r=4.15$, $\tan\delta=0.013$). The axis coincide with those illustrated in Fig. 6.4a. 217

- Fig. 6.20 Left) Correlation coefficient computed regarding radiation patterns (6.9) and S-parameters (6.10). In this case the S-parameters computation considers the matching networks illustrated in Fig. 6.19; Right) Radiation and antenna efficiency for each radiating system. Number 1 refers to the coupled monopoles whereas number 2 refers to the hexa-band PIFA. 218
- Fig. 6.21 E-total regarding the main cuts of the radiation patterns associated to the radiating systems of Fig. 6.20. a) $\phi=0^\circ$ ($f=900\text{MHz}$); b) $\phi=90^\circ$ ($f=900\text{MHz}$); c) $\phi=0^\circ$ ($f=1900\text{MHz}$); d) $\phi=90^\circ$ ($f=1900\text{MHz}$). Note that the null appearing at $\phi=90^\circ$, $\theta=90^\circ$ is due to the infinite FR4 piece considered in the simulation. In practice, when finite dielectrics are regarded, the $\phi=90^\circ$ cut is omnidirectional. 218
- Fig. 6.22 a)-b) Current distribution when the coupled monopoles are excited and the hexa-band PIFA is connected to a 50Ω load for the center frequency of the low (900MHz) and high frequency region (1900MHz), respectively; c)-d) Current distribution when the hexa-band PIFA is excited and the coupled monopoles are connected to a 50Ω load for the center frequency of the low (900MHz) and high frequency region (1900MHz), respectively. Max-E current is 5A/m and the dynamic range is 30dB's. The axis coincide with those illustrated in Fig. 6.4a. 219
- Fig. 6.23 Geometry and S-parameters associated to a multi-band MIMO system comprising a ground plane booster (5 mm x 5 mm x 5 mm) and a dual-band PIFA antenna according to the arrangement of the ground plane booster with respect to the antenna. The ground plane and the PIFA are etched over a 1 mm thick FR4 piece ($\epsilon_r=4.15$, $\tan\delta=0.013$), respectively. The axis coincide with those illustrated in Fig. 6.4a. 220
- Fig. 6.24 Left) Correlation values computed through radiation patterns (6.9) for each one of the cases illustrated in Fig. 6.23; Right) Antenna and radiation efficiency values regarding case Fig. 6.23c. Number 1 refers to the ground plane booster whereas number 2 refers to the dual-band PIFA. 220
- Fig. 6.25 Left) Geometry of the proposed multi-band MIMO system comprising a dual-band PIFA and a booster for the low frequency region. The ground plane and the PIFA are etched over a 1 mm thick FR4 piece ($\epsilon_r=4.15$, $\tan\delta=0.013$); Right) S-parameters. The axis coincide with those illustrated in Fig. 6.4a. 221
- Fig. 6.26 Left) Correlation coefficient computed regarding radiation patterns (6.9) and S-parameters (6.10); Right) Antenna and radiation efficiency values corresponding to the MIMO system illustrated in Fig. 6.25. Number 1 refers to the ground plane booster, whereas number 2 refers to the dual-band PIFA. 221
- Fig. 6.27 Left) Geometry of the proposed multi-band MIMO system comprising a set of coupled monopoles and two ground plane boosters. The coupled monopoles are etched over a 1 mm thick FR4 piece ($\epsilon_r=4.15$, $\tan\delta=0.013$); Right) S-parameters. The axis coincide with those illustrated in Fig. 6.4a. 222
- Fig. 6.28 Left) Geometry of the proposed multi-band MIMO system comprising a set of coupled monopoles and two ground plane boosters. The coupled monopoles are etched over a 1 mm thick FR4 piece ($\epsilon_r=4.15$, $\tan\delta=0.013$); Right) S-parameters. The axis coincide with those illustrated in Fig. 6.4a. 223
- Fig. 6.29 a)-b) Radiation and antenna efficiency for each one of the radiating systems under study for the low and the high frequency region, respectively; c)-d) Correlation coefficient computed regarding radiation patterns (6.9) for the low and high frequency region, respectively. 223
- Fig. 6.30 a)-b) E-total regarding the $\phi=0^\circ$ and $\phi=90^\circ$ cuts associated to the radiating systems of Fig. 6.27 at the frequency of 0.9GHz; c)-d) E-total regarding the $\phi=0^\circ$ and $\phi=90^\circ$ cuts associated to the radiating systems of Fig. 6.28 at the frequency of 0.9GHz. Note that the null appearing at $\phi=90^\circ$, $\theta=90^\circ$ is due to the infinite FR4 piece considered in the simulation. In practice, when finite dielectrics are regarded, the $\phi=90^\circ$ cut is omnidirectional. 224

- Fig. 6.31 a)-b) Current distribution without the slot when the coupled monopoles and the ground plane booster for the low frequency region are excited, respectively. Port 3 is connected to a 50Ω load; c)-d) Current distribution regarding the slot when the coupled monopoles and the ground plane booster for the low frequency region are excited, respectively. Port 3 is connected to a 50Ω load. Max-E current is 5A/m and the dynamic range is 30dB's. The axis coincide with those illustrated in Fig. 6.4a. 225
- Fig. 6.32 a) Geometry of the proposed multi-band MIMO system. The coupled monopoles and the ground plane are etched over a 1 mm thick FR4 piece ($\epsilon_r=4.15$, $\tan\delta=0.013$), respectively; b) S-parameters. Port 1 refers to the coupled monopoles, whereas port 2 and 3 relate to the ground plane booster intended for the low frequency region and the high frequency region, respectively; c) Detailed view of the ground plane booster and the matching network for the low frequency region d) Schematic representation of the implemented matching networks containing the commercial values of the reactive elements (Murata SMD0402) connected to port 2 and port 3. 226
- Fig. 6.33 Left) Geometry of the proposed multi-band MIMO system incorporating a miniaturized slot as isolation technique. The coupled monopoles and the ground plane are etched over a 1 mm thick FR4 piece ($\epsilon_r=4.15$, $\tan\delta=0.013$); Right) S-parameters. Port 1 refers to the coupled monopoles, whereas port 2 and 3 relate to the ground plane booster intended for the low frequency region and the high frequency region, respectively. 227
- Fig. 6.34 a)-b) Radiation and antenna efficiency for each one of the radiating systems under study regarding the low and the high frequency region, respectively; c)-d) Correlation coefficient computed regarding radiation patterns (6.9) for the low and high frequency region, respectively. 227
- Fig. 6.35 Comparison of the radiation patterns associated to the ground plane booster intended for the low frequency region (port 2) and to the coupled monopoles (port 1) at a frequency where the correlation null appears regarding both configurations, with and without the slot. 228
- Fig. 6.36 Left) Geometry of the proposed multi-band MIMO system comprising four ground plane boosters placed at the corners of a ground plane (120 mm x 50 mm). The ground plane is etched over a 1 mm thick FR4 piece ($\epsilon_r=4.15$, $\tan\delta=0.013$). The matching network connected to each port contains a series inductor, a broadband matching network, and a series capacitor as a fine tuning stage; Right) S-parameters. The axis coincide with those illustrated in Fig. 6.4a. 230
- Fig. 6.37 Radiation and antenna efficiency corresponding to the MIMO system illustrated in Fig. 6.36. Port 1 and 3 refer to the ground plane booster intended for the low frequency region, whereas port 2 and 4 relate to those boosters in charge of the high frequency region. 231
- Fig. 6.38 Left) Geometry of the proposed multi-band MIMO system comprising four ground plane boosters and two slots inspired in the Hilbert fractal. The ground plane is etched over a 1 mm thick FR4 piece ($\epsilon_r=4.15$, $\tan\delta=0.013$). The matching network connected to each port contains a series inductor, a broadband, and a series capacitor as a fine tuning stage; Right) S-parameters. The axis coincide with those illustrated in Fig. 6.4a. 231
- Fig. 6.39 Radiation and antenna efficiency corresponding to the MIMO system illustrated in Fig. 6.38. Port 1 and 3 refer to the ground plane booster intended for the low frequency region, whereas port 2 and 4 relate to those boosters in charge of the high frequency region. 232
- Fig. 6.40 a) Comparison of the correlation coefficient with (Fig. 6.38) and without the Hilbert-based slots (Fig. 6.36) computed through radiation patterns (6.9) for the low and high frequency region. 232
- Fig. 6.41 a)-b) E-total regarding the $\phi=0^\circ$ and $\phi=90^\circ$ cuts associated to the radiating systems of Fig. 6.36 at the frequency of 0.94 GHz; c)-d) E-total regarding the $\phi=0^\circ$ and $\phi=90^\circ$ cuts associated to the radiating systems of Fig. 6.38 at the frequency of 0.94 GHz. Note that the null appearing at $\phi=90^\circ$, $\theta=90^\circ$ is due to the infinite FR4 piece considered in the simulation. In practice, when finite dielectrics are regarded, the $\phi=90^\circ$ cut is omnidirectional. 233

- Fig. 6.42 a)-b) Current distribution at 0.9GHz and 1.9GHz without the slot when the ground plane boosters for the low and high frequency region are excited; c)-d) Current distribution regarding the slots inspired in the Hilbert fractal when the ground plane boosters for the low and high frequency region are excited. Port 3 and port 4 are connected to a 50Ω load. Max-E current is 5A/m and the dynamic range is 30dB's. The axis coincide with those illustrated in Fig. 6.4a. 234
- Fig. 6.43 a) Geometry of the proposed multi-band MIMO system comprising four ground plane boosters. The ground plane is etched over a 1 mm thick FR4 piece ($\epsilon_r=4.15$, $\tan\delta=0.013$); b) S-parameters. Port 1 and port 3 relate to the ground plane boosters intended for the low frequency region whereas port 2 and port 4 refers to those in charge of the high frequency range; c) Detailed view; d) Schematic representation of the implemented matching networks containing the commercial values of the reactive elements (Murata 0402). 235
- Fig. 6.45 a) Geometry of the proposed multi-band MIMO system comprising the four ground plane boosters and two slots inspired in the Hilbert geometry. The ground plane is etched over a 1 mm thick FR4 piece ($\epsilon_r=4.15$, $\tan\delta=0.013$); b) S-parameters..... 236
- Fig. 6.49 Comparison of the radiation patterns associated to each one of the ports of the low frequency region at a frequency where the correlation null appears regarding both configurations, with and without slots. 238

LIST OF TABLES

Table 2.1 Measured radiation and antenna efficiency for a PIFA antenna in a ground plane 100 mm x 40 mm without and with a conductive strip 40 mm x 33 mm x 3 mm (Fig. 2.19). Measurements are obtained using 3D pattern integration with the anechoic chamber Satimo Stargate-32.	50
Table 2.2 Q values at 900 MHz regarding a dipole configuration (Fig. 2.24) and regarding the ground plane (Fig. 2.23).	56
Table 2.3 Overview of the main methods and conclusions extracted from this chapter	64
Table 3.1 Frequency Bands and Bandwidths.	97
Table 3.2 Measured isolation between bands. Worst value is shown.	102
Table 3.3 Summary of the proposed radiating system based on the ground plane booster antenna technology.	121
Table 4.1 SAR Measurements.	140
Table 4.2 SAR and Absorption Losses regarding “Boosters Up”.	142
Table 4.3 SAR and Absorption Losses regarding “Boosters Down”.	142
Table 4.4 SAR (1g) Comparison for “Antenna Down” Position	143
Table 4.5 Summary of the main results related to the dual-band PIFA, the hexa-band PIFA on a slotted ground plane, the coupled monopoles, and the compact radiating system including ground plane boosters, when regarding the human head.	145
Table 5.1 Summary of Results.	163
Table 5.2 Out-of-phase Distributed Solution versus Single Monopole.	166
Table 5.3 In-phase Distributed Solution versus Single Monopole.	167
Table 5.4 Matching Network Components (SMD 0402).	171
Table 5.5 Reactive component values (lumped components SMD0402 high Q type illustrated in Fig. 5.39).	185
Table 5.6 In-phase (In), out-of-phase (Out), single element (Single). In/Out refers to the prototype using the in-phase feeding scheme for the LFR and the out-of-phase feeding scheme for the HFR.	188
Table 5.7 Summary of the proposed radiating systems intended for improving the performance in free-space as well as regarding finger loading.	191
Table 6.1 LTE Frequency Bands (FDD (Frequency Division Duplex).	199
Table 6.2 Summary of the proposed MIMO solutions based on ground plane boosters.	240
Table 7.1 Summary and Conclusions	253

CHAPTER 1 INTRODUCTION

1.1. Introduction

This thesis is framed in the wireless communications market and more specifically in handset antennas for wireless handheld devices.

Communication has evolved from the primary smoke signals to nowadays where sophisticated wireless handheld devices flood the society. The wireless technology appears, as a disruptive concept, in the early 70's and becomes consolidated in the 90's as a solution to provide mobility capabilities to the already existing Public Switched Telephone Network (PSTN). This fact becomes an important milestone that sets forth the starting point of the evolution history of wireless handheld devices and consequently of handset antennas as the fundamental part of a wireless communication system. In their early stages, the antennas developed for wireless handheld devices were conceived with the aim of providing operability in a single communication standard (GSM (Global System for Mobile Communications)) mainly developed to offer basic voice and short messaging services, and being allocated in a narrow frequency region of the electromagnetic spectrum. These primary handset antennas were essentially external antennas (antennas that protruded the handset phone (Fig. 1.1a)).



Fig. 1.1 Handset antenna evolution: a) Example of an external antenna and a handset including such external antenna; b) Example of two internal antennas and handsets including internal antennas.

Nevertheless, the impact caused by such technology in the society and the great market share achieved by mobile communication operators, fostered the need to develop new communication standards in order to solve the limitations not only found in terms of capacity for assuming the great number of user demands, but also in terms of functionalities since innovative services were continuously required. Such new mobile communication standards were allocated in a wide frequency region of the electromagnetic spectrum involving a great challenge for providing multi-band handset antennas capable of operating in said wide frequency range. Thus, and as a second important milestone, a novel generation of internal antennas (antennas integrated inside the handset phone (Fig. 1.1b)) appears to provide operability in such multiple communication standards and to satisfy user requirements regarding aesthetic, functional, and

operational factors. From those days until now, the wireless handset market is consolidated as a powerful economic market sector always in constant evolution with more than 5.6 billion of users.

This fast growing has fostered the need to still develop more communication standards integrating not only new access techniques to take full advantage of the available frequency spectrum but also new smart antenna technologies such as Multiple Input Multiple Output (MIMO) to provide sophisticated services demanding high data rates and high quality, such as video on demand, video streaming, video conference, voice over IP, high definition video, interactive games, web 2.0, etc. In this sense, and in order to offer the above services, it is expected that new multifunctional wireless devices or smartphones integrate a great number of mobile communication standards such as for example GSM850, GSM900, GSM1800, GSM1900, UMTS, CDMA, W-CDMA, LTE, etc., multiple connectivity standards such as for instance WiFi, IEEE802.11 standards, Bluetooth, WiMAX, WiBro, etc., and multiple broadcast standards such as FM, DAB, DVB-H, DMB or other related digital or analog video and/or audio standards, which at the same time have to coexist with already offered functionalities such as music players (MP3, MP4), camera, Global Positioning System (GPS), etc. (Fig. 1.2).



Fig. 1.2 Multiple mobile communication standards offering a great number of services and functionalities integrated in the new multifunctional wireless devices commonly known as smartphones.

Furthermore, the aforementioned requirements force the need of integrating a great number of handset components (batteries, speakers, shieldings, micro-processors, memory modules, communication circuits, multiplexors, LCD displays, QWERTY keyboards, etc.) in such multifunctional wireless devices while aesthetic and functional limitations appear mainly in terms of ultra slim, low weight, and low energy consumption platforms. Therefore, the dare lies in integrating such great number of functionalities and services into the reduced space available in current handset platforms (Fig. 1.3).

These needs considerably make even more difficult the antenna design, since antenna engineers have to face the challenge of providing handset antennas capable of operating in such multiple communication standards while restricted by physical constraints in terms of available space. This fact

directly faces up to the physic limits since the radiation properties associated to antennas are inversely proportional to the antenna size [1]-[2].

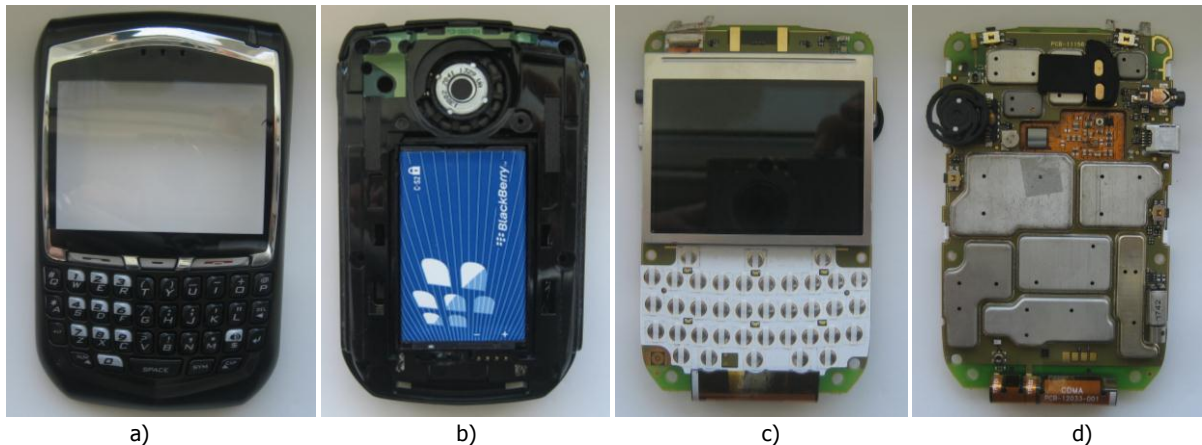


Fig. 1.3 Handset components associated to the handset phone BlackBerry 8703e: a) Image showing the keyboard; b) Image showing the speaker, the battery, and a handset antenna (top edge); c) Image showing the LCD display; d) Image showing several shieldings containing memory modules, microprocessors, communication circuits, multiplexors, etc., and another handset antenna (bottom edge).

In order to overcome the aforementioned shortcomings, this thesis proposes a new generation of radiating systems where no dedicated antenna is required for providing operability in multiple communication standards. The technology is based on the proper excitation of a structure already existing in the handset phone, the ground plane, which usually appears etched in the Printed Circuit Board (PCB). This excitation is carried out through the use of small non-resonant elements featured by considerable reduced dimensions. The term ground plane booster is used along this thesis to refer to these non-resonant elements that feature poor stand-alone radiation properties. Accordingly, the here called ground plane boosters are intended for exciting an efficient radiating mode of the ground plane, avoiding the need of including a dedicated antenna while preserving the radiation performance. As a result, the PCB space devoted to the prior handset antennas is considerably reduced and the integration capability of new services, functionalities, and handset components is further increased.

This thesis is divided in seven chapters, namely:

- Introduction
- Fundamental Principles
- Ground Plane Booster Antenna Technology
- Human Interaction
- Distributed Radiating Systems
- Ground Plane Boosters in MIMO Systems
- Conclusions

Chapter 1 introduces the scope and objectives of the present research and discloses the initial hypothesis as well as the preliminary results that will set forth the grounds of the proposed technology. The methodology followed up to develop the thesis is also presented along this chapter. In addition, an analysis of the state of the art is presented with the aim of determining the benefits and limitations of

handset antenna solutions used nowadays. Finally, a list of the derived publications in scientific journals, international and national conferences as well as patent applications is detailed.

Chapter 2 is more focused on discussing the fundamental principles of the proposed technology, which are mainly based on the characteristic modes theory. In this sense, the chapter firstly introduces the principles of this theory and continues with the discussion of how this theory could be applied to the handset antenna design. Characteristic modes are defined as the electrical current eigenfunctions linked to the boundary conditions of an arbitrary shaped conducting object. These characteristic modes are only dependent on the shape and size of the conducting object and not on the feeding mechanism. Thus, their knowledge becomes significantly useful, since they provide a relevant physical insight into the radiation properties of a particular conducting object just through the knowledge of its shape and size. Although the information provided is very valuable, in some cases their computation becomes cumbersome and particularly complex. In order to provide a simplified computation method, this chapter also proposes a Radar Cross Section analysis (RCS) to estimate the radiation properties of the fundamental modes for a given conducting structure such as a ground plane of a wireless handheld device. As previously indicated and as will be discussed later in more detail, the main objective of this thesis is focused on providing a radiating system capable of using the inherent ground plane of any handset platform as main radiator. The solution removes the need of including additional radiating antenna elements, thus providing supplementary space in the handset platform to integrate other handset components intended for increasing the number of services and functionalities of the wireless handheld or portable device. The challenge of the proposal not only relies on determining the suitable ground plane size and shape capable of producing efficient wave modes at mobile frequencies, but also on the elements used to excite said potential wave modes. In this sense, this chapter further analyzes the advantages and disadvantages of using resonant antennas or non-resonant elements to excite the ground plane radiation modes as well as discusses how the size and geometry of these elements affect the performance of the radiating system.

Chapter 3 describes in a first stage, a multi-band radiating system capable of providing penta-band operation (GSM850, GSM900, GSM1800, GSM1900, and UMTS). Two non-resonant elements performing considerable small dimensions of just 5 mm x 5 mm x 5 mm are used to excite the ground plane modes of the typical handset platform of a bar-type mobile phone (100 mm x 40 mm). These elements are called ground plane boosters and they should not be considered antennas mainly due to their poor stand-alone radiation properties (very high quality factor (Q) at the frequencies of operation). Thus, the solution removes the need of integrating large resonant antenna elements that occupy a considerable PCB space. Impedance matching is attained through the addition of a radiofrequency system based on a systematic matching network design, which is deeply explained along the chapter. As previously introduced, in the context of this thesis, the term ground plane booster is used to refer to those non-resonant elements featured by considerably poor stand-alone radiation properties due to their reduced electrical dimensions. In a similar manner the term radiofrequency system relates to those reactive

components, either lumped or distributed, used to attain impedance matching at the desired operating frequencies.

The second stage presents an alternative solution, which substitutes the volumetric ground plane boosters by coplanar ground plane boosters, thus simplifying significantly the manufacturing process of the solution while maintaining the radiation properties. This stage also introduces a systematic method to determine in advance the required size and shape of the ground plane booster as a function of the shape and size of the ground plane. The previous proposals, shown in this chapter, are based on capacitive elements, which couples energy to the ground plane through electric fields. Nevertheless, this coupling could be made otherwise through magnetic fields by using inductive elements. Accordingly, the chapter is completed with the study of the effect introduced by inductive ground plane boosters on the radiation properties. Finally, a novel concept of radiofrequency system that presents a simplified matching architecture capable of reducing the number of reactive components in a factor around 2.5 with respect to other solutions also proposed along this thesis is provided.

Chapter 4 is intended for analyzing the effects of the human interaction over the suggested radiating system from two main perspectives, functional and biological. On one hand, the performance of the proposed ground plane booster solution is compared with already consolidated handset antenna technologies, more particularly with a Planar Inverted F Antenna (PIFA), a set of coupled monopoles, and a PIFA over a slotted ground plane in the presence of the human head. The solutions are compared in functional terms, i.e. the effects produced by the presence of the human head over the performance of the radiating system are analyzed in order to determine the robustness of each solution. These effects mainly translate into detuning and efficiency decrements. Nevertheless, not only the effects that the proximity of the human head produces over the performance of a particular radiating system should be considered, but also biological aspects caused by the radiation of the handset device must be taken into account. In this sense, the Specific Absorption Rate (SAR) as the main relevant biological parameter is provided for each one of the proposed solutions in order to better characterize them.

Chapter 5 is also oriented to provide robust radiating systems to human interaction, but in contrast to the previous chapter, in this case the proximity of the human hand is analyzed. The chapter proposes solutions to overcome the detuning and efficiency decrements that the proximity of the user hand produces over the performance of radiating systems. The concept is based on introducing redundancy by adding different radiating elements in such a way that when a radiating element is blocked by the user hand the remaining element could still operate properly. The main advantage of this completely passive antenna solution relies on the fact that it not only enhances the robustness of the radiating system to hand loading but also improves its performance in terms of bandwidth and efficiency proportionally to the number of the redundant radiating elements added. Different feeding schemes (namely, an out-of-phase and an in-phase feeding scheme) to combine signals into a single Input/Output port are deeply discussed in order to determine their advantages and disadvantages. The distributed radiating system is finally expanded to a distributed ground plane booster antenna solution, which enhances the electromagnetic

properties of previous booster based solutions by providing hepta-band operation capable of covering nine communication standards, namely LTE700, GSM850, GSM900, GSM1800, GSM1900, UMTS, LTE2100, LTE2300, and LTE2500).

Chapter 6 is oriented to enable MIMO in emergent multifunction wireless devices. The chapter discusses the shortcomings associated to representative state of the art solutions and presents MIMO technologies based on ground plane boosters capable of overcoming aforementioned shortcomings. MIMO technology requires the use of multiple antennas in transmission and reception in order to increase the channel capacity. Thus, the bottle neck in cellular wireless networks is found in the user terminal rather than in the terrestrial base station. This is mainly due to the fact that handset devices are featured by strict size constraints imposed by strong user demands based on functional and aesthetical reasons. More particularly, the challenge of integrating MIMO in handset platforms further exacerbates in the low frequency region comprising the widespread communication standards (GSM850 and GSM900) as well as important emergent standards such as LTE700. In this frequency region, resonant antennas require a considerable size that makes unfeasible or even prevents the integration of multiple antennas into a single handset platform. This chapter explains that these size limitations could be solved by the use of ground plane boosters capable of exciting different ground plane radiation modes or even the same ground plane radiation mode with acceptable correlation levels as for guarantying the proper performance of the MIMO system.

Chapter 7 presents the main conclusions derived throughout the research.

1.2. Hypothesis and Preliminary Results

From a technical point of view, the fundamental principle of the proposal is based on the use of non-resonant ground plane boosters (Fig. 1.4) to excite the efficient radiation mode of the ground plane, reusing in this sense an existing handset structure as a main radiator.

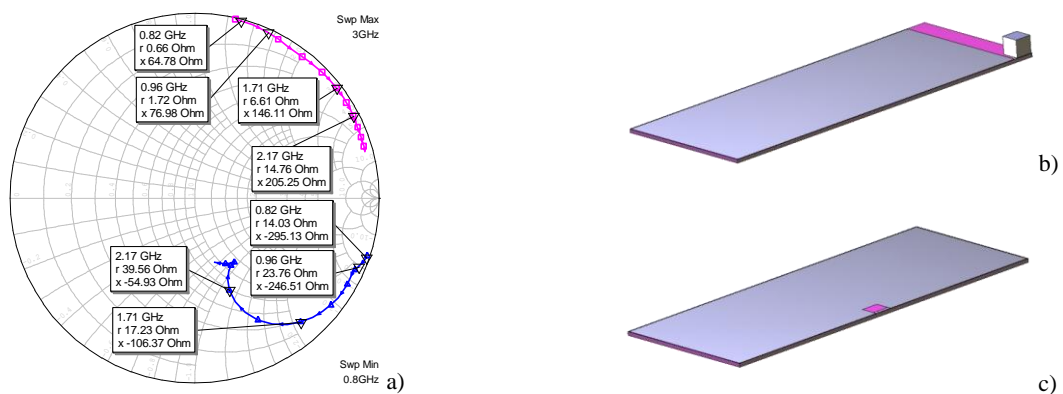


Fig. 1.4 a) Input impedance associated to the simulated geometry b) including a non-resonant capacitive ground plane booster on a ground plane having a size of 100 mm x 40 mm according to a typical bar-type phone (featuring capacitive input impedance) (triangular markers) and input impedance associated to the simulated geometry c) including a non-resonant inductive ground plane booster element (featuring inductive input impedance) (square markers).

However, the proper excitation of the predominant mode is not enough for providing multi-band behavior since its inherent bandwidth (BW_0) (1.1) calculated from its quality factor (Q_a) (1.2) (Fig. 1.5),

according to reference [3], is not enough to provide operation in the desired frequency range. In order to provide operability in the main communication standards GSM850, GSM900, GSM1800, GSM1900, and UMTS a bandwidth (BW) around 15% in the low frequency region and 24% in the high frequency region is required. Consequently, a matching network is needed to guarantee operability in the aforementioned communication standards.

With this aim, a systematic method for broadening the BW_0 of RLC circuits in a factor around one half of Fano's limit [4] is proposed in [5] for parallel RLC circuits and in [6] for circuits featuring RLC series input impedances as a result of this thesis development. However, the proposed radiating structures (Fig. 1.4) also demand a preceding step in order to allow the application of this broadband method. Thus, a series inductor, regarding the radiating structure corresponding to Fig. 1.4b, is used to compensate the capacitive reactance in order to model the input impedance locus according to that provided by a resonant RLC series circuit. In the case of Fig. 1.4c, a series capacitance would be needed. Such broadband mechanism applied over non-resonant ground plane booster is further disclosed in [7]-[9] where some results associated to the first stage of this thesis are gathered demonstrating the feasibility of the proposal. Accordingly and in order to achieve the enhanced bandwidth (BW_f), a parallel capacitor and inductor is used as a broadband matching network. The proper values of these reactances (C_m and L_m) gathered in equations (1.3) and (1.4) are readily obtained through an accurate mathematical analysis already developed in [9] using the associated electrical model (Fig. 1.6a).

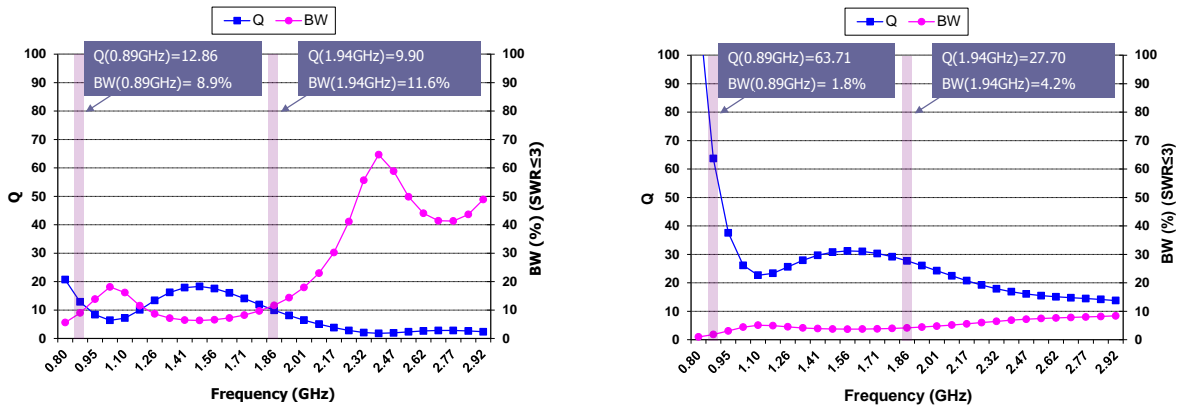


Fig. 1.5 Inherent bandwidth and quality factor versus frequency calculated regarding the radiating structures shown in Fig. 1.4 b) (left plot) and c) (right plot) through the corresponding input impedances according to equations (1.1) and (1.2).

$$BW_0 = \frac{f_2 - f_1}{f_0} = \frac{S-1}{Q_a \cdot \sqrt{S}} \quad (1.1)$$

$$Q_a(\omega) = \frac{\omega}{2R(\omega)} \sqrt{\left[\frac{dR(\omega)}{d\omega} \right]^2 + \left[\left[\frac{dX(\omega)}{d\omega} \right] + \left| \frac{X(\omega)}{\omega} \right| \right]^2} \quad (1.2)$$

$$C_m = \frac{1}{\omega_0^2 \cdot L_m} \quad (1.3)$$

$$L_m = \frac{(f_1^2 - f_r^2) \cdot Z_0 \cdot (1 + (Q_a \cdot v_1)^2)}{S \cdot Q_a \cdot (f_1^2 - f_r^2) \cdot 2 \cdot \pi \cdot f_r} \quad (1.4)$$

Where f_2 and f_1 are the frequencies where $S_{11}(f_2)=S_{11}(f_1)$ has a Standing Wave Ratio (*SWR*) equal to S ; f_0 is the central frequency between f_2 and f_1 , Q_a is the antenna Q , $R(\omega)$ and $X(\omega)$ are the real and imaginary part of the input impedance, respectively; and $v_l=f_1/f_0=f_0/f_1$.

Such suitable values provide the expected bandwidth by satisfying the condition represented graphically and defined mathematically in the illustrated equations (Fig. 1.6b). On one hand and as previously exposed, the reactance cancellation element allows the impedance locus feature input impedance similar to that provided by a resonant *RLC* series circuit. On the other hand, the two stages matching network based on a parallel inductor and capacitor turns the curve into a multi-resonance loop providing a bandwidth enhancement factor (F) around 2.45 (1.5) considering a $SWR \leq 3$ (Fig. 1.6c). Note that parameter S illustrated along this section directly refers to *SWR*.

The aforementioned process obtained during this thesis development, allows simplifying the matching network design, since the antenna engineer is able to know in advance if the radiating structure would be able to offer a potential bandwidth (BW_f) capable of providing operability in the desired communication standards. In this sense, the systematic broadband matching network becomes a powerful tool that not only provides a wide bandwidth with the minimum number of reactive elements but also avoids the cumbersome matching network methodologies based on trial and error.

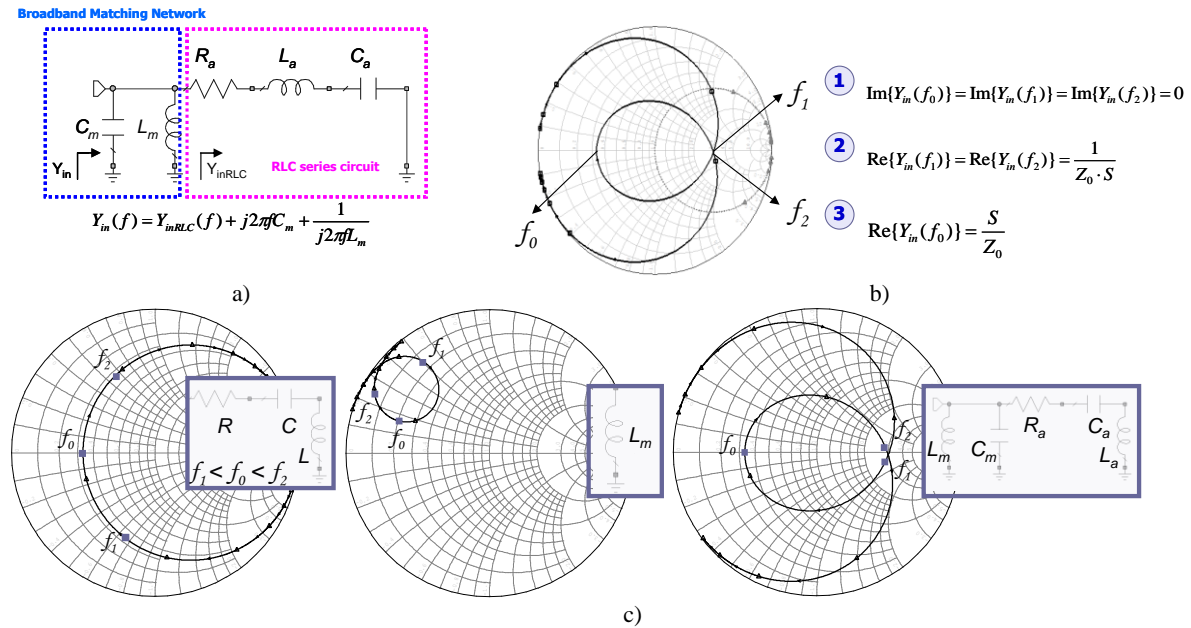


Fig. 1.6 a) Equivalent electrical circuit associated to the radiating structure of Fig. 1.4b after the addition of the reactance cancellation element (*RLC* series circuit) and the two stages broadband matching network; b) Conditions required to attain a broadband matching network capable of increasing the inherent bandwidth of a radiating structure featuring a *RLC* series input impedance in a factor around 2.45 for $S \leq 3$; c) Step by step input impedance sequence starting by the addition of the reactance cancellation element and concluding with the two stages matching network with the proper C_m and L_m values that allow inscribing the impedance loop in a circle of $S \leq 3$.

The radiating structure and the radiofrequency system including such broadband matching network as a whole (Fig. 1.7) will constitute one of the radiating systems disclosed in this thesis. The feasibility of the proposal has been already analyzed by prototyping (Fig. 1.8) and the promising results are gathered in [9]. The aforementioned limitations of current handset antenna mainly in terms of required volume to achieve multi-band behavior are solved by this proposal that provides a penta-band behavior operating in

the main worldwide communication standards GSM850, GSM900, GSM1800, GSM1900, and UMTS thanks to the use of two capacitive ground plane booster elements featured by a small volume of only 250 mm³. This fact implies a volume reduction with respect to current technologies offering penta-band behavior of a factor around 20 (Fig. 1.9).

$$F = \frac{BW_f}{BW_0} = \frac{\left(\sqrt{S^2 - 1} / Q_a\right)}{(S - 1) / (Q_a \cdot \sqrt{S})} = \frac{\sqrt{S^3 - S}}{S - 1} \quad (1.5)$$

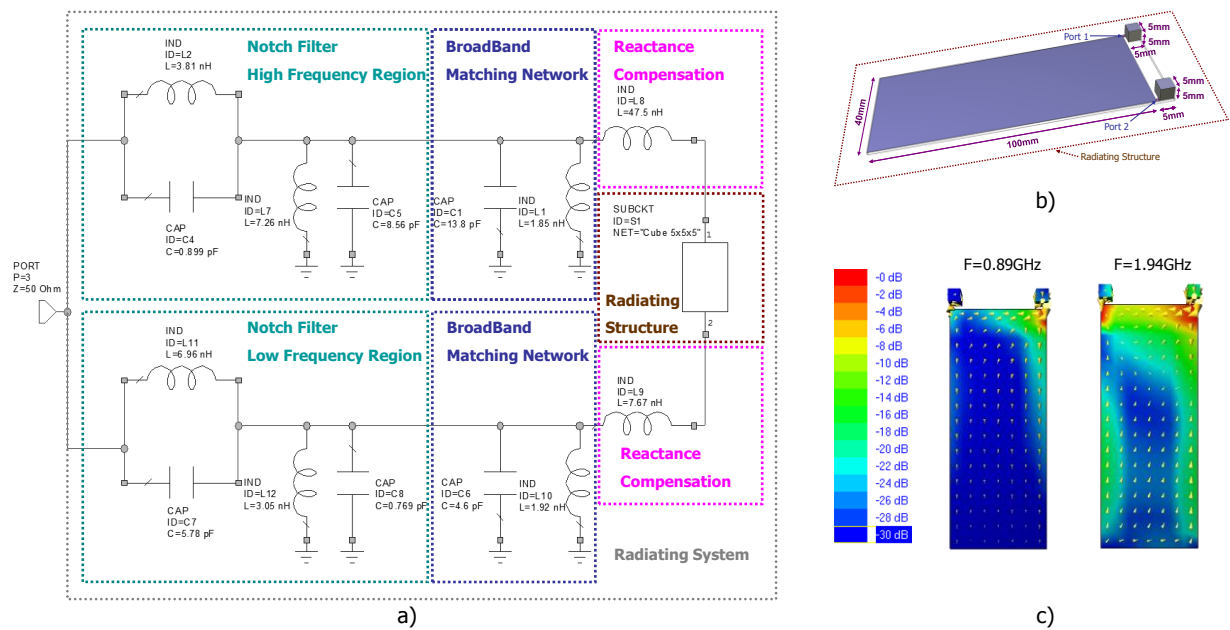


Fig. 1.7 a) Radiating system designed for achieving a penta-band behavior consisting in a reactance cancellation element, a broadband matching network, and a notch filter for each frequency region [7]-[9]. Note that the first stage of the notch filter and the broadband matching network can be simplified using only two components. The two-port box is the simulated input impedance of the radiating structure shown in b); b) Detailed view of the radiating structure obtained from the simulated layout comprising two non-resonant ground plane boosters with dimensions 5 mm x 5 mm x 5 mm each one in charge of the ground plane (100 mm x 40 mm) excitation for each frequency region (low frequency region comprising the communication standards (GS850 and GSM900) and high frequency region comprising the communication standards (GSM1800, GSM1900, and UMTS)); c) Current distribution associated to the radiating structure at the central frequencies of both frequency regions ($f=0.89$ and $f=1.94$ GHz) that demonstrates the effectiveness of the boosters in exciting efficient radiation modes of the ground plane.

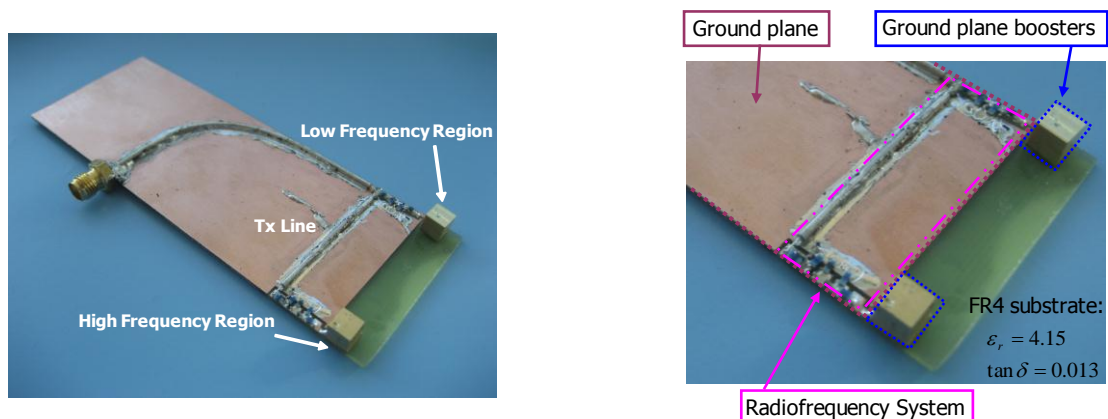


Fig. 1.8 Penta-band prototype designed according to the schematic shown in a) including besides the reactance cancellation inductor and the broadband matching network, the notch filters required for providing isolation between both frequency regions.

This penta-band radiating system is slightly introduced here in order to briefly illustrate the technical aspects that mainly support the scope and objectives of this thesis. Its design is further analyzed and discussed along chapter 3. In addition to the size advantages (Fig. 1.9), the proposal of this thesis is also oriented to provide an innovative solution focused on becoming a standard product able to be integrated in a handset platform independently from its form factor (bar, tablet, phablet, clamshell, slider, swivel, sidekick, laptop, etc.). Until recently now, handset antenna design presents an important customization phase where the antenna has to be designed according to the handset platform.

In this way, current handset antenna designs could not be extended to all platforms since especial considerations must be taken into account regarding not only the form factor but also the distribution and arrangement of other handset components. Consequently, the aim of this thesis is also focused on providing a standard solution that can be implemented without the need of a customization phase in any handset platform. It is possible on one hand, by the reduced space required by the ground plane boosters, and on the other hand by the fact that the ground plane used as main radiator is present in all current handset platforms (Fig. 1.10).



Fig. 1.9 Comparison between current internal antenna technologies and the technology proposed in this thesis. Note that the PCB space is considerable increased when the dedicated antenna (framed in dashed line (left)) is replaced by the non-resonant ground plane boosters (framed in dashed line (right)).

Once the feasibility of the proposal from functional and mechanical aspects is performed and its advantages with respect to previous technologies are demonstrated (chapter 3), the question that arises and that will be treated along the thesis is related to the robustness of the proposed radiating systems to the effects associated to the human interaction (chapter 4). It is well known that the analysis of the electromagnetic performance related to a specific radiating system in free-space is not enough to fully characterize the device, since the human interaction strongly affects to its performance. In fact, the simple action of holding the handset during a phone call introduces undesired effects such as detuning and efficiency decrements that can jeopardize considerably the performance of the radiating system. Consequently, handset antennas have to be evaluated regarding not only free-space conditions but also realistic situations emulating the effects of the human presence.

For previous reasons, the human interaction is tackled in this thesis from two main aspects: biological and functional (Fig. 1.11). On one hand, the biological compatibility of some of the solutions

presented along the thesis development will be analyzed in terms of Specific Absorption Rate (SAR). The SAR is a measure of the maximum electromagnetic field inside the human head per unit of mass and is directly related with health aspects.



Fig. 1.10 Left: Example of several handset platforms featuring different form factors and consequently dissimilar internal antennas especially customized for being integrated in such specific handset platforms; Right: Ground plane booster elements as the promising standard solution that enables the integration in any handset platform without the need of a complex customization process.

The relevance of the SAR measurements regarding medical aspects lies in the fact that the electromagnetic field entering inside the human head is the main responsible of undesired temperature increments that could derive in health problems. Consequently, a regulation is required. Such regulation related to the radiofrequency exposure is performed by several standardization organisms such as European Committee for Electrotechnical Standardization (CENELEC) in Europe or the Federal Communications Commission (FCC) in the United States, which are in charge of determining the standards that ensure the acceptable limits.

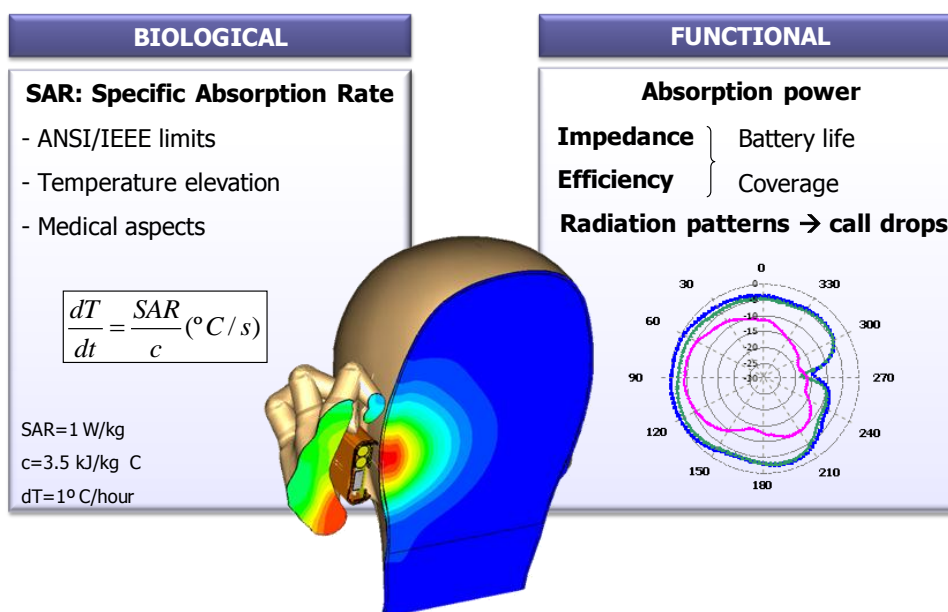


Fig. 1.11 Main aspects regarding human interaction considered along this thesis: biological and functional.

On the other hand, the human presence modifies the electromagnetic performance of the radiating system regarding functional aspects as for example, alteration of bandwidth, efficiency, and radiation patterns. The human head acts as a lossy reflector at mobile frequencies causing power absorption that directly translate into efficiency drops. The same occurs with the human hand, which in addition to the power losses can perform detuning effects.

In this sense, it is possible to conclude that the electromagnetic performance of any radiating system must be studied regarding the human presence in order to set forth a faithful environment closer to realistic situations. Not considering these effects could produce damaging consequences related to the performance of the system, which entails negative quality of service perceptions produced by the lack of coverage, call drops, or reduction of the duration of the battery among others. This thesis makes a special emphasis in this aspect, since the developed radiating systems are evaluated regarding not only free-space conditions but also taking into account the human presence. In addition, special care is taken in providing a solution for reducing the SAR values, in order to minimize the temperature elevation inside the human head. Other solutions are focused on providing distributed antenna systems based on boosters capable of minimizing the effects of hand loading (chapter 5). The fundamental principle of this proposal consists in adding redundancy to the radiating systems, in such a way that when the finger of a user blocks part of a radiating structure, other part of the same radiating structure can still radiate properly.

A further aspect of this thesis deals with the development of innovative radiating system capable of providing smart antenna technologies such as MIMO (chapter 6). The proposals are also based on the excitation of the ground plane through ground plane boosters strategically located to favor efficient radiation. The small PCB volume occupied by such boosters allows the integration of multiple of such elements required to provide MIMO systems. This fact becomes a considerable advantage with respect to current technologies, which are strongly limited by the antenna volume, more significantly when operation in the low frequency region is demanded. Nevertheless, not only the technology undergoing in this thesis will enable high data rate services but also high quality, since redundancy could be included based on the same principle to provide diversity systems.

To sum up, it is an object of the present thesis to provide radiating systems robust to the human presence for being integrated as a standard solution in new multifunctional or smartphones wireless devices independently from its form factor and capable of operating in the main communication standards. At the same time, the proposed radiating systems minimize the required PCB volume, favor the integration of new and multiple functionalities, and enable high data rate as well as high quality services.

1.3. Methodology

The thesis combines a theoretical phase including the following stages:

- Focalized research in the field of handset antennas in order to determine the needs (the main information sources regarded are those gathered in Fig. 1.12)
- Conception of the idea

- Study of the fundamental behavior through a deep physical insight mainly focused on the development of electrical models regarding concentrated and/or distributed elements, as well as on the theory of characteristic modes and RCS analysis

The aforementioned phase is completed with electromagnetic simulations carried out through the specialized electromagnetic software IE3D based on MoM (Method of Moments) (Fig. 1.12) which comprise the following summarized steps:

- Design of the proposed radiating structures
- Electromagnetic simulation of these radiating structures
- Extraction of the main antenna parameters (impedance bandwidth, radiation and antenna efficiency, radiation patterns, directivity, gain, and current distribution...)
- Study of the non-resonant ground plane booster effect (inductive or capacitive nature, location, size, resonant frequency, and geometry) over the performance of the radiating structure
- Study of the non-resonant ground plane booster effect over several platforms featuring different form factors (bar and smartphone)
- Study of the suitable matching network topologies according to the specific radiating structure
- Study of the interaction and combination of ground plane boosters featuring the same or different natures
- Study of the interaction and combination of ground plane boosters with current handset antennas



Fig. 1.12 Tools used along the different phases that compose this thesis.

To conclude, the feasibility of the proposals is evaluated through prototypes, and the main antenna parameters (impedance bandwidth, radiation efficiency, antenna efficiency, radiation patterns, directivity, and gain) are measured thanks to Fractus facilities (Fig. 1.12) regarding:

- Free-space conditions
- Human presence: Head and Hand
- Real platforms: Nearby components (such as shielding and speaker)

In addition SAR, measurements are provided by the DASY4 equipment (Fig. 1.12).

Therefore, this thesis envisages a new revolution in the handset antenna field: first generation of external antennas (back in 1990), internal antennas (back in 2000), and the proposed ground plane booster antenna technology (2013) (Fig. 1.13). The novel architecture introduced herein only requires ground plane boosters featured by a small electrical size, a high quality factor and extremely poor stand-alone radiation properties in combination with a matching network for providing simultaneous operability in the main communication standards.

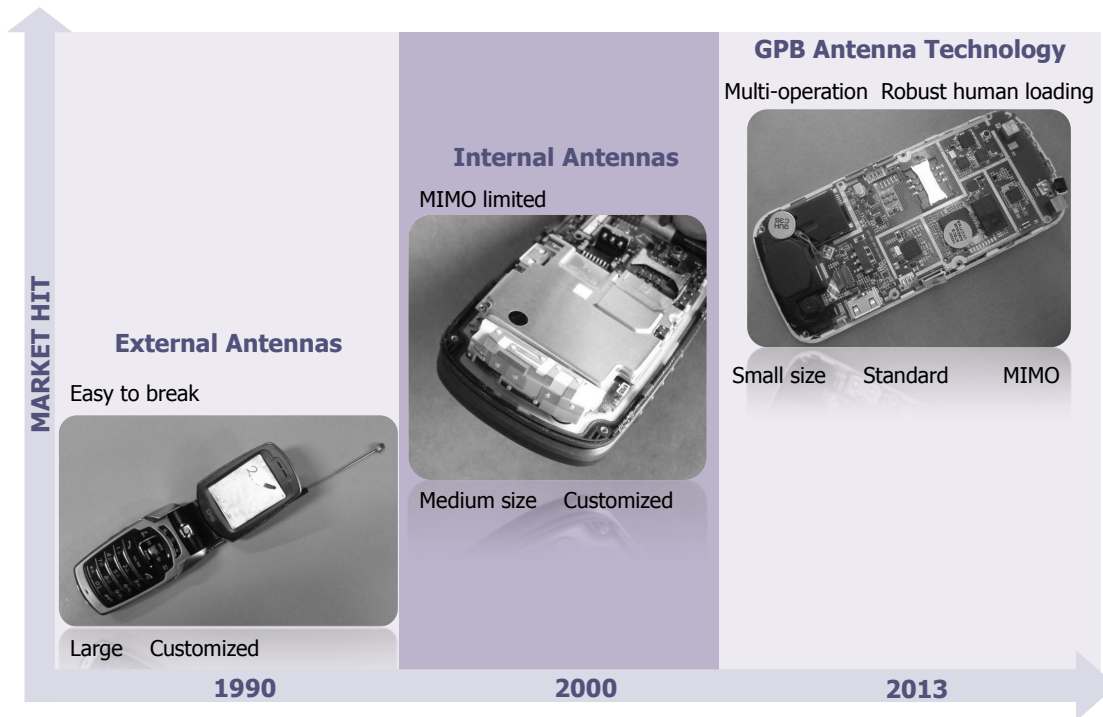


Fig. 1.13. Handset antenna evolution envisaged in this thesis.

The main advantages of this technology, which will be further explained in the following sections, can be summarized as follows:

- Multi-band performance and reduced size.
- Integration capabilities through the removal of customized antennas. This is an advantage not only for antenna manufacturers but also for handset phones manufacturers. Up to date, a new phone means a new antenna. This is a time consuming process as far as antenna engineering and mechanical engineering are concerned.

- Robustness to the human loading mainly due to the small ground plane booster size, which minimizes the interaction with the human hand (one of the most critical part when dealing with human interaction).

Smart systems (MIMO) are enabled because of the very small volume of ground plane booster elements. Many boosters may be integrated within a handset platform allowing high data rates technologies.

1.4. Objectives

As a global objective, this thesis proposes a new generation of handset antenna technology conceived to be integrated in new multifunctional wireless devices or smartphones. The main objective of such technology consists in achieving the convergence between laptops functionalities and handheld mobility capabilities strongly required by handset users. Accordingly, it is an object of the present thesis to allow the integration of a great number of functionalities as well as communication services in handset platforms thanks to the PCB space increment obtained by removing the need of integrating a dedicated antenna. The technology developed is based on the use of an existing part of the handset phone to perform the radiation. This fact allows increasing the integration capabilities while preserving the electromagnetic performance in the multiple communication standards already demanded by the handset market. More specific objectives are summarized in the following paragraphs (Fig. 1.14).

It is an object of the present research to achieve a solution capable of providing simultaneous operation in multiple mobile communication standards such as for example GSM850, GSM900, GSM1800, GSM1900, UMTS, CDMA, W-CDMA, LTE, etc., multiple connectivity standards such as for instance WiFi, IEEE802.11 standards, Bluetooth, WiMAX, WiBro, etc., and multiple broadcast standards such as FM, DAB, DVB-H, DMB or other related digital or analog video and/or audio standards. The challenge lies in attaining the great bandwidth required to cover such wide frequency range of the electromagnetic spectrum through the use of electrically small non-resonant ground plane boosters.

It is a further object of the present thesis to provide miniature and non-radiating ground plane boosters capable of exciting an efficient radiation mode of the ground plane while providing operability in multiple communication standards. The aim consists in removing the need of including a dedicated antenna in the radiating system through the use of such electrically small non-resonant ground plane boosters capable to excite the ground plane of a handset phone. Thus, as no dedicated antenna is required, the available PCB space is further increased (Fig. 1.9) for including:

- New and multiple functionalities (Fig. 1.2)
- New and multiple services requiring high data rates, and high quality of services (Fig. 1.2)
- Nearby components (for example, larger LCD displays enabling touch screens) (Fig. 1.3)

In this case, the challenge consists in reducing the occupied PCB volume substituting the dedicated antenna by such low-volume ground plane boosters while preserving the electromagnetic performance. It is well-known in the antenna field that the electromagnetic properties of handset antennas are directly

proportional to the antenna volume [1]-[2]. The first solution attained in this thesis with the proposed technology achieves a reduction factor around 20 with respect to current antenna technologies according to [9].

The aforementioned objectives in terms of providing electrically small ground plane boosters to perform the radiation in combination with the ground plane structure directly leads to the third objective of this thesis, which is focused on enhancing the integration capabilities of these radiating systems in current handset platforms. Thus, and as aforementioned, since no antenna is required, the PCB space is further increased to include more handset components, more functionalities or more communication services. However, another objective appears focused on enhancing the integration aspects provided by such ground plane boosters based solutions. These objectives can be summarized as follows:

- To reduce the volume as well as the weight to enable the integration of the proposed radiating system in ultra-slim multifunctional platforms or smartphones
- To facilitate the integration of handset components as well as to enhance the robustness of the radiating system to the effects caused by such nearby handset components (detuning effects and efficiency decrements)
- To attain a standard solution in order to avoid the required customization process according to the form factor corresponding to a specific handset platform
- To simplify the fabrication process not only in terms of designing stages but also in terms of materials and costs



Fig. 1.14 Thesis Objectives.

This thesis is also focused on providing a robust solution to the human interaction regarding two main aspects:

- Functional aspects: It is an object of the present research to provide a solution robust to the effects caused by the human interaction in order to avoid a performance degradation of the radiating system in terms of detuning effects and power absorption
- Biological aspects: It is a further object of the present thesis to provide a solution to minimize the electromagnetic field entering the human head in order to avoid undesired temperature elevations for the sake of ensuring the users security

Another important objective of the present thesis consists in providing radiating systems featuring smart antenna technology such as MIMO for enabling high data rates and high quality services. In this sense, and mainly due to the volume reduction achieved by the proposed technology, it will be possible to integrate multiple ground plane boosters to achieve high data rates services overcoming, in this way, the limitations found in current antenna technologies [10].

1.5. State of the Art

The primary handset phones including external antennas and initially conceived with a limited number of functionalities have evolved to a novel concept of multifunctional wireless devices or smartphones. The emergence of such devices is fostered by the user demands focused on achieving the total convergence between the functionalities offered by current laptops and those in terms of mobility provided by handheld devices. In order to satisfy such requirements, powerful micro-processor, great memory cards, large touch screens, camera, music players (MP3, MP4) between others are demanded. Nevertheless, the integration of such functionalities is constrained by aesthetic and mechanical aspects in terms of ultra slim, low weight, robust, and low consumption platforms, fact that considerable difficult the integration. Thus, the challenge lies in providing such great number of functionalities in the limited space offered by a handset platform and strictly restricted to preserve the portability feature.

Nevertheless, such challenge is still more noticeable for antenna designers who have to design multi-band antennas capable of providing operability in a great number of communication standards while constrained by physical limitations. Therefore, the trade-off lies in providing small antennas capable of being incorporated in such multifunctional platforms to facilitate the integration of big displays enabling touch screens, cameras, batteries, speakers, micro-processors, memory cards, etc., while operating in multiple communication standards such as for example GSM850, GSM900, GSM1800, GSM1900, UMTS, CDMA, W-CDMA, LTE, etc., multiple connectivity standards such as for instance WiFi, IEEE802.11 standards, Bluetooth, WiMAX, WiBro, etc., and multiple broadcast standards such as FM, DAB, DVB-H, DMB or other related digital or analog video and/or audio standards. This great number of communication standards directly translates into a huge spectrum bandwidth that has to be covered in order to ensure such multi-band operation.

Nowadays, internal antennas can be grouped into patch/PIFAs [11], monopoles/IFAs (Inverted F Antenna) [12]-[14], slots [15]-[17], and a combination of them [18] as the most common designs for handsets (Fig. 1.15). Nevertheless, they are constrained by the fundamental limits of small antennas that imply an inherently narrow impedance bandwidth [1]-[2].

The first ones, patch/PIFA antennas, are featured by a specific volume and are generally located over the ground plane at a certain height ('on-ground'). This fact increases the complexity of the design and makes difficult its integration in slim platforms. Several well-known techniques, that complicate the geometry, are used to provide dual-band or multi-band operation such as including several radiating paths, using slotted ground planes [19]-[27] or introducing conductive strips [28]-[30] (Fig. 1.16). Handset monopole antennas and slots become the alternative to provide multi-band operation in slim platforms mainly due to its characteristic low profile provided by its 'off-ground' characteristic. In this way, most of the ground plane is removed underneath the antenna enabling substantially coplanar structures, which become especially suitable for ultra slim platforms [12]-[14], [26]-[27].

However, and mainly due to the market trends, previous antenna technologies are not enough to guarantee sufficient space in the handset platform to integrate other handset functionalities and/or operation in the new frequency bands appeared for allocating those communication standards capable of providing high data rates and high quality services. In this sense, the antenna designs have to evolve to satisfy user requirements.

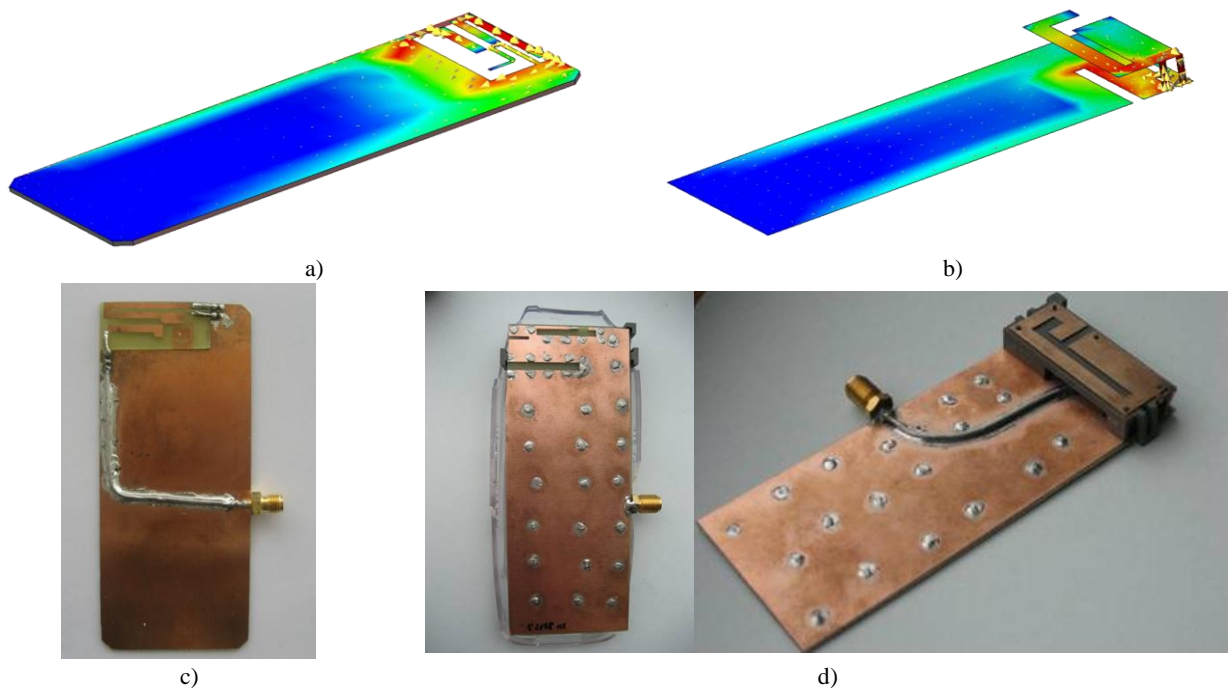


Fig. 1.15 Two representative examples of current internal antenna technologies: a) Current distribution associated to coupled monopoles representing 'off-ground' coplanar structures; b) Current distribution associated to PIFA antenna over a slotted ground plane illustrating 'on-ground' technology together with ground plane shaping techniques; c) Coupled monopoles prototype [12],[14]; d) PIFA antenna prototype[19]-[27]. These handset antenna designs are also being analyzed in this thesis for comparison purposes.

Until relatively recently, the efforts in antenna design were mainly addressed to the antenna geometry and not to the ground plane, since its relevance in the radiation process was underestimated.

Accordingly, the antenna element was typically a self-resonant element that provided an efficient radiation independently from the ground plane structure. Nevertheless, the ground plane is progressively acquiring relevance, since several studies have demonstrated its strong contribution to the radiation properties [19]-[35]. In this way, the study presented in [31], proposes an equivalent circuit model that provides a quantitative view of the effect of the combination of a single-resonant antenna and chassis over the most significant antenna parameters. The theoretical effect of the coupling factor and the resonant frequencies is demonstrated through simulation regarding self-resonant antennas such as patch antennas and PIFA antennas. The bandwidth increases as long as the resonant frequency of the antenna approximates that of the ground plane and as long as the coupling between both elements increases.

At the same time, reference [32] presents a folded radiating ground plane fed with a bowtie-shaped planar monopole specially selected to properly excite the desired ground plane modes. However, the folded ground plane can be understood as a PIFA antenna over a finite ground plane (100 mm x 40 mm) with significant physical dimensions (49.5 mm x 35 mm x 10 mm), which are too large for practical purposes in modern handheld wireless devices. Again, the radiation becomes a combination of the PIFA antenna and the ground plane modes.

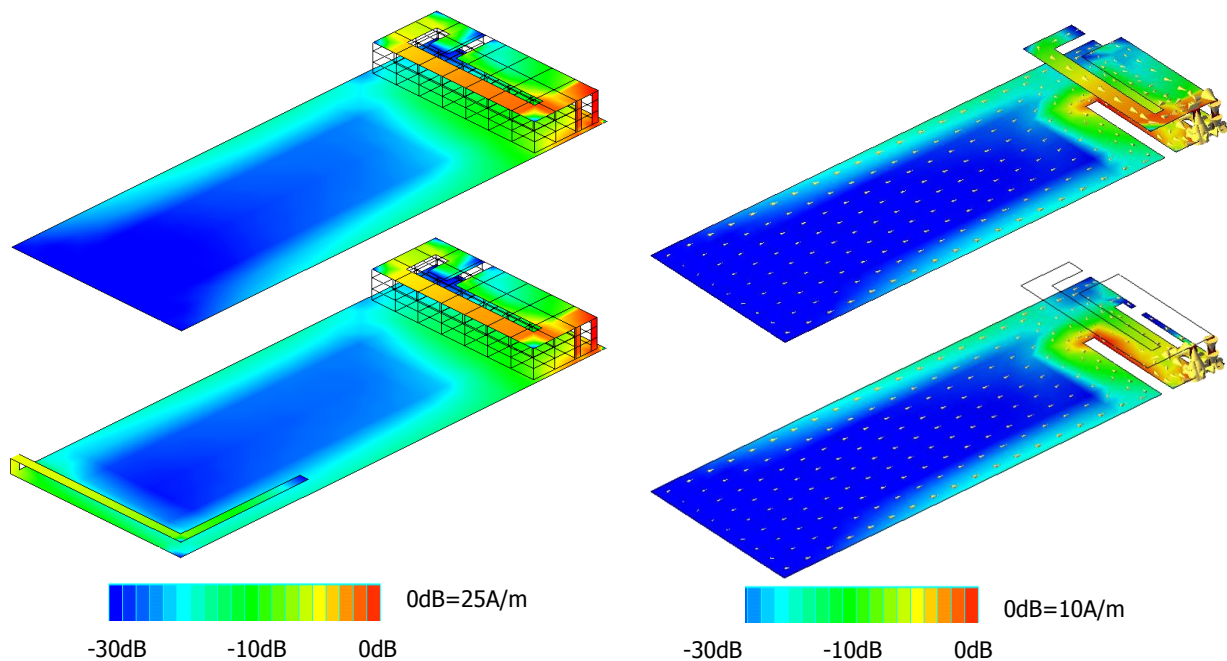


Fig. 1.16 Current distribution associated to existing antenna technologies intended for providing intelligence to the ground plane by electrically enlarging it through the addition of a conductive strip (left) [28]-[30] or by the insertion of slots (right) [19]-[27].

In [33], resonant elements are used for simultaneous tuning of two different ground plane modes. On one hand, the resonance of the first ground plane mode is adjusted by strategically loading the ground plane with a resonant screen acting as a quarter-wave slot resonator for the GSM1800 and GSM1900 bands. In this sense an electrical enlargement of the ground plane is achieved for the low frequency region (0.84-0.96GHz). On the other hand, the resonant frequency at the high frequency region (1.71-2.17GHz) is obtained by reducing the electrical length of the chassis for this frequency region. Similar proposals are found in [19]-[27] where a slot is used for tuning the resonant mode to lower frequencies by

providing a long current path, or in [28]-[30] where a conductive strip directly connected to the ground plane allows tuning such resonant frequency. On the contrary, in [35] the resonant mode is tuned to the high frequency region. At the same time, in [36] a distributed antenna system is proposed for enhancing the radiation efficiency of the ground plane mode while providing robustness to the performance degradation caused by the human interaction. On the contrary, in the present thesis, the efficient radiation is entirely provided by the proper excitation of the ground plane modes since no antenna is regarded [7]-[9].

Regarding [34], two antenna structures based on coupling elements designed to transfer energy to the ground plane mode are presented. They are intended for covering the communication standards GSM900 and GSM1800 separately by means of a single-resonant matching circuit based on distributed matching elements (Fig. 1.17a). Other reference based on coupling elements is given in [37] where an antenna structure consisting in two coupling elements and two resonant circuits is proposed (Fig. 1.17b). The proposal achieves a quad-band behavior. Nevertheless, the coupling elements presented for covering each frequency region (624 mm^3 and 64 mm^3 respectively), and specially that in charge of providing operability in the low frequency region, still presents a considerable volume compared with the 250 mm^3 disclosed herein for providing penta-band operation [9]. In [38], the penta-band behavior is achieved by means of two small antenna elements and two matching networks capable to provide multi-band operation at each frequency region.

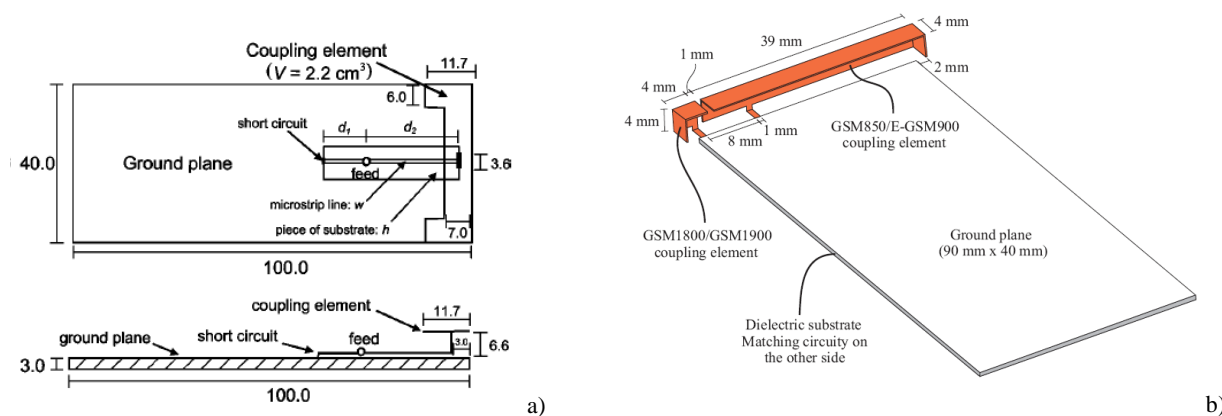


Fig. 1.17 a) Image of the coupling elements given in [34] where an antenna structure consists of coupling elements and two resonant circuits to provide operation in two frequency regions separately; b) Image corresponding to [37] showing the two coupling elements with volumes 624 mm^3 and 64 mm^3 , presented for covering each frequency region respectively.

As previously explained, in the present thesis, the self-resonant antenna element is replaced by non-resonant ground plane boosters featuring a very low volume, such as for instance of only 250 mm^3 [9], (regarding the solution presented in Fig. 1.18, which will be further disclosed in chapter 3). Therefore, the efforts are oriented to reuse an already existing part of the handset to radiate/receive electromagnetics signals in order to avoid the need of including a dedicated antenna.

In this sense, the present research is focused on providing multi-band wireless handheld device architectures based on the proper excitation of the ground plane without the need of an antenna element [7]-[9]. The fundamental basics of the proposal rely on the characteristics mode theory [39]-[42], which becomes a useful tool to understand the ground plane contribution. At the same time, and as will be

illustrated along this thesis, it can be used to perform systematic analysis and design of handset antennas. Accordingly, the preliminary solution briefly presented along this section, demonstrates that the efficient radiation mode associated to a ground plane with dimensions 100 mm x 40 mm can be excited through the use of non-resonant ground plane boosters [9]. This solution will be analyzed in more detail along chapter 3 but some illustrative results are presented below (Fig. 1.18) in order to demonstrate the feasibility of the proposal.

This first solution [7]-[9] reveals that no handset antenna is required for effectively exciting the radiation modes of the ground plane. On the contrary, the novel architecture introduced here only requires small ground plane boosters (Fig. 1.18), featured by a high quality factor ($Q=2250$ for the low frequency region and $Q=265$ for the high frequency region) and extremely poor stand-alone radiation properties in combination with a matching network for providing simultaneous operability in the main communication standards (GSM850, GSM900, GSM1800, GSM1900, and UMTS).



Fig. 1.18 a) Geometry and dimensions associated to the radiating structure, as a first solution of this thesis development comprising two non-resonant ground plane boosters, each one in charge of the ground plane excitation for each frequency region. Current distribution referred to the excited ground plane mode at $f=0.892\text{GHz}$; b) Prototype associated to the geometry shown in a).

Commonly, handset antenna specifications are given regarding free-space conditions. However, in practice, the handset antenna performance is strongly affected by other important factors such as hand interaction [43]-[44] and human head effect [45]-[53]. The user strongly interacts with the radiating system, especially during a phone call, affecting its performance and causing radiation losses as well as detuning effects. Thus, free-space measurements are not enough to correctly characterize handset antenna performance. The significant effects of the human head interaction over the performance of handset antennas have to be considered and accordingly, they are analyzed along the thesis. With this regard, another purpose of this thesis consists in evaluating the performance of the proposed solutions taking into account human interaction. In addition, the results are compared with other current handset antenna technologies already consolidated in the handset market which have been also analyzed regarding the human interaction. In this sense, the performance of three representative prototypes based on ‘off-ground’ solutions (monopoles), ‘on-ground’ solutions (PIFA), and ‘on-ground’ solutions (PIFA) over slotted ground planes are compared with the ground plane booster antenna technology proposed along this thesis not only in free-space but also regarding the human interaction.

Another important aspect of the present research is that concerning to smart antenna technologies such as MIMO. The operation principle of MIMO systems lies in the use of multiple antennas in both transmission and reception to provide an increment in the data rate, which is desirable for emergent applications requiring these high data rates. The arrangement of several conventional handset antennas in a specific mobile handset in order to provide MIMO capabilities becomes a challenge since their volume is too large. It is known that reducing the size of an antenna results in a penalty on the attainable bandwidth and radiation efficiency, which might severely drop below the minimum required in cellular and wireless systems if the antennas are too small.

Therefore, antennas for a MIMO enabled handset need to keep a certain size to fully operate within the entire bandwidth of the multiple frequency bands. Even if a few mid-size antennas fit inside a handset, another challenge is to ensure that the multiple antennas are sufficiently uncoupled and uncorrelated to benefit from the MIMO gain. The challenge is multiplied when the system has to operate at multiple frequency bands, since the dependence of the antenna performance with the electrical size makes even more difficult to achieve multi-band operation in a reduced space.

The solutions found in the literature regarding the integration of smart antennas in handheld wireless devices are mainly based on resonant antennas featuring physical dimensions comparable to a quarter of a wavelength [54]-[57]. Those solutions provide operability in the high frequency region and are mainly oriented to the communication standards LTE (3400-3600MHz), UMTS (1920-2170MHz), WiFi (2.5GHz), respectively. The property of being resonant at the operation frequencies, strictly limits the performance of such antenna technologies at lower frequency regions (~900MHz), since the physical dimensions that would be required to provide operation in such frequency range prevent the integration of multiple antenna elements in mobile platforms as shown in [58].

At the same time, those solutions based on non-resonant coupling elements are limited to single-band operation in the high frequency region where several different orthogonal modes appear, and can be excited to provide low correlation [59]-[60]. In [61], a MIMO system is proposed for covering the broadcast standard DVB-H located at a low frequency region (470-800MHz). Although the solution proposed is able for reception purposes it would not be able to provide acceptable performance in the transmission band since the reported antenna efficiency is insufficient for transmission purposes.

It is a further object of the present research to provide a MIMO solution capable of being integrated with current handset antenna technologies. Furthermore, this thesis will be focused on providing MIMO systems entirely provided by non-resonant ground plane boosters [10]. This new solution based on miniature ground plane boosters for MIMO operation allows the integration of multiple radiating structures in a single platform due to their characteristic small dimensions. In the present thesis the MIMO system is extended to multi-band operation including low and high frequency communication standards, such as LTE700, GSM850, GSM900, GSM1800, GSM1900, UMTS, LTE2100, LTE2300, and LTE2500.

1.6. Publications

This section gathers the publications derived from this thesis.

1.6.1 Patents

- [1] J. Anguera, A. Andújar, C. Puente, and J. Mumbrú, “Antennaless Wireless Device”, International Publication Number WO2010015365A2.
- [2] J. Anguera, A. Andújar, C. Puente, and J. Mumbrú, “Antennaless Wireless Device capable of Operation in Multiple Frequency Regions”, International Publication Number WO2010015364A2.
- [3] J. Anguera, C. Borja, C. Picher, and A. Andújar, “Wireless Device providing Operability for Broadcast Standards and Method Enabling such Operability”, International Publication Number WO2010145825A1.
- [4] J. Anguera and A. Andújar, “Antennaless Wireless Device comprising One or More Bodies”, International Publication Number WO2011095330A1.
- [5] A. Andújar, J. Anguera, C. Puente, and C. Picher, “Wireless Device capable of Multi-band MIMO Operation” International Publication Number WO2012017013A1.
- [6] A. Andújar and J. Anguera, “Compact Radiating Array for Wireless Handheld or Portable Devices”, Patent Application Number US 61/661,885.
- [7] J. Anguera, C. Picher, A. Andújar, and C. Puente, “Concentrated Antennaless Wireless Device providing Operability in Multiple Frequency Regions”, Patent Application Number US 61/671,906.
- [8] A. Andújar and J. Anguera, “Scattered Virtual Antenna Technology for Wireless Devices”, Patent Application Number US 61/837,265.
- [9] J. Anguera, A. Andújar, and C. Puente, “Wireless Handheld Devices, Radiation Systems, and Manufacturing Methods”, Patent Application Number US 13/946,922.

1.6.2 Journals

- [1] A. Andújar, J. Anguera, and C. Puente, “On the Radiation Pattern of the L-shaped Wire Antenna”, *Progress in Electromagnetic Research M*, vol. 6, pp. 91-105, 2009.
- [2] J. Anguera, A. Camps, A. Andújar, and C. Puente, “Enhancing Robustness of Handset Antennas to Finger Loading Effects”, *IEE Electronics Letters*, vol. 45, n° 15, July 2009, pp. 770-771.
- [3] S. Risco, J. Anguera, A. Andújar, A. Pérez, and C. Puente, “Coupled Monopole Antenna Design for Multi-band Handset Devices”, *Microwave and Optical Technology Letters*, vol. 52, n° 2, February 2010, pp. 359-364.

- [4] A. Pladevall, C. Picher, A. Andújar, and J. Anguera, "Some Thoughts on Human Body Effects on Handset Antenna at the FM Band", *Progress in Electromagnetic Research M*, vol. 19, 2011, pp. 121-132.
- [5] A. Andújar, J. Anguera, and C. Puente, "Ground Plane Boosters as a Compact Antenna Technology for Wireless Handheld Devices", *IEEE Transactions on Antennas and Propagation*, vol. 59, n° 5, May 2011, pp. 1668-1677.
- [6] J. Anguera, A. Andújar, and C. Puente, "A Mechanism to Electrically Enlarge the Ground Plane of Handset Antennas: a Bandwidth Enhancement Technique", *Microwave and Optical Technology Letters*, vol. 53, n° 7, July 2011, pp. 1512-1517.
- [7] S. Risco, J. Anguera, A. Andújar, C. Picher, and J. Pajares, "Comparison of a Monopole and a PIFA Handset Antenna in the Presence of the Human Head", *Microwave and Optical Technology Letters*, vol. 54, n° 2, February 2012, pp. 454-459.
- [8] C. Picher, J. Anguera, A. Andújar, C. Puente, and S. Kahng, "Analysis of the Human Head Interaction in Handset Antennas with Slotted Ground Planes", *IEEE Antennas and Propagation Magazine*, vol. 54, n° 2, April 2012, pp. 36-56.
- [9] C. Picher, A. Andújar, C. Borja, J. Anguera, C. Puente, and S. Kahng, "Integração de antenas de FM a celulares", *Brazilian Magazine*, April 2012, pp. 64-73.
- [10] A. Andújar, J. Anguera, C. Picher, and C. Puente, "Human Head Interaction over Ground Plane Booster Antenna Technology: Functional and Biological Analysis", *Progress in Electromagnetic Research B*, vol. 41, 2012, pp. 153-185.
- [11] A. Andújar and J. Anguera, "On the Radio-Frequency System of Ground Plane Booster Antenna Technology", *IEE Electronics Letters*, vol. 48, n° 14, July 2012, pp. 815-817.
- [12] J. Anguera, A. Andújar, C. Picher, L. González, C. Puente, and S. Kahng, "Behavior of Several Antenna Topologies Near the Human Head at the 2.4-2.5GHz Band", *Microwave and Optical Technology Letters*, vol. 54, n° 8, August 2012, pp. 1911-1916.
- [13] A. Andújar, J. Anguera, Y. Cobo, and C. Picher, "Distributed Antenna Systems for Wireless Handheld Devices Robust to Hand Loading", *IEEE Transactions on Antennas and Propagation*, vol. 60, n° 10, October 2012, pp. 4830-4837.
- [14] A. Andújar and J. Anguera, "Magnetic Boosters for Multi-band Operation", *Microwave and Optical Technology Letters*, vol. 55, n° 1, January 2013, pp. 65-75.
- [15] J. Anguera, A. Andújar, M. Huynh, C. Orlenius, C. Picher, and C. Puente, "Advances in Antenna Technology for Wireless Handheld Devices", *International Journal on Antennas and Propagation*, Volume 2013, ID 838364.
- [16] A. Andújar, J. Anguera, J. L. Leiva, and C. Picher, "In-phase versus Out-of-phase Distributed Antenna Systems for Wireless Handheld Devices", *IEEE Transactions on Antennas and Propagation*, vol. 61, n° 1, January 2013, pp. 346-353.

- [17] C. Picher, J. Anguera, and A. Andújar, “Analysis of a multi-band Monopole Handset Antenna combined with a Slotted Ground Plane”, *Microwave and Optical Technology Letters*, vol.55, n° 1, January 2013, pp. 173-180.
- [18] A. Andújar and J. Anguera, “Multiband Coplanar Ground Plane Booster Antenna Technology”, *IEE Electronics Letters*, vol. 48, n° 21, October 2012, pp. 1326-1328.
- [19] J. Anguera, A. Andújar, and C. García, “Multiband and Small Coplanar Antenna System for Wireless Handheld Devices”, *IEEE Transactions on Antennas and Propagation*, vol. 61, n° 7, July 2013, pp. 3782-3789.
- [20] A. Bujalance, C. Picher, J. Anguera, A. Andújar, and C. Puente, “Influence of handset components into the behavior of a Handset Antenna in a Slotted Ground Plane”, *Microwave and Optical Technology Letters*, vol.55, n° 8, August 2013, pp. 1770-1779.
- [21] J. Anguera and A. Andújar, “Ground Plane Contribution in Wireless Handheld Devices using Radar Cross Section Analysis”, *Progress In Electromagnetics Research M*, vol.26, 2012, pp-101-114.
- [22] C. Picher, J. Anguera, A. Andújar, and C. Puente, “Concentrated Ground Plane Booster Antenna Technology for Multiband Operation in Handset Devices”, Submitted to *Microwave and Optical Technology Letters*.
- [23] A. Andújar, J. Anguera, and Y. Cobo, “Distributed Systems Robust to Hand Loading based on Non-Resonant Elements”, *Microwave and Optical Technology Letters*, vol.55, n°10, October 2013, pp-2307-2317.
- [24] J. M. J. W. Jayasinghe, J. Anguera, D.N. Uduwawala, A. Andújar, “Genetic Algorithm Optimization of Microstrip Patch Antennas for High-Directivity Applications”, submitted to *Microwave and Optical Technology Letters*, in press 2013.
- [25] C. Picher, J. Anguera, A. Andújar, A. Bujalance, “Non-Resonant Element in a Slotted Ground Plane for Multiband Operation”, Submitted to *IEE Electronics Letters*.
- [26] A. Andújar and J. Anguera, “MIMO Multiband Antenna System Combining Resonant and Non-Resonant Elements”, submitted to *Microwave and Optical Technology Letters*.

1.6.3 International Conferences

- [1] M. García-Lozano, S. Ruiz-Boqué, A. Andújar-Linares, and N. Oller-Camaute, “Automatic Tuning of Soft Handover Parameters in UMTS Networks”, TD(07) COST 2100, COST, 2007, pp. 1-13.
- [2] J. Anguera, L. González, A. Andújar, and C. Puente, “Analysis of Several Antenna Topologies Operating at 2.4GHz Band close to human head”, *IEEE Antennas and Propagation Society International Symposium*, Charleston, South Carolina, USA, June 2009.

- [3] A. Andújar, J. Anguera, C. Puente, "A Systematic Method to Design Broadband Matching Networks", *IEEE Antennas and Propagation Society International Symposium*, Charleston, South Carolina, USA, June 2009.
- [4] J. Anguera, J. Arenas, A. Andújar, C. Puente, and S. Kahng, "Comparing Balanced and Single-Ended Handset Antennas in Free Space and Human Loading Scenarios", *IEEE Antennas and Propagation Society International Symposium*, Charleston, South Carolina, USA, June 2009.
- [5] J. Anguera, A. Andújar, C. Puente, A. Camps, and C. Picher, "Mitigation of Finger Loading Effect in Handset Antennas", *Proceedings of the Fourth European Conference on Antennas and Propagation*, EuCAP 2010, Barcelona, Spain, April 2010, pp. 1-4.
- [6] I. Sanz, J. Anguera, A. Andújar, C. Puente, and C. Borja, "The Hilbert Monopole Revisited", *Proceedings of the Fourth European Conference on Antennas and Propagation*, EuCAP 2010, Barcelona, Spain, April 2010, pp. 1-4.
- [7] C. Picher, J. Anguera, A. Andújar, C. Puente, and S. Kahng, "Analysis of the Specific Absorption Rate in Antennas with Slotted Ground Planes", *Proceedings of the Fourth European Conference on Antennas and Propagation*, EuCAP 2010, Barcelona, Spain, April 2010, pp. 1-5.
- [8] A. Andújar, J. Anguera, and C. Puente, "A Systematic Method to Design Broadband matching Networks", *Proceedings of the Fourth European Conference on Antennas and Propagation*, EuCAP 2010, Barcelona, Spain, April 2010, pp. 1-5.
- [9] J. Anguera, L. González, A. Andújar, C. Picher, C. Puente, and SungTek Kahng, "Comparison of several antenna topologies near the Human Head: a 2.4GHz case Study", *IEEE Antennas and Propagation Society International Symposium*, Toronto, Canada, July 2010.
- [10] A. Andújar, J. Anguera, and C. Puente, "Ground Plane Boosters to provide Multi-Band Operation in Wireless Handheld Devices", *Proceedings of the Fifth European Conference on Antennas and Propagation*, EuCAP 2011, Rome, Italy, April 2011, pp. 599-603.
- [11] J. Anguera, A. Andújar, Y. Cobo, C. Puente, and C. Picher, "Handset Antenna Array to Mitigate the Finger Loading Effect", *Proceedings of the Fifth European Conference on Antennas and Propagation*, EuCAP 2011, Rome, Italy, April 2011, pp. 611-614.
- [12] C. Picher, J. Anguera, A. Andújar, C. Borja, C. Puente, and S. Kahng, "Reuse of the Mobile Communication Antenna for FM Reception", *Proceedings of the Fifth European Conference on Antennas and Propagation*, EuCAP 2011, Rome, Italy, April 2011, pp. 324-327.
- [13] A. Andújar, J. Anguera, C. Picher, and C. Puente, "Ground Plane Booster Antenna Technology. Human Head Interaction: Functional and Biological Analysis", *Proceedings of the Sixth European Conference on Antennas and Propagation*, EuCAP 2012, Prague, Czech Republic, March 2012, pp. 2745-2749.

- [14] C. Picher, J. Anguera, A. Andújar, A. Bujalance, and C. Puente, “Multi-band Handset Antennas by Combining Monopoles and Intelligent Ground Planes”, *Proceedings of the Sixth European Conference on Antennas and Propagation*, EuCAP 2012, Prague, Czech Republic, March 2012, pp. 2741-2744.
- [15] J. Anguera, A. Andújar, C. Picher, C. Puente, and S. Kahng, “Analysis of Some Techniques to Enhance the Bandwidth of Handset Antennas using Metallic Strips”, *Proceedings of the Sixth European Conference on Antennas and Propagation*, EuCAP 2012, Prague, Czech Republic, March 2012, pp. 2730-2733.
- [16] A. Andújar and J. Anguera, “Coplanar Non-Resonant Elements for Multiband Operation”, *Proceedings of the Seventh European Conference on Antennas and Propagation*, EUCAP 2013, Gothenburg, Sweden, April 2013.
- [17] A. Andújar and J. Anguera, “Non-Resonant Elements with a Simplified Radiofrequency System for Handset Devices”, *Proceedings of the Seventh European Conference on Antennas and Propagation*, EUCAP 2013, Gothenburg, Sweden, April 2013.
- [18] J. Anguera, C. Picher, A. Andújar, S. Kahng, and C. Puente, “Compact Multiband Antenna System for Smartphone Platforms”, *Proceedings of the Seventh European Conference on Antennas and Propagation*, EUCAP 2013, Gothenburg, Sweden, April 2013.

1.6.4 National Conferences

- [1] S. Risco, J. Anguera, A. Andújar, A. Pérez, C. Puente, “Análisis y Diseño de Monopolos Acoplados para Dispositivos Móviles Multi-banda”, *Proceedings of the XXIII National Symposium of the Scientific International Union of Radio*, URSI 2008, Madrid, Spain, September 2008.
- [2] S. Risco, J. Anguera, A. Andújar, C. Picher, C. Puente, “Análisis del comportamiento de antenas móviles en presencia del cuerpo humano”, *Proceedings of the XXIV National Symposium of the Scientific International Union of Radio*, URSI 2009, Santander, Spain, September 2009.
- [3] C. Picher, J. Anguera, A. Andújar, C. Puente, S. Risco, S. Kahng, “Diseño de una antena multi-banda con ranuras en el plano de masa: una técnica para facilitar la integración de la línea de alimentación”, *Proceedings of the XXIV National Symposium of the Scientific International Union of Radio*, URSI 2009, Santander, Spain, September 2009.
- [4] A. Andújar, J. Anguera, C. Puente, C. Picher, “Conformación del diagrama de radiación de un monopolo en L”, *Proceedings of the XXIV National Symposium of the Scientific International Union of Radio*, URSI 2009, Santander, Spain, September 2009.
- [5] Y. Cobo, A. Andújar, J. Anguera, “Sistema de Antenas Distribuido para Dispositivos Móviles”, *Proceedings of the XXVI National Symposium of the Scientific International Union of Radio*. URSI 2011. Leganés, September 2011.

1.7. References

- [1] J.S. McLean, "A Re-Examination of the Fundamental Limits on the Radiation Q of Electrically Small Antennas", *IEEE Transactions on Antennas and Propagation*, AP-44, May 1996, pp. 672-676.
- [2] M. Geissier, D. Heberling, and I. Wolff, "Bandwidth and Radiating Properties of Internal Handset Antennas", *IEEE Antennas and Propagation Society International Symposium*, vol. 4, July 2000, pp. 2246-2249.
- [3] S. R. Best, "The Inverse Relationship between Quality Factor and Bandwidth in Multiple Resonant Antennas", *IEEE Antennas and Propagation Society International Symposium*, 2006, pp. 623-626.
- [4] R. C. Hansen, "Fano Limits on Matching Bandwidth", *IEEE Antennas and Propagation Magazine*, vol. 47, n° 3, June 2005, pp. 89-90.
- [5] J. Anguera, C. Puente, C. Borja, G. Font, and J. Soler, "A Systematic Method to Design Single-Patch Broadband Microstrip Patch Antennas", *Microwave and Optical Technology Letters*, vol. 31, n°3, November 2001, pp. 185-188.
- [6] A. Andújar, J. Anguera, and C. Puente, "A Systematic Method to Design Broadband Matching Networks", *Proceedings of the Fourth European Conference on Antennas and Propagation*, EuCAP 2010, Barcelona, Spain, 2010.
- [7] J. Anguera, A. Andújar, C. Puente, and J. Mumbrú, "Antennaless Wireless Device", *Patent Application* WO2010/015365, July 31, 2009.
- [8] J. Anguera, A. Andújar, C. Puente, and J. Mumbrú, "Antennaless Wireless Device Capable of Operation in Multiple Frequency Regions", *Patent Application* WO2010/015364, July 31, 2009.
- [9] A. Andújar, J. Anguera, and C. Puente, "Ground Plane Boosters as a Compact Antenna Technology for Wireless Handheld Devices", *IEEE Transactions on Antennas and Propagation*, vol.59, n°5, May 2011, pp.1668-1677.
- [10] A. Andújar, J. Anguera, and C. Puente, "Antennaless Wireless Device Capable of MIMO Multi-band Operation", *Patent Application* WO 2012/017013, August 3, 2011.
- [11] K. L. Wong, *Planar Antennas for Wireless Communications*, New York, John Wiley & Sons, 2003.
- [12] C. Puente, J. Anguera, J. Soler, and A. Condes, "Coupled Multi-band Antennas", *Patent Application* WO2004/025778, September 10, 2002.
- [13] C. Lin and K. L. Wong, "Printed Monopole Slot Antenna for Internal Multi-band Mobile Phone Antenna", *IEEE Transactions on Antennas and Propagation*, vol. 55, n°12, December 2007, pp. 3690-3697.
- [14] S. Risco, J. Anguera, A. Andújar, A. Pérez, and C. Puente, "Coupled Monopole Antenna Design for Multi-band Handset Devices", *Microwave and Optical Technology Letters*, vol. 52, n° 2, February 2010, pp. 359-364.
- [15] J. Anguera and C. Puente, "Shaped Ground Plane for Radio Apparatus", *Patent Application* WO2006/070017, December 29, 2005.

- [16] C. Puente and J. Anguera “Slotted Ground-Plane used as a Slot Antenna or used for a PIFA Antenna”, *Patent Application* WO2006/097496, September 21, 2006.
- [17] C. Wu and K. Wong, “Hexa-band Internal Printed Slot Antenna for Mobile Phone Application”, *Microwave and Optical Technology Letters*, vol. 50, n°1, January 2008, pp. 35-38.
- [18] J. Anguera, I. Sanz, J. Mumbrú, and C. Puente, “Multi-Band Handset Antenna with a Parallel Excitation of PIFA and Slot Radiators”, *IEEE Transactions on Antennas and Propagation*, vol.58, n°2, February 2010, pp.348-356.
- [19] J. Anguera, I. Sanz, A. Sanz, A. Condes, D. Gala, C. Puente, and J. Soler, “Enhancing the performance of handset antennas by means of ground plane design”, *IEEE International Workshop on Antenna Technology: Small Antennas and Novel Metamaterials (iWAT 2006)*, New York, USA, March 2006.
- [20] J. Anguera, A. Cabedo, C. Picher, I. Sanz, M. Ribó, and C. Puente, “Multi-band Handset Antennas by Means of Ground plane Modification”, *IEEE Antennas and Propagation Society International Symposium*, Honolulu, Hawaii, USA, June 2007.
- [21] C. Picher, J. Anguera, A. Cabedo, C. Puente, and S. Kahng, “Multi-band Handset Antenna Using Slots on the Ground Plane: Considerations to Facilitate the Integration of the Feeding Transmission Line”, *Progress In Electromagnetics Research C*, vol. 7, 2009, pp. 95-109.
- [22] A. Cabedo, J. Anguera, C. Picher, M. Ribó, and C. Puente, “Multi-Band Handset Antenna Combining a PIFA, Slots, and Ground Plane Modes”, *IEEE Transactions on Antennas and Propagation*, vol.57, n°9, Sep. 2009, pp. 2526-2533.
- [23] R. Quintero and C. Puente, “Multilevel and Space-Filling Ground Planes for Miniature and Multi-band Antennas”, *Patent Application* WO2003/023900, September 13, 2001.
- [24] C. Picher, J. Anguera, A. Andújar, C. Puente, and S. Kahng, “Analysis of the Specific Absorption Rate in Handset Antennas with Slotted Ground Planes”, *Proceedings of the Fourth European Conference on Antennas and Propagation*, EuCAP 2010, Barcelona, Spain, April 2010.
- [25] C. Picher, J. Anguera, A. Andújar, C. Puente, and S. Kahng, “Analysis of the Human Head Interaction in Handset Antennas with Slotted Ground Planes”, *IEEE Antennas and Propagation Magazine*, vol. 54, n°2, April 2012, pp. 37-54.
- [26] C. Picher, J. Anguera, A. Andújar, C. Puente, and A. Bujalance, “Multi-band Handset Antennas by Combining Monopoles and Intelligent Ground Planes”, *Proceedings of the Sixth European Conference on Antennas and Propagation*, EuCAP 2012, Prague, Czech Republic, March 2012, pp. 2741-2744.
- [27] C. Picher, J. Anguera, A. Bujalance, A. Andújar, and C. Puente, “Analysis of a Multi-band Monopole Handset Antenna Combined with a Slotted Ground Plane”, *Microwave and Optical Technology Letters*, vol. 55, n°1, January 2013, pp. 173-180.

- [28] J. Anguera and A. Condes, "Antenna Set, Portable Wireless Device, and use of a Conductive Element for Tuning the Ground-plane of the Antenna set", Patent Application WO 2007/039071, September 15, 2006.
- [29] J. Anguera, A. Andújar, and C. Puente, "A Mechanism to Electrically Enlarge the Ground Plane of Handset Antennas: A Bandwidth Enhancement Technique", *Microwave and Optical Technology Letters*, vol. 53, n°7, July 2011, pp. 1512-1517.
- [30] J. Anguera, A. Andújar, C. Picher, C. Puente, and S. Kahng, "Analysis of Some Techniques to Enhance Bandwidth of Handset Antennas using Metallic Strips", *Proceedings of the Sixth European Conference on Antennas and Propagation*, EuCAP 2012, Prague, Czech Republic, March 2012, pp. 2730-2733.
- [31] P. Vainikainen, J. Ollikainen, O. Kivekäs, and I. Kelder, "Resonator-Based Analysis of the Combination of Mobile Handset Antenna and Chassis", *IEEE Transactions on Antennas and Propagation*, vol. 50, n° 10, October 2002, pp. 1433-1444.
- [32] M. Cabedo-Fabrés, E. Antonino-Daviu, A. Valero-Nogueira, and M. Ferrando Bataller, "The Theory of Characteristic Modes Revisited: A Contribution to the Design of Antennas for Modern Applications", *IEEE Antennas and Propagation Magazine*, vol. 49, n° 5, October 2007, pp. 52-68.
- [33] W. L. Schroeder, C. T. Fandie, and K. Solbach, "Utilization and Tuning of the Chassis Modes of a Handheld Terminal for the Design of Multi-band Radiation Characteristics", *IEE Wideband and Multi-band Antennas and Arrays*, September 2005, pp. 117-121.
- [34] J. Villanen, J. Ollikainen, O. Kivekäs, and P. Vainikainen, "Coupling Element Based Mobile Terminal Antenna Structures", *IEEE Transactions on Antennas and Propagation*, vol. 54, n° 7, July 2006, pp. 2142-2153.
- [35] C. Puente and J. Anguera, "Handset with Electromagnetic Bra", *Patent Application* WO2005/083833, February 28, 2005.
- [36] J. Anguera and C. Puente, "Distributed Antenna System Robust to Human Body Loading Effects", *Patent Application* WO2007/141187, June 08, 2006.
- [37] S. Ozden, B. K. Nielsen, C. H. Jorgensen, J. Villanen, C. Icheln, and P. Vainikainen, "Quad-Band Coupling Element Antenna Structure", *U.S. Patent* 7,274,340, September 25, 2007.
- [38] J. Anguera, I. Sanz, and C. Puente, "Wireless Device Including a Multi-band Antenna System", *Patent Application* WO2008/119699, March 30, 2007.
- [39] R. J. Garbacz and R.H. Turpin, "A generalized expansion for radiated and scattered fields", *IEEE Transactions on Antennas and Propagation*, vol. AP-19, May 1971, pp. 348-358.
- [40] R.F. Harrington and J.R. Mautz, "Theory of Characteristic Modes for Conducting Bodies", *IEEE Transactions on Antennas and Propagation*, AP-19, n° 5, September 1971, pp. 622-628.
- [41] E.H. Newman, "Small Antenna Location Synthesis Using Characteristic Modes", *IEEE Transactions on Antennas and Propagation*, vol. AP-27, n° 4, July 1979, pp. 530-531.

- [42] C. T. Famdie, W. L. Schroeder, and L. Solbach, "Numerical analysis of characteristic modes on the chassis of mobile phones", *Proceedings of the First European Conference on Antennas and Propagation*, EuCAP 2006, Nice, France, 2006.
- [43] J. M. Jung, S. Kim, K. Kong, J. Lee, and B. Lee, "Designing Ground Plane to Reduce Hand Effects on Mobile Handsets", *IEEE Antennas and Propagation Society International Symposium*, Honolulu, USA, June 2007, pp. 1040-1043.
- [44] C. Su, C. Wu, and K. Wong, "User's Hand Effects on EMC internal GSM/DCS mobile phone antenna", *IEEE Antennas and Propagation Society International Symposium*, Albuquerque, USA, July 2006, pp. 2097-2100.
- [45] P.S. Kildal and C. Carlsson, "Comparison between Head Losses of 20 Phones with External and Built-in Antennas Measured in Reverberation Chamber", *IEEE Antennas and Propagation Society International Symposium*, vol. 1, August 2002, pp. 436-439.
- [46] K. R. Boyle, Y. Yuan, and L. P. Ligthart, "Analysis of Mobile Phone Antenna Impedance Variations with User Proximity", *IEEE Transaction on Antennas and Propagation*, vol.55, n°2, February 2007, pp. 364-372.
- [47] T. Huang and K. R. Boyle, "User Interaction Studies on Handset Antennas", *Proceedings of the Second European Conference on Antennas and Propagation*, EuCAP2007, Edinburgh, United Kingdom, 2007.
- [48] D. Lu, D. Fisk, and A. Wang, "A Mobile Antenna Design for Optimal Performance in Human Head and Hand Configuration", *IEEE Antennas and Propagation Society International Symposium*, Honolulu, USA, June 2007, pp. 1048-1048.
- [49] M. A. Ebrahimi-Ganjeh and A. R. Attari, "Interaction of Dual Band Helical and PIFA Handset Antennas with Human Head and Hand", *Progress In Electromagnetics Research*, PIER 77, pp. 225-242, 2007.
- [50] A. Schiavoni, P. Bertotto, G. Richiardi, and P. Bielli, "SAR Generated by Commercial Cellular Phones –Phone Modeling, Head Modeling, and Measurements", *IEEE Transactions on Microwave Theory and Techniques*, vol.18, n°11, November 2000, pp. 2064-2071.
- [51] P. Bernardi, M. Cavagnaro, S. Pisa, and E. Piuze, "Power Absorption and Temperature Elevations Induced in the Human Head by a Dual-Band Monopole-Helix Antenna Phone", *IEEE Transactions on Microwave Theory and Techniques*, vol. 49, n°12, December 2001, pp. 2539-2546
- [52] H. Khodabakhshi and A. Cheldavi, "Human Head Interaction with a PIFA in Cellular Mobile Communication", *Proceedings of the Fourth European Conference on Antennas and Propagation*, EuCAP2010, Barcelona, Spain, 2010.
- [53] Basic standard for the measurement of Specific Absorption Rate related to human exposure to Electromagnetic fields from mobile phones (300 MHz-3GHz) CENELEC-European Committee for Electro technical Standardization Std. EN 50 361, Jul. 2001.

- [54] A. A. H. Azremi, M. Kyrö, J. Ilvonen, J. Holopainen, S. Ranvier, C. Icheln, and P. Vainikainen, "Five-Element Inverted-F Antenna Array for MIMO Communications and Radio Direction Finding on Mobile Terminal", *IEEE Antennas and Propagation Conference*, Loughborough UK, November 2009, pp. 557-560.
- [55] Z. Li, Z. Du and K. Gong, "Compact Reconfigurable Antenna Array for Adaptive MIMO Systems", *IEEE Antennas and Wireless propagation Letters*, vol.8, 2009, pp. 1317-1320.
- [56] Y. Gao, X. Chen, Z. Ying, and C. Parini, "Design and Performance Investigation of a Dual-Element PIFA Array at 2.5 GHz for MIMO Terminal", *IEEE Transactions on Antennas and Propagation*, vol. 55, n°12, December 2007, pp. 3433-3441.
- [57] J. Guterman, A. Moreira, and C. Peixeiro, "Microstrip Fractal Antennas for Multistandard Terminals", *IEEE Antennas and Wireless Propagation Letters*, vol.3, 2004, pp. 351-354.
- [58] R. Glogowski and C. Peixeiro, "Multiple Printed Antennas for Integration Into Small Multistandard Handsets", *IEEE Antennas and Wireless Propagation Letters*, vol.7, 2008, pp. 632-635.
- [59] S. K. Chaudhury, H. J. Chaloupka, and A. Ziroff, "Novel MIMO Antennas for Mobile Terminal", *Proceeding of the 38th European Microwave Conference*, 2008, pp-330-333.
- [60] S. Kabir Chaudhury, W. L. Schroeder, and H. Chaloupka, "Multiple Antenna Concept Based on Characteristic Modes of Mobile Phone Chassis", *Proceedings of the Second European Conference on Antennas and Propagation*, EuCAP2007, Edinburgh, United Kingdom, November 2007.
- [61] M. Kyrö, M. Mustonen, C. Icheln, and P. Vainikainen, "Dual-Element Antenna for DVB-H Terminal", *IEEE Antennas and Propagation Conference*, Loughborough UK, March 2008, pp. 265-268.

CHAPTER 2 FUNDAMENTAL PRINCIPLES

2.1. Introduction

As introduced in the previous chapter, the trend in the handset market more and more is focused on integrating a large number of functionalities and services in handset devices with considerable space constraints. Consequently, antenna designers have to face the challenge of not only providing miniature antennas with multi-band capabilities, but also of allowing the integration of multiple antenna elements in this limited space. These challenges exacerbate when resonant antenna elements are considered. For this reason, and as indicated in the introductory section, this thesis proposes the use of the ground plane, inherently present in any handset platform, as the main radiator. This proposal, removes the need of integrating resonant antenna elements inside the handset platform, thus reducing considerably the Printed Circuit Board (PCB) space devoted to the radiating system. This fact becomes significantly advantageous for integrating multiple handset components and functionalities as well as for leaving more space to integrate a great number of radiating system such as those required by the emergent MIMO technology.

Since the main objective relies on exciting the ground plane, this chapter proposes the use of the characteristic modes theory [1]-[3] to determine the electromagnetic properties of this conducting object. Firstly, a brief review of the theory is presented in section 2.2. This theory will be applied later on along section 2.2.1, to analyze representative handset platforms. Handset platforms have rapidly evolved to new form factors, such as smartphones featured by a large display, which are substituting more and more, other well-known form factors such as for example small bar-type phones, sliders, and clamshells. Different shaped handset platforms integrate different shaped ground planes that potentially could produce different electromagnetic performance. In order to characterize said electromagnetic performance, section 2.3 computes the characteristic modes associated to three representative handset platforms of nowadays (a bar-type with dimensions of 100 mm x 40 mm, a smartphone of larger dimensions close to 120 mm x 50 mm, and a clamshell-type handset platform having two PCBs being adapted to be folded together, each one comprising a ground plane with dimensions of 80 mm x 40 mm).

Section 2.3 proposes a new method to compute the resonant frequency of the fundamental mode of arbitrary shaped conducting objects. The method is based on Radar Cross Section (RCS). It relies on illuminating the conducting structure with a plane wave linearly polarized in the direction of the long axis of the conducting structure. Consequently, the method only applies for determining the behavior of those radiating modes having linear current distributions. More particularly, for the analyzed topologies, the proposed method becomes useful for determining the behavior of the fundamental radiating mode, which at the end is the mode of interest at mobile frequencies, more significantly when operation in the low frequency region is regarded. The advantage with respect to the mathematical procedure required by the characteristic modes theory mainly relies on its simplicity, especially when ground planes of complex

shapes are regarded. In order to illustrate this fact, this section further computes the fundamental radiating modes of a slotted ground plane and a ground plane having an additional conducting strip. Both methods are intended for enlarging the electrical size of the ground plane without affecting its physical dimensions. The feasibility of the RCS computation will be demonstrated since it will allow an easy comparison of the advantages and disadvantages of the aforementioned techniques. Once the potential electromagnetic properties of the inherent ground planes of current handset platforms have been determined, the question that arises is how to transfer energy to these ground plane radiating modes, i.e. which elements are more suitable for exciting these ground plane radiating modes. Section 2.4 is intended for solving this question and compares the effect produced by resonant and non-resonant elements in the excitation of the ground plane modes, and consequently in the performance of the whole radiating system.

2.2. Characteristic Modes Theory

Characteristic modes theory was initially introduced by Garbacz and later developed by Harrington and Mautz in the early 70's. The theory allows determining the wave modes that are supported by a particular conducting body just as a function of their shape and size [1]-[4]. This fact provides a significant physical insight into the radiation properties of a particular conducting object.

The theory is based on the impedance matrix (\hat{Z}), which relates a surface current density (J_s) to the tangential components of the electrical field on the surface S of the conducting body (2.1).

$$E_{\text{tan}} = \hat{Z} \cdot J_s = (\hat{R} + j\hat{X}) \cdot J_s \quad (2.1)$$

Note that \hat{R} and \hat{X} represent the real and imaginary part of the impedance matrix \hat{Z} , respectively. The reciprocity theorem states that if \hat{Z} is a linear symmetric operator, its parts \hat{R} and \hat{X} , will be also real and symmetric operators. Accordingly, all the eigenvalues are real and all the eigencurrents are real or equiphasal over the surface in which they are defined. This problem formulation developed in detail in [2]-[4], leads via the generalized eigenvalue problem to real eigenvalues λ_n and real eigenfunctions or eigencurrents $J_{s,n}$, which present orthogonal properties (2.2). In practice this formulation can be reduced to a matrix form (2.3) that can be solved using standard algorithms for eigenvalues problems.

The solution of equation (2.3) provides the corresponding eigenvalues associated to each particular characteristic mode and their knowledge offers a relevant physical insight into their radiation properties. A characteristic mode is in resonance when its corresponding eigenvalue is zero whereas a mode contributes to store electric energy or magnetic energy when its eigenvalue is lower than zero ($\lambda_n < 0$) and larger than zero ($\lambda_n > 0$), respectively.

$$\hat{X} \cdot J_{s,n} = \lambda_n \cdot \hat{R} \cdot J_{s,n} \quad (2.2)$$

$$[X] \cdot \vec{J}_n = \lambda_n \cdot [R] \cdot \vec{J}_n \quad (2.3)$$

Similarly, the electric fields produced by these eigencurrents can be derived from (2.1) according to (2.4). The electric fields produced by two currents J_m and J_n are also equiphasal and they also present orthogonal properties, which become apparent from the Poynting theorem (2.5).

$$E_n(\vec{J}_n) = Z(\vec{J}_n) = R(\vec{J}_n) + jX(\vec{J}_n) = R(\vec{J}_n) \cdot (1 + j\lambda_n) \quad (2.4)$$

$$P(J_m, J_n) = \iint_{S'} \vec{E}_m \times \vec{H}_n^* ds + j\omega \iiint_{\tau'} (\mu \vec{H}_m \cdot \vec{H}_n^* - \epsilon \vec{E}_m \cdot \vec{E}_n^*) d\tau = (1 + j\lambda_n) \delta_{mn} \quad (2.5)$$

Due to the orthogonal properties of both, electric fields and surface currents, each characteristic mode radiates power independently from one another. Thus, they can be used as a basis set in which to expand the total current J on the surface of the conducting body according to (2.6).

$$J = \sum_n \frac{V_n^i \cdot J_n}{1 + j\lambda_n} \quad (2.6)$$

It is worth noticing that characteristic modes are independent from the source excitation (V_n^i). Nevertheless, this source excitation (V_n^i) influences the total current on the surface of the conducting body (J) and determines if a characteristic mode will be properly excited or not. The total current surface is directly proportional to the term, $\frac{1}{1 + j\lambda_n}$, and its modulus is well known in the field as modal significance (MS). This term represents the normalized amplitude of the characteristic modes as well as an alternative representation of their electromagnetics properties. In this sense, insofar the modal significance approaches one, the more effectively the characteristic mode contributes to the radiation process.

$$Q_{rad} = \frac{\omega_{\max} (\langle W_{mag} \rangle, \langle W_{el} \rangle)}{P_{rad}} \quad (2.7)$$

$$Q_{rad,n} = \frac{1}{2} Q_{s,n} = \frac{\omega_n}{2} \left| \frac{d\lambda_n}{d\omega} \right|_{\omega=\omega_n} \quad (2.8)$$

Of further importance is the quality factor associated to each characteristic mode, which is defined according to [5] as illustrated in (2.7) and (2.8). The quality factor of a characteristic mode at a particular frequency provides a valuable information since it allows determining its inherent bandwidth (1.1). Thus, it is possible to know in advance if the proper excitation of this mode would produce the required bandwidth to provide operation in the desired communication standards.

Once the most relevant parameters arising from the characteristic modes theory have been presented, the following sections will be focused on demonstrating the great potential of this theory in practical applications.

2.2.1 Characteristic Modes of Representative Handset Platforms

The procedure followed along this thesis to compute characteristic modes can be summarized as follows. Firstly, the conducting object under study is created and triangularly meshed regarding a cell size criterion of one twentieth of the operating wavelength. The election of the cell size strongly depends on the size of the conducting object to characterize. In this case, since the conducting objects are handset platforms, this cell size becomes sufficient to model them properly. The Partial Differential Equation Toolbox (PDEtool) of Matlab is the software used to create and mesh the conducting object. Once the conducting object is meshed, the complex input impedance matrix $[Z]$ can be derived for each frequency. As indicated in (2.3), the eigenvalues are defined as the ratio between the imaginary part and the real part of this complex input impedance matrix. Thus, its knowledge for each frequency allows obtaining readily the eigenvalues according to (2.9).

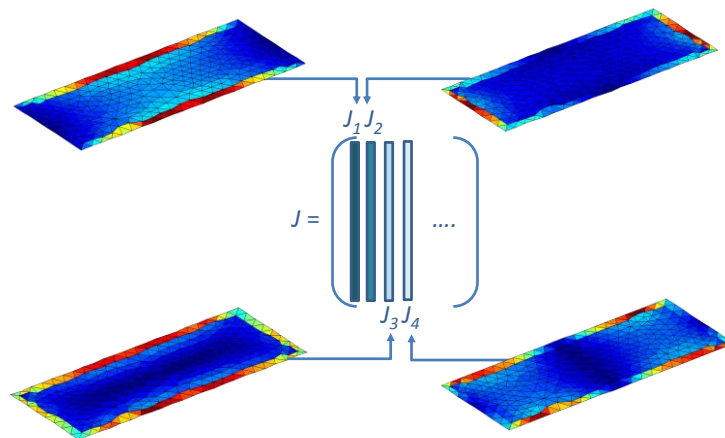


Fig. 2.1 Physical interpretation of the matrix J . The columns of the matrix correspond to each characteristic mode and they contain information about its current distribution. In this case, the conducting structure is a rectangular conducting body of dimensions 100 mm x 40 mm.

The diagonal elements of the matrix D correspond to the eigenvalues. These values have to be ordered due to the non-continuous behavior of the eigenvalues after the decomposition of the Z matrix using the “eig” operator of Matlab. At the same time, the column elements of the matrix J correspond to the eigenvectors which are useful to represent the current distribution of a mode for a given conductive structure (Fig. 2.1). The modal significance is readily obtained according to equation (2.10). Following

the theoretic principles and the mathematical procedure presented above, the characteristic modes associated to a bar type handset platform with dimensions 100 mm x 40 mm have been computed.

$$[J, D] = \text{eig}(X, R) \text{ where } R = \Re\{Z\} \text{ and } X = \Im\{Z\} \quad (2.9)$$

The results reveal that the first and the fourth characteristic modes (J_1 and J_4) become effective radiating modes at the frequencies near the resonance. In fact, the modal significance of the fundamental radiating mode (J_1) remains close to the normalized maximum value for a large range of frequencies, hence contributing to the radiation process actively along this frequency range (Fig. 2.2).

$$MS_n = \left| \frac{1}{1 + j\lambda_n} \right| \quad (2.10)$$

Nevertheless the second and the third (J_2 and J_3) characteristic modes do not contribute actively to the radiation process in the mobile frequencies under study. This fact is further illustrated in the eigenvalues representation, which depicts that the second radiating mode contributes to store electric energy along the low frequency region (690-960MHz) and the high frequency region (1710-2690MHz) ($\lambda_2 < 0$) whereas the third radiating mode contributes to store magnetic energy at these same frequency ranges ($\lambda_3 > 0$) (Fig. 2.3). Each mode presents a particular current distribution (Fig. 2.4).

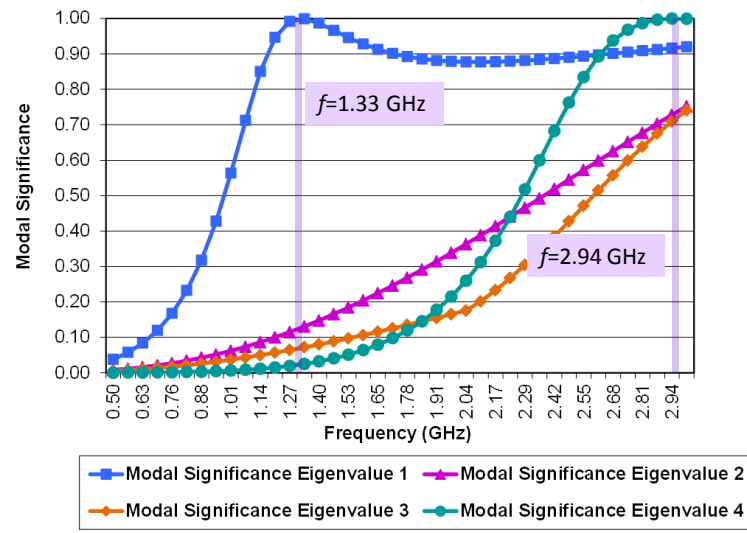


Fig. 2.2 Modal significance associated to the characteristic modes J_1, J_2, J_3, J_4 of a bar type handset platform having dimensions of 100 mm x 40 mm.

The current distribution of the fundamental radiating mode (J_1) approximates that featured by a half-wavelength dipole since it presents maximums of current at the center of the longitudinal edges of the ground plane and minimums in its transversal edges (Fig. 2.4a). At the same time, the current distribution of the fourth radiating mode can be compared to that produced by a wavelength dipole with an asymmetric excitation (Fig. 2.4d) [6]. These results are completely aligned with those illustrated in [5].

The fact of increasing the length of the handset platform produces a shifting in the resonant frequencies of the characteristic modes to lower frequencies (Fig. 2.5), but does not modify the corresponding current distributions (Fig. 2.6). Namely, the resonance of the fundamental radiating mode (J_1) shifts from approximately 1.33GHz to 1.08GHz, and the resonance of the fourth radiating mode (J_4) moves from approximately 2.94GHz to 2.49GHz (Fig. 2.2 and Fig. 2.5).

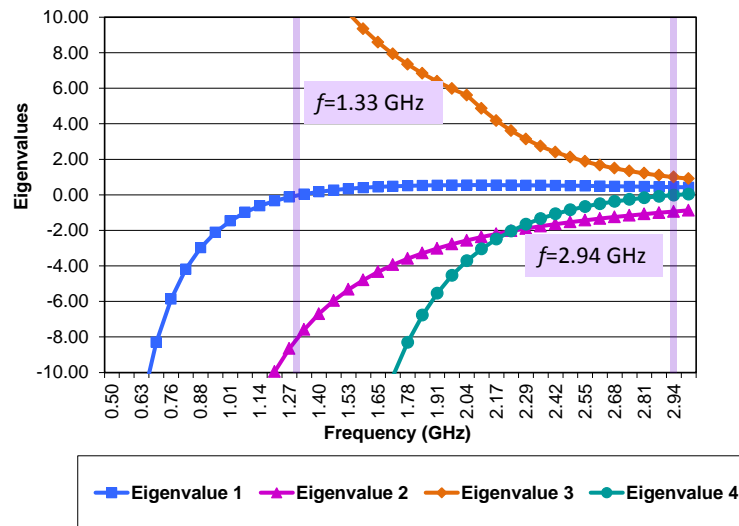


Fig. 2.3 Eigenvalues associated to the characteristic modes J_1, J_2, J_3, J_4 of a bar type handset platform having dimensions of 100 mm x 40 mm.

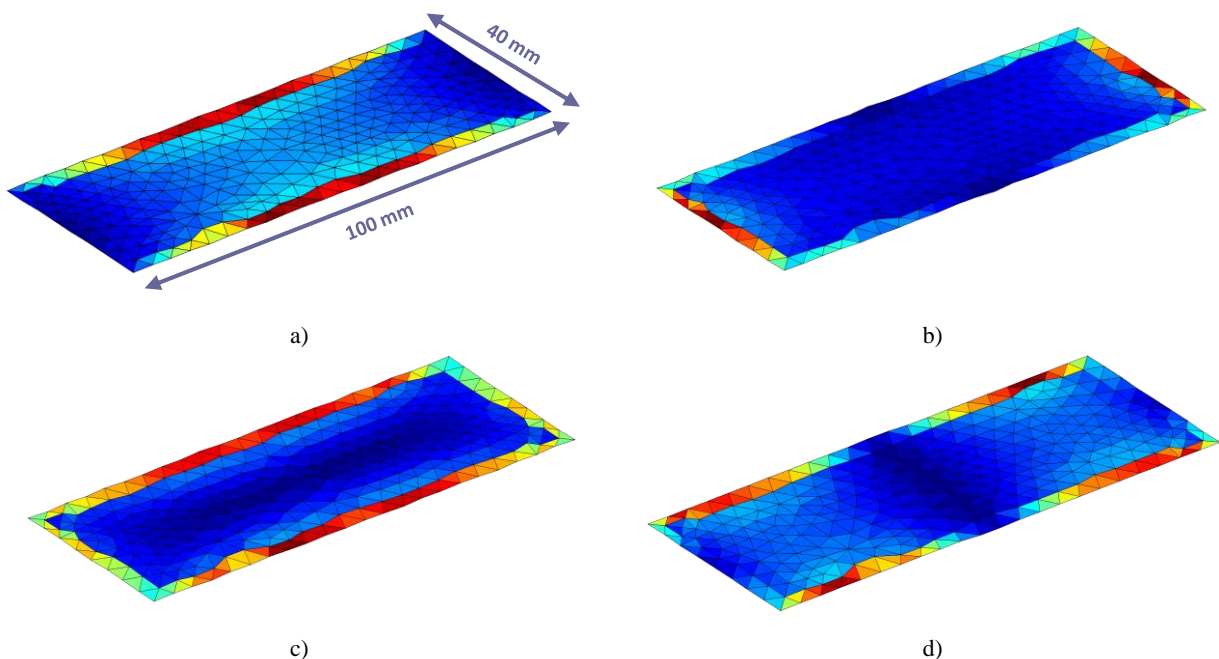


Fig. 2.4 Current distribution regarding a bar type handset platform having dimensions of 100 mm x 40 mm corresponding to a) Characteristic mode J_1 ; b) Characteristic mode J_2 ; c) Characteristic mode J_3 ; d) Characteristic mode J_4 .

This frequency shifting is really advantageous when designing multi-band radiating systems for mobile phones. The reason, as will be further demonstrated along the next sections, mainly relies on the fact that the performance of the radiating system improves considerably when the resonance of the radiating modes is close to the operating bands. This modification does not alter the current distribution

associated to each radiating mode since its trend remains equal to that presented above in connection with the bar type platform with dimensions of 100 mm x 40 mm (Fig. 2.4).

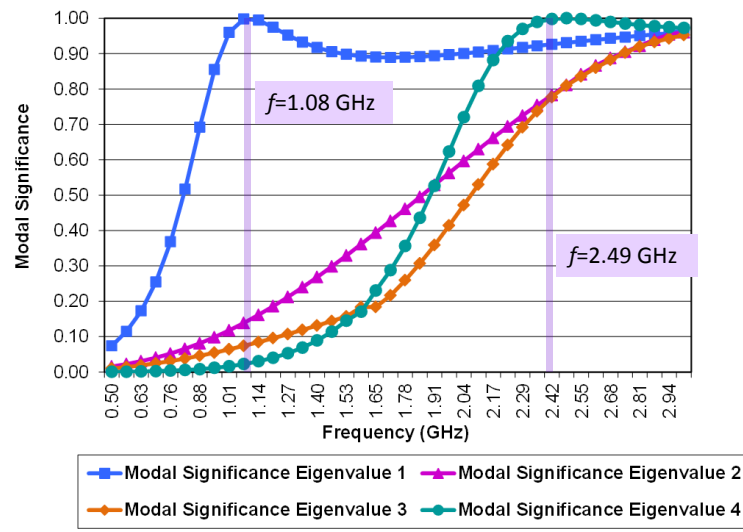


Fig. 2.5 Modal significance associated to the characteristic modes J_1 , J_2 , J_3 , J_4 of a bar type handset platform having dimensions of 120 mm x 50 mm.

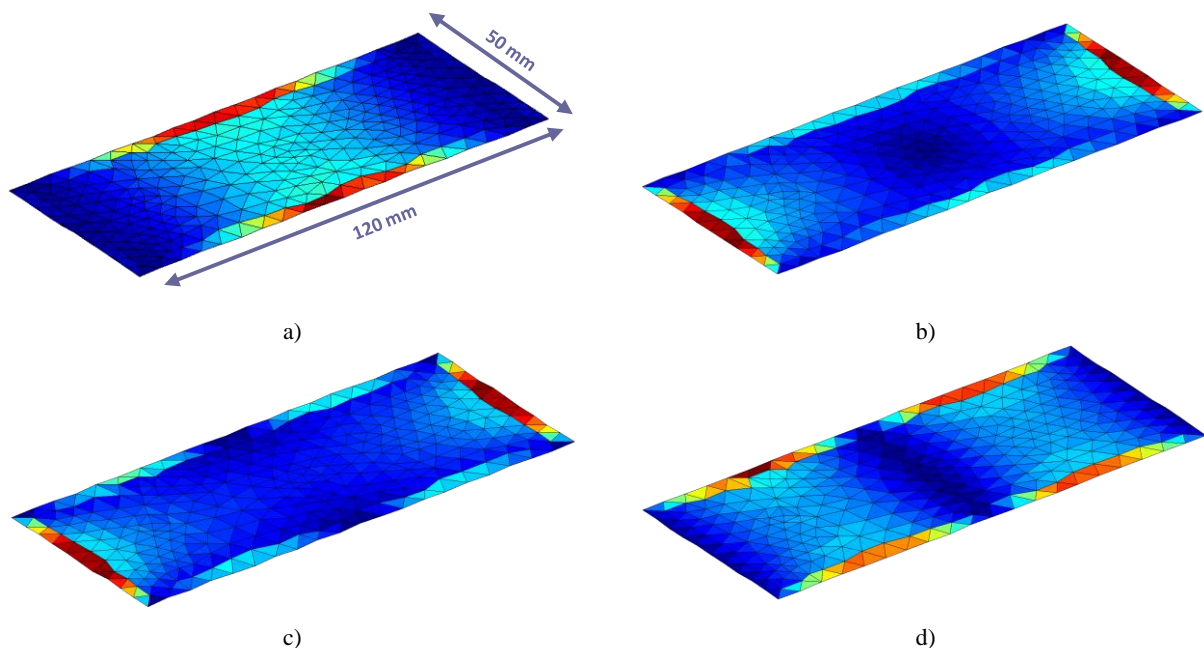


Fig. 2.6 Current distribution regarding a bar type handset platform having dimensions of 120 mm x 50 mm corresponding to a) Characteristic mode J_1 ; b) Characteristic mode J_2 ; c) Characteristic mode J_3 ; d) Characteristic mode J_4 .

The current distribution associated to the fundamental mode (J_1) of a bar type phone of larger dimension (120 mm x 50 mm) is also similar to that featured by a half-wavelength dipole (Fig. 2.6a) whereas the trend of that associated to the fourth characteristic modes (J_4) is comparable to that produced by a wavelength dipole with an asymmetric excitation (Fig. 2.6d) [6]. This fact is further advantageous, since as it is well known in the art, omnidirectional radiation patterns such as those produced by a half-wavelength or a wavelength dipole are preferred for mobile communications. Accordingly, not only the first and the fourth radiating modes present advantageous resonances near the mobile communication standards, but also their current distribution become useful for mobile applications. In this sense, the

challenge of this thesis regarding these potential features is mainly focused on exciting these efficient radiating modes in order to use the ground plane as the main radiator, thus avoiding the need of including additional quarter-wavelength resonant elements.

In addition to the bar type handset platforms previously introduced, the performance of a clamshell type platform has also been analyzed. The results reveal that three potential radiating modes with resonances around 0.63GHz, 1.59GHz, and 2.10GHz appear for the open position [7].

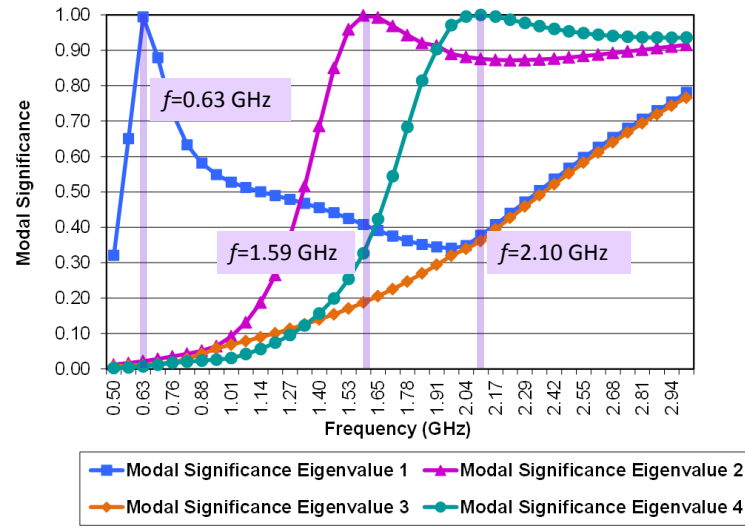


Fig. 2.7 Modal significance associated to the characteristic modes J_1 , J_2 , J_3 , J_4 of a clamshell type handset platform having two PCBs being adapted to be folded together, each one comprising a ground plane with dimensions of 80 mm x 40 mm.

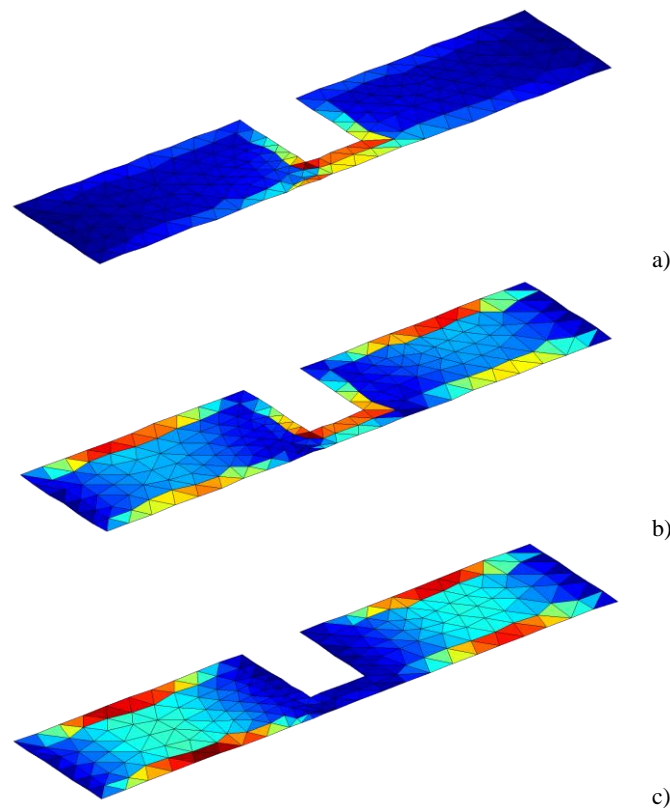


Fig. 2.8 Current distributions regarding a clamshell type handset platform having two PCBs being adapted to be folded together, each one comprising a ground plane with dimensions of 80 mm x 40 mm. a) Characteristic mode J_1 ; b) Characteristic mode J_2 ; c) Characteristic mode J_3 .

The advantage of the clamshell platform in open position mainly relies on the fact that the fundamental radiating mode resonance is shifted down to lower frequencies (0.63GHz) (Fig. 2.7), which becomes advantageous for providing operation in communication standards placed at lower frequencies such as for instance FM, DVB-H, or DMB [7]. The current distribution associated to the characteristic mode J_l corresponds again to that featured by a half-wavelength dipole. It means that it presents a sinusoidal current distribution, having maximums at the center of the longitudinal edges of the PCB and minimums in its transversal edges (Fig. 2.8).

The previous characteristic modes analysis reveals that typical handset platforms feature efficient radiating modes for a wide range of frequencies that could be potentially excited. Each radiating mode presents a particular current distribution, whose knowledge will become a key factor to properly transfer energy to them. The following sections will propose on one hand, and alternative procedure to compute and analyze the behavior of said ground plane modes. The proposal will allow the simplification of the complex mathematical method described above. On the other hand, they will deal with a parametric study based on the geometric properties and the size of the elements used to transfer energy to these ground plane modes and more particular, they will show how these parameters strongly condition the performance of the whole radiating system.

2.3. Ground Plane Contribution using Radar Cross Section Analysis (RCS)

As previously illustrated, current handset platforms support efficient radiating modes at mobile frequencies. The proper excitation of these ground plane modes plays a very important role in determining bandwidth, efficiency, and radiation patterns. The significance of the ground plane contribution needs to be better understood in order to determine not only which are the most important parameters to consider when designing a radiating system based on the excitation of the ground plane modes but also how these parameters condition its electromagnetic performance. With this aim the present section proposes an alternative method to readily compute the fundamental radiating modes of conventional handset platforms and proposes techniques to modify the electromagnetic properties of these ground plane modes.

So far, the ground plane contribution was underestimated and the main efforts of the antenna engineers were focused on providing antennas capable of maximizing the operating bandwidth while minimizing the volume occupied in the PCB. The appearance of studies dealing with the relevance of the ground plane in the radiation process forced the antenna engineers to focus their attention on the ground plane design. In this way, the bandwidth limitations of conventional PIFA antennas such as the one provided in [8] could be overcome by adding mechanisms to electrically enlarge the ground plane. The radiating modes analysis of the former section indicates that the fundamental mode is in resonance when the length of the ground plane is approximately 0.4λ (Fig. 2.2, Fig. 2.5, and Fig. 2.7). Accordingly, if operation in the low frequency region containing the consolidated communication standards GSM850, GSM900 and the emergent LTE700 was demanded, a ground plane size of at least 144.7mm (regarding

the center frequency of this frequency region (825MHz) would be required. This size is too large for current handset platforms and for this reason some authors have proposed mechanisms to enlarge the ground plane by using slots or conductive strips. These mechanisms allow solving these size limitations while providing enhanced excitation of the fundamental radiating mode, fact that mainly translates into larger bandwidth and efficiency [9]-[26]. This fact will be further illustrated along this section by analyzing the effect introduced by these enlarging mechanisms in the fundamental modes of the handset platforms under study. The simplified method proposed along this section is focused on the RCS parameter, which is used to compute the frequency at which maximum back-scattering occurs [27]. The method allows knowing the electromagnetic properties of some characteristic modes without requiring the complex mathematical process presented above in section 2.2. To validate the proposed method, the three platforms previously presented are also considered for carrying out the analysis, namely a bar-type of 100 mm x 40 mm, a smartphone of 120 mm x 50 mm, and a clamshell (two connected plates of 80 mm x 40 mm).

2.3.1 Radar Cross Section (RCS) Analysis

The proposed RCS method to compute the resonant frequency of the fundamental mode consists in illuminating the platform of the wireless device by a plane wave impinging from the normal direction. As illustrated in the former section, the current distribution associated to the fundamental radiating mode of a bar-type handset platform is completely aligned with the longitudinal edges of the ground plane (Fig. 2.4a and Fig. 2.6a). Thus and in order to find out the fundamental mode of this bar-type handset platform, the polarization of the incoming wave should be aligned with the longest dimensions of the ground plane, i.e. with its longitudinal edges (Fig. 2.9). The same effect occurs for the clamshell type wireless device (Fig. 2.8), thus the same polarization is used.

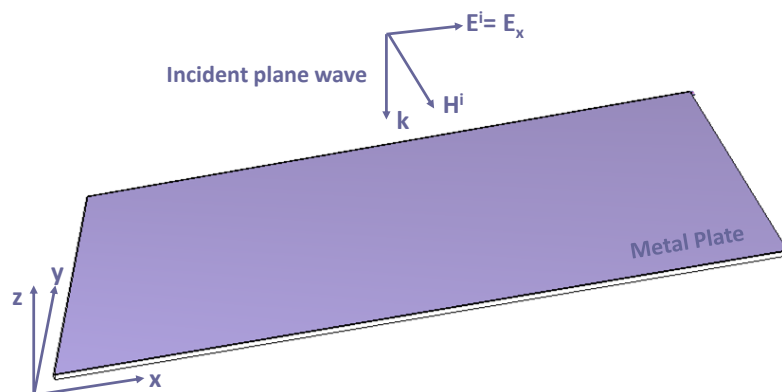


Fig. 2.9 Polarization of the incident wave used to determine the fundamental mode of a metal plate with dimensions of a ground plane associated to a bar-type wireless handheld device.

The RCS versus frequency is computed by means the software IE3D based on the Method of Moments (MoM) for each one of the platforms under analysis, i.e. for two bar-type phones of dimensions 100 mm x 40 mm and 120 mm x 50 mm, respectively, as well as for a clamshell platform. The RCS is normalized in all cases to its maximum value. Therefore, RCS ranges from 1 to 0 where the maximum

value 1, indicates the maximum backscattering, which coincides with the better excitation of the metal plate, whereas 0 means transparency, i.e. no scattering is produced by the metal plate (Fig. 2.10). The MS parameter is used for comparison purposes and is computed according to equation (2.10) by using a MoM Matlab-based code [28]. MS ranges from 0 to 1, where the maximum values 1 means that the mode can be excited in its maximum amplitude [2]. Note that just the RCS associated to the fundamental mode is computed. The reason mainly relies on the fact that it becomes a radiating mode at the frequencies of interest, since its MS value remains close to one for a large range of mobile frequencies (Fig. 2.4). In addition, it is important to emphasize that this method can be easily applied to this radiating mode due to the simplicity of its current distribution which is mainly aligned with the longitudinal edges of the platform. More complex current distributions would make considerably difficult, if not impossible, the determination of the ground plane resonance through the RCS analysis, since to obtain acceptable results, the impinging wave must be polarized according to the current distribution.

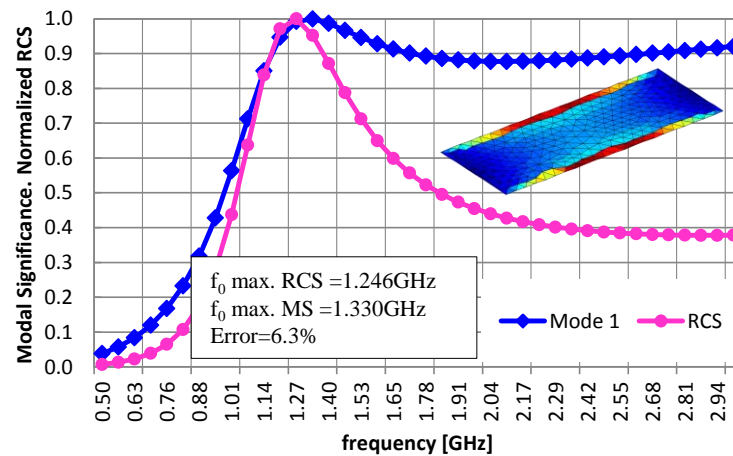


Fig. 2.10 Comparison between normalized RCS and modal significance for a bar-type platform 100 mm x 40 mm.

The results of the comparison between both methods, RCS and MS, conclude that RCS is a good alternative for determining easily the resonance of some characteristic modes such as the fundamental mode. The prediction of the resonant frequency of the fundamental mode is in good agreement (error less than 6.3% worst case (Fig. 2.10)) with that obtained through the MS analysis.

It should be pointed out that both RCS and MS agree from the very low frequency region up to the resonance of the fundamental mode. Beyond that, more modes are supported. This means that for frequencies beyond the fundamental mode, the backscattering results become the contribution from not only the backscattering due to the fundamental mode but also from higher order modes. These higher order modes do not radiate in the perpendicular direction to the metal plate. Therefore, this produces a decrement of the RCS computed in the normal direction (Fig. 2.10). The RCS results also confirm that the resonance of the fundamental mode decreases when the ground plane length is larger. For example, for the bar-type platform (Fig. 2.10), the resonance based on the RCS method occurs at 1.246GHz while it is 1.030GHz for the smartphone platform (Fig. 2.11). In this sense, an antenna operating in the low frequency region (690-960MHz) would offer better performance when integrated in the smartphone platform, since the RCS indicates that the ground plane resonance is placed at lower frequencies.

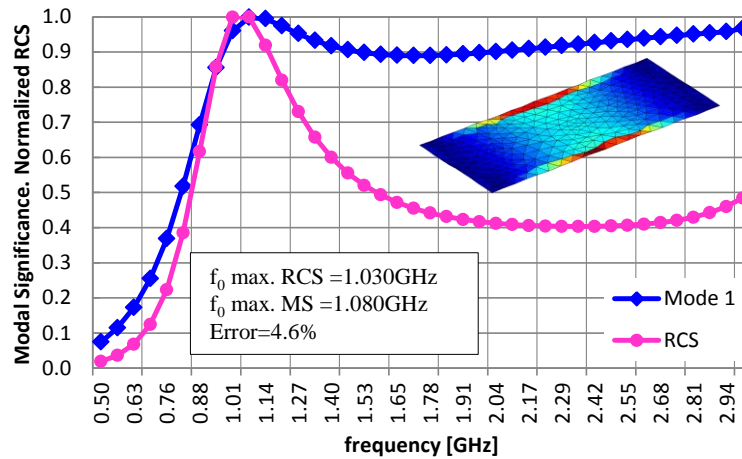


Fig. 2.11 Comparison between normalized RCS and modal significance for a smartphone platform 120 mm x 50 mm.

Owing to the clamshell phone in open position, the fundamental mode is highly excited at frequencies around 0.63GHz (Fig. 2.12). The results are aligned with aforementioned predictions based on MS, since it demonstrates that the larger the longitudinal dimension, the lower the resonant frequency. This particular platform can become advantageous for integrating antennas operating in lower frequency ranges such as DVB-H (470-700MHz), i.e. for integrating antennas intended for TV reception [29].

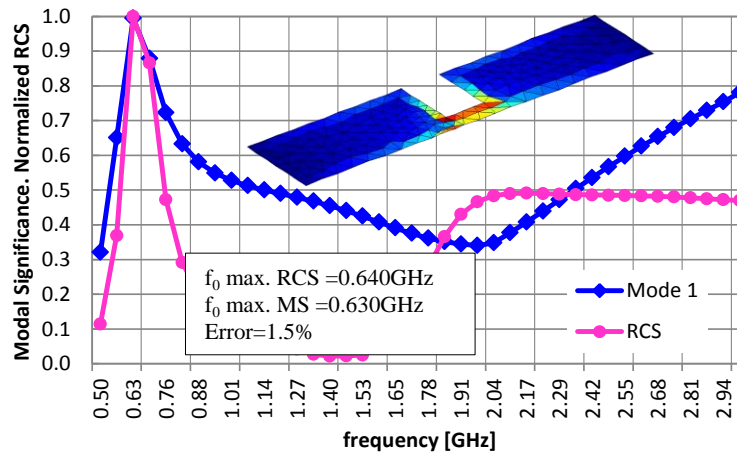


Fig. 2.12 Comparison between normalized RCS and modal significance for a clamshell having two PCBs being adapted to be folded together, each one comprising a ground plane with dimensions of 80 mm x 40 mm.

For all cases, the current distribution associated to the fundamental mode presents the typical half-wavelength sinusoidal behavior, maximum at the center of the longitudinal edges and minimum in the transversal edges. Such current distribution determines the radiation pattern, which presents an omnidirectional behavior with a null in the direction of the longest edge of the metal plate, i.e. similar to that produced by a half-wavelength dipole. It is also interesting to note that below the maximum, the amplitude of both RCS and MS decreases which means that the excitation of the fundamental mode becomes more difficult. This fact, clearly limits the performance of integrated antennas in terms of bandwidth and efficiency below the resonance of the fundamental mode since both the antenna and the ground plane are electrically small.

Finally, ground planes of wireless handheld devices are usually printed on a thin substrate layer of a low-cost material (FR4, 1mm thick and $\epsilon_r=4.15$). The effect of the dielectric coating can also be taken

into account by the RCS analysis proposed herein. For instance, for the bar-type (Fig. 2.10), if the dielectric coating having the same size as the ground plane is used, the frequency of the maximum RCS shifts from 1.246GHz down to 1.140GHz which represents a shift of 8% approximately.

2.3.2 Practical Application

This section gathers some experiments carried out for the sake of illustrating the relevance of the ground plane size in the electromagnetic performance. Firstly, the performance of a radiating system comprising the typical ground plane of a bar-type phone having dimensions of 100 mm x 40 mm is compared with the performance of a radiating system comprising a larger ground plane such as the one found in current smartphones (120 mm x 50 mm). Once the relevance of the ground plane length is demonstrated, two techniques are proposed for enlarging the electrical length of the ground plane without affecting its physical dimensions.

2.3.2.1. Ground Plane Size

The size of the ground plane, and more particularly its length, strongly conditions the resonance of the fundamental ground plane radiating mode. As previously discussed, this resonance moves to lower frequencies as long as the length of the ground plane increases (Fig. 2.13). This shifting is particularly advantageous for radiating systems intended for operation in the low frequency region (690-960MHz), since the proximity of the ground plane resonance to the operating bandwidth considerably enhances the electromagnetic performance of the whole radiating system. With the aim of validating this effect, the performance of two radiating systems having different ground plane lengths has been evaluated.

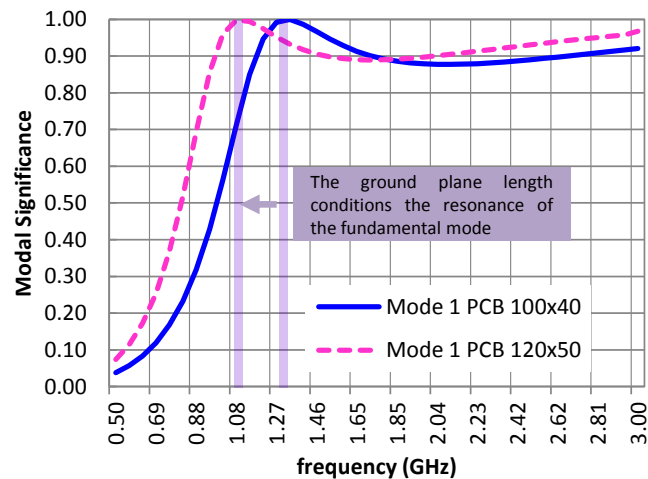


Fig. 2.13 Comparison between the resonance of the fundamental mode of a bar-type platform with dimensions 100 mm x 40 mm and the resonance of the fundamental mode of a smartphone platform (120 mm x 50 mm).

As slightly introduced in section 2.1, this thesis is mainly focused on using the ground plane of a handset platform as main radiator taking profit of the efficient radiating modes that it presents at mobile frequencies (Fig. 2.10, Fig. 2.11, and Fig. 2.12). With this aim, this thesis substitutes conventional resonant antennas by small non-resonant ground plane boosters having substantially reduced stand-alone

radiation properties [30]-[32]. Although this technique will be further developed in the following chapter, more specifically in section 3.2, this current section anticipates some results in order to demonstrate the ground plane length effect. In this way, a non-resonant ground plane booster featured by considerably small dimensions of just 5 mm x 5mm x 5 mm is placed at the corner of the two ground planes under study in order to excite their corresponding fundamental radiating modes. The impedance matching of the radiating system is attained by the use of a simple broadband matching network such as the one described in detail in the introductory section 1.2 as well as in [32].

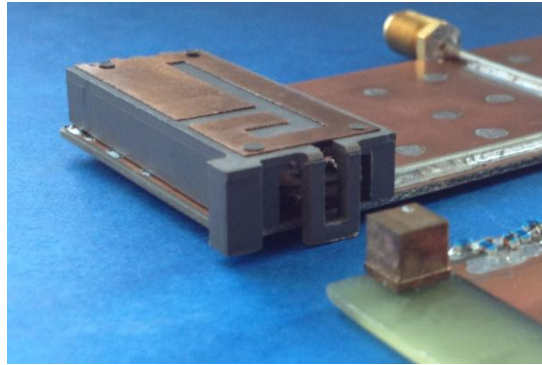


Fig. 2.14 Comparison of a PIFA and a ground plane booster both for GSM850 and GSM900 operation. The size of the PIFA is 40 mm x 15 mm x 6 mm whereas the size of the ground plane booster is just 5 mm x 5 mm x 5 mm.

It is significant to emphasize that since the ground plane becomes an effective means for radiation, conventional antennas such as PIFAs can be substituted by ground plane boosters such as the ones proposed herein, which advantageously contribute to reduce the volume occupied in the PCB (Fig. 2.14).

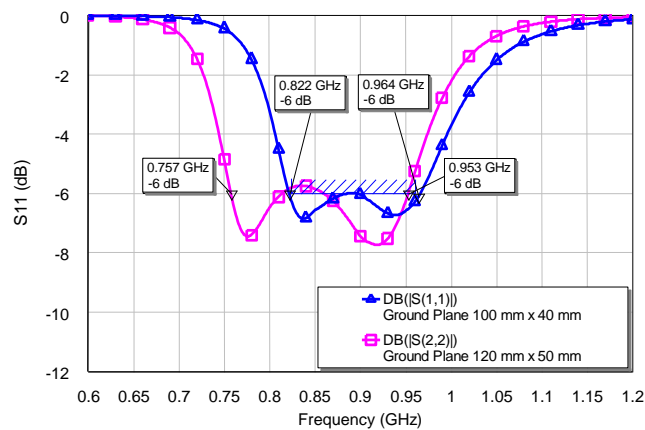


Fig. 2.15 Measured reflection coefficient for a non-resonant element of 5 mm x 5 mm x 5mm including a broadband matching network and regarding two ground planes of different size.

As predicted, the smartphone platform having a larger ground plane length enhances the performance of the radiating system with respect to that attained by the conventional bar-type platform of smaller dimensions. In this way, the smartphone offers a bandwidth of 26.3% ($SWR \leq 3$) whereas the ground plane of dimensions 100 mm x 40 mm just provides a bandwidth around 17.7% ($SWR \leq 3$) (Fig. 2.15). Despite this bandwidth is enough for covering some communication standards such as GSM850 and GSM900, it becomes insufficient for providing operation in emergent communication standards such as LTE700. For this reason, larger ground planes would be preferable for allowing the operation of the radiating system in communication standards allocated in lower frequency

regions. Nevertheless, the market trends in some cases do not allow this ground plane enlargement and other techniques such as those presented in section below are required.

2.3.2.2. Enlarging the Ground Plane through Conductive Strips

The analysis carried out in former sections demonstrates that the length of the ground plane strongly conditions the resonant frequency of the fundamental mode. The performance of the radiating system significantly improves by placing this resonance near the desired operating frequencies. Nevertheless, in some cases these operating frequencies are allocated in low frequency regions. Operation in low frequency regions require lowering the resonance of the ground plane to improve the performance of the whole radiating system, which usually translates into increasing its length. Nevertheless, in many situations this ground plane length cannot be increased due to the mechanical constraints imposed by the form factors currently demanded by the market trends. Alternative solutions to improve the performance of the radiating systems by placing the resonance of the ground plane close to the desired operating frequencies, without requiring a physical enlargement of the ground plane are deeply disclosed in the literature. With this aim, some techniques appear for adding intelligence in the ground plane, such as for example those based on including slots [9]-[20] or those consisting in the addition of conductive strips [21]-[26].

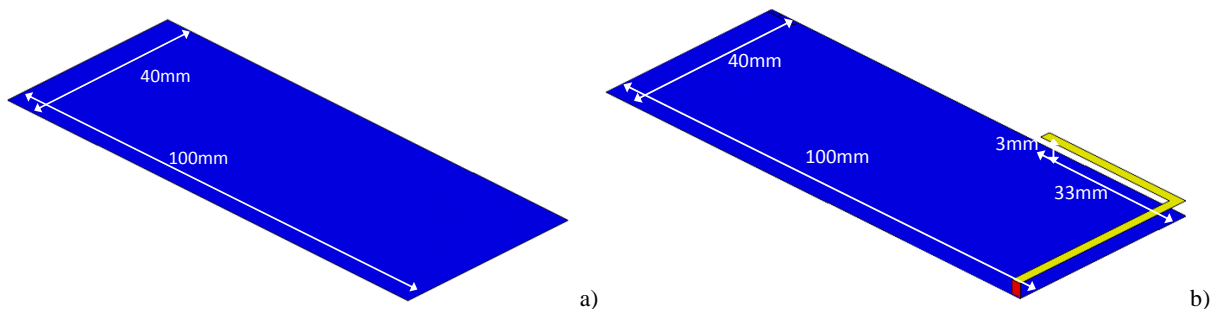


Fig. 2.16 a) Ground plane of dimensions 100 mm x 40 mm; b) the same ground plane having a conductive strip of 40 mm x 33 mm x 3 mm. Both ground planes are supported by a thin dielectric slab of 1mm thick with $\epsilon_r=4.15$.

One of the main advantages of the proposed method based on the RCS analysis is that it can be applied to more complex platforms such as the ones proposed in [14], [23]. This fact becomes significantly advantageous since it allows determining the effect produced by the addition of a conductive strip into the resonance of the ground plane mode readily, without requiring complex mathematical procedures. The outcomes of the RCS analysis provide an important physical insight into the potential radiation properties of platforms integrating enlarging mechanisms. The use of the characteristic modes theory would complicate this analysis considerably. In this way and in order to illustrate this fact, the RCS has been computed for a ground plane having dimensions of 100 mm x 40 mm as well as for the same ground plane including the conductive strip (Fig. 2.16). For the two ground planes the RCS is computed regarding a planar electric wave linearly polarized along the longitudinal edges of the ground plane (Fig. 2.9). For the ground plane having 100 mm x 40 mm, the maximum RCS is found at 1.14GHz (Fig. 2.17), whereas for the case regarding the conductive strip, the maximum RCS is found at 0.96GHz.

Both cases have been normalized to the maximum value. From the results, several conclusions can be drawn (Fig. 2.17):

a) The addition of the conductive strip allows tuning the resonant frequency of the ground plane mode to lower frequencies, mainly due to the increment produced in the electrical path.

b) In the frequency range from 824MHz to 960MHz where the communication standards GSM850 and GSM900 are allocated, the RCS for the ground plane with the conductive strip is larger. Therefore, more impedance bandwidth is expected.

c) A minimum of RCS appears at 1.02GHz concerning the ground plane with the conductive strip. This null is produced by the resonance appearing in the conductive strip, which at this frequency features approximately a quarter-wavelength length. This low RCS value also evidences that at this frequency the ground plane is not properly excited, hence not being an effective radiator. Due to this RCS drop, poor electromagnetic performance is expected at this frequency region. This fact will be further illustrated next.

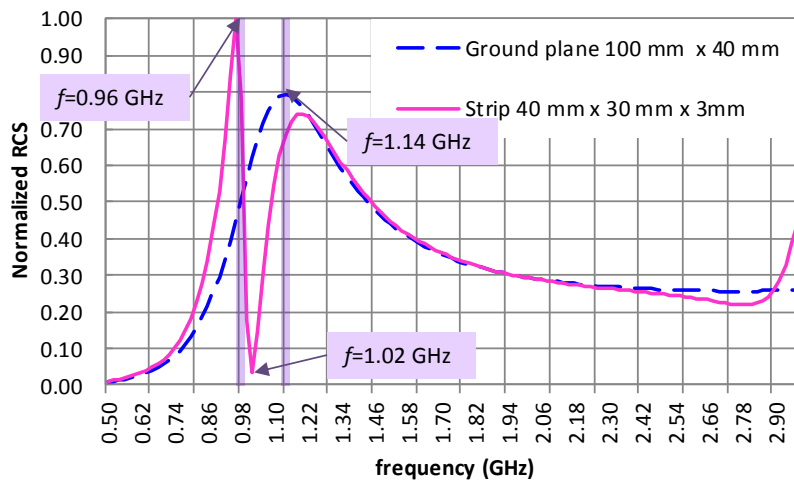


Fig. 2.17 Comparison of the normalized RCS for a ground plane of 100 mm x 40 mm and the same ground plane with the conductive strip (Fig. 2.16).

The results remark the relevance of the RCS method in determining the electromagnetic properties of the ground plane, even if considering tuning mechanisms such as slots or conductive strips. In the latest, it further allows determining the effects of the conductive strip over the ground plane performance. This knowledge is particularly relevant for properly designing the conductive strip. In effect, if the conductive strip were tuned at the central frequency of the frequency region 824MHz-960MHz, i.e. if its length were selected to be a quarter of a wavelength at this frequency, a null of RCS will appear and consequently, poor performance would be expected in said frequency region. Accordingly, the design can be optimized by adjusting the length of the conductive strip so as to obtain a better RCS in the frequency region of interest, in this case 824MHz-960MHz, while keeping the null of RCS out of the band.

The conductive strip does not alter the current distribution at the maximum of RCS (0.96GHz) (Fig. 2.18), since it follows that presented above in connection with a ground plane of dimensions 100 mm x 40 mm (Fig. 2.4). In this sense, this technique allows maintaining the current aligned with the longitudinal edges of the ground plane, which produces the desired omnidirectional radiation patterns

[23], with the advantage of lowering the resonance of the ground plane without increasing its physical size. As previously introduced, the analysis of the current distribution regarding the frequency where the RCS null appears ($f=1.02\text{GHz}$) (Fig. 2.18), confirms that the conductive strip alters the radiation properties of the ground plane, thereby converting it in a non-effective radiator. In fact, at 1.02GHz , the strip becomes a resonant structure with a length of approximately a quarter of the wavelength (73 mm is approximately $\lambda/4$ at 1.02GHz). These results confirm the initial hypothesis that suggested that the electromagnetic performance of a radiating system comprising a resonant antenna and a ground plane strongly depends on the electrical properties of the antenna element at its resonant frequency and on its effectiveness of transferring energy to the ground plane [10]. Therefore, if an antenna on a ground plane operates at 1.02GHz , the behavior will depend mainly on the antenna and not on the ground plane, since it would not be properly excited. This fact is clearly observed when regarding a PIFA antenna placed on a ground plane of $100\text{ mm} \times 40\text{ mm}$ comprising the proposed conductive strip (Fig. 2.18 and Fig. 2.19). The radiation efficiency (η_r) of this radiating system presents a pronounced drop in the frequency where the RCS presents a minimum, thus confirming again that at this frequency, the ground plane is weakly excited (Fig. 2.18) and as a consequence, poor electromagnetic performance is obtained (Fig. 2.19).

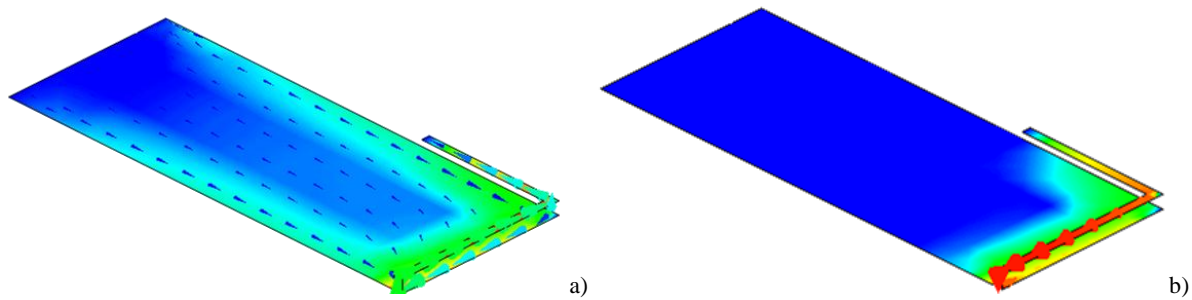


Fig. 2.18 Induced current (A/m) for a plane wave excitation according to Fig. 2.9 at a) $f=0.96\text{GHz}$; b) and $f=1.02\text{GHz}$. Same maximum and dynamic range is used for both illustrations.

Thanks to the RCS analysis, the operation of the conductive strip to enhance the bandwidth in the $824\text{MHz}-960\text{MHz}$ is better understood. It is important to emphasize that this method stands out over the method presented in section 2.2 when regarding complex structures. The conductive strip is tuned so as to have the maximum of the RCS in the frequency region of interest while avoiding the minimum of RCS to be in said frequency region. By following this procedure, a PIFA on a ground plane $100\text{ mm} \times 40\text{ mm}$ having a bandwidth of 8.3% at 900MHz ($SWR \leq 3$) is improved up to 14.6% [23]. Moreover, since the RCS at the frequency region $824\text{MHz}-960\text{MHz}$ is larger when using the conductive strip (Fig. 2.19), not only the bandwidth improves but also the radiation efficiency.

A larger RCS translates in a better excitation of the ground plane mode when an antenna operates in conjunction with the ground plane and therefore, larger radiation efficiency can be obtained. Better matching and radiation efficiency translates into more antenna efficiency ($\eta_a = \eta_r \cdot (1 - |S_{11}|^2)$). Measured radiation and antenna efficiencies of the PIFA antenna with and without the conductive strip (Fig. 2.19) shows how the radiation efficiency increases around 1dB across the GSM850-GSM900 frequency region. At the same time, due to the larger bandwidth provided by the conductive strip, the antenna efficiency

also increases almost 2 dB (Table 2.1) [23]. It is interesting to point out that the use of the conductive strip is not only useful for enhancing the bandwidth at the low frequency region but also to provide robustness to hand loading [33] as well as for controlling the near field for hearing-aid [34].

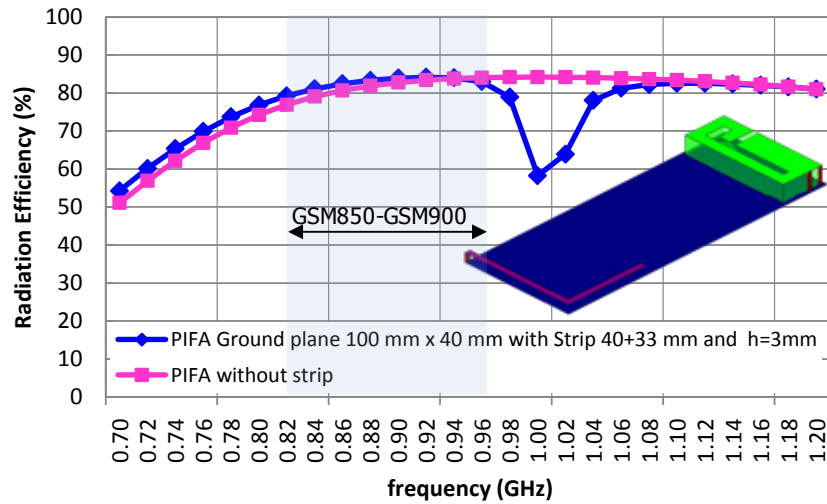


Fig. 2.19 Simulated radiation efficiency for a PIFA on a ground plane 100 mm x 40 mm and the conductive strip 40 mm x 33 mm x 3mm.

Table 2.1 Measured radiation and antenna efficiency for a PIFA antenna in a ground plane 100 mm x 40 mm without and with a conductive strip 40 mm x 33 mm x 3 mm (Fig. 2.19). Measurements are obtained using 3D pattern integration with the anechoic chamber Satimo Stargate-32.

$f(\text{MHz})$	η_r (%)			η_a (%)		
	Without strip	With strip	$\Delta\eta_r$ (dB)	Without strip	With strip	$\Delta\eta_r$ (dB)
820	31.1	38.8	0.96	16.2	23.5	1.62
850	37.5	51.3	1.36	27.1	41.2	1.82
880	39.3	56.0	1.54	33.8	51.6	1.84
890	45.2	65.9	1.64	40.7	62.2	1.84
920	55.4	75.3	1.33	46.7	67.4	1.59
960	62.3	74.0	0.75	44.4	62.0	1.45

2.3.2.3. Enlarging the Ground Plane with Slots

The integration of slots in the ground plane also becomes an efficient technique to enlarge the electrical length of the handset platform without affecting its physical dimensions [9]-[20]. As previously illustrated, this enlargement considerably contributes to enhance the electromagnetic properties of the radiating system, namely in terms of impedance bandwidth and efficiency. This section gathers the analysis of a slotted ground plane through the proposed RCS method. The simplicity of the proposal allows comparing easily the characteristic modes variations produced by different techniques focused on increasing the electrical length of the ground plane, such as the one presented above based on the integration of a conductive strip and the one proposed herein based on the integration of slots (Fig. 2.20).

The operation principle of a slotted ground plane is equivalent to that illustrated in the case of the conductive strip. In this sense, when a slot is printed or etched over a ground plane, the currents are forced to travel a longer path, thus contributing to increase the electrical length of the ground plane. This increment mainly shifts the fundamental mode resonance to lower frequencies. The length of this slot allows tuning the resonant frequency of the fundamental radiating mode to the desired operating

frequency, for instance, to 890 MHz, which corresponds to the central frequency of the low frequency region allocating the communication standards GSM850 and GSM900 (Fig. 2.21).

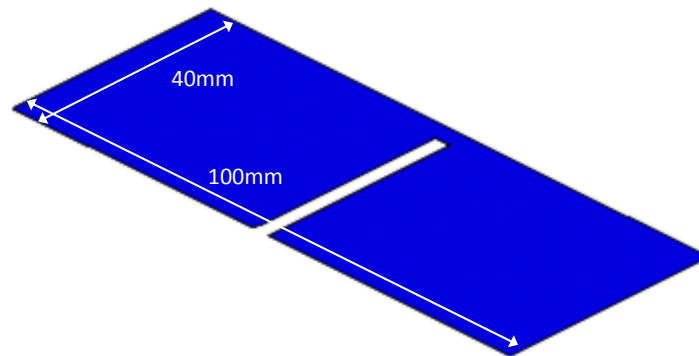


Fig. 2.20 Ground plane having dimensions of 100 mm x 40 mm and integrating an open slot with dimensions of 38 mm x 3 mm. The ground plane is etched on a thin dielectric slab of 1mm thick and $\epsilon_r=4.15$, $\tan\delta=0.013$.

The RCS analysis reveals that the slot technique stands out over the previous proposal consisting in the integration of a conductive strip and becomes advantageous to tune the resonant frequency of the ground plane mode to 900MHz. Moreover, this technique does not present a null as it was the case of the conductive strip. However, it may be more challenging to be integrated into a wireless handheld device due to the presence of other components such as a display or a battery.

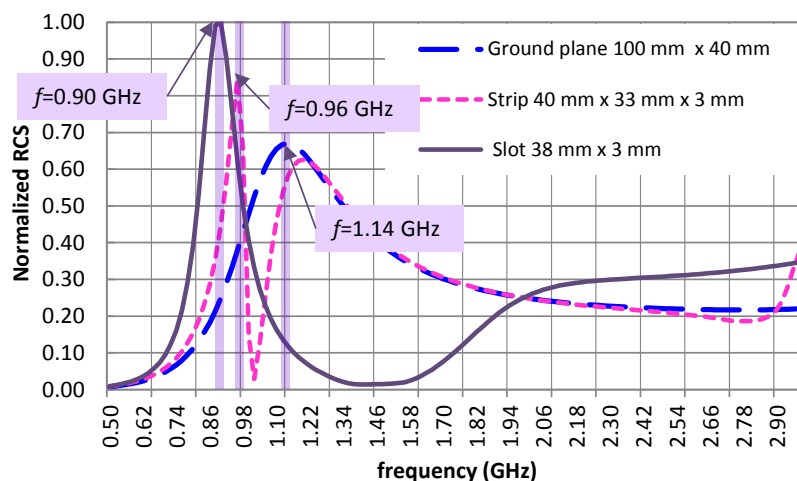


Fig. 2.21 Comparison of RCS for three different ground planes: 100 mm x 40 mm, 100 mm x 40 mm with a conductive strip as shown (Fig. 2.16), and a ground plane 100 mm x 40 mm with slot 38 mm long and 3mm width (Fig. 2.20). The plane wave impinges the ground plane according to Fig. 2.9. All ground planes are etched on a thin dielectric slab of 1mm thick and $\epsilon_r=4.15$, $\tan\delta=0.013$.

It should be pointed out that the RCS bandwidth is larger for the slot case than for the conductive strip case (Fig. 2.21). Thus, one would expect to obtain more bandwidth using a slot in the ground plane rather than using a conductive strip. In particular, the bandwidth using the conductive strip is 14.6% for the PIFA in the 100 mm x 40 mm ground plane [23] whereas the same PIFA with a slot in the ground plane [13] has a bandwidth around 35.1%. These results clearly agree with the RCS curves of Fig. 2.21.

From a quantitative point of view, it is interesting to link the impedance bandwidth obtained with the RCS bandwidth predicted by using a -3dB RCS bandwidth computation (frequency at which the RCS drops 3dB). The RCS_{-3dB} bandwidth for the ground plane with strip and with the slot is 8.0% and 18.0%,

respectively. This results in a ratio of 2.3 which agrees with the impedance bandwidth ratio of 2.4 (35.1% over 14.6%). This makes the RCS method useful not only to determine the frequency at which the best excitation of the ground plane mode occurs, but also to estimate the bandwidth of several ground plane configurations.

2.4. Resonant Elements versus Non-Resonant Elements

Previous section demonstrates that the inherent ground plane of current handset platforms present efficient radiating modes at mobile frequencies. The question that arises at this point relies on determining which elements become preferable for exciting said efficient radiating modes.

Many techniques including PIFAs [35]-[36], monopoles [37]-[40], loops [41], slots [42]-[43], balanced antennas [44], combinations thereof [45], arrays of small antennas [46]-[47], and ground plane modifications [9]-[26], [48]-[52] have been proposed in the literature as well as in the industry. These solutions are mainly based on resonant antennas. Accordingly, when they are integrated in a handset platform, the radiation becomes the combination between the radiation properties of the antenna itself and those of the ground plane mode if it has been properly excited.

This section is then focused on determining if resonant antennas, such as the ones cited above, properly excite the radiating modes of the ground plane or if in contrast, non-resonant solutions are preferred. It is important to outline that non-resonant solutions are *per se* small structures since no resonance is achieved in any frequency of operation when no other components are connected to the non-resonant solution. It is important to emphasize that along this section, several situations are analyzed. First, antenna elements having a resonant frequency (f_r) lower to the resonant frequency of the fundamental mode of the ground plane (f_{GP}), i.e. $f_r < f_{GP}$. Second, those elements accomplishing $f_r = f_{GP}$, and finally those elements satisfying $f_r > f_{GP}$. Usually, for the current platforms analyzed along this section, f_{GP} is above the upper frequency of the low frequency region comprising 690MHz to 960MHz where some of the main communication standards are allocated (LTE700, GSM850, and GSM900). Therefore, those elements having $f_r > f_{GP}$ are called herein as non-resonant elements.

Not only is the resonance analyzed, but also the role that the antenna geometry plays in the performance of the whole radiating system. Previous research such as the one disclosed in [53], demonstrates that the geometry affects the electromagnetic performance of monopole antennas when they are placed over a ground plane with considerable dimensions. Therefore, it is indeed interesting to analyze the role of the geometry when the ground plane actively contributes to the radiation process.

In this sense, this section analyzes the ground plane interaction with resonant antenna elements performing different geometries (Hilbert-based monopoles of two and three iterations and spiral monopoles) as well as such interaction when small non-resonant elements are regarded instead. The parameter used to compare the performance of the radiating system is the inherent bandwidth (BW_0). As slightly introduced in section 1.2, the quality factor (Q) can be computed through the input impedance of a particular radiating structure and allows determining readily its BW_0 [54]-[55]. This method becomes

significantly advantageous since it removes the need of matching each frequency independently, usually highly influenced by the skills of the antenna engineer in designing the matching network. By computing the Q associated to the radiating structure through equation (1.2), the BW_0 for a wide range of frequencies can be readily obtained according to (1.1). This procedure will be deeply explained along section 3.2 but is slightly introduced here for the sake of allowing the comparison between the different radiating structures. The study will demonstrate that non-resonant elements are preferable for exciting ground plane radiating modes since they maximize the attainable BW_0 . This conclusion sets forth the basis of this thesis and for this reason the elements used to excite the ground plane radiating modes are small non-resonant elements with significantly poor stand-alone radiation properties.

2.4.1 On the Behavior of Several Geometries

Usually, the most challenging situation when designing multi-band and small radiating systems for wireless handheld devices occurs at the low frequency region (690-960MHz where some communications standards such as LTE700, GSM850, and GSM900 are allocated). In this frequency region, the ground plane is small in terms of the operating wavelength and in many situations, it does not support an efficient radiating mode, i.e. the first resonance of the fundamental mode commonly appears at a frequency above the frequency region allocating the aforementioned communication standards (Fig. 2.2 and Fig. 2.5). For this reason, this section is focused on this particular frequency region and is intended for determining which element becomes preferable for exciting these radiating modes as a function of its geometry and its resonant properties [56]. Four elements are analyzed: a spiral, two fractal-inspired elements based on the Hilbert geometry (second iteration (H2) and third iteration (H3)) [57], and a non-resonant element, called hereafter pad. The four elements present a footprint of 15 mm x 15 mm and are placed in a corner of a ground plane having dimensions of 90 mm x 40 mm. Both, the ground plane and the geometries under study are printed on a thin FR4 substrate of 1mm thick ($\epsilon_r=4.15$, $\tan\delta=0.013$) (Fig. 2.22). Note that regarding this ground plane dimensions, the first characteristic mode (J_1) resonates at 1170MHz. This resonance has been calculated using characteristic mode analysis according to section 2.2.1, namely computing the zero crossing of the eigenvalue λ_l [1]-[4]. Taking into account this resonant frequency, three different experiments have been carried out for determining how the geometry and the resonant frequency of the element used to excite the ground plane, influences the performance of the whole radiating system. The experiments are performed by means of the software IE3D based on MoM.

In a first experiment, the spiral and the two Hilbert-based antennas are tuned to resonate at 900MHz (approximately the center frequency of the frequency region of operation comprising the communication standards GSM850 and GSM900), whereas the pad presents its first resonance at 1921MHz, well above the frequency region of operation. Note that elements having a resonance well above the resonance of the ground plane radiating mode would be identified along this section as non-resonant elements. In the second experiment, the spiral, H2, and H3 are tuned to resonate at 1170MHz, i.e. at the same frequency as the eigenmode J_1 . The basis for this experiment is found on the electrical

circuit modeling of the antenna and the ground plane disclosed in [10], [14], [48], which stated that the bandwidth of a radiating system is improved when the resonant frequency of the antenna is similar to that of the ground plane. Finally, in the third experiment, the resonant frequency is shifted to a frequency above the resonance of the ground plane (1170MHz). Note that in each case, the geometry of all the elements, except the pad, has been modified to allow the resonant frequency shifting.

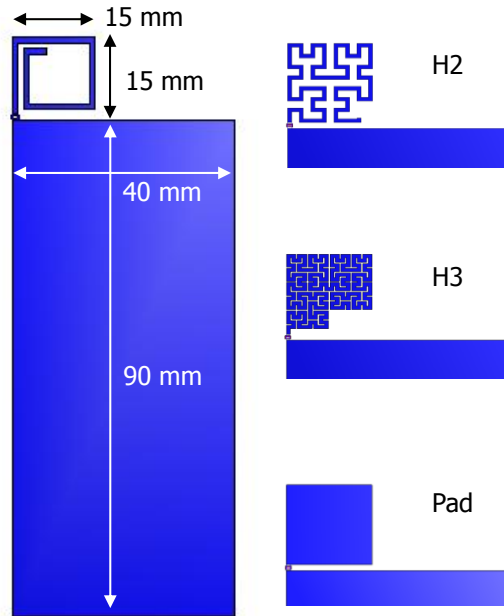


Fig. 2.22 Geometry of the proposed structures (spiral, H2, H3, and pad) placed in a corner of a ground plane having dimensions of 90 mm x 40 mm etched in a 1mm FR4 substrate $\epsilon_r=4.15$ $\tan\delta=0.013$. For this case, spiral, H2, and H3 resonate at 900MHz whereas the pad element presents a higher resonant frequency around 1921MHz.

In order to compare the behavior of the four elements, the BW_0 and the Q is computed from input impedance according to equations (1.1) and (1.2) [54]-[55]. The advantages of this procedure lie in its simplicity since by a single simulation of the input impedance, the bandwidth across a large frequency range can be obtained without the need of matching the antenna element at each frequency. This last procedure is undesirable since usually a matching can misrepresent the potential bandwidth (BW_f). It should be taken into account that the validity of this method holds as long as the input impedance presents a behavior similar to a series or parallel RLC circuit [54]. For those cases, where the input impedance presents small loops as the ones caused by couplings between different radiators, the validity of the method is not guaranteed.

2.4.1.1. Resonance of the Element (f_r) equal to 900MHz

The spiral and the two Hilbert-based antennas are tuned to resonate at 900MHz whereas the pad, as indicated above, presents a first resonant at 1921MHz. The conclusions that can be extracted from the results (Fig. 2.23) can be summarized as follows:

a) When the elements are resonating at a frequency below the resonance of the eigenmode J_1 (1170MHz), the maximum BW_0 is obtained close to the resonant frequency of the element. In this case around 900MHz.

b) When the elements resonate at a frequency above the resonance of the eigenmode J_1 (1170MHz), as is the case of the pad, the maximum BW_0 is obtained close to this resonance, i.e. the maximum BW_0 appears at the resonance of the fundamental mode of the ground plane (1170MHz).

c) Those elements having the resonance below that of the ground plane (spiral, H2, and H3), do not effectively excite the ground plane at the resonant frequency of the eigenmode J_1 (1170MHz).

d) The maximum BW_0 for the cases resonating at 900MHz is dependent on the geometry. In this case, H3 stands out over H2 and the spiral geometry, being the last the worst case.

e) The pad has the maximum BW_0 at the resonance of the ground plane reaching very large values around 62%. It should be noted that at this point the Q method is not accurate but indicative. The semi loop that appears in the input impedance avoids having an exact quantitative value but provides a qualitative result that suggests a large value. In order to obtain the exact BW_0 at this frequency the conjugate matching technique is used and the results coincide with the predictions, since a large BW_0 around 44% is obtained.

f) The pad also offers slightly better BW_0 around the center frequency of the operating region, i.e. around 900MHz. In fact, the behavior from 650MHz to 880MHz is very similar to that provided by H3, however, it becomes better than that provided by H3 beyond 880MHz.

As a first glance, the previous results lead to the conclusion that the simplest geometry, i.e. the pad, would be preferable for two main reasons. On one hand, it performs similar to the best resonant case (H3) close to the center frequency of the operating region (around 900MHz) and slightly better as long as the frequency of operation approximates the resonance of the ground plane. On the other hand, its simplicity makes the fabrication process easier.

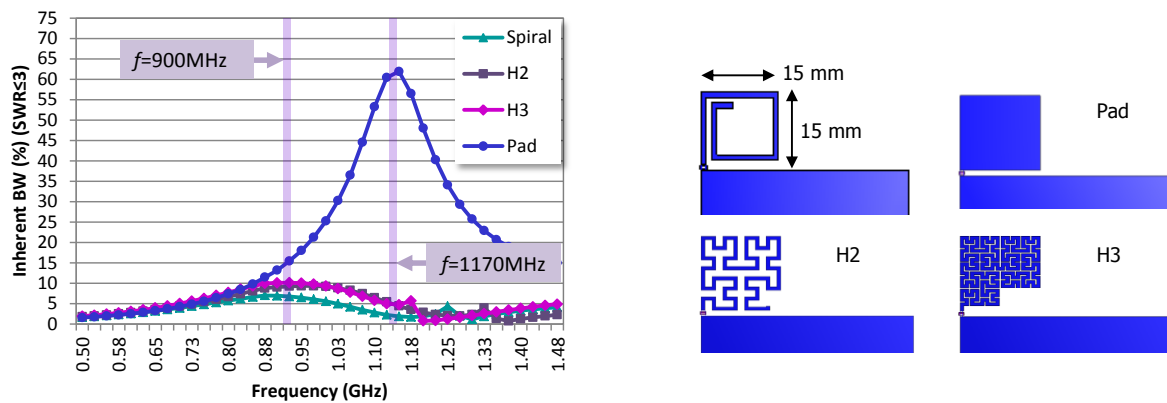


Fig. 2.23 BW_0 associated to the spiral, H2, and H3 when they are resonating at 900MHz, and to a pad resonating at 1920MHz. All the elements considered, are placed in a corner of a ground plane having dimensions of 90 mm x 40mm and being etched in a 1 mm FR4 substrate ($\epsilon_r=4.15$, $\tan\delta=0.013$).

At this point, an interesting question to address is to determine if the pad itself is an efficient element or actually is the one that better excites the fundamental mode of the ground plane. In order to answer this question, the Q is computed for the pad element as well as for the spiral case in a dipole configuration (Fig. 2.24). The spiral dipole resonates at 900MHz whereas the pad dipole resonates at upper frequencies around 2330MHz. Both dipoles feature the same footprint and radiation efficiency (η_r) of 24.0% and 42.3% for the spiral and pad, respectively. At the frequency of interest (900MHz), the Q of

the pad-based dipole is larger than the one of the spiral dipole (Table 2.2), thus, being the latest the one that offers better performance at 900MHz. Nevertheless, as illustrated above, the situation changes completely when the ground plane is considered. In this case, the Q of the pad is lower than that obtained by the spiral (Fig. 2.23). These results suggest that the element is not the main contributor to the performance of a radiating system comprising a ground plane of resonant dimensions.

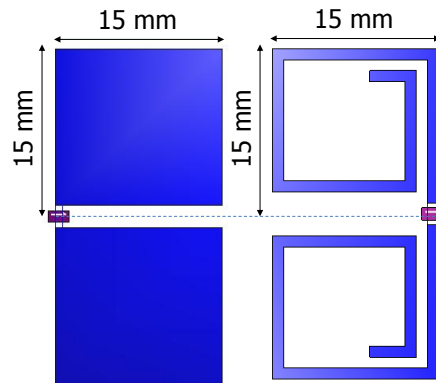


Fig. 2.24 Dipole configurations for the pad and spiral used to compute the Q of the element itself. A dipole arm corresponds to the element used in Fig. 2.22.

Accordingly, the relevant aspect is the way the element excites a mode or modes in the ground plane and not the radiation effectiveness of the element itself. For this particular case, the Q for the pad placed in the corner of the ground plane is around 12.2 (BW_0 ($SWR \leq 3$) around 9.5%) whereas the Q for the spiral regarding the same ground plane is around 20.1 (BW_0 ($SWR \leq 3$) around 5.7%). Therefore concluding, that the pad element, despite not being the best candidate when regarding its stand-alone radiation properties, becomes the best candidate when concerning the ground plane excitation (Table 2.2), attaining a BW_0 67% times larger than the spiral case.

Table 2.2 Q values at 900 MHz regarding a dipole configuration (Fig. 2.24) and regarding the ground plane (Fig. 2.23).

Element	Q for the dipole configuration at 900MHz	Q regarding the ground plane at 900MHz
Spiral	80.5	20.1
Pad	101.1	12.2

2.4.1.2. Resonance of the Element (f_r) equal to the Resonance of the Ground Plane (f_{GP})

As previously introduced, the second experiment is focused on analyzing the performance of the radiating system when the geometries under study are tuned to resonate at the frequency of 1170MHz, i.e. the frequency associated to the resonance of the fundamental mode of a ground plane having dimensions of 90 mm x 40 mm. The footprint for all the cases is maintained as in the previous experiments and the geometry has been adapted to produce a resonance around 1170MHz. The conclusions that can be extracted from the results (Fig. 2.25 and Fig. 2.26) can be summarized as follows:

a) When the elements are resonating at a frequency equal to the resonance of the eigenmode J_1 (1170MHz), the maximum BW_0 is obtained at this resonant frequency, in this case around 1170MHz.

b) When the elements resonate at a frequency above the resonance of the eigenmode J_1 (1170MHz), as is the case of the pad, the maximum BW_0 is obtained close to this resonance, i.e. the maximum BW_0 appears at the resonance of the fundamental mode of the ground plane (1170MHz).

c) The geometry conditions the performance, more significantly near the resonance of the ground plane. Near this frequency, the maximum BW_0 is obtained for the Hilbert antennas, being H3 the one attaining the largest value. The results confirm again that the spiral antenna is the worst candidate, since it presents the lowest inherent BW_0 .

d) The pad directly competes with the Hilbert antennas, since it still obtains large BW_0 with the advantage of being geometrically simpler.

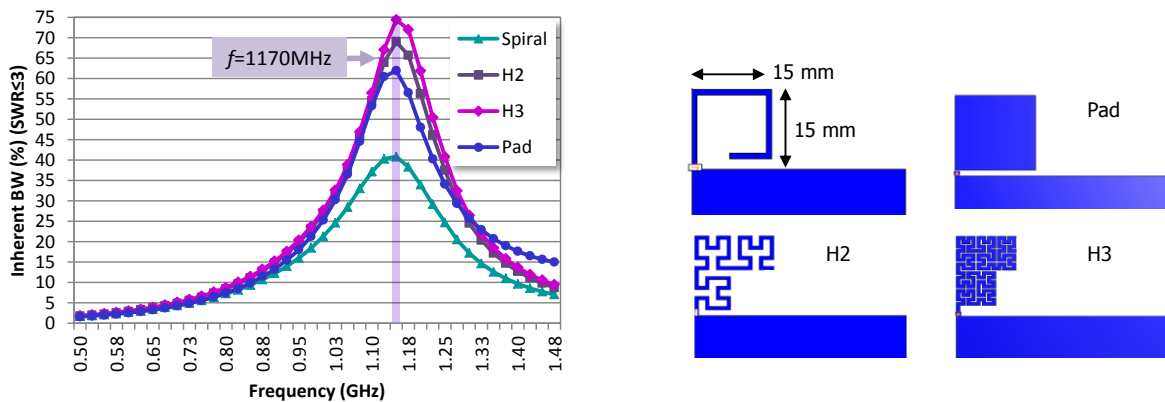


Fig. 2.25 BW_0 for the spiral, H2, H3, and pad when the resonant frequency of the antenna element becomes equal to the resonance of the ground plane mode ($f_r=f_{GP}=1170\text{MHz}$).

It is important to underline, the benefits of having the resonant frequency of the antenna element close to the resonant frequency of the ground plane, as initially taught in [10], [48]. For instance, the results when regarding the resonant elements (i.e. those elements presenting $f_r \leq f_{GP}$) depict that the bandwidth at the 690-960MHz frequency range is lower for those cases having $f_r < f_{GP}$. Therefore and contrarily to what was initially believed, it is preferable to locate the resonance of the antenna element close to the resonance of the ground plane rather than to approximate it to the center frequency of the frequency region to match (Fig. 2.23 and Fig. 2.25). In order to better illustrate this fact, the results for the best case of the resonant elements (H3) are compared in both situations (Fig. 2.26) and they clearly shown a significant bandwidth enhancement for the case where $f_r=f_{GP}$. In this sense, if operation in the frequency region close to 900MHz is required, the best option would consists in modifying the ground plane length as for achieving a resonance shifting to lower frequencies. As demonstrated in the former section, the resonance of the fundamental mode of the ground plane appears when its longitudinal dimension reaches values close to approximately 0.4λ [35], which results in approximately 133 mm at 900MHz. In order to reduce the physical size without modifying the electrical length, previous literature [9]-[26], as well as the previous section teaches that the resonant frequency of short ground planes (around 100 mm), can be shifted down to 900MHz by introducing slots or by adding conductive strips that force the currents to travel a longer electrical path (Fig. 2.17 and Fig. 2.21). In the present section, the approach is not focused

on manipulating the ground plane, but on determining which element better contributes to the excitation of the radiating mode of the ground plane.

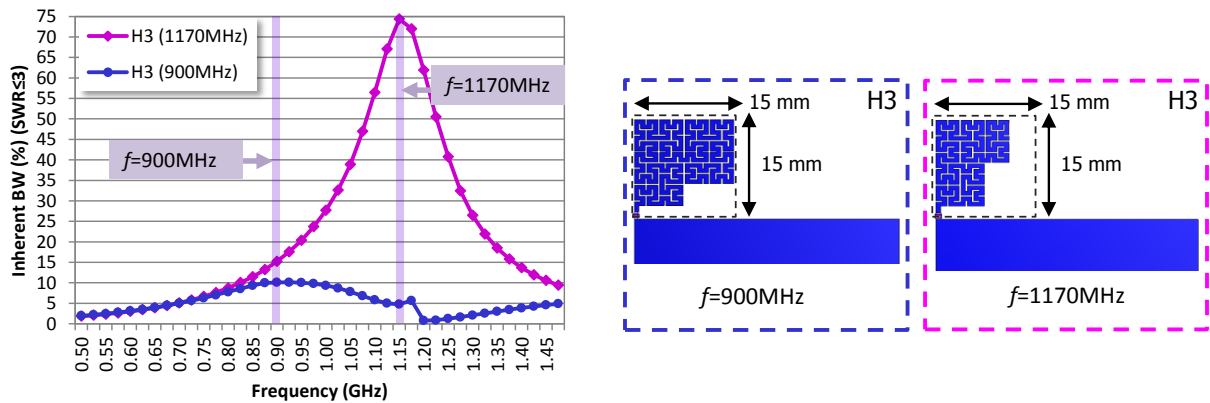


Fig. 2.26 Comparisons of the BW_0 attained by H3 when it is designed to resonate at 900MHz and at 1170MHz, which coincides with the ground plane resonance.

Contrarily to what was initially believed, resonant antennas should not be designed to resonate at the center frequency of the frequency region of interest, but at the resonant frequency of the ground plane mode in order to maximize inherent BW_0 . This conclusion is completely aligned with that obtained from the electrical model presented in [14] where the bandwidth was maximized if the resonant frequency of the antenna matched that of the ground plane. The results further illustrate that non-resonant elements are also good candidates for exciting efficiently the ground plane mode without a significant loss of performance (Fig. 2.25) as well as with the advantage of its geometrical simplicity. In fact, the pad element offers a larger BW_0 at 900MHz even when the other antenna elements are tuned to resonate at this particular frequency (Fig. 2.23). Therefore, a new conclusion is derived from the results, since if the resonant frequency of the element is placed above that of the ground plane, the bandwidth can be large enough and very similar to that obtained in those cases where both resonances become the same (Fig. 2.25) and even larger than that offered by resonant elements tuned at the central frequency of the operating region (900MHz) (Fig. 2.23). The following section will deeply explain the advantages of using non-resonant elements ($f_r > f_{GP}$) instead of commonly used resonant elements. It is worth to outline that the basis for replacing conventional resonant antennas by non-resonant elements, called along the thesis as ground plane boosters, is found in the physical insight provided along this section.

2.4.1.3. Resonance of the Element (f_r) above the Resonance of the Ground Plane (f_{GP})

For the third experiment and in order to demonstrate the advantage of using non-resonant elements ($f_r > f_{GP}$), the spiral, H2, and H3 are tuned to a resonant frequency placed above $f_{GP}=1170\text{MHz}$. For this case, all the elements feature a footprint of 5 mm x 5 mm. The resonant frequencies for the spiral, H2, H3, and pad are 2500MHz, 3800MHz, 2300MHz, and 5800MHz, respectively, which are well above 1170MHz (Fig. 2.27). For this experiment, all cases present similar BW_0 at the frequency region of 690-960MHz. Nevertheless, they slightly differ near the resonant frequency of the ground plane (Fig. 2.27), similarly to what happened when the resonance of the elements were aligned with that of the ground

plane (Fig. 2.25). The previous experiments demonstrate that the better BW_0 appears at the frequencies nearer the resonant frequency of the ground plane, which for this case is placed at 1170MHz. In order to reduce this resonance, the length of the ground plane should be increased, as illustrated in the former sections. If the length of the ground plane is increased up to 120 mm, the ground plane resonance shifts to values close to the operating frequencies (Fig. 2.28), thus providing an enhanced performance at these frequency regions.

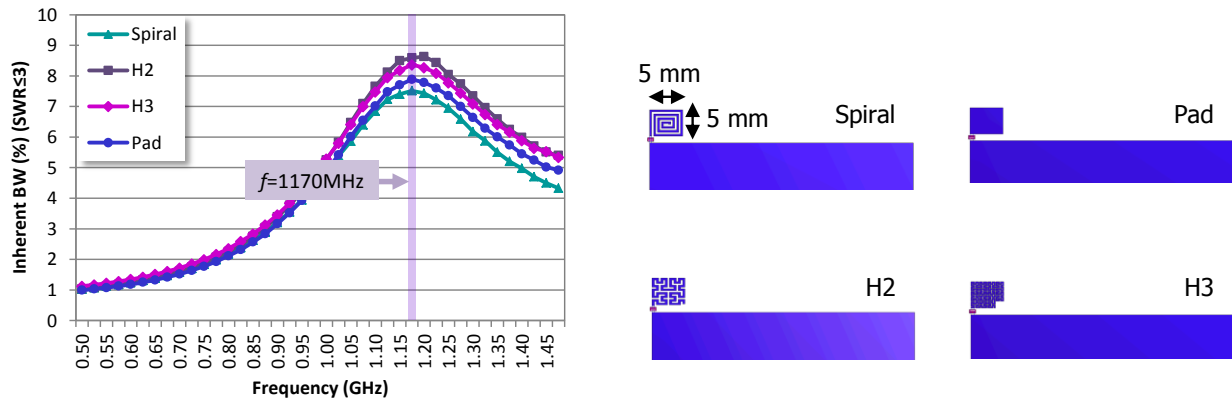


Fig. 2.27 Comparison of the BW_0 attained by the four geometries under study when they are designed to resonate above the resonant frequency of a ground plane having dimensions of 90 mm x 40 mm and being etched over a 1 mm thick FR4 substrate ($\epsilon_r=4.15$, $\tan\delta=0.013$) ($f_{GP}=1170\text{MHz}$).

These results lead to the conclusion that solutions having a resonant frequency equal or above the ground plane resonance are preferable for enhancing the electromagnetic performance of the radiating system at those frequencies close to the resonant frequency of the ground plane. In order to reduce this resonant frequency, larger ground planes or techniques capable of electrically enlarging them are strongly required.

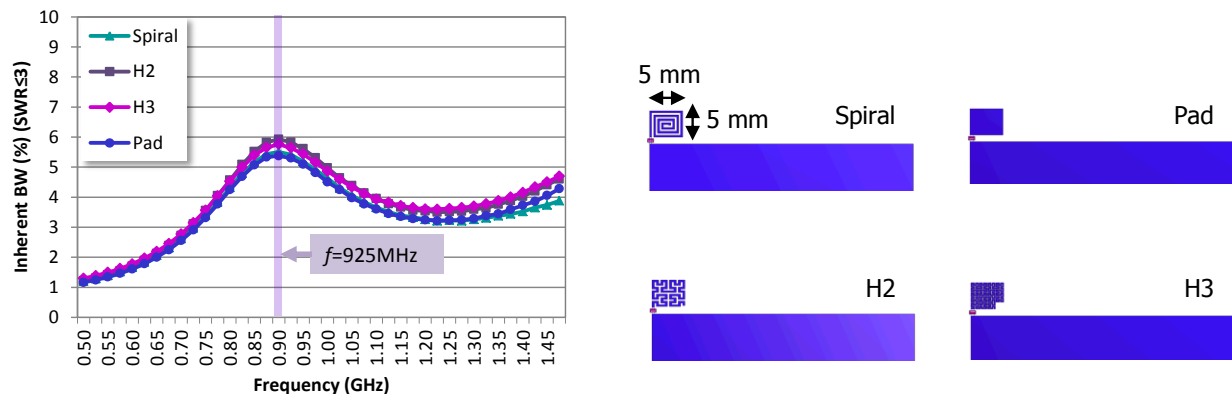


Fig. 2.28 Comparison of the BW_0 attained by the four geometries under study when they are designed to resonate above the resonant frequency of a ground plane having dimensions of 120 mm x 50 mm and being etched over a 1 mm thick FR4 substrate ($\epsilon_r=4.15$, $\tan\delta=0.013$) ($f_{GP}=925\text{MHz}$).

Finally it is possible to conclude that the geometry of the non-resonant element plays a role at frequencies close to the resonant frequency of the ground plane when the elements are tuned to this frequency. If the resonance of the ground plane is placed above the operating frequencies, the geometry loses its relevance and different geometries performs similarly (Fig. 2.27 and Fig. 2.28). This fact allows the use of geometrically simpler structures to provide operation at these frequency regions. Further to the

geometry and size effect, the following section will provide a physical insight into the feeding location effect by approximating the radiating structure to an asymmetric dipole.

2.5. Physical Approximation to an Asymmetric Dipole

This section is intended for providing a physical insight into the behavior of radiating systems fundamentally based on the excitation of the ground plane as main radiator. Previous section analyzes the effect that the geometry, size, and resonant frequency of the element used to excite the ground plane plays in the radiation properties of the whole radiating system. This section goes a step further and provides a physical insight into their radiation properties by approximating it to a dipole.

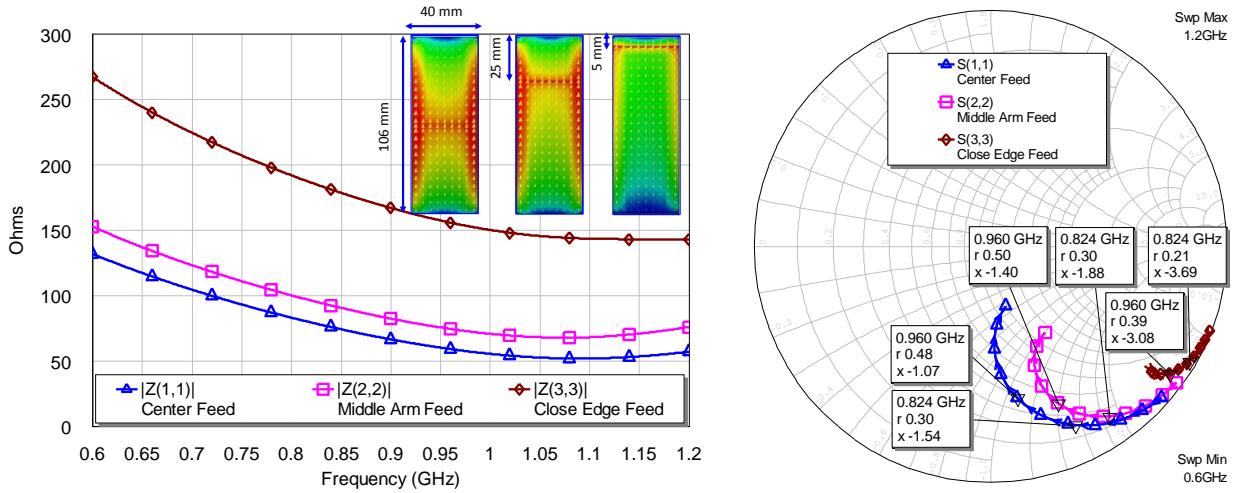


Fig. 2.29 Left: Modulus of the input impedance according to the feeding arrangement. The current distribution relates to the frequency of 825 MHz, which corresponds, approximately, to the center frequency of the frequency range (690-960MHz). The current maximum is fixed to 0.5A/m and the dynamic range is 30dBs; Right: Smith Chart representation of the input impedance.

The location of the feeding point in a dipole configuration plays a significant role in the performance of the radiating structure [6]. It could condition the input impedance value, the current distribution, the radiation pattern or even the radiation efficiency. In order to determine the effects produced by the feeding arrangement in the radiating properties, a dipole antenna of dimensions comparable to the ground plane of a bar-type handset phone, such as the one presented in the former section, has been considered.

$$I_{in} = I_0 \cdot \sin\left(k\left(\frac{l}{2} - |z'|\right)\right) \quad (2.11)$$

$$|Z_{in}| \propto \frac{R_r}{\sin^2\left(k\left(\frac{l}{2} - |z'|\right)\right)} \quad (2.12)$$

As long as the feeding approximates the edge of the dipole (Fig. 2.29), the input impedance modulus increases and varies according to equations (2.11) and (2.12). In this case, this impedance variation affects the quality factor of the structures. Nevertheless, no significant changes are appreciated

in the radiation efficiency which remains substantially close to 100% at the frequency regions under study (0.6-3GHz).

The performance of the radiating structures proposed along the thesis could be approximated to that provided by an asymmetric dipole, understanding asymmetric dipole as that dipole having an off-center feed. The main difference with respect to an ideal asymmetric dipole [6] mainly relies in the asymmetries between the arms that constitute the dipole, which usually entails significant performance variations as deeply presented in section 2.4. The literature asserts that the location of the feeding conditions the current distribution when longer dipoles are considered (larger than $\lambda/2$). Nevertheless, it does not alter the current distribution in shorter dipoles (lower than $\lambda/2$) [6]. Accordingly, since the size of the structure under analysis presents an electrical length smaller than $\lambda/2$ at the low frequency region, the current distribution mode is not significantly altered, since it continues aligned with the longitudinal edge of the radiating structure (Fig. 2.29 and Fig. 2.30).

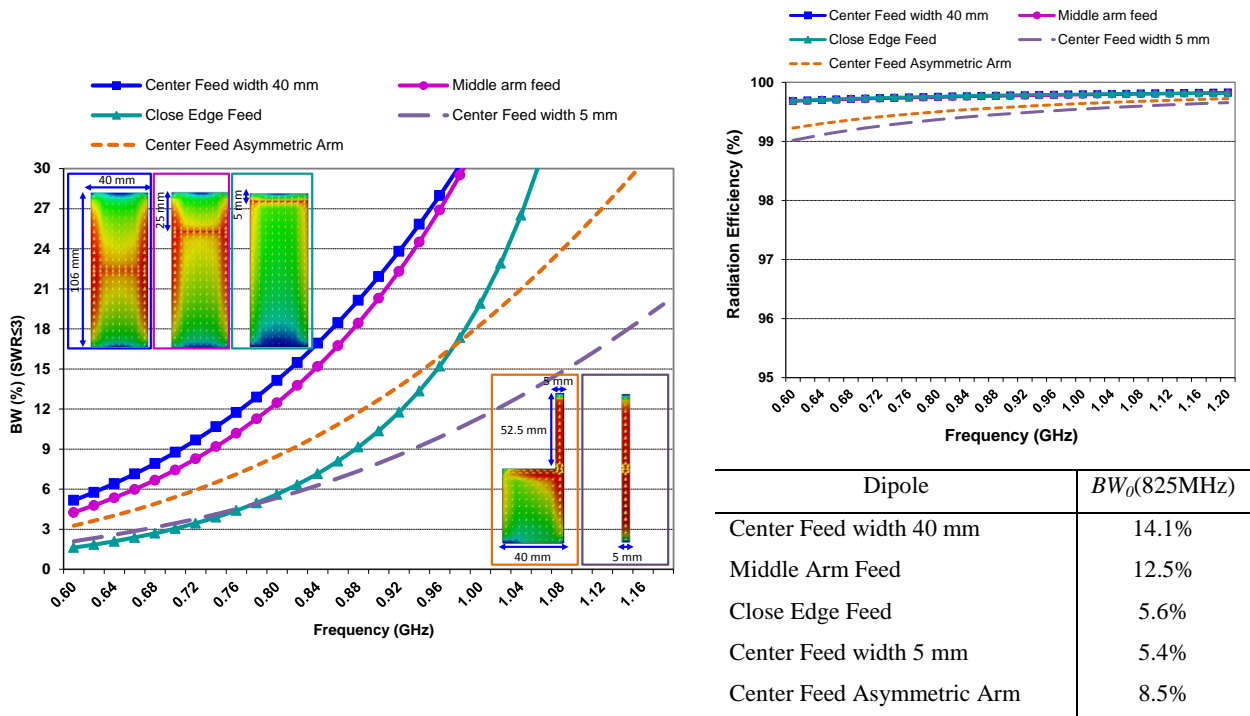


Fig. 2.30 Left: BW_0 according to the feeding arrangement and the dipole arms width. The current distribution relates to the frequency of 825 MHz, which corresponds, approximately, to the center frequency of the frequency range (690-960MHz). The current maximum is fixed to 0.5A/m and the dynamic range is 30dBs; Right: Radiation efficiency and quantitative BW_0 .

The shifting of the feeding location to the shorter edge of the structure mainly translates into a decrement of the BW_0 but neither alters the current distribution nor the radiation efficiency, being the last almost the same, independently of the feeding position (Fig. 2.30).

The previous results illustrate that the center feed solution having a width of 40 mm would be preferable since it attains larger impedance bandwidths. Nevertheless and regarding the implementation perspective, it would significantly complicate the design of current handsets. On one hand, it would make difficult the integration of other handset components, such as the battery, without affecting significantly the performance of the structure. On the other hand, the line routing of the layout would also become a significant challenge. This inconvenience could be overcome by providing an asymmetric solution such

as those proposed along this thesis. These solutions try to reduce as much as possible the size of one arm, or in other words, try to locate the feeding as close as possible to the short edge in order to not only simplify the integration of other handset components, but also to provide a common grounding reducing, in this way, the interaction of other handset components with the radiating structure.

2.6. Conclusions

The characteristics modes theory provides a significant physical insight into the radiation properties of conducting objects as a function of their shape and size. The application of this analysis to the ground plane of some current handset platforms, namely to a bar-type, a smartphone, and a clamshell, reveals that these structures are capable of supporting efficient radiating modes along the frequency region typically used for mobile communication services.

The fundamental radiating mode is the one that predominates in the low frequency region and its current distribution is completely aligned with the longitudinal edges of these ground planes. Accordingly, its length mainly determines the resonance of the fundamental mode, i.e. the larger the length of the ground plane, the lower the resonant frequency, and vice versa. In the higher frequency region, other higher order radiating modes contribute to the radiation process as well.

In addition, this section further demonstrates the effectiveness of the proposed RCS analysis in determining the radiation properties of the fundamental mode of the ground plane. The main advantage of the method mainly relies on its simplicity for determining its resonant frequency without the need of resorting to the tedious mathematical processes required by the characteristic modes theory. The results of the method are completely aligned with those obtained by the mathematical procedure proposed in the characteristic modes theory.

Since the electrical dimensions of the ground plane condition the appearance of the resonance of its radiating modes, this section further proposes methods to reduce its resonant frequency without modifying its physical dimensions. In this sense, this section demonstrates that the addition of slots as well as conductive strips in the ground plane of these typical handset platforms become suitable techniques for increasing the electrical length of the ground plane without affecting its physical dimensions. The RCS method can also be readily applied to those ground planes including these enlarging techniques. The results allow knowing the effect that the addition of these mechanisms introduces into the radiation properties of the fundamental mode. The slotted solution would be preferred over ground planes integrating conductive strips, since it provides larger normalized RCS bandwidth, which mainly translates into larger impedance and efficiency bandwidth. The proposed RCS method also allows better determining how the physical parameters of the solutions affect the excitation of the ground plane mode. In this sense, when a conductive strip is properly designed, the RCS shows a maximum in the frequency region of interest and a minimum at a quarter of the wavelength of the strip, hence, selectively allowing the placement of this minimum out of the frequency region of interest. The RCS method further demonstrates that the slot technique disclosed herein not only presents more bandwidth

for handset antenna design but also avoids the minimum of RCS appearing at the resonant dimensions of the conductive strip, which hardly limits the bandwidth of this solution. Note that the RCS allows taking into account the frequency shifting produced by the dielectric material where the ground plane is usually etched. In this sense, it is possible to state that the RCS method becomes appropriate for providing a better understanding of the behavior of the ground plane which strongly conditions the electromagnetic performance of the whole radiating system.

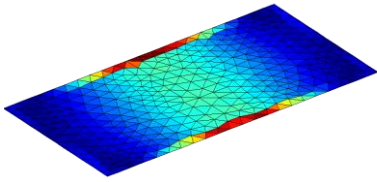
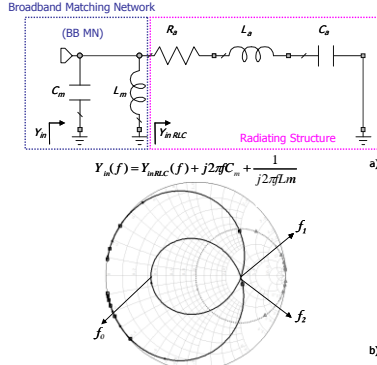
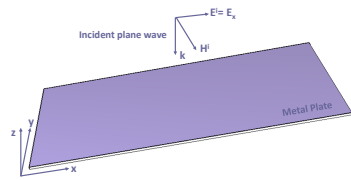

Once the existence of efficient ground plane radiating modes at mobile frequencies is demonstrated, the question that this section addresses, consists in determining the effect of the resonant frequency, the size, and the geometry of the element used to excite this ground plane radiating mode. The performed study demonstrates that the resonance of the element used to excite the ground plane strongly conditions the performance of the whole radiating system. The study reveals that the resonance of these elements should coincide with the resonance of the ground plane mode in order to significantly enhance the performance of the radiating system, and particularly its inherent bandwidth. Contrarily to what was initially believed, the performance of the radiating system is considerably degraded if the resonance of the element is tuned to the center frequency of the frequency region of operation when it is below the resonance of the ground plane mode. In these cases, the geometry plays a role, being the spiral the worst candidate, and the monopole inspired in the Hilbert curve either of two or three interactions, the best candidate. It is important to underline that the radiation properties of a particular element considerably changes in the presence of the ground plane.

The analysis further proves that non-resonant elements can perfectly substitute resonant geometries since their performance is comparable to the resonant cases regarding $f_r = f_{GP}$, with the significant advantage of their simpler geometry. When no-resonant elements are regarded, the geometry loses its relevance and reinforces the benefits of the simplest geometry, i.e. the benefits of the pad element over more complex geometries. Thus, the pad becomes the element that presents the best trade-off between electromagnetic performance and geometry simplicity. In order to determine the preferred ratio between resonant frequencies, several experiments have been carried out and they coincide in the fact that as long as the resonant frequency is above the resonance of the ground plane mode, the performance will remain equal, independently of the ratio between resonances.

The proposed radiating structures could be approximated to an asymmetric dipole. The asymmetric dipole analysis reveals that the best performance is attained when the feeding is arranged at the center of the radiating structure. Nevertheless, this feeding arrangement supposes significant challenges from the integration perspective, since the location of other handset components, such as batteries or displays would significantly degrade the performance of the system. The input impedance modulus increases as far the feeding approximates the short edge of the ground plane, thus increasing the quality factor of the radiating structure. This feeding arrangement neither alters the current distribution nor the radiation patterns of the structure considering structures smaller or comparable to $\lambda/2$. The challenge at this point mainly relies on shifting the feeding point or in a similar manner on modifying the size of the non-

resonant element as for accomplishing the minimum inherent bandwidth capable of providing operation in the desired frequency bands.

Table 2.3 Overview of the main methods and conclusions extracted from this chapter.

Method of Analysis	Features	Results
<p>Characteristic modes</p> 	<ul style="list-style-type: none"> The theory allows determining the wave modes supported by a particular conducting body just as a function of their shape and size. Computation does not need to take into account a feeding mechanism. Eigenvalues (λ) provides information about the nature of the mode. If $\lambda < 0$, the mode is capacitive, if $\lambda > 0$, the mode is inductive, if $\lambda = 0$, the mode is in resonance. Values close to $\lambda = 0$ are desired across the frequency region of operation. 	<ul style="list-style-type: none"> For smartphone platforms having 120mm to 135mm length, the fundamental mode presents a λ close to 0 across the frequency region of interest (690MHz up to 3GHz). The fundamental mode presents minimums of current at the shortest edges of the ground plane, being the ideal position for capacitive ground plane boosters. Maximums of current are located at the center of the longest edges, being this position ideal for inductive ground plane boosters (chapter 3).
<p>Broadband matching network</p> 	<ul style="list-style-type: none"> Electrical circuit models the input impedance of a non-resonant element in a wireless handheld device. Equations for optimum values of a LC broadband matching circuit are derived which allows a systematic design. A fundamental bandwidth enhancement limit is derived which permits to know the boundary of the bandwidth improvement. 	<ul style="list-style-type: none"> A simple broadband matching circuit comprising a LC resonator allows creating an input impedance loop. A bandwidth improvement of 2.45 for SWR=3 is achieved. This systematic technique is used for impedance broadband matching of the several ground plane booster architectures proposed throughout the thesis.
<p>Radar Cross Section</p> 	<ul style="list-style-type: none"> Easy computation. Suitable to determine the resonant frequency of the fundamental mode for a given platform. The backscattering depends on the angle of arrival of the incoming plane wave. Useful to analyze complex platforms such as those having slots or strips in the ground plane. Useful to consider the shifting effect produced by the dielectric support where the ground plane is usually etched. 	<ul style="list-style-type: none"> The RCS method has been compared with characteristic mode analysis to determine the resonant frequency of the fundamental mode of several platforms (bar, smartphone, and clamshell) concluding differences less than 7%. The method has been used to calculate the frequency displacement of the resonant frequency of the ground plane due to a dielectric coating such as those existing in the PCB of wireless handheld devices.
<p>Resonant vs. non-resonant</p> 	<ul style="list-style-type: none"> Computation of the Q using input impedance for a given element on a ground plane, allows determining the best element capable of maximizing the BW_0. 	<ul style="list-style-type: none"> For a typical smartphone platform, the largest bandwidth for the most critical frequency region (690MHz-960MHz), is obtained when the resonance of the element is equal or even above the resonance of the ground plane and not when the element resonates at the frequency of interest.

This conclusion sets forth the basis of this thesis (Table 2.3), which is mainly focused on replacing resonant structures by small non-resonant elements having reduced stand-alone radiation properties in order to excite the efficient radiating modes of the ground planes of typical handset platforms. The following section will demonstrate the effectiveness of the method in providing multi-band radiating systems featured by significantly small dimensions.

2.7. References

- [1] R. J. Garbacz and R.H. Turpin, "A generalized expansion for radiated and scattered fields", *IEEE Transactions on Antennas and Propagation*, vol. AP-19, May 1971, pp. 348-358.
- [2] R.F. Harrington and J.R. Mautz, "Theory of Characteristic Modes for Conducting Bodies", *IEEE Transactions on Antennas and Propagation*, AP-19, n° 5, September 1971, pp. 622-628.
- [3] R.F. Harrington and J.R. Mautz, "Computation of Characteristic Modes for Conducting Bodies", *IEEE Transactions on Antennas and Propagation*, AP-19, n° 5, September 1971, pp. 629-639.
- [4] M. Cabedo, E. Antonino, A. Valero, and M. Ferrando, "The Theory of Characteristic Modes Revisited: A Contribution to the Design of Antennas for Modern Applications", *IEEE Antennas and Propagation Magazine*, vol. 49, n°5, October 2007, pp.52-68.
- [5] C. T. Famdie, W. L. Schroeder, and L. Solbach, "Numerical analysis of characteristic modes on the chassis of mobile phones", *Proceedings of the First European Conference on Antennas and Propagation*, EuCAP 2006, Nice, France, 2006.
- [6] W.L. Stutzman and G. A. Thiele, "Antenna Theory and Design", 2nd Edition, John Wiley, 1998.
- [7] J. Anguera and A. Andújar, "Antennaless Wireless Device comprising One or More Bodies", *Patent Application* WO2011095330, February 2, 2011.
- [8] T. Y. Wu and K. L. Wong, "On the impedance bandwidth of a planar inverted-F antenna for mobile handsets", *Microwave and Optical Technology Letters*, vol.32, Feb.20, 2002, pp.249-251.
- [9] R. Quintero and C. Puente, "Multilevel and Space-Filling Ground Planes for Miniature and Multi-band Antennas", *Patent Application* WO2003/023900, September 13, 2001.
- [10] P. Vainikainen, J. Ollikainen, O. Kivekäs, and I. Kelder, "Resonator-Based Analysis of the Combination of Mobile Handset Antenna and Chassis," *IEEE Transactions on Antennas and Propagation*, vol. 50, n°10, October 2002, pp. 1433-1444.
- [11] M. F. Abedin and M. Ali, "Modifying the Ground Plane and Its Effect on Planar Inverted-F Antennas (PIFAs) for Mobile Phone Handsets", *IEEE Antennas and Wireless Propagation Letters*, vol. 2, 2003, pp.226-229.
- [12] R. Hossa, A. Byndas, and M. E. Bialkowski, "Improvement of Compact Terminal Antenna Performance by Incorporating Open-End Slots in Ground Plane", *IEEE Microwave and Wireless Components Letters*, vol. 14, n° 6, June 2004, pp.283-285.
- [13] J. Anguera, I. Sanz, A. Sanz, A. Condes, D. Gala, C. Puente, and J. Soler, "Enhancing the performance of handset antennas by means of groundplane design". *IEEE International Workshop*

- on Antenna Technology: Small Antennas and Novel Metamaterials* (iWAT 2006), pp.29-32, New York, USA, March 2006.
- [14] A. Cabedo, J. Anguera, C. Picher, M. Ribó, and C. Puente, "Multi-Band Handset Antenna Combining a PIFA, Slots, and Ground Plane Modes", *IEEE Transactions on Antennas and Propagation*, vol.57, n°9, Sep. 2009, pp.2526-2533.
- [15] C. Picher, J. Anguera, A. Cabedo, C. Puente, and S. Kahng, "Multi-band handset antenna using slots on the ground plane: considerations to facilitate the integration of the feeding transmission line", *Progress In Electromagnetics Research C*, vol. 7 , 2009.pp. 95-109.
- [16] C. Picher, J. Anguera, A. Andújar, C. Puente, and A. Bujalance, "Multi-band Handset Antennas by Combining Monopoles and Intelligent Ground Planes", *Proceedings of the Sixth European Conference on Antennas and Propagation*, EuCAP 2012, Prague, Czech Republic, March 2012, pp. 2741-2744.
- [17] C. Picher, J. Anguera, A. Bujalance, A. Andújar, and C. Puente, "Analysis of a Multi-band Monopole Handset Antenna Combined with a Slotted Ground Plane", *Microwave and Optical Technology Letters*, vol. 55, n°1, January 2013, pp. 173-180.
- [18] A. R. Razali and M. E. Bialkowski, "Coplanar Inverted-F with Open-End Ground Slots for Multi-band Operation", *IEEE Antennas and Wireless Propagation Letters*, 8, 2009, pp. 1029-1032.
- [19] J. Anguera, I. Sanz, J. Mumbrú, and C. Puente, "Multi-Band Handset Antenna with a Parallel Excitation of PIFA and Slot Radiators", *IEEE Transactions on Antennas and Propagation*, vol.58, n°2, pp.348-356, February 2010.
- [20] C. Picher, J. Anguera, A. Andújar, C. Puente, and S. Kahng, "Analysis of the Human Head Interaction in Handset Antennas with Slotted Ground Planes", *IEEE Antennas and Propagation Magazine*, vol.54, n°2, pp.36-56, April 2012.
- [21] J. Anguera and A. Condes, "Antenna Set, Portable Wireless Device, and use of a Conductive Element for Tuning the Ground-plane of the Antenna set", Patent *application*, WO 2007/039071. September 15, 2006.
- [22] C.H. Chang and K.L. Wong, "Bandwidth enhancement of internal WWAN antenna using an inductively coupled plate in the small-size mobile phone", *Microwave and Optical Technology Letters*, vol. 52, n°6, , June 2010, pp.1247–1253.
- [23] J. Anguera, A. Andújar, and C. Puente, "A Mechanism to Electrically Enlarge the Ground Plane of Handset Antennas: a Bandwidth Enhancement Technique", *Microwave and Optical Technology Letters*, vol.53, n°7, July 2011, pp.1512-1517.
- [24] P. Lindberg and E. Öjefors, "A Bandwidth Enhancement Technique for Mobile Handset Antennas Using Wavetraps", *IEEE Transactions on Antennas and Propagation*, vol. 54, n°8, August 2006, pp.2226-2233.
- [25] J. Maoz and M. Kadichevitz, "Apparatus and method for Enhancing Low-Frequency Operation of Mobile Communication Antennas", *Patent US* 6,940,460.

- [26] C. Puente and J. Anguera, "Handset with Electromagnetic Bra", *Patent Application* WO2005/083833, February 28, 2005.
- [27] J. Anguera and A. Andújar, "Ground Plane Contribution in Wireless Handheld Devices using Radar Cross Section Analysis", *Progress In Electromagnetics Research M*, vol.26, 2012, pp-101-114.
- [28] S. N. Makarov, "Antenna and EM Modeling with Matlab," *Wiley-Interscience*, John Wiley & Sons, New York, July 2002.
- [29] J.H. Jo, B. Yu, K.H. Kong, K. Jung, I.Y. Lee, M.J. Park, and B. Lee, "Multi-band internal antenna including DVB-H band" *IEEE Antennas and Propagation Society International Symposium*, 9-15 June 2007, pp.972-975.
- [30] J. Anguera, A. Andújar, C. Puente, and J. Mumbrú, "Antennaless Wireless Device", *Patent Application* WO2010/015365, July 31, 2009.
- [31] J. Anguera, A. Andújar, C. Puente, and J. Mumbrú, "Antennaless Wireless Device Capable of Operation in Multiple Frequency Regions", *Patent Application* WO2010/015364, July 31, 2009.
- [32] A. Andújar, J. Anguera, and C. Puente, "Ground Plane Boosters as a Compact Antenna Technology for Wireless Handheld Devices", *IEEE Transactions on Antennas and Propagation*, vol. 59, n°5, May 2011, pp.1668-1677.
- [33] J. M. Jung, S. J. Kim, K. H. Kong, J. S. Lee, and B. Lee, "Designing Ground Plane to Reduce Hand Effects on Mobile Handsets", *IEEE Antennas and Propagation Society International Symposium*, Honolulu, Hawaii, USA, June 2007.
- [34] J. Holopainen, J. Ilvonen, O. Kivekäs, R. Valkonen, C. Icheln, and P. Vainikainen, "Near-Field Control of Handset Antennas Based on Inverted-Top Wavetraps: Focus on Hearing-Aid Compatibility", *IEEE Antennas and Wireless Propagation Letters*, vol. 8, 2009, pp. 592-595.
- [35] K.L.Wong, "Planar Antennas for Wireless Communications", *Wiley Inter-Science* 2003.
- [36] M. Martínez-Vázquez, O. Litschke, M. Geissler, D. Heberling, A. M. Martínez-González, and D. Sánchez-Hernández, "Integrated Planar Multi-band Antennas for Personal Communication Handsets", *IEEE Transactions on Antennas and Propagation*, vol. 54, n°2, February 2006, pp.384-391.
- [37] K.L. Wong, G.Y. Lee, and T.W. Chiou, "A low-profile planar monopole antenna for multi-band operation of mobile handsets", *IEEE Transactions on Antennas and Propagation*, vol.51, n°1, January 2003, pp. 121- 125.
- [38] K.L. Wong and S.C. Chen, "Printed Single-Strip Monopole using a Chip Inductor for Penta-Band WWAN Operation in the Mobile Phone", *IEEE Transactions on Antennas and Propagation*, vol. 58, n°3, March 2010, pp. 1011-1014.
- [39] H. Kanj and S.M. Ali, "Compact Multi-band Folded 3-D Monopole Antenna," *IEEE Antennas and Wireless Propagation Letters*, vol.8, pp.185-188, 2009.

- [40] J. Ma, Y. Z. Yin, J.L. Guo, and Y.H. Huang, "Miniature Printed Octaband Monopole Antenna for Mobile Phones", *IEEE Antennas and Wireless Propagation Letters*, vol.9, pp.1033-1036, 2010.
- [41] K.L. Wong and C.H. Huang, "Printed Loop Antenna with a Perpendicular Feed for Penta-band Mobile Phone Application", *IEEE Transactions on Antennas and Propagation*, vol. 56, n°7, July 2008, pp. 2138-2141.
- [42] C. Lin and K.L. Wong, "Printed Monopole Slot Antenna for Internal Multi-band Mobile Phone Antenna", *IEEE Transactions on Antennas and Propagation*, vol.55, n°2, Dec.2007, pp.3690-3697.
- [43] C.H. Wu and K.L. Wong "Hexa-band internal printed slot antenna for mobile phone application," *Microwave and Optical Technology Letters*, vol.50, January 2008, pp. 35-38.
- [44] B.S. Collins, S.P. Kingsley, J.M. Ide, S.A. Saario, R.W. Schlub, and S.G. O'Keefe, "A multi-band hybrid balanced antenna", *IEEE International Workshop on Antenna Technology: Small Antennas and Novel Metamaterials*, New York, March 6-8, 2006, pp.100-103.
- [45] C. Lin and K. L. Wong, "Printed Monopole Slot Antenna for Internal Multi-band Mobile Phone Antenna", *IEEE Transactions on Antennas and Propagation*, vol. 55, n°12, December 2007, pp. 3690-3697.
- [46] J. Anguera, A. Camps, A. Andújar, and C. Puente, "Enhancing the robustness of handset antennas to finger loading effects", *IEE Electronics Letters*, vol.45, n°15, July 2009, pp-770-771.
- [47] R. Valkonen, S. Myllymaki, A. Huttunen, J. Holopainen, J. Ilvonen, P. Vainikainen, and H. Jantunen, "Compensation of finger effect on a mobile terminal antenna by antenna selection", *International Conference on Electromagnetics in Advanced Applications (ICEAA)*, September 2010, pp.364-367.
- [48] J. Villanen, J. Ollikainen, O. Kivekäs, and P. Vainikainen, "Coupling Element Based Mobile Terminal Antenna Structures", *IEEE Transactions on Antennas and Propagation*, vol. 54, n° 7, July 2006, pp. 2142-2153.
- [49] B. Sanz-Izquierdo, J. Batchelor, and R. Langley, "Multi-band printed PIFA antenna with ground plane capacitive resonator", *IEE Electronics Letters* 28th, vol. 40 n°22, October 2004 , pp.1391-1392.
- [50] M. Cabedo, E. Antonino, V. Rodrigo, and C. Suárez, "Análisis Modal de un Plano de Masa Radiante Doblado y con una Ranura para Terminales Móviles", *Proceedings of the XXI National Symposium URSI '06*. Oviedo, Spain, September 2006.
- [51] W.L. Schroeder, T. Famdie, and K. Solbach, "Utilisation and tuning of the chassis modes of a handheld terminal for the design of multi-band radiation characteristics", *IEE Wideband and Multi-band Antennas and Arrays*, September 2005, pp. 117-121.
- [52] P. Lindberg and E. Öjefors, "A Bandwidth Enhancement Technique for Mobile Handset Antennas Using Wavetraps", *IEEE Transactions on Antennas and Propagation*, vol. 54, n° 8, August 2006, pp.2226-2233.

-
- [53] I. Sanz, J. Anguera, A. Andújar, C. Puente, and C. Borja, “The Hilbert Monopole Revisited”, *Proceedings of the Fourth European Conference on Antennas and Propagation*, EuCAP 2010, April 2010, Barcelona, Spain.
- [54] S.R. Best, “The Inverse Relationship between Quality Factor and Bandwidth in Multiple Resonant Antennas”, *IEEE Antennas and Propagation Society International Symposium*, 2006, 623-626.
- [55] H.F. Pues and A.R. Van de Capelle, “An Impedance-Matching Technique for Increasing the Bandwidth of Microstrip Antennas”, *IEEE Transactions on Antennas and Propagation*, vol. 37, n°11, Nov. 1989, pp. 1345-1354.
- [56] J. Anguera, A. Andújar, C. García, “Multiband and Small Coplanar Antenna System for Wireless Handheld Devices”, *IEEE Transactions on Antennas and Propagation*, vol. 61, n° 7, July 2013, pp. 3782-3789.
- [57] J. Anguera, C. Puente, E. Martínez, and E. Rozan, “The fractal Hilbert monopole: A two-dimensional wire”. *Microwave and Optical Technology Letters*, vol.36, n°2, Jan. 2003, pp.102-104.

CHAPTER 3 GROUND PLANE BOOSTER ANTENNA TECHNOLOGY

3.1. Introduction

The theoretical principles of the characteristic modes that set forth the grounds of the proposed antenna technology are presented in detail in the former chapter. The theory demonstrates that it is possible to compute the wave modes supported by any conductive structure as a function of their shape and size, i.e. only the shape and size of a conducting structure determines the wave modes that it can support. In addition, the theory also allows knowing in advance the radiation properties associated to said modes, i.e. its computation determines if a particular mode contributes to store electric/magnetic energy, or if in contrast, said mode is a radiating mode, which means that it is capable of properly radiating the energy to the space.

In order to apply the potential advantages of this theory, previous chapter presented the computation of the characteristic modes associated to several handset platforms such as bar and smartphone. The results reveal that the ground plane of said platforms presents an efficient radiating mode at mobile frequencies. The technology proposed along this chapter is focused on properly exciting this efficient radiating mode without requiring the use of conventional antennas having resonant dimensions close to a quarter of the operating wavelength. The use of the ground plane as the main radiator provides the advantages of reducing the space required by the radiating system in the handset platform. The manufacturers considers the integration of the antenna element into the handset platform as a toll to pay, thus its size reduction is strongly demanded. This reduction allows not only the integration of other handset components and functionalities but also the addition of multiple antenna elements strongly required in emergent technologies such as MIMO.

As previously discussed, the shape and size of the ground plane of the handset platform strongly condition the radiation modes that could be excited. Once the shape and size has been selected as for supporting the desired radiation modes, the challenge moves toward the way of properly transfer energy to the efficient radiating ground plane modes. Previous chapter demonstrate that the energy transferred is strongly dependent on the geometry, size, and resonance of the element used. The results further reveal that non-resonant elements stand out over resonant elements not only due to their size benefits but also to their geometry simplicity (section 2.4.1.3).

In this regard, this chapter is focused on providing a radiating system based on the excitation of the efficient radiating modes of a handset platform by means of a set of ground plane boosters strategically arranged along the ground plane of said handset platform. The proposed radiating system further comprises a radiofrequency system based on broadband matching networks, which provides a useful systematic design. The elements used to excite the ground plane are referred along this thesis as ground plane boosters mainly due its limited stand-alone radiation properties. In particular, the ground plane

boosters presented along this chapter cannot be considered antennas since they feature a considerably high Q at the frequencies of interest.

The particular content of each section that conforms this chapter can be summarized as follows: Section 3.2 is focused on demonstrating the feasibility of providing a radiating system based on the excitation of the efficient fundamental radiating mode of the ground plane by using small ground plane boosters featured by their reduced dimensions of just 5 mm x 5 mm x 5 mm. The proposed radiating system comprises a radiofrequency system including broadband matching networks and notch filters for each frequency region, namely a low frequency region (824-960MHz) and a high frequency region (1710-2170MHz), in such a way that each ground plane booster is intended for a particular frequency region. The proposal attains penta-band operation and allows covering the communication standards GSM850, GSM900, GSM1800, GSM1900, and UMTS while reducing the volume occupied in the Printed Circuit Board (PCB).

Several studies emphasize the need of using L-shaped coupling elements having a volumetric geometry to increase the transfer of energy to the efficient ground plane radiation mode. Nevertheless, section 3.3, demonstrate that volumetric ground plane boosters such as the one described in section 3.2 can be substituted by coplanar ground plane boosters without a loss of performance. Two coplanar radiating systems are proposed. The first one attains octo-band operation and allows covering the communication standards GSM850, GSM900, GSM1800, GSM1900, UMTS, LTE2100, LTE2300, and LTE2500. The second one is intended for increasing the number of operating frequency bands up to nine in order to cover ten communication standards LTE700, GSM850, GSM900, GPS, GSM1800, GSM1900, UMTS, LTE2100, LTE2300, and LTE2500.

Section 3.4 will further demonstrate that the geometry, size, and resonance of the element used to excite the ground plane mode are not the only factors that condition the excitation thereof. In particular, the location of the booster element as a function of its nature (inductive/capacitive) plays a significant role. In order to illustrate this effect, this section analyzes the performance of inductive boosters as a function of their placement with respect to the ground plane.

Finally, section 3.5 describes an alternative radiofrequency system capable of minimizing the number of reactive elements (either lumped components or distributed elements) in a factor around 2.5 with respect to previous proposals based on broadband matching networks and notch filters. In particular, the proposed solution attains octo-band operation (GSM850, GSM900, GSM1800, GSM1900, UMTS, LTE2100, LTE2300, and LTE2500) using only 5 reactive components.

3.2. Volumetric Ground Plane Boosters: Capacitive Elements

As previously explained in the introductory section of this thesis, the handset phones initially conceived with a limited number of functionalities have evolved to a novel concept of multifunctional wireless devices or smartphones, which must integrate a great number of services in a limited space in order to satisfy the user demands. Furthermore, new frequency bands appear for allocating new

communication standards for which the antenna has to guarantee operability. In this sense, the antenna design becomes more and more a challenging effort since it has to provide multi-band operation while dealing with the constraints associated to physical limitations. On one hand, small size antennas are required for allowing the integration of other components in the handset platform, such as big displays enabling touch screens, cameras, batteries, speakers, etc. On the other hand, a low profile and low weight design is preferable in order to ensure slim multifunctional platforms. Nowadays, internal antennas such as patch/PIFAs (Planar Inverted F Antenna) and monopoles are the most common designs for handsets [1]. Nevertheless, they are constrained by the fundamental limits of small antennas that imply an inherently narrow bandwidth (BW) [2]. For PIFAs, several well-known techniques are used to provide dual-band or multi-band operation such as inserting slits in the radiating path or using slotted ground planes. This fact increases the complexity of the design and difficult the integration in slim platforms, since to guarantee good performance, the antenna has to be arranged at a certain height with respect to the ground plane occupying a considerable volume ($\approx 3600 \text{ mm}^3$). Handset monopole antennas are an alternative to provide multi-band operation in slim platforms mainly due to its characteristic low profile [3]-[5].

Until relatively recently, the efforts on the antenna design were mainly addressed to the antenna geometry and not to the ground plane, since its relevance in the radiation process was underestimated. Accordingly, the antenna element was typically a self-resonant element that provided an efficient radiation independently from the ground plane structure. Nevertheless, as previously discussed the ground plane is progressively acquiring relevance and several studies have demonstrated its strong contribution to the radiation properties [6]-[29]. In this way, the study presented in [6], proposes an equivalent circuit model that provides a quantitative view of the effect of the combination of a single-resonant antenna and a chassis over the most significant antenna parameters. The theoretical effect of the coupling factor and the resonant frequencies is demonstrated through simulation regarding self-resonant antennas such as patch and PIFA antennas. At the same time, [7] presents a folded radiating ground plane fed with a bowtie-shaped planar monopole specially selected to properly excite the desired ground plane modes. However, the folded ground plane can be understood as a PIFA antenna over a finite ground plane (100 mm x 40 mm) with significant physical dimensions (49.5 mm x 35 mm x 10 mm), which are too large for practical purposes in modern handheld wireless devices. Again the radiation becomes a combination of the PIFA antenna and the ground plane modes. In the present study, the radiation is entirely provided by the proper excitation of the ground plane modes since no antenna is regarded.

In [8], resonant elements are used for simultaneous tuning of two different ground plane modes. On one hand, the resonance of the first ground plane mode is adjusted by strategically loading the ground plane with a resonant screen acting as a quarter-wave slot resonator for the GSM1800 and GSM1900 bands. In this sense, an electrical enlargement of the ground plane is achieved for the low frequency region (0.84-0.96GHz). On the other hand, the resonant frequency at the high frequency region (1.71-2.17GHz) is obtained by reducing the electrical length of the chassis for this frequency region. Other

proposals are found in [9]-[17] where a slot is used for tuning the resonant mode to lower frequencies by providing a longer current path, whereas in [18] the resonant mode is tuned to the high frequency region. Regarding [19], two antenna structures based on coupling elements designed to transfer energy to the ground plane mode are presented. They are intended for covering the communication standards GSM900 and GSM1800 separately by means of a single-resonant matching circuit based on distributed matching elements. Other reference based on coupling elements is given in [20] where an antenna structure consisting in two coupling elements and two resonant circuits is proposed. The proposal achieves a quad-band behavior. Nevertheless, the coupling elements presented for covering each frequency region (624mm^3 and 64mm^3 respectively), and specially that in charge of providing operation in the low frequency region, still presents a considerable volume compared with the 250mm^3 of the new solution disclosed herein for providing penta-band operation. In [21], the penta-band behavior is achieved by means of two radiating elements and two matching networks capable to provide multi-band operation at each frequency region.

In the present thesis, the self-resonant antenna element is replaced by non-resonant ground plane boosters. In this sense, a challenge appears since the ground plane resonance is not coupled to the antenna resonance. Thus, the present research is focused on providing multi-band wireless handheld device architectures based on the proper excitation of the ground plane without the need of an antenna element [22]-[24]. This chapter demonstrates that no handset antenna is required for effectively exciting the radiation modes of the ground plane. On the contrary, the novel architecture introduced here only requires small ground plane boosters featured by a high quality factor ($Q \approx 2250$ for the low frequency region and $Q \approx 265$ for the high frequency region) and extremely poor stand-alone radiation properties in combination with a matching network for providing simultaneous operability in the main communication standards (GSM850, GSM900, GSM1800, GSM1900, and UMTS).

This section is structured in the following manner: firstly, the characteristic modes theory as a base of this study is briefly reviewed in subsection 3.2.1. Subsequently, the radiating system comprising both the radiating structure electrical model and the matching network design are presented in subsection 3.2.2. Secondly, the proposal is evaluated through simulations using the software IE3D based on MoM (Method of Moments) (3.2.3). In a third stage, a prototype is built for the sake of validating the simulations with the experimental results (3.2.4).

3.2.1 Theoretic Principles

Characteristic modes theory [30]-[32] becomes a useful tool to understand the ground plane contribution and can be used to perform systematic analysis and design of handset antennas. As deeply analyzed in the former chapter, they are described as the electrical current eigenfunctions linked to the boundary conditions established by an arbitrary shaped conducting body. Thus, they provide a physical insight into the radiation properties of a specific radiating structure and are only dependent on the shape and size of the conducting object. Accordingly, the behavior of the radiating structure can be described as

a combination of the radiation and impedance characteristics of the wave modes associated to the antenna element and those associate to the ground plane. In this sense, once the shape of the radiating structure is determined, the radiation modes can be computed and the optimum feeding configuration can be selected in order to correctly excite the desired radiation modes [33].

A predominant longitudinal mode is provided by a conventional ground plane layer with typical handset dimensions (100 mm x 40 mm) in the operation range (Fig. 3.1), which is perfectly aligned with the results shown in [34]. From (Fig. 3.1) it is possible to determine that a mode is in resonance when its associated eigenvalue is zero. At the same time, the smaller the magnitude of the eigenvalue, the higher is the contribution to the total surface current density. In addition, the sign of the eigenvalue determines whether the mode contributes to store magnetic energy ($\lambda_n > 0$) or electric energy ($\lambda_n < 0$). It is important to notice that the modal significance (2.10) of the eigenvalue λ_l predominates in the entire frequency range of interest.

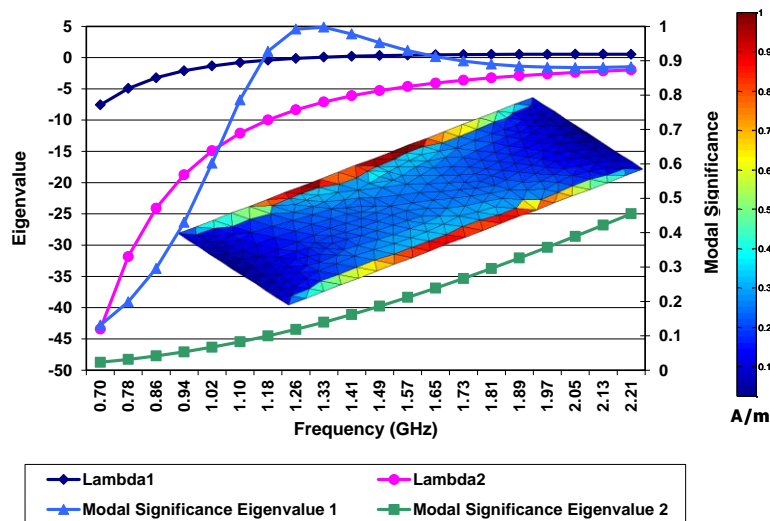


Fig. 3.1 Eigenvalues (λ^1) and modal significance versus frequency associated to the first and second predominant modes (λ_1 and λ_2) regarding a PCB with dimensions 100 mm x 40 mm. Current distribution (A/m) at the frequency of $f=892$ MHz provided by the first radiating mode J_1 .

In the low frequency region, the ground plane is featured by a longitudinal radiation mode characterized by a low quality factor ($Q=1.51$ at the resonance of the first eigenmode (1.3GHz) computed according to (2.8) provided by its resonant dimensions at this frequency range (Fig. 3.1). If a self-resonant antenna element is used, the radiation becomes a combination of the wave mode associated the antenna element and those associated to this longitudinal radiation mode. Consequently, the resulting radiation strongly depends on the efficiency of the radiation mode provided by the antenna element if the ground plane mode is not correctly excited. In this sense, the main idea of this proposal consists in maximizing the energy transfer to the efficient radiation mode of the ground plane by means of a non-resonant ground plane booster with a high Q around 2250 for the low frequency region and 265 for the high frequency region. This non-resonant element merely acts as a ground plane booster for both frequency regions.

¹ Note that λ in subsection 3.2.1 is defined as the eigenvalue and must not be confused with the wavelength.

3.2.2 Concept Definition

This section is intended for describing the proposed radiating system which is mainly composed by a radiating structure and a radiofrequency system. The radiating structure comprises the ground plane of the handset platform, which behaves as the main radiator, as well as the ground plane boosters, which are intended for transferring energy to said ground plane. At the same time, the radiofrequency system is mainly formed by a reactance compensation stage (series inductor for the present case), broadband matching networks, and notch filters. The systematic design of the proposed radiofrequency system will be described in detail along this section, in particular, the broadband matching network employed to enhance the bandwidth, since it plays a key role in obtaining the sufficient bandwidth to cover the required communication standards.

3.2.2.1. Electrical Model of the Radiating Structure

The excitation of the radiation modes of the ground plane can be made either via its magnetic or electrical fields. The suitable location of the non-resonant ground plane booster is only dependent of the fields distribution associated to the radiation modes. The predominant mode of the proposed radiating structure presents a current distribution (Fig. 3.2) similar to that produced by a $\lambda/2$ thick dipole, having its maximum at the center of the longest edges of the ground plane not only for the low frequency region, but also for the high frequency region. In this sense and in order to correctly excite the mode, an electric element should be located at a short edge of the ground plane where the maximum of the electric field distribution takes place. The proposed radiating structure is designed following these considerations and high radiation efficiency around 80% is attained at both frequency regions. More particularly, the radiating structure comprises two non-resonant ground plane boosters featured by their reduced dimensions of just 5 mm x 5 mm x 5 mm, which entails a very low volume (125 mm^3), and a ground plane (100 mm x 40 mm) (Fig. 3.2). Said non-resonant ground plane boosters, characterized by a high Q (≈ 2250 for the low frequency region and ≈ 265 for the high frequency region), are used to couple energy to the ground plane in order to correctly excite its predominant radiation modes [22]-[24].

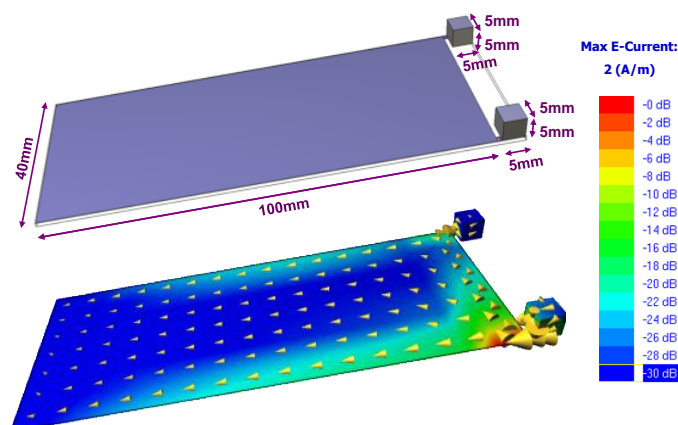


Fig. 3.2 Geometry and dimensions associated to the radiating structure comprising two non-resonant ground plane boosters located at a 2 mm distance from the ground plane edge, each one in charge of the ground plane excitation for each frequency region. Current distribution referred to the excited ground plane mode at $f=0.892\text{GHz}$. The ground plane is supported by a thin FR4 substrate layer of 1mm thick having $\epsilon_r=4.15$ and $\tan\delta=0.013$.

Thus, the ground plane acts as main radiator taking profit of its high radiation efficiency for a wide range of frequencies (Fig. 3.1), concerning both the low and high frequency regions. However, the proper excitation of the predominant mode is not enough for providing penta-band behavior and a matching network is required in order to guarantee operability in the aforementioned communication standards, GSM850, GSM900, GSM1800, GSM1900, and UMTS. In this sense, two non-resonant ground plane boosters are preferable in order to match each one to each one of the frequency regions of interest. Hereafter, the radiating structure and the matching network as a whole will constitute the radiating system.

3.2.2.2. Broadband Matching Network Design

The input impedance associated to the radiating structure presents a capacitive behavior regarding the whole frequency range (0.8-3GHz). The Q_a of the structure (Fig. 3.3) and its inherent BW (BW_0) can be calculated from its input impedance according to equations (3.1)² and (3.2)³ derived in [35].

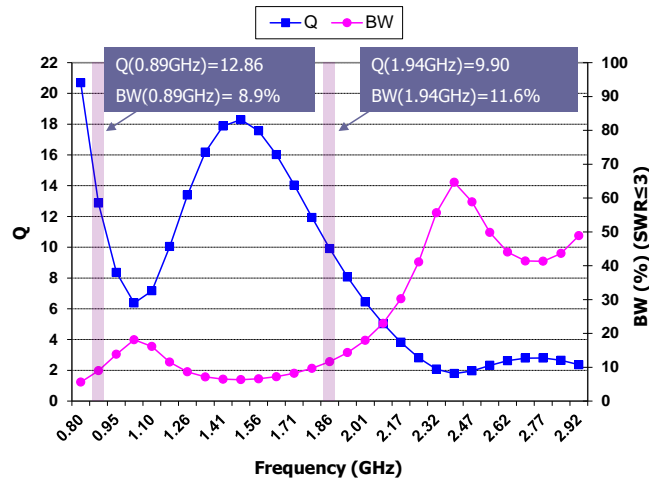


Fig. 3.3 Q_a and related BW_0 versus frequency referred to the radiating structure of Fig. 3.2.

The BW_0 for a (Standing Wave Ratio ($SWR \leq 3$)) referred to the central frequency of both regions of operation is around 8.9% and 11.6%, respectively (Fig. 3.3), which is not enough for covering the bandwidth associated to the communication standards (GSM850, GSM900) (15.2%), and (GSM1800, GSM1900, UMTS) (23.7%).

$$Q_a(\omega) = \frac{\omega}{2R(\omega)} \sqrt{\left[\frac{dR(\omega)}{d\omega} \right]^2 + \left[\left[\frac{dX(\omega)}{d\omega} \right] + \left| \frac{X(\omega)}{\omega} \right| \right]^2} \quad (3.1)$$

$$BW_0 = \frac{f_2 - f_1}{f_0} = \frac{S - 1}{Q_a \cdot \sqrt{S}} \quad (3.2)$$

² ω is the angular frequency. $R(\omega)$ and $X(\omega)$ is the real and imaginary part of the input impedance, respectively.

³ S is the SWR (Standing Wave Ratio).

A systematic method for broadening the BW_0 of RLC circuits in a factor around one half of Fano's limit [36] is proposed in [37] for parallel RLC circuits and in [38] for circuits featuring RLC series input impedances. Thus, before applying the method a previous step is required. A series inductor is used to compensate the capacitive reactance of the radiating structure.

In this sense, the input impedance can be modeled as an RLC series circuit and the broadband mechanism developed in [38] can be applied. Accordingly and in order to achieve the enhanced bandwidth (BW_f), a parallel capacitor and a parallel inductor are used to constitute the proposed broadband matching network, whose input admittance is defined according to equations (3.3) and (3.4). The proper values of these reactances are readily obtained through an accurate mathematical analysis developed using the associated electrical model (Fig. 3.4). The suitable values, that provide the expected BW_f , are those that satisfy the condition represented graphically in Fig. 3.4 and defined mathematically in equations (3.5), (3.6), and (3.7).

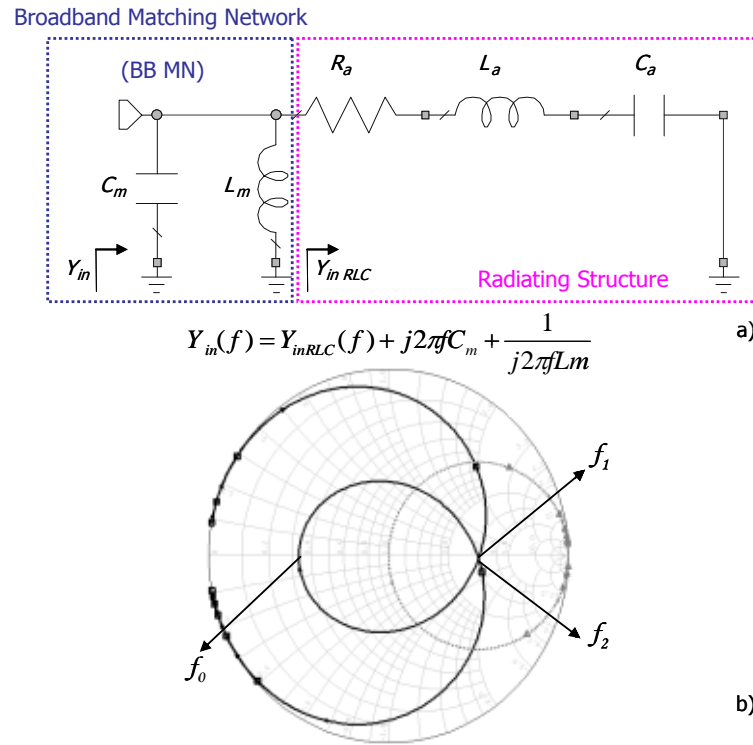


Fig. 3.4 a) Equivalent circuit regarding the input impedance referred to the radiating structure, the reactance compensation (series inductor (L)) stage and the broadband matching network; b) Condition required for achieving a BW enhancement around one half of Fano's limit.

$$\text{Im}\{Y_{in}(f)\} = \frac{-R_a Q_a v}{R_a^2 + (R_a Q_a v)^2} + \omega C_m - \frac{1}{\omega L_m} \quad (3.3)$$

$$\text{Re}\{Y_{in}(f)\} = \frac{G_a}{1 + (Q_a v)^2} \quad (3.4)$$

Where R_a refers to input impedance at f_0 , G_a refers to the conductance at f_0 , and v is defined as $v = \frac{f}{f_0} - \frac{f_0}{f}$.

It is important to note that if the imaginary part of the input admittance (3.3) is equated to 0, three resonant frequencies appear (f_0 , f_1 and f_2). In order to maximize the BW , the input impedance locus has to be forced to fulfill the following requirements that will condition the L_m and C_m values (Fig. 3.4):

$$\text{Im}\{Y_{in}(f_0)\} = \text{Im}\{Y_{in}(f_1)\} = \text{Im}\{Y_{in}(f_2)\} = 0 \quad (3.5)$$

$$\text{Re}\{Y_{in}(f_1)\} = \text{Re}\{Y_{in}(f_2)\} = \frac{1}{Z_0 \cdot S} \quad (3.6)$$

$$\text{Re}\{Y_{in}(f_0)\} = \frac{S}{Z_0} \quad (3.7)$$

The first solution to the equation (3.3) gives in a straightforward manner the relationship required between L_m and C_m (3.8). At the same time, the value of L_m (3.9) can be easily obtained substituting equation (3.8) into equation (3.3).

$$C_m = \frac{1}{\omega_0^2 \cdot L_m} \quad (3.8)$$

$$L_m = \frac{(f_1^2 - f_r^2) \cdot Z_0 \cdot (1 + (Q_a \cdot v_1)^2)}{S \cdot Q_a \cdot (f_1^2 - f_r^2) \cdot 2 \cdot \pi \cdot f_r} \quad (3.9)$$

Where f_1 and f_2 are computed according to equations (3.10) and (3.11), respectively:

$$f_1 = \frac{-f_0 \cdot \sqrt{G \cdot Z_0 \cdot S - 1} + f_0 \sqrt{G \cdot Z_0 \cdot S - 1 + 4 \cdot Q_a^2}}{2 \cdot Q_a} \quad (3.10)$$

$$f_2 = \frac{f_0 \cdot \sqrt{G \cdot Z_0 \cdot S - 1} + f_0 \sqrt{G \cdot Z_0 \cdot S - 1 + 4 \cdot Q_a^2}}{2 \cdot Q_a} \quad (3.11)$$

Theoretically, the BW_f obtained with the addition of the proposed broadband matching network can be defined according to equation (3.12) as:

$$BW_f = \frac{f_2 - f_1}{f_0} = \frac{\sqrt{S^2 - 1}}{Q_a} \quad (3.12)$$

$$F = \frac{BW_f}{BW_0} = \frac{(\sqrt{S^2 - 1}/Q_a)}{(S-1)/(Q_a \cdot \sqrt{S})} = \frac{\sqrt{S^3 - S}}{S-1} \quad (3.13)$$

The enhancement factor F given by (3.13) presents the same shape as that given by the Fano's limit for an ideal network having an infinite number of reactive components [39]. The F obtained in this case is

around 2.45 ($SWR=3$), which supposes a significant enhancement regarding that only a pair of reactive elements is used. Equation (3.12) allows determining the theoretical BW_f that can be achieved.

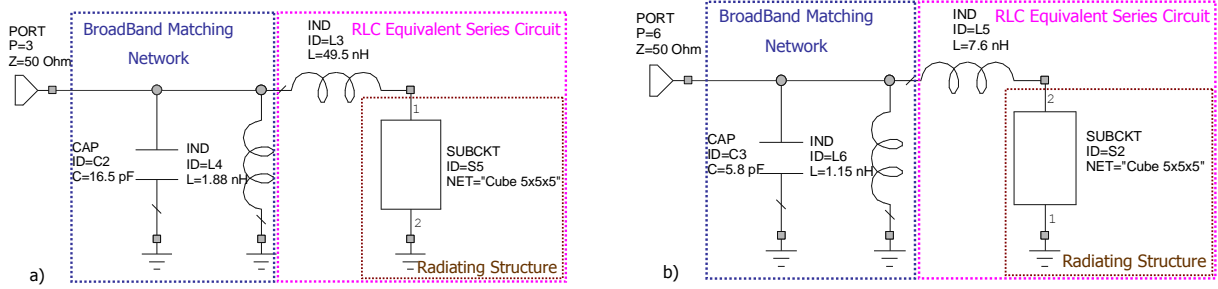


Fig. 3.5 a) Equivalent circuit regarding the input impedance referred to the radiating structure, the reactance compensation (series inductor (L)) stage and the broadband matching network for the low frequency region; b) The same sequence but regarding the high frequency region.

In this sense and as given by Fig. 3.3, the inherent BW_0 equal to 8.9% and 11.6% regarding low and high frequency region, respectively, can be enhanced in a factor around 2.45 for $SWR=3$ (3.13), for each frequency region, resulting in 21.8% and 28.4%, which is enough for covering the communication standards GSM850, GSM900, GSM1800, GSM1900, and UMTS.

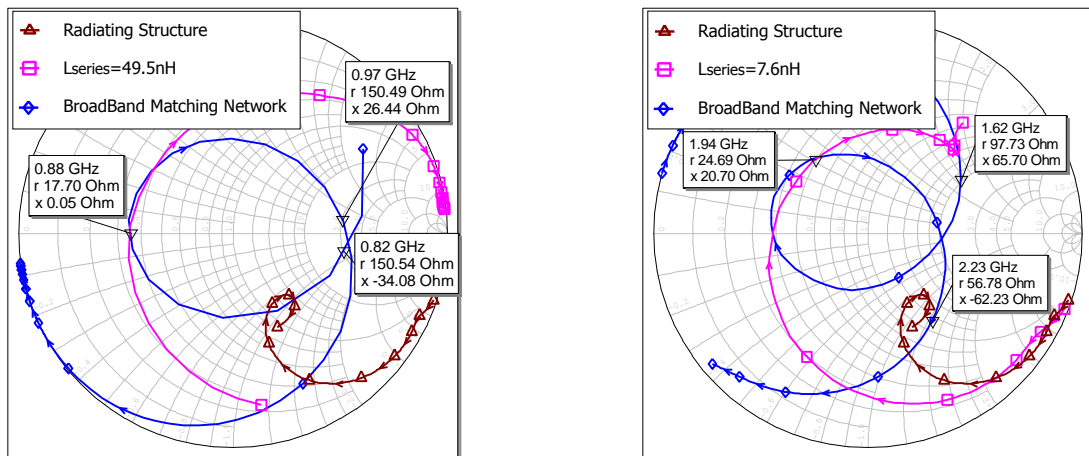


Fig. 3.6 a) Impedance associated to the radiating structure (triangular markers); Impedance after the addition of the series inductor as a reactance compensation element for the low frequency region (square markers); Impedance according to the schematic shown in (Fig. 3.5a) (rhombus marker); b) The same sequence but regarding the high frequency region (Fig. 3.5b).

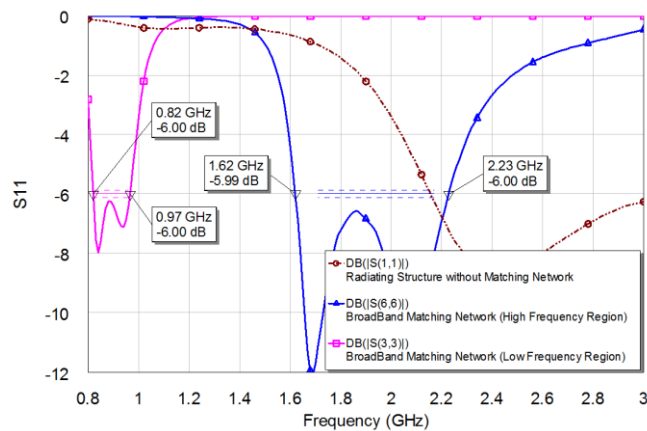


Fig. 3.7 Reflection coefficient associated to the radiating structure without any components (dashed line); Reflection coefficient associated to the schematic shown in (Fig. 3.5a) designed for covering the low frequency region (solid line with square markers); Reflection coefficient associated to the schematic shown in (Fig. 3.5b) designed for covering the high frequency region (solid line with triangular markers).

As aforementioned, two non-resonant ground plane boosters are proposed in order to provide penta-band behavior. In this sense, each booster is matched separately since one is used to provide operability in the low frequency region while the other is in charge of the high frequency region. Thus, the value of the series inductor is adjusted for tuning the resonance of the radiating structure at a frequency belonging on one hand to the low frequency region (Fig. 3.5a) and on the other hand to the high frequency region (Fig. 3.5b), according to [22]-[24].

The addition of this reactance compensation inductor tunes the resonant frequency whereas the broadband matching network allows inscribing the impedance locus at the center of the Smith chart (Fig. 3.6) providing the expected BW_f (Fig. 3.7).

3.2.3 Multi-Band Design: Simulated Results

Previous section demonstrates the feasibility of providing operability in both frequency regions separately, i.e. each ground plane boosters is matched at a particular frequency region, thus a first ground plane booster is capable of providing operation in the low frequency region (GSM850, and GSM900), whereas a second ground plane booster is intended for the high frequency region (GSM1800, GSM1900, and UMTS).

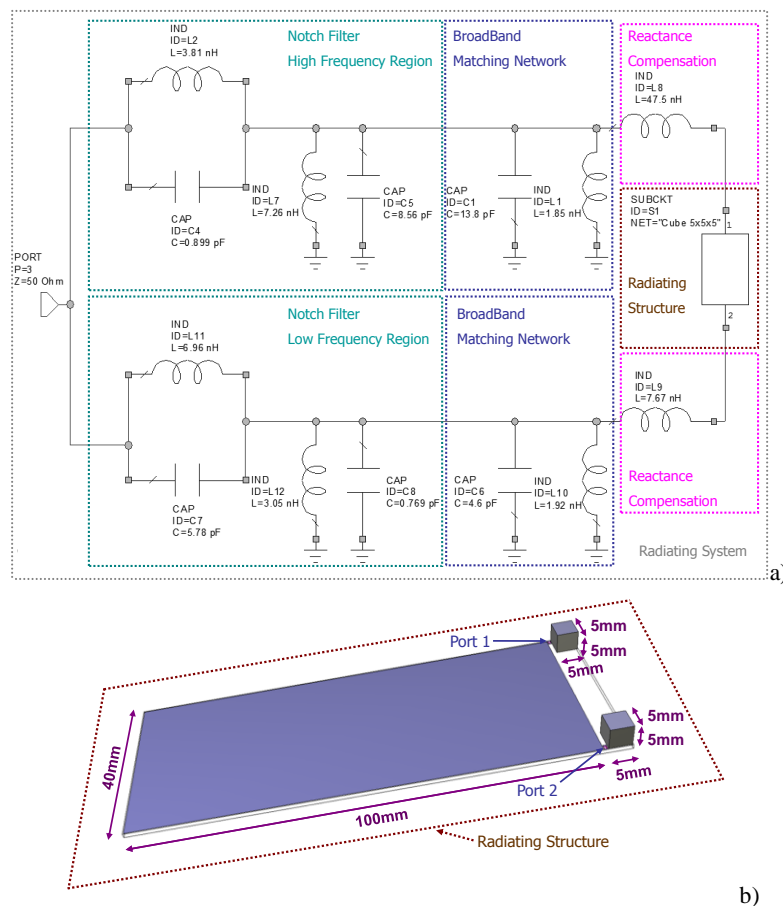


Fig. 3.8 a) Radiating system designed for achieving a penta-band behavior consisting in a reactance cancellation element, a broadband matching network, and a notch filter for each frequency region. Note that the first stage of the notch filter and the broadband matching network can be simplified using only two components. The two-port box is the simulated input impedance of the radiating structure shown in Fig. 3.2; b) Detailed view of the radiating structure obtained from the simulated layout comprising two non-resonant ground plane boosters with dimensions 5 mm x 5 mm x 5 mm, and a ground plane with dimension 100 mm x 40 mm. The ground plane boosters are located at a 2 mm distance from the edge of the ground plane.

This section goes beyond and proposes a matching architecture suitable to afford penta-band behavior simultaneously using a single input/output port [23]-[24]. Besides the reactance compensation element and the broadband matching network, the radiating system also comprises a notch filter for the low frequency region as well as for the high frequency region. The integration of the notch filters provides high isolation between both frequency regions, which is preferable in order to avoid coupling effects that would make difficult the matching network process (Fig. 3.8). This systematic network design provides a standard solution for matching all those non-resonant ground plane boosters featuring capacitive input impedance.

The topology remains equal to that used for the single ground plane booster solution for each frequency region. Thus, the simulated analysis demonstrates the feasibility of the proposal since the designed radiating system provides operability in five of the main communication standards, namely GSM850, GSM900, GSM1800, GSM1900, and UMTS (Fig. 3.9 and Fig. 3.10).

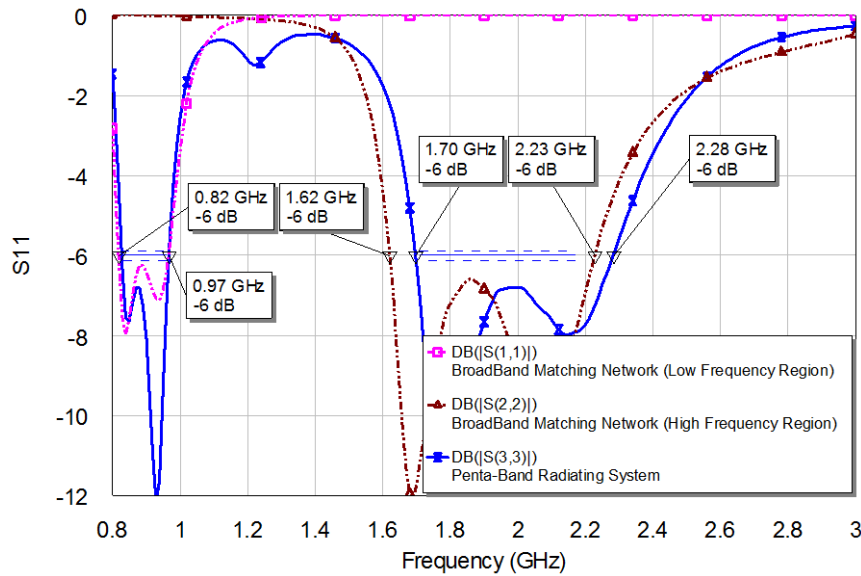


Fig. 3.9 Reflection coefficient associated to the schematic shown in Fig. 3.5a (dashed line with square markers) and in Fig. 3.5b (dashed line with triangular markers) for providing operability in both frequency regions separately; Reflection coefficient to provide penta-band operation simultaneously achieved with the radiating system proposed in Fig. 3.8 (solid line).

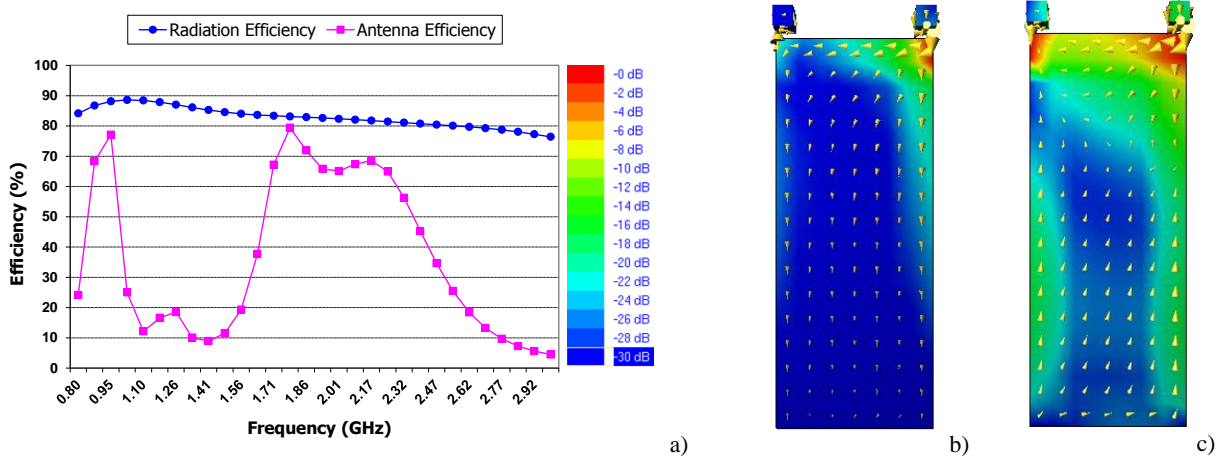


Fig. 3.10 a) Radiation efficiency (η_r), and antenna efficiency (η_a); b)-c) Current distribution associated to the radiating structure at the central frequencies of both frequency regions ($f=0.89$ and $f=1.94$ GHz), respectively. The antenna efficiency takes into account the mismatch losses since it is defined as $\eta_a = \eta_r \cdot (1 - |S_{11}|^2)$.

It is important to remark the relevance of the ground plane boosters since their nature, location, and size clearly conditions the correct excitation of the ground plane mode and consequently, the performance of the radiating system. In this sense, if the size of the ground plane boosters is reduced from 5 mm x 5 mm up to 3 mm x 3 mm x 3 mm, the radiating system limits the frequency range of operation from a penta-band radiating system to a tri-band radiating system (GSM900, GSM1900, and UMTS) (Fig. 3.11), still becoming encouraging results taking into account the reduced volume of the ground plane boosters (54 mm^3).

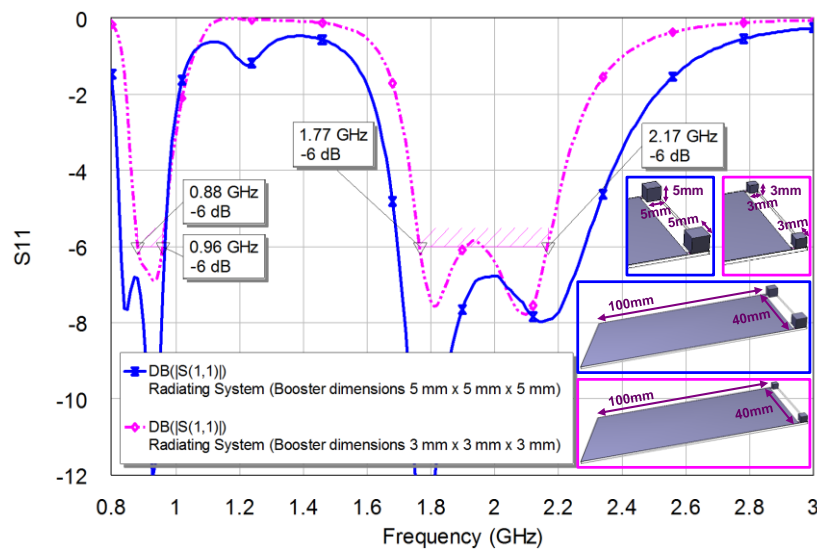


Fig. 3.11 Reflection coefficient to provide penta-band operation simultaneously achieved with the radiating system proposed in Fig. 3.8 (solid line). Reflection coefficient associated to the same radiating structure (Fig. 3.8b) but with the difference that the size of the ground plane boosters (previously 5 mm x 5 mm x 5 mm) has been reduced to only 3 mm x 3 mm x 3 mm (dashed line). The topology of the radiofrequency system remains equal and corresponds to that illustrated in Fig. 3.8a, whereas the values of the reactive components have been adjusted.

3.2.4 Multi-Band Design: Experimental Results

The previous simulated results are validated through an experimental procedure. Accordingly, several prototypes have been built and tested for the sake of demonstrating the effectiveness of the proposal. On one hand, a ground plane (100 mm x 40 mm) is etched over a 1mm thickness FR4 piece ($\epsilon_r=4.15$ and $\tan\delta=0.013$) and several pads are arranged in the upper side of the long edge in order to facilitate the integration of the matching network components. On the other hand, a non-resonant ground plane booster featured by its reduced physical dimensions (solid cube of 5 mm x 5 mm x 5 mm made of brass) is soldered at a 2 mm distance from the edge of the ground plane layer (Fig. 3.12).

The radiating system consisting in a single element provides operability in a specific frequency region and consequently no filter is required. However, the challenge of the proposal lies in achieving a penta-band behavior and for this reason, a prototype have been manufactured integrating two non-resonant ground plane boosters featuring the same characteristics previously described (Fig. 3.13).

The radiofrequency system comprises the reactance cancellation elements, the broadband matching networks, the filtering stages and a transmission line that interconnects both non-resonant ground plane boosters in order to provide a single input/output port system. In this configuration (Fig. 3.13) the

radiofrequency system occupies a certain space in the PCB. However, it is worth to outline that such integration can be further improved by soldering pads in line with the shorter edge of the PCB diminishing, in this sense, not only the required PCB space but also the transmission line length. Furthermore, it is important to remark that lumped components can be arranged in a reduced space according to current soldering techniques.

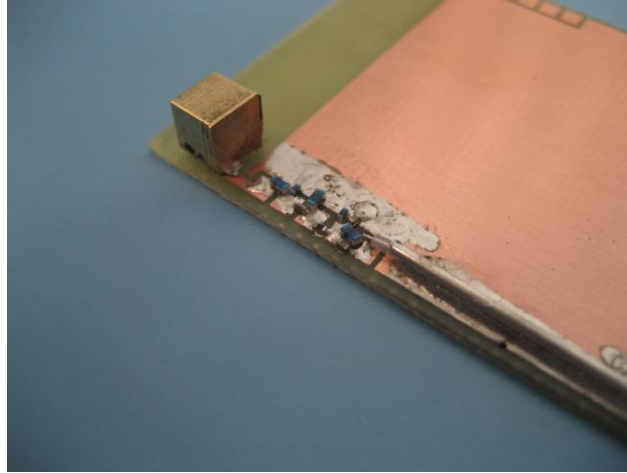


Fig. 3.12 Prototype including the reactance cancellation inductor and the broadband matching network used for covering one frequency region. The components of the matching circuit are SMD 0402 type.

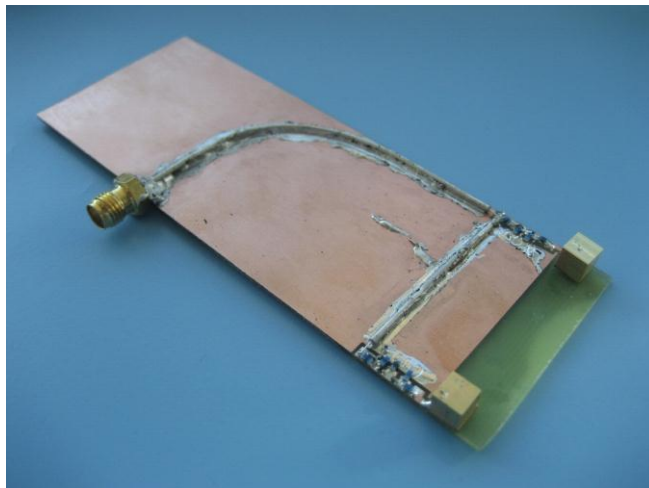


Fig. 3.13 Penta-band prototype designed according to the schematic shown in Fig. 3.8 including besides the reactance cancellation inductor and the broadband matching network, the notch filters required for providing isolation between both frequency regions.

In order to completely characterize the radiating performance of the proposed prototype, the main antenna parameters have been measured and they are gathered in the following subsections.

3.2.4.1. Reflection Coefficient and Efficiency

A network analyzer has been used for measuring the reflection coefficient associated to the penta-band prototype shown in Fig. 3.13. As expected, the proposed radiating system is able to provide operability in the main communication standards (GSM850, GSM900, GSM1800, GSM1900, and UMTS) since the reflection coefficient remains below -6dB ($SWR \leq 3$) for both operating regions (Fig. 3.14). As seen, the measured results (Fig. 3.14) are in good agreement with the simulations (Fig. 3.9).

The antenna efficiency has been measured in the anechoic chamber Satimo Stargate-32 by means of the integration of the 3D radiation pattern (Fig. 3.15). Regarding the high frequency region, the reduction in the antenna efficiency with respect to the simulated case is negligible since it remains around 70% for all the frequency range. However, in the low frequency region the difference between simulated and measured results becomes significant (the simulated values around 70% drop to approximately 40% in the measured case). This reduction is mainly due to the fact that in the simulated case the matching network components are considered to be lossless. However, in practice they present a Q value which is smaller for the low frequency region than for the high frequency region. In this sense, their effect becomes more significant in the low frequency region. Nevertheless, this antenna efficiency value is still acceptable for mobile communications [40]-[43].

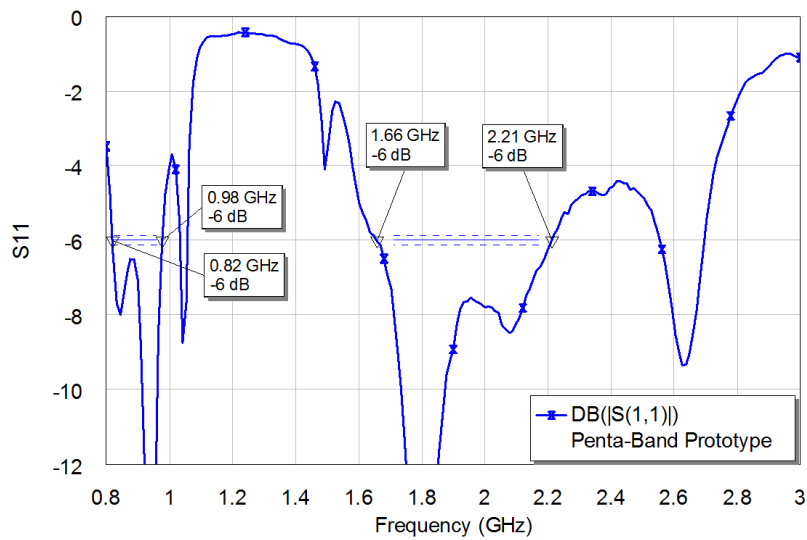


Fig. 3.14 Reflection coefficient related to the penta-band prototype (Fig. 3.13).

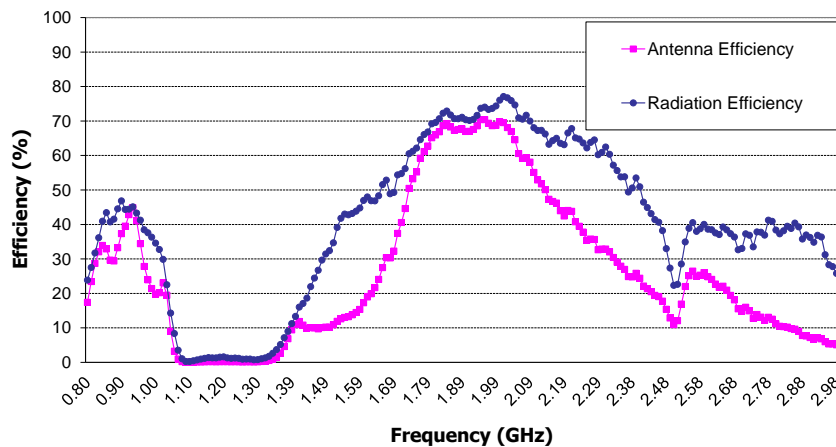


Fig. 3.15 Radiation efficiency (η_r) and antenna efficiency (η_a) related to the penta-band prototype (Fig. 3.13). The antenna efficiency takes into account the matching losses since $\eta_a = \eta_r \cdot (1 - |S_{11}|^2)$.

3.2.4.2. Radiation Patterns

As aforementioned, the radiation patterns have been also measured using the anechoic chamber Satimo Stargate-32 located in the Fractus lab (Fig. 3.16). The main cuts normalized to the maximum gain

($\varphi=0^\circ$ and $\varphi=90^\circ$) are obtained for the frequencies $f=900\text{MHz}$, $f=1800\text{MHz}$, and $f=2000\text{MHz}$. They show an omnidirectional behavior for both frequency regions (Fig. 3.17), which is highly desirable for a handset antenna. The radiation is associated to that produced by a conventional dipole antenna having a null in the y-axis, especially in the low frequency region. The gain is computed regarding the antenna efficiency. It means that, the losses introduced by the matching network as well as the mismatching losses are considered.

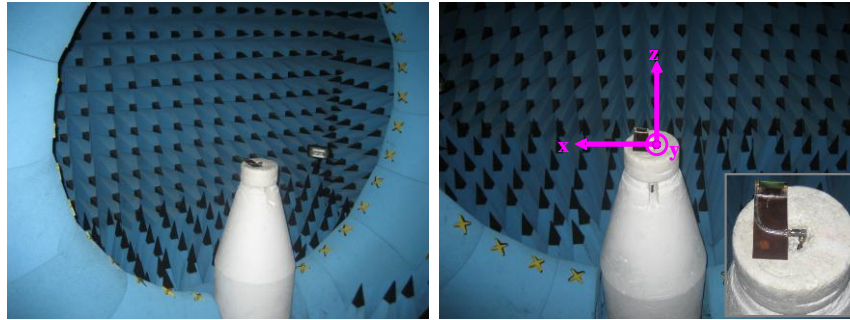


Fig. 3.16 Set-up for radiation measurement in the Fractus' anechoic chamber Satimo Stargate-32 showing the coordinate system. The ground plane lies in the XY plane having the longest dimension aligned with the Y-axis.

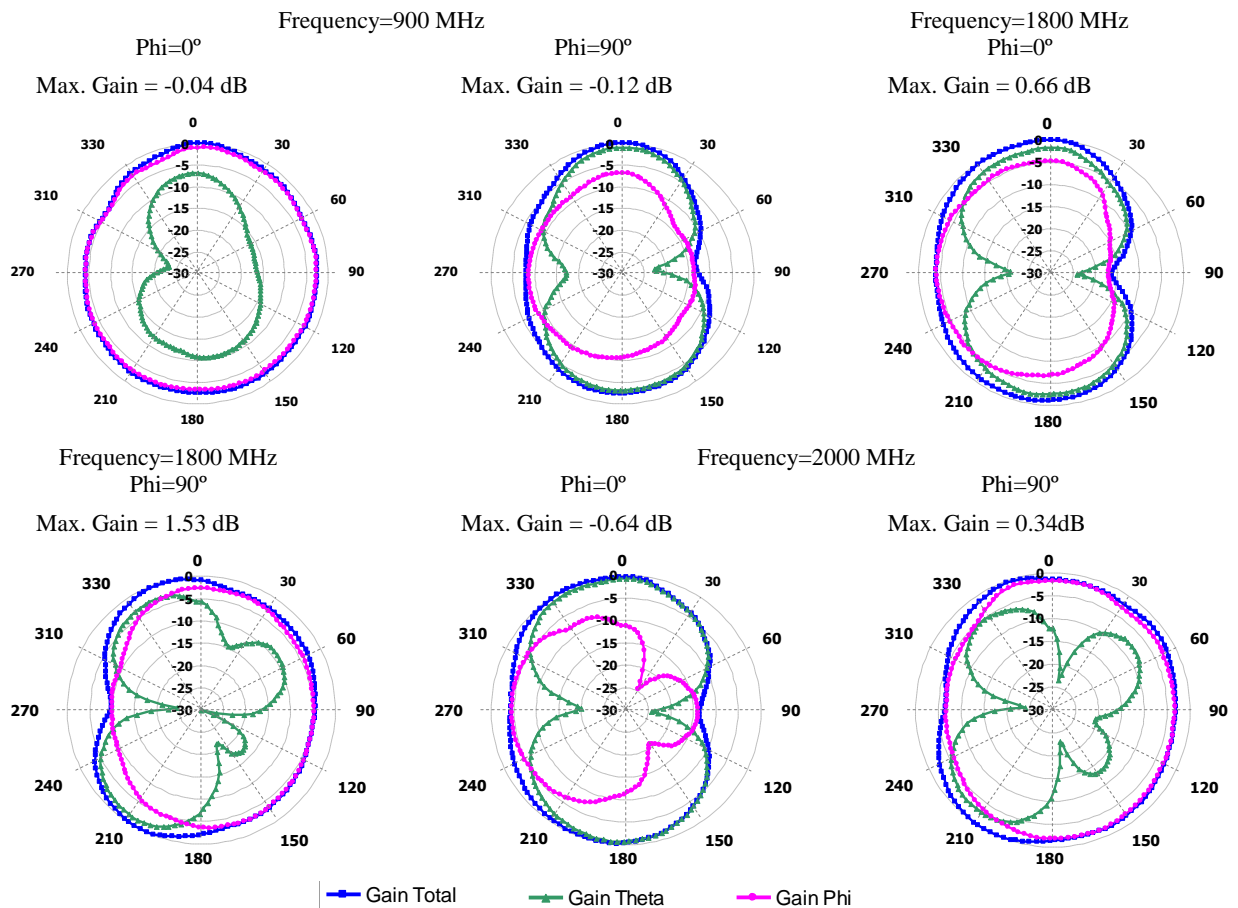


Fig. 3.17 Main cuts ($\Phi=0^\circ$ and $\Phi=90^\circ$) of the radiation pattern provided by the penta-band prototype (Fig. 3.13) measured at the frequencies of $f=900\text{MHz}$, $f=1800\text{MHz}$, and $f=2000\text{MHz}$.

3.2.4.3. SAR Measurement

Once the feasibility of the proposal is demonstrated, the biological compatibility of the prototype in terms of SAR is analyzed. The SAR is a measure of the localized maximum value of the power absorbed

by the human head. It is defined as the absorbed RF energy by unity of mass, and its dimensions are mW/g. Due to the fact that this absorption is produced in the near field, SAR can be computed from the electric near field according to equation (3.14), where σ_{eff} , and ρ are the human tissue effective conductivity and the tissue volumetric density, respectively.

$$SAR = \frac{\sigma_{\text{eff}}}{\rho} \cdot |\vec{E}|^2 \quad (3.14)$$

In this sense, the SAR values associated to the prototype under study (Fig. 3.13) have been measured using the DASY4 equipment. The prototype is arranged in the right cheek of the phantom head and the ground plane is spaced apart 1mm from it thanks to the use of a methacrylate piece. Two different positions have been evaluated for this location. On one hand, the non-resonant ground plane boosters are placed near the right ear of the phantom head (“Boosters Up” position) and on the other hand, the prototype is rotated 180° (“Boosters Down” position).

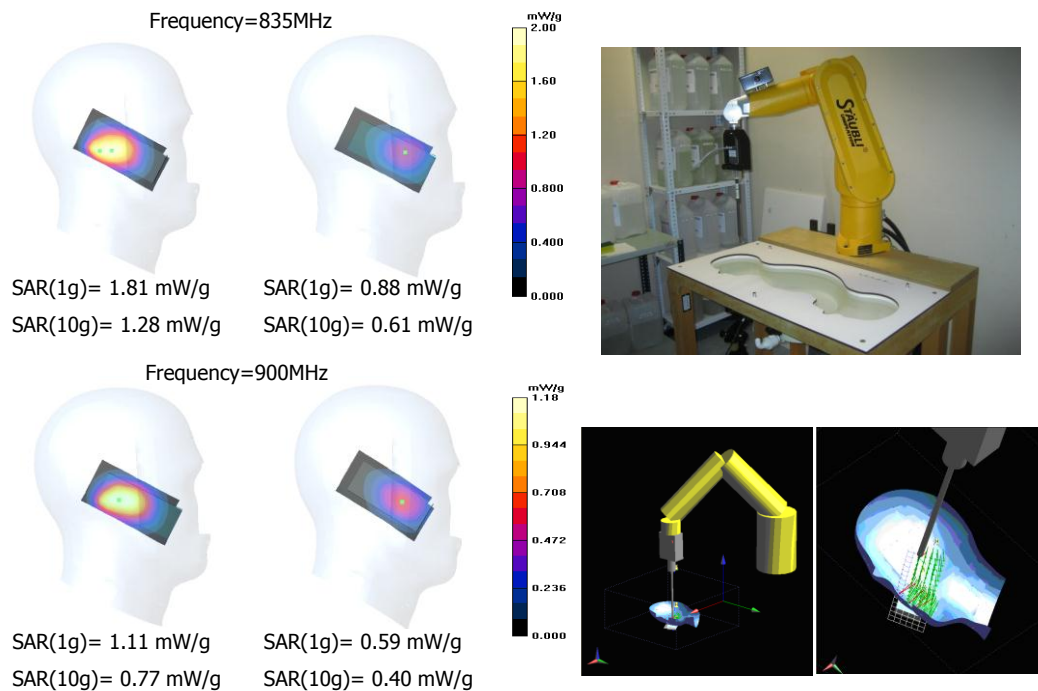


Fig. 3.18 SAR measurements for the low frequency region at the specific frequencies of $f=835\text{MHz}$ and $f=900\text{MHz}$ regarding both positions: left (“Boosters Up”) and right (“Boosters Down”). Right cheek position is tested.

Two main conclusions can be extracted from the results (Fig. 3.18 and Fig. 3.19). On one hand, SAR values are strongly dependent not only on the geometry and the distribution of the radiation mode excited in the ground plane, but also on the way that other handset components are connected to the PCB. For instance, a plastic back-cover may absorb some radiated power decreasing as a consequence the SAR value.

On the other hand, as the excited mode presents a localized maximum field value placed in the vicinity of the shorter ground plane edge at a certain distance from its center, the rotation reduces

considerably the SAR values for both frequency regions but in a significant way for the high frequency region. In this sense, at high frequencies, the hot spot is located near the non-resonant ground plane boosters. This fact produces higher SAR values in the booster up position mainly due to the proximity between such maximum field value and the human head. Accordingly, the booster down position considerable diminishes these SAR values since in this context the hot spot is located at a larger distance from the human head. In the case of the low frequency region the SAR values regarding both positions are located below the standards (American standard (ANSI/IEEE): 1.6mW/g (1g) and European standard (ICNIRP) 2mW/g (10g)). However, for the high frequency region the antenna down position is preferred.

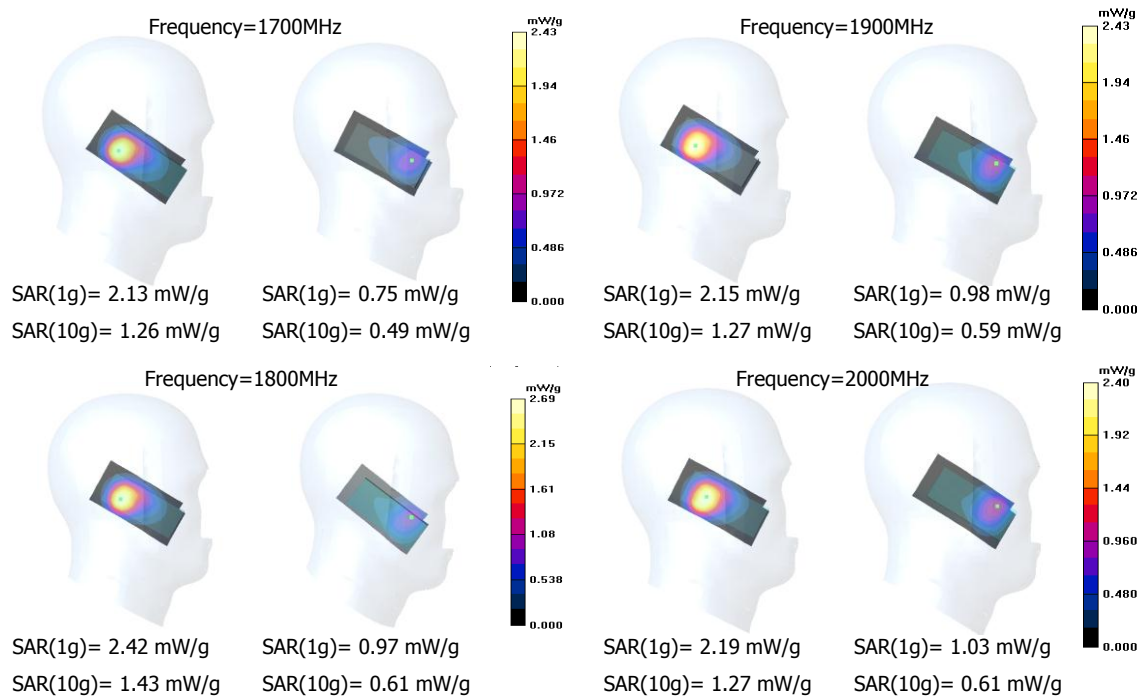


Fig. 3.19 SAR measurements for the high frequency region at the specific frequencies of $f=1700\text{MHz}$, $f=1800\text{MHz}$, $f=1900\text{MHz}$ and $f=2000\text{MHz}$ regarding both positions: left (“Boosters Up”) and right (“Boosters Down”).

It is worth to outline that previous set-up regards the worst situation since the ground plane is only spaced a distance of 1 mm from the human head. In practice, said distance is considerably larger reaching values larger than 20 mm mainly due to the cover and the integration of other handset components. Said increment in distance allows lowering aforementioned SAR values.

As a summary, an ultra-compact radiating system capable of providing operability in the main communication standards (GSM850, GSM900, GSM1800, GSM1900 and UMTS) has been presented. The conventional handset antenna featured by a considerable volume ($\approx 3600\text{ mm}^3$) has been replaced by two low-volume non-resonant ground plane boosters (250 mm^3) and a matching topology with a systematic design. The next section deals with a 2D ground plane booster approach.

3.3. Coplanar Ground Plane Boosters: Capacitive Elements

As discussed in previous section, multifunction wireless devices require, more and more, miniature antennas for providing multi-band operation in order to not only increase the available PCB space to

incorporate as much functionalities as possible, but also to enable the integration of other handset antenna technologies such as MIMO, which require multiple antenna elements. Current handset antenna technologies are based on the integration of resonant antenna elements inside the handset platform. As it is well known, the antennas are strictly constrained by the fundamental limits that directly relate their size in terms of wavelength with their electromagnetic performance [2]. In this sense, some widely spread resonant antennas such as PIFAs, monopoles or slots require a considerable volume to provide proper operation [44]-[52]. This self-resonance feature leads to large antenna elements, more significantly when operation in the low frequency region is required (824-960MHz). This fact increases the complexity not only for integrating multiple handset components but also for providing large number of antenna elements. As previously discussed, recent techniques capable of overcoming aforementioned disadvantages mainly rely on the proper excitation of the ground plane modes through coupling elements [19]-[20]. However, the proposed coupling elements are still volumetric L-shaped structures that require a certain height. Their performance is strongly conditioned by this height, which varies according to the ground plane dimensions [25]. On the contrary, the present thesis proposes the use of ground plane boosters with poor stand-alone radiation properties. Previous section demonstrates the feasibility of using two small ground plane boosters, each one featured by a reduced size of just (5 mm x 5 mm x 5 mm) (Fig. 3.13) to provide penta-band operation (Fig. 3.14) [24]. Nevertheless, the solutions presented in the former section are still based on volumetric structures. In contrast, the proposal described along this section removes the need of including volumetric structures in the handset platform, since it demonstrates that proper ground plane excitation can be obtained through the addition of two coplanar ground plane boosters featured by considerable reduced dimensions of just 6 mm x 6 mm [28]. The first proposal (section 3.3.1) provides operation in the communication standards GSM850, GSM900, GSM1800, GSM1900, UMTS, LTE2100, LTE2300, and LTE2500. The second solution also based on coplanar ground plane boosters (section 3.3.2) is capable of providing nona-band operation, thus covering besides the aforementioned standards, the emergent LTE700 and the GPS band, hence attaining a full wireless solution [29].

3.3.1 Hepta-Band Solution

The proposal described along this section provides operation in seven frequency bands capable of allocating eight communication standards GSM850, GSM900, GSM1800, GSM1900, UMTS, LTE2100, LTE2300, and LTE2500 through the use of two small coplanar ground plane boosters with an area of just 72 mm² [28].

3.3.1.1. Simulated Results

In booster-based antenna technology, the size of the handset platform, namely the size of the ground plane, mainly determines the performance of the whole radiating system, more critically in the low frequency region where the communication standards LTE700, GSM850, GSM900 are allocated. As

seen along chapter 2, the fundamental radiating modes are strongly conditioned by the longest dimension of the ground plane (Fig. 3.20). In this case, the radiating modes are considered to be the first and the fourth radiating modes, i.e. the radiating mode associated to the eigenvalue λ_1 and that corresponding to the eigenvalue λ_4 , respectively. These are the modes that produce a larger contribution to the radiation process. In contrast, the second and the third ground plane modes mainly contribute to store energy at the frequency bands of interest (2.2.1). The longest dimension of the ground plane allows tuning the resonant frequency of these radiating modes (Fig. 3.20). The reason mainly relies on the current distribution (Fig. 3.21), which for these radiating modes is completely aligned with the longest edges of the ground plane. Thus, any modification applied to these dimensions contributes to modify the frequency response of the fundamental radiating modes. Accordingly, the increment of the longest dimension of the ground plane produces a resonance shifting to lower frequencies (Fig. 3.20). This fact allows placing the resonant frequency of these radiating modes nearer the operating bands, hence contributing to an enhancement of the behavior of the radiating system at these frequency bands.

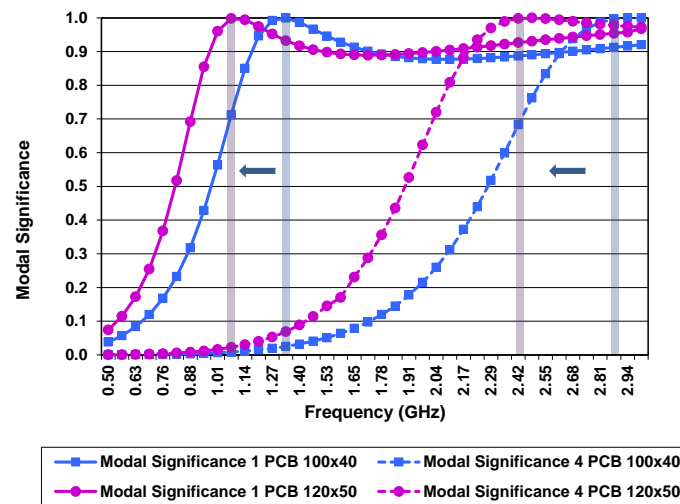


Fig. 3.20 Effect of the ground plane size over the first and the fourth radiating mode. Note that the second and the third radiating modes have not been illustrated due to the fact that they mainly contribute to store energy rather than to radiate it (see section 2.2.1). Note that the dielectric support is omitted in this calculus; its consideration would produce a further shifting to lower frequencies.

Nevertheless, not only the ground plane plays a significant role but also the nature (electric or magnetic), location, and size of the ground plane boosters clearly condition the ground plane mode excitation and consequently the inherent bandwidth [22]-[24], [27]-[29]. The effect of the magnetic ground plane boosters over the performance of the radiating system will be explained in detail along next section (3.4).

In the same way as in the previous section (3.2), this section will still deal with capacitive ground plane boosters. As previously discussed, capacitive ground plane boosters should be arranged close to electrical field maximums. Therefore, and according to the current distribution of the radiating modes to be excited, they should be located at the corners of the shortest edges of the ground plane where minimums of current distribution take place for both radiating modes (Fig. 3.21). Accordingly, the proposed radiating structure comprises a ground plane having dimensions comparable to that featured by

emergent smartphones (120 mm x 50 mm) and two coplanar ground plane boosters. The ground plane boosters are placed at the corners of one of the shortest edge of the ground plane and are etched in the same plane as that containing the ground plane layer, thus becoming coplanar structures (Fig. 3.22). Nevertheless, the size of the ground plane booster further determines the electromagnetic behavior of the radiating system. A systematic method slightly introduced in previous section and detailed herein, is proposed to determine which will be the size that will enable the operation of the radiating system in the desired frequency bands. The systematic method consists in computing the Q and the BW_0 associated to different-sized coplanar ground plane boosters through their input impedance computed using the software IE3D based on MoM [35].

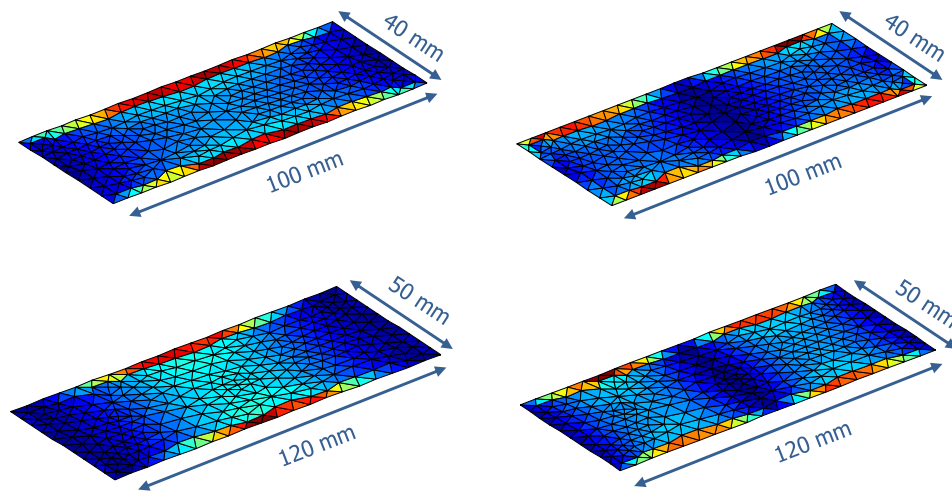


Fig. 3.21 Current distribution associated to the first and fourth radiating modes of a ground plane having dimensions of 100 mm x 40 mm and 120 mm x 50 mm.

The input impedance associated to this kind of radiating structure approximates the input impedance curve of an ideal RLC series circuit for the low (824-960MHz) and high frequency region (1710-2690MHz) (Fig. 3.23). Accordingly, previous theory [35] and [38] can be easily applied.

Once the BW_0 is known, the potential bandwidth could be obtained through the systematic design proposed in [38], which disclose a broadband matching network capable of producing an enhancement factor around 2.45 for a $SWR \leq 3$ (Fig. 3.24). This method allows knowing in advance if a radiating structure will be capable of providing the required operating bandwidth. The method just requires knowing the input impedance of the radiating structure and the enhancement factor of a particular matching network. In this case, the broadband matching network is selected for being the one that maximizes impedance bandwidth while minimizes the number of reactive elements. The proposal removes the need of requiring cumbersome trial and error methods based on the testing of different matching networks for each radiating structure. It is important to underline that the reliability of equations (3.1) and (3.2) applies as long as the input impedance of the system under study approximates that produced by an RLC series or shunt circuit. In other situations where loops or semi-loops appear, the outcomes could at most give a qualitative prediction [35].

The parametric study consists in reducing the size of the coplanar ground plane boosters with the aim of demonstrating its effect over the radiating system performance. The results demonstrate that the larger the booster size, the larger the BW_0 associated to the radiating system (Fig. 3.24 and Fig. 3.25).

However, not only the size of the boosters is an important parameter to consider but also the radiofrequency system plays an important role in the performance of the radiating system. The number of reactive elements required to match the input impedance of a particular radiating system clearly conditions its performance. Reactive elements are not ideal components, hence they tend to introduce losses that affect radiation efficiency, and more significantly at critical frequencies such as those found in the low frequency region. In this case, the challenge lies in attaining the maximum performance with the least number of reactive elements. Thus and as previously mentioned, this section follows the teachings of the former one and proposes the use of broadband matching networks [38] for being the ones that attain an acceptable trade-off between achievable bandwidth and matching network complexity (Fig. 3.26). In addition, the systematic method carefully described in section 3.2.2.2 is further validated since the computation of the BW_0 together with the knowledge of the enhancement factor produced by a broadband matching network (3.13) allows knowing in advance if the size of the ground plane boosters will be enough for covering the desired communication standards.

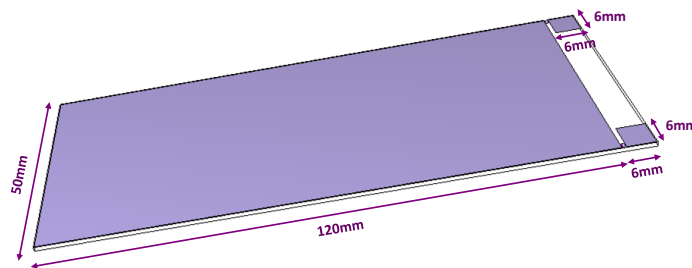


Fig. 3.22 Detailed view of a radiating structure comprising two coplanar non-resonant ground plane boosters with dimensions 6 mm x 6 mm, and a ground plane with dimension 120 mm x 50 mm. The ground plane boosters are located at 1 mm distance from the shortest edge of the ground plane. The ground plane is supported by a thin FR4 substrate layer of 1 mm thick having $\epsilon_r=4.15$ and $\tan\delta=0.013$.

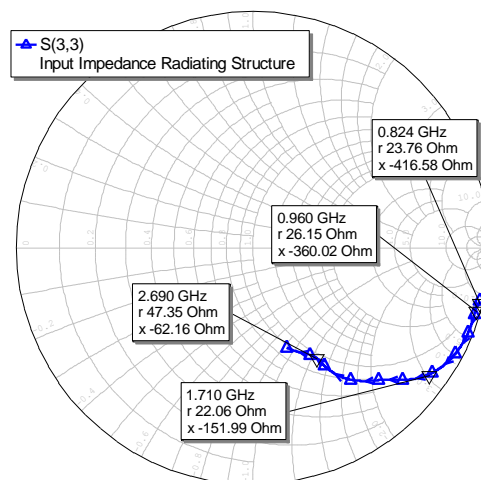


Fig. 3.23 Input impedance associated to the radiating structure shown in Fig. 3.22 regarding one ground plane booster.

The BW_0 analysis (Fig. 3.24) regarding the theoretical enhancement factor (2.45 for $SWR=3$) of a broadband matching network topology demonstrates that the minimum ground plane booster size able of

providing operation in the low frequency region (824-960MHz) is 6 mm x 6 mm (Fig. 3.22), since it features at the central frequency of the low frequency region an inherent bandwidth around 8.3% regarding a $SWR \leq 3$ (Fig. 3.24a). Once the broadband matching network is applied, this inherent bandwidth can be increased by a theoretical factor around 2.45 (3.13), thus resulting in a potential bandwidth of 20.3%. This potential bandwidth becomes sufficient for covering the low frequency region (15.2%). Similarly, for the high frequency region (1710-2690MHz) (Fig. 3.25), a coplanar ground plane booster with dimensions 6 mm x 6 mm is capable of offering an inherent bandwidth around 29.5%, which results in a potential bandwidth of 72.3%. This bandwidth is larger than that required for covering the high frequency region (44.5%), thus suggesting that smaller ground plane booster dimensions could be used. Note that at this frequency region, the method just provides a qualitative vision since the input impedance presents a semi-loop (Fig. 3.23). However, for the sake of just validating the feasibility of the proposal, two coplanar ground plane boosters of 6 mm x 6 mm each one intended for a particular frequency region are selected. Due to their 2D profile, the ground plane boosters are called here as pads.

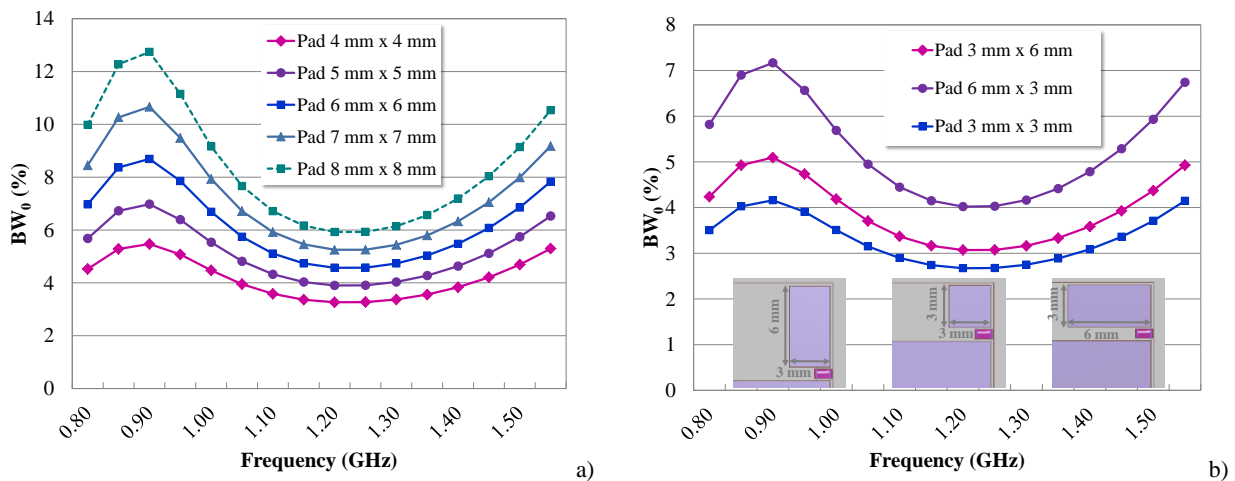


Fig. 3.24 BW_0 associated to a handset platform featuring dimensions of 120 mm x 50 mm as a function of the booster size regarding the low frequency region. a) comparison for several square-shaped pads; b) comparison for two pads having the same area but different orientation. A smaller pad is included also as a reference.

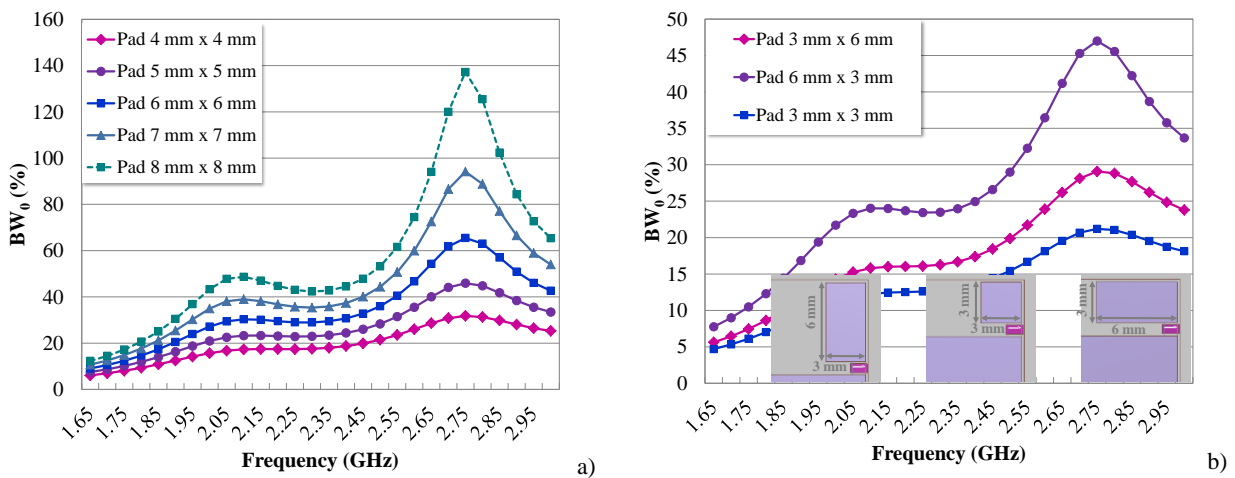


Fig. 3.25 BW_0 associated to a handset platform featuring dimensions of 120 mm x 50 mm as a function of the booster size regarding the high frequency region. a) comparison for several square-shaped pads; b) comparison for two pads having the same area but different orientation. A smaller pad is included also as a reference.

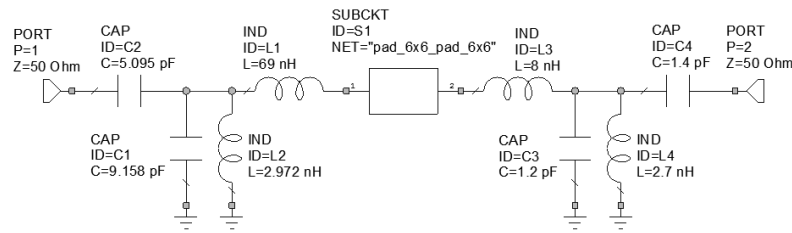


Fig. 3.26 Radiofrequency system proposed including two broadband matching networks (LC resonators) each one intended respectively for the low and high frequency regions. The series C is used to allocate the impedance loop at the center of the Smith chart.

It is worth to outline, that coplanar boosters having the same area do not affect equally to the radiation characteristics and particularly to the inherent bandwidth (Fig. 3.24b and Fig. 3.25b). The experiments carried out demonstrate that the larger the longitudinal dimension, the larger the attainable inherent bandwidth. This behavior could be compared with that featured by an asymmetrical dipole since as demonstrated in section 2.5, the Q of the dipole decreases insofar the feeding point approximates the center.

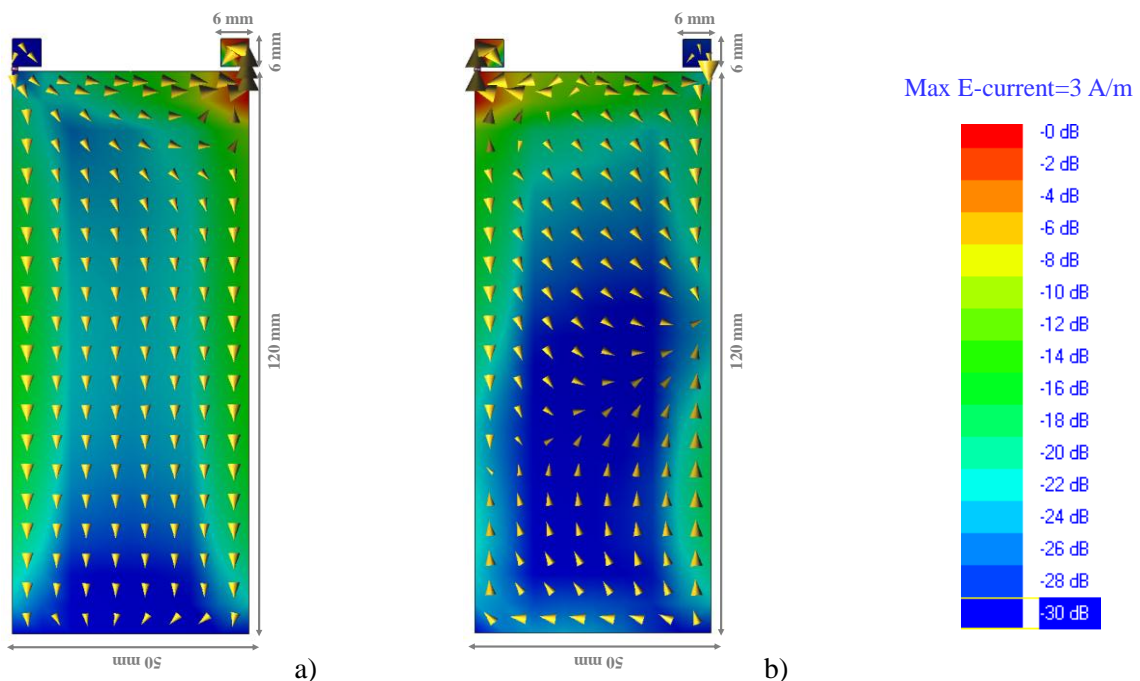


Fig. 3.27 a) Current distribution at $f=0.9\text{GHz}$ and b) at $f=2.2\text{GHz}$ when considering the proposed radiofrequency system depicted in Fig. 3.26.

As indicated above and in order to demonstrate the benefits of the proposal, two coplanar electric ground plane boosters having dimensions of just 6 mm x 6 mm are respectively placed at the corners of a transversal edge of the ground plane where maximums of electrical field take place (Fig. 3.27a-b). This configuration forms the two-port box structure associated to the radiating structure (Fig. 3.26). As previously discussed, broadband matching networks are selected to maximize the attainable bandwidth while minimizing not only the required matching network components but also undesired power losses (Fig. 3.26). In the low frequency region, the fundamental ground plane radiation mode having a half-

wavelength dipole type current distribution is excited (Fig. 3.27a), whereas in the high frequency region a higher order mode is attained (Fig. 3.27b). The proposed solution provides octo-band operation by satisfying the bandwidth requirements associated to the communication standards GSM850, GSM900, GSM1800, GSM1900, UMTS, LTE2100, LTE2300, LTE2500 (Fig. 3.28). Note that both ports are highly isolated attaining transmission coefficient values below -32 dB. According to the previous teachings they could also be combined into a single port through the addition of notch filters as those described in [24]. It should be pointed out that nowadays some wireless device architectures support two front end modules for each low and high frequency regions. Therefore, the present solution can be readily adopted into current wireless handheld devices.

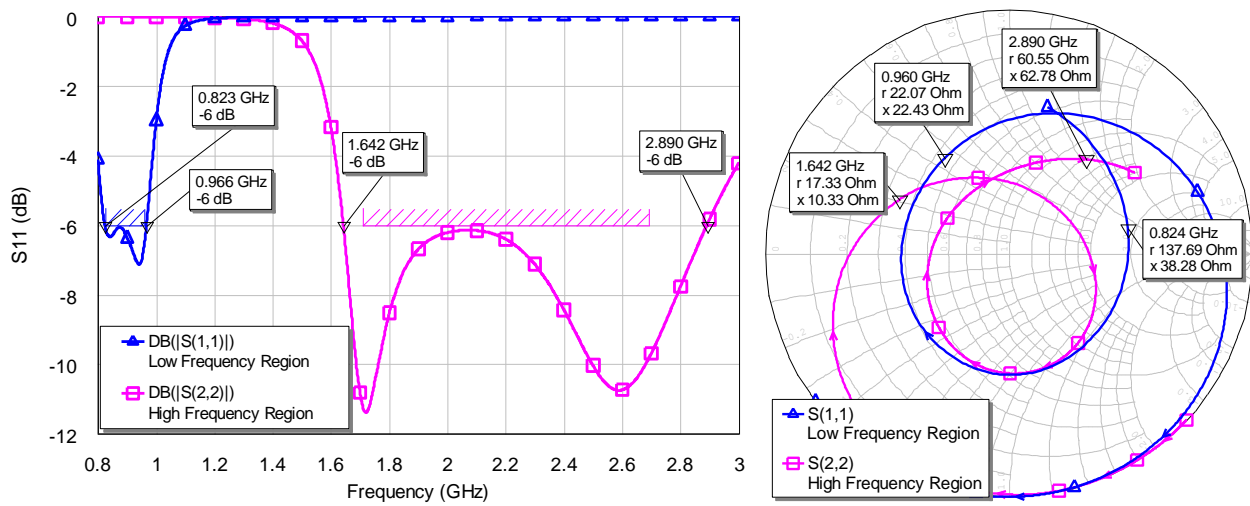


Fig. 3.28 Simulated reflection coefficient (S_{11}) and input impedance after the addition of the proposed radiofrequency system depicted in Fig. 3.26.

3.3.1.2. Measured Results

This section gathers the results obtained from a prototype built with the aim of validating the feasibility of the proposal. A ground plane featuring dimensions of 120 mm x 50 mm and two electric ground plane boosters of just 6 mm x 6 mm are etched over a 1 mm thick FR4 piece ($\epsilon_r=4.15$, $\tan\delta=0.013$) (Fig. 3.29). The implemented radiofrequency system comprises respectively for the low and high frequency region a reactance cancellation element (series inductor of 56nH, 6.8nH), a broadband matching network (shunt inductor of 2.9nH, 3.9nH and shunt capacitor of 9pF, 0.5pF), and a fine tuning stage (series capacitor of 5.1pF, 0.85pF) using the topology shown in Fig. 3.26. Measured results (Fig. 3.30 and Fig. 3.31) are significantly aligned with the simulated results (Fig. 3.28) since the frequency ranges for which the reflection coefficient remains below -6 dB's extend to the previously defined low and high frequency regions, hence allowing the operation of the radiating system in eight of the main communication standards (GSM850, GSM900, GSM1800, GSM1900, UMTS, LTE2100, LTE2300, LTE2500). In addition, the measured antenna efficiency using 3D pattern integration by means of the anechoic chamber Satimo Stargate-32, attains acceptable values of 47% and 61% in average in the low and high frequency region, respectively.

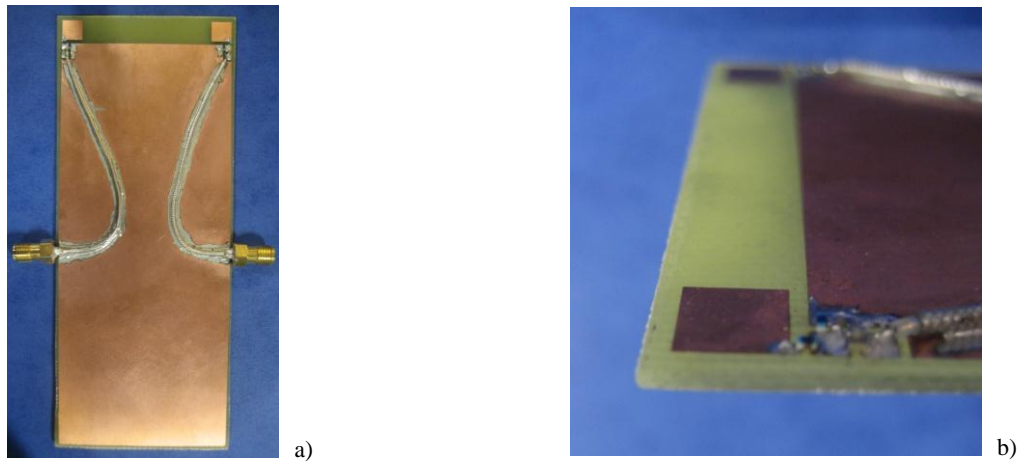


Fig. 3.29 a) Front-view of a radiating system comprising two coplanar ground plane boosters; b) Detailed view of the radiating system depicting the integration of the radiofrequency system described in Fig. 3.26.

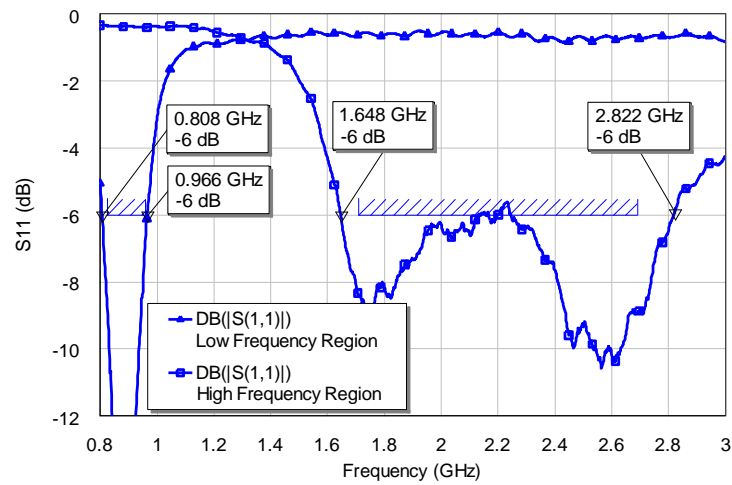


Fig. 3.30 Measured reflection coefficient (S_{11}) of the prototype depicted in Fig. 3.29.

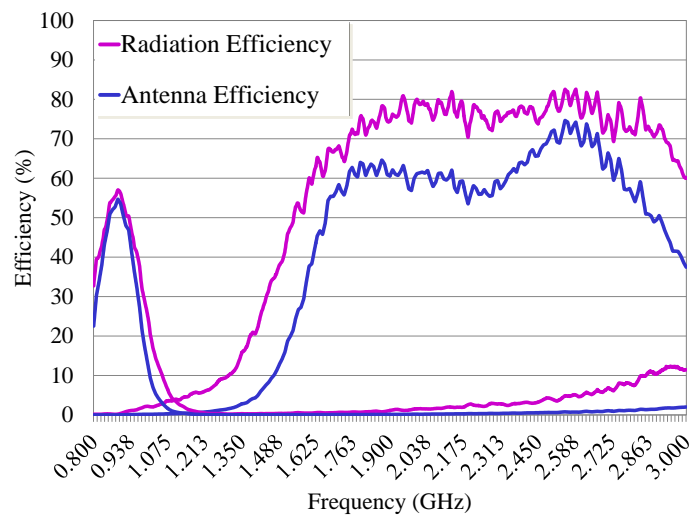


Fig. 3.31 Measured radiation (η_r) and antenna efficiency ($\eta_a = \eta_r \cdot (1 - |S_{11}|^2)$) of the prototype depicted in Fig. 3.29.

3.3.2 Nona-Band Solution

This section presents a radiating system based on the concepts previously exposed but capable of increasing the number of operating bands from seven to nine. In this case, the ground plane boosters are

distributed along the PCB and each one of them is intended for a particular frequency region in such a way that the proposed radiating system is capable of providing operation in nine frequency bands capable of allocating ten of the main mobile communication standards LTE700, GSM850, GSM900, GPS, GSM1800, GSM1900, UMTS, LTE2100, LTE2300, and LTE2500. For simplicity purposes, the pad terminology will be adopted herein to refer to the coplanar ground plane boosters.

3.3.2.1. Simulated Results

The radiating structure in this case, also comprises a ground plane representative of that associated to a smartphone device, i.e. the ground plane dimensions are 120 mm x 50 mm. Four coplanar ground plane boosters are arranged in the four corners of the ground plane where minimums of current distribution take place (Fig. 3.21). The size of each pad is designed according to the aforementioned rules of thumb as the one that allows covering the required bandwidth at each operating region. For this particular case, the mobile communication systems considered are LTE700, GSM850, GSM900, GPS, GSM1800, GSM1900, UMTS, LTE2100, LTE2300, and LTE2500 (Table 3.1).

As discussed, the size of the coplanar ground plane booster clearly conditions the performance of the radiating system, for instance in terms of inherent bandwidth (Fig. 3.24 and Fig. 3.25). With the aim of determining the required size to fulfill the bandwidth specifications in the low frequency region, a parametric analysis has been carried out. The potential candidates, two pads having dimensions of 12 mm x 6 mm and 6 mm x 6mm, respectively, are compared in terms of bandwidth at the low frequency region (Fig. 3.32). The inherent BW_0 computed from the input impedance [35] for a pad of 6 mm x 6 mm is approximately 8% at the center frequency of the low frequency region (900MHz). This BW_0 neither becomes sufficient to cover LTE700 nor to cover GSM850 and GSM900. However as previously suggested, the BW_0 can be enhanced in a factor around 2.45 regarding a $SWR \leq 3$ by the use of a broadband matching network consisting of an LC resonator (Fig. 3.32) [38].

Table 3.1 Frequency Bands and Bandwidths.

Mobile Communication Systems	f_1 (MHz)	f_2 (MHz)	f_0 (MHz)	BW (%)
LTE700	698	787	743	11.9
GSM850/GSM900	824	960	892	15.2
GPS	1563	1587	1575	1.5
GSM1800/GSM1900/UMTS/LTE2100/LTE2300/LTE2500	1710	2690	2200	44.5

Accordingly, the potential bandwidth increases up to approximately 20% at 900MHz, thus becoming enough to provide operation in the communication standards GSM850 and GSM900 but not for covering the emergent LTE700 system. In this sense, an additional larger pad is required to provide operation at this frequency band (LTE700 ($f_0=743$ MHz)). The simulated results demonstrate that to increase the size of the pad to 12 mm x 6mm would be sufficient for covering the bandwidth specifications of the LTE700 communication system. It should be pointed out that both, the pad of 12 mm x 6 mm and the pad of 6 mm x 6 mm present a resonant frequency of 3076MHz and 4244MHz, respectively. This resonant frequency is well above the resonant frequency of the eigenmode J_1 of the ground plane 120 mm x 50 mm which is located around 964MHz (section 2.3). Note that in this case the

FR4 dielectric piece where the ground plane is etched is taken into account when computing the resonant frequency. This condition satisfies the criteria disclosed in section 2.4.1.3, where was demonstrated that non-resonant elements stand out over resonant solutions.

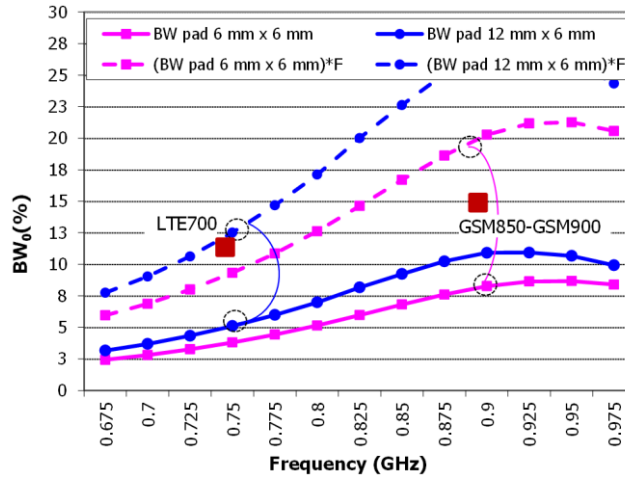


Fig. 3.32 BW_0 for a pad of 12 mm x 6 mm and a pad of 6 mm x 6mm on a ground plane of 120 mm x 50mm (solid line). The dashed line represents the potential bandwidth enhancement (BW_F) due to the broadband matching network. The square represents the required bandwidth at a given frequency band (see Table 3.1).

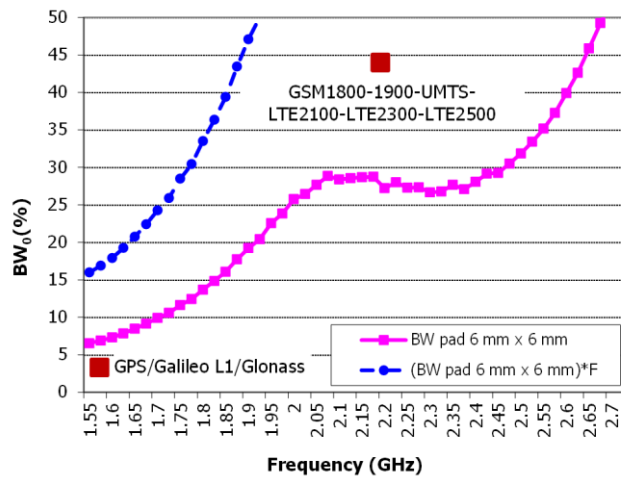


Fig. 3.33 BW_0 for a pad of 6 mm x 6 mm in a ground plane of 120 mm x 50 mm (square markers). The line with circular markers represents the potential bandwidth enhancement (BW_F) due to the broadband matching network. The square represents the required bandwidth at a given frequency band (Table 3.1).

For the high frequency region, a pad of 6 mm x 6mm presents a BW_0 of 8.8% at GPS (Fig. 3.33), which is well above the required specifications. Therefore, this element is reduced in size down to 3 mm x 3mm. In relation to GSM1800, GSM1900, UMTS, LTE2100, LTE2300, and LTE2500, a pad of 6 mm x 6mm presents a BW_0 around 30% at 2200MHz (the central frequency of the frequency region between 1710-2690MHz). When this BW_0 is multiplied by the enhancement factor of the broadband matching network ($F=2.45$), the resulting bandwidth ($30\% \cdot 2.45=73.5\% > 44.5\%$, Table 3.1) is large enough for covering the frequency range allocating the aforementioned communication standards. (Fig. 3.33). It is worth to outline that a pad of 6 mm x 6mm in a dipole configuration such as in Fig. 2.24 has a $Q=141$ and $Q=50$ for $f=900\text{MHz}$ and $f=2200\text{MHz}$, respectively, meaning that the pad itself has a high- Q when the ground plane is not considered. This high- Q is not enough for covering any of the communication

standards depicted in Table 3.1. Therefore the pad cannot be considered an antenna but a ground plane booster intended for transfer energy to the ground plane.

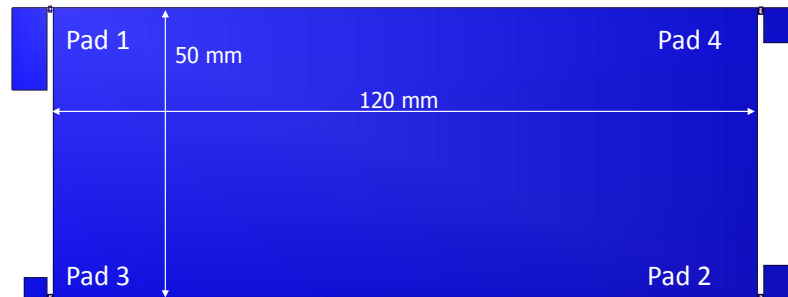


Fig. 3.34 Architecture of the proposed small, multi-band, and planar radiating structure, comprising four pads placed at the corners of a ground plane of 120 mm x 50 mm etched on a thin layer of FR4 having 1mm thick, $\epsilon_r=4.15$, $\tan\delta=0.013$. Pad 1 is designed for LTE700; pad 2 for GSM850 and GSM900; pad 3 for GPS; and pad 4 for GSM1800 up to LTE2500. The distance between the pad and the transversal edge of the ground plane is 1mm. The total area occupied by the pads is only 153mm².

Once the geometry and dimension have been determined, the proposed radiating system comprises one pad for each set of communication standards (Table 3.1), i.e. four pads are used to provide operation in LTE700, GSM850/GSM900, GPS, and GSM1800/GSM1900/LTE2100/2300/2500, respectively. They are strategically arranged at the corners of the ground plane (Fig. 3.34). Since LTE700 and GSM850/GSM900 are close in frequency, the pad for LTE700 (pad 1) is located in an opposite corner with respect to the pad for GSM850/GSM900 (pad 2) in order to obtain high isolation.

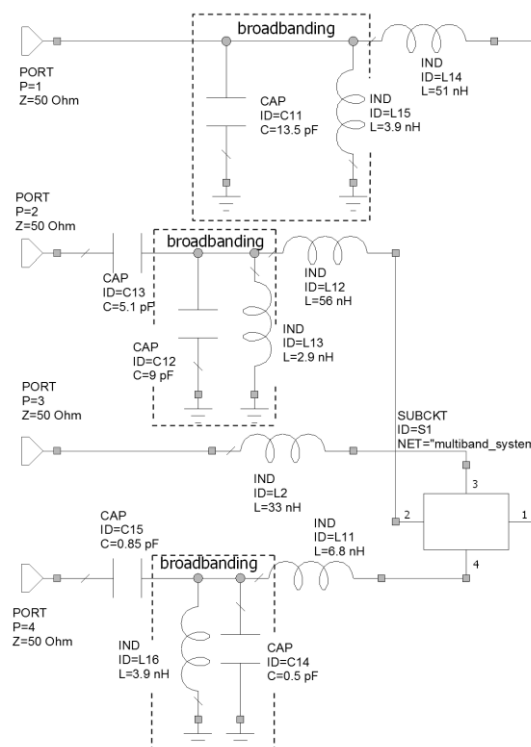


Fig. 3.35 Radiofrequency system selected for the radiating structure of Fig. 3.34. Port 1, 2, 3, and 4 correspond to LTE700, GSM850/GSM900, GPS, and GSM1800/GSM1900/UMTS/LTE2300/LTE2500, respectively. Port 1, 2 and 4 includes broadband matching networks whereas port 3 (GPS) include a single series component. The values shown are those selected for the built prototype.

As previously discussed, a broadband matching network is required for all the pads except for the GPS pad (Fig. 3.35 and Fig. 3.36). The results demonstrate the effectiveness of the proposed systematic design, since the bandwidth predictions are aligned with the results obtained after the addition of the broadband matching network (Fig. 3.36b). The isolation between ports has been computed showing that the worst case presents an isolation of 10.9dB between the LTE700 and GSM850/900 ports.

Finally, current distribution is computed for several representative frequencies across the operating bands (Fig. 3.37). The outcomes confirm again the results of the former sections. In particular, for the low frequency region (690-960MHz) the fundamental mode is excited which corresponds to an almost linear current distribution aligned with the longitudinal edges of the ground plane. In the high frequency region (1710-2690MHz), higher order modes appear. It is important to emphasize that in this kind of radiating systems where the ground plane is the main contributor, the radiation patterns are mainly determined by the current distribution of the wave modes of the ground plane and they are not influenced by the non-resonant elements used to excite these wave modes. This fact reinforces again the perspective that the ground plane boosters presented herein should not be considered antennas.

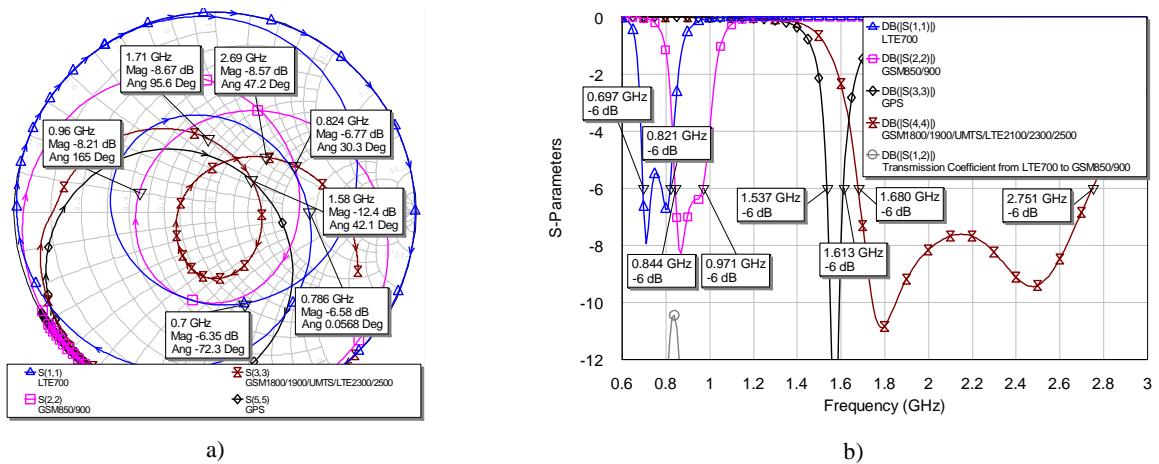


Fig. 3.36 a) Simulated input impedance for all the ports showing the input impedance loops due to the addition of a broadband matching network (Fig. 3.35), except for the GPS pad, which only requires a single series reactive element; b) Simulated S-parameters for the proposed radiating system (Fig. 3.35).

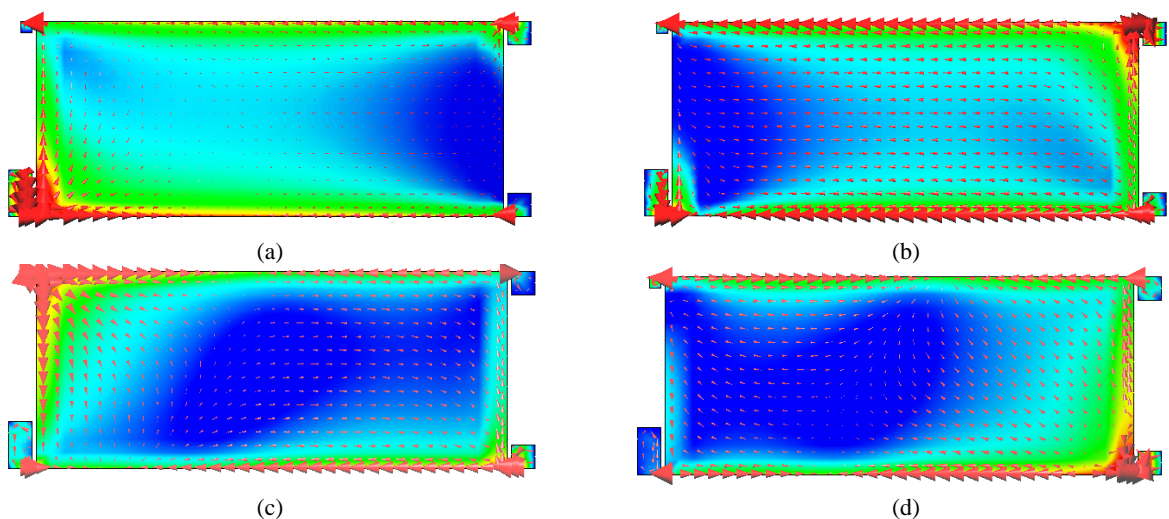


Fig. 3.37 Computed surface current distributions at several frequencies. a) $f=750\text{MHz}$ port 1 excited; b) $f=950\text{MHz}$ port 2 excited; c) $f=1575\text{MHz}$ port 3 excited; d) $f=2200\text{MHz}$ port 4 excited. Each pad is connected to the matching network illustrated in Fig. 3.35.

3.3.2.2. Measured Results

A prototype is built for the sake of validating the simulation analysis (Fig. 3.38). As described above, a broadband matching network is connected to the three pads intended for mobile communication services whereas for the GPS pad just a single inductor is required (Fig. 3.35).

The measured results (Fig. 3.39) are aligned with those obtained by simulation (Fig. 3.36). In particular, the measured reflection coefficient demonstrates that the proposed configuration allows the operation of the radiating system in the frequency ranges listed in Table 3.1 with a $SWR \leq 3$ (Fig. 3.39). The isolation between ports shows that the worst case is above 18.5dB ensuring low coupling among them (Table 3.2). At the same time, antenna efficiency has been measured in the anechoic chamber Satimo Stargate-32 by integration of the 3D radiation pattern (Fig. 3.40). For these measurements, 50Ω loads are connected to each one of the ports not under test. It is worth noting that each pad can be connected to a different front-end-module (FEM) in charge of providing operation in a given number of bands. The use of this FEMs is widely spread in the commercial mobile phones.

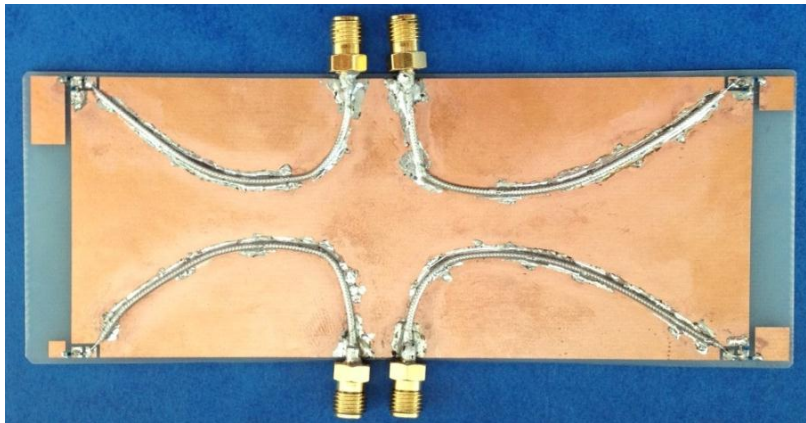


Fig. 3.38 Prototype using the four proposed pad elements. The ground plane and the pads are etched over a 1 mm thick FR4 piece.

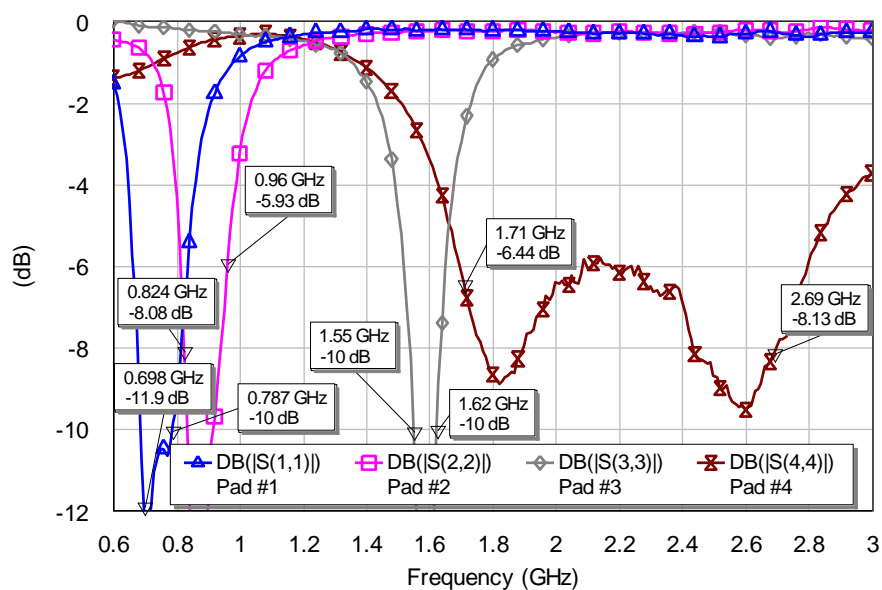
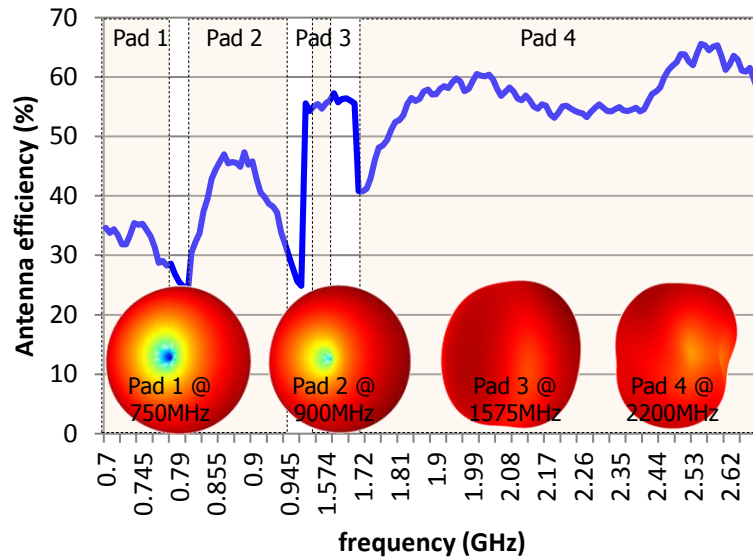


Fig. 3.39 Measured reflection coefficient for the prototype of Fig. 3.38.

Table 3.2 Measured isolation between bands. Worst value is shown.

Isolation (dB)	LTE700	GSM850-900	GPS	GSM1800-LTE2500
LTE700	-	18.5	31.9	42.6
GSM850-900	18.5	-	28.4	40.3
GPS	31.9	28.4	-	21.8

Antenna efficiency is moderate for the low frequency region but still acceptable for mobile communications [40]-[43]. It should be pointed out that pad 1 and pad 2 are operating below the resonant frequency of the eigenmode J_1 , which is 964MHz. For larger smartphones as those nowadays appearing in the market, the resonant frequency of the eigenmode J_1 will be close the operating frequencies, hence enhancing the antenna efficiency. This fact is clearly observed in pad 3 which attains an antenna efficiency of 58% at 1575MHz with a pad of only 3 mm x 3mm. It becomes the smallest known GPS antenna with such antenna efficiency values. For pad 4, the efficiencies are even higher despite its considerable small dimensions (0.034λ at 1710MHz), thus emphasizing again that pad elements are just ground plane boosters that effectively excite the ground plane radiation modes. Measured radiation patterns presents omni-directionality with similar measured directivities $D(750\text{MHz})=2.8\text{dB}$, $D(900\text{MHz})=2.7\text{dB}$, $D(1757\text{MHz})=1.9\text{dB}$, $D(1800\text{MHz})=4.5\text{dB}$, $D(2200\text{MHz})=3.8\text{dB}$, $D(2600\text{MHz})=3.8\text{dB}$ (Fig. 3.40).

Fig. 3.40 Measured antenna efficiency η_a ($\eta_a = \eta_r \cdot (1 - |S_{11}|^2)$) and radiation patterns for the prototype of Fig. 3.38.

3.4. Coplanar Ground Plane Boosters: Inductive Elements

The previous section, substitutes the volumetric ground plane boosters introduced in section 3.2 by coplanar ground plane boosters with the aim of providing an ultra-slim booster-based antenna technology. Both solutions, demonstrate the feasibility of the initial proposal of this thesis that is focused on removing the need of including large resonant antenna elements to provide multi-band operation. Nevertheless, the previous solutions are only based on capacitive ground plane boosters. In contrast, this section is focused on analyzing the performance of inductive ground plane boosters. Note that in the context of this thesis, a capacitive element is defined as a ground plane booster that presents capacitive input impedance within

the frequency range associated to the frequency regions of operation. In contrast, inductive elements are classified as those ground plane boosters whose input impedance is predominantly inductive in the frequency regions of operation. In some situations, the capacitive and inductive ground plane boosters can also be called electric and magnetic boosters, respectively. This nomenclature has to do with the way the elements couple energy to the ground plane, through the electric fields in the first case, and through the magnetic fields in the second one.

So far and as introduced in former sections, the most common designs of handset antennas can be roughly classified in two categories according to the arrangement of the antenna with respect to the ground plane. Thus, internal antennas can be arranged over a ground plane (e.g. PIFA (Planar Inverted F Antenna) and patch antenna) [1] or in a ground plane clearance (e.g. monopoles and slots). PIFA and patch antennas require a certain volume and particularly a certain height for providing acceptable performance whereas monopoles and slots need a certain dedicated PCB area also known as clearance area [3]-[5]. Regarding slot antennas, several studies have proposed the integration of said antenna elements in handsets as being compact and coplanar solutions particularly suitable for ultra-slim platforms [49]-[66]. Thus, [49] presents a slot antenna with two closed ends operating as a half-wavelength resonant structure. However, this sort of structures still occupy a considerable PCB area (45 mm x 21 mm) and are not proper for current handsets demanding more and more available PCB space to integrate not only multiple components but also a large number of antenna elements capable of improving functionalities and performance. More compact slot antenna solutions are proposed in [50]-[58]. Nevertheless, these solutions are still quarter wavelength resonators that require a considerable PCB area and despite the large bandwidth attained, they are not able of providing operability in the low frequency region, where common communication standards such as GSM850 and GSM900 are allocated. In other situations, slot antennas are used for enhancing the electromagnetic performance of a particular radiating system and in these cases they are combined with other type of antenna elements [9]-[16], [59]. Further solutions based on quarter-wavelength resonant slot antennas use the characteristic modes theory to improve their electromagnetic behavior [60]. Nevertheless, all the aforementioned techniques are still based on structures having dimensions comparable to a half of a wavelength or a quarter of a wavelength. This fact leads to large antenna elements when operation in the low frequency region is demanded. In order to overcome these shortcomings, recent research is focused on exciting the ground plane radiating modes since several studies have demonstrated its relevance in the radiation process [6]-[21]. Namely, most of them demonstrate that it is possible to provide multi-band operation through this ground plane excitation in such a way that no additional radiating elements are required [19]-[29]. In fact, the research deeply explained in former sections reveals that the inherent ground plane of any handset platform can be used integrally as main radiator, thus removing the need of including additional antenna elements. Thus and contrarily to what was thought so far, the efforts of the antenna engineers should not only concentrate on an antenna element but on the ground plane as for attaining the desired efficient radiation modes. For instance, the resonance of the fundamental mode of the typical ground plane of a handset platform can be

tuned to low or high frequencies by properly modifying its electrical length through the addition of slots or conductive strips [9]-[18]. In this new frame, the most relevant elements besides the ground plane are the elements used to excite it, since its size, nature and placement clearly condition the performance of the whole radiating system [22]-[24], [27]-[29]. In this sense, electric ground plane boosters, such as the ones described in sections 3.2 and 3.3 must be arranged in the corners of the shorter edge of the ground plane where maximums of electric field take place. Note, that the current distribution of the ground plane mode to be excited will condition the proper placement of the ground plane boosters.

This section proposes the excitation of the effective dipole type ground plane radiation mode through the use of small magnetic ground plane boosters placed at the center of said ground plane. This arrangement is particularly suitable for magnetic boosters since the ground plane fundamental mode presents a maximum of current distribution at this location (Fig. 3.21). The proposed arrangement is consistent with other kind of radiators such as dielectric antennas [67]. For those antennas, a mode inside the dielectric cavity having a maximum of electric field in a certain location can be excited by placing an electric probe at that location. On the contrary, if the mode has a maximum of magnetic field at a certain location, a magnetic probe can excite such mode by placing the probe at said location [67]. A similar situation occurs in this case, the magnetic booster effectively excites the fundamental radiating mode of the ground plane when said magnetic ground plane booster is located in a position having maximum magnetic field, which in the case of handsets coincides with the center portion of the longitudinal edges. Other solutions based on half-wavelength or quarter-wavelength resonant slots are not desirable to be placed at the center of the PCB since they make difficult the signal line routing of the PCB layout. However, the present proposal allows simplifying the line routing as well as the integration of other handset components such as big displays due to the reduced electrical dimensions of the magnetic boosters. In addition, the interaction with other components is also minimized. In this sense, the present section proposes the use of inductive non-resonant ground plane boosters capable of effectively exciting the dipole type ground plane radiating mode without requiring a considerable dedicated PCB area and without affecting significantly the complexity of the PCB layout. As well as in the previous cases, the radiofrequency system is based on broadband mechanisms capable of making the solution useful for covering the main communication standards GSM850, GSM900, GSM1800, GSM1900, and UMTS.

The section is structured in the following manner: firstly, the characteristic modes theory as a base of this study is briefly reminded. Subsequently, the radiating system is evaluated through simulations using the software IE3D based on MoM. Electrical models as well as matching network designs are also presented along section 3.4.1. Simulated results as well as measured results are presented in section 3.4.2 and section 3.4.3, respectively.

3.4.1 Theoretical Background and Concept Definition

The characteristic modes theory has been deeply analyzed in the literature and provides a significant physical insight into the radiation process of a particular conducting structure [30]-[32]. The

studies demonstrate that the radiating and non-radiating modes that a particular structure could support can be determined by just knowing the shape and size of said conducting structure. Particularly, a ground plane with dimensions 100 mm x 40 mm, which represents the typical dimensions of a bar type handset, presents a main radiating mode at mobile frequencies that features a longitudinal current distribution having a maximum at the center of the longest edges of the ground plane (Fig. 3.1) [24]. Then, the challenge lies in taking full advantage of the radiating properties associated to such efficient ground plane radiating mode. As discussed above, the efficient ground plane radiating mode appearing at mobile frequencies presents a current distribution similar to that produced by a half-wavelength dipole, i.e. featuring a maximum at the center of the longitudinal edges of the ground plane and a minimum in its transversal edges (Fig. 3.1). The knowledge of the current distribution associated to a particular radiating mode becomes an important aspect since it allows determining the proper placement of the corresponding ground plane boosters as a function of their nature. The ground plane radiating mode can be excited either via the magnetic or the electric fields. In order to take full advantage, electric boosters must be placed near the electric field maximum of the ground plane radiating mode whereas magnetic boosters must be placed near the magnetic field maximum [22]-[24], [27]-[29]. Said location guarantees the alignment of the electric or magnetic fields of the ground plane booster with the electric and magnetic fields of the ground plane radiating mode, respectively, fact that ensures an effective excitation. The relevance of the proper placement of the ground plane boosters for providing suitable performance will be demonstrated in the following sections.

3.4.1.1. On the location of Magnetic Boosters

The previous sections demonstrate the existence of an efficient ground plane radiating mode at mobile frequencies.

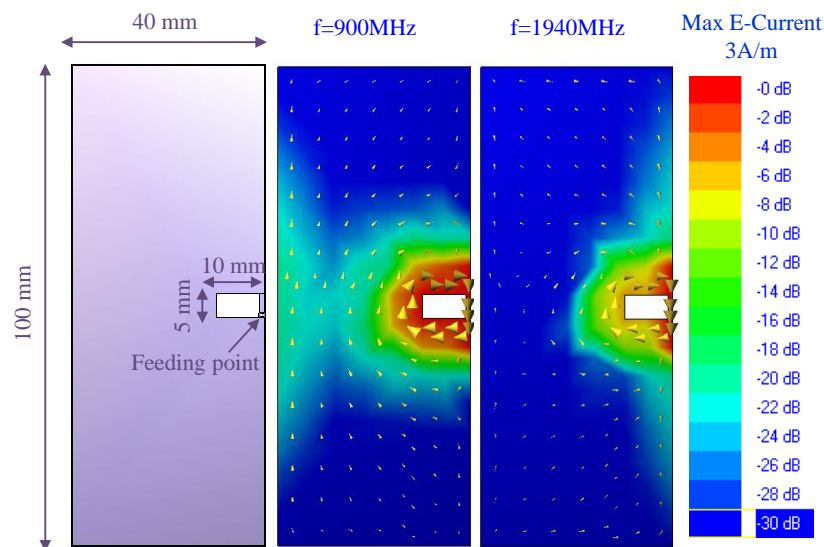


Fig. 3.41 Geometry and dimensions associated to the radiating structure comprising a magnetic booster located at the center of the longitudinal edge of the ground plane. Current distribution referred to the excited ground plane radiating mode at $f=900\text{MHz}$ and $f=1940\text{MHz}$. The ground plane is etched over a 1mm thickness FR4 piece ($\epsilon_r=4.15$ and $\tan\delta=0.013$).

However, the challenge lies in exciting said efficient ground plane radiating mode, which according to the present study strongly depends on several factors such as the nature, the placement, and the radiating properties associated to the element used for transferring energy to the ground plane.

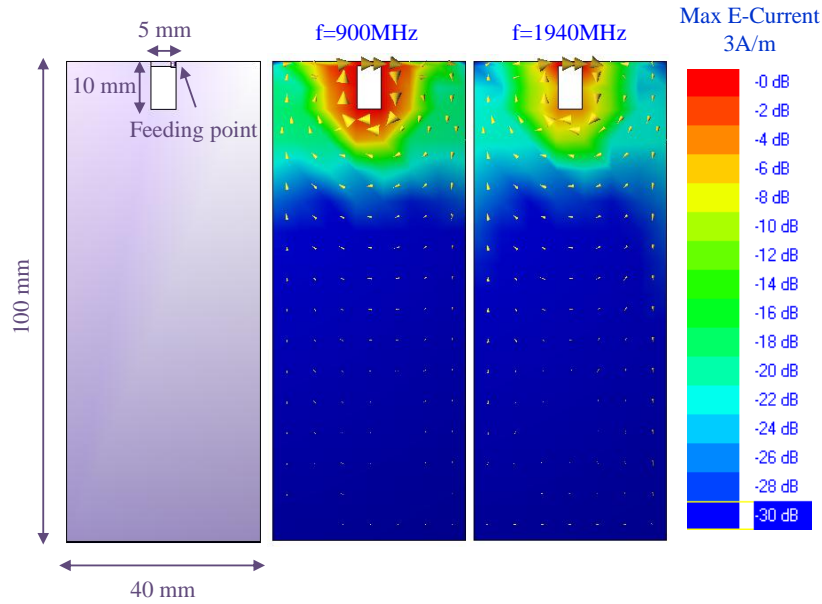


Fig. 3.42 Geometry and dimensions associated to the radiating structure comprising a magnetic booster located at the center of the transversal edge of the ground plane. Current distribution referred to the excited ground plane radiating mode at $f=900\text{MHz}$ and $f=1940\text{MHz}$. The ground plane is etched over a 1mm thickness FR4 piece ($\epsilon_r=4.15$ and $\tan\delta=0.013$).

This section proposes the use of magnetic boosters featuring extremely poor stand-alone radiation properties to properly excite the fundamental mode of a ground plane featuring dimensions of 100 mm x 40 mm, which corresponds with the typical dimensions associated with a bar-type handset phone. As aforementioned, the nature, size, and placement of the ground plane boosters play an important role in effectively exciting the ground plane radiating mode.

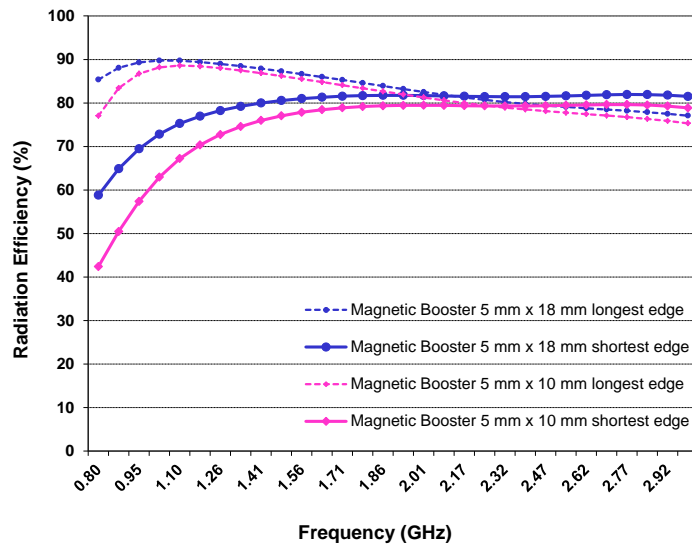


Fig. 3.43 Effect of the size and the arrangement of the magnetic booster over the radiation efficiency (η_r) of the radiating structure.

Accordingly, when the magnetic boosters are arranged in the center of the longitudinal edge of the ground plane, the fundamental mode is better excited since the current distribution appears stronger along

the longitudinal edge (Fig. 3.41). However, this same magnetic booster placed in the center of the transversal edge of the ground plane does not attain as good excitation since in this case the current concentrates in the vicinity of the magnetic booster rather than along the longitudinal edge (Fig. 3.42). This effect is further appreciated through the radiation efficiency (Fig. 3.43). While the first arrangement (Fig. 3.41) provides radiation efficiency values around 80%-90% for the whole frequency range (0.8-3GHz), the second one (Fig. 3.42) diminishes the attainable radiation efficiency more significantly in the low frequency region where the ground plane radiating mode excitation is critical for a suitable performance.

Nevertheless, the proper excitation of the ground plane radiating mode does not ensure operation at mobile frequencies, since to provide operation, acceptable input impedance levels are required. In this sense, the following subsection is focused on computing the Q of the proposed radiating structures in order to assess their potential performance in terms of impedance bandwidth.

3.4.1.2. Electrical Model and Matching Network Design

Contrary to what happened with the previous solutions based on electric boosters (Sections 3.2 and 3.3), the proposed radiating structure presents an input impedance comparable to that provided by a non-resonant RL series circuit. Thus, its input impedance features a significant inductive behavior for the whole frequency range of interest (0.8-3GHz). The Q of the radiating structure and its BW_0 can be calculated from its input impedance according to equations (3.1) and (3.2) derived in [35], where S is a particular value of SWR .

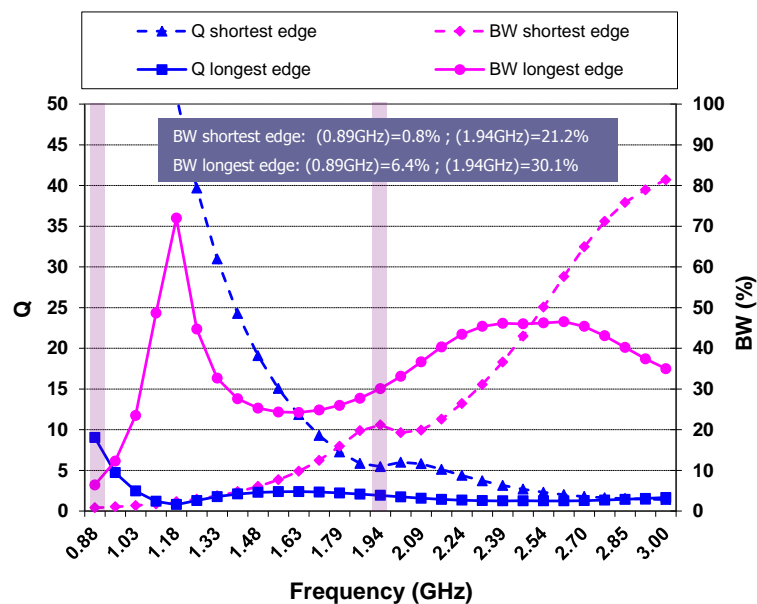


Fig. 3.44 Q and BW_0 versus frequency referred to the radiating structure comprising a magnetic booster with dimensions 5 mm x 18 mm as a function of their placement with respect to a ground plane with dimensions 100 mm x 40 mm.

Once more, the influence of the arrangement of the ground plane booster over the electromagnetic performance becomes apparent in view of Q and BW_0 (Fig. 3.44 and Fig. 3.45). When the magnetic booster is placed in the center of the shortest edge of the ground plane, BW_0 considerably decreases, more

significantly in the low frequency region. However, not only the arrangement of the magnetic booster strongly influences the performance, but also the size of the magnetic booster modifies the input impedance of the radiating structure and consequently the attainable BW_0 (Fig. 3.44 and Fig. 3.45). Namely, a magnetic booster with dimensions of 5 mm x 18 mm and regarding the low frequency region features a BW_0 of 6.4% when placed at the center of the longest edge, whereas its BW_0 is considerably reduced down to 0.8% when it is arranged at the center of the shortest edge. Similar effects are appreciated when a magnetic booster with a reduced size of 5 mm x 10 mm is considered. In order to assess if a particular radiating structure will be able to provide operation in a particular frequency region, the systematic analysis already introduced in the previous section is proposed. Once the attainable BW_0 is known (Fig. 3.44 and Fig. 3.45), the potential bandwidth (BW_f) provided by a broadband matching network can be computed following the methods presented in section 3.2.2.2.

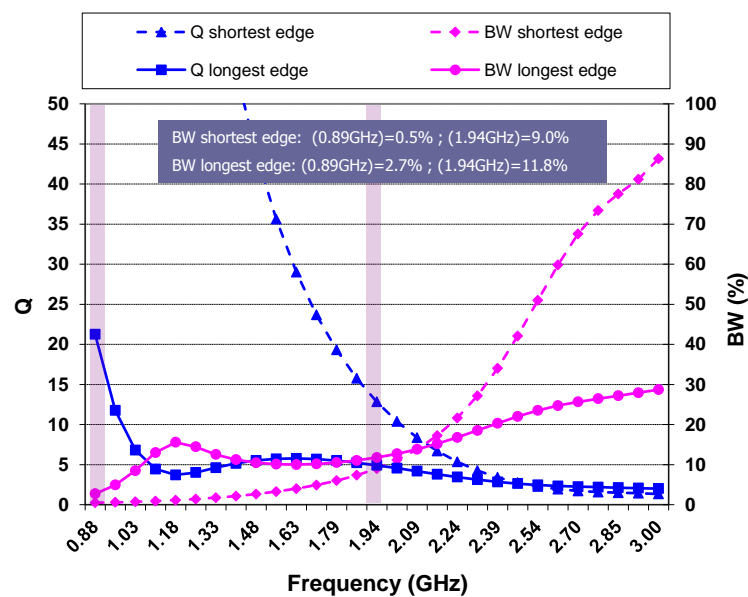


Fig. 3.45 Q and BW_0 versus frequency referred to the radiating structure comprising a magnetic booster with dimensions 5 mm x 10 mm as a function of their placement with respect to a ground plane with dimensions 100 mm x 40 mm.

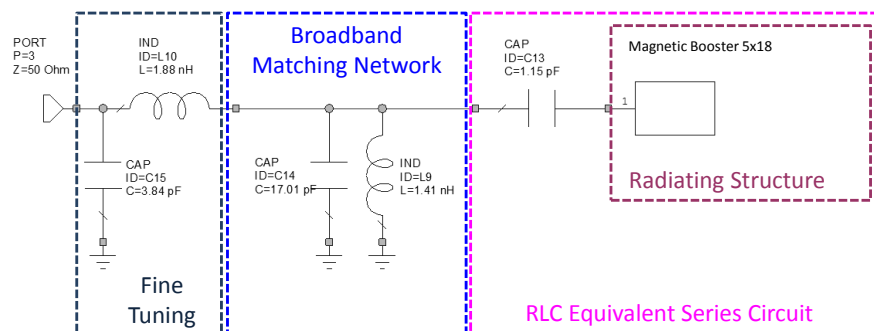


Fig. 3.46 Radiofrequency system including a reactance compensation and a broadband matching network for the low frequency region. The one-port box corresponds to the simulated impedance of the radiating structure comprising a magnetic booster of 5 mm x 18 mm placed in the center of the longest edge of the PCB (100mm x 40mm).

As demonstrated, this technique allows broadening the bandwidth around one half of Fano's limit [36], which translates into an enhancement factor of 2.45 regarding a $SWR=3$. Thus, by knowing the BW_0 and the enhancement factor it is possible to determine the capabilities of a particular radiating structure

without the need of requiring trial and error methods. The application of this systematic analysis reveals that the two proposed radiating structures (Fig. 3.44 and Fig. 3.45) will be able, after the addition of a broadband matching network, to provide operation separately in both low (824-960MHz) and high (1710-2170MHz) frequency regions comprising the communication standards GSM850, GSM900, GSM1800, GSM1900, and UMTS. More particularly, a magnetic booster having dimensions of 5 mm x 18 mm presents a BW_0 at 0.89GHz of 6.4% (Fig. 3.44) which is enhanced approximately 2.45 times by adding a broadband matching network resulting in a BW_f of 15.6% capable of covering the communication standards GSM850 and GSM900. Similarly, a magnetic booster having dimensions of 5 mm x 10 mm presents a BW_0 at 1.94GHz of 11.8% (Fig. 3.45) which is enhanced approximately 2.45 times by adding a broadband matching network resulting in a BW_f of 28.9% capable of covering the communication standards GSM1800, GSM1900, and UMTS.

In this case, the proposed matching network comprises in a first stage a series capacitor rather than a series inductor as required in [38]. The series capacitor is in charge of not only compensating the inductance of the input impedance but also of attaining an impedance locus similar to that produced by an RLC series circuit. Said impedance locus is required to accomplish the conditions forced by the broadband matching network method, which are described in further detail in section 3.2.2.2. The broadband matching network creates an impedance loop that can be inscribed in the circle of $SWR=3$ resulting in an enhanced bandwidth. In some situations, a fine tuning network is needed to allocate such loop inside said circle. Practical details are presented in the following section.

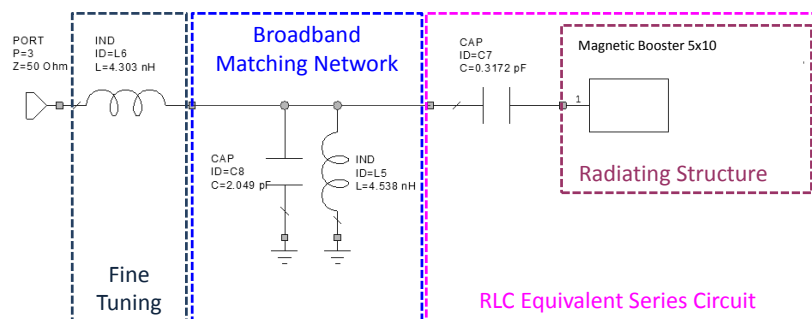


Fig. 3.47 Radiofrequency system including reactance compensation and broadband matching network for the high frequency region. The one-port box corresponds to the simulated impedance of the radiating structure comprising a magnetic booster of 5 mm x 10 mm placed in the center of the longest edge of the PCB (100mm x 40mm).

3.4.2 Simulated Results

The former section presented a systematic analysis to determine the inherent BW_0 of a particular radiating structure as a function of its input impedance. At the same time the potential BW_f when adding a broadband matching network can be directly estimated by knowing the theoretical enhancement factor without the need of testing multiple matching network topologies. The proposed matching networks for the low and high frequency regions (Fig. 3.46 and Fig. 3.47) comprise three stages, respectively. The first one is intended for compensating the reactance of the input impedance associated to the center frequency of the frequency region of operation. The broadband matching network provides an impedance loop in the Smith chart having smaller dimensions than the reference circle of $SWR=3$. Finally, the fine tuning stage

allows inscribing said impedance loop in the circle of $SWR=3$ (Fig. 3.48). As aforementioned, a radiating structure comprising a magnetic ground plane booster featuring dimensions 5 mm x 18 mm and located at the center of the longest edge of the ground plane presents a BW_0 of 6.4% (Fig. 3.44), which becomes insufficient for covering the communication standards GSM850 and GSM900, which demand a bandwidth of approximately 15.2%. The addition of the proposed broadband matching network results in a bandwidth around 16.4%, which translates into an enhancement factor of 2.56^4 close to the theoretical value. The enhanced bandwidth allows the operation of the radiating system in the communication standards GSM850 and GSM900 (Fig. 3.49).

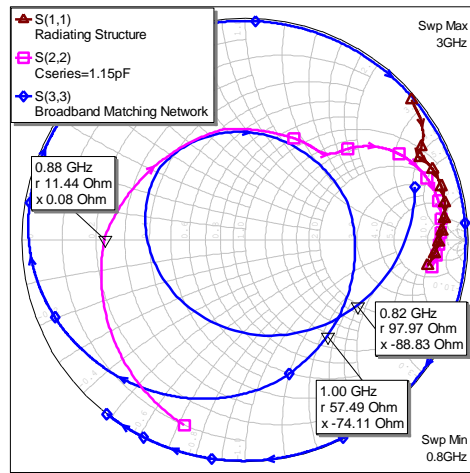


Fig. 3.48 Impedance associated to the radiating structure comprising a magnetic booster of 5 mm x 18 mm (triangular markers); Impedance after the addition of the series capacitor as a reactance compensation element for the low frequency region (square markers); Impedance attained through the radiofrequency system shown in Fig. 3.46 (rhombus markers).

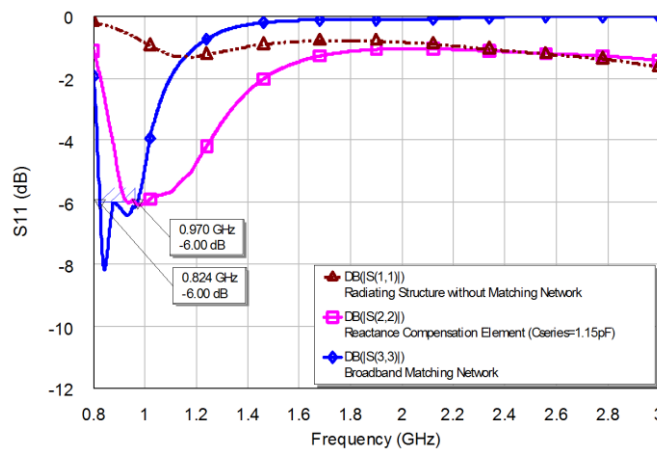


Fig. 3.49 Reflection coefficient associated to the radiating structure (dashed line); Reflection coefficient regarding the addition of the reactance compensation element (solid line with square markers); Reflection coefficient associated to the radiofrequency system shown in Fig. 3.46 designed for covering the low frequency region (solid line with rhombus markers).

A similar matching network design is proposed for the high frequency region (Fig. 3.47). The movements in the Smith chart produced by the different stages are equivalent to those already presented for the low frequency region (Fig. 3.50). In this case, the same radiating structure as that used for the low

⁴ This value exceeds the theoretical BW enhancement factor. The explanation resides in the nature of the input impedance curve which can be only approximated to an RLC series circuit for a limited range of frequencies. Therefore, the enhancement factor holds as long as the input impedance is equal to a series RLC circuit. In other cases, as the one shown here, the enhancement factor can exceed the theoretical one.

frequency region could be used since it presents an inherent BW_0 around 30.1% (Fig. 3.44) for the high frequency region. However, the object is focused on providing the solution that attains the maximum performance regarding the minimum possible size. In this sense, the magnetic booster of dimensions 5 mm x 18 mm implemented for the low frequency region has been replaced by a magnetic ground plane booster featuring dimensions of just 5 mm x 10 mm as being the option that guarantees a trade-off between performance and size.

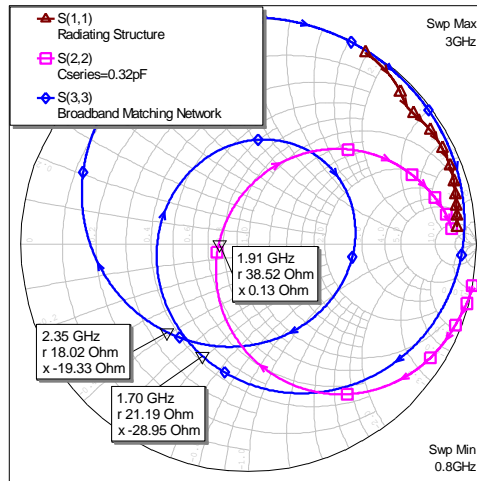


Fig. 3.50 Impedance associated to the radiating structure (triangular markers); Impedance after the addition of the series capacitor as a reactance compensation element for the high frequency region (square markers); Impedance attained through the radiofrequency system shown in Fig. 3.47 (rhombus markers).

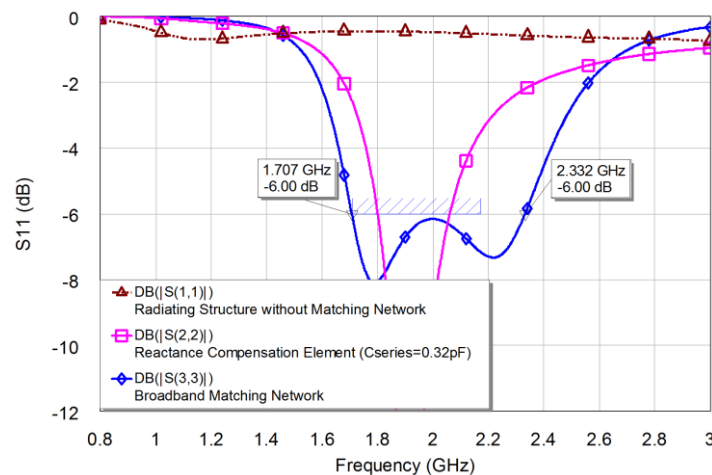


Fig. 3.51 Reflection coefficient associated to the radiating structure (dashed line); Reflection coefficient regarding the addition of the reactance compensation element (solid line with square markers); Reflection coefficient associated to the radiofrequency system shown in Fig. 3.47 designed for covering the high frequency region (solid line with rhombus markers).

Again, the influence of the magnetic ground plane booster size over the electromagnetic performance of the radiating system is stressed. In this case, the radiating structure performs an inherent BW_0 of 11.8% (Fig. 3.45), whereas the radiating system including the proposed matching network (Fig. 3.47) attains an enhanced bandwidth of 30.7% (Fig. 3.51). Simulated results are aligned with the theory since said bandwidth enhancement corresponds to a factor around 2.60, which is close to the theoretical value of 2.45. The results demonstrate that the ground plane radiating mode can be effectively excited through magnetic boosters featuring considerable reduced dimensions. The solutions proposed are not

only able of covering the bandwidth demanded by the main communication standards (GSM850, GSM900, GSM1800, GSM1900, and UMTS), but also of presenting high antenna efficiency between 60-70% (Fig. 3.52) for both frequency regions. It is important to remark that the electrical length of the magnetic boosters is just 0.05λ and 0.06λ for the low and high frequency region, respectively, which supposes a significant size reduction in a factor around five with respect to the previous solutions based on 0.25λ or even 0.5λ .

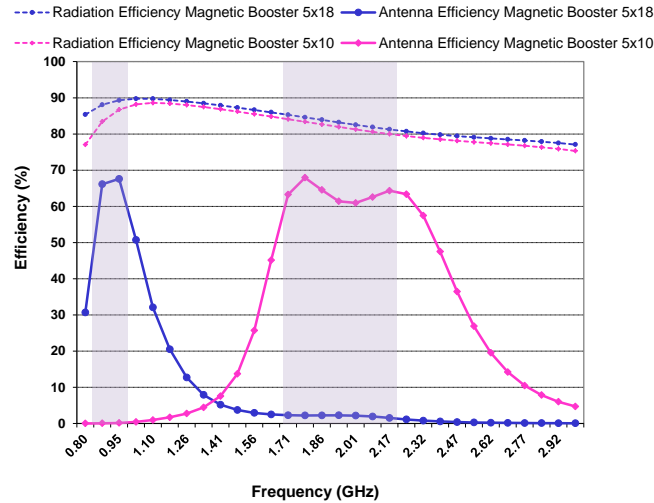


Fig. 3.52 Radiation efficiency (η_r) associated to the proposed radiating structures and antenna efficiency (η_a) referred to the radiating systems presented in Fig. 3.46 and Fig. 3.47. The antenna efficiency takes into account the matching losses since it is defined as $\eta_a = \eta_r \cdot (1 - |S_{11}|^2)$. The dashed area corresponds to the frequency ranges associated to the low frequency region (824-960MHz) and to the high frequency region (1710-2170MHz).

3.4.3 Experimental Results

For the sake of validating the simulated results, two prototypes are built. The first one comprises a magnetic booster featuring dimensions of 5 mm x 18 mm and intended for providing operation in the low frequency region (824-960MHz) whereas the second one includes a magnetic booster with dimensions of 5 mm x 10 mm and proposed for covering the high frequency region (1710-2170MHz).

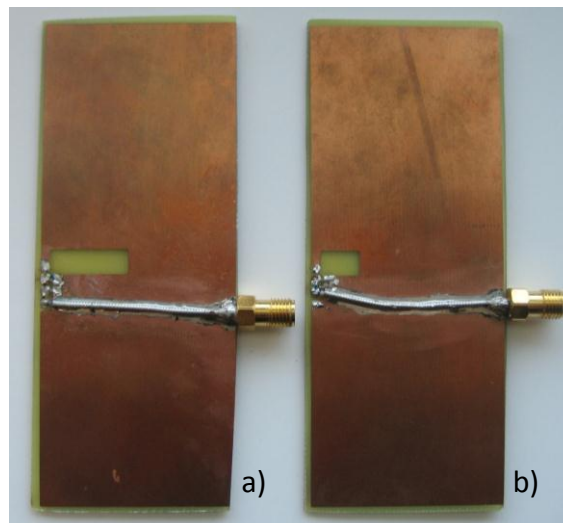


Fig. 3.53 a) Prototype intended for the low frequency region comprising a magnetic booster with dimensions of 5 mm x 18 mm and the radiofrequency system depicted in Fig. 3.46; b) Prototype intended for the high frequency region comprising a magnetic

booster with dimensions of 5 mm x 10 mm and the radiofrequency system depicted in Fig. 3.47. Ground plane size is 100 mm x 40 mm. Both magnetic boosters are located at the center of the longest edge.

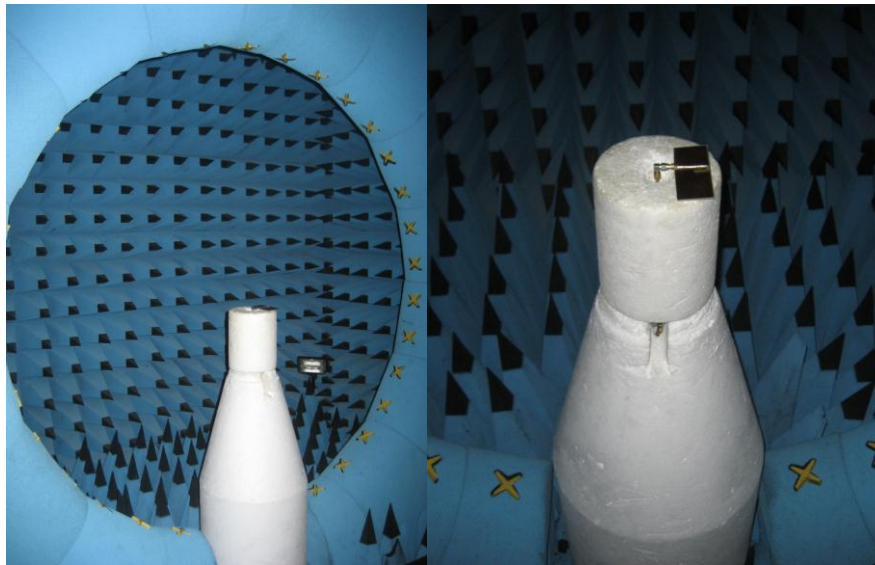


Fig. 3.54 Set-up measurement in the anechoic chamber Satimo Stargate-32.

Both prototypes include a ground plane with dimensions of 100 mm x 40 mm etched over a 1mm thick FR4 piece ($\epsilon_r=4.15$ and $\tan\delta=0.013$) (Fig. 3.53). The components of the matching circuit are SMD 0402 type. The capacitor used for the low frequency region ($C=17\text{pF}$) features a Q of 50. The rest of components present a Q larger than 100.

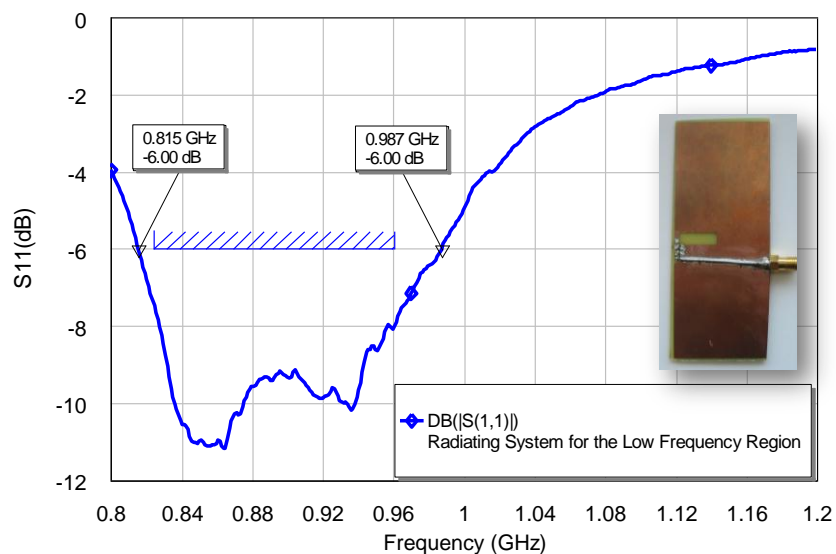


Fig. 3.55 Measured reflection coefficient associated to the prototype depicted in Fig. 3.53a.

Reflection coefficients of the proposed solutions have been measured through a network analyzer whereas antenna efficiency is obtained by integration of 3D radiation patterns by means of the anechoic chamber Satimo Stargate-32 (Fig. 3.54). The measured results demonstrate the feasibility of the proposal since the radiating system based on a single magnetic booster featuring dimensions of 5 mm x 18 mm (approximately an electrical length of 0.05λ) is able of satisfying the impedance bandwidth required by the communication standards GSM850 and GSM900 (824-960MHz) (Fig. 3.55). At the same time, the radiating system proposed for the high frequency region comprising a magnetic booster featured by

considerable reduced dimensions of just 5 mm x 10 mm is able to provide the impedance bandwidth required by the communication standards GSM1800, GSM1900, and UMTS (1710-2170MHz) (Fig. 3.56). Finally and in order to complete the assessment of the performance of the proposed radiating systems, 3D radiation patterns and antenna efficiencies are measured by means of the anechoic chamber Satimo Stargate-32 (Fig. 3.54).

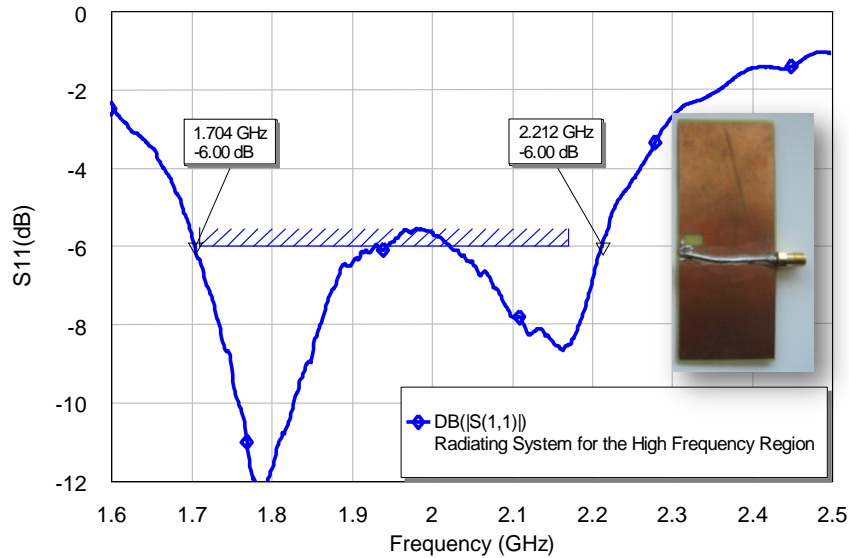
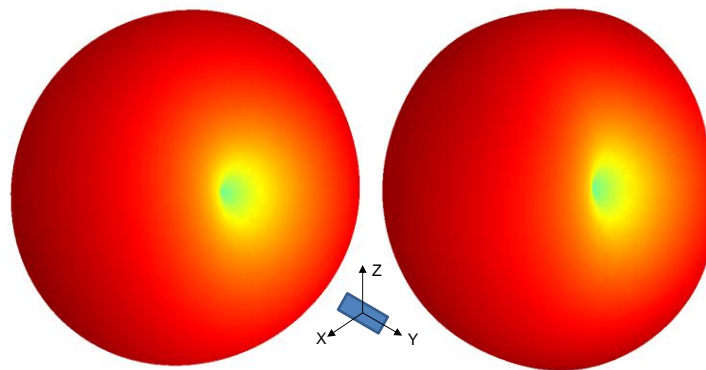


Fig. 3.56 Measured reflection coefficient associated to the prototype depicted in Fig. 3.53b.

The radiation patterns obtained demonstrate the effectiveness of the magnetic boosters in exciting the fundamental mode of the ground plane. As presented in section 2.2.1, the first radiating mode of the ground plane features a current distribution similar to that produced by a half-wavelength dipole having current maximums in the center of the longest edges and minimums in the shortest edges.



Frequency: 900MHz
Maximum Gain: 0.61 dB
Directivity: 2.8 dB

Frequency: 1900MHz
Maximum Gain: 0.77 dB
Directivity: 2.4 dB

Fig. 3.57 3D radiation patterns for approximately the central frequency of the low frequency region (900MHz) and the high frequency region (1900MHz).

In this sense, the radiation patterns at both frequency regions correspond to those provided by a half-wavelength dipole, i.e. they present an omni-directional behavior in the x-z plane and a null in the y direction that corresponds to the axis of the longest edge of the ground plane (Fig. 3.57). The antenna efficiency for both frequency regions further demonstrates the feasibility of the proposal since it remains

around 50% in average with maximum values of 60% for the low frequency region and around 65% in average with maximum values of 80% for the high frequency region (Fig. 3.58 and Fig. 3.59).

The reduction of the radiation efficiency with respect to the simulated case is mainly produced by the non-ideal feature of the matching network components, which was considered ideal during simulation. Finally, measured antenna efficiency results are aligned with simulated results (section 3.4.2) and they validate the proposal. The radiating systems based on magnetic ground plane boosters are able to provide operation in the main communication standards while minimizing the required PCB area.

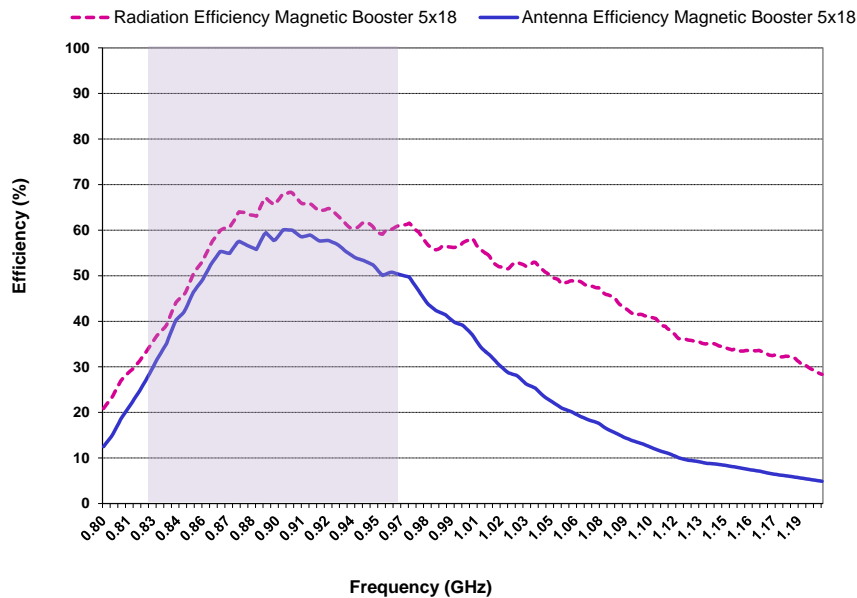


Fig. 3.58 η_r and η_a referred to the radiating system presented in Fig. 3.53a. The dashed area corresponds to the frequency ranges associated to the low frequency region (824-960MHz).

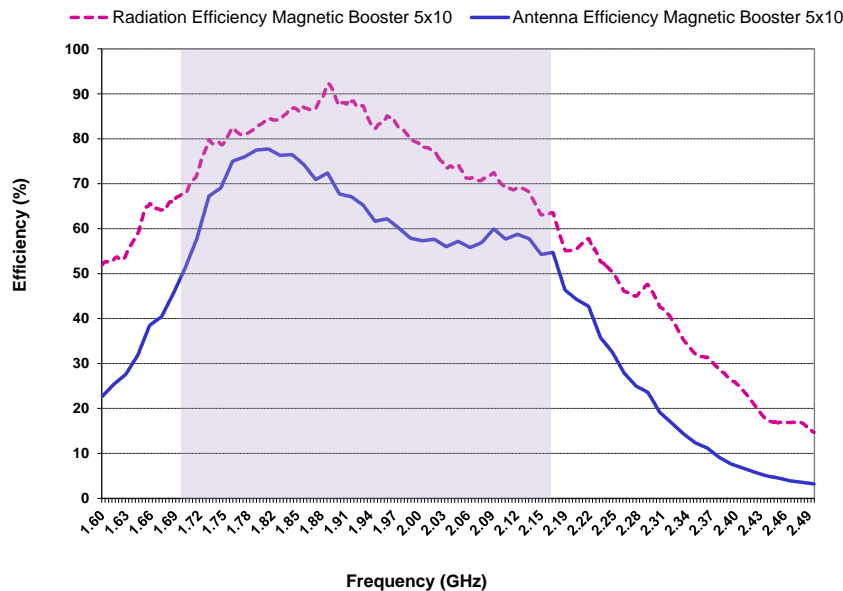


Fig. 3.59 η_r and η_a associated to the radiating system presented in Fig. 3.53b. The dashed area corresponds to the frequency ranges associated to the high frequency region (1710-2170MHz).

The coplanar feature of the proposals make them especially suitable for being integrated in ultra-slim handset platforms. The disclosed solutions attain a significant size reduction with respect to prior

proposals based on slots, namely the dimensions are reduced in a factor larger than five. In addition, less sensitiveness to the hand loading is expected in this case since the radiation is mainly provided by the ground plane mode. Thus, it is unlikely that the human hand block the whole radiating system, namely the whole ground plane as usually occurs in the case of a resonant antennas such as a PIFA.

3.5. On the Radiofrequency System

The previous results reveal that a reconsideration of the radiating system known so far is strongly demanded in order to satisfy current demands focused on providing operability in multiple communication standards while minimizing the required PCB space. Until now, the efforts were focused on the antenna element itself since the ground plane contribution was underestimated. However, in this new scenario, such efforts move toward the proper design of the ground plane, the elements used to excite said ground plane, as well as to the radiofrequency system used to provide impedance matching. Accordingly, recent advancements in the antenna field are focused on substituting resonant antennas by non-resonant elements featuring reduced dimensions [19]-[29]. Said non-resonant solutions are usually forced to integrate a radiofrequency system capable of modifying the input impedance of the radiating structure to attain the desired bandwidth. This is the case of [19]-[20], which provides impedance matching through the addition of a radiofrequency system based on distributed elements such as transmission lines.

However, the use of distributed elements as matching components undesirably contributes to increase the PCB space required by the radiating system. Other efforts [22]-[29] are focused on using lumped components capable of minimizing such PCB space, thus providing a compact antenna solution. Nevertheless a trade-off exists between the attainable bandwidth and the number of stages of the radiofrequency system. In this sense, [24] proposes a radiofrequency system including three stages intended for providing penta-band operation, GSM850, GSM900 and GSM1800, GSM1900, and UMTS. Namely, the stages that constitute the radiofrequency system comprise reactance cancellation elements, broadband matching networks, and notch filters which translates into 15 reactive elements. With the aim of simplifying said architecture, this section proposes the use of a radiofrequency system capable of minimizing the number of reactive components in a factor around 3, with respect to the solution illustrated in section 3.2, while preserving the systematic design and enhancing the electromagnetic performance.

The section is structured in the following manner. First, a non-resonant ground plane booster solution suitable for emergent smartphone platforms is proposed. In a second stage the impedance response of the radiating structure is analyzed through the electromagnetic software IE3D based on MoM. Subsequently the proposed radiating system and the simulated results are presented. Finally and in order to validate simulated results, a prototype is built and main antenna parameters (reflection coefficient and efficiency) are measured.

3.5.1 Physical Insight and Simulated Results

The proposed radiating structure comprises two ground plane boosters featured by their reduced dimensions of just 5 mm x 5 mm x 5 mm and their high quality factors ($Q \approx 2250$ for the low frequency region (824-960MHz) and $Q \approx 265$ for the high frequency region (1710-2690MHz)).

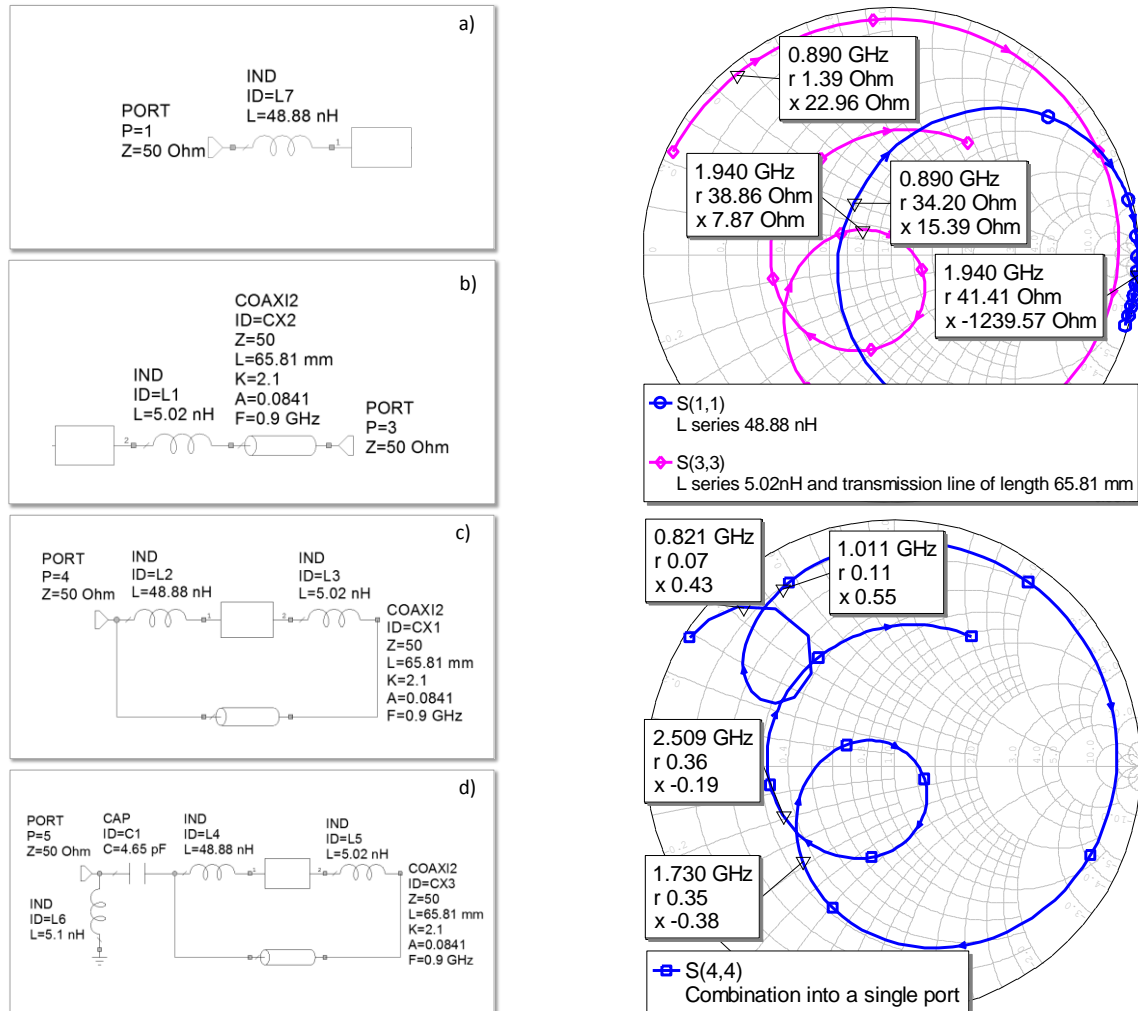


Fig. 3.60 Matching network topology and input impedance response associated to the different stages that constitute the proposed radiofrequency system. a) reactive cancellation for the low frequency region; b) reactive cancellation for the high frequency region; c) combination into a single port; d) fine-tuning stage that place the impedance loops at the center of the Smith chart.

Said boosters are distributed along the shortest edge of a ground plane having similar dimensions to those presented by current smartphone platforms (120 mm x 50 mm). They are capable of exciting the efficient radiation mode that the inherent ground plane of any handset platform features at mobile frequencies. However, as stated above, the simple excitation of said ground plane mode is not sufficient to guarantee operability since a radiofrequency system capable of providing appropriate bandwidth able to satisfy the specifications of multiple communication standards is needed. The proposed radiating structure is not resonant in any of both frequency regions. Thus, it is featured by an important capacitive behavior that can be readily compensated through the addition of a series inductance (Fig. 3.60a). Unlike the radiofrequency system proposed in section 3.2.3, this case neither needs broadband matching networks nor notch filters for providing hepta-band operation. On the contrary, the proposal attains

compact impedance loops centered in the circle $SWR \leq 3$ by the combination of properly shifted input impedances [68]-[69].

More specifically, the proposal relies on providing reactance cancellation stages at the input port of both ground plane boosters in order to make them resonant at the center frequencies of the low and high frequency regions (824-960MHz and 1710-2690MHz), respectively (Fig. 3.60a and Fig. 3.60b). Said input impedances are combined into a single input/output port through the addition of a phase delay, in this case a transmission line (Fig. 3.60c). Said phase delay allows the creation of compact impedance loops in both frequency regions, which can be easily centered through the addition of a fine-tuning stage composed by an LC circuit, thus, attaining hepta-band operation capable of allocating eight communication standards (GSM850, GSM900, GSM1800, GSM1900, UMTS, LTE2100, LTE2300, and LTE2500) (Fig. 3.60d and Fig. 3.61).

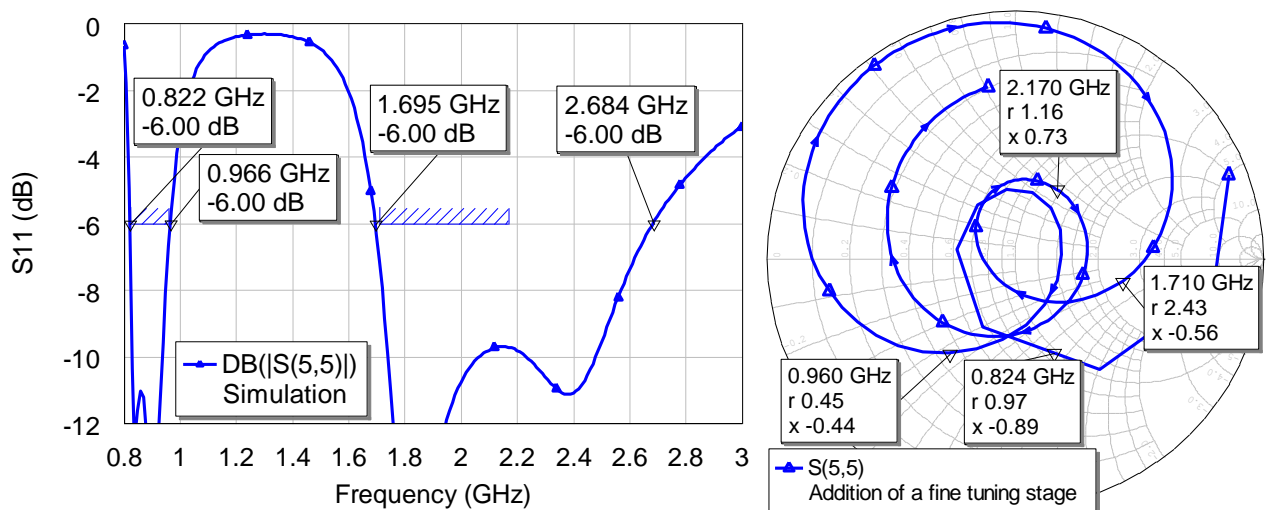


Fig. 3.61 Reflection coefficient and input impedance obtained from the proposed radiofrequency system depicted in Fig. 3.60d.

3.5.2 Measured Results

In order to validate simulated results, a prototype is built and main antenna parameters are measured (Fig. 3.62). As presented in the former section, the topology of the radiofrequency system mainly consists of two reactance cancellation elements, a phase delay, and a fine tuning stage of two elements. Each ground plane booster has dimensions of 5 mm x 5 mm x 5 mm and is soldered at a distance of 2 mm with respect to the edge of the ground plane. Note that the soldered microcoaxial transmission line can be replaced by commercial UFL cables, widely spread in the handset industry.

In this case, the phase delay is a micro-coaxial transmission line having a characteristic impedance of 50Ω . The results demonstrate the effectiveness of the proposal since the radiating system is able of providing operation in the low and high frequency regions (824-960MHz and 1710-2690MHz), which allocate the main communication standards (GSM850, GSM900, GSM1800, GSM1900, UMTS, LTE2100, LTE2300, and LTE2500) with enhanced electromagnetic performance (Fig. 3.63 and Fig. 3.64). The antenna efficiency reaches peaks of 60% in the low frequency region and remains around 65%, in average, in the high frequency region.

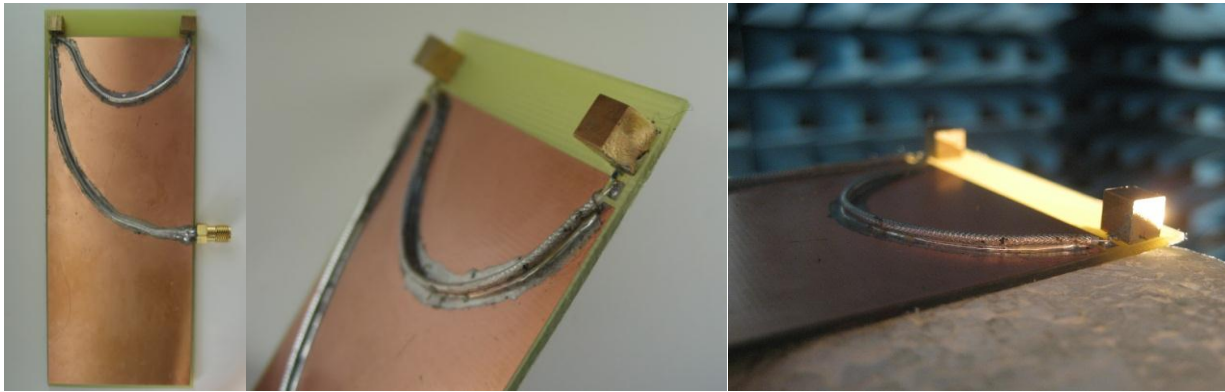


Fig. 3.62 Radiating structure comprising two ground plane boosters (5 mm x 5 mm x 5 mm) and a ground plane (120 mm x 50 mm) etched over a 1 mm thick FR4 piece (left); radiation properties are measured using anechoic chamber Satimo Stargate-32 (right).

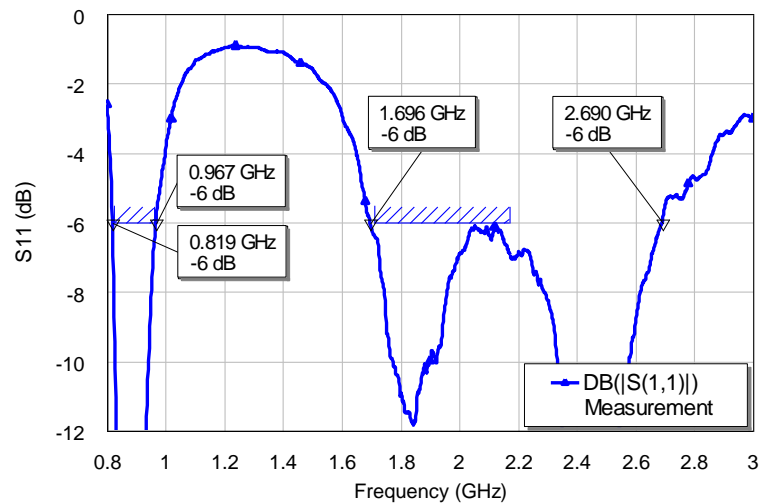


Fig. 3.63 Measured reflection coefficient (S_{11}) associated to the prototype depicted in Fig. 3.62.

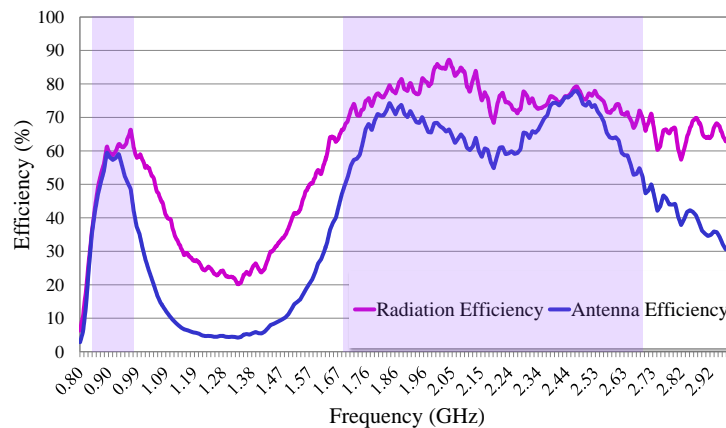


Fig. 3.64 Measured radiation (η_r) and antenna efficiency ($\eta_a = \eta_r (1 - |S_{11}|^2)$) associated to the prototype depicted in Fig. 3.62.

3.6. Conclusions

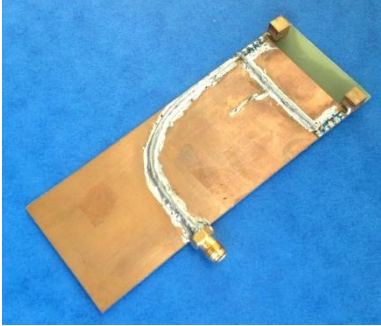

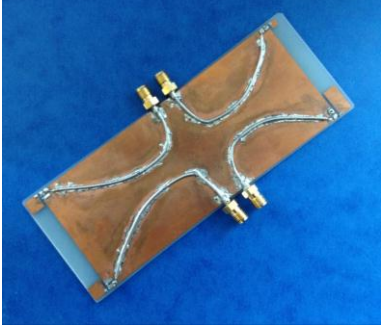
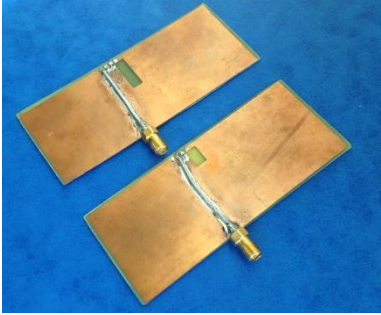

The first proposal presented along this chapter demonstrates that volumetric ground plane boosters become suitable solutions for providing an ultra-compact radiating system capable of operating in the main communication standards (GSM850, GSM900, GSM1800, GSM1900 and UMTS). In this sense, the conventional handset antennas featured by a considerable volume ($\approx 3600 \text{ mm}^3$) could be replaced by two low-volume non-resonant ground plane boosters (250 mm^3) and a matching topology with a systematic

design. These elements are in charge of properly exciting the efficient radiation mode of the ground plane, which presents high radiation efficiency and low Q at the frequencies of interest, especially in the low frequency region. The proposed systematic matching network design enables the operability in the desired frequency regions. The radiation contribution provided by such small ground plane boosters is negligible and they should not be considered antennas. Consequently their integration in the handset platform removes the need of including additional dedicated antenna elements featured by resonant dimensions. This first proposal becomes an alternative to the traditional antenna technology and appears as a promising standard solution for being integrated in the emergent multifunctional wireless devices. In this regard, the available space in handset platforms for integrating new functionalities is further increased while the radiating performance is preserved.

The second solution presented along this chapter further demonstrates that the efficient radiation modes associated to a ground plane can be effectively excited through a set of coplanar ground plane boosters. Thus, removing the belief that volumetric structures are always required for providing a proper coupling. The coplanar feature considerably simplifies their integration in emergent ultra-slim handset platforms. The solution demonstrates on one hand, that volumetric structures can be substituted by coplanar solutions, thus dispelling the belief that proper coupling to ground plane radiation modes is just attained by volumetric structures. On the other hand, the proposal confirms that the systematic design based on broadband matching networks becomes a feasible solution for being integrated in booster-based radiating systems. Two solutions based on ground plane boosters have been presented. The first one attains octo-band operation (GSM850, GSM900, GSM1800, GSM1900, UMTS, LTE2100, LTE2300, LTE2500) whereas the second one further adds to the aforementioned standards the emergent LTE700 system and the GPS service. For the first proposal, two coplanar ground plane boosters featuring small dimensions of just 6 mm x 6 mm, or equivalently occupying an area of 72 mm², are placed at the corners of a ground plane featuring typical dimensions of current smartphones 120 mm x 50 mm. In the second solution, two additional coplanar ground plane boosters are added for covering the additional communication services. This fact leads to a distributed antenna system capable of providing operation in ten communication standards while minimizing the occupied PCB space due to its reduced area of just 153 mm². Conventional antenna solutions, such as PIFAs tend to occupy a volume around 3600 mm³.

The integration of a coplanar booster-based technology in a handset platform allows reducing the required volume in a factor around fifty, which supposes a substantial size reduction. The proposed solutions just require small PCB areas, thus enabling easily the integration of other handset components inside the handset platform. Once the feasibility of relying on non-resonant ground plane boosters to effectively excite the ground plane radiation modes is demonstrated, the third solution is focused on analyzing the effects of the nature, placement, and size of said ground plane boosters over the performance of the radiating system. The study reveals that a proper location to place said non-resonant ground plane boosters exists and demonstrates that it is highly dependent on their nature (electric or magnetic).

Table 3.3 Summary of the proposed radiating system based on the ground plane booster antenna technology.

Architecture	Features	Performance
	<ul style="list-style-type: none"> • Electric Ground Plane Booster each one with dimensions of 5 mm x 5 mm x 5 mm. • Number of components of the radiofrequency system: 14 including notch filter to end up with a single input/output port. • Ground plane 100 mm x 40 mm. 	GSM850, GSM900, GSM1800, GSM1900, and UMTS.
	<ul style="list-style-type: none"> • Electric Ground Plane Booster: each one with dimensions of 6 mm x 6 mm (coplanar). • Number of components of the radiofrequency system: 4 for each frequency region. • Ground plane 120 mm x 50 mm. 	GSM850, GSM900, GSM1800, GSM1900, UMTS, LTE2100, LTE2300, and LTE2500
	<ul style="list-style-type: none"> • Electric Ground Plane Booster: one of 6 mm x 12 mm, one of 3 mm x 3 mm, and two of 6 mm x 6 mm (coplanar). • Number of components of the radiofrequency system: 12. • Ground plane 120 mm x 50 mm. 	LTE700, GSM850, GSM900, GPS, GSM1800, GSM1900, UMTS, LTE2100, LTE2300, LTE2500
	<ul style="list-style-type: none"> • Magnetic Ground Plane Booster: one of 18 mm x 5 mm and one of 10 mm x 5 mm (coplanar). • Number of components of the radiofrequency system: 5 and 4 for the low and high frequency region, respectively. • Ground plane 100 mm x 40 mm. 	GSM850, GSM900, GSM1800, GSM1900, and UMTS
	<ul style="list-style-type: none"> • Electric Ground Plane Booster each one with dimensions of 5 mm x 5 mm x 5 mm. • Number of components of the radiofrequency system: 5. • Ground plane 120 mm x 50 mm. 	GSM850, GSM900, GSM1800, GSM1900, UMTS, LTE2100, LTE2300, and LTE2500

Accordingly, electric ground plane boosters must be placed in the electrical field maximum of the radiating mode whereas magnetic ground plane boosters must be placed in the maximum of the magnetic field in order to ensure the proper ground plane radiating mode excitation.

The proposal further demonstrates that it is possible to efficiently excite the fundamental mode of the ground plane through magnetic ground plane boosters strategically arranged in the center of the longest edge of the PCB. Nevertheless said excitation is not enough to provide operation since a matching network is strongly required to ensure proper input impedance levels. The physical insight through electrical models and quality factor assessment as well as the use of a broadband technique allows simplifying the matching network design of this sort of radiating structures avoiding cumbersome trial and error methods.

The proposed radiating systems are completely planar solutions and enable the operation in the main communication standards GSM850, GSM900, GSM1800, GSM1900, and UMTS through the use of magnetic boosters featured by considerable reduced dimensions of approximately 0.05λ . In this sense, the use of radiating systems comprising magnetic ground plane boosters becomes a suitable option to minimize the required PCB space while preserving the electromagnetic performance since it implies a reduction factor around five with respect to previous solutions based on resonant elements.

As previously discussed, the efficient radiation mode associated to handset platforms can be effectively excited through non-resonant elements. However, said excitation does not guarantee the proper performance since a radiofrequency system capable of matching the resulting input impedance is strongly required. In this sense, the proper design of these radiofrequency systems becomes an essential part of emergent radiating systems based on non-resonant elements. The proposed radiofrequency system in the last section not only allows minimizing the number of reactive components in a factor around 3 with respect to the previous solutions but also simplifying the integration while enhancing the electromagnetic performance. With the proposed technique, octo-band operation (GSM850, GSM900, GSM1800, GSM1900, UMTS, LTE2100, LTE2300, and LTE2500) is achieved by two small ground plane boosters of 5 mm x 5 mm x 5 mm and a radiofrequency system of only five reactive components.

The radiating systems proposed along this chapter provide operation in the main communication standards while considerably reduce the space occupied in the PCB. Thus, they become suitable solutions to satisfy the multi-band and miniature requirements strongly demanded by the market trends (Table 3.3).

3.7. References

- [1] K. L. Wong, *Planar Antennas for Wireless Communications*, New York, *John Wiley & Sons*, 2003.
- [2] J.S. McLean, "A Re-Examination of the Fundamental Limits on the Radiation Q of Electrically Small Antennas", *IEEE Transactions on Antennas and Propagation*, AP-44, May 1996, pp. 672-676.
- [3] C. Puente, J. Anguera, J. Soler, and A. Condes, "Coupled Multi-band Antennas", *Patent Application WO2004/025778*, September 10, 2002.

- [4] C. Lin and K. L. Wong, "Printed Monopole Slot Antenna for Internal Multi-band Mobile Phone Antenna", *IEEE Transactions on Antennas and Propagation*, vol. 55, n°12, December 2007, pp. 3690-3697.
- [5] S. Risco, J. Anguera, A. Andújar, A. Pérez, and C. Puente, "Coupled Monopole Antenna Design for Multi-band Handset Devices", *Microwave and Optical Technology Letters*, vol. 52, n°2, February 2010, pp. 359-364.
- [6] P. Vainikainen, J. Ollikainen, O. Kivekäs, and I. Kelder, "Resonator-Based Analysis of the Combination of Mobile Handset Antenna and Chassis", *IEEE Transactions on Antennas and Propagation*, vol. 50, n°10, October 2002, pp. 1433-1444.
- [7] M. Cabedo-Fabrés, E. Antonino-Daviu, A. Valero-Nogueira, and M. Ferrando Bataller, "The Theory of Characteristic Modes Revisited: A Contribution to the Design of Antennas for Modern Applications", *IEEE Antennas and Propagation Magazine*, vol. 49, n°5, October 2007, pp. 52-68.
- [8] W. L. Schroeder, C. T. Fandie, and K. Solbach, "Utilization and Tuning of the Chassis Modes of a Handheld Terminal for the Design of Multi-band Radiation Characteristics", *IEEE Wideband and Multi-band Antennas and Arrays*, September 2005, pp. 117-121.
- [9] J. Anguera, I. Sanz, A. Sanz, A. Condes, D. Gala, C. Puente, and J. Soler, "Enhancing the performance of handset antennas by means of groundplane design", *IEEE International Workshop on Antenna Technology: Small Antennas and Novel Metamaterials (iWAT 2006)*. New York, USA, March 2006.
- [10] J. Anguera, A. Cabedo, C. Picher, I. Sanz, M. Ribó, and C. Puente, "Multi-band Handset Antennas by Means of Groundplane Modification", *IEEE Antennas and Propagation Society International Symposium*, Honolulu, Hawaii, USA, June 2007.
- [11] C. Picher, J. Anguera, A. Cabedo, C. Puente, and S. Kahng, "Multi-band Handset Antenna Using Slots on the Ground Plane: Considerations to Facilitate the Integration of the Feeding Transmission Line", *Progress In Electromagnetics Research C*, vol. 7, 2009, pp. 95-109.
- [12] C. Picher, J. Anguera, A. Andújar, C. Puente, and A. Bujalance, "Multi-band Handset Antennas by Combining Monopoles and Intelligent Ground Planes", *Proceedings of the Sixth European Conference on Antennas and Propagation*, EuCAP 2012, Prague, Czech Republic, March 2012, pp. 2741-2744.
- [13] C. Picher, J. Anguera, A. Bujalance, A. Andújar, and C. Puente, "Analysis of a Multi-band Monopole Handset Antenna Combined with a Slotted Ground Plane", *Microwave and Optical Technology Letters*, vol. 55, n°1, January 2013, pp. 173-180.
- [14] A. Cabedo, J. Anguera, C. Picher, M. Ribó, and C. Puente, "Multi-Band Handset Antenna Combining a PIFA, Slots, and Ground Plane Modes", *IEEE Transactions on Antennas and Propagation*, vol.57, n°9, Sep. 2009, pp. 2526-2533.
- [15] J. Anguera, I. Sanz, J. Mumburú, and C. Puente, "Multi-band Handset Antenna with a Parallel Excitation of PIFA and Slot Radiators", *IEEE Transactions on Antennas and Propagation*, vol. 58, n°2, February 2010, pp. 348-355.

- [16] R. Quintero and C. Puente, "Multilevel and Space-Filling Ground Planes for Miniature and Multi-band Antennas", *Patent Application* WO2003/023900, September 13, 2001.
- [17] J. Anguera and C. Puente, "Shaped Ground Plane for Radio Apparatus", *Patent Application* WO2006/070017, December 29, 2005.
- [18] C. Puente and J. Anguera, "Handset with Electromagnetic Bra", *Patent Application* WO2005/083833, February 28, 2005.
- [19] J. Villanen, J. Ollikainen, O. Kivekäs, and P. Vainikainen, "Coupling Element Based Mobile Terminal Antenna Structures", *IEEE Transactions on Antennas and Propagation*, vol. 54, n^o7, July 2006, pp. 2142-2153.
- [20] S. Ozden, B. K. Nielsen, C. H. Jorgensen, J. Villanen, C. Icheln, and P. Vainikainen, "Quad-Band Coupling Element Antenna Structure", *U.S. Patent* 7,274,340, September 25, 2007.
- [21] J. Anguera, I. Sanz, C. Puente, and J. Mumbrú, "Wireless Device including a Multi-band Antenna System", *Patent Application* WO2008/119699, March 26, 2008.
- [22] J. Anguera, A. Andújar, C. Puente, and J. Mumbrú, "Antennaless Wireless Device", *Patent Application* WO2010/015365, July 31, 2009.
- [23] J. Anguera, A. Andújar, C. Puente, and J. Mumbrú, "Antennaless Wireless Device Capable of Operation in Multiple Frequency Regions", *Patent Application* WO2010/015364, July 31, 2009.
- [24] A. Andújar, J. Anguera, and C. Puente, "Ground Plane Boosters as a Compact Antenna Technology for Wireless Handheld Devices", *IEEE Transactions on Antennas and Propagation*, vol. 59, n^o5, May 2011, pp.1668-1677.
- [25] J. Holopainen, J. Ilvonen, R. Valkonen, A. Azremi, and P. Vainikainen, "Study on the Minimum Required Size of the Low-Band Cellular Antenna in Variable-Sized Mobile Terminals", *Proceedings of the Sixth European Conference on Antennas and Propagation*, EuCAP2012, Prague, Czech Republic, March 2012, pp. 2754-2758.
- [26] J. Rahola and J. Ollikainen, "Optimal Antenna Placement for Mobile Terminals using Characteristic Mode Analysis", *Proceedings of the First European Conference on Antennas and Propagation*, EuCAP 2006, Nice, France.
- [27] A. Andújar and J. Anguera, "Magnetic Boosters for Multi-band Operation", *Microwave and Optical Technology Letters*, vol.55, n^o1, Jan.2013, pp.65-75.
- [28] A. Andújar and J. Anguera, "Multi-band Coplanar Ground Plane Booster Antenna Technology", *IEE Electronics Letters*, vol.48, n^o21, October 2012, pp.1326-1328.
- [29] J. Anguera, A. Andújar, and C. García, "Multiband and Small Coplanar Antenna System for Wireless Handheld Devices", *IEEE Transactions on Antennas and Propagation*, vol. 61, n^o 7, July 2013, pp. 3782-3789.
- [30] R. J. Garbacz and R.H. Turpin, "A generalized expansion for radiated and scattered fields", *IEEE Transactions on Antennas and Propagation*, vol. AP-19, May 1971, pp. 348-358.

- [31] R.F. Harrington and J.R. Mautz, "Theory of Characteristic Modes for Conducting Bodies", *IEEE Transactions on Antennas and Propagation*, AP-19, n°5, September 1971, pp. 622-628.
- [32] R.F. Harrington and J.R. Mautz, "Computation of Characteristic Modes for Conducting Bodies", *IEEE Transactions on Antennas and Propagation*, AP-19, n°5, September 1971, pp. 629-639.
- [33] E.H. Newman, "Small Antenna Location Synthesis Using Characteristic Modes", *IEEE Transactions on Antennas and Propagation*, vol. AP-27, n°4, July 1979, pp. 530-531.
- [34] C. T. Fandie, W. L. Schroeder, and L. Solbach, "Numerical analysis of characteristic modes on the chassis of mobile phones", *Proceedings of the First European Conference on Antennas and Propagation*, EuCAP 2006, Nice, France, 2006.
- [35] S. R. Best, "The Inverse Relationship between Quality Factor and Bandwidth in Multiple Resonant Antennas", *IEEE Antennas and Propagation Society International Symposium*, 2006, pp. 623-626.
- [36] R. C. Hansen, "Fano Limits on Matching Bandwidth", *IEEE Antennas and Propagation Magazine*, vol. 47, n° 3, June 2005, pp. 89-90.
- [37] J. Anguera, C. Puente, C. Borja, G. Font, and J. Soler, "A Systematic Method to Design Single-Patch Broadband Microstrip Patch Antennas", *Microwave and Optical Technology Letters*, vol. 31, n°3, November 2001, pp. 185-188.
- [38] A. Andújar, J. Anguera, and C. Puente, "A Systematic Method to Design Broadband Matching Networks", *Proceedings of the Fourth European Conference on Antennas and Propagation*, EuCAP 2010, Barcelona, Spain, 2010.
- [39] H. F. Pues and A.R. Van de Capelle, "An Impedance-Matching Technique for Increasing the Bandwidth of Microstrip Antennas", *IEEE Transactions on Antennas and Propagation* vol. AP-37, n° 11, November 1989, pp. 1345-1354.
- [40] M. Martínez, O. Litschke, M. Geissler, D. Heberling, A. M. Martínez, and D. Sánchez, "Integrated Planar Multi-band Antennas for Personal Communication Handsets", *IEEE Transactions on Antennas and Propagation*, vol. 54, n° 2, February 2006, pp. 384-391.
- [41] B. Kim, S. Park, Y. Yoon, J. Oh, K. Lee, and G. Koo, "Hexaband Planar Inverted-F Antenna with Novel Feed Structure for Wireless Terminals", *IEEE Antennas and Wireless Propagation Letters*, vol. 6, 2007, pp. 66-69.
- [42] H. Hsieh, Y. Lee, K. Tiong, and J. Sun, "Design of a Multi-band Antenna for Mobile Handset Operations", *IEEE Antennas and Wireless Propagation Letters*, vol. 8, 2009, pp. 200-203.
- [43] Z. Li and Y. Rahmat-Samii, "Optimization of PIFA-IFA Combination in Handset Antenna Designs", *IEEE Transactions on Antennas and Propagation*, vol. 53, n° 5, May 2005, pp. 1770-1778.
- [44] C. Lin and K. L. Wong, "Printed Monopole Slot Antenna for Internal Multi-band Mobile Phone Antenna", *IEEE Transactions on Antennas and Propagation*, vol. 55, n°12, December 2007, pp. 3690-3697.

- [45] R. A. Bhatti and S. O. Park, "Hepta-Band Internal Antenna for Personal Communication Handsets", *IEEE Transactions on Antennas and Propagation*, vol. 55, n° 12, December 2007, pp. 3398-3403.
- [46] S. Hong, W. Kim, H. Park, S. Kahng, and J. Choi, "Design of Internal Multiresonant Monopole Antenna for GSM900/DCS1800/US-PCS/S-DMB", *IEEE Transactions on Antennas and Propagation*, vol. 56, n°5, May 2008, pp. 1437-1443.
- [47] Y. Chi and K. Wong, "Quarter-Wavelength Printed Loop Antenna with an Internal Matching Circuit for GSM/DCS/PCS/UMTS Operation in the Mobile Phone", *IEEE Transactions on Antennas and Propagation*, vol. 57, n° 9, September 2009, pp. 2541-2547.
- [48] M. Zheng, H. Wang, and Y. Hao, "Internal Hexa-band Folded Monopole/Dipole/Loop Antenna with Four Resonances for Mobile Device", *IEEE Transactions on Antennas and Propagation*, vol. 60, n° 6, June 2012, pp. 2880-2885.
- [49] K. L. Wong, Y. W. Chi, and S. Y. Tu, "Printed Folded Slot Antenna for Internal Multi-band Mobile Phone Antenna", *IEEE Antennas and Propagation Society International Symposium*, June 2007, pp. 2622-2625.
- [50] C. I. Lin and K. L. Wong, "Printed monopole slot antenna for internal multi-band mobile phone antenna", *IEEE Transactions on Antennas and Propagation*, vol. 55, n°12, December 2007, pp. 3690-3697.
- [51] K. L. Wong and P.W. Lin, "Simple Printed Monopole Slot Antenna for WWAN Mobile Handset", *International Workshop on Antenna Technology (iWAT)*, March 2011, pp. 186-189.
- [52] A. Zhao and J. Rahola, "Quarter-Wavelength Wideband Slot Antenna for 3-5GHz Mobile Applications", *IEEE Antennas and Wireless Propagation Letters*, vol. 4, 2005, pp. 421-424.
- [53] A. Zhao and J. Rahola, "Numerical and Experimental Study of a Quarter-Wavelength Wideband Slot Antenna for Mobile Applications", *IEEE Microwave Conference Proceedings (APMC) Asia-Pacific*, December 2005.
- [54] S. K. Sharma, L. Shafai, and N. Jacob, "Investigation of Wide-Band Microstrip Slot Antenna", *IEEE Transactions on Antenna and Propagation*, vol. 52, n° 3, March 2004, pp. 865-872.
- [55] F. H. Chu and K. L. Wong, "Simple folded monopole slot antenna for penta-band clamshell mobile phone application", *IEEE Transactions on Antennas and Propagation*, vol. 57, n°11, November 2009, pp. 3680-3684.
- [56] C. Lin and K.L.Wong, "Printed Penta-Band Monopole Slot Antenna for Application in the Folder-Type Mobile Phone", *IEEE Antennas and Propagation Society International Symposium*, July 2008.
- [57] A. Zhao, "Wideband and Low-profile Antenna for Mobile Terminals", *Microwave and Optical Technology Letters*, vol. 52, n°12, December 2012, pp. 2724-2728.

- [58] P. Lindberg, E. Öjefors, and A. Rydberg, "Wideband Slot Antenna for Low-Profile Hand-held Terminal Applications", *Proceedings of the 36th European Microwave Conference*, September 2006, Manchester UK, pp. 1698-1701.
- [59] S. H. Lee, Y. Lim, Y. J. Yoon, C. B. Hong, and H. I. Kim, "Multi-band Folded Slot Antenna with Reduced Hand Effect for Handsets", *IEEE Antennas and Wireless Propagation Letters*, vol. 9, 2010, pp. 674-677.
- [60] M. Cabedo, E. Antonio, A. Valero, and M. Ferrando, "Wideband Radiating Ground Plane with Notches", *IEEE Antennas and Propagation Society International Symposium*, July 2005, pp. 560-563.
- [61] H.C. Choi, O. Cho, and H.M. Jang, "Ground radiator using capacitor", *US Patent Publication*, 2011/0193757 A1, Aug. 11, 2011.
- [62] R. Martens, E. Safin, and D. Manteuffel, "Selective excitation of characteristic modes on small terminals", *Proceedings of the Fifth European Conference on Antennas and Propagation*, EUCAP 2011, Rome, Italy, April 2011, pp. 2492–2496.
- [63] K. R. Boyle, "Improvements in or Relating to Wireless Terminals", *Patent Application* WO2003/0817, Feb. 12, 2003.
- [64] J. Holopainen, J. Villanen, C. Icheln, and P. Vainikainen, "Mobile Terminal Antennas Implemented by using Direct Coupling", *Proceeding of the First European Conference on Antennas and Propagation*, EuCAP2006, Nice, France.
- [65] R. Hossa, A. Byndas, and M. E. Bialkowski, "Improvement of Compact Terminal Antenna Performance by Incorporating Open-End Slots in Ground Plane", *IEEE Microwave and Wireless Component Letters*, vol. 14, n° 6, June 2004, pp. 283-285.
- [66] M. F. Abedin and M. Ali, "Modifying the Ground Plane and Its Effect on Planar Inverted-F Antennas (PIFAs) for Mobile Phone Handsets", *IEEE Antennas and Wireless Propagation Letters*, vol.2, 2003, pp. 226-229.
- [67] A. Petosa, "Dielectric Resonator Antenna handbook", *Artech House*, 2007.
- [68] A. Andújar and J. Anguera, "On the Radiofrequency System of Ground Plane Booster Antenna Technology", *IEE Electronics Letters*, vol. 48, n°14, July 2012.
- [69] A. Andújar and J. Anguera, "Compact Radiating Array for Wireless Handheld or Portable Devices", *Patent Application* US 61/661,885, June 20, 2012.

CHAPTER 4 HUMAN HEAD INTERACTION

4.1. Introduction

As deeply discussed along this thesis, the mobile industry is constantly growing and handset antennas are subject to the new requirements demanded by the market trends based on ultra-slim multifunctional wireless devices [1]. In this sense, handset antennas have to be as small as possible to satisfy not only these requirements, but also to allow the integration of other handset components capable of providing multiple functionalities and services [2]. In addition, these handset antennas have to fulfill the human interaction requirements from two main perspectives, functional and biological. Accordingly, the challenge not only relies on providing multi-band antennas capable of operating in multiple communication standards sufficiently small as for being integrated inside the handset platform, but also on ensuring robustness in front the human interaction.

As introduced along chapter 1, and as a rough approximation, handset antennas can be grouped into patch/PIFA (Planar Inverted-F Antenna) antennas [3], monopole/IFA (Inverted-F Antenna) antennas [4]-[6], slots [7], and a combination of them [8]. On one hand, the first ones are featured by a specific volume and are generally located ‘on-ground’, i.e., placed over the ground plane at a certain height. Several techniques have been described to provide dual-band or multi-band operation such as for instance shaping the PIFAs radiating path or using slotted ground planes [9]-[16]. On the other hand, monopoles and slots are designed to be ‘off-ground’ in such a way that most of the ground plane is removed underneath the antenna, enabling, in some cases, substantially coplanar structures which become especially suitable for ultra slim platforms.

As deeply discussed along this thesis, the theory of characteristic modes [17]-[18] is acquiring relevance in the handset field and several proposals are focused on the excitation of some efficient radiation modes associated to the ground plane of current handset platforms. With this aim, [9]-[14] propose solutions based on slots capable of tuning said resonant mode to lower frequencies by providing a longer current path, whereas in [19] the resonant mode is tuned to higher frequencies. The proper excitation of the ground plane mode leads to an enhancement of the handset antenna performance regarding impedance bandwidth and radiation efficiency. Other handset antenna designs are presented in [20]-[21], which are based on coupling and small antennas capable of efficiently exciting the radiation mode of the ground plane. The solutions provide quad-band and penta-band behavior, respectively by the addition of a specific matching network for each frequency region. With the aim of taking full advantage of the excitation of these ground plane modes, this thesis proposes the use of ground plane boosters featured by considerable reduced dimensions and poor stand-alone radiation properties [22]-[24]. As suggested in section 3.2, the use of two ground plane boosters with considerable small dimensions allow multi-band operation when they are used in combination with a ground plane having the typical

dimensions of a bar platform (100 mm x 40 mm), and a proper radiofrequency system. The ground plane, the ground plane boosters, and the radiofrequency system compose a compact radiating system capable of providing operability in the main communication standards GSM850, GSM900, GSM1800, GSM1900, and UMTS. In this case, the challenge lies in the fact that the ground plane resonance is not coupled to the antenna resonance so the efficient radiation is entirely provided by the proper excitation of the ground plane modes. The radiation contribution provided by such small boosters is negligible and they should not be considered antennas. This architecture [22]-[24] becomes a promising alternative to current antenna technologies since its fundamental principle based on the correct excitation of the ground plane, which is inherent anyway, in any wireless device, removes the need of including a dedicated antenna, such as PIFAs or monopoles. Nevertheless, the human interaction over these kind of solutions must be carefully considered and this chapter is intended for analyzing it from two main perspectives, biological and functional [25].

Commonly, handset antenna specifications are given regarding free-space conditions. However, in practice, the handset antenna performance is strongly affected by other important factors such as hand interaction [26]-[28] and human head effect [29]-[37]. The user significantly interacts with the radiating system, especially during a phone call, affecting its performance and causing radiation losses as well as detuning effects. Thus, free-space measurements are not enough to correctly characterize handset antennas and the effects of the human head interaction over their performance have to be considered. The purpose of this chapter consists in evaluating the performance of the booster-based antenna technology proposed along this thesis concerning the human head interaction. For the sake of comparison, three representative handset antenna topologies together with the booster-based solution are analyzed not only in free-space but also regarding the human head presence.

The chapter is structured as follows. In section 4.2, the geometry of the four selected prototypes for comparison purposes is described. The study of the human head effect over the performance of these prototypes regarding the detuning effect and the power absorption is analyzed along section 4.3. In section 4.4, the biological impact caused by the electromagnetic fields radiated by the antenna into the human head is presented. Subsequently, a criterion for evaluating the performance of a handset and a figure of merit are proposed in Section 4.5. Finally, the conclusions are discussed along section 4.6.

4.2. Description of the Radiating Systems

Conventionally, the main antenna parameters are evaluated regarding free-space conditions. However, this environment emulates an ideal situation that does not occur in practice. For instance, when holding the phone during a call, the proximity of the human head strongly affects the performance of the antenna. At the same time, the electromagnetic fields radiated by the handset antenna produce biological effects over the human head that have to be measured and restricted. Accordingly, the human head interaction assessed along this chapter considers not only the effect of the human head over the antenna

performance but also the biological effect of the antenna over the human head in terms of Specific Absorption Rate (SAR).

With this regard, four representative prototypes have been selected for carrying out the study: a dual-band PIFA antenna for GSM900 and GSM1900; an hexa-band PIFA antenna for covering the mobile bands GSM850, GSM900, GSM1800, GSM1900, UMTS and LTE2300 [14]; a penta-band coupled monopole set [4], [6], and a penta-band compact radiating system for GSM850, GSM900, GSM1800, GSM1900, and UMTS [22]-[24] (Fig. 4.1). The election of these prototypes as case studies has been done taking into consideration that most of handset antennas can be grouped into two categories, patch/PIFA antennas and monopole antennas. The main difference between both designs lies in the fact that PIFA antennas present a ground plane portion underneath the antenna area and they have to be located at a certain height from the ground plane in order to guarantee proper performance. On the other hand, monopole antennas do not present a ground plane portion underneath the antenna and consequently they can be coplanar to it, i.e. they can lie in the same plane as the ground plane, hence featuring a very low profile.



Fig. 4.1 Geometry of the four radiating systems proposed. All prototypes are etched over a 1 mm thick FR4 piece ($\epsilon_r=4.15$, $\tan\delta=0.013$). Penta-band coupled monopoles set (left), penta-band compact radiating system (2nd column), dual-band PIFA (top right), and hexa-band PIFA with a slotted ground plane (bottom right).

In this sense, two PIFAs and a set of coupled monopoles are compared not only between them but also with the booster-based proposal. The dual-band PIFA antenna is used as a reference antenna. It is featured by a width (W) and a length (L) of 15 mm and 40 mm respectively, and is located at a height (h) of 6 mm over a ground plane with dimensions 100 mm x 40 mm (Fig. 4.1 (top right)). The hexa-band PIFA antenna differs from the conventional PIFA in the addition of a mechanism conceived to electrical enlarge the ground plane. Said mechanism is based on the integration of slots in the ground plane and is intended to enlarge the current path in the low frequency region (824-960MHz) and for featuring resonant dimensions in the high frequency region (1710-2170MHz) (Fig. 4.1 (bottom right)). As aforementioned,

coupled monopoles are evaluated as a representative sample of a penta-band antenna specially designed for being integrated in slim platform thanks to its characteristic low profile (Fig. 4.1 (left)).

Finally, the proposed booster-based antenna technology is compared with the former techniques, already consolidated in the handset market. Along this chapter the proposed booster-based solution will be referred as compact radiating system. The compact radiating system under study coincides with that presented along section 3.2. Accordingly, the solution comprises two ground plane boosters with very small dimensions of just 5 mm x 5 mm x 5 mm, soldered at a distance of 2 mm from the edge of a ground plane (100 mm x 40 mm) (Fig. 4.1 (2nd column)). The proposal considerably reduces the volume with respect to the other topologies under consideration. In fact, it supposes around one order of magnitude less than the PIFA solutions, which requires a volume around 3600mm³ with respect to the 250mm³ required to attain penta-band operation by the compact radiating systems based on the ground plane booster antenna technology.

4.3. Functional Analysis

This section is focused on analyzing the human head effect over the handset antenna performance. With this regard, the main antenna parameters (reflection coefficient, efficiency, radiation pattern, and directivity) are measured regarding free space conditions and human head interaction. For the last case, right-cheek talk positions, included in the new European Standard for SAR measurements [37], have been tested. In order to complete the study, for this right location two different arrangements of the prototypes have been evaluated (Fig. 4.2): on one hand, the antenna or the ground plane boosters are arranged near the phantom ear (“Antenna Up” or “Boosters Up”), and on the other hand, the prototypes are rotated 180° with respect to the previous position (“Antenna Down” or “Boosters Down”).

The Printed Circuit Board (PCB) is spaced apart 1 mm from the phantom head for all the prototypes under study thanks to the use of a methacrylate piece. It is important to notice that this is a critical situation because in practice the distance between the PCB and the human head is usually higher.

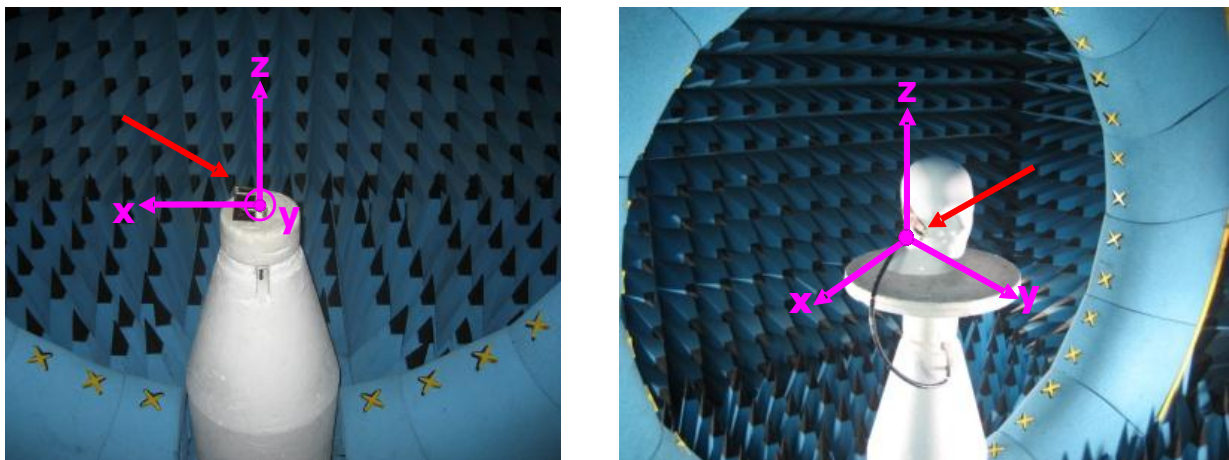


Fig. 4.2 Set-up for radiation measurement in the anechoic chamber Satimo Stargate-32 showing the coordinate system regarding free-space and the human head presence for the “Antenna Down” position.

The phantom head is filled with lossy liquids emulating the electromagnetic properties of the human tissue for the frequency ranges under study: low frequency region comprising the communication standards GSM850 and GSM900 (824-960MHz), and high frequency region allocating the communication standards GSM1800, GSM1900, and UMTS (1710-2170MHz) [37].

4.3.1 Reflection Coefficient: S_{11}

As the lossy liquids are frequency dependent, the reflection coefficient has to be measured in two steps by means of a network analyzer. Firstly the low frequency region is measured regarding CENELEC liquid @ 900 MHz ($\epsilon_r=41.5$, $\sigma=0.97S/m$) and secondly CENELEC liquid @ 1800 MHz ($\epsilon_r=40$, $\sigma=1.4 S/m$) is used for the high frequency region [37].

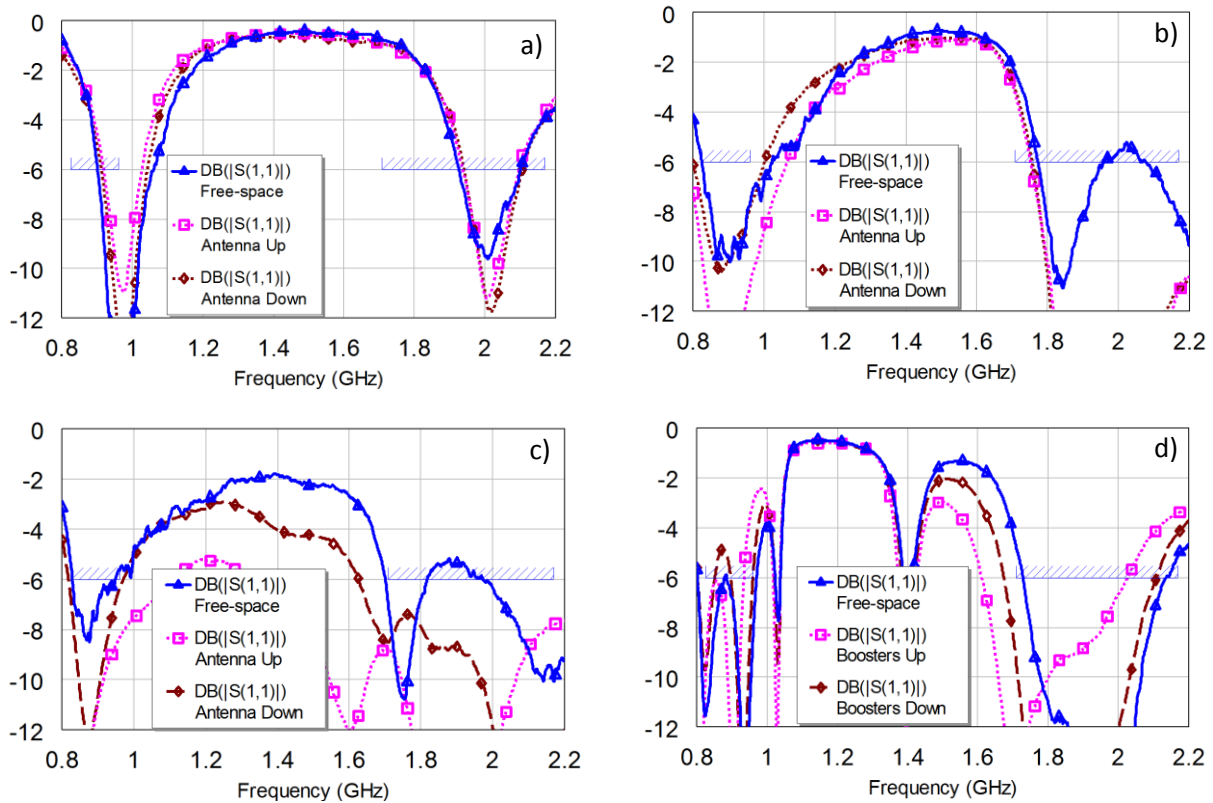


Fig. 4.3 S_{11} regarding free-space and head interaction. a) Dual-band PIFA; b) Hexa-band PIFA with a slotted ground plane; c) Coupled Monopoles; d) Compact radiating system.

As a common trend observed in the four prototypes, the impedance bandwidth increases with respect to the free-space conditions when the phantom head is considered (Fig. 4.3). This increment is directly related to an increment of the power losses, mainly produced by the power absorbed by the human head. This effect is more significant in the low frequency region and substantially higher for the “Antenna Up” position, as it will be further demonstrated along section 4.3.2. Analyzing each prototype particularly, it is possible to state that the presence of the human head does not significantly disturb the low frequency region and even less the high frequency region provided by the dual-band PIFA (Fig. 4.1 (top right)), since no significant detuning effects are observed (Fig. 4.3a).

For the hexa-band PIFA case (Fig. 4.1 (bottom right)) higher losses are likely for the low frequency region and regarding the “Antenna Up” position. However, no significant detuning effect, either in the low frequency region or in the high frequency region is observed (Fig. 4.3b). Regarding the coupled monopoles (Fig. 4.1 (left)), higher losses are expected for both frequency regions since a significant bandwidth increment is observed (Fig. 4.3c).

In the compact radiating system case (Fig. 4.1 (2nd column)), some detuning effect is observed in both frequency regions but more significantly in the high frequency region when the “Boosters Up” position is evaluated (Fig. 4.3d). It is important to notice that for PIFA-based solutions and coupled monopoles no mismatching effect is appreciated, which means that the bandwidth in all cases is equal or larger. However, for the compact radiating system and regarding the “Boosters Up” position a detuning effect to lower frequencies is observed. The quantitative values of the power absorbed by the human head are discussed in the following section.

4.3.2 Absorption Ratios and Free-space Efficiency

The free-space antenna efficiency (Fig. 4.4) of the four prototypes has been measured using the anechoic chamber Satimo Stargate-32. Subsequently, these values have been processed according to the reflection coefficients measured in free space (Fig. 4.3) in order to obtain the radiation efficiency $\eta_r = \eta_a / (1 - |S_{11}|^2)$. In this sense, the mismatching effect is removed and the prototypes can be compared just taking into account losses without the need of regarding whether the antenna is well matched or not (Fig. 4.5).

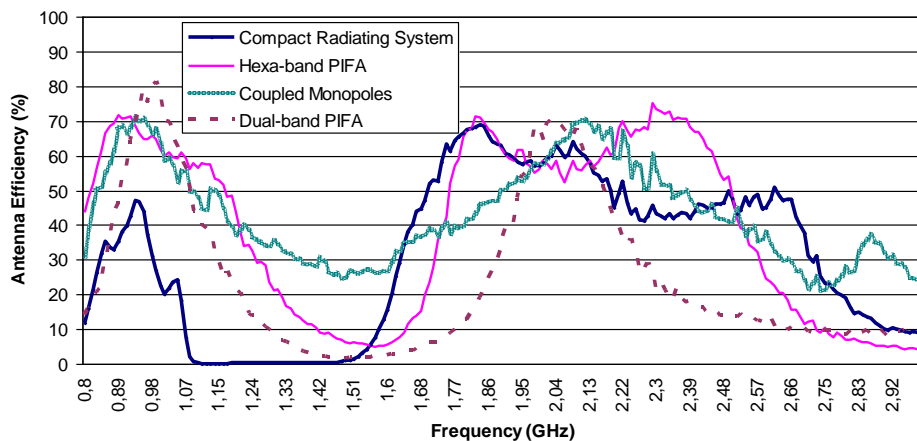


Fig. 4.4 Antenna efficiency measured by 3D integration pattern in the anechoic chamber Satimo Stargate-32 regarding the: dual-band PIFA (Fig. 4.1 (top right)), hexa-band PIFA (Fig. 4.1 (bottom right)), coupled monopoles (Fig. 4.1 (left)), and compact radiating system (Fig. 4.1 (2nd column)) in free-space. The antenna efficiency takes into account the mismatch losses, since it is defined as $\eta_a = \eta_r (1 - |S_{11}|^2)$.

The four prototypes present similar radiation efficiency (Fig. 4.5) in the high frequency region but not in the low frequency region, where the radiation efficiency of the compact radiating system drops to lower values. In this case, the reactive elements that compose the radiofrequency system present a finite Q , fact that contributes to increase losses, more significantly in the low frequency region. However, these efficiency values are still considered acceptable for mobile communications [38]-[41].

The power absorption caused by the human head presence considerably reduces the radiation efficiency in all cases (Fig. 4.6) with respect to those values achieved in free-space conditions (Fig. 4.5). The ratio between the radiation efficiency values obtained in free-space and those obtained taking into account the phantom head gives a quantitative vision of the losses introduced by the human head. In order to carefully analyze the losses experimented by each radiating system, the power absorption ratios associated to each prototype are calculated according to equation (4.1).

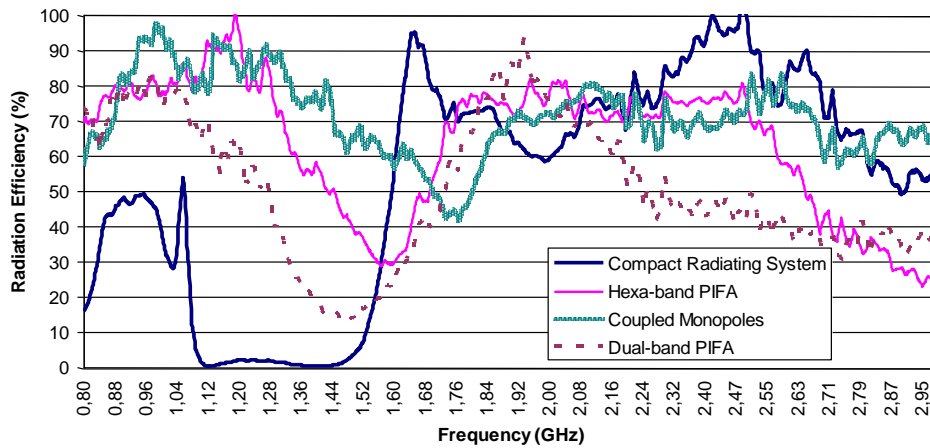


Fig. 4.5 Radiation efficiency associated to the dual-band PIFA (Fig. 4.1 (top right)), the hexa-band PIFA (Fig. 4.1 (bottom right)), the coupled monopoles (Fig. 4.1 (left)), and the compact radiating system (Fig. 4.1 (2nd column)) regarding free-space.

The results reveal that although the radiation efficiency of the compact radiating system in free-space is lower than that offered by the other handset antenna designs when regarding the low frequency region (Fig. 4.5); its performance remains comparable to the other prototypes when the interaction of the human head is considered (Fig. 4.6). Particularly, when regarding “Antenna Up” position, the radiation efficiency of the compact radiating system is comparable to that obtained by the coupled monopoles in the low frequency region, thus revealing that the latest is more sensitive to the human interaction (Fig. 4.6a). The results are even better when regarding the “Antenna Down” position, since in this case the compact radiating system offers larger efficiency values than the coupled monopoles, thus highlighting again the sensitiveness of the latest to the human interaction. In view of the outcomes, it is possible to conclude that the proposed compact radiating system is more robust to the human head presence in the low frequency region, since it suffers lower efficiency losses.

$$Absorption_ratio[dB] = 10 \cdot \log_{10} \left(\frac{\eta_{rad_free_space}}{\eta_{rad_head_position}} \right) \quad (4.1)$$

In the high frequency region and when regarding the “Antenna Up” location, the losses are larger than those experimented by the other prototypes. Nevertheless, in the “Antenna Down” position in this frequency region, the behavior remains comparable to that presented by the other designs, and more particularly to the hexa-band PIFA. In this sense, the results analyzed at both frequency regions and regarding all the prototypes conclude that the power absorption is higher for the “Antenna Up” position

than for the “Antenna Down” position. This last becomes preferred since for this position the distance between the antenna and the human head is larger.

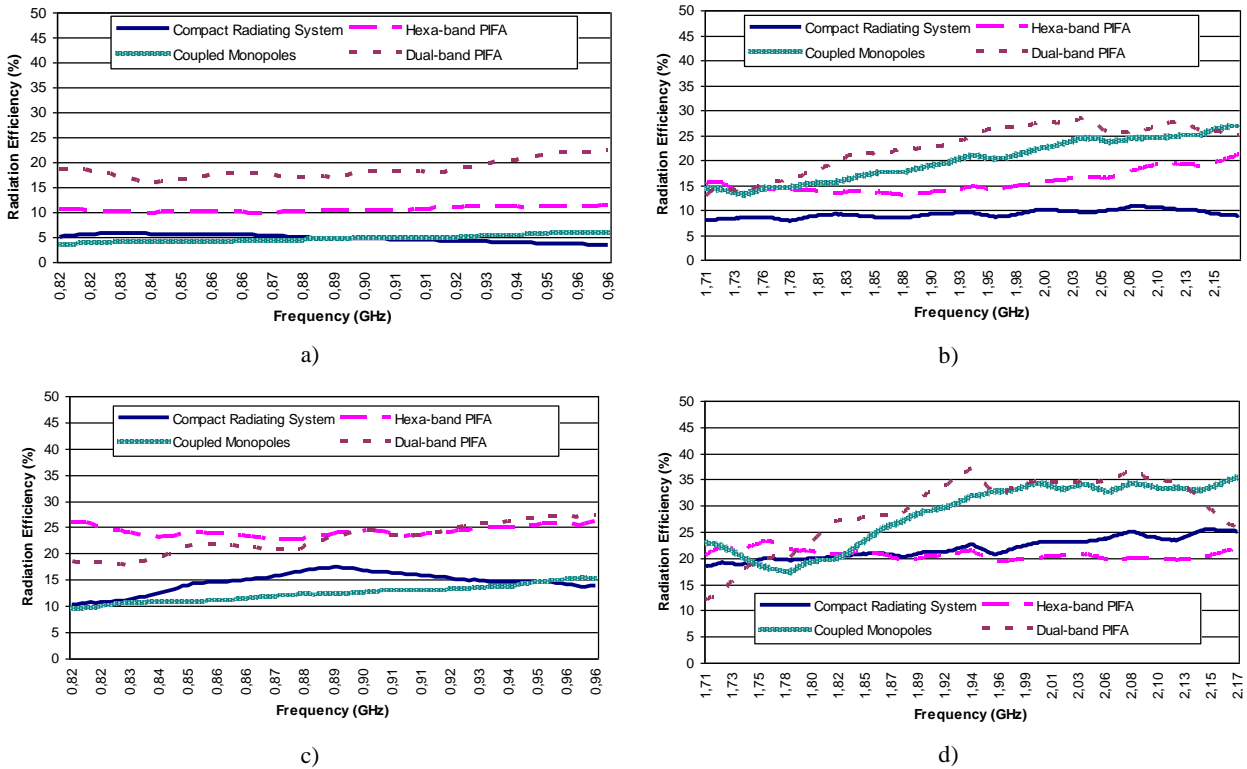


Fig. 4.6 Measured radiation efficiency in the low and high frequency region for the dual-band PIFA (Fig. 4.1 (top right)), the hexa-band PIFA (Fig. 4.1 (bottom right)), the coupled monopoles (Fig. 4.1 (left)), and the compact radiating system (Fig. 4.1 (2nd column)) regarding a)-b) “Antenna Up” position and c)-d) “Antenna Down” position.

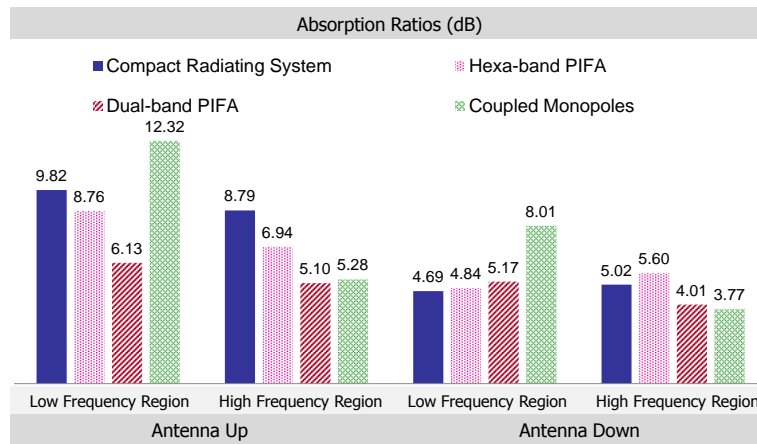


Fig. 4.7 Average absorption ratios across the low frequency region (824-960 MHz) and the high frequency region (1710-2170MHz) regarding both positions “Antenna Up” and “Antenna Down”.

At the same time and perfectly aligned with the results gathered in the previous section, the absorption ratio is higher in the low frequency region than in the high frequency region (Fig. 4.7). In particular and as stated above, losses are higher for the coupled monopoles, being around 12 dB in average, when regarding the low frequency region and the worst configuration (“Antenna Up”) (Fig. 4.7). This fact coincides with the predictions extracted from the reflection coefficient measurements (Fig. 4.3) where a considerable bandwidth increment was observed. In the preferred situation (“Antenna Down”), the compact radiating system becomes the best option concerning losses, operation, and volume.

4.3.3 Antenna Efficiency regarding Human Head

In this section the antenna efficiency is measured taken into account the human head interaction. Thus, losses associated to the amount of power absorbed by the human head are considered as well as the mismatching effects regarding both talking positions under study: “Antenna Up” and “Antenna Down”.

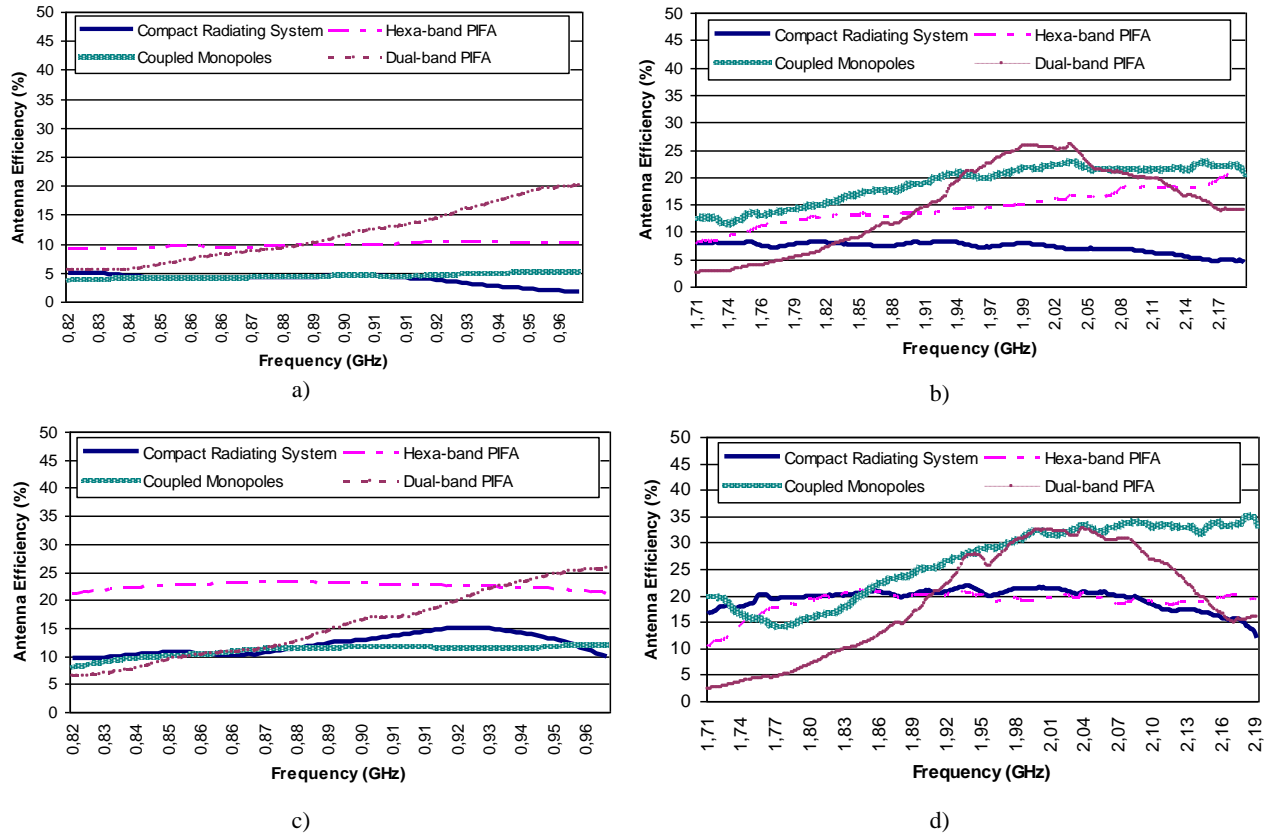


Fig. 4.8 Measured antenna efficiency in the low and high frequency region for the dual-band PIFA (Fig. 4.1 (top right)), the hexa-band PIFA (Fig. 4.1 (bottom right)), the coupled monopoles (Fig. 4.1 (left)), and the compact radiating system (Fig. 4.1 (2nd column)) regarding a)-b) “Antenna Up” position and c)-d) “Antenna Down” position.

As aforementioned, the “Antenna Up” position is the configuration that suffers higher losses in all cases mainly due to the proximity of the antenna to the human head. Thus, the antenna efficiency is noticeably reduced with respect to the free-space conditions (Fig. 4.4) regarding both frequency regions (Fig. 4.8a-b). It is important to remark that despite the antenna efficiency of the compact radiating system prototype is lower than that presented by the other cases referring free-space measurements, the difference diminishes when the human head presence is considered. In this sense, the antenna efficiency attained in the low frequency region is comparable to that obtained by the coupled monopoles especially in the frequency band associated to the communication standard GSM850, taking into account that the starting point in the coupled monopole case was an antenna efficiency around 60% whereas the compact radiating system offered values around 40%. These results confirm again that coupled monopoles present higher absorption losses than the booster-based antenna technology. In the high frequency region, the antenna efficiency concerning the compact radiating system could be improved if the detuning effect is corrected through the appropriate adjustment of the matching network components.

In the preferred configuration (“Antenna Down”), the compact radiating system prototype experiments less additional losses than the other antenna designs and as expected, the antenna efficiency achieved in the low frequency region is comparable to that values attained by other common handset antenna designs such as the coupled monopoles (Fig. 4.8c-d). The best values are those achieved by the hexa-band PIFA and are comparable to that obtained by the dual-band PIFA regarding those frequencies for which the antenna is matched. In the high frequency region, the compact radiating system prototype competes directly with the hexa-band PIFA prototype since similar values are obtained with the added advantage of its reduced volume (250mm^3) compared to the 3600mm^3 of the hexa-band PIFA.

4.3.4 Radiation Patterns

Following with the study of the human head effect over the main antenna parameters, radiation patterns are evaluated and presented along this section. Although the four prototypes have been measured regarding free-space conditions and human head interaction for both positions: “Antenna Up” and “Antenna Down”, only the most significant results related to the compact radiating system prototype are presented herein (Fig. 4.9).

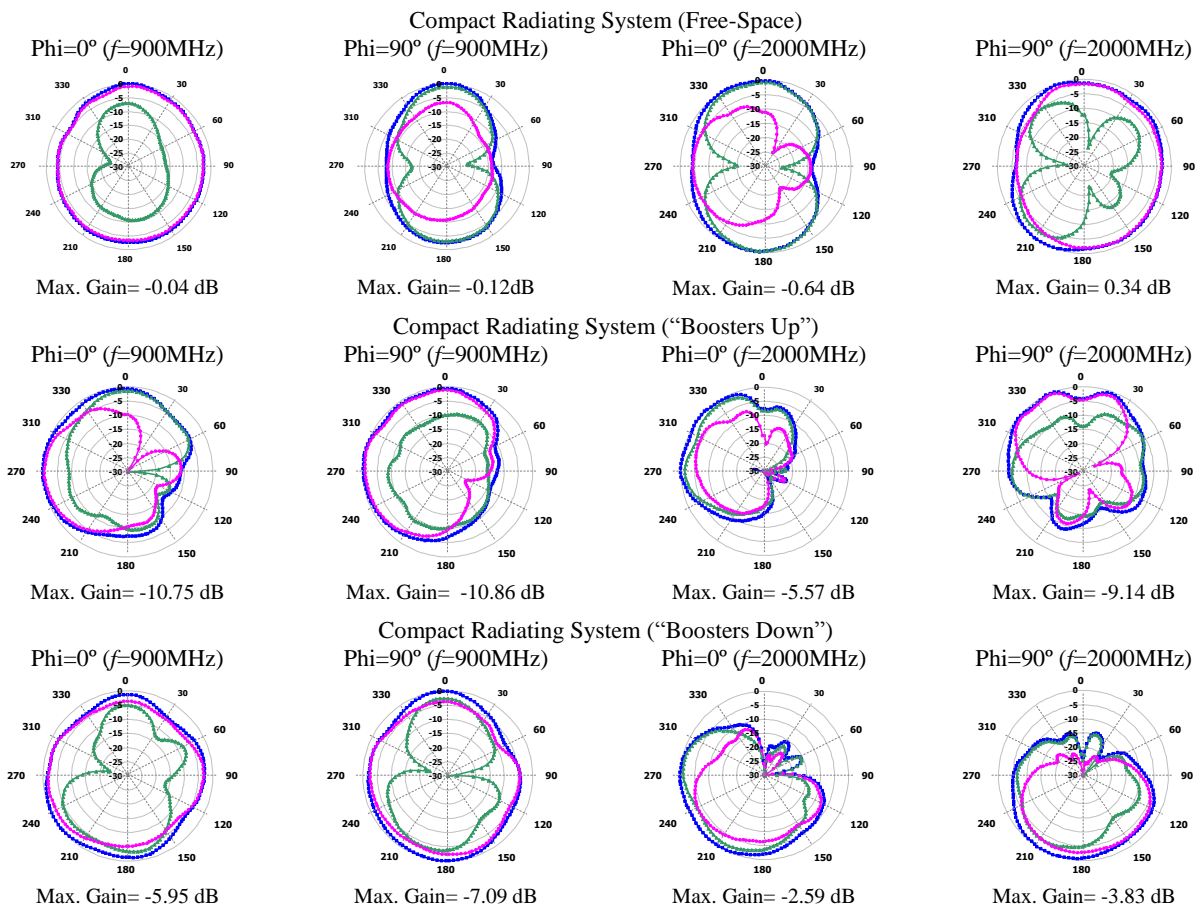


Fig. 4.9 Main cuts ($\Phi=0^\circ$ and $\Phi=90^\circ$) of the radiation patterns provided by the compact radiating system prototype (Fig. 4.1 (2nd column)) measured at the frequency of 900MHz and 2000MHz regarding free-space and human head for both positions: “Boosters Up” and “Boosters Down”. See coordinate axis at Fig. 4.2.

The effect of the human head over the radiation pattern is quite similar for all the cases. The omnidirectional behavior found in free-space conditions is modified with the human head presence

resulting in a directivity increment (depicted in Fig. 4.10 and Fig. 4.11 as an average Δ) for all the prototypes under study. This effect is mainly produced by the fact that at these frequencies the phantom head acts as a lossy reflector. The impact is more evident in the high frequency region since for this frequency range the head is electrically larger.

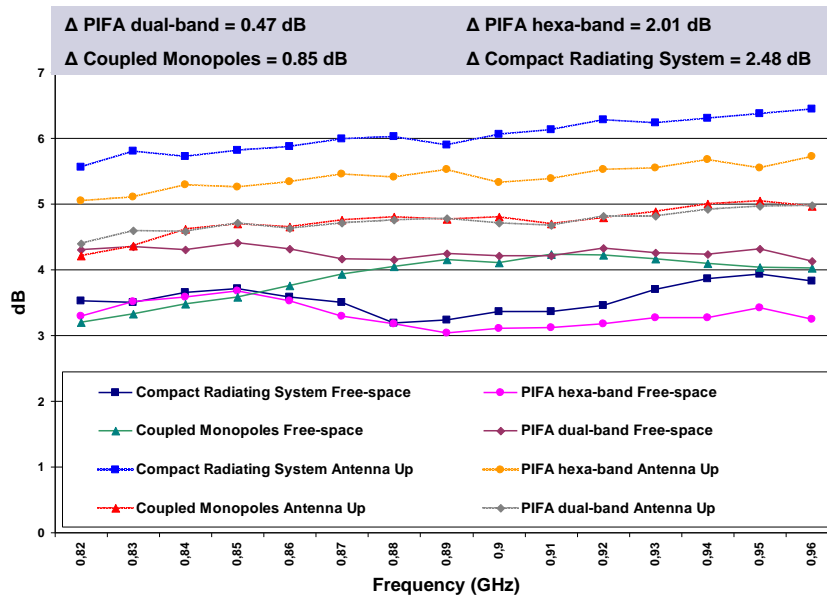


Fig. 4.10 Measured directivity in the low frequency region regarding the four prototypes in free-space and human head conditions.

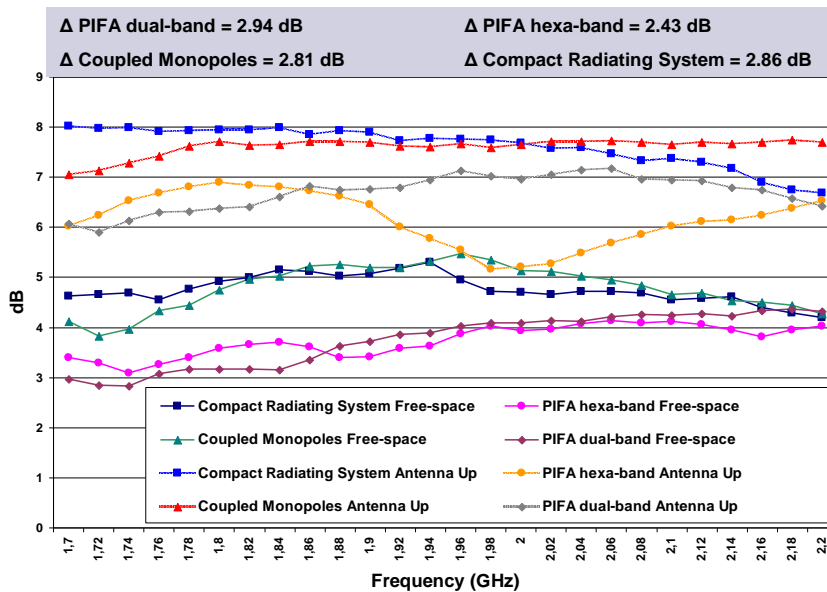


Fig. 4.11 Measured directivity in the high frequency region regarding the four prototypes in free-space and human head conditions.

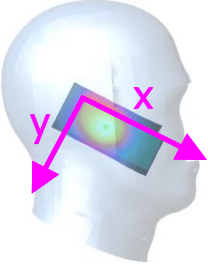

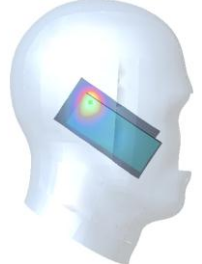
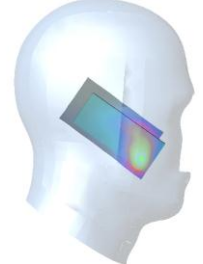
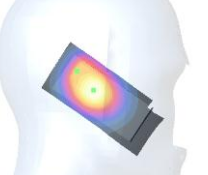
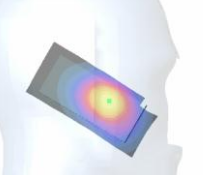
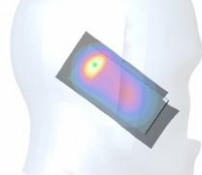
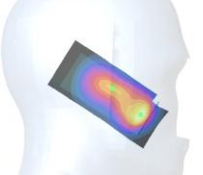
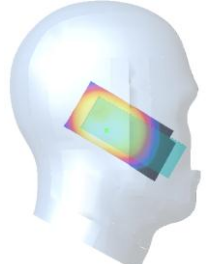
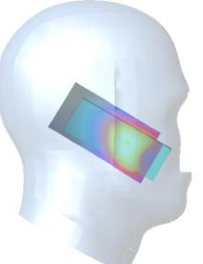
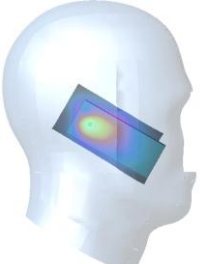
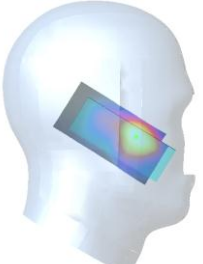
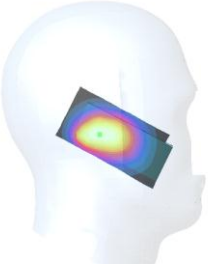


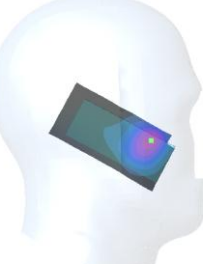
As previously mentioned, the directivity for the three prototypes regarding free-space conditions remains around 3.5 dB in the low frequency region and slightly increases as long the frequency increases. The effect caused by the human head presence traduces in a directivity increment regarding both frequency regions for all the prototypes under study, concluding that it affects in a similar way to their radiation patterns. Note that for simplicity purposes the “Antenna Up” position is considered since it

produces more significant effects over the directivity. The “Antenna Down” case also increases the directivity but their effects are not so noteworthy.

4.4. Biological Compatibility

The assessment of the human head impact must be carried out regarding two main aspects. On one hand, the effect over the performance of the handset antenna, which takes into account absorption losses and detuning effects (former section), and on the other hand, the biological impact over the human head, which is the object of the present section.

Table 4.1 SAR Measurements. The hotspot coordinates (x,y) are referred to top right corner of the ground plane.

	Antenna Up ($f=900\text{MHz}$)	Antenna Down ($f=900\text{MHz}$)	Antenna Up ($f=1900\text{MHz}$)	Antenna Down ($f=1900\text{MHz}$)
Dual-band PIFA				
	(1g):2.46mW/g (10g):1.65mW/g Hotspot: (38,20)	(1g):2.29mW/g (10g):1.52mW/g Hotspot: (64,14)	(1g):2.68mW/g (10g):1.36mW/g Hotspot: (9,8)	(1g):0.79mW/g (10g):0.44mW/g Hotspot: (91,30)
Hexa-band PIFA				
	(1g):2.42mW/g (10g):1.61mW/g Hotspot: (35,19)	(1g):2.02mW/g (10g):1.39mW/g Hotspot: (65,13)	(1g):3.28mW/g (10g):1.50mW/g Hotspot: (13,14)	(1g):1.63mW/g (10g):0.89mW/g Hotspot: (92,20)
Coupled Monopoles				
	(1g):3.58mW/g (10g):2.48mW/g Hotspot: (27,29)	(1g):2.36mW/g (10g):1.67mW/g Hotspot: (68,18)	(1g):2.93mW/g (10g):1.66mW/g Hotspot: (18,23)	(1g):1.47mW/g (10g):0.92mW/g Hotspot: (68,16)
Compact Radiating System				
	(1g):1.11mW/g (10g):0.77mW/g Hotspot: (26,26)	(1g):0.59mW/g (10g):0.41mW/g Hotspot: (66,16)	(1g):2.15mW/g (10g):1.27mW/g Hotspot: (24,27)	(1g):0.98mW/g (10g):0.59mW/g Hotspot: (79,5)

SAR is the parameter used to evaluate the biological impact over the human head caused by the electromagnetic fields radiated by a handset antenna. SAR is a measure of the localized maximum value of the power absorbed by the human head by unity of mass and its dimensions are mW/g. Due to the fact that this absorption is produced in the near field, SAR can be measured from the electric near field according to equation (4.2), where σ_{eff} , and ρ are the human tissue effective conductivity and the tissue volumetric density, respectively.

$$SAR = \frac{\sigma_{eff}}{\rho} |\vec{E}|^2 \quad (4.2)$$

In this sense, the SAR values associated to the four prototypes under study have been measured using the DASY4 equipment. SAR distribution is depicted at two representative frequencies, one associated to the low frequency region (900MHz) and the other one located in the high frequency region (1900MHz) regarding both positions: “Antenna Up” and “Antenna Down” (Table 4.1).

As a common feature, SAR values are higher in the “Antenna Up” position since the antenna is nearer the human head. In this sense, the fact of rotating the prototype 180° causes a significant reduction of the SAR values. This effect is observed in all the prototypes and more significantly in the high frequency region where the maximum electric field appears localized in the shorter edge of the PCB at a certain distance from its center. Otherwise, in the low frequency region, SAR reduction is less significant, since for these frequencies the electric field is distributed along the PCB and the hot-spot is located nearer the PCB center.

In the case of the low frequency region, the SAR values regarding both positions are located below the standards (American standard (ANSI/IEEE): 1.6mW/g (1g) and European standard (ICNIRP) 2mW/g (10g)). However, for the high frequency region the “Antenna Down” position is preferred.

4.5. Evaluation Criteria

As previously discussed, human interaction must be carefully considered when assessing the performance of a particular prototype. The effects produced by this human interaction must be considered from two main perspectives. On one hand, the functional analysis, i.e. the effects that the human head produce over the antenna performance, which usually translate into detuning and efficiency decrements. On the other hand, the biological analysis, i.e. the effects that the electromagnetic radiation produce over the human head. This section analyzes the relationship between these functional and biological effects and proposes a figure of merit with the aim of determining the solution that minimizes SAR while becomes robust to detuning effects and efficiency decrements.

4.5.1 SAR versus Power Absorption and Antenna Efficiency

In order to complete the study it is interesting to deeply analyze the correlation between the SAR values and the power absorption. A priori, the statement, the higher the SAR, the higher the absorption

losses, seems reasonable. However, the experiments carried out demonstrate that this is an invalid affirmation because this statement is not always true.

SAR is a measure of the peak power absorption per unit of mass as defined in (4.2). Consequently, it only gives information about the maximum value of absorption and the location where it takes place. On the contrary, the total power absorption, as given in (4.3), is calculated as the integral along all the head volume (V') so it is directly connected with the distribution of the near electrical fields. On one hand, SAR is an electromagnetic magnitude useful for biological analysis since it is directly related to temperature elevations inside the human's head [35]. On the other hand, power absorption is referred to the antenna performance that at the end, determines the phone behavior. Power absorption could determine functional parameters, such as the duration of the handset battery as well as coverage.

$$Power_absorption = \int_{V'} \sigma_{eff} \cdot |E|^2 dV' \quad (4.3)$$

In this sense, it is possible to find a prototype having maximum SAR but minimum power absorption. This is the case of the hexa-band PIFA, which presents at a frequency of 2000MHz regarding the "Antenna Up" position a high level of SAR (2.81 mW/g (1g)) and losses around 7.11 dBs. On the contrary, the behavior of the compact radiating system prototype at 900 MHz shows that it is possible to have low SAR (1.11 mW/g (1g)) but higher losses (around 10.07 dB). This fact demonstrates that both values are not necessarily directly proportional, high values of SAR do not imply high losses, since they are only defined by the distribution of the near fields along the PCB.

The conclusion that can be extracted from the compact radiating system results (Table 4.2 and Table 4.3) is that as long as the frequency increases, the near electric field distribution concentrates nearer the ground plane boosters providing high values of SAR. At the same time since the hot-spot is located nearer the booster and at a significant distance from the PCB midpoint, the rotation of the PCB ("Boosters Down" position) not only reduces the SAR values but also the power absorption levels.

Table 4.2 SAR and Absorption Losses regarding "Boosters Up".

Compact Radiating System	Boosters Up			
	Frequency(MHz)	SAR(1g) (mW/g)	Hot Spot (x,y)	Absorption Losses (dB)
835	1.81	32,28	7.06	4.75
900	1.11	26,26	10.07	4.58
1800	2.42	20,28	9.23	7.82
1900	2.15	24,27	8.57	8.03
2000	2.19	26,23	7.71	7.90

Table 4.3 SAR and Absorption Losses regarding "Boosters Down".

Compact Radiating System	Boosters Down			
	Frequency(MHz)	SAR(1g) (mW/g)	Hot Spot (x,y)	Absorption Losses (dB)
835	0.88	66,12	4.03	9.91
900	0.59	66,16	4.61	13.01
1800	0.97	81,6	5.62	19.85
1900	0.98	79,5	4.91	20.76
2000	1.03	79,5	4.14	21.41

The compact radiating system presents lower SAR values for the preferred position ("Boosters Down") when it is compared with those achieved by the other prototypes. This fact, depicted in Table 4.4,

leads to an important conclusion since for approximately the same antenna efficiency (especially comparing the compact radiating system with the coupled monopole in the low frequency region and with the hexa-band PIFA in the high frequency region (Fig. 4.8c-d) the SAR values obtained are noticeably reduced (Table 4.4).

Table 4.4 SAR (1g) Comparison for “Antenna Down” Position.

Prototype	(900MHz)	(1900MHz)
Dual-band PIFA	2.29 mW/g	0.79 mW/g
Hexa-band PIFA	2.02 mW/g	1.63 mW/g
Coupled monopoles	2.36 mW/g	1.47 mW/g
Compact Radiating System	0.59 mW/g	0.98 mW/g

Accordingly and in order to define a criteria for evaluating the performance of the four prototypes regarding both biological and functional effects in terms of SAR and power absorption, a new figure of merit is proposed and discussed in the following section.

4.5.2 Figure of Merit

The proposed figure of merit is defined as the ratio between the antenna efficiency and the SAR values for a given frequency. As aforementioned, the absorption ratios and SAR values are not necessarily directly linked. However, SAR values are directly related to the antenna efficiency. Thus, for a given device, the higher the power radiated by the antenna, the higher the SAR values.

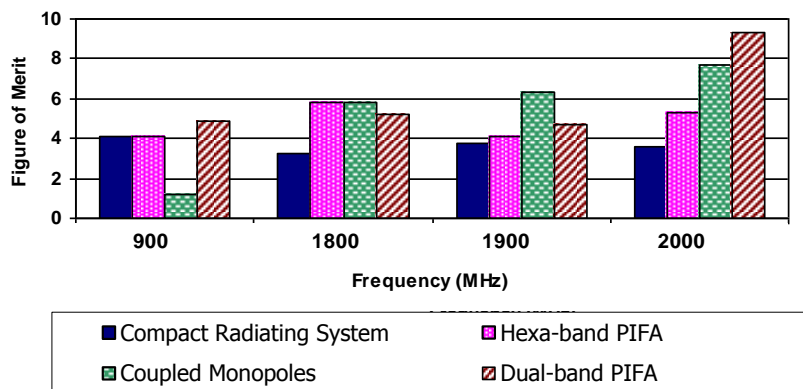


Fig. 4.12 Figure of Merit regarding “Antenna Up” position.

In this sense and in order to establish a fair comparison between prototypes, a figure of merit that relates antenna efficiency and SAR is provided regarding both positions: “Antenna Up” and “Antenna Down”, respectively (Fig. 4.12 and Fig. 4.13). Accordingly, the prototype with better performance is the one that presents higher antenna efficiency and lower SAR values.

In the “Antenna Up” case, the compact radiating system does not present the best trade-off. However, for the low frequency region the values obtained are comparable with those achieved by the hexa-band PIFA. In this case, the dual-band PIFA is the prototype that maximizes antenna efficiency while minimizing SAR at those frequencies for which the antenna is well-matched. Otherwise coupled monopoles and hexa-band PIFA alternate their performance since for the low frequency region, the hexa-

band PIFA would be preferred while for frequencies around 1900MHz, coupled monopoles perform better.

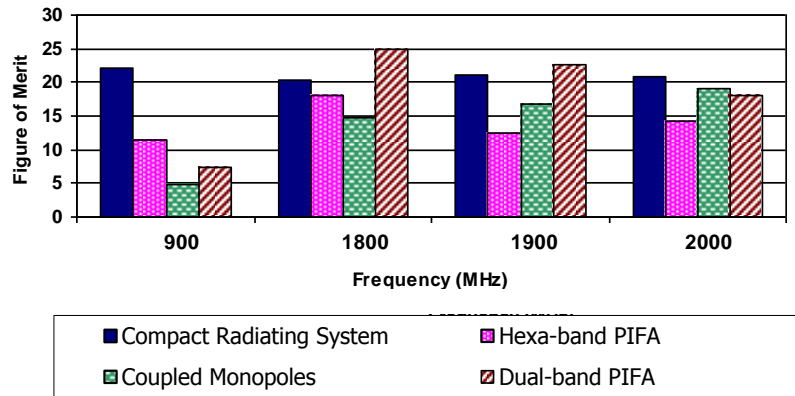


Fig. 4.13 Figure of Merit regarding “Antenna Down” position.

Nevertheless and taking into account the preferred position: “Antenna Down”, the compact radiating system stands out over the hexa-band PIFA and the coupled monopoles as the better solution regarding both frequency regions, but especially for the low frequency region. In the high frequency region, the values obtained are comparable with those achieved by the dual-band PIFA but with the advantage of the reduced volume and the penta-band operation of the compact radiating system. This fact turns the compact radiating system in a good alternative to the already existing handset antennas technologies since it is able not only to provide penta-band operation with a reduced volume (250 mm^3) but also to ensure robustness to the human head effect guarantying low SAR values.

4.6. Conclusions

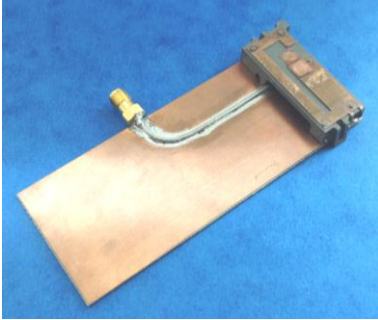

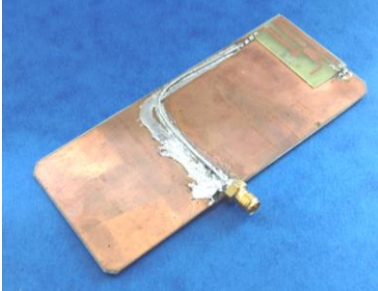
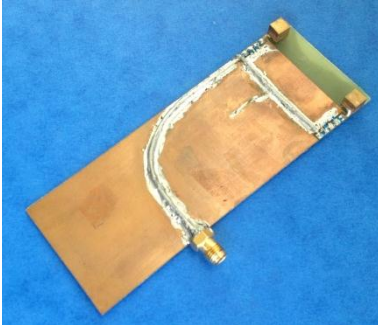
Free-space measurements are not enough to fully characterize a handset device since the presence of the human head in the vicinity of a handset antenna strongly affects its performance. This effect must be taken into account regarding two main aspects: functional and biological. The first one considers the effect of the human head over the main antenna parameters whereas the second one relates to the effect of the radiated fields into the human head in terms of SAR and temperature elevation.

On one hand, power absorption losses and SAR values can be minimized if the antenna is placed in the PCB edge located at a higher distance from the human cheek. On the other hand, the results show that SAR values are not necessarily associated with power absorption, since while SAR is a measure of the peak power absorption per unit of mass, the power absorption is defined as the integral along all the head volume so it is directly connected to the near electrical fields distribution. It means that a prototype can present high losses but low SAR values, and in this sense, a figure of merit is required for the sake of comparison since the best solution is the one that maximizes antenna efficiency while minimizing SAR.

Regarding the preferred arrangement (“Antenna Down”), the compact radiating system using ground plane boosters stands out over the other prototypes in the low frequency region, since is the one that minimizes SAR while maximizes antenna efficiency. For instance, the coupled monopoles present significantly higher SAR(1g) values (2.36 mW/g (900MHz)) than the compact radiating system

(0.59mW/g (900MHz)) while offering similar antenna efficiencies, around 11.58% and 13.01% at 900MHz for the coupled monopoles and the compact radiating system, respectively.

Table 4.5 Summary of the main results related to the dual-band PIFA, the hexa-band PIFA on a slotted ground plane, the coupled monopoles, and the compact radiating system including ground plane boosters, when regarding the human head.

Architecture	Features	Performance
	<ul style="list-style-type: none"> PIFA antenna 40 mm x 15 mm x 6 mm. Ground plane 100 mm x 40 mm. 	<ul style="list-style-type: none"> GSM900 and GSM1900 SAR_{down} (900MHz)=2.29mw/g SAR_{down} (1900MHz)=0.79mW/g Antenna Efficiency_{down} (900MHz)=16.76% Antenna Efficiency_{down} (1900MHz)=17.80%
	<ul style="list-style-type: none"> PIFA antenna 40 mm x 15 mm x 6 mm on a slotted ground plane Ground plane 100 mm x 40 mm 	<ul style="list-style-type: none"> GSM850, GSM900, GSM1800, GSM1900, UMTS, and LTE2300 SAR_{down} (900MHz)=2.02mw/g SAR_{down} (1900MHz)=1.63mW/g Antenna Efficiency_{down} (900MHz)=22.88% Antenna Efficiency_{down} (1900MHz)=20.20%
	<ul style="list-style-type: none"> Coupled monopoles formed by a driven monopole and two parasitic elements (15 mm x 33 mm) Ground plane 110 mm x 47 mm 	<ul style="list-style-type: none"> GSM850, GSM900, GSM1800, GSM1900, and UMTS SAR_{down} (900MHz)=2.36mw/g SAR_{down} (1900MHz)=1.47mW/g Antenna Efficiency_{down} (900MHz)=9.03% Antenna Efficiency_{down} (1900MHz)=24.85%
	<ul style="list-style-type: none"> Electric Ground Plane Boosters, each one with dimension of 5 mm x 5 mm Ground plane 100 mm x 40 mm 	<ul style="list-style-type: none"> GSM850, GSM900, GSM1800, GSM1900, and UMTS SAR_{down} (900MHz)=0.59mw/g SAR_{down} (1900MHz)=0.98mW/g Antenna Efficiency_{down} (900MHz)=9.91% Antenna Efficiency_{down} (1900MHz)=20.76%

In the high frequency region, the dual-band PIFA presents slightly better results from the figure of merit point of view. Nevertheless, the compact radiating system is still preferable at this frequency region not only by the considerable size reduction offered (a reduction of approximately one order of magnitude, from 3600 mm³ up to 250 mm³), but also, because it increases the number of operating frequency bands

in said high frequency region, from single band operation (GSM1900) offered by the dual-band PIFA to a tri-band operation (GSM1800, GSM1900, and UMTS).

The summary of the main results extracted from this section (Table 4.5), illustrate that the proposed compact radiating system based on the excitation of the ground plane modes becomes a suitable solution that directly competes with other common handset antenna designs regarding functional performance and with the advantage of a reduced volume (250 mm³). In particular, the solution is capable of providing penta-band operation (GSM850, GSM900, GSM1800, GSM1900, and UMTS) while reducing SAR values in both frequency regions with respect to those presented by the other handset antenna architectures.

4.7. References

- [1] F. Frost & Sullivan, *Antennas Systems 2006*, Washington, USA, 2006.
- [2] M. Geissier, D. Heberling, and I. Wolff, "Bandwidth and Radiating Properties of Internal Handset Antennas", *IEEE Antennas and Propagation Society International Symposium*, vol. 4, July 2000, pp. 2246-2249.
- [3] K. L. Wong, *Planar Antennas for Wireless Communications*, New York, John Wiley & Sons, 2003.
- [4] C. Puente, J. Anguera, J. Soler, and A. Condes, "Coupled Multi-band Antennas", *Patent Application WO2004/025778*, September 10, 2002.
- [5] C. Lin and K. L. Wong, "Printed Monopole Slot Antenna for Internal Multi-band Mobile Phone Antenna", *IEEE Transactions on Antennas and Propagation*, vol. 55, n°12, December 2007, pp. 3690-3697.
- [6] S. Risco, J. Anguera, A. Andújar, A. Pérez and C. Puente, "Coupled Monopole Antenna Design for Multi-band Handset Devices", *Microwave and Optical Technology Letters*, vol. 52, n° 2, February 2010, pp. 359-364.
- [7] C. Wu and K. Wong, "Hexa-band Internal Printed Slot Antenna for Mobile Phone Application", *Microwave and Optical Technology Letters*, vol. 50, n°1, January 2008, pp. 35-38.
- [8] J. Anguera, I. Sanz, J. Mumbrú, and C. Puente, "Multi-Band Handset Antenna with a Parallel Excitation of PIFA and Slot Radiators", *IEEE Transactions on Antennas and Propagation*, vol.58, n°2, February 2010, pp.348-356.
- [9] J. Anguera, I. Sanz, A. Sanz, A. Condes, D. Gala, C. Puente, and J. Soler, "Enhancing the performance of handset antennas by means of groundplane design", *IEEE International Workshop on Antenna Technology: Small Antennas and Novel Metamaterials (iWAT 2006)*. New York, USA, March 2006.
- [10] J. Anguera, A. Cabedo, C. Picher, I. Sanz, M. Ribó, and C. Puente, "Multi-band Handset Antennas by Means of Groundplane Modification", *IEEE Antennas and Propagation Society International Symposium*, Honolulu, Hawaii, USA, June 2007.

- [11] C. Picher, J. Anguera, A. Cabedo, C. Puente, and S. Kahng, "Multi-band Handset Antenna Using Slots on the Ground Plane: Considerations to Facilitate the Integration of the Feeding Transmission Line", *Progress In Electromagnetics Research C*, vol. 7, 2009, pp. 95-109.
- [12] C. Picher, J. Anguera, A. Andújar, C. Puente, and A. Bujalance, "Multi-band Handset Antennas by Combining Monopoles and Intelligent Ground Planes", *Proceedings of the Sixth European Conference on Antennas and Propagation*, EuCAP 2012, Prague, Czech Republic, March 2012, pp. 2741-2744.
- [13] C. Picher, J. Anguera, A. Bujalance, A. Andújar, and C. Puente, "Analysis of a Multi-band Monopole Handset Antenna Combined with a Slotted Ground Plane", *Microwave and Optical Technology Letters*, vol. 55, n°1, January 2013, pp. 173-180.
- [14] A. Cabedo, J. Anguera, C. Picher, M. Ribó, and C. Puente, "Multi-Band Handset Antenna Combining a PIFA, Slots, and Ground Plane Modes", *IEEE Transactions on Antennas and Propagation*, vol.57, n°9, Sep. 2009, pp. 2526-2533.
- [15] R. Quintero and C. Puente, "Multilevel and Space-Filling Ground Planes for Miniature and Multi-band Antennas", *Patent Application* WO2003/023900, September 13, 2001.
- [16] J. Anguera and C. Puente, "Shaped Ground Plane for Radio Apparatus", *Patent Application* WO2006/070017, December 29, 2005.
- [17] M. Cabedo-Fabrés, E. Antonino-Daviu, A. Valero-Nogueira, and M. Ferrando Bataller, "The Theory of Characteristic Modes Revisited: A Contribution to the Design of Antennas for Modern Applications", *IEEE Antennas and Propagation Magazine*, vol. 49, n°5, October 2007, pp. 52-68.
- [18] W. L. Schroeder, C. T. Famdie, and K. Solbach, "Utilization and Tuning of the Chassis Modes of a Handheld Terminal for the Design of Multi-band Radiation Characteristics", *IEEE Transactions on Antennas and Propagation*, vol. 50, n°10, October 2002, pp. 1433-1444.
- [19] C. Puente J. Anguera, "Handset with Electromagnetic Bra", *Patent Application* WO2005/083833, February 28, 2005.
- [20] S. Ozden, B. K. Nielsen, C. H. Jorgensen, J. Villanen, C. Icheln, and P. Vainikainen, "Quad-Band Coupling Element Antenna Structure", *U.S. Patent* 7,274,340, September 25, 2007.
- [21] J. Anguera, I. Sanz, C. Puente, and J. Mumbrú, "Wireless Device including a Multi-band Antenna System", *Patent Application* WO2008/119699, March 26, 2008.
- [22] J. Anguera, A. Andújar, C. Puente, and J. Mumbrú, "Antennaless Wireless Device", *Patent Application* WO2010/015365, July 31, 2009.
- [23] J. Anguera, A. Andújar, C. Puente, and J. Mumbrú, "Antennaless Wireless Device Capable of Operation in Multiple Frequency Regions", *Patent Application* WO2010/015364, July 31, 2009.
- [24] A. Andújar, J. Anguera, and C. Puente, "Ground Plane Boosters as a Compact Antenna Technology for Wireless Handheld Devices", *IEEE Transactions on Antennas and Propagation*, vol. 59, n°5, May 2011, pp. 1668-1677.

- [25] A. Andújar, J. Anguera, C. Picher, and C. Puente, "Human Head Interaction over Ground Plane Booster Antenna Technology: Functional and Biological Analysis", *Progress in Electromagnetic Research B*, vol. 41, 2012, pp. 153-185.
- [26] J. Anguera, A. Camps, A. Andújar, and C. Puente, "Enhancing the robustness of handset antennas to finger loading effects", *IEE Electronics Letters*, vol.45, n°15, July 2009, pp. 770-771.
- [27] J. M. Jung, S. Kim, K. Kong, J. Lee, and B. Lee, "Designing Ground Plane to Reduce Hand Effects on Mobile Handsets", *IEEE Antennas and Propagation Society International Symposium*, Honolulu, USA, June 2007, pp. 1040-1043.
- [28] C. Su, C. Wu, and K. Wong, "User's Hand Effects on EMC internal GSM/DCS mobile phone antenna", *IEEE Antennas and Propagation Society International Symposium*, Albuquerque, USA, pp. 2097-2100, July 2006.
- [29] P. S. Kildal and C. Carlsson, "Comparison between Head Losses of 20 Phones with External and Built-in Antennas Measured in Reverberation Chamber", *IEEE Antennas and Propagation Society International Symposium*, vol. 1, August 2002, pp. 436-439.
- [30] K. R. Boyle, Y. Yuan, and L. P. Ligthart, "Analysis of Mobile Phone Antenna Impedance Variations with User Proximity", *IEEE Transaction on Antennas and Propagation*, vol.55, n°2, February 2007, pp. 364-372.
- [31] T. Huang and K. R. Boyle, "User Interaction Studies on Handset Antennas", *Proceedings of the Second European Conference on Antennas and Propagation*, EuCAP2007, Edinburgh, United Kingdom, 2007.
- [32] D. Lu, D. Fisk, and A. Wang, "A Mobile Antenna Design for Optimal Performance in Human Head and Hand Configuration", *IEEE Antennas and Propagation Society International Symposium*, Honolulu, USA, June 2007, pp. 1048-1048.
- [33] M. A. Ebrahimi-Ganjeh and A. R. Attari, "Interaction of Dual Band Helical and PIFA Handset Antennas with Human Head and Hand", *Progress In Electromagnetics Research*, PIER 77, 2007, pp. 225-242.
- [34] A. Schiavoni, P. Bertotto, G. Richiardi, and P. Bielli, "SAR Generated by Commercial Cellular Phones –Phone Modeling, Head Modeling, and Measurements", *IEEE Transactions on Microwave Theory and Techniques*, vol.18, n°11, November 2000, pp. 2064-2071.
- [35] P. Bernardi, M. Cavagnaro, S. Pisa, and E. Piuzzi, "Power Absorption and Temperature Elevations Induced in the Human Head by a Dual-Band Monopole-Helix Antenna Phone", *IEEE Transactions on Microwave Theory and Techniques*, vol. 49, n°12, December 2001, pp. 2539-2546.
- [36] H. Khodabakhshi and A. Cheldavi, "Human Head Interaction with a PIFA in Cellular Mobile Communication", *Proceedings of the Fourth European Conference on Antennas and Propagation*, EuCAP2010, Barcelona, Spain, 2010.

- [37] Basic standard for the measurement of Specific Absorption Rate related to human exposure to Electromagnetic fields from mobile phones (300 MHz-3GHz. CENELEC-European Committee for Electro technical Standardization Std. EN 50 361, Jul. 2001.
- [38] M. Martínez, O. Letschke, M. Geissler, D. Heberling, A. M. Martínez, and D. Sánchez, “Integrated Planar Multi-band Antennas for Personal Communication Handsets”, *IEEE Transactions on Antennas and Propagation*, vol. 54, n°2, February 2006, pp. 384-391.
- [39] B. Kim, S. Park, Y. Yoon, J. Oh, K. Lee, and G. Koo, “Hexaband Planar Inverted-F Antenna with Novel Feed Structure for Wireless Terminals”, *IEEE Antennas and Wireless Propagation Letters*, vol. 6, 2007, pp. 66-69.
- [40] H. Hsieh, Y. Lee, K. Tiong, and J. Sun, “Design of a Multi-band Antenna for Mobile Handset Operations”, *IEEE Antennas and Wireless Propagation Letters*, vol. 8, 2009, pp. 200-203.
- [41] Z. Li and Y. Rahmat-Samii, “Optimization of PIFA-IFA Combination in Handset Antenna Designs”, *IEEE Transactions on Antennas and Propagation*, vol. 53, n°5, May 2005, pp. 1770-1778.

CHAPTER 5 DISTRIBUTED RADIATING SYSTEMS

5.1. Introduction

The previous chapters prove that the inherent ground planes of conventional handset platforms present efficient radiating modes at mobile frequencies. In addition, it has been demonstrated the feasibility of providing multi-band radiating systems by properly exciting the radiating modes of these inherent ground planes through the use of either magnetic or electric ground plane boosters. The challenge in this kind of radiating systems, mainly relies not only on the proper election of the element used to excite the ground plane, but also on the radiofrequency system used to provide impedance matching. Broadband matching networks have been selected in the former sections as being the ones that attain the best trade-off between performance and simplicity. They are capable of providing enhancement factors around 2.45 ($SWR \leq 3$) (Standing Wave Ratio) regarding a reduced number of reactive elements, namely a reactance cancellation element (inductor or capacitor according to the nature of the input impedance provided by the ground plane booster element), a shunt capacitor, and a shunt inductor. This bandwidth enhancement supposes around one half of Fano's limit.

The solutions presented along the former chapter, can be easily integrated in current handset platforms including multi-band Front-End Modules (FEMs), since they can be readily combined into a single input/output port through the addition of notch filters for the low (690-960MHz) and high frequency regions (1710-2690MHz), respectively. In a similar manner, they can also provide different input/output ports according to the number of frequency regions to cover. One example would be the coplanar solutions provided in section 3.3 and 3.4, where instead of combining the two frequency regions into a single input/output port, two or even four different ports are provided according to the number of frequency regions. The proposals become useful for providing very compact solutions, while considerably simplifying the complexity of the FEMs. It is important to underline that in some of the previous solutions, each ground plane booster and the radiofrequency system associated to it, work independently for each frequency region, i.e. when the ground plane booster intended for the low frequency region operates, the ground plane booster intended for the high frequency region does not operate, and vice versa. This effect does not happen in the latest compact solution (section 3.5). In this case, the input impedance of both ground plane boosters is combined into a single input/output port in a particular manner as for providing the desired response. Both elements interact, since one element charges the other and, vice versa.

Following this principle, this chapter is focused on combining the input impedances of different resonant and non-resonant elements in a single input/output port not only for improving the impedance bandwidth at a particular frequency region but also to provide a better excitation of the fundamental radiating mode and higher robustness to hand loading.

With this aim, section 5.2 discloses a distributed antenna system formed by two resonant monopole antennas, whose input impedance is combined into a single input/output port. This proposal not only increases the impedance bandwidth with respect to that provided by a single monopole antenna with a broadband matching network, but also offers robustness to human loading effects, more particularly to finger loading. In this sense, when a user blocks one of the monopoles of the proposed distributed system, the other one can still radiate properly, and vice versa. However, if the finger blocks the single monopole antenna, the performance is significantly degraded. This section further proposes a distributed antenna system of three monopoles and demonstrates that the bandwidth enhancement is directly proportional to the number of elements of the distributed system.

Section 5.3 goes and step further and analyze the effect that the feeding scheme produces in the behavior of the distributed systems. In this case, two feeding schemes, namely an in-phase and an out-of-phase feeding mechanism are analyzed in order to determine the advantages and disadvantages of each one.

Finally, section 5.4 substitutes previous resonant monopoles by ground plane boosters according to the spirit of this thesis. Whereas previous solutions are mainly focused on the low frequency region (690-960MHz), this proposal expands the results to the high frequency region (1710-2690MHz). In this case, the performance of in-phase feeding schemes and out-of-phase feeding schemes are not only compared between them but also with the behavior of a single ground plane booster solution having the equivalent volume of the proposed distributed systems based on ground plane boosters. The results demonstrate that the distributed antenna system allows enhancing the transfer of energy to the fundamental ground plane radiating mode, thus significantly improving the performance of the radiating system.

5.2. Distributed Antenna Technology based on Resonant Elements

The challenges in the antenna community are further exacerbated when regarding human interaction. In this sense, antenna engineers are not only forced to provide small and multi-band radiating systems capable of operating in a larger number of frequency bands, but also robust systems capable of minimizing the effects of the human interaction over their behavior.

In this sense, it is not sufficient to guarantee the performance of handset antenna solutions in free-space since the effects of the human interaction, and particularly the hand interaction, must also be carefully considered. On one hand, radiating systems need to fulfill the so-called free-space requirements in terms of efficiency and impedance bandwidth, as well as the active test measurements such as TRP (Total Radiated Power) and TIS (Total Isotropic Sensitivity). On the other hand, the effects of the presence of the human body in the vicinity of the radiating system must be also taken into consideration regarding not only biological aspects in terms of SAR (Specific Absorption Rate), but also functional effects in terms of electromagnetic performance [1]-[23]. Owing to functional aspects, the human presence mainly translates into impedance mismatching and power absorption that causes efficiency decrements. The hand of the user when holding the phone, is one of the main contributors to these

efficiency decrements, so that many handset antenna manufacturers are forced to advertise how a handheld device should be grabbed in order to mitigate the negative effects produced by the human hand over the electromagnetic performance. Consequently, research focused on handset antenna architectures capable of providing robustness to the human loading effect is strongly required.

The present section proposes handset antenna architectures based on an array of small monopoles strategically arranged along the PCB (Printed Circuit Board) of a wireless handheld device. The proposed architecture is intended not only for increasing the bandwidth but also for providing robustness to human loading and in particular, to the finger loading effect [11]. Electrical models are used to give a physical insight into the bandwidth enlargement mechanism provided by the distributed antenna systems. In the present case, a distributed system including an array of two monopoles is presented [12]-[13], and its behavior is compared with that obtained by an array of three monopoles [14]-[15]. The proposed systems are completely passive, which in terms of simplicity and battery consumption is considerably advantageous. The previous schemes found in the literature propose the compensation of the finger effect by an antenna selection which requires a switching mechanism that involves an undesired increment in the battery consumption [17]-[18].

The section is divided in three main parts. Physical insight using electrical models is given in section 5.2.1. The bandwidth and antenna efficiency measurements of several prototypes, both in free-space and regarding a hand phantom, are shown in section 5.2.2 and 5.2.3, respectively. Finally, the conclusions on the robustness of the proposed solution are presented.

5.2.1 Theoretical Analysis

The main purpose of a distributed antenna system is based on improving the robustness of the radiating system to the hand loading effect and more particularly to the finger loading effect, which is responsible for the impedance mismatching and power absorption. At the same time, the proposal is also focused on enhancing the electromagnetic performance of the radiating system by increasing the bandwidth with respect to that attained by a single antenna element. The physical principle used to increase the bandwidth relies on combining two equivalent single monopole antennas by applying a proper phase difference between their input impedances (Fig. 5.1).



Fig. 5.1 Schematic example of a distributed antenna system consisting of a passive array of two monopole antennas placed at the corners of the ground plane of a handset device. A phase delay ϕ is used to optimize the bandwidth.

A monopole antenna features input impedance comparable to that produced by a series *RLC* circuit around its first resonant frequency f_0 (Z_1 in Fig. 5.2 and Fig. 5.3). The first distributed antenna system described herein, combines two monopole antennas into a single input/output port (Fig. 5.2a), whereas the second proposal combines three monopole antennas (Fig. 5.2b).

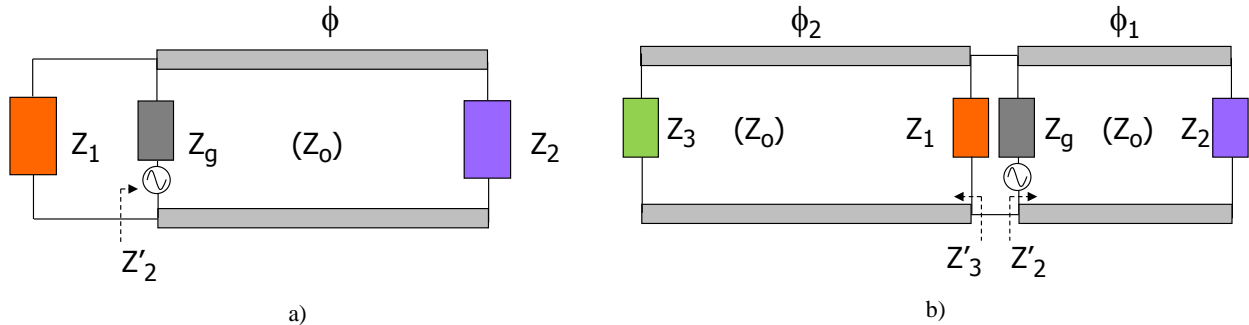


Fig. 5.2 a) Electrical model for a distributed antenna system similar to that schematically depicted in Fig. 5.1. Z_1 and Z_2 correspond to the complex input impedances of monopoles 1 and 2, respectively, which are connected through a transmission line with characteristic impedance $Z_0=50 \Omega$ and electrical length ϕ ; b) Electrical model for a distributed antenna system comprising three monopoles.

For the first case, the first monopole maintains the common series *RLC* input impedance whereas the second monopole is connected to a phase delay, such as for instance a transmission line. When the second monopole, which also operates in its first resonant frequency f_0 and presents the same input impedance $Z_2=Z_1$ (Fig. 5.2a), is connected to a phase delay of 90° at f_0 , its input impedance becomes Z_2' , resulting in a parallel *RLC* circuit response (Z_2' in Fig. 5.2a and Fig. 5.3). Thus, Z_1 and Z_2' become substantially complementary impedances (i.e. Z_1 follows a series *RLC* response and Z_2' follows a parallel *RLC* response (Fig. 5.3)). If both impedances are connected into a single input/output port, an input impedance loop appears as a consequence of the cancellation of the reactance associated to Z_1 and Z_2' .

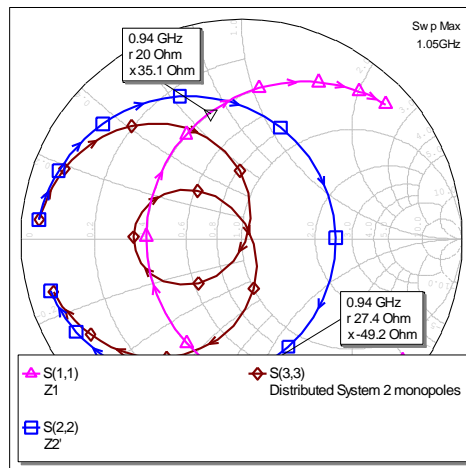


Fig. 5.3 Simulated impedance for the electrical circuit of Fig. 5.2a. a) Input impedance Z_1 of a monopole antenna (triangular markers); b) Z_2' which is the resulting input impedance Z_2 after the addition of a transmission line featuring 90° at f_0 (square markers); c) distributed system with $Z_1=Z_2$, $\phi=90^\circ$ at 900 MHz (rhombus markers).

This reactance cancellation produces an increment of the impedance bandwidth that can be further demonstrated theoretically by computing the bandwidth of the equivalent electrical circuit. For example, the combination of two series *RLC* circuits having a resonant frequency $f_0=900\text{MHz}$, $R(f_0)=20\Omega$, and

quality factors $Q_1=Q_2=20$ can at most produce a bandwidth of 5.7%. ($SWR \leq 3$), as computed according to (1.1) and following the approaches of [24]. Nevertheless, the bandwidth increases up to 16.5% when the distributed antenna concept based on the addition of a transmission line featuring 90° at 900MHz is applied (Fig. 5.2a). In this sense, the theory as well as the simulation results demonstrates that the bandwidth of a single monopole can be increased approximately two times by the proper design of the phase delay between two equivalent monopole antennas.

Note that L and C values for the suggested RLC equivalent circuits, once f_0 , R , and Q are fixed, can be obtained according to equation (5.1) and (5.2), respectively.

$$L = \frac{Q \cdot R}{2\pi \cdot f_0} \quad (5.1)$$

$$C = \frac{1}{(2\pi f_0)^2 \cdot L} \quad (5.2)$$

In addition, a further advantage that will be demonstrated in the following sections relies on the robustness that the proposal offers to undesired finger loading effects, since it is expected that when the finger loads the first monopole, the second one can still be radiating because it is not obstructed by the finger, and vice versa.

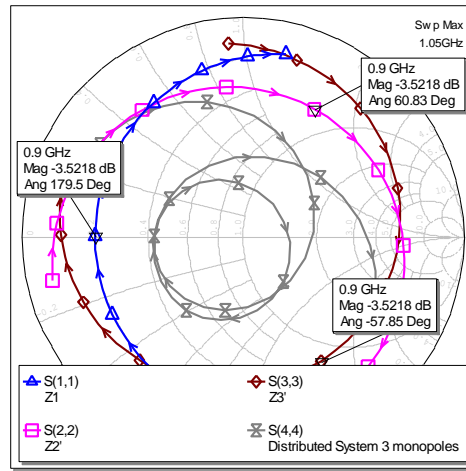


Fig. 5.4 Simulated impedance for the electrical circuit of Fig. 5.2b. a) Input impedance Z_1 of a monopole antenna (triangular markers); b) Z_2' which is the resulting input impedance Z_2 after the addition of a transmission line featuring 60° at f_0 (square markers); c) Z_3' which is the resulting input impedance Z_3 after the addition of a transmission line featuring 120° at f_0 (rhombus markers); d) distributed system with $Z_1=Z_2=Z_3$, $\phi_1=60^\circ$ and $\phi_2=120^\circ$ at 900MHz (double triangle markers).

In the present section, the idea of combining two monopole antennas in a single input/output port is expanded to three monopoles in order to both increase bandwidth and provide more robustness to hand loading effects. In this regard, the proposed electrical model contains a second transmission line having an electrical length ϕ_2 and capable of connecting the third monopole to the common input/output port (Fig. 5.2b). In addition, since the third monopole is geometrically equal to the first and the second monopole, its input impedance Z_3 is also identical to Z_1 and Z_2 . In this case, in order to maximize the bandwidth, the phase delay of each line is selected to be $\phi_1=60^\circ$ and $\phi_2=120^\circ$ at the resonant frequency

under study ($f_0=900\text{MHz}$). This condition ensures the minimum attainable reflection coefficient at the feeding port and consequently higher bandwidth (Fig. 5.4). Using this condition and the aforementioned circuit values, the reflection coefficients of the suggested schemes (Fig. 5.2) are compared demonstrating that the single monopole bandwidth of 5.7% is enhanced up to 16.5% and 25.7% for the distributed system using two and three monopoles, respectively (Fig. 5.5).

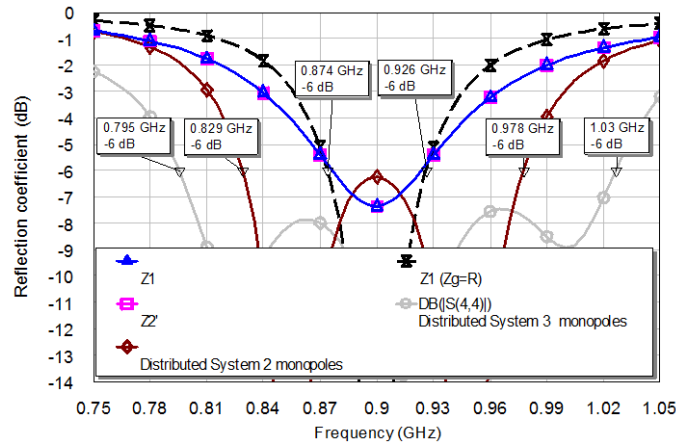


Fig. 5.5 Simulated reflection coefficient (S_{11}) associated to an impedance Z_1 corresponding to a series RLC circuit featuring $f_0=900\text{MHz}$, $R=20\Omega$, $Q=20$ (triangular markers); S_{11} regarding Z_2 (square markers); S_{11} regarding Z_1 connected to a generator having an internal impedance $Z_g=R$ (double triangle markers); S_{11} for the distributed antenna system of Fig. 5.2a (2 monopoles) connecting two equal impedances $Z_1=Z_2$ with a $\phi=90^\circ$ (900MHz) transmission line having a characteristic impedance $Z_0=50\Omega$ (rhombus markers); and S_{11} for the distributed antenna system of Fig. 5.2b (3 monopoles) having $Z_1=Z_2=Z_3$ and $\phi_1=60^\circ$ and $\phi_2=120^\circ$ at 900MHz (circular markers).

The following sections are focused on demonstrating the advantages of a distributed antenna system having three monopoles in terms of bandwidth and efficiency both in free-space and considering hand loading conditions.

5.2.2 Distributed Antenna System Design

The proposed distributed antenna system comprising two and three monopoles are designed according to the principles explained in the former section (Fig. 5.6). A single monopole is used for comparison purposes. Main antenna parameters, namely bandwidth and antenna efficiency, are measured and compared in free-space for all the prototypes. The comparison is made in the 824 MHz to 960 MHz frequency range, where some of the main communication standards are allocated such as GSM850 and GSM900.

Circuit theory [25]-[26] demonstrates that the bandwidth of a single monopole can be enhanced in a factor around 2.45 regarding a $SWR=3$, which involves a considerable increment taking into consideration that only two reactive components are required. For this reason, the selected single monopole solution comprises a spiral-shaped geometry and a broadband matching network comprising a shunt LC circuit ($L_m=1.6\text{nH}$, $C_m=21.5\text{pF}$), which is capable of enhancing the bandwidth to provide operation in the communication standards GSM850 and GSM900 (Fig. 5.7). As the literature and the previous sections demonstrate, such broadband matching network is particularly useful to increase the

bandwidth of antennas featuring a series RLC circuit response, as it is the case of a single monopole in its first resonant mode [25].

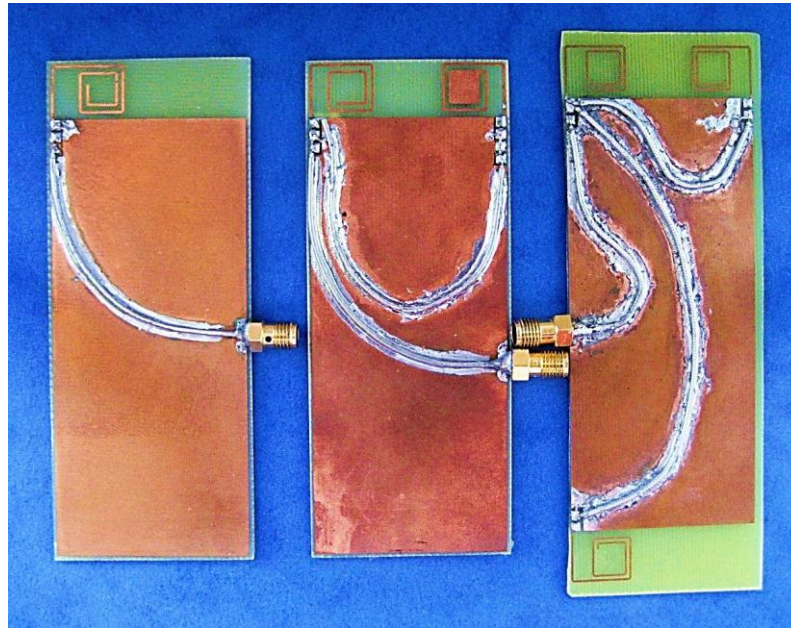


Fig. 5.6 Left) single monopole; middle) distributed antenna system comprising two monopoles; right) distributed antenna system of three monopoles. The ground plane in all cases presents dimensions of 90 mm x 40 mm and is printed on a FR4 substrate 1 mm thick. The footprint for the monopoles is 13 mm x 11 mm.

The design of the proposed distributed antenna systems follow the approaches found in the former section. On one hand, in the case of the distributed antenna system of two monopoles, a transmission line is added to connect both monopole antennas. As previously discussed, a transmission line of 90° at the central frequency of operation provides a cancellation of the waves reflected from each monopole antenna at the input/output port. Said cancellation increases the bandwidth with respect to that provided by a single monopole antenna without the need of requiring other broadband techniques, such as the broadband matching network described above.

On the other hand, the distributed antenna system comprising three monopoles requires two transmission lines. In this case, the theoretical phase delay for each one of the transmission lines is 60° and 120° , respectively, in order to ensure the cancellation of the three waves reflected from each monopole antenna at the central frequency of operation according to the results presented in the former section. It should be pointed out that many commercially available handset phones comprise micro-coaxial transmission lines for allowing the interconnection of the antenna with the FEM when both, the antenna and the FEM are spaced apart. Therefore, it seems feasible to bring into practice the present proposal by using market available transmission lines widely used in the handset industry.

A comparison between the previous solutions is established and the measured results demonstrate the effectiveness in terms of bandwidth associated to the proposed distributed antenna systems. In this sense, the single monopole including the broadband matching network only attains a bandwidth of 15.6%, whereas the distributed systems comprising two and three monopoles present bandwidths around 23.6%, and 34.0%, respectively (Fig. 5.7). In all cases, it is possible to cover the standards GSM850 and

GSM900 but it is worth to outline that the distributed antenna system of three monopoles is also able of providing operation in the emergent LTE700 system (698-798MHz).

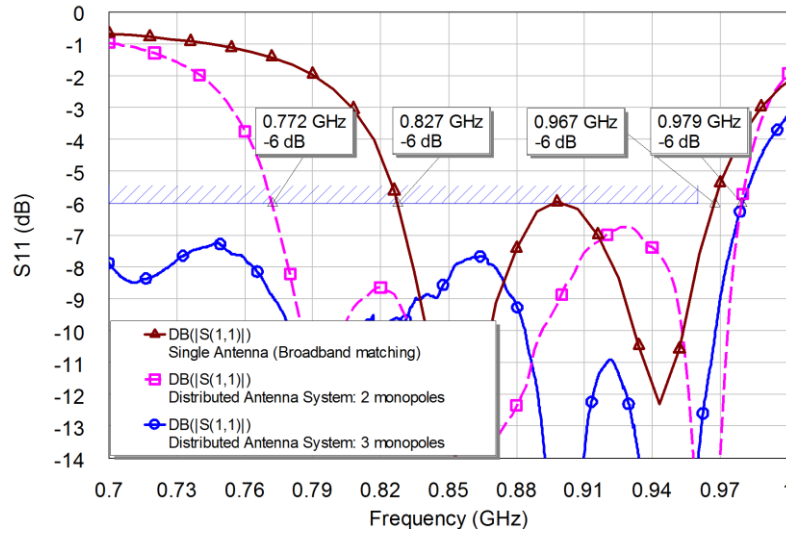


Fig. 5.7 Measured reflection coefficient for the radiating systems of Fig. 5.6.

The antenna efficiency (η_a) of the proposals has also been measured using 3D radiation pattern integration through the anechoic chamber Satimo Stargate-32. Due to a limitation of the anechoic chamber, antenna efficiency cannot be measured below 800MHz. However, for the present purpose of demonstrating the robustness of the distributed antenna system with respect to those solutions based on single antenna elements, the assessment of the performance in the frequency range of 824-960MHz allocating the standards GSM850 and GSM900 is fair enough. The average antenna efficiency in the 824-960MHz frequency range is 34.6% for the single monopole, 46.1%, and 48.1%, for the distributed antenna systems of two and three monopoles, respectively. This fact emphasizes again that the distributed antenna systems stand out over the single element solution, since they provide better averaged antenna efficiencies (Fig. 5.8).

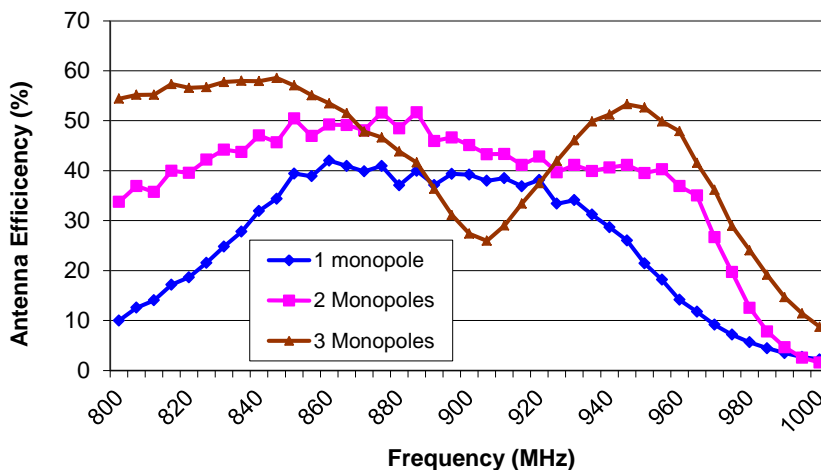


Fig. 5.8 Measured antenna efficiency for the radiating systems shown in Fig. 5.6. The antenna efficiency takes into account both radiation efficiency and mismatch losses $\eta_a = \eta_r (1 - |S_{11}|^2)$.

Since the distributed antenna system is an array of antenna elements, array theory could be employed to analyze the shape of the radiation patterns of each one of the radiating systems under study.

From the array theory, one could conclude that the distributed antenna system having three monopoles could present more directivity than the one using two monopoles because it is electrically larger. However, the three cases under study present similar directivities, which suggest that the array theory could not be fairly applied in this kind of radiating systems. The reason mostly relies on the ground plane, which, as emphasized along this thesis, becomes the main radiator at this frequency region (824-960MHz), mainly due to its electrical size comparable to the wavelength of operation. Accordingly, the radiation pattern is determined by the current distribution of the fundamental ground plane radiating mode, which is mainly aligned with the longitudinal edges of the ground plane and approximates that produced by a half-wavelength dipole. Therefore, the resulting radiation pattern features a dipole-type pattern, omnidirectional in one plane and with a null along the longitudinal axis of the ground plane (Fig. 5.9). This fact is further emphasized by the directivity values, which remain around 2.5-3.0dBi across the 824-960MHz frequency range in all cases, contrary to what was initially predicted by the array theory. The directivity values correspond to the typical values of a half-wavelength dipole confirming again the influence of the ground plane radiating mode into the radiation process. Finally, an alternative physical insight can be addressed by simulating the current distribution (Fig. 5.10).

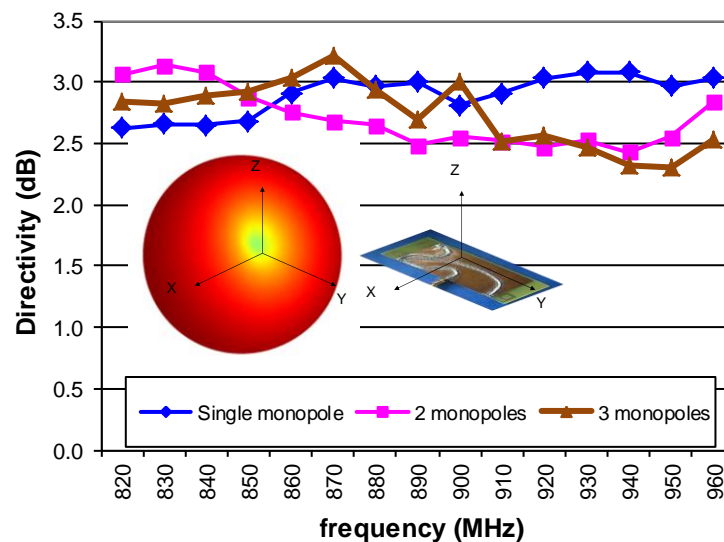


Fig. 5.9 Measured directivity for the single monopole and the distributed antenna systems of two and three monopoles. Measured 3D radiation pattern at 900MHz showing the typical $\lambda/2$ dipole-type pattern for the distributed system of three monopoles.

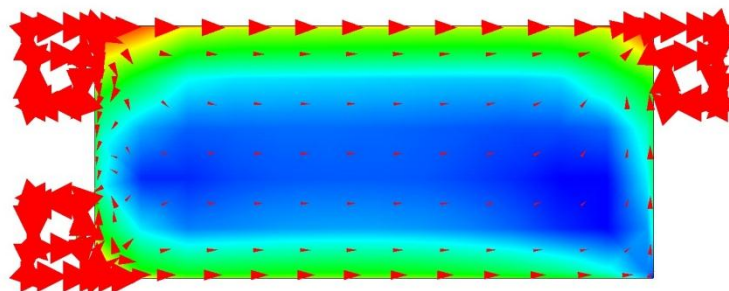


Fig. 5.10 Simulated current distribution at $f=850\text{MHz}$ depicting the current aligned with the longitudinal edges of the ground plane, hence approximating that of a typical half-wavelength mode, null at the transversal edges and maximum at the center of the longitudinal edges.

Current distribution along the ground plane confirms the theory, since it follows that of a half-wavelength dipole, (i.e. halved sinusoidal current distribution), being the null located at the transversal edges of the ground plane and the maximum at the middle of its longitudinal edges. As stated above, this current distribution determines the radiation pattern of the radiating systems, since the ground plane is the main contributor to the radiation process at this frequency region.

Once the benefits of the distributed antenna systems in free-space have been presented, their advantages in front of the human loading effect are discussed in the next section.

5.2.3 Human Hand Effect

The effect of the finger loading is analyzed using a phantom hand emulating a real human hand holding the phone in talking position (Fig. 5.11). The phantom is filled with a liquid performing the electromagnetic properties of the human tissues at the frequencies of interest ($\epsilon_r'=41.1$, $\sigma=0.88$ S/m at 835MHz and $\epsilon_r'=40.3$, $\sigma=0.93$ S/m at 900MHz) [20].

In order to analyze the robustness of the distributed antenna system, the finger is located at three different positions along the shortest edge of the ground plane, namely left, center, and right positions. For each position and prototype, the antenna efficiency is measured inside the anechoic chamber Satimo Stargate-32 (Fig. 5.11-Fig. 5.17). It should be outlined that these experiments consider a critical scenario in which the finger is only spaced apart 1 mm from the antenna using a methacrylate piece of 1 mm thick placed above the PCB.

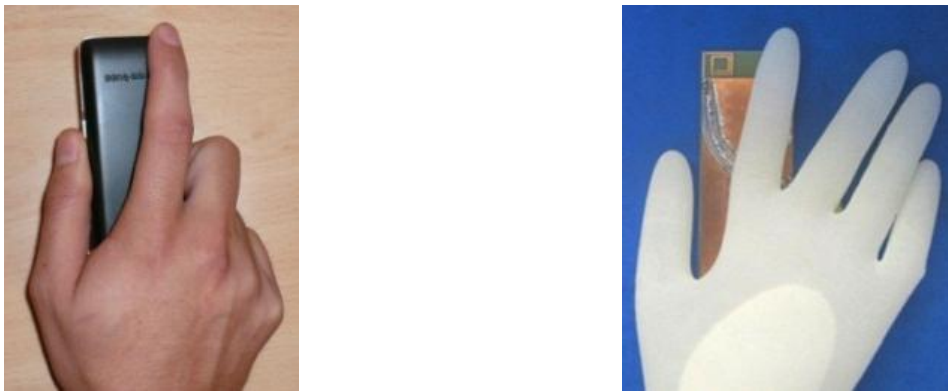


Fig. 5.11 Left: common holding position during a call; right: the phantom hand emulating the real situation illustrated in the figure on the left.

For the single monopole antenna, the finger in the left position is critical since the finger totally covers the antenna, whereas for the right position, the finger is further away. This effect is clearly appreciated in the measured results. For the right case, the antenna efficiency reaches an efficiency peak of 30%, whereas for the left position, it is not more than 3% (Fig. 5.12-Fig. 5.17).

Regarding the distributed system of two monopoles, antenna efficiency is better compared to the single monopole for all cases except for the right position where the single monopole does not suffer the finger effect since it is further away from the antenna. However, in the best case (finger right, Fig. 5.13), average antenna efficiencies for the single monopole and the distributed system of two monopoles remain comparable. The benefits of the distributed antenna system of two monopoles becomes apparent for the

other cases (finger middle and left), where the efficiency is clearly above the efficiency of the single monopole. Thus, it is possible to conclude that the distributed antenna system of two monopoles offers better performance than that based on a single monopole regarding the presence of the phantom hand.

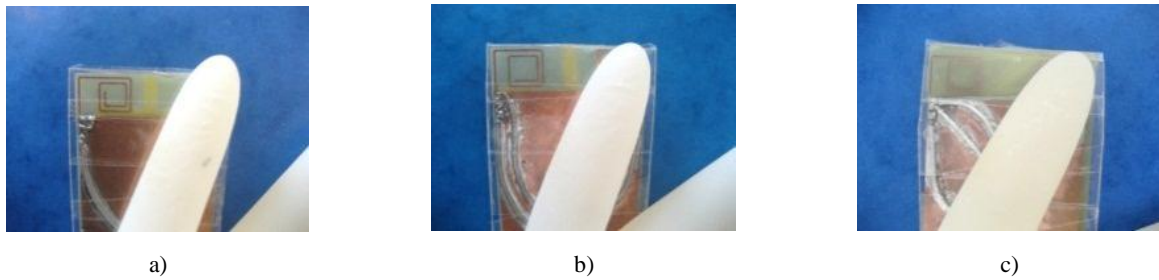


Fig. 5.12 Detail of the phantom finger covering the upper right corner of the PCB for the three prototypes under consideration: a) single monopole; b) two monopoles; c) three monopoles.

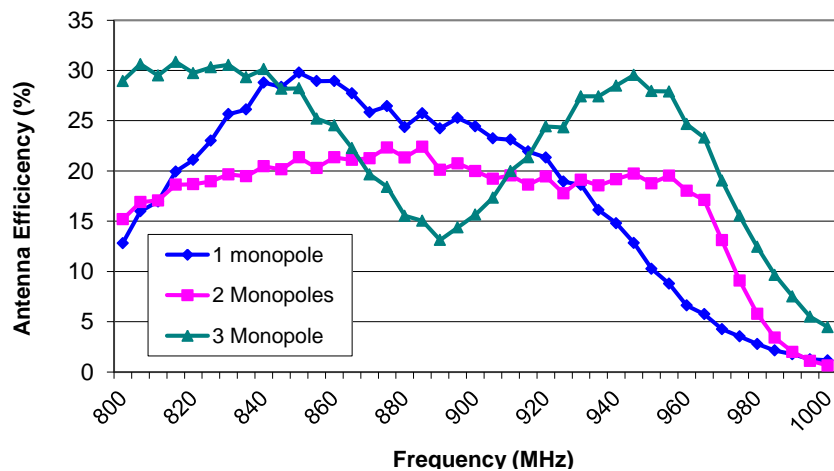


Fig. 5.13 Measured antenna efficiency taking into account the phantom hand over the PCB and the finger in the right position.

Concerning the distributed system of three monopoles, the advantages are even better since it presents the best results among the three prototypes. For example, for the left case, the average efficiency in the 824-960MHz frequency range is 2.5dB higher than the distributed system having two monopoles and 7.9dB higher than the single monopole case (Table 5.1). It is worth noting that besides the best performance in terms of antenna efficiency, the distributed system of three monopoles presents minor variations in antenna efficiency behavior regarding the three positions under study (Table 5.1 and Fig. 5.18).

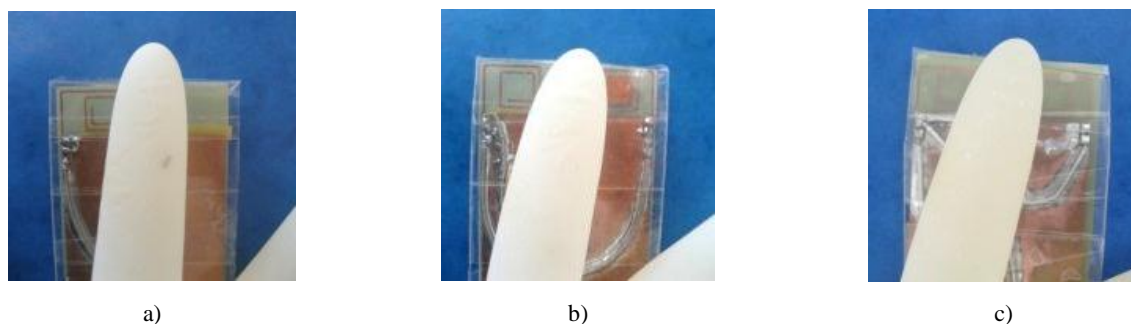


Fig. 5.14 Detail of the phantom finger covering the upper middle area of the PCB for the three prototypes under consideration: a) single monopole; b) two monopoles; c) three monopoles.

Once the measured antenna efficiency values are obtained, the hand losses can be estimated as the ratio between the averaged antenna efficiency in free-space and regarding hand-loading. These losses take into account both the power absorbed by the hand and the mismatching effect (Table 5.1, Fig. 5.18, and Fig. 5.19).

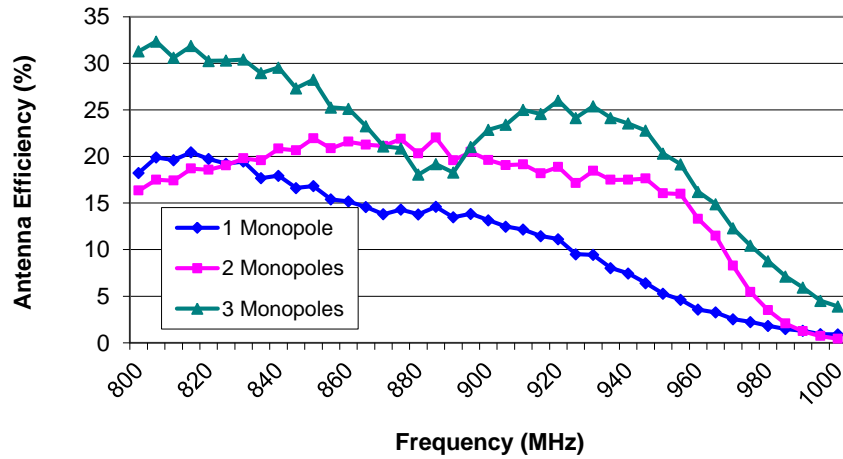


Fig. 5.15 Measured antenna efficiency taking into account the phantom hand over the PCB and the finger in the middle position.

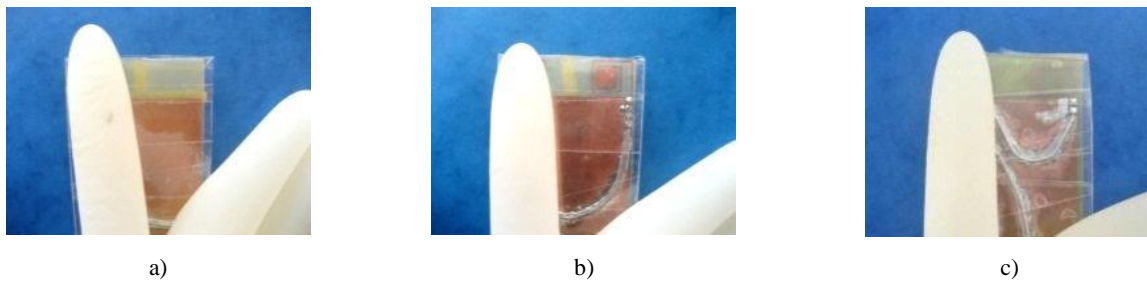


Fig. 5.16 Detail of the phantom finger covering the upper left corner of the PCB for the three prototypes under consideration: a) single monopole; b) two monopoles; c) three monopoles.

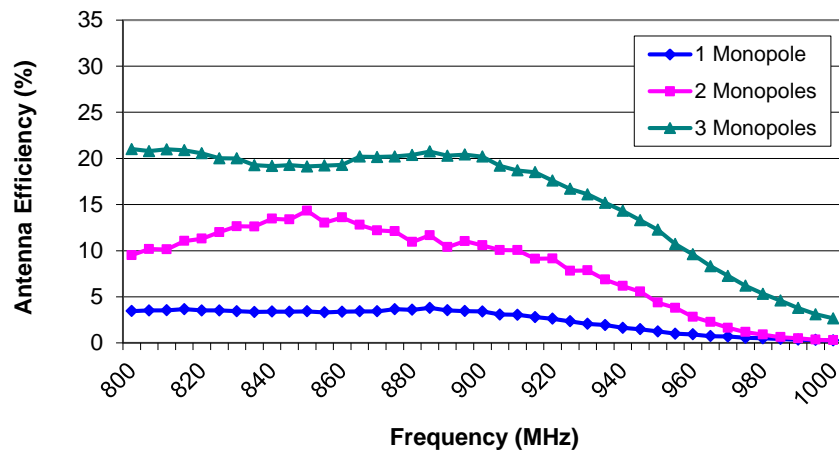


Fig. 5.17 Measured antenna efficiency taking into account the phantom hand over the PCB and the finger in the left position.

As previously asserted, the effect of the hand (impedance mismatching and power absorption) is severe when the finger is over the single monopole area reaching 10.6dB losses, which results in antenna efficiency of only 3.0%. Nevertheless, the distributed antenna systems mitigate considerably this effect. For example, the worst case for the distributed system of two monopoles and three monopoles are 6.5dB

and 4.1dB, respectively. Furthermore, the distributed system of three monopoles not only mitigates said effect, but also maintains power losses significantly independent from the finger position. In this way, the power losses go from 4.1dB regarding the left position to 2.9dB for the other cases.

Table 5.1 Summary of Results.

Antenna System	1 monopole	2 monopoles	3 monopoles
BW ($SWR \leq 3$) (%)	15.6	23.6	34.0
Average η_a in free-space (%) (824-960MHz)	34.6	46.1	48.1
Average η_a (%) (824-960MHz) regarding hand loading	Left: 3.0 Middle: 13.0 Right: 23.0	Left: 10.4 Middle: 20.0 Right: 20.7	Left 18.5 Middle 24.6 Right 24.5
Absorption losses (dB)	Left: 10.6 Middle: 4.3 Right: 1.8	Left: 6.5 Middle: 3.6 Right: 3.5	Left: 4.1 Middle: 2.9 Right: 2.9

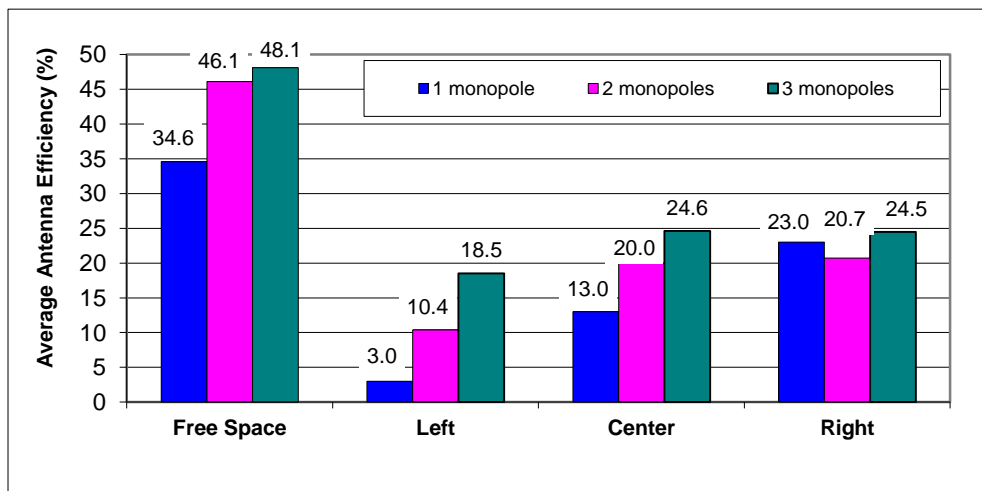


Fig. 5.18 Average antenna efficiency (824-960MHz) in free-space and regarding hand loading for the proposed antenna systems (Fig. 5.6) and regarding the three finger positions analyzed.

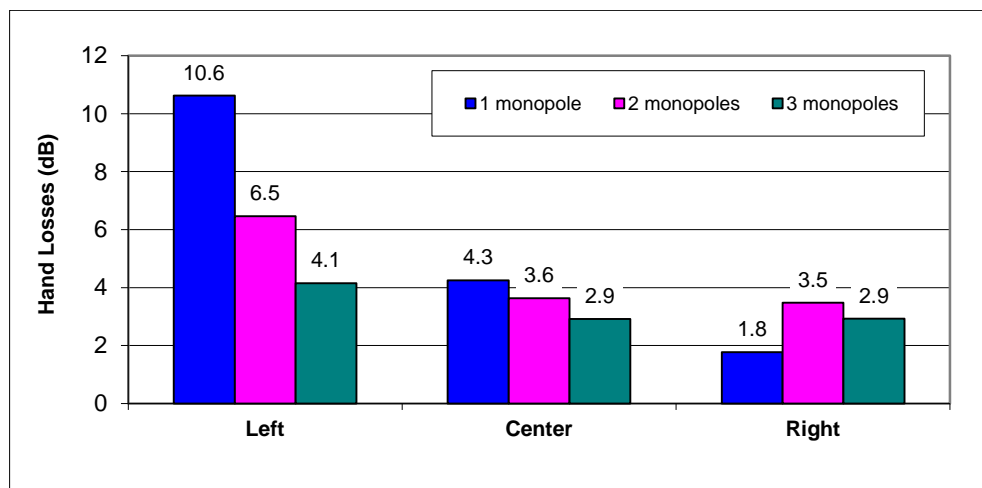


Fig. 5.19 Hand losses averaged in the 824-960MHz frequency range for the proposed antenna systems (Fig. 5.6) and regarding the three finger positions analyzed.

These results demonstrate that this technique is useful to reduce the efficiency decrement produced by the finger loading directly related to a decrement of the battery life, signal coverage, and eventual call drops.

5.3. In-phase versus Out-of-phase Distributed Antenna Systems

As previously illustrated, human interaction and particularly hand loading is a relevant aspect to consider when designing handset antennas, since the common holding of handset phones usually degrades their performance. Their vulnerability is not only related to talking positions since it also extends to texting positions, for which handset phones are increasingly being used for. Several studies are focused on determining the radiated power losses as a function of the holding and close proximity of the human hand regarding different form factors and different antenna elements [1]-[23], [27]-[39]. In all cases, the results demonstrate that hand loading introduces losses to the radiated power, which are highly dependent on the hand and finger location with respect to the antenna. Some attempts to mitigate hand loading effects are focused on providing balanced structures such as slots, loops, or monopole antennas capable of minimizing the ground plane contribution to the radiation process [1]-[2], [22], [37], [38].

Other efforts mainly rely on switching mechanisms that involve an undesired increment of the battery consumption [17]. This challenge further exacerbates when considering human head interaction. Usually, the handset antenna arrangement capable of mitigating hand loading opposes the one preferable for minimizing head loading effects. Thus, in some cases the location of the antenna in the bottom part of the handset becomes preferable for minimizing not only power losses, but also SAR values. However, this antenna arrangement is highly degraded by the users' hand since in this position the antenna can be completely covered by the users' palm. Following this reasoning, some proposals are focused on providing two separate antenna elements each one intended for a particular frequency region and placed in an opposite shorter edge of a handset ground plane [18]. Nevertheless, this solution undesirably increases the size of the whole radiating system. Other trends mitigate hand loading by modifying the ground plane in order to produce directional radiation patterns in the opposite direction of the user hand [39]. Although this solution can overcome the aforementioned inconvenient, it does not become appropriate for free-space radiation where omni-directional radiation patterns are preferable. The problem further exacerbates in the low frequency region (824-960MHz) since in this frequency range, the ground plane contribution becomes essential. In this sense, the aforementioned techniques, and in particular balanced structures, do not result appropriate. In order to overcome these shortcomings, this thesis proposes the use of distributed antenna systems consisting of a passive antenna array of two or more monopoles operating in the same frequency range. A phase delay between monopoles, i.e. out-of-phase feeding scheme, is introduced with the purpose of maximizing the bandwidth. The proposal, as discussed in the former section, becomes a feasible solution to increase impedance bandwidth while providing robustness to the finger loading [11]-[15]. However, although the out-of-phase feeding mechanism proposed in the former section allows significant bandwidth enhancement, it does not provide a symmetric solution since hand loading effects are clearly dependent on the finger location. This results in non-uniform situation as the one shown in Fig. 5.18 where the antenna efficiency is 10.4% and 20.7% for the left and right cases, respectively. Although these values are better than the single monopole case, a power balance is required to avoid the performance dependence to the finger location.

With the objective of solving these drawbacks, the present section proposes a distributed antenna system where the monopoles are fed in-phase [16]. This feeding mechanism allows solving the asymmetries introduced by previous out-of-phase solutions while maintaining an acceptable input impedance bandwidth. As indicated above, this section is focused on the low frequency region (824-960MHz) comprising the communication standards GSM850 and GSM900, although the teachings can be as well extended to the LTE-Advanced communication service and to the high frequency region (1710-2690MHz). The reason mainly relies on the fact that the low frequency region is the most challenging for attaining high efficiency values due to the limited size of current wireless platforms. Thus, antennas operating at this frequency range must be further protected to face power losses due to hand loading.

The section is divided in three main parts. Physical insight using electrical models is given in section 5.3.1 for providing a better understanding of the behavior of out-of-phase and in-phase feeding mechanisms. Section 5.3.2 is focused on describing the proposal and gathers simulated and measured results. The performance of the proposed in-phase system is compared with the out-of-phase scheme and with a single monopole including a broadband matching network. The robustness in front of hand loading is assessed in section 5.3.3. Finally, the conclusions are presented..

5.3.1 Theoretical Analysis

As previously discussed, human interaction and particularly hand loading considerably affects the performance of handset antennas by introducing impedance mismatch and power absorption. Consequently, some efforts of this thesis are addressed to increase the robustness of the radiating systems to the hand presence by adding multiple antennas, which are combined into a single input/output port through some phase delay mechanisms such as transmission lines. This is the case of the distributed antenna systems disclosed in the former section [12]-[15], which are based on an out-of-phase feeding mechanism.

However, although the previous technique considerably increases impedance bandwidth with respect to that provided by a single monopole antenna including a broadband matching network (Fig. 5.7), its robustness to the hand loading is still dependent on the finger location (Fig. 5.18). In this sense and in order to solve the aforementioned limitations, the present proposal is focused on improving impedance bandwidth while providing a robust solution immune to the finger location thanks to the use of in-phase feeding mechanisms [16]. With the aim of providing a physical insight, the following sections analyze the performance of distributed antenna systems as a function of the feeding mechanism through electrical models.

5.3.1.1. Out-of-phase Distributed Antenna Systems

The principle of operation of a distributed antenna system relies on the combination of two equivalent monopole antennas into a single input/output port through a phase delay mechanism (Fig. 5.2a). The input impedance response of a monopole antenna can be modeled as an *RLC* series circuit in

its first resonance (Fig. 5.20). Thus, the introduction of a phase delay between both monopoles allow the creation of an input impedance loop in the Smith chart, which translates into a considerable bandwidth increment when compared to that provided by a single monopole antenna (Fig. 5.20).

In the present example, the first monopole maintains the common series RLC input impedance whereas the transmission line connected to the second one, modifies its input impedance resulting in a parallel RLC circuit response (Z_2' in Fig. 5.20). Thus, bandwidth increases when both input impedances (Z_1 and Z_2') are connected into a single input/output port mainly due to their complementary character that produces an input impedance loop as a consequence of the reactance cancellation. The aforementioned bandwidth increment can be further demonstrated theoretically by computing the bandwidth of the equivalent electrical circuit through equation (1.1) (Table 5.2) [24].

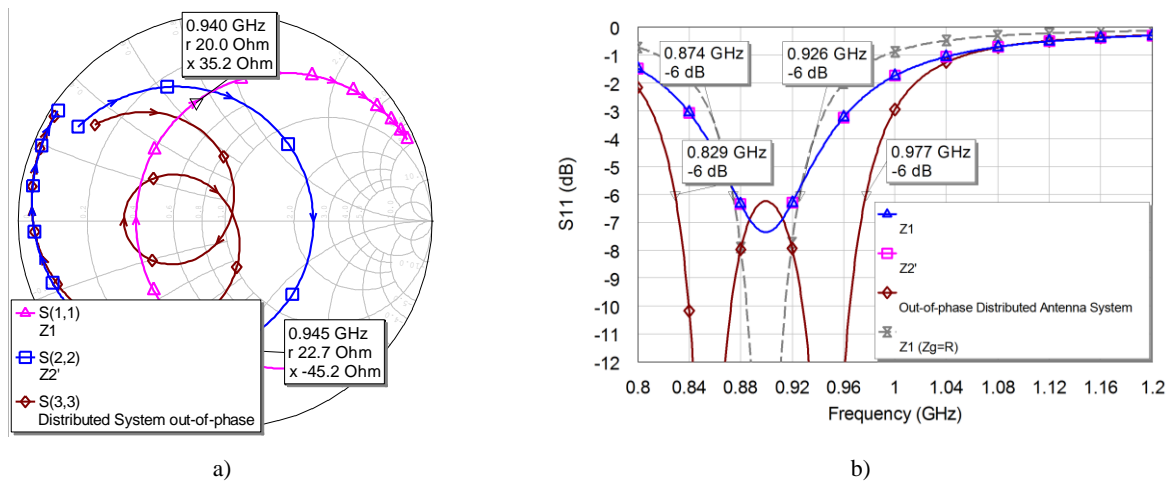


Fig. 5.20 Simulated impedance for the electrical circuit of Fig. 5.2a. Input impedance Z_1 of a monopole (triangular markers); Z_2' which is the resulting input impedance Z_2 after the addition of a transmission line featuring 90° at f_0 (square markers); distributed system with $Z_1=Z_2$, $\phi=90^\circ$ at 900 MHz (rhombus markers). Both RLC series circuits Z_1 and Z_2 are characterized by an input resistance $R=20\Omega$, quality factor $Q=20$, and resonant frequency $f_0=900\text{MHz}$.

Note that L and C values for the suggested RLC equivalent circuits, once f_0 , R , and Q are fixed, can be obtained according to equation (5.1) and (5.2), respectively.

Table 5.2 Out-of-phase Distributed Solution versus Single Monopole.

	f_0	$Q_1=Q_2$	$R(f_0)$	$BW(SWR\leq 3)$
Single Monopole	900MHz	20	20Ω	6.0%
Distributed Out-of-phase	900MHz	20	20Ω	16.5%

Previous theory demonstrates that the bandwidth of a distributed antenna system can be increased approximately three times by the proper design of a phase delay between two equivalent monopole antennas. In fact, the former section demonstrates that the impedance bandwidth increases directly proportional to the number of monopole antennas combined (section 5.2). However, as the next section will present, its robustness to the hand loading effect is sensitive to the finger location mainly due to the impedance imbalance.

5.3.1.2. In-phase Distributed Antenna Systems

In order to mitigate previous impedance imbalance, this section proposes an in-phase feeding mechanism capable of providing robustness to undesired finger loading effects with certain independence

of the finger location (Fig. 5.21). In the out-of-phase technique, the input power is not equally distributed between monopole 1 and monopole 2 due to the difference between Z_1 and Z_2' . This fact considerably affects the symmetry of the radiating system and consequently the effects of the finger loading clearly depend on its location, i.e. on the obstructed monopole.

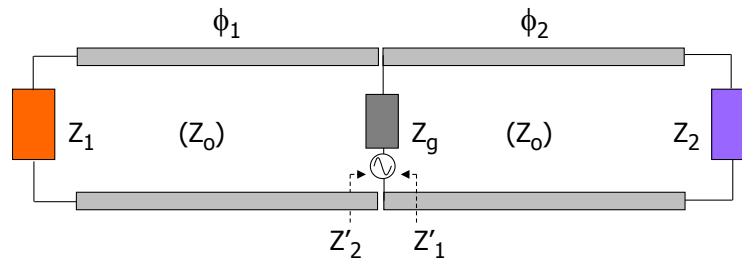


Fig. 5.21 Electrical model of a distributed antenna system comprising a passive array of two monopoles fed in-phase when $\phi_1=\phi_2$. Z_1 and Z_2 correspond to the complex input impedances of monopoles 1 and 2, respectively, which are connected through two transmission lines with characteristic impedances $Z_0=50 \Omega$ and electrical length ϕ_1 and ϕ_2 , respectively.

In contrast to the distributed antenna system fed out-of-phase, the monopole antennas of an in-phase distributed antenna system present equivalent input impedances, since no phase delay is added between them (Fig. 5.22). Thus, both input impedances Z_1 and Z_2 suffer the same phase delay since $\phi_1=\phi_2$, resulting in $Z_1'=Z_2'$.

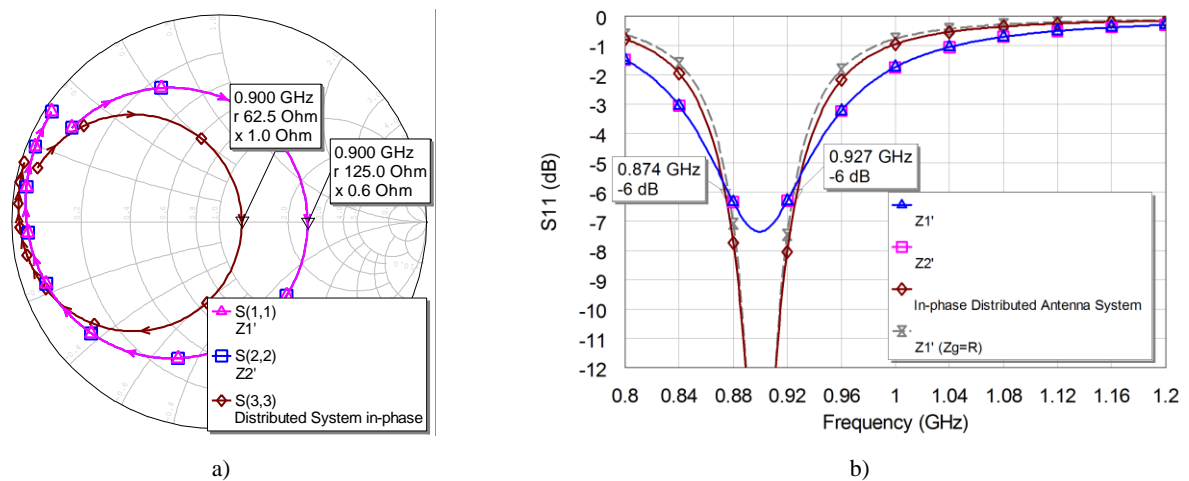


Fig. 5.22 Simulated impedance for the electrical circuit of Fig. 5.21. Input impedance Z_1' and Z_2' are respectively, the resulting input impedances Z_1 and Z_2 after the addition of two transmission lines, each one featuring 90° at f_0 (square and triangular markers); distributed system with $Z_1=Z_2$, $\phi_1=\phi_2=90^\circ$ at 900 MHz (rhombus markers). $Z_1=Z_2$ have $R=20\Omega$, $Q=20$, and $f_0=900\text{MHz}$.

Table 5.3 In-phase Distributed Solution versus Single Monopole.

	f_0	$Q_1=Q_2$	$R(f_0)$	$BW(SWR\leq 3)$
Single Monopole	900MHz	20	20Ω	6.0%
Distributed In-phase	900MHz	20	20Ω	6.0%

From the electrical model analysis, the fact of having two equal input impedances combined into a single input/output port does not provide, at a first glance, the benefit of a bandwidth increment (Fig. 5.22 and Table 5.3). However, as the following section will demonstrate, an in-phase feeding mechanism achieves more bandwidth than a single monopole after the addition of the proper matching network design. The reason is that the ground plane is more excited for the in-phase system when compared to the single monopole solution.

5.3.2 In-phase Distributed Antenna System Design

The theoretical analysis presented in the previous section demonstrates that the out-of-phase distributed antenna system provides greater impedance bandwidth than the single monopole or even than the in-phase distributed antenna system. Nevertheless, the previous study must be complemented with simulated and measured results in order to analyze the effects of the feeding mechanism over the antenna efficiency. In this sense, this section is focused on validating the feasibility of the proposal by disclosing the benefits of the suggested in-phase distributed antenna system not only in terms of impedance bandwidth, but also in terms of efficiency and robustness.

5.3.2.1. Simulations

The proposed distributed antenna system comprises two Hilbert monopoles intended for resonating at 900MHz, which corresponds approximately to the central frequency of the low frequency region (824-960MHz) comprising the communication standards GSM850 and GSM900 (Fig. 5.23). Hilbert geometry has been selected due to its miniaturization capabilities [40]-[41]. Both Hilbert monopoles are combined into a single input/output port following the techniques theoretically described in section 5.3.1 (Fig. 5.24). The proposals have been simulated using the software IE3D based on MoM (Method of Moments).

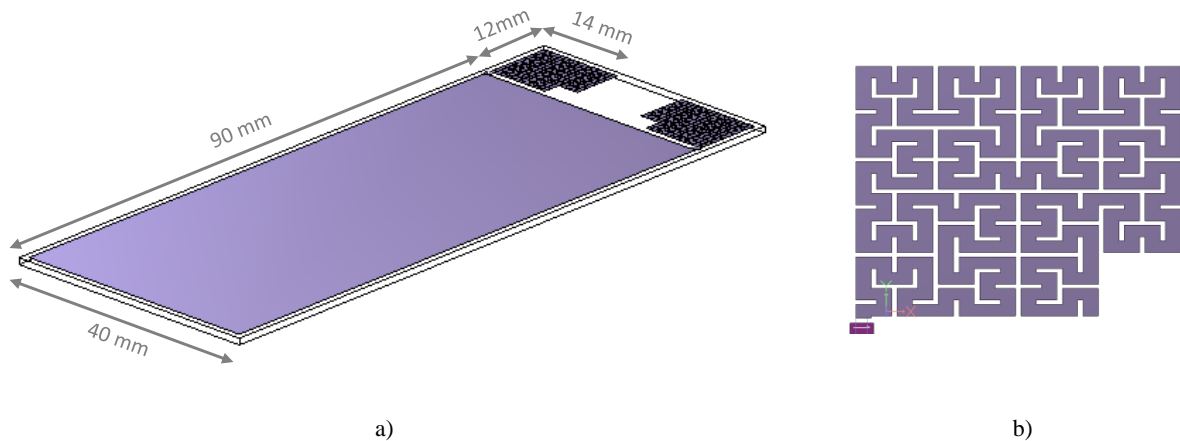


Fig. 5.23 Geometry associated to the proposed radiating system composed by two Hilbert monopoles having a footprint area of 12 mm x 14 mm. The Hilbert monopoles are arranged at the corners of the shorter edge of a ground plane having dimensions of 90 mm x 40 mm.

The performance in terms of bandwidth of the proposed distributed antenna systems (in-phase versus out-of-phase) (Fig. 5.24b-c) is compared with a single Hilbert monopole which is properly matched following the broadband circuit theory described in [25]-[26] (Fig. 5.24a). As theoretically demonstrated in section 5.3.1, the out-of-phase distributed antenna system offers greater bandwidth (30% ($SWR \leq 3$)) than the single monopole (18% ($SWR \leq 3$)) and the in-phase solution (26% ($SWR \leq 3$)) (Fig. 5.25). Note that a fine-tuning stage is used in the out-of-phase scheme for inscribing the impedance loop in the circle of $SWR=3$, whereas for the in-phase solution a π -network is used.

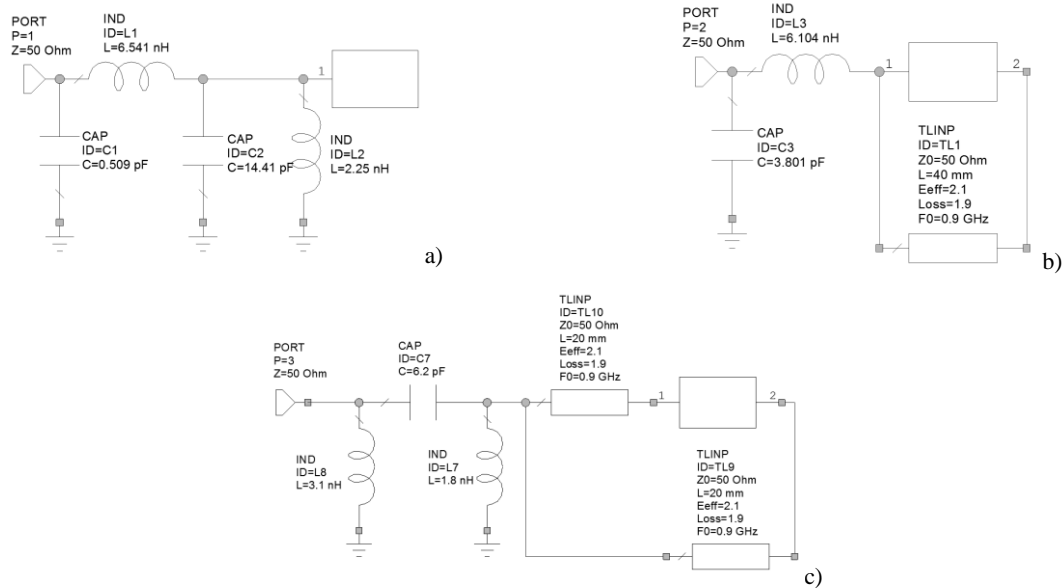


Fig. 5.24 Proposed radiofrequency systems. a) Broadband matching network and fine-tuning stage for a single Hilbert monopole; b) Out-of-phase distributed antenna system; c) In-phase distributed antenna system. Both, in-phase and out-of-phase schemes include a matching network after the combination of the response into a single input/output port. Note that the one-port box depicted in a) corresponds to the input impedance associated to a single Hilbert monopole while the two port-box shown in b) and c) corresponds to the distributed antenna system depicted in Fig. 5.23.

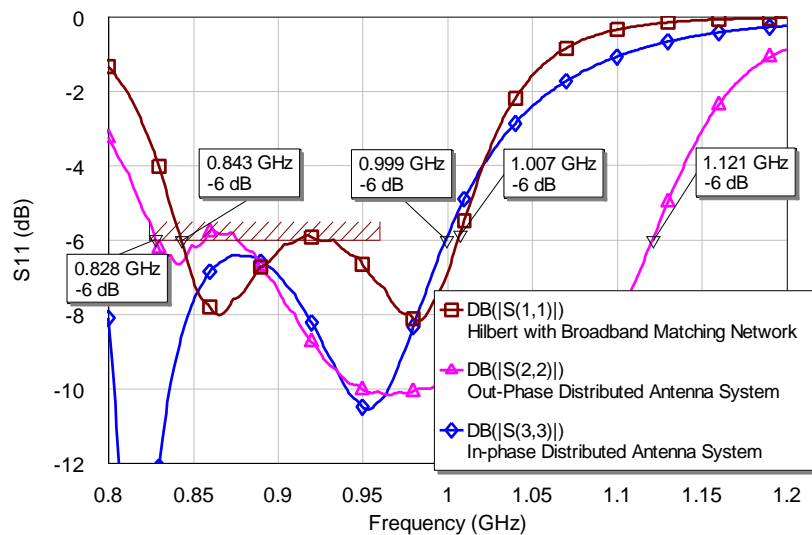


Fig. 5.25 Reflection coefficient corresponding to the radiating structures and the radiofrequency systems depicted in Fig. 5.23 and Fig. 5.24.

In order to attain a complete assessment, efficiency values must be computed. Different feeding schemes produce different current distributions (Fig. 5.26) and consequently different radiation efficiency values (Fig. 5.27). In this way, the out-of-phase distributed antenna system excites each element with a different phase resulting in a power imbalance. This fact mainly produce two different effects, on one hand, at certain particular frequencies, current at the input ports of the Hilbert monopoles present opposite phases (Fig. 5.26b), which produces significant radiation efficiency drops (Fig. 5.27). On the other hand, current is not distributed equally at both Hilbert monopoles (Fig. 5.26e) and consequently ground plane mode is not symmetrically excited, hence resulting in lower efficiency values along a significant frequency range of the low frequency region (824-960MHz).

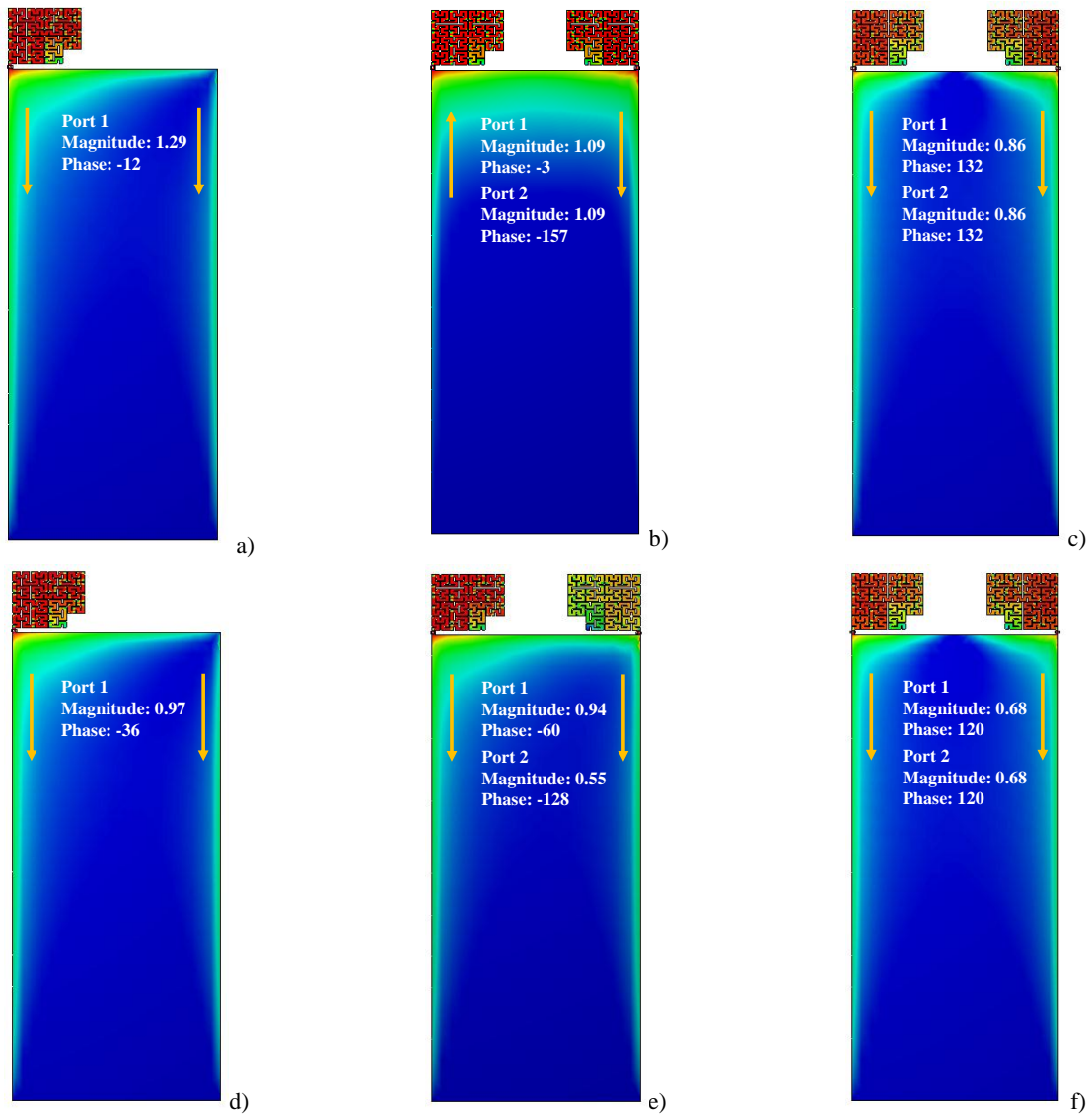


Fig. 5.26 Current distribution at frequencies 850 MHz (a-c) and 900 MHz (d-f); a) and d) single Hilbert monopole (Fig. 5.24a); b) and e) out-of-phase distributed antenna system (Fig. 5.24b); c) and f) in-phase distributed antenna system (Fig. 5.24c). Amplitude (in volts) and phase (in degrees) information for each port takes into account the radiofrequency systems of Fig. 5.24. The arrows represent schematically the sense of the current vectors.

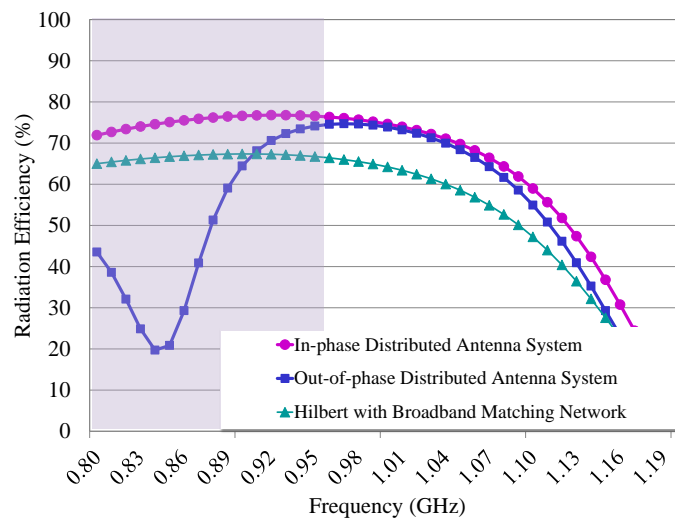


Fig. 5.27 Simulated radiation efficiency (η_r) associated to the radiating systems under study taking into account the corresponding radiofrequency systems of Fig. 5.24.

Accordingly, and contrarily to what happen with the proposed in-phase solution, the out-of-phase distributed antenna system presents an important trade-off between bandwidth and efficiency. In this way, the proposed in-phase distributed antenna system is capable of solving the aforementioned trade-off since it allows maximizing the bandwidth (26% ($SWR \leq 3$)) while maintaining high efficiency values ($\eta_r=75\%$ in average) and symmetric operation.

5.3.2.2. Measurements

In order to validate the simulated results and particularly the symmetric operation of the in-phase technique, a prototype comprising a single Hilbert monopole and a ground plane having dimensions $90\text{ mm} \times 40\text{ mm}$ is built (Fig. 5.28a). Both, the Hilbert monopole and the ground plane are etched over a 1 mm thick FR4 piece ($\epsilon_r=4.15$, $\tan\delta=0.013$).

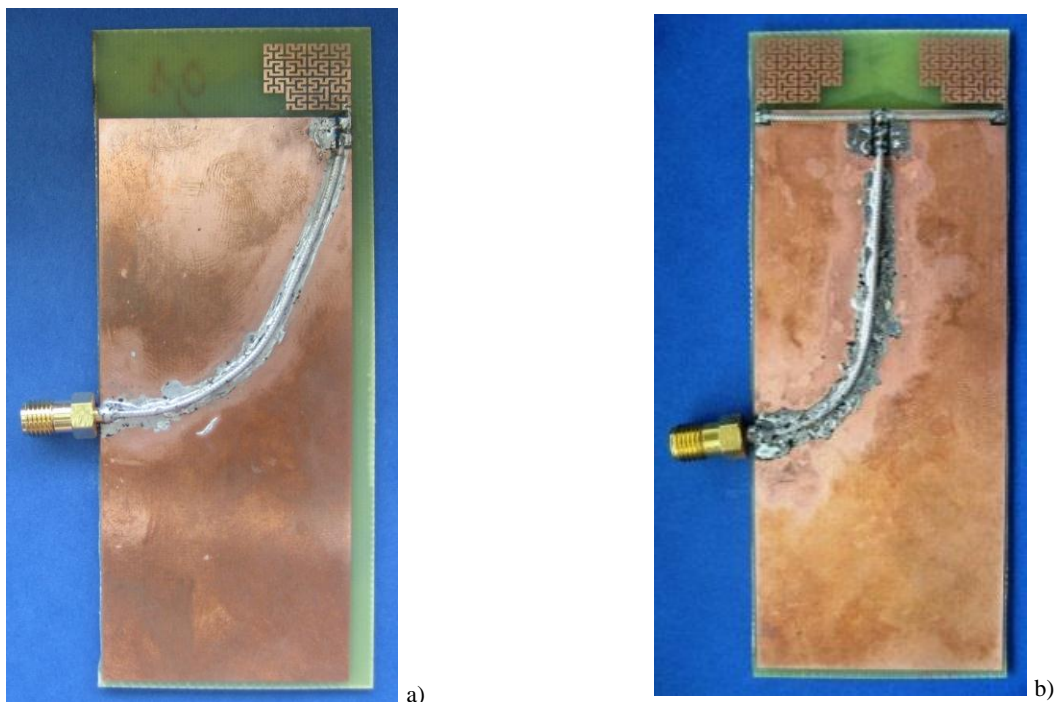


Fig. 5.28 a) Single Hilbert monopole connected to the radiofrequency system depicted in Fig. 5.24a; b) In-phase distributed antenna system comprising two identical Hilbert monopoles and connected to the radiofrequency system defined in Fig. 5.24c; The ground plane in all cases presents dimensions of $90\text{ mm} \times 40\text{ mm}$ and is printed on a FR4 substrate 1 mm thick. The footprint of the monopoles is $14\text{ mm} \times 12\text{ mm}$.

Table 5.4 Matching Network Components (SMD 0402).

	L_p	C_p	C_s	L_p
Single Monopole	2.7nH	4.7pF	3.3pF	6.2nH
Distributed In-phase	L_{TX}	L_p	C_s	L_p
	20 mm	4.3nH	4.7pF	9.1nH

The same fabrication process is used for the distributed antenna system. In this case, two identical Hilbert monopoles are arranged in the corners of the shorter edge of the ground plane (Fig. 5.28b). A broadband matching network and a fine tuning stage are used to match the Hilbert monopole (Fig. 5.24a). At the same time, the distributed antenna system is combined into a single input/output port through the addition of two equal transmission line sections of just 20 mm , which ensure the symmetry of the radiating system. In addition and in order to obtain sufficient bandwidth as for providing operation in the

communication standards GSM850 and GSM900, a π -network is added (Fig. 5.24c). The commercial values of the reactive components used in the prototype are gathered in Table 5.4.

Main antenna parameters have been measured and the results demonstrate that the distributed antenna system fed in-phase stands out over the prototype based on a single Hilbert monopole since it attains higher impedance bandwidth (Fig. 5.29). While the single Hilbert monopole attains a bandwidth around 19% regarding $SWR \leq 3$ (805-972MHz), the distributed antenna system increases impedance bandwidth up to approximately 26% regarding $SWR \leq 3$ (772-1007 MHz). Note that the measured results are aligned with the simulated results presented in the former section.

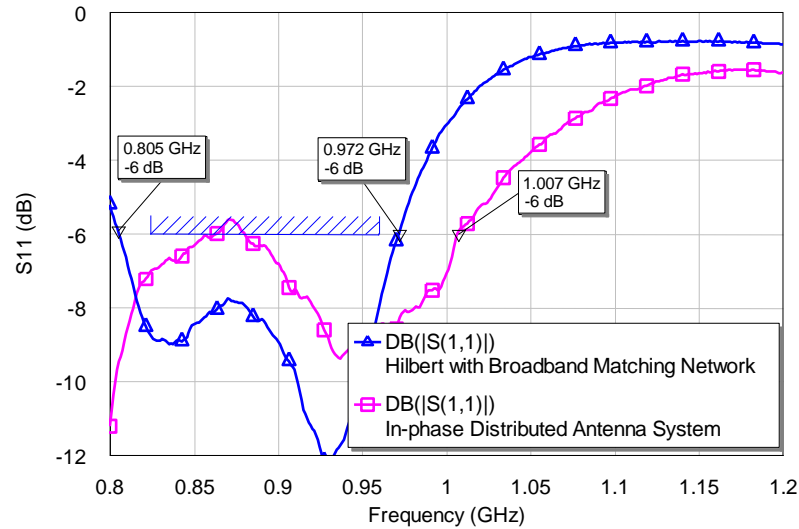


Fig. 5.29 Measured reflection coefficient for the radiating systems of Fig. 5.28.

The antenna efficiency (η_a) of the proposals has also been measured in the anechoic chamber Satimo Stargate-32 by means of 3D radiation pattern integration. Antenna efficiency takes into account both radiation efficiency (η_r) and mismatch losses (Fig. 5.30). Owing to the antenna efficiency, the proposed in-phase solution provides an average value around 43% for the low frequency region (824-960MHz), whereas the Hilbert monopole presents values around 40%. Note that these values differ from the simulated results (Fig. 5.27) since for the last, ideal reactive components with infinite Q were considered. At this point, it is important to emphasize that although slightly better antenna efficiency values are obtained in free-space, the performance of both radiating systems considerably differs when regarding hand loading. In that case, the distributed system stands out over the single monopole. These benefits will be discussed in the next section. In regards to the radiation patterns and directivity values, they are conditioned by the excited ground plane radiation mode, which, as repetitively discussed along this thesis, presents a current distribution similar to that provided by a half-wavelength dipole (Fig. 5.26).

Thus and as discussed in the previous section as well as in [15], array theory does not apply in distributed antenna system intended for wireless handheld devices since the ground plane radiating mode presents an important role in the radiation process that clearly conditions the radiation pattern. In this sense, the resulting radiation pattern at these mobile frequencies (824-960MHz) mainly presents an omnidirectional behavior in one plane and a null along the long axis of the ground plane (Fig. 5.31).

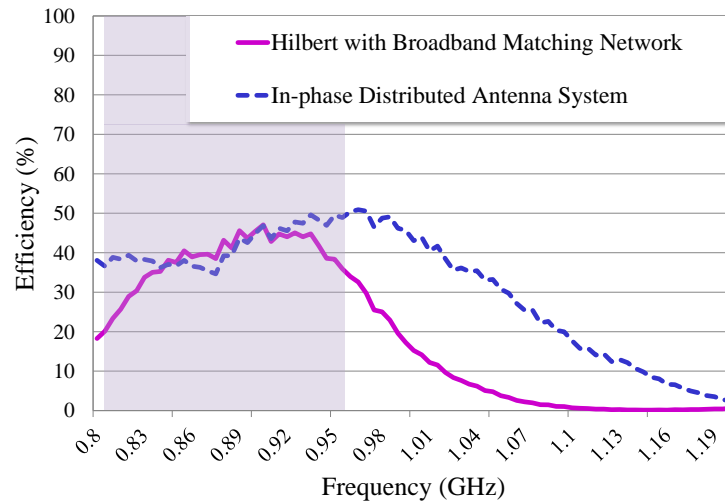


Fig. 5.30 Measured antenna efficiency (η_a) for the radiating systems shown in Fig. 5.28. The antenna efficiency takes into account both ohmic losses and mismatch losses, $\eta_a = \eta_r \cdot (1 - |S_{11}|^2)$. Shaded area ranges from 824 to 960MHz.

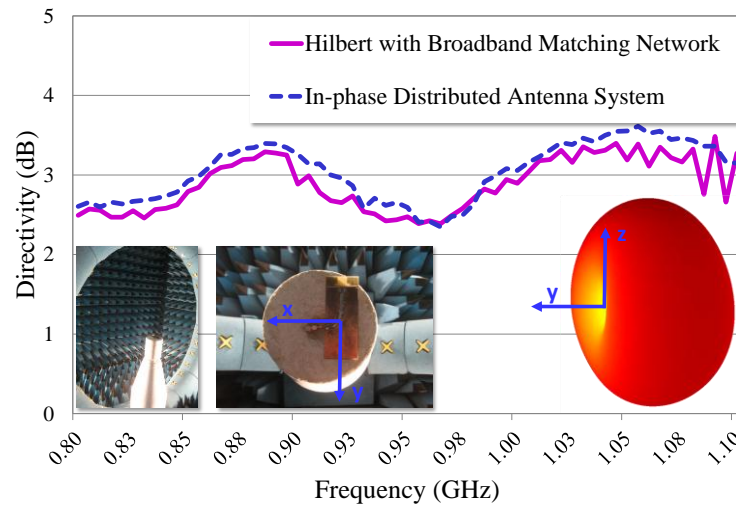


Fig. 5.31 Measured directivity (dB) for the Hilbert monopole and the in-phase distributed antenna system. Measured 3D radiation pattern at 900MHz showing the typical $\lambda/2$ dipole-type pattern for the in-phase distributed antenna system.

The benefits of the distributed antenna system in front of the human loading effect are discussed in the next section.

5.3.3 Human Hand Effect

As previously indicated, the performance of radiating systems integrated in wireless handheld devices is clearly conditioned by the human presence. Particularly, the radiation of an internal handset antenna is considerably affected by the interaction with the user hand when performing a phone call. In order to overcome the aforementioned shortcomings, this section proposes the use of a distributed antenna system capable of mitigating the undesirable detuning and power absorption effects produced by the human hand. Namely this section, in particular, proposes a distributed system fed in-phase for solving the drawbacks of the prior out-of-phase distributed antenna systems discussed above in section 5.2.

A phantom hand filled with lossy liquids ($\epsilon_r' = 41.1$ $\sigma = 0.88$ S/m at 835MHz and $\epsilon_r' = 40.3$ $\sigma = 0.93$ S/m) [20] is used to emulate the electromagnetic properties of the human hand at the frequencies under

study (824-960MHz). Antenna efficiency is measured regarding three finger positions (left, middle, right). Three finger locations have been selected for being considered the most common holding positions. It should be outlined that these experiments consider a critical scenario in which the finger is only spaced apart 1 mm from the antenna using a methacrylate spacer of 1 mm thick placed above the PCB. The distance to the palm is fixed to 20 mm through a foam spacer.

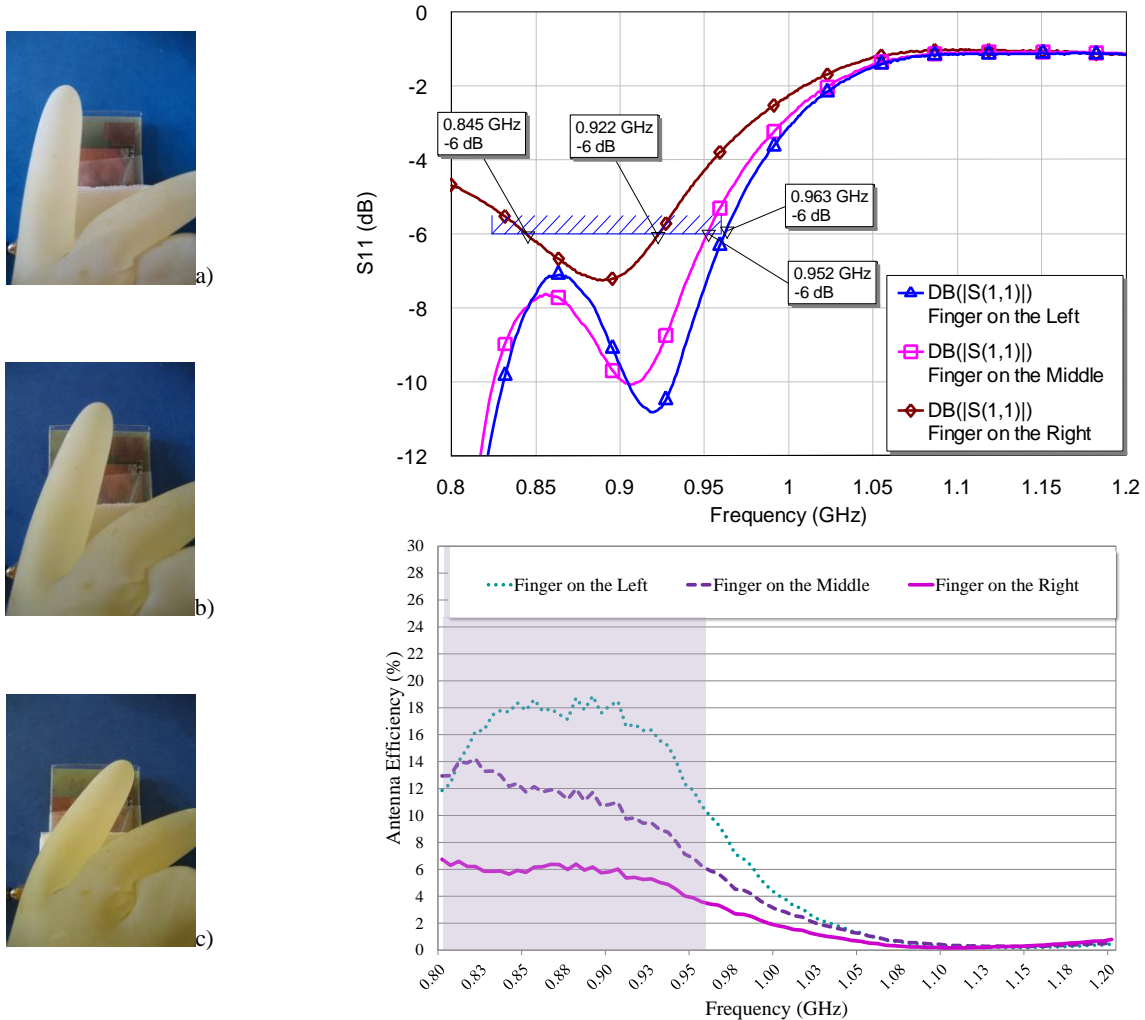


Fig. 5.32 Measured reflection coefficient and antenna efficiency taking into account the phantom hand over the PCB; Detail of the phantom finger covering the upper part of the single Hilbert monopole prototype for the three positions under study: a) Left; b) Middle; c) Right.

The results demonstrate that the distributed system in-phase presents higher robustness to the finger loading than the single Hilbert monopole. On one hand, the single Hilbert monopole is clearly detuned when the finger is placed above the antenna element (finger on the right position) (Fig. 5.32). In contrast, the distributed system fed in-phase does not suffer significant detuning effects in none of the three finger positions analyzed (Fig. 5.33). On the other hand, owing to power losses and consequently to efficiency decrements, the proposed distributed antenna system stands out over the single Hilbert monopole since while the first one is clearly more sensitive to the finger location (average efficiency values around 16%, 10%, 5% for the left, middle, and right positions, respectively), the second one offers the required robustness while guarantying average efficiency values around 18% for the three finger positions. It would also be worth noting, that although with the in-phase arrangement, the efficiency drops from

approximately 50% without the hand, down to 20%, the solution is consistent, independent of the finger location and better than the single antenna and the out-of-phase distributed antenna system.

Finally, it is interesting to compare the proposed distributed system with a single monopole antenna occupying a similar area than the two Hilbert monopoles. For this comparison a coupled monopole is tested using the same hand-loading conditions described above (Fig. 5.34) [42]. The single Hilbert monopole is also included. The total area for the distributed system using the Hilbert monopole is 336 mm^2 (regarding two Hilbert monopoles of $12 \text{ mm} \times 14 \text{ mm}$) whereas the area for the coupled monopole antenna is 495 mm^2 , that is, 48% larger.

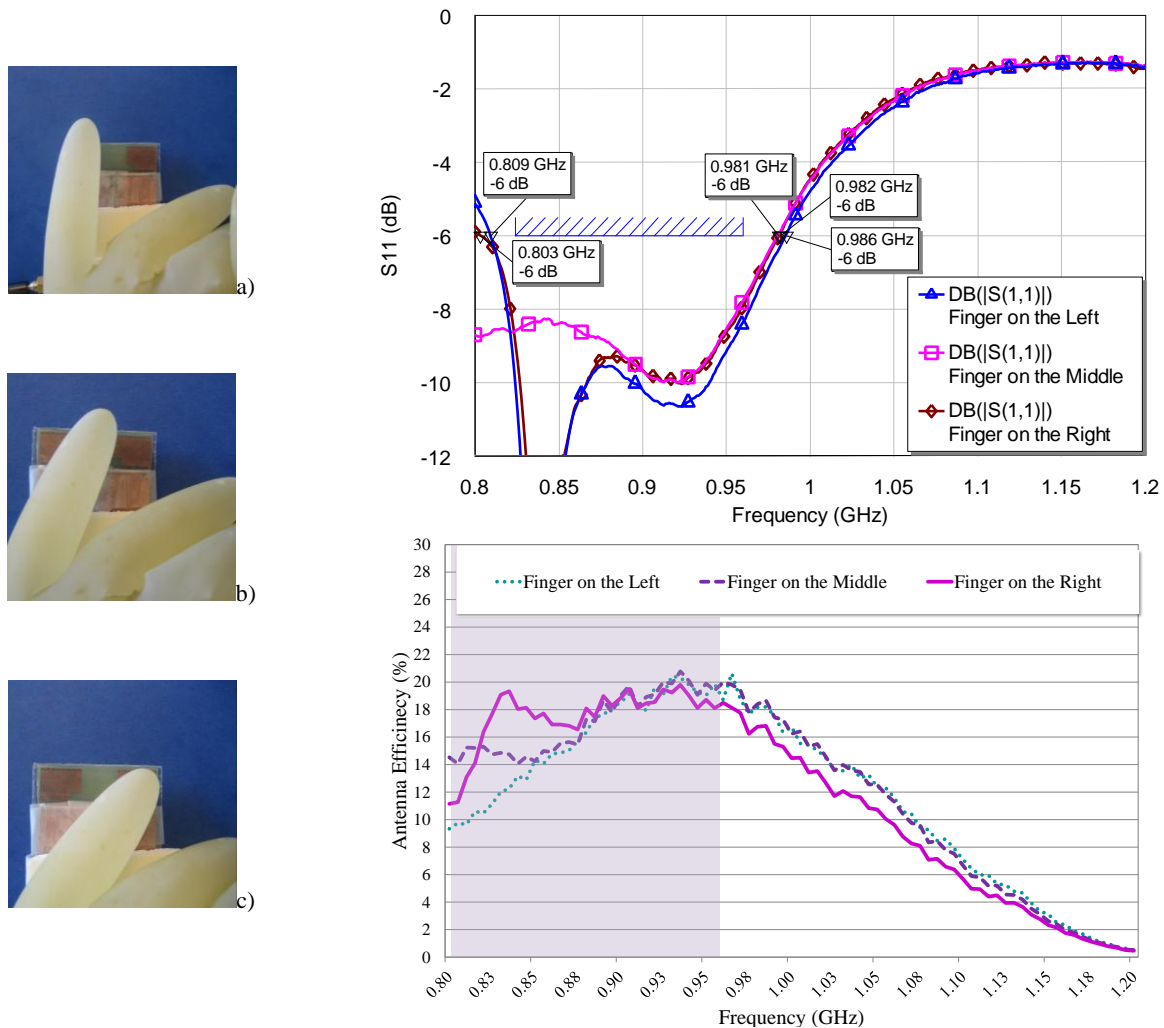


Fig. 5.33 Measured reflection coefficient and antenna efficiency taking into account the phantom hand over the PCB; Detail of the phantom finger covering the upper part of the distributed system prototype for the three positions under study: a) Left; b) Middle; c) Right.

The antenna efficiency results averaged from 824 to 960 MHz illustrate that the coupled monopole antenna performs better than the single Hilbert monopole (the area of the coupled monopole is 94% larger than the Hilbert monopole area), more significantly in the right position when the finger covers the Hilbert monopole. In this case, the single Hilbert monopole becomes the worst solution since its efficiency drops to low values around 5%. However, the proposed distributed system, despite occupying a smaller area, offers slightly higher antenna efficiency values than the coupled monopole antenna as well as consistency with respect to the finger location. This fact demonstrates the potential of the proposed

distributed system as a robust technique in front of the hand loading effects. The proposal could be also extensible to the high frequency region where most of current communication standards, such as GSM1800, GSM1900, and UMTS, are allocated.

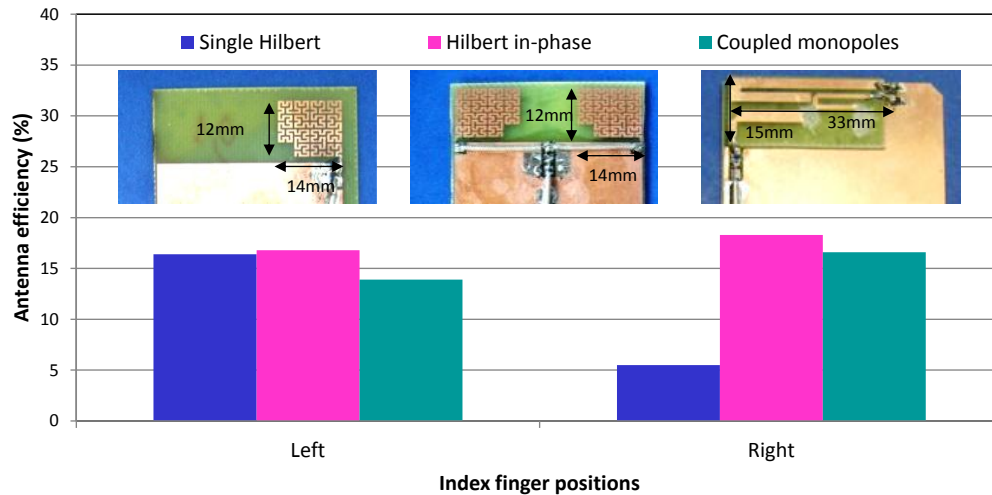


Fig. 5.34 Measured average antenna efficiency (824-960MHz) for the single Hilbert monopole, the in-phase distributed system, and a coupled monopoles taking into account the phantom hand.

5.4. Distributed System based on Ground Plane Boosters

So far, multi-band handset antenna solutions are mainly based on the use of resonant elements, similar to those previously presented, and featured by dimensions comparable to an integer multiple of a quarter of a wavelength at the frequencies of operation [43]-[49]. As discussed in former chapters, when resonant antennas are considered, the behavior of the radiating system is described as the combination of the radiation and impedance characteristics of the wave modes associated to the antenna and those associated to the ground plane [50]-[51]. Thus, the performance of the whole radiating system is strongly conditioned by the antenna itself. These resonant antennas usually present the disadvantage of featuring a complex geometry and a large size, which makes difficult their integration in wireless handheld devices, more significantly when operation in the low frequency region (LFR) (690-960MHz) is demanded. According to the spirit of this thesis, this section is focused on miniaturizing as much as possible the size of the antenna element by substituting resonant antennas by non-resonant elements featured by reduced dimensions. In this sense, the resonant elements used in the former distributed antenna systems are replaced by ground plane boosters of reduced dimensions capable of providing robustness to hand loading by adding redundancy, in particular, two ground plane boosters are used for each frequency region of operation.

At the same time the performance is evaluated regarding the two feeding schemes under study, namely the in-phase feeding and the out-of-phase feeding scheme [52]-[53]. This section further proposes the use of a third feeding mechanism, which suggests a phase difference between input impedances capable of attaining the best trade-off between the former in-phase and out-of-phase solutions [52]-[53]. The proposal maximizes the impedance bandwidth while provides symmetric robustness to finger loading by avoiding impedance imbalance. In this section, the study is not only focused on the LFR, but also it is

expanded to the high frequency region (HFR) (1710-2690MHz). The proposal attains operation in three communication standards (LTE700, GSM850, and GSM900) allocated in the LFR (690-960MHz) and in six communication standards (GSM1800, GSM1900, UMTS, LTE2100, LTE2300, and LTE2500) allocated in the HFR.

The reason behind the use of distributed ground plane boosters in this section is not only focused on miniaturizing the size of the elements used for providing robustness in front of hand loading, but also on enhancing the performance of the system by properly designing the radiofrequency system. Usually, a radiofrequency system based on filters and resonators that integrate a large number of reactive elements (either lumped components or distributed elements) is required to provide impedance matching at multiple frequency bands when non-resonant elements are used [54]-[61]. In order to improve the ground plane mode excitation while simplifying the required radiofrequency system, the present section proposes the use of two paired ground plane boosters (5 mm x 5 mm x 5 mm) located in the corners of a rectangular ground plane featuring typical dimensions of current smartphones (120 mm x 50 mm). Each pair is intended for a particular frequency region and their particular arrangement and combination into a single input/output port increases the bandwidth in a factor around two, with respect to the previous solutions such as those carefully described in chapter 3 [58].

The section is structured in the following manner: firstly, the radiating system comprising both the radiating structure and the proposed radiofrequency systems is presented in section 5.4.1. Secondly, the two proposals based on two different feeding schemes (in-phase and out-of-phase) are assessed through simulations using the software IE3D based on MoM. At the same time, these solutions are compared with a larger single element including a broadband matching network (section 5.4.2). In a third stage, three prototypes are built for the sake of validating the simulations. The experimental results also include the human interaction analysis in terms of hand loading (section 5.4.3). Finally, the conclusions are discussed in section 5.5.

5.4.1 Radiating Structure and Radiofrequency System

The proposed radiating structure comprises a rectangular ground plane (120 mm x 50 mm) capable of supporting at least two efficient radiating modes with resonances at 1.08 GHz and 2.49 GHz, respectively (Fig. 5.35)⁵. The fundamental radiating mode (J_1) features a longitudinal current distribution comparable to that produced by a half wavelength dipole, whereas the current distribution of mode (J_4) could be approximated to that produced by a wavelength dipole with an asymmetric excitation [62] (Fig. 5.35). In order to excite these radiating modes, four non-resonant elements having small dimensions of just 5 mm x 5 mm x 5 mm are arranged in the corners of the ground plane where minimums of current distribution appear (Fig. 5.36). Due to the highly reactive behavior of the non-resonant elements, the challenge of these radiating systems mainly relies on attaining impedance matching. The previous

⁵ Note that this computation does not take into account the dielectric support where, in practice, the ground plane is etched, whose consideration would produce a resonance shifting to lower frequencies. For a thin dielectric slab of 1mm thick and $\epsilon_r=4.15$, the resonance is shifted down approximately a 8% (section 2.3.1).

techniques propose the use of two elements and two matching networks, each one intended for a particular frequency region [54]-[61]. However, although these solutions provide a considerable bandwidth enhancement, the results are still away from the attainable bandwidth that can be computed from the theoretical quality factor (Q) of the radiating structure (2.8)⁶[63].

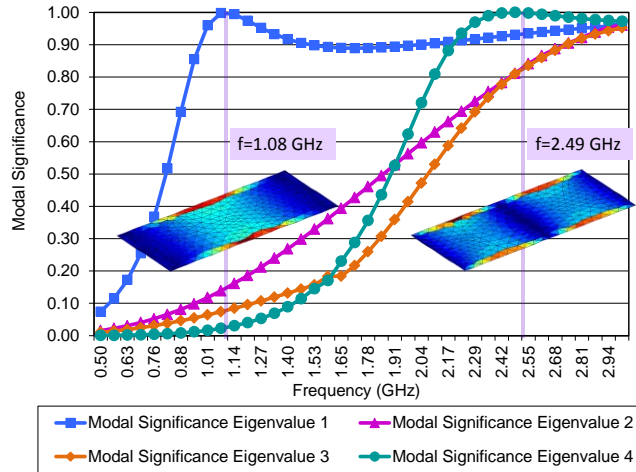


Fig. 5.35 Modal significance associated to the current modes J_1, J_2, J_3, J_4 supported by a ground plane having dimensions of 120 mm x 50 mm. The modal significance represents the normalized amplitude associated to the current modes and provides a physical insight into their radiation properties. As long as the curve approaches the maximum value of one, radiation efficiency increases. The current distributions for the modes J_1 and J_4 are shown.

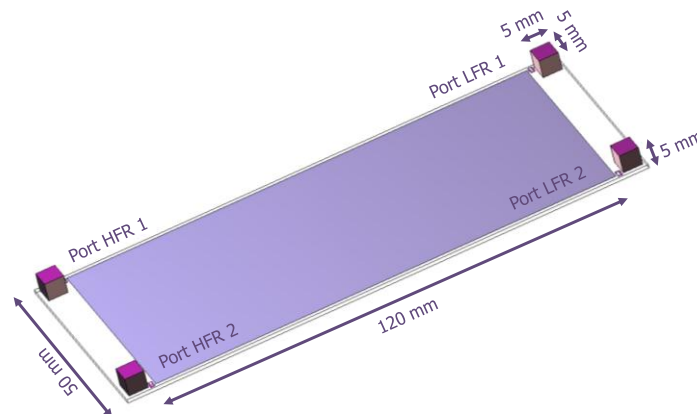


Fig. 5.36 Geometry and dimensions associated to the radiating structure comprising four non-resonant ground plane boosters located at the corners of the rectangular ground plane having typical dimensions of current smartphones 120 mm x 50 mm. Each ground plane booster is a square metallic cube comprising six faces of 5 mm length.

According to equation (1.22.8), a theoretical Q_I around 3.8, hence a theoretical bandwidth of 30.4% $(1.1)^7$ is expected at the center frequency (825MHz) of the LFR regarding a $SWR \leq 3$ [63]. Nevertheless, the size, the nature, and the placement of the non-resonant elements clearly condition these radiation properties. In this sense, if the Q is computed from the input impedance (1.2)⁸ [64], which takes into account the non-resonant element effect, its value increases up to 13.2, thus reducing the inherent bandwidth in a factor around 3.5 (8.7%). Consequently, a radiofrequency system capable of providing

⁶ Q = Quality factor; ω =Angular frequency; λ =Eigenvalue; n =order of the current mode (eigenvector).

⁷ S = Standing Wave Ratio (SWR).

⁸ $R(\omega)$ and $X(\omega)$ (Real and Imaginary part of the input impedance, respectively).

impedance match is strongly demanded. However, its election becomes a relevant aspect to consider since it will strongly condition the performance of the whole radiating system.

In this sense, the challenge and the purpose of this section relies on properly designing a radiofrequency system capable of increasing the bandwidth and capable of approaching it to the theoretical one while providing robustness to the hand loading.

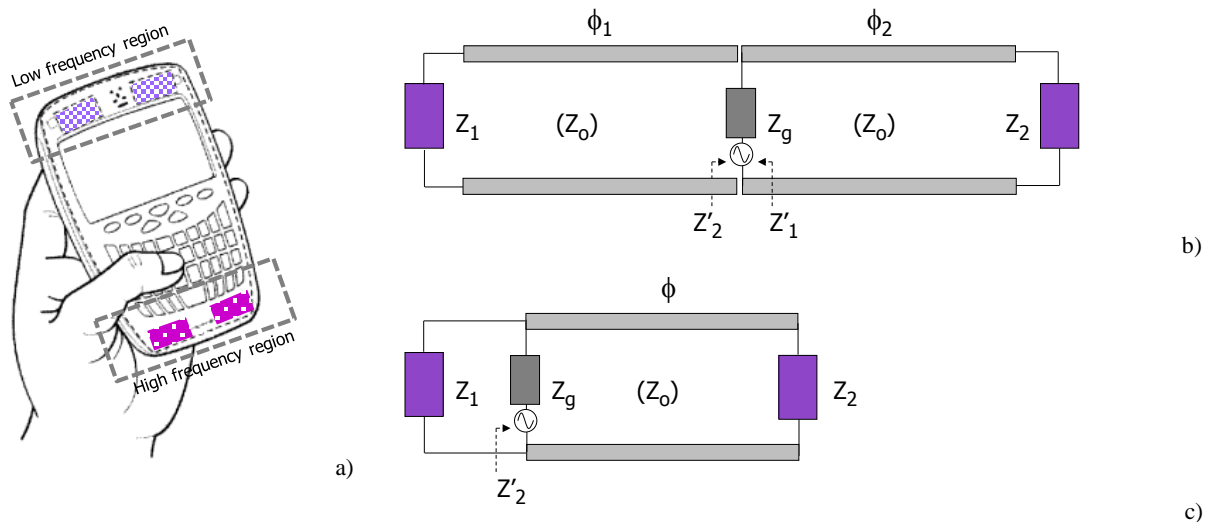


Fig. 5.37 a) Schematic example of a distributed antenna system; b) In-phase feeding scheme ($\phi_1=\phi_2$); c) Out-of-phase feeding scheme (ϕ phase difference between Z_1 and Z_2). Z_1 and Z_2 correspond to the complex input impedances of the first and second non-resonant elements, respectively.

The solution includes two paired ground plane boosters strategically arranged at the corners of the ground plane. Each pair is intended for a particular frequency region (Fig. 5.37a). The responses of each ground plane booster that constitute a pair are combined into a single input/output port through a radiofrequency system including on one hand, an in-phase feeding scheme (Fig. 5.37b and Fig. 5.38a) and on the other hand, an out-of-phase feeding scheme based on conjugated input impedances (Fig. 5.37c) [52]-[53]. The proposals not only improve the excitation of the ground plane modes, but also provide robustness to hand loading. A further object of the present section is focused on demonstrating the relevance of the radiofrequency system in the performance of the whole radiating system. For this reason the behavior of the proposed solutions is compared with the behavior of an out-of-phase feeding scheme based on complementary input impedances [11]-[16], [65] and with a single element having a size comparable to two paired ground plane boosters.

When an out-of-phase system such as the one described in former sections as well as in [11]-[16] is considered, two impedances Z_1 and Z_2 are connected by a transmission line of 90° so as Z_2' is complementary to Z_1 at the central frequency of the intended operating frequency region (Fig. 5.38b). Z_1 and Z_2' are complementary impedances because $Z_1/Z_0=1/(Z_2/Z_0)$ where Z_0 is the reference impedance. The phase delay enhances the bandwidth considerably but causes a significant power unbalance. In effect, for the typical impedances described in [12]-[16], $Z_1=Z_2=20\Omega$. Therefore, $Z_2'=125\Omega$, which supposes a different power distribution in Z_1 and Z_2 . In a similar way, the input impedances in the present case, become also unbalanced (Fig. 5.38b), fact that again would translate into different efficiency values in the

presence of the human hand, as demonstrated in [12]-[16]. In addition these differences can introduce efficiency drops in the operating frequency region [16]. Consequently, this solution is discarded and a new out-of-phase scheme based on conjugated input impedances is proposed to overcome previous shortcomings.

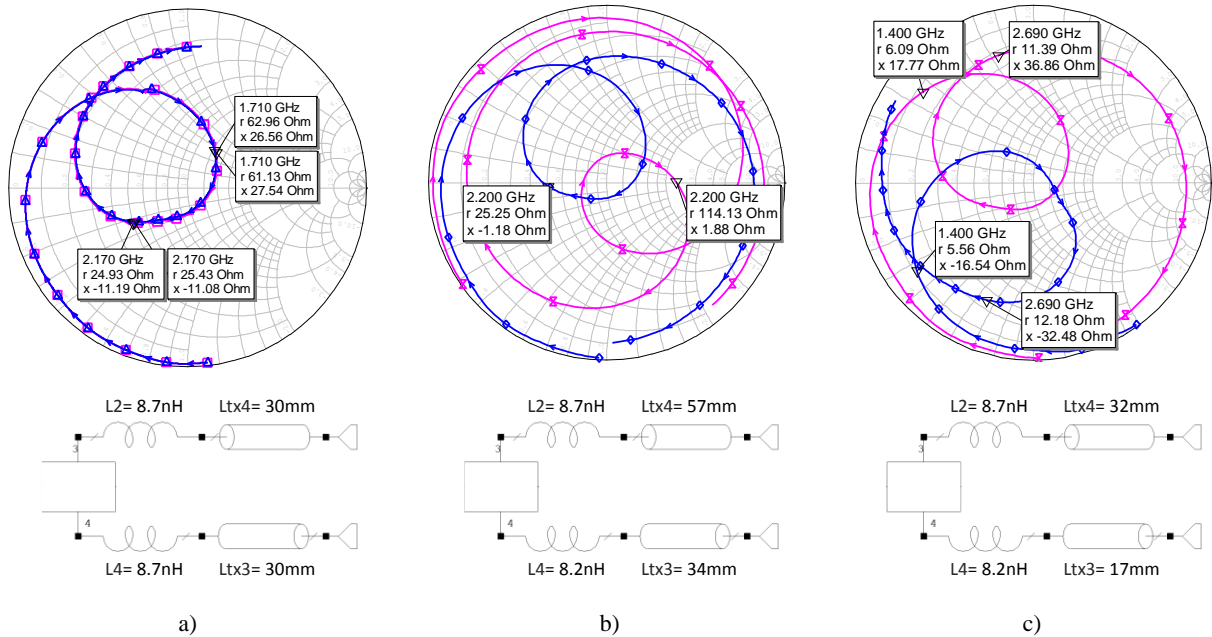


Fig. 5.38 a) In-phase feeding mechanism applied to the HFR; Out-of-phase feeding mechanism where b) the impedances are substantially complementary; c) the impedances are substantially conjugated. The two input impedances illustrated in each Smith chart correspond to the input impedance measured at the corresponding input port of the circuit schematics depicted below each Smith chart.

In the proposal, Z_1 and Z_2 are no longer complementary but conjugated at a frequency of the operating frequency region, that is $Z_1' = Z_2^*$. As $|Z_1'| = |Z_2^*|$ there is no significant power unbalance whereas a bandwidth enhancement is still obtained because of the phase delay between impedances. Along the next sections, the out-of-phase feeding scheme will always refer to this case, i.e. to the case having conjugated impedances. As indicated above and as an alternative solution for overcoming the power unbalance, an in-phase feeding scheme is further proposed in the present section. Both schemes, namely the in-phase and the out-of-phase feeding scheme based on conjugated input impedances are compared not only between them but also with a single element solution featuring a size of 5 mm x 10 mm x 5 mm. This size is selected to set forth a fair comparison between the volume occupied by the pair of ground plane boosters and that required by the single element solution. A broadband matching network such as the one presented in [25], [58] is used to match the single element solution.

5.4.2 Multi-Band Design: Simulated Results

The radiofrequency system proposed for the in-phase feeding scheme combines two equal input impedances into a single port through two transmissions lines of equal length in order to feed the antennas with the same phase (Fig. 5.39a). The length of a first (L_{tx1}) and a second transmission line (L_{tx2}) are equal (36 mm) for the LFR (Port 2). At the same time, the length of a third (L_{tx3}) and a fourth transmission line

(L_{tx4}) are fixed to 30 mm for the HFR (Port 1) (Fig. 5.39a). Note that all the transmission lines have a characteristic impedance of $Z_0=50\Omega$.

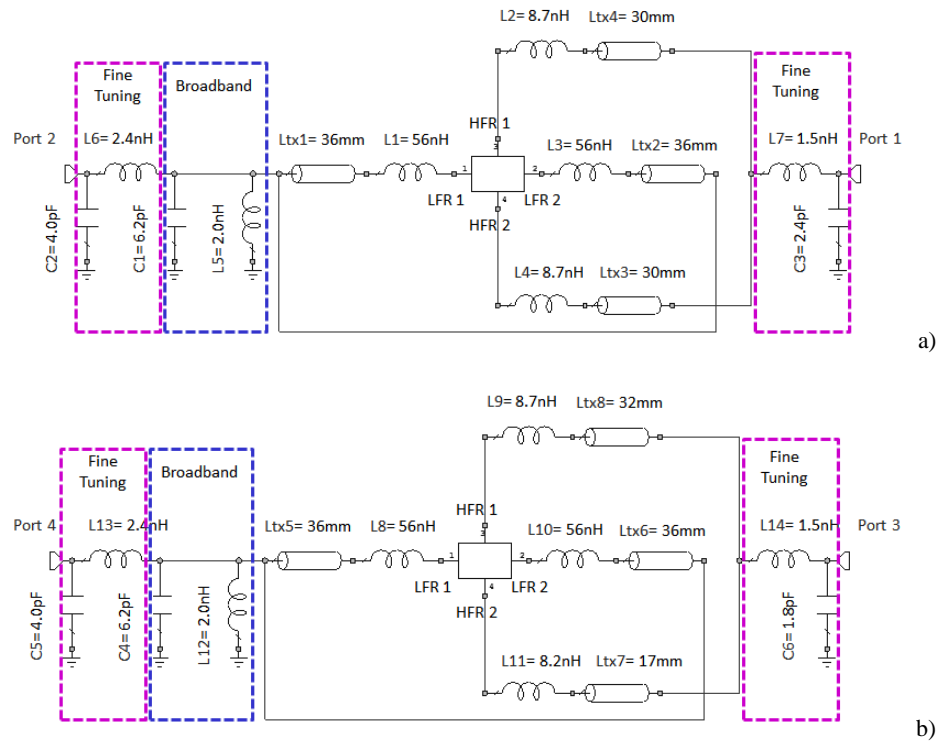


Fig. 5.39 Proposed radiofrequency system based on: a) in-phase feeding scheme for the LFR and HFR, and b) out-of-phase feeding scheme for the HFR and in-phase feeding scheme for the LFR. Ports LFR 1, LFR 2, HFR 1, and HFR 2 represent the ports of Fig. 5.36.

A broadband matching network [25] and a fine tuning stage are added for providing operation in the LFR whereas the HFR just requires a fine tuning stage formed by a series inductor and a parallel capacitor (Fig. 5.39a). The proposal allows the operation of the radiating system in three communication standards LTE700, GSM850, and GSM900 in the LFR (Fig. 5.40). It supposes a bandwidth around 38.6%, which approximates the theoretical value computed from equation (2.8). At the same time, it increases the inherent bandwidth (1.1) computed from Q (1.2) in a factor around 4.5, which almost doubles the potential bandwidth that could be achieved by the addition of just a broadband matching network such as the one described in [58], [25]. A single broadband matching network just provides enhancement factors around 2.45. Similarly, a bandwidth around 35.3% is attained at the HFR, which allows operation in four frequency bands capable of allocating five communication standards (GSM1800, GSM1900, UMTS, LTE2100, and LTE2300) (Fig. 5.40). The transmission coefficient between ports remain below -16dB in both frequency regions, thus guarantying the proper performance of the radiating system.

The simulated results (Fig. 5.41) for the out-of-phase mechanism (Fig. 5.39b) demonstrate that the bandwidth in the HFR can be increased considerably with respect to the in-phase solution (Fig. 5.40). Note that in this case, the in-phase scheme is maintained in the LFR. An out-of-phase feeding scheme has also been tested for the LFR but as will be demonstrated later, it has been discarded due to integration reasons.

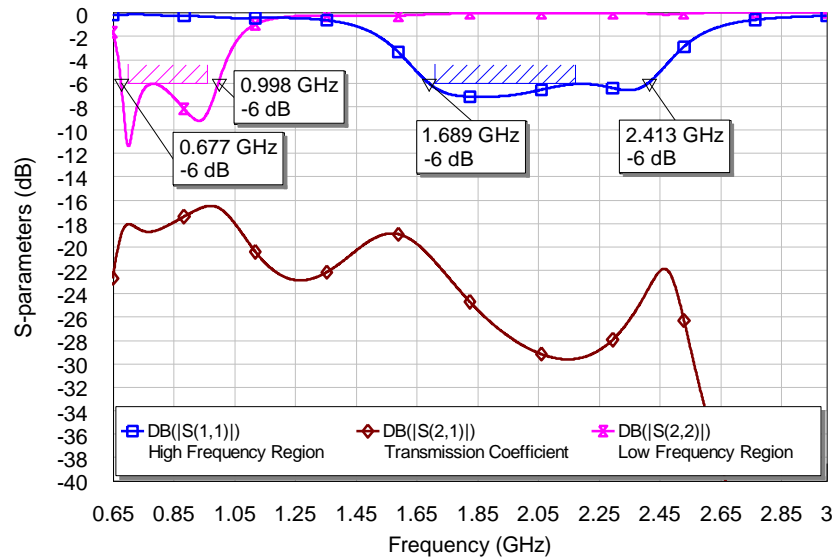


Fig. 5.40 S-parameters resulting from the radiating system gathered in Fig. 5.39a. Solid line with bowtie markers corresponds to the S_{11} measured at the input/output port 2, whereas solid line with square markers refers to port 1. Transmission coefficient (S_{21}) between ports is represented by a solid line with rhombus markers.

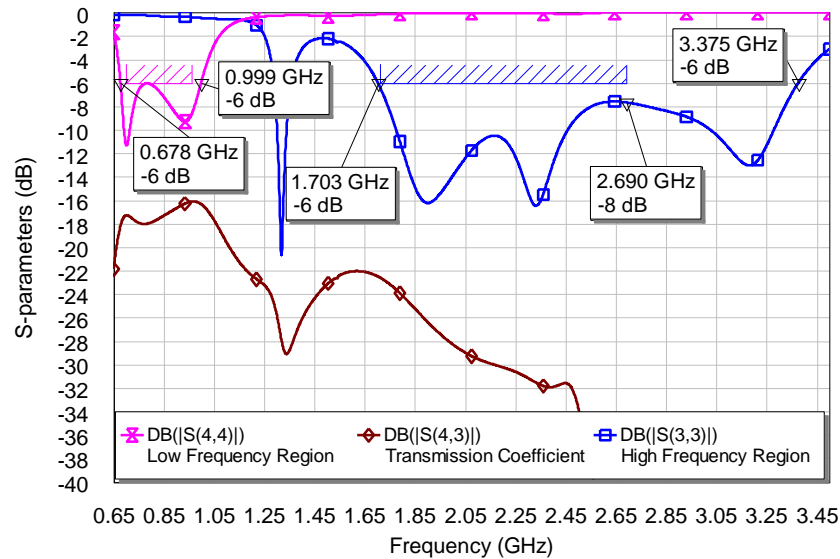


Fig. 5.41 S-parameters resulting from the radiating system gathered in Fig. 5.39b. Solid line with bowtie markers corresponds to the S_{11} measured at the input/output port 4, whereas solid line with square markers refers to port 3. Transmission coefficient (S_{21}) between ports is represented by a solid line with rhombus markers.

With this new configuration the radiating system is capable of providing operation in more than eight frequency bands capable of allocating nine communication standards, namely LTE700, GSM850, GSM900, GSM1800, GSM1900, UMTS, LTE2100, LTE2300, and LTE2500 while preserving the properties of the in-phase feeding schemes in terms of robustness. Again, the transmission coefficient between ports remain below -16dB s for both frequency regions (Fig. 5.41). In order to demonstrate the effectiveness of the proposal in exciting aforementioned ground plane radiating modes (Fig. 5.35), the current distribution is computed at the center frequency of both frequency regions not only for the aforementioned configurations, but also for the single element solution. The results demonstrate that the fundamental longitudinal radiating mode is excited in the LFR, whereas in the HFR a current distribution similar to that produced by a wavelength dipole featured by an asymmetric excitation predominates (Fig.

5.42). On one hand, the in-phase proposal (Fig. 5.39a) is preferable in the LFR since it offers a similar bandwidth than the out-of-phase solution with the advantage of higher robustness and easier integration (Fig. 5.43).

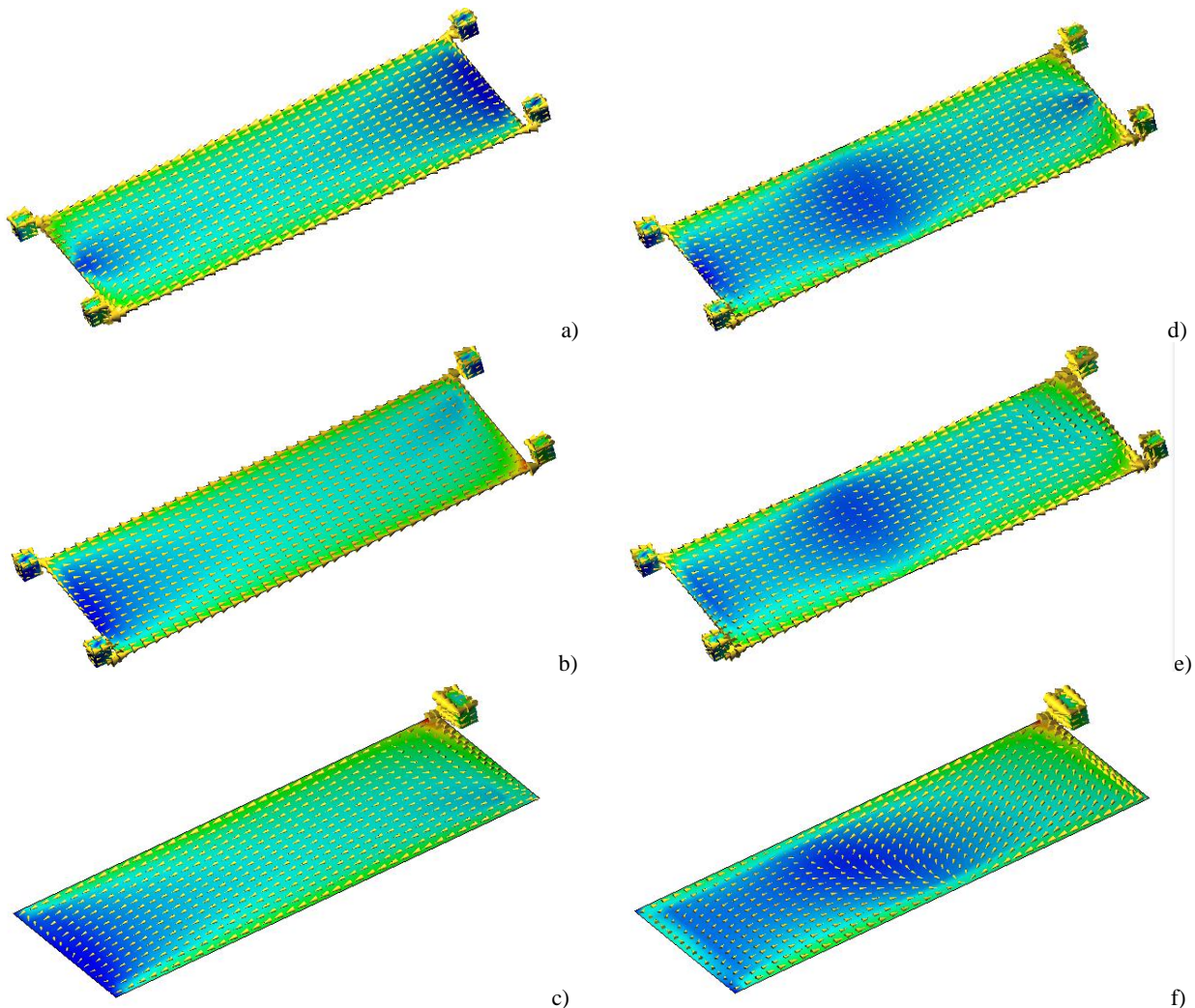


Fig. 5.42 a)-c) Current distribution regarding an in-phase feeding scheme (Fig. 5.39a), an out-of-phase feeding scheme (Fig. 5.39b), and a single element with a broadband matching network, for the center frequency of the LFR (825MHz), respectively, and d)-f) for the center frequency of the HFR (2100MHz), respectively.

The integration simplicity is due to the fact that the out-of-phase scheme for the LFR requires two transmission lines of length 18mm and 5mm, respectively, i.e. the length of the transmission lines capable of producing the required bandwidth enhancement is shorter than the length of the shortest edge of the ground plane (50mm), thus making difficult the combination of both non-resonant elements into a single input/output port. In this frequency region, the distributed systems perform better than the single element solution because the longitudinal mode is better excited. This result is consistent with similar principles applied to monopole antennas where a dual-fed system attains more bandwidth than a single-fed due to a better excitation of a longitudinal mode [51]. On the other hand, in the HFR, the out-of-phase proposal (Fig. 5.39b) stands out over the in-phase proposal (Fig. 5.39a). Note, that at this frequency region it maintains a similar performance with respect to the broadband solution although the latest is more sensitive to the finger position (Fig. 5.43). In this way, it is possible to conclude that the out-of-phase feeding scheme and the single element solution performs better than the in-phase solution in the HFR

whereas in the LFR the in-phase mechanism is the one that attains the best trade-off between implementation simplicity, robustness, and bandwidth.

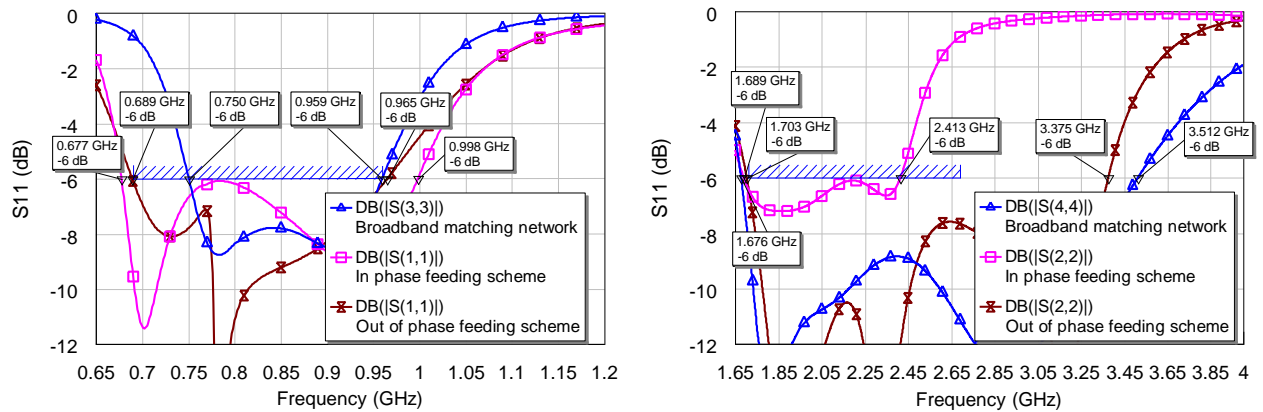


Fig. 5.43 Comparison between the impedance bandwidth attained by an in-phase feeding scheme (solid line with square markers), an out-of-phase feeding scheme based on conjugated input impedances (solid line with bowtie markers), and a single element solution (5 mm x 10 mm x 5 mm) with a broadband matching network (solid line with triangular markers).

5.4.3 Multi-Band Design: Experimental Results

In order to validate the simulated results, three prototypes incorporating the former feeding schemes have been built. They comprise a ground plane having dimensions comparable to that featured by current smartphones (120 mm x 50 mm). The distributed systems include four ground plane boosters of reduced dimensions of just 5 mm x 5 mm x 5 mm whereas the single element solution includes just a larger ground plane booster. The ground plane boosters are respectively placed at the corners of the ground plane where minimums of current distribution appear (Fig. 5.44). The ground plane is etched over a FR4 piece of 1 mm thick and the ground plane boosters are soldered at a distance of 2 mm with respect to its transversal edges.



Fig. 5.44 Prototyped solution including a) in-phase feeding scheme for both frequency regions; b) in-phase feeding scheme for the LFR (upper edge) and out-of-phase feeding scheme for the HFR (bottom edge); c) Single element 5 mm x 10 mm x 5 mm with a broadband matching network (note that for the single element case the component values of the matching network are adapted according to the frequency region of operation). The reactive elements used are SMD0402.

The topology of the proposed radiofrequency systems for the in-phase feeding scheme (Fig. 5.44a) and for the out-of-phase feeding scheme (Fig. 5.44b) corresponds to that illustrated in section 5.4.2 (Fig.

5.39a and Fig. 5.39b, respectively), except for the LFR where the broadband and fine tuning stage have been replaced by a π -network. Similarly, the values of the components have been slightly adjusted (Table 5.5) with respect to that estimated by simulation. This value adjustment obeys to the fact that the simulation considers an ideal scenario where no losses are taken into account. It is important to emphasize that the proposal can be readily integrated in current wireless handheld devices since the use of micro coaxial transmission lines is a widely spread connection technique in commercial handset phones.

5.4.3.1. Free-Space Measurements

Measured results are in good agreement with simulations (Fig. 5.45 and Fig. 5.46). As previously discussed, the in-phase feeding scheme becomes the best solution for the LFR since it attains greater bandwidth than the single element solution (5 mm x 10 mm x 5 mm) (Fig. 5.43).

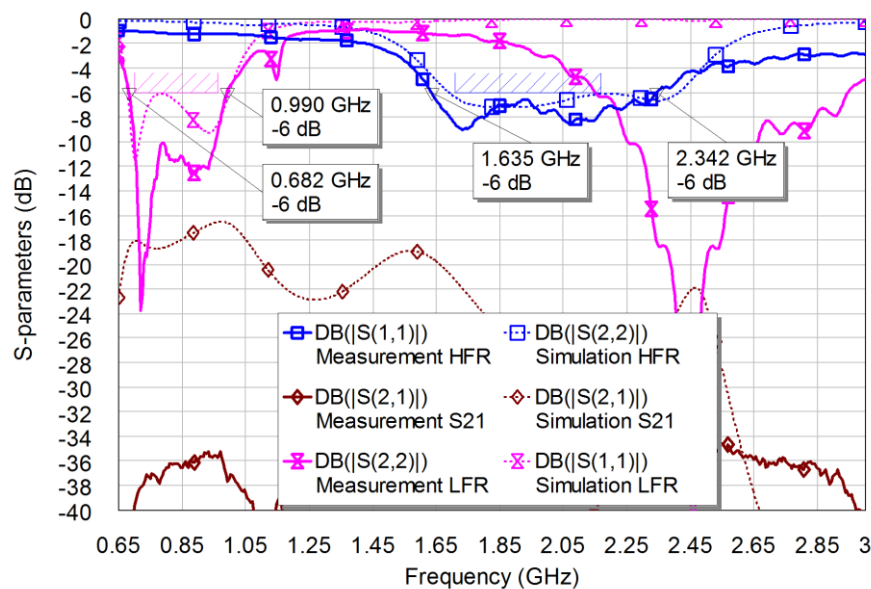


Fig. 5.45 S-parameters resulting from the radiating system gathered in Fig. 5.44a (solid lines) compared with those extracted from simulations (dashed lines) (Fig. 5.40). Solid line with bowtie markers corresponds to the reflection coefficient measured at the input/output port 2 (Fig. 5.39a), whereas solid line with square markers refers to port 1 (Fig. 5.39a). Transmission coefficient between ports (solid line with rhombus markers).

Table 5.5 Reactive component values (lumped components SMD0402 high Q type illustrated in Fig. 5.39).

In-phase feeding scheme for both frequency regions							
Low Region	L1	L3	CX1	CX2	C_{1shunt}	$C_{1series}$	L_{1shunt}
	56nH	56nH	36mm	36mm	4.8pF	15pF	5.5nH
High Region	L2	L4	CX3	CX4	L_{shunt}	C_{series}	
	7.5nH	7.5nH	30mm	30mm	1.6nH	4.1pF	
In-phase feeding scheme for the LFR/Out-of-phase feeding scheme for the HFR							
Low Region	L8	L10	CX5	CX6	C_{1shunt}	$C_{1series}$	L_{1shunt}
	56nH	56nH	36mm	36mm	4.8pF	15pF	5.5nH
High Region	L9	L11	CX7	CX8	L_{series}	C_{shunt}	
	5.6nH	15nH	27mm	24mm	5.4nH	2.2pF	

In addition, it provides higher robustness since in a distributed antenna system if a non-resonant element is blocked, the second one can still operate properly. Furthermore, the in-phase solution stands out over the out-of-phase proposal since it simplifies the integration process. The latest requires two transmission lines, whose length is smaller than the length of the shortest edges of the ground plane, thus

preventing the proper connection of both non-resonant elements. In accordance with the simulated results, the in-phase solution attains triple band operation LTE700, GSM850, and GSM900 (Fig. 5.45 and Fig. 5.46). For the HFR the results demonstrate that the out-of-phase feeding scheme stands out over the in-phase solution, since it allows maximizing the impedance bandwidth while avoiding efficiency drops and power unbalance. It is important to emphasize that these results could be comparable to those obtained by the broadband matching network regarding free-space conditions. However, in the presence of the human hand the single element solution is more sensitive to the finger position as it will be shown next.

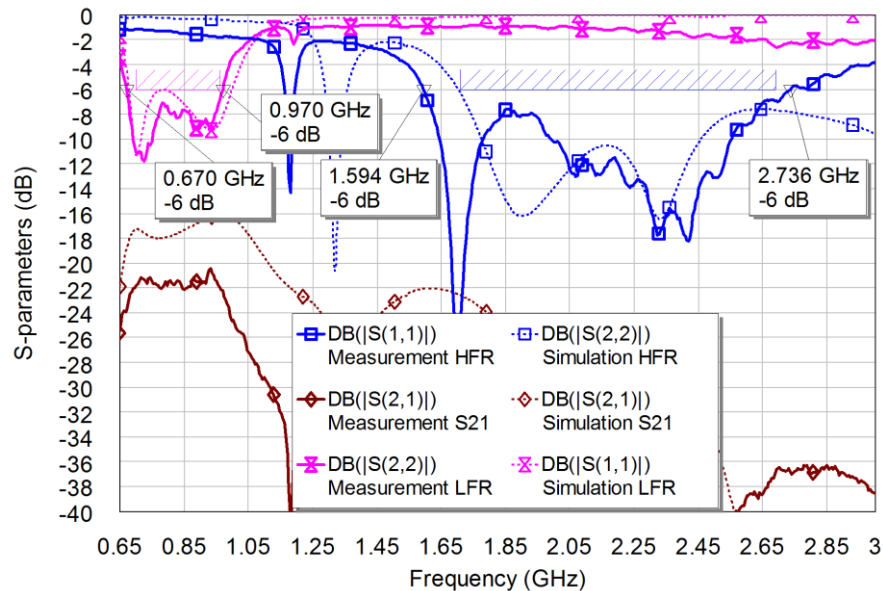


Fig. 5.46 S-parameters resulting from the radiating system gathered in Fig. 5.44b (solid lines) compared with those extracted from simulations (dashed lines) (Fig. 5.41). Solid line with bowtie markers corresponds to the reflection coefficient measured at the input/output port 4 (Fig. 5.39b), whereas solid line with square markers refers to port 3 (Fig. 5.39b). Transmission coefficient between ports (solid line with rhombus markers).

5.4.3.2. Hand Loading

This section is focused on studying the effects of hand loading over the proposed solutions, in-phase, out-of-phase, and single element. With this aim, the aforementioned prototypes are assessed regarding a phantom hand filled with lossy liquids emulating the electromagnetic properties of the human tissue at the frequencies of interest ($\epsilon_r'=41.5$ $\sigma=0.9$ S/m at 835MHz, $\epsilon_r'=40.0$ $\sigma=1.4$ S/m at 1800/1900MHz, and $\epsilon_r'=39.2$ $\sigma=1.8$ S/m at 2450MHz) [20].



Fig. 5.47 Phantom hand holding the prototype. a) finger in the left; b) finger in the middle; c) finger in the right.

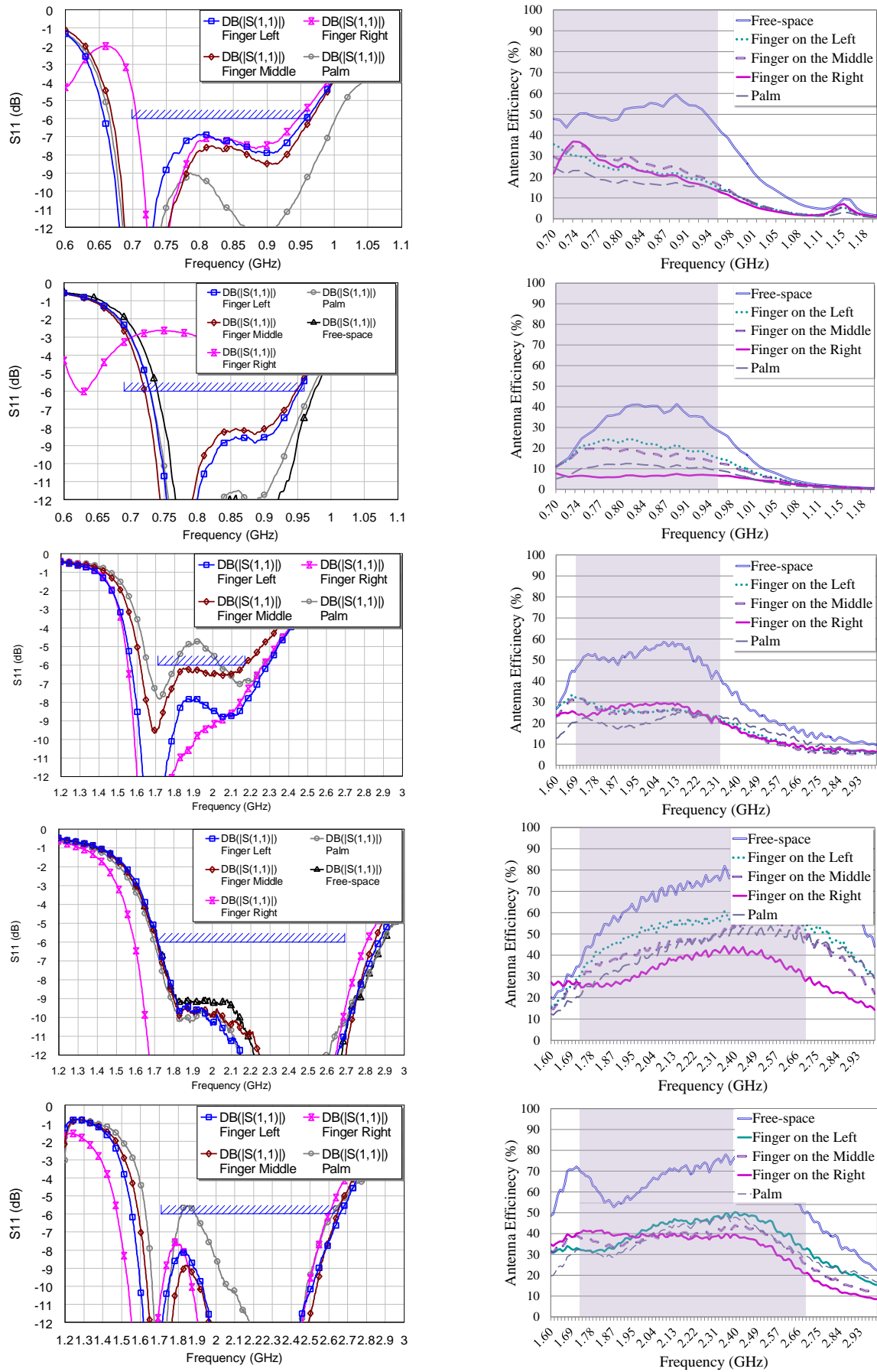


Fig. 5.48 Left: Measured S_{11} (up to down): In-phase and single element solutions regarding LFR and HFR, and out-of-phase scheme for the HFR; Right: Measured η_a in free-space and regarding hand loading.

In a first case, the elements intended for the LFR are located at the upper portion of the PCB, thus placing the HFR in the bottom portion. In a second case, the PCB is rotated 180°, thus locating the LFR in the bottom portion and the HFR in the upper portion of the PCB. When regarding the upper portion, three different finger positions (left, middle, right) are tested according to the common holding of current phones (Fig. 5.47). In this case, the phantom finger is spaced apart 1 mm from the ground plane boosters thanks to the use of a methacrylate piece of 1 mm thick. When the elements are arranged in the bottom portion, the phantom palm is spaced apart 20 mm from the radiating structure. In this sense, the measurements labeled as finger left, middle, and right refer to the upper position, whereas those labeled as palm refer to the bottom position. The results when regarding the upper position demonstrate that the robustness provided by the in-phase feeding scheme is independent of the finger location for both frequency regions.

As discussed previously, the in-phase solution guarantees a similar power distribution at both frequency regions. This power balance translates into similar antenna efficiency values (finger left, middle, and right). The out-of-phase solution overcomes the shortcomings found in [12]-[16], since it produce a large impedance bandwidth while preserving an acceptable power distribution. In this way, the independence of the robustness of the radiating system to the finger location is still preserved.

Table 5.6 In-phase (In), out-of-phase (Out), single element (Single). In/Out refers to the prototype using the in-phase feeding scheme for the LFR and the out-of-phase feeding scheme for the HFR⁹.

	Low Frequency Region					High Frequency Region				
	Free	Left	Middle	Right	Palm	Free	Left	Middle	Right	Palm
In										
η_r (%)	58.5	28.2	30.5	28.5	19.5	69.5	30.5	33.1	30.9	27.9
η_a (%)	51.1	23.9	26.7	24.0	18.1	53.6	26.6	26.0	27.6	20.8
Loss (dB)	---	3.2	2.8	3.1	4.7	---	3.6	3.2	3.5	3.9
In/Out										
η_r (%)	66.5	29.6	32.3	27.3	24.0	74.4	45.5	40.9	40.4	44.1
η_a (%)	56.3	23.7	26.3	20.0	20.6	66.1	41.8	38.0	37.0	38.7
Loss (dB)	---	3.5	3.1	3.9	4.4	---	2.1	2.6	2.7	2.3
Single										
η_r (%)	36.7	23.6	19.7	12.4	11.8	74.2	56.6	49.4	35.9	45.6
η_a (%)	32.7	20.1	16.8	6.6	10.5	68.8	53.0	46.2	35.1	42.8
Loss (dB)	---	1.9	2.7	4.7	4.9	---	1.2	1.7	3.2	2.1

Contrarily, in the single element solution the results are strongly conditioned by the position of the finger. In this way, the right position, that considers the finger completely covering the single element, introduces higher losses (computed between radiation efficiency losses) than the middle and left position in both frequency regions (Fig. 5.48 and Table 5.6). When the elements are placed at the bottom position, the palm introduces higher losses in all cases, except for the single element. In this case, to place the finger over the single element is even more critical than to place the palm. The results further demonstrate

⁹ Note that the table gathers average values. The frequency range considered is 690-960MHz for the LFR and 1710-2690MHz for the HFR except for the in-phase case in the HFR where this range has been adapted to 1710-2170MHz according to the impedance bandwidth ($SWR \leq 3$).

that the in-phase feeding scheme stands out over the single element solution in the LFR. It provides larger impedance bandwidth and well-balanced robustness (Fig. 5.48 and Table 5.6). Note that the out-of-phase feeding scheme for the LFR was discarded in former sections due to implementation reasons.

The results further reveal that the in-phase solution for the LFR suffers lower losses in the upper position. In this configuration, the elements intended for the HFR would be placed in the bottom portion. Regarding this arrangement, the single solution and the out-of-phase feeding scheme would offer a comparable behavior and would perform better than the in-phase case (Fig. 5.48 and Table 5.6).

5.5. Conclusions

Hand loading is a relevant aspect to consider when designing handset antennas since it could introduce significant detuning effects and efficiency decrements. In this sense, radiating systems capable of providing robustness to hand loading are particularly relevant, especially for the low frequency region where the performance is more critical. The placement of the antenna element in the upper part of the handset is preferable since in the bottom part, the antenna may be completely covered by the users' palm, hence suffering significant losses. Nevertheless, at this location, the finger position plays a significant role since the completely obstruction of the antenna element also produces significant efficiency decrements.

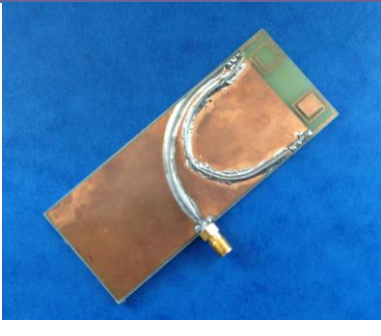
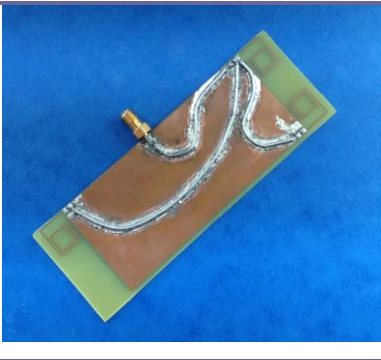



The proposed distributed antenna systems based on a passive array of several antenna elements become an effective solution to improve the performance of the wireless device in the presence of the human hand by overcoming the aforementioned limitations. In particular, the proposal provides redundancy to the system in such a way that when the finger blocks an antenna element, the other elements constituting the array can still operate properly. Particularly, the proposed distributed antenna systems based on complementary input impedances significantly increase the impedance bandwidth while minimize efficiency losses. This bandwidth increment is proportional to the number of elements to combine. In this way, a single monopole attains an impedance bandwidth around 15.6%, whereas a distributed system of two and three monopoles increases it up to 23.6% and 34.0%, respectively. The bandwidth increment of the proposed distributed system of three monopoles supposes enhancement factors around 1.5 over the distributed antenna system of two monopoles, and 2.2 over the single monopole solution. At the same time, the solution based on three monopoles further enhances the antenna efficiency in free space, with an average of 48.1% versus the 46.1% of the distributed system of two monopoles and the 34.6% of the single monopole calculated in the same frequency margin. In addition, it significantly increases the robustness against the loading effects introduced by the user's hand since losses are greatly reduced from 10.6dB for the single monopole solution to 4.1dB for the distributed system of three monopoles. It is worth noting the usefulness of the electrical models to understand not only the broadbanding mechanism but also the combination of impedances having different phases. Due to the substantial improvement in bandwidth, the proposal based on three monopoles cover the standards LTE700, GSM850, and GSM900.

The distributed systems based on complementary input impedances, significantly increases impedance bandwidth and improves robustness in front of hand loading with respect to a single monopole solution. Their operation principle is based on combining two or more equal input impedances into a single input/output by providing a phase difference between them capable of producing a compact impedance loop. Thus, for the two element solution, the proper phase difference is around 90° at the center frequency of the operating region, whereas for the three elements, a phase difference close to 60° becomes preferred. Although, these phases allow the creation of compact impedance loops, they provide some impedance imbalance that produce different efficiency losses according to the element blocked by the finger. In order to overcome the dependence of the radiating system performance to the finger location, the use of a distributed antenna system fed-in-phase has been proposed. It allows increasing bandwidth and robustness in front of hand loading while providing a symmetric solution independent of the finger location. This solution removes the finger position dependence of previous out-of-phase distributed systems. In the in-phase case, Hilbert monopoles were used instead of spiral monopoles due to their performance advantages. In this case, the two monopoles are combined into a single input/output port through two transmission lines of equal length. In this way, each transmission line introduces the same phase to each input impedance. Contrarily to what happened with the out-of-phase feeding schemes, this combination does not produce a compact impedance loop. Nevertheless, the lack of sufficient impedance bandwidth to cover the desired communication standards is overcome by the addition of a matching network. The results demonstrate that this design provides greater freedom to the user since the random location of the finger does not produce different performance. The solution avoids critical situations where the finger causes a significant efficiency drop, which produces more battery consumption and eventual call drops.

The aforementioned solutions mainly based on resonant monopoles are substituted by ground plane boosters in order to demonstrate the feasibility of providing miniaturized distributed systems. Radiating systems based on the excitation of ground plane modes through ground plane boosters become a promising solution to provide multi-band performance while minimizing the required printed circuit board area. The challenge of this kind of radiating systems mainly relies on enhancing the transfer of power to the efficient ground plane radiating modes not only by the proper placement of the ground plane boosters, but also by the proper election of the radiofrequency system.

This section proposes the use of distributed antenna systems based on two different feeding schemes (in-phase and out-of-phase) for enhancing the ground plane mode excitation while increasing the robustness of the radiating system to hand loading. In this case, the out-of-phase solution is not based on complementary input impedances but on conjugated ones, i.e. at a proximately the center frequency of the frequency region of operation the input impedances present similar real part but conjugated imaginary part, thus resulting in a similar input impedance modulus. This solution overcomes the disadvantages of the previous out-of-phase feeding schemes based on complementary input impedances, since it attains the best trade-off between bandwidth enhancement and efficiency balance.

Table 5.7 Summary of the proposed radiating systems intended for improving the performance in free-space as well as regarding finger loading.

Architecture	Features	Performance
	<ul style="list-style-type: none"> • Two monopoles of 13 mm x 11 mm. • Ground plane: 90 mm x 40 mm. • Out-of-phase feeding scheme. 	<ul style="list-style-type: none"> • GSM850, GSM900 • Robust to finger loading. • Response depends on the finger location.
	<ul style="list-style-type: none"> • Three monopoles of 13 mm x 11 mm. • Ground plane: 90 mm x 40 mm. • Out-of-phase feeding scheme. 	<ul style="list-style-type: none"> • LTE700, GSM850, GSM900 • Robust to finger loading • Response depends on the finger location
	<ul style="list-style-type: none"> • Two Hilbert-based monopoles of 14 mm x 12 mm. • Ground plane: 90 mm x 40 mm. • In-phase feeding scheme. 	<ul style="list-style-type: none"> • GSM850, GSM900 • Robust to finger loading. • Response is independent of the finger location.
	<ul style="list-style-type: none"> • Two ground plane boosters in-phase for the low frequency region: 5 mm x 5 mm x 5 mm. • Two ground plane booster in-phase for the low frequency region: 5 mm x 5 mm x 5 mm. • Ground plane: 120 mm x 50 mm. 	<ul style="list-style-type: none"> • LTE700, GSM850, GSM900 and GSM1800, GSM1900, UMTS, LTE2100, LTE2300 • Robust to finger loading. • Response is independent of the finger location.
	<ul style="list-style-type: none"> • Two ground plane boosters in-phase for the low frequency region: 5 mm x 5 mm x 5 mm. • Two ground plane booster in-phase for the high frequency region: 5 mm x 5 mm x 5 mm. • Ground plane: 120 mm x 50 mm. 	<ul style="list-style-type: none"> • LTE700, GSM850, GSM900 and GSM1800, GSM1900, UMTS, LTE2100, LTE2300, and LTE2500 • Robust to finger loading. • Response is independent of the finger location.

For the low frequency region, the results demonstrate that although the out-of-phase feeding scheme based on conjugated input impedances provides similar bandwidth than that obtained by the in-phase feeding scheme, the last is preferable from an integration perspective. Whereas the out-of-phase solution requires two transmission lines of length 18 mm and 5 mm, respectively (too shorts regarding the length of the transversal edge of the ground plane (50mm)), the in-phase solution uses two transmission lines each one having a length of 36 mm, which easily allows the interconnection of both ground plane boosters. The performance of the proposed distributed systems is compared with a single ground plane booster solution having a volume equivalent to the volume occupied by the two ground plane boosters that form the distributed system. The single ground plane booster solution is matched with a broadband matching network and the results demonstrate that the distributed systems stand out over the single ground plane booster solution in the low frequency region, since they attain a higher excitation of the ground plane mode, which mainly translate into an increment of the impedance bandwidth. Concerning the high frequency region, the single ground plane booster solution performs similar than the out-of-phase feeding scheme based on conjugated input impedances in free-space. Nevertheless, the distributed system becomes preferable when regarding hand loading, since it is not conditioned by the finger position. The proposed solution is capable of providing octo-band operation, capable of allocating nine communication standards LTE700, GSM850, GSM900, GSM1800, GSM1900, UMTS, LTE2100, LTE2300, and LTE2500 while minimizing the required PCB area.

It is important to emphasize that the distributed systems do not alter the omnidirectional radiation properties of the radiation pattern required in wireless handheld devices, since the half-wavelength dipole type radiating mode of the ground plane is preserved and is the one that mainly contributes to the radiation process mainly on the low frequency region. Finally, it is important to underline that the proposed distributed systems are completely passive, being advantageous in terms of simplicity and battery consumption. Due to all aforementioned advantages and the obtained encouraging results, it is possible to state that distributed systems are suitable solutions to be integrated into mobile platforms to ensure the performance of the antenna system in the presence of the human hand. Some features and the performance of the prototypes proposed along this chapter are summarized in Table 5.7.

5.6. References

- [1] H. Morishita, H. Furuchi, and K. Fujimoto, "Characteristics of a balance-fed loop antenna system for handsets in the vicinity of human head or hand", *IEEE Antennas and Propagation Society International Symposium*, Salt Lake City, USA July 2000, pp.2254-2257.
- [2] B.S. Collins, S.P. Kingsley, J.M. Ide, S.A. Saario, R.W. Schlub, and S.G. O'Keefe, "A multi-band hybrid balanced antenna", *IEEE International Workshop on Antenna Technology: Small Antennas and Novel Metamaterials*, White Plains, New York, March 6-8, 2006, pp.100-103.

- [3] M.I. Kitra, C.J. Panagamuwa, P. McEvoy, J.C. Vardaxoglou, and J.R. James, "Low SAR Ferrite Handset Antenna Design", *IEEE Transactions on Antennas and Propagation*, vol. 55, n° 4, April 2007, pp.1155-1164.
- [4] M. Bank and B. Levin, "The Development of a Cellular Phone Antenna with Small Irradiation of Human-Organism Tissues", *IEEE Antennas and Propagation Magazine*, vol. 49, n° 4, August 2007, pp.65-73.
- [5] K.M. Lee and R.S. Chu, "Analysis of Mutual Coupling Between a Finite Phased Array of Dipoles and Its Feed Network", *IEEE Transactions on Antennas and Propagation*, vol. 36, n°12, December 1988, pp.1681-1699.
- [6] M.A. Stuchly, M. Okoniewski, M. Rahman, and K. Capula "Modeling of Human Interaction with Antennas Using the Finite Difference Time Domain Technique", *IEEE APS Conference on Antennas and Propagation of Wireless Communications*, November 1998, pp.73.76.
- [7] W. J. Krzysztofik, "Meandered Double-PIFA Antenna-Handset/Human Interaction", *International Conference on Microwaves, Radar & Wireless Communications*, May. 2006, pp.119-122.
- [8] A. Hirata, K. Shirai, and O.Fujiwara, "On Averaging Mass of SAR Correlating with Temperature Elevation due to a Dipole Antenna", *Progress In Electromagnetic Research (PIER)* 84, 2008, pag. 221-237.
- [9] A. Hirata and T. Shiozawa, "Correlation of Maximum Temperature Increase and Peak SAR in the Human Head Due to Handset Antennas", *IEEE Transactions on Microwave Theory and Techiques*, vol. 51, n° 7, Jul. 2003, pp.1834-1841.
- [10] K. R. Boyle, Y. Yuan, and L. P. Lighthart, "Analysis of Mobile Phone Antenna Impedance Variations With User Proximity", *IEEE Transactions on Antennas and Propagation*, vol. 55,n°2, February 2007, pp.364-372.
- [11] J. Anguera and C.Puente, "Distributed Antenna System Robust to Human Loading Effects", *Patent Application*,WO 2007/141187, May 31, 2007.
- [12] J. Anguera, A. Camps, A. Andújar, and C. Puente, "Enhancing the robustness of handset antennas to finger loading effects", *IEE Electronics Letters*, vol.45, n°15, July 2009, pp-770-771.
- [13] J. Anguera, A. Andújar, C. Puente, A. Camps, and C. Picher, "Mitigation of Finger Loading Effect in Handset Antennas", *Proceedings of the Fourth European Conference on Antennas and Propagation*, EuCAP 2010, Barcelona, Spain, April 2010.
- [14] J. Anguera, A. Andújar, Y. Cobo, C. Picher, and C. Puente, "Handset Antenna Array to Mitigate the Finger Loading Effect", *Proceedings of the Fifth European Conference on Antennas and Propagation*, EuCAP 2011, Rome, Italy, pp.611-614.
- [15] A. Andújar, J. Anguera, Y. Cobo, and C. Picher, "Distributed Antenna Systems for Wireless Handheld Devices Robust to Hand Loading", *IEEE Transactions on Antennas and Propagation*, vol. 60, n°10, October 2012, pp. 4830-4837.

- [16] A. Andújar, J. Anguera, and J.L. Leiva, "In-phase versus Out-of-phase Distributed Antenna Systems for Wireless Handheld Devices", *IEEE Transactions on Antennas and Propagation*, vol. 61, n°1, January 2013, pp. 346-353.
- [17] R. Valkonen, S. Myllymaki, A. Huttunen, J. Holopainen, J. Ilvonen, P.Vainikainen, and H. Jantunen, "Compensation of finger effect on a mobile terminal antenna by antenna selection", *International Conference on Electromagnetics in Advanced Applications (ICEAA)*, 2010, 20-24 Sept. 2010, pp.364-367.
- [18] D. Lu, D. Fisk, and A. Wang, "A Mobile Antenna Design for Optimal Performance in Human Head and Hand Configuration", *IEEE Antennas and Propagation Society International Symposium*, Honolulu, USA, June 2007, pp. 1048-1048.
- [19] T. Huang and K. R. Boyle, "User Interaction Studies on Handset Antennas", *Proceedings of the Second European Conference on Antennas and Propagation*, EuCAP 2007, Edinburgh, United Kingdom, November 2007.
- [20] Basic standard for the measurement of Specific Absorption Rate related to human exposure to Electromagnetic fields from mobile phones (300 MHz - 3 GHz. J, CENELEC-European Committee for Electrotechnical Standardization Std. EN 50 361, July 2001.
- [21] A. Schiavoni, P. Bertotto, G. Richiardi, and P. Bielli "SAR generated by commercial cellular phones-phone modeling, head modeling, and measurements", *IEEE Transactions on Microwave Theory and Techniques*, vol. 48, n°11, November 2000, pp.2064-2071.
- [22] J.J. Arenas, J. Anguera, and C. Puente, "Balanced and single-ended handset antennas: free space and human loading comparison", *Microwave and Optical Technology Letters*, vol.51, n°9, September 2009, pp.2248-2254.
- [23] J. Vergés, J. Anguera, C. Puente, and D. Aguilar, "Analysis of the human body on the radiation of FM handset antenna", *Microwave and Optical Technology Letters*, vol.51, n°11, November 2009, pp.2588-2590.
- [24] H. F. Pues and A.R. Van de Capelle, "An Impedance-Matching Technique for Increasing the Bandwidth of Microstrip Antennas", *IEEE Transactions on Antennas and Propagation*, vol. AP-37, n° 11, November1989, pp. 1345-1354.
- [25] A. Andújar, J. Anguera, and C. Puente, "A Systematic Method to Design Broadband matching Networks", *Proceedings of the Fourth European Conference on Antennas and Propagation*, EuCAP 2010, Barcelona, Spain, April 2010.
- [26] J. Anguera, C. Puente, C. Borja, G. Font, and J. Soler "A systematic method to design single-patch broadband microstrip patch antennas", *Microwave and Optical Technology Letters*, vol.31, n°3, November 2001, pp.185-188.
- [27] C. Li, E. Ofli, N. Chavannes, and N. Kuster, "Effects of Hand Phantom on Mobile Phone Antenna Performance", *IEEE Transactions on Antennas and Propagation*, vol. 57, n°9, 2009, pp. 2763-2770.

- [28] V. Plicanic, B. Lau, A. Derneryd, and Z. Ying, "Actual Diversity Performance of a Multi-band Diversity Antenna with Hand and Head Effects", *IEEE Transactions on Antennas and Propagation*, vol. 57, n°5, 2009, pp.1547-1556.
- [29] H. AbuTarboush, R. Nilavalan, T. Peter, and S. Cheung, "Multi-band Inverted-F Antenna with Independent Bands for Small and Slim Cellular Mobile Handsets", *IEEE Transactions on Antennas and Propagation*, vol. 59, n°7, 2011, pp. 2636-2645.
- [30] M. Pelosi, O.Franek, M. Knudsen, G. Pedersen, and J. Andersen, "Antenna Proximity Effects for Talk and Data Modes in Mobile Phones", *IEEE Antenna and Propagation Magazine*, vol. 52, n° 3, 2010, pp. 15-27.
- [31] S. Myllymaki, A. Huttunen, M. Berg, M. Komulainen, and H. Jantunen, "Method for Measuring User-Induced Load on Mobile Terminal Antenna", *IEE Electronics Letters*, vol. 45, 2009, pp. 1065-1066.
- [32] Wei Yu, Shiwen Yang, Chia-Lun Tang, and Danny Tu, "Accurate Simulation of the Radiation Performance of a Mobile Slide Phone in a Hand-Head Position", *IEEE Antennas and Propagation Magazine*, vol. 52, 2010, pp. 168-177.
- [33] S. Ali, A. Mobasher and P. Lusina, "Users Effects on MIMO Performance: From an Antenna to a Link Perspective", *International Journal of Antennas and Propagation*, Article ID 918315, 2011.
- [34] M. Koubeissi, M. Mouhamadou, C. Decroze, D. Carsenat, and T. Monédière, "Triband Compact Antenna for Multistandard Terminals and User's Hand Effect", *International Journal of Antennas and Propagation*, Article ID 491262, 2009.
- [35] C. Su, C. Wu, and K. Wong, "User's Hand Effects on EMC internal GSM/DCS mobile phone antenna", *IEEE Antennas and Propagation Society International Symposium*, Albuquerque, USA, July 2006, pp. 2097-2100.
- [36] M. A. Ebrahimi-Ganjeh and A. Attari, "Interaction of Dual Band Helical and PIFA Handset Antennas with Human Head and Hand", *Progress In Electromagnetics Research*, PIER 77, 2007, pp. 225-242.
- [37] S. Lee, Y. Lim, Y. Joong, C. Hong, and H. Kim, "Multi-band Folded Slot Antenna With Reduced Hand Effect for Handsets", *IEEE Antennas and Wireless propagation Letters*, vol. 9, 2010, pp. 674-677.
- [38] J.Ilvonen, R.Valkonen, O.Kivekäs, P.Li, and P.Vainikainen, "Antenna shielding method reducing interaction between user and mobile terminal antenna", *IEE Electronics Letters*, vol. 47, 2011, pp. 896-897.
- [39] J. M. Jung, S. Kim, K. Kong, J. Lee, and B. Lee, "Designing Ground Plane to Reduce Hand Effects on Mobile Handsets", *IEEE Antennas and Propagation Society International Symposium*, Honolulu, USA, June 2007, pp. 1040-1043.
- [40] C.Puente, E.Rozan, and J.Anguera, "Space Filling Miniature Antennas", patent app. WO 01 54225, January 10, 2000.

- [41] I. Sanz, J. Anguera, A. Andújar, C. Puente, and C. Borja, "The Hilbert Monopole Revisited", *Proceedings of the Fourth European Conference on Antennas and Propagation*, EuCAP 2010, Barcelona, Spain, April 2010.
- [42] S. Risco, J. Anguera, A. Andújar, A. Pérez, and C. Puente, "Coupled Monopole Antenna Design for Multi-band Handset Devices", *Microwave and Optical Technology Letters*, vol.52, n°10, February 2010, pp.359-364.
- [43] C. Lin and K. L. Wong, "Printed Monopole Slot Antenna for Internal Multi-band Mobile Phone Antenna", *IEEE Transactions on Antennas and Propagation*, vol. 55, n°12, December 2007, pp. 3690-3697.
- [44] R. A. Bhatti and S. O. Park, "Hepta-Band Internal Antenna for Personal Communication Handsets", *IEEE Transactions on Antennas and Propagation*, vol. 55, n°12, December 2007, pp. 3398-3403.
- [45] S. Hong, W. Kim, H. Park, S. Kahng, and J. Choi, "Design of Internal Multiresonant Monopole Antenna for GSM900/DCS1800/US-PCS/S-DMB", *IEEE Transactions on Antennas and Propagation*, vol. 56, n°5, May 2008, pp. 1437-1443.
- [46] A. Cabedo, J. Anguera, C. Picher, M. Ribó, and C. Puente "Multi-band Handset Antenna combining a PIFA, Slots, and Ground Plane Modes", *IEEE Transactions on Antennas and Propagation*, vol. 57, n°9, September 2009, pp. 2526-2533.
- [47] Y. Chi and K. Wong, "Quarter-Wavelength Printed Loop Antenna with an Internal Matching Circuit for GSM/DCS/PCS/UMTS Operation in the Mobile Phone", *IEEE Transactions on Antennas and Propagation*, vol. 57, n°9, September 2009, pp. 2541-2547.
- [48] J. Anguera, I. Sanz, J. Mumbrú, and C. Puente, "Multi-band Handset Antenna with a Parallel Excitation of PIFA and Slot Radiators", *IEEE Transactions on Antennas and Propagation*, vol. 58, n° 2, February 2010, pp. 348-355.
- [49] M. Zheng, H. Wang, and Y. Hao, "Internal Hexa-band Folded Monopole/Dipole/Loop Antenna with Four Resonances for Mobile Device", *IEEE Transactions on Antennas and Propagation*, vol. 60, n°6, June 2012, pp. 2880-2885.
- [50] P. Vainikainen, J. Ollikainen, O. Kivekäs, and I. Kelder, "Resonator-Based Analysis of the Combination of Mobile Handset Antenna and Chassis", *IEEE Transactions on Antennas and Propagation*, vol. 50, n°10, October 2002, pp. 1433-1444.
- [51] M. Cabedo-Fabrés, E. Antonino-Daviu, A. Valero-Nogueira, and M. Ferrando Bataller, "The Theory of Characteristic Modes Revisited: A Contribution to the Design of Antennas for Modern Applications", *IEEE Antennas and Propagation Magazine*, vol. 49, n°5, October 2007, pp. 52-68.
- [52] A. Andújar, J. Anguera, "Scattered Virtual Antenna Technology for Wireless Devices", *Patent Pending* 2013.
- [53] A. Andújar, J. Anguera, Y. Cobo, "Distributed Systems Robust to Hand Loading based on Non-Resonant Elements", *Microwave and Optical Technology Letters*, in press 2013.

- [54] J. Villanen, J. Ollikainen, O. Kivekäs, and P. Vainikainen, "Coupling Element Based Mobile Terminal Antenna Structures", *IEEE Transactions on Antennas and Propagation*, vol. 54, n° 7, July 2006, pp. 2142-2153.
- [55] S. Ozden, B. K. Nielsen, C. H. Jorgensen, J. Villanen, C. Icheln, and P. Vainikainen, "Quad-Band Coupling Element Antenna Structure", *U.S. Patent 7,274,340*, September 25, 2007.
- [56] J. Anguera, A. Andújar, C. Puente, J. Mumbrú, "Antennaless Wireless Device", *Patent Application WO2010/015365*, July 31, 2009.
- [57] J. Anguera, A. Andújar, C. Puente, and J. Mumbrú, "Antennaless Wireless Device Capable of Operation in Multiple Frequency Regions", *Patent Application WO2010/015364*, July 31, 2009.
- [58] A. Andújar, J. Anguera, and C. Puente, "Ground Plane Boosters as a Compact Antenna Technology for Wireless Handheld Devices", *IEEE Transactions on Antennas and Propagation*, vol. 59, n°5, May 2011, pp. 1668-1677.
- [59] J. Holopainen, J. Ilvonen, R. Valkonen, A. Azremi, and P. Vainikainen, "Study on the Minimum Required Size of the Low-Band Cellular Antenna in Variable-Sized Mobile Terminals", *Proceedings of the Sixth European Conference on Antennas and Propagation, EUCAP 2012*, Prague, Czech Republic, March 2012, pp. 2754-2758.
- [60] A. Andújar and J. Anguera, "Magnetic Boosters for Multi-band Operation", *Microwave and Optical Technology Letters*, vol.55, n°1, Jan.2013, pp.65-75.
- [61] A. Andújar and J. Anguera, "Multi-band Coplanar Ground Plane Booster Antenna Technology", *IEE Electronics Letters*, vol.48, n°21, 2012, pp.1326-1328.
- [62] W.L.Stutzman and G. A.Thiele, "Antenna Theory and Design", 2nd Edition, *John Wiley*, 1998.
- [63] C. T. Fandie, W. L. Schroeder, and L. Solbach, "Numerical Analysis of Characteristic Modes on the Chassis of Mobile Phones", *Proceedings of the First European Conference on Antennas and Propagation, EuCAP 2006*, Nice, France, 2006.
- [64] S. R. Best, "The Inverse Relationship between Quality Factor and Bandwidth in Multiple Resonant Antennas", *IEEE Antennas and Propagation Society International Symposium*, 2006, pp. 623-626.
- [65] R. An, L. Youyuan, and L. Shou, "An Antenna Arrangement", *Patent Application WO2008/075208*.

CHAPTER 6 GROUND PLANE BOOSTERS IN MIMO SYSTEMS

6.1. Introduction

The rapid growth of mobile communications has fostered the appearance of new communication standards capable of providing high data rates. This is the case of LTE (Long Term Evolution), which consolidates as the 4G solution that will naturally follow today's 3G UMTS Technology. The great success of handset devices mainly obeys to their capabilities of integrating large number of functionalities and services in a portable device. Nowadays, handset's users can perform from speech and video calls to streaming media and web browsing all over a common platform. Nevertheless, the handset market is more and more demanding and requiring high data rates capable of enabling a wide variety of Internet protocol services such as video on demand, video streaming, video conference, voice over IP, high definition video, interactive games, web 2.0, etc.

In this sense, the radiating system integrated in a 4G wireless handheld or portable device must provide enough bandwidth to satisfy the strict demands of these emergent applications. However, the bandwidth associated to the cellular communication standards, wireless connectivity standards, and broadcast standards is already allocated and cannot be increased mainly due to the well-known electromagnetic spectrum limitations.

Table 6.1 LTE Frequency Bands (FDD (Frequency Division Duplex)).

Band - Name	Uplink	Downlink	Band - Name	Uplink	Downlink
(1) 2100MHz	1920-1980MHz	2110-2170MHz	(13) Up700MHz	777-787MHz	746-756MHz
(2) 1900MHz	1850-1910MHz	1930-1990MHz	(14) Public Safety	788-798MHz	758-768MHz
(3) 1800MHz	1710-1785MHz	1805-1880MHz	(17) Low700MHz	704-716MHz	734-746MHz
(4) AWS	1710-1755MHz	2110-2155MHz	(18) Japan800	815-830MHz	860-875MHz
(5) 850MHz	824-849MHz	869-894MHz	(19) Japan800	830-845MHz	875-890MHz
(6) Japan	830-840MHz	875-885MHz	(20) 800EDD	832-862MHz	791-821MHz
(7) 2500MHz	2500-2570MHz	2620-2690MHz	(21) 1.5GHz	1447.9- 1462.9MHz	1495.9- 1510.9MHz
(8) 900MHz	880-915MHz	925-960MHz	(22) 3.5GHz	3410-3490MHz	3510-3590MHz
(9) 1700MHz	1749.9- 1784.9MHz	1844.9- 1879.9MHz	(23) S-Band	2000-2020MHz	2180-2200MHz
(10) Extend. AWS	1710-1770MHz	2110-2170MHz	(24) L-Band	1626.5- 1660.5MHz	1525-1559MHz
(11) Japan1.5	1427.9- 1447.9MHz	1475.9- 1495.9MHz	(25) US-PCS	1850-1915MHz	1930-1995MHz
(12) Low700MHz	698-716MHz	728-746MHz	(26) Up 850MHz	814-849MHz	859-894MHz

LTE appears in this context with the aim of providing further frequency bands as well as new access techniques. Nevertheless, the assignment of new frequency bands of the electromagnetic spectrum (Table 6.1) as well as the proposed new access techniques such as OFDM (Orthogonal Frequency

Division Multiplexing) must to work together with a new handset antenna technology called MIMO (Multiple Input Multiple Output) in order to ensure these high data rates, ideally close to 100Mb/s for high mobility, such as mobile access, and up to approximately 1 Gb/s for low mobility, such as local wireless access [1]-[2]. Accordingly, MIMO technology appears as a particularly promising solution to increase data throughput, without additional bandwidth or increased transmit power. In a MIMO system, the capacity of the channel is directly proportional to the number of paired antennas. For instance, two antennas in the transmitter ($M=2$) and two antennas in the receiver ($M=2$) would lead to a MIMO system ($M \times M$) of MIMO order (M) equal to two, which means that the MIMO system is capable of increasing the channel capacity in a factor around two with respect to that provided by a SISO system (Single Input Single Output) composed by a single antenna in the transmitter ($M=1$) and a single antenna in the receiver ($M=1$).

This section deals with the challenge of enabling multi-band MIMO systems in current smartphones (Fig. 6.1). First of all and in order to allow the proper assessment of MIMO systems, the MIMO concept as well as the most relevant MIMO parameters, such as MIMO capacity, correlation, diversity gain, etc. are introduced in section 6.2.

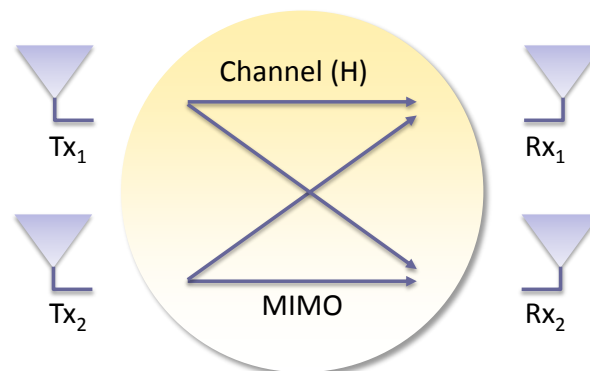


Fig. 6.1 Schematic representation of a MIMO System with a MIMO order of two.

Section 6.3 is intended for analyzing some of the current state of the art solutions in order for determining both, their advantages and limitations. This section further discusses current isolation techniques, such as spatial diversity, radiation patterns diversity, polarization diversity, slotted ground planes, dielectric antennas, decoupling networks, neutralization lines, and parasitic radiators, which are intended for reducing mutual coupling and correlation between radiating systems.

Section 6.4 analyzes the feasibility of integrating a multi-band MIMO system in a handset platform being formed by some representative current handset technologies. The radiating systems are mainly based on antenna elements featuring resonant dimensions. The proposals are intended for determining the performance of conventional “on-ground” and “off-ground” solutions. With this aim, a dual-band PIFA (Planar Inverted F Antenna) antenna, as an “on-ground” solution, is compared with a similar PIFA design placed over a slotted ground plane and finally with a set of coupled monopoles, as a representative sample of “off-ground” solutions.

Section 6.5 combines the previous radiating systems with the non-resonant elements proposed along this thesis. In this sense, the previous designs are combined with a radiating system based on ground plane boosters, similar to that illustrated in section 3.2, and their performance as a MIMO system is assessed. An isolation technique based on the insertion of slots in the ground plane is proposed for reducing mutual coupling. A parametric study is carried out for determining the location and size of the slot that maximizes isolation.

Finally, section 6.6 provides a MIMO solution fully based on ground plane boosters. The proposal also employs the isolation technique described above. Nevertheless, in this case the geometry of the slots is inspired in the Hilbert fractal, hence allowing their miniaturization. This miniaturization is further increased through the addition of reactive elements. A 2x2 multi-band MIMO system capable of providing MIMO operation in the communication standards GSM850 (band 5), GSM900 (band 8), GSM1800 (band 3), GSM1900 (band 2), UMTS, and LTE2100 (band 1) is finally achieved (Table 6.1).

6.2. MIMO Concept and Relevant Parameters

As slightly introduced in the previous section, MIMO technology requires the integration of multiple antennas in transmission as well as in reception. These antenna elements must be capable of providing independent propagation paths for enabling significant data rate increments. In this sense, MIMO systems only work properly in rich multipath propagation environments, i.e. when regarding low correlation channels. In these cases, the data rate increment is ideally proportional to the number of antennas used in transmission and reception. Thus, in ideal conditions, MIMO technology is capable of increasing the channel capacity in an M factor (6.1) with respect to that attained by a SISO system (6.2). The M factor corresponds to the MIMO order of the MIMO System. Note that multiple antenna systems do not always increase channel capacity proportionally to the number of antenna elements. In fact, multiple antenna systems can be as well used to improve BER (Bit Error Rate) for a fixed transmission data or to improve data transmission for a fixed BER. The latest corresponds to the MIMO technology, which, in ideal conditions, produces an increment of the channel capacity directly proportional to the number of paired antennas in transmission and reception according to (6.1). It means that if a 2x2 MIMO system is going to be designed, two antennas must be used for transmission and two antennas must be used for reception. If the number of antennas in transmission and reception is not equal, the system will lead to a SIMO (Single Input Multiple Output) or MISO (Multiple Input Single Output) system (Fig. 6.2). This kind of systems usually increase the channel capacity by providing an improvement of the Signal to Noise Ratio (SNR), i.e. are used to improve BER for a fixed transmission data but not to improve data transmission for a fixed BER.

A SISO system comprises a single antenna for transmission and a single antenna for reception. If this system operates in a multipath propagation channel (as the one characteristic of wireless environments), the transmitted signal is spread out in multiple signals that arrive at the receiver with different angles, amplitudes, and phases. This phenomenon is mainly produced by the obstacles that the

transmitted signal finds in their way, which produce scattering, reflection, refraction, diffraction, etc. At the end, multiple signals arrive at the receiver, and these signals could be added constructively in the best situation or destructively in the worst case depending on their amplitudes and phases. Destructive additions yield to signal fadings that considerably degrade the performance of the transceiver.

$$C_{MIMO} = M \cdot \left(B \cdot \log \left(1 + \frac{S}{N} \right) \right) \text{bits} / s \quad (6.1)$$

$$C_{SISO} = B \cdot \log \left(1 + \frac{S}{N} \right) \text{bits} / s \quad (6.2)$$

In order to avoid these signals fadings, diversity schemes such as those composed by multiple antennas in the receiver (SIMO) or multiple antennas in the transmitter (MISO) are widely used (Fig. 6.2). Multiple antennas in reception, for instance, allow having multiple independent paths as long as these antennas are sufficiently uncorrelated. It means that each antenna sees a different channel, thus making highly unlikely the appearance of simultaneous fadings in these multiple paths. Many techniques are used in the receiver to combine these signals, such as MRC (Maximum Ratio Combining) or SC (Selection Combining). All of them are intended for improving BER for a fixed transmission data, i.e. for improving the SNR, hence the channel capacity according to (6.2). Note that the capacity increment obtained by these diversity schemes is not comparable to that attained by a MIMO system, since in ideal conditions it is capable of multiplying the channel capacity proportionally to the number of antenna elements, whereas diversity schemes are just intended for improving signal quality.

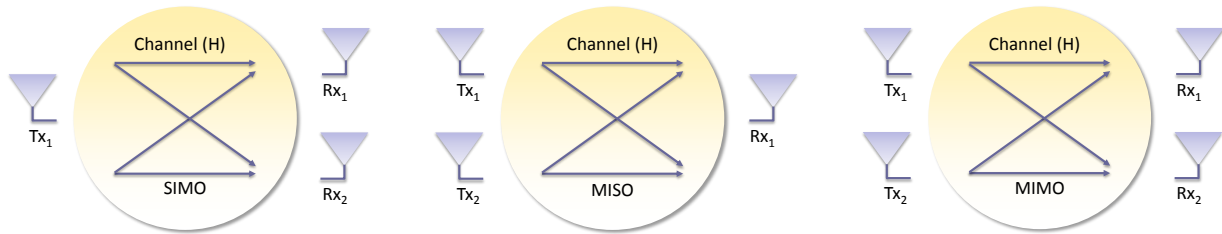


Fig. 6.2 Schematic illustration of a SIMO, MISO, and MIMO system, respectively.

$$DG = SNR_{combined} - SNR_{alone}(dB) \quad (6.3)$$

$$EDG = SNR_{combined} - SNR_{ref_antenna}(dB) \quad (6.4)$$

$$ADG = SNR_{combined} - SNR_{one_branch}(dB) \quad (6.5)$$

$$IDG = SNR_{combined} - SNR_{ideal_Rayleigh_one_branch}(dB) \quad (6.6)$$

Diversity gain (DG) is the most relevant parameter for these diversity schemes. It is defined as the ratio between the SNR measured when a diversity scheme is used, such as for example one antenna for transmission and two antennas for reception, and the SNR measured when just a single antenna in transmission and a single antenna in reception is considered.(6.3). Other ratios such as Effective Diversity Gain (EDG) (6.4), Apparent Diversity Gain (ADG) (6.5), and Ideal Diversity Gain (IDG) (6.6) are also

proposed in the literature. It is important to underline once again that in the same manner as the aforementioned diversity schemes (SIMO or MISO), MIMO technology also requires operation in rich multipath propagation environments for performing properly. Nevertheless and as previously mentioned, in contrast to diversity schemes it is intended for attaining channel capacity increments directly proportional to the number of paired antennas thanks to the use of spatial multiplexing (Fig. 6.3).

MIMO technique based on spatial multiplexing requires the same number of transmitting and receiving antennas. They must operate in a rich multipath propagation environment in order to enable sufficient number of uncorrelated paths. The signal is divided according to the number of transmitting and receiving antennas, in such a way that the number of symbols transmitted simultaneously to the channel is proportional to the number of paired antennas. In this sense, the receiving antennas are capable of recovering as much symbols as transmitting antennas at the same time, thus multiplying the channel capacity proportionally to the number of paired antennas (Fig. 6.3) [1].

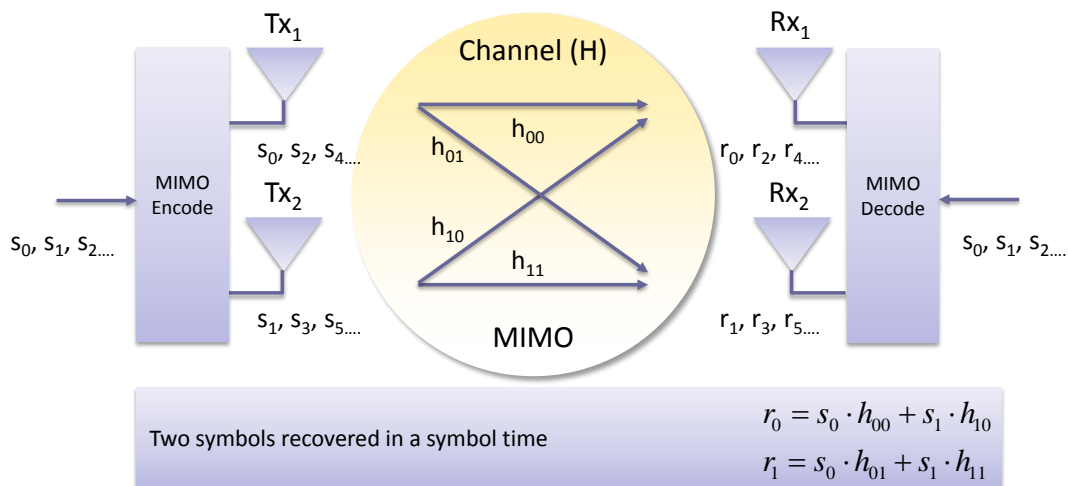


Fig. 6.3 MIMO Technique: Spatial multiplexing.

In addition to the typical handset antenna requirements in terms of impedance bandwidth, efficiency, radiation patterns, etc., the antennas forming the MIMO system should also satisfy strict specifications in terms of mutual coupling and correlation in order to avoid a penalty of the MIMO capacity.

MIMO antennas must be as uncorrelated as possible in order to preserve independent propagation paths. In this sense, they should be as uncoupled as possible since mutual coupling between antenna elements considerably degrades correlation as well as decreases the radiated power. Ideally, the correlation between antennas should be zero, although values smaller than 0.5 are also acceptable [3]-[4]. Several methods are disclosed in the literature capable of reducing correlation and mutual coupling between antenna elements. These methods will be deeply explained along the following section.

In the present chapter, correlation coefficient is derived from the far-field radiation patterns regarding the characteristic of the propagation environment, the terminating input impedances, as well as the mutual coupling between antenna elements [5]. The mutual coupling describes the electromagnetic interaction between antenna elements. The relation between the currents (I) and the voltages (V) at the

antenna ports are given by (6.7). The correlation coefficient between two antenna elements will depend on these coupling effects as well as on the propagation environment. When an isotropic environment with a uniform distribution is considered it can be described according to (6.8) or alternatively according to (6.9) regarding $XPR = 1$ and, P_θ and P_ϕ uniform [6]-[8]. The parameter XPR stands for the cross-polarization ratio, which is the ratio of mean power of incident θ -polarized and ϕ -polarized waves. At the same time, the angular power distribution of the signals in elevation and azimuth are denoted with P_θ and P_ϕ , respectively.

$$\begin{aligned} V_1 &= Z_{11} \cdot I_1 + Z_{12} \cdot I_2 \\ V_2 &= Z_{21} \cdot I_1 + Z_{22} \cdot I_2 \end{aligned} \quad (6.7)$$

An efficient approach to compute envelope correlation without requiring the previous knowledge of the radiation patterns is that based on the scattering parameters [6]-[8]. Nevertheless this approximation is only valid when isotropic distribution is assumed and the antenna system is lossless. In this kind of environments, the envelope correlation based on S-parameters (6.10) corresponds to that given by (6.8), where $\vec{F}_i(\theta, \phi)$ is the field radiation pattern of the antenna system when port i is excited and $\vec{F}_1(\theta, \phi) \cdot \vec{F}_2^*(\theta, \phi)$ denotes the Hermitian product. It is important to emphasize that in the context of handset devices, the S-parameters method could not replace previous radiation pattern method (6.8) and (6.9), which allows the possibility of better characterize the propagation environment. The reason relies on the fact that the efficiency of handset antennas unlikely reaches 100% due to the limited constraints in terms of size. Consequently, the assumed energy conservation principle in the envelope correlation expression does not hold (6.10).

$$\rho_e = \frac{\left| \iint_{4\pi} [\vec{F}_1(\theta, \phi) \cdot \vec{F}_2^*(\theta, \phi)] d\Omega \right|^2}{\iint_{4\pi} |\vec{F}_1(\theta, \phi)|^2 d\Omega \cdot \iint_{4\pi} |\vec{F}_2(\theta, \phi)|^2 d\Omega} \quad (6.8)$$

$$\rho_e = \frac{\left| \iint_{4\pi} [E_{1\theta} \cdot E_{2\theta}^* \cdot P_\theta + XPR \cdot E_{1\phi} \cdot E_{2\phi}^* \cdot P_\phi] d\Omega \right|^2}{\iint_{4\pi} [|E_{1\theta}|^2 \cdot P_\theta + XPR \cdot |E_{1\phi}|^2 \cdot P_\phi] d\Omega \cdot \iint_{4\pi} [|E_{2\theta}|^2 \cdot P_\theta + XPR \cdot |E_{2\phi}|^2 \cdot P_\phi] d\Omega} \quad (6.9)$$

$$\rho_e = \frac{|S_{11}^* \cdot S_{12} + S_{12}^* \cdot S_{22}|^2}{\left(1 - (|S_{11}|^2 + |S_{21}|^2)\right) \cdot \left(1 - (|S_{12}|^2 + |S_{22}|^2)\right)} \quad (6.10)$$

Mean Effective Gain (MEG) is also an important parameter for assessing MIMO performance. It provides a statistical measure of the antenna gain in a given mobile environment and defines the power

received by an antenna, accounting for the effects of the radiation pattern, the antenna efficiency, and the propagation effects (6.11) [7]. P_θ and P_ϕ are the angular density functions of the incident power. XPR represents the cross-polarization ratio. G_θ and G_ϕ are the polarized components of the antenna power gain patterns, respectively.

$$MEG = \int_0^{2\pi} \int_0^\pi \left(\frac{XPR}{1+XPR} G_\theta(\theta, \phi) P_\theta(\theta, \phi) + \frac{1}{1+XPR} G_\phi(\theta, \phi) P_\phi(\theta, \phi) \right) \sin \theta d\theta d\phi \quad (6.11)$$

Another important MIMO parameter is the gain or power unbalance. In a MIMO system and in order to preserve the MIMO benefits, all the antennas forming the system must present similar electromagnetic performance. As the gain imbalance increases, the benefit of MIMO decreases. The effects of power unbalance over the diversity gain of a MIMO system are analyzed in [9] showing that if power unbalance is close to zero, high diversity gains are obtained. In contrast if power unbalance is high, the diversity gain drops to zero. More particularly, the specifications require ratios less than 3 dBs for ensuring proper performance, i.e. the ratio between the MEG values measured at each antenna port should be less than 3 dBs [4].

6.3. State of the Art

As discussed in the previous chapters, the integration of a single multi-band antenna capable of providing multi-band operation with an acceptable radio electric behavior in a small wireless device becomes significantly challenging due to the reduced space available in current handset platforms. The challenge is further exacerbated when shifting from a single antenna system to a multiple antenna MIMO system. The antennas for a MIMO enabled handset, need to keep a certain size to fully operate within the entire bandwidth of several frequency bands. Nevertheless, usually this size prevents the integration of multiple antenna elements. Even if this integration is attained, strict coupling and correlation requirements need to be fulfilled as to benefit from the MIMO gain.

The prior art solutions disclosed in the literature for providing a wireless handheld or portable device integrating the MIMO technology are usually based on antenna elements with a size comparable to the wavelength of operation [10]-[13]. These MIMO solutions usually operate at a frequency located in a high frequency region where the operating wavelength is small enough to allow the integration of several antenna elements with dimensions close to a quarter of a wavelength. Therefore, these proposals are still antenna-based solutions since the contribution to the radiation is predominantly provided by the antenna. This limitation prevents the possibility of arranging large number of antenna elements, since on one hand, the available space in the wireless handheld or portable device is limited, and on the other hand, undesired coupling effects appear due to the proximity between the antenna elements, more significantly when operation in low frequency regions, such as those allocating the LTE700 communication standard, is demanded.

In addition and as discussed in chapter 4, an antenna element having resonant dimensions is typically very sensitive to external effects (such as for instance the presence of plastics or dielectric covers that constitute the wireless handheld or portable device), to components of the wireless handheld or portable device (such as for instance, a speaker, a microphone, a connector, a display, a shield can, a vibrating module, a battery, or an electronic module or subsystem) placed either in the vicinity of, or even underneath, the antenna element, and/or to the presence of the user of the wireless handheld or portable device. Furthermore, usually these elements require a complex geometry able to package the operating wavelength in such limited space.

Other attempts are focused on antenna elements not requiring a complex geometry while still providing some degree of miniaturization by using an antenna element that is not resonant in the frequency regions of operation of the wireless handheld or portable device [14]-[18]. The solution presented in [14] is based on this concept and provides operation in DVB-H communication standard, which is located in a low frequency region (470MHz-862MHz). Although some miniaturization is achieved, such a solution is not enough to provide low correlation and low coupling or high isolation between these antenna elements. Owing to such limitations, while the MIMO performance of the former solution may be sufficient for reception of electromagnetic wave signals, the antenna elements still could not provide an adequate MIMO behavior (for example, in terms of input return losses or gain) for a cellular communication standard requiring also the transmission of a significant amount of power in the form of electromagnetic wave signals. At the same time, those solutions providing suitable transmission and reception of electromagnetic wave signals, such as those described in [15]-[17], are limited to single band operation.

Many are the efforts in the literature focused on reducing mutual coupling and correlation. The most common techniques rely on spacing the multiple antennas a sufficient distance, preferably larger than 0.5λ , as for achieving high port-to-port isolation [19]-[20]. Although this mechanism becomes suitable for high frequency operation, the limited dimensions of current handset platforms make it unsuitable for antennas operating at low frequency regions. Other techniques reduce the correlation between antenna elements by providing significantly different radiation patterns or polarizations [21]. This solution proposes quarter-wavelength resonant antennas placed over a ground plane with dimensions of 105 mm x 55 mm. The antenna elements operate at the 2.6GHz LTE/WiFi band (2.5-2.7GHz) and are oriented orthogonally to each other. It becomes particularly appropriate at this frequency region where the contribution of the antenna elements to the radiation is significant. Nevertheless, at low frequency regions below 1GHz where the ground plane behaves as the main radiator, the required orthogonal feature is considerably difficult to achieve.

Balanced antennas appear as an alternative solutions for reducing mutual coupling [22]-[23]. They prevent the appearance of currents in the ground plane, which leads to high isolation values between antenna ports. However, the main inconvenience of these solutions is again found in frequency regions

below 1 GHz. At these frequencies, the excitation of the ground plane is strongly advisable in order to satisfy mechanical and functional specifications.

Other studies deal with the reduction of the mutual coupling and the correlation values by providing modifications in the ground plane such as adding quarter wavelength slots [24]-[25] or quarter-wavelength stubs [26]-[28]. Alternatively, several attempts address this challenge by integrating hybrid couplers [29]-[32], decoupling networks [33]-[34], or neutralization lines [35]-[37] inside the handset platform in order to enhance the correlation and isolation. The main current disadvantages of decoupling circuits mainly rely on their size, usually large for being integrated in current handset platforms, as well as in the severe losses they introduce, which considerably degrades the efficiency of the system. At the same time, neutralization lines also involve a considerable handset space as well as an extensive iterative and simulation process to find out the proper wire dimension. Finally, other attempts suggest the use of dielectric antennas due to their capabilities of near-field confinement [38]. Nevertheless, some cost, complexity and losses problems arise when regarding this kind of antenna elements.

In order to overcome space limitations, this thesis proposes a wireless handheld or portable device not requiring an antenna featured by resonant dimensions for multi-band operation. This solution is advantageous since more space is available to integrate other wireless handheld components such as batteries, displays, speakers, front-end modules and the like. Nevertheless, since the ground plane acts as the main radiator, there could appear to be a challenge in providing sufficiently uncorrelated current paths in order to preserve the benefits of the MIMO technology.

Another limitation of current wireless handheld or portable devices relates to the fact that the design and integration of an antenna element for a radiating structure in a wireless device is typically customized for each device. Different form factors or platforms, or a different distribution of the functional blocks of the device will force to redesign the antenna element and its integration inside the device almost from scratch.

For at least the above reasons, wireless device manufacturers regard the volume dedicated to the integration of the radiating structure, and in particular to the antenna element, a toll to pay in order to provide wireless capabilities to the wireless handheld or portable device.

In order to solve the aforementioned limitations, this chapter provides a new solution based on miniature ground plane boosters and their arrangement in MIMO systems inside a wireless handheld or portable device, which benefits from their reduced volume to enable a standardized solution capable of multi-band operation suitable for several wireless handheld or portable device platforms.

6.4. MIMO Systems based on Resonant Antennas

This chapter analyzes the feasibility of integrating multi-band antennas having resonant dimensions in current handset platforms in order to provide a MIMO system. In particular, widely spread “on-ground” solutions such as PIFAs are proposed as representative samples of current handset antenna technologies. On one hand, a dual-band PIFA operating in the communication standards GSM900 and

GSM1900 is proposed. On the other hand, an hexa-band PIFA capable of operating in seven communication standards (GSM850, GSM900, GSM1800, GSM1900, UMTS, LTE2100, and LTE2300) acting in cooperation with a slotted ground plane is analyzed in order to determine the effects produced by these ground plane modifications into the MIMO performance. The study is completed with an “off-ground” solution, namely a set of coupled monopoles capable of operating the communication standards GSM850, GSM900, GSM1800, GSM1900, UMTS, LTE2100, and LTE2300.

The performance of each radiating system in free-space regarding the main antenna parameters (impedance bandwidth, antenna efficiency, and radiation patterns) is presented along section 6.4.1. At the same time, section 6.4.2 gathers, in addition to the previous antenna parameters, some relevant MIMO parameters such as correlation and isolation when regarding the combination of two of these radiating systems inside the handset platform.

6.4.1 Description of the Radiating Systems

The proposed radiating systems are selected as a representative sample of current handset antenna technologies. The first proposal consists of a dual-band PIFA featuring dimensions of 40 mm x 15 mm x 6 mm and being placed over a ground plane with a size comparable to current handset platforms (100 mm x 40 mm). The ground plane is etched over an FR4 piece of 1 mm thick ($\epsilon_r=4.15$, $\tan\delta=0.013$), whereas the PIFA is stamped over a plastic carrier ($\epsilon_r=2.55$, $\tan\delta=0.013$) able of supporting the metal piece (Fig. 6.4a). The radiating system is matched at the communication standards GSM900 and GSM1900, hence providing dual-band operation (Fig. 6.4b).

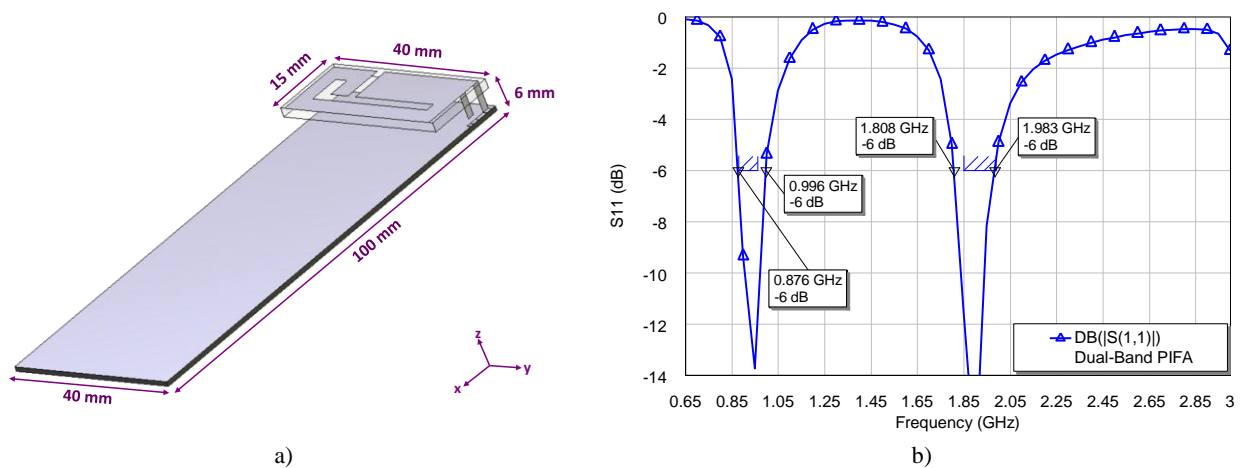


Fig. 6.4 a) Geometry of the proposed dual-band PIFA etched over a plastic carrier of 1 mm thick ($\epsilon_r=2.55$, $\tan\delta=0.013$) and being placed over a ground plane etched over an FR4 piece of 1 mm thick ($\epsilon_r=4.15$, $\tan\delta=0.013$); b) Reflection coefficient.

In the second proposal, the PIFA antenna is placed over a slotted ground plane (Fig. 6.5a) capable of enhancing its performance as for allowing hexa-band operation (Fig. 6.5b). This solution is selected for being a technology that integrates an “on-ground” solution with mechanisms capable of electrically enlarging the ground plane. A matching network is used for centering the operating bands at the frequency regions of interest (Fig. 6.5a). Finally, a set of coupled monopoles is selected to represent “off-ground” solutions featured by a very low profile, hence, capable of being integrated in ultra-slim

platforms (Fig. 6.6a). In this case, no matching network is required for providing penta-band operation when a ground plane having dimensions of 110 mm x 47 mm is regarded (Fig. 6.6b).

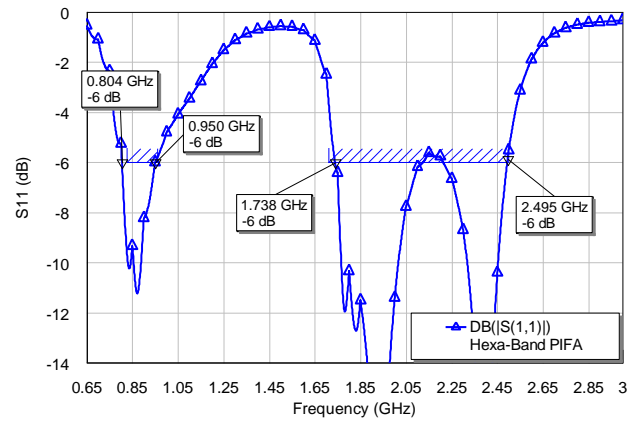
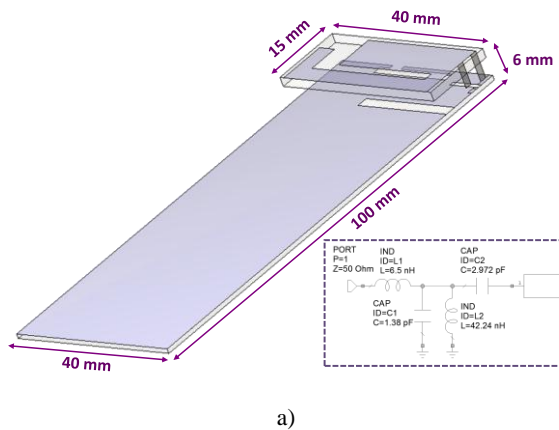


Fig. 6.5 a) Geometry of the proposed hexa-band PIFA etched over a plastic carrier of 1 mm thick ($\epsilon_r=2.55$, $\tan\delta=0.013$) and being placed over a ground plane etched over an FR4 piece of 1 mm thick ($\epsilon_r=4.15$, $\tan\delta=0.013$). In this case, a matching network is used for providing the hexa-band operation; b) Reflection coefficient. The axis coincide with those illustrated in Fig. 6.4a.

The radiation efficiency is computed for each one of the radiating systems under study (Fig. 6.7) and it remains around 80% in average for the low frequency region and around 65% in average for the high frequency region in all three cases. The average values are obtained according to the frequency region of operation of each radiating systems.

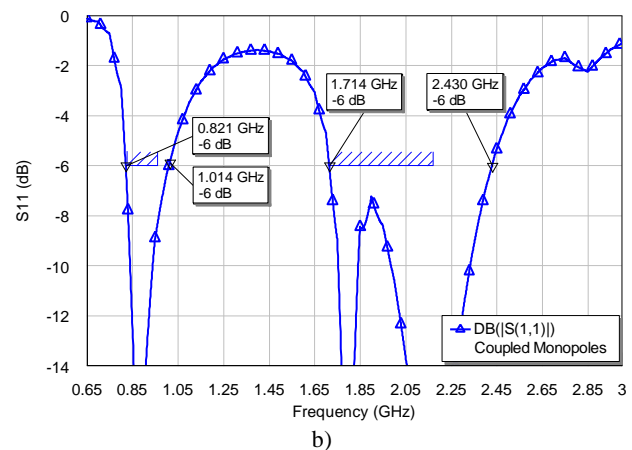
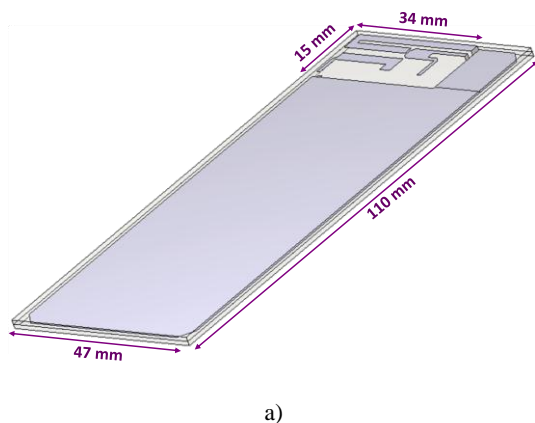


Fig. 6.6 a) Geometry of the proposed coupled monopoles etched over an FR4 piece of 1 mm thick ($\epsilon_r=4.15$, $\tan\delta=0.013$) and being placed over a ground plane also etched over an FR4 piece of 1 mm thick ($\epsilon_r=4.15$, $\tan\delta=0.013$); b) Reflection coefficient. The axis coincide with those illustrated in Fig. 6.4a.

In this sense, the dual-band PIFA, the hexa-band PIFA over a slotted ground plane, and the coupled monopoles are averaged in the frequency range of 880-960MHz, 824-960MHz, 824-960MHz, respectively, when regarding the low frequency region, and in the frequency ranges 1850-1990MHz, 1710-2400MHz, 1710-2400MHz, respectively, when the high frequency region is considered. It is important to underline that unlike radiating systems based on non-resonant elements, in this case, the radiation efficiency presents efficiency drops usually produced by a non-radiating mode of the antenna (Fig. 6.7). In contrast, when non-resonant elements are used, the radiation efficiency remains at high values for the whole frequency range, since the fundamental mode of the ground plane predominates in the radiation process.

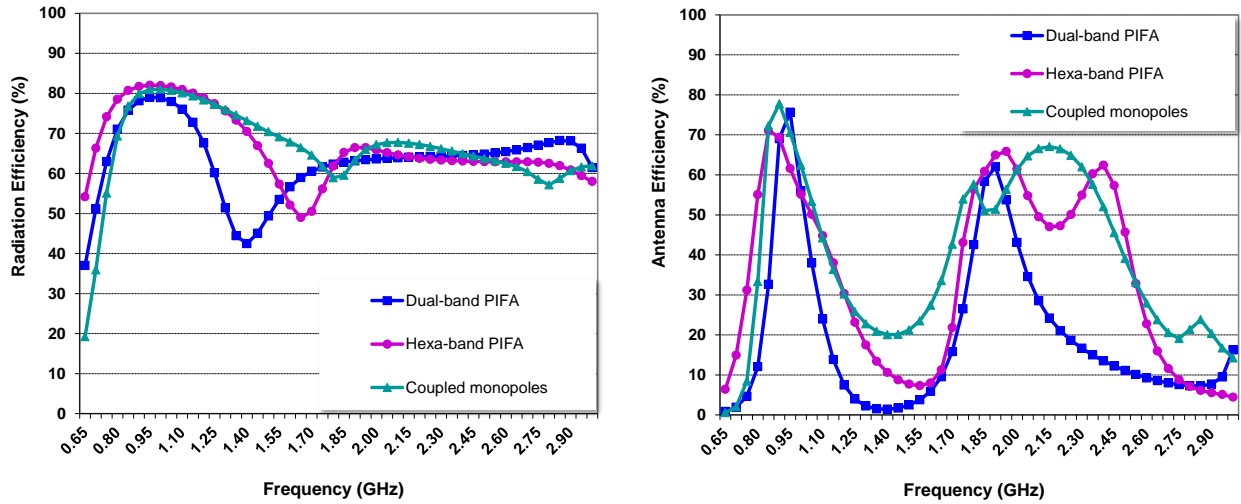


Fig. 6.7 Radiation efficiency and antenna efficiency corresponding to the proposed radiating systems.

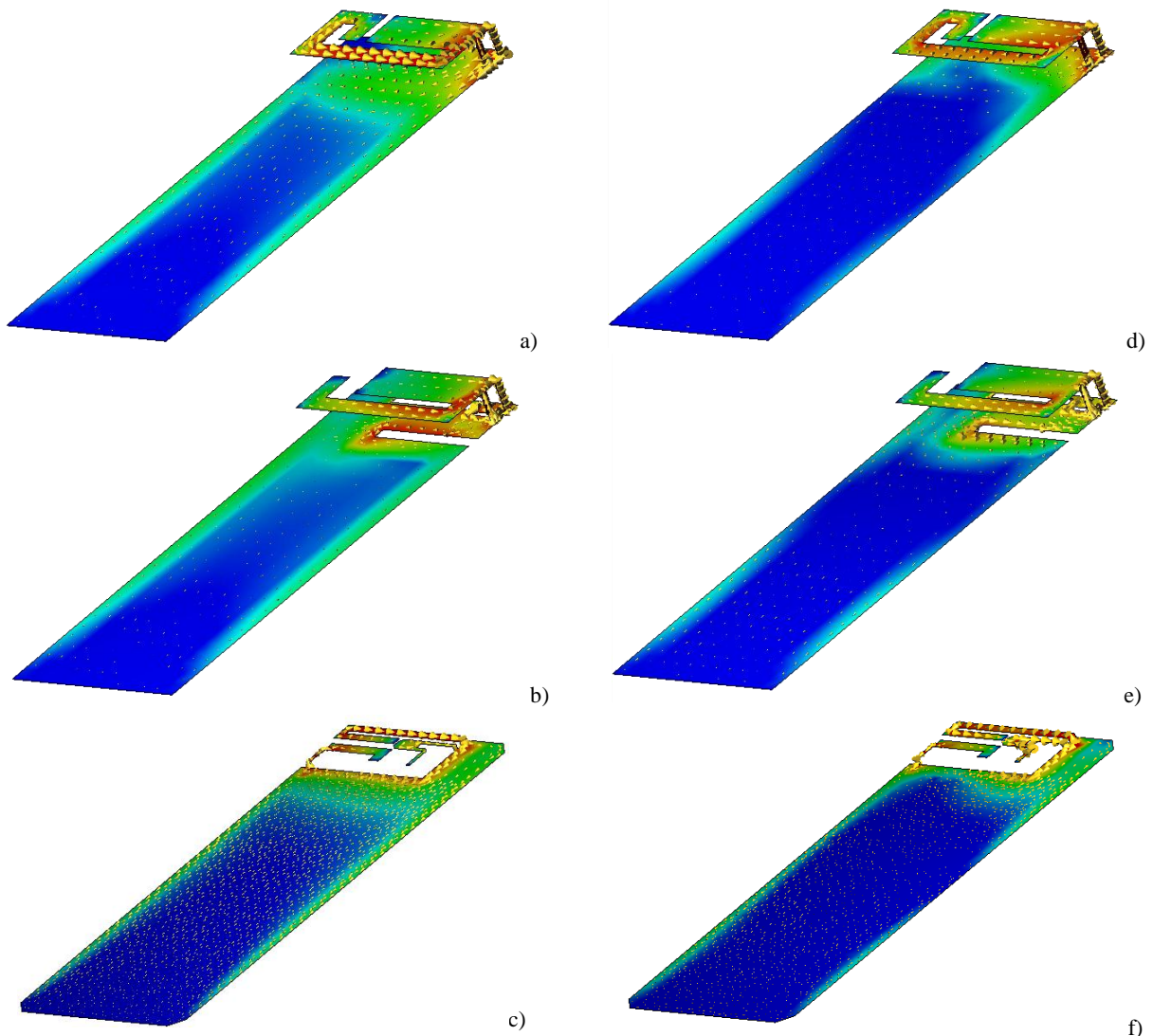


Fig. 6.8 a)-c) Current distribution at 900MHz regarding the dual-band PIFA, the hexa-band PIFA, and the coupled monopoles, respectively; d)-f) Current distribution at 1900MHz regarding the dual-band PIFA, the hexa-band PIFA, and the coupled monopoles, respectively. Max E-current is fixed to 8 A/m and the dynamic range is 30dBs. The axis coincide with those illustrated in Fig. 6.4a.

The antenna efficiency is averaged in the same manner and the results also remain comparable in the three cases. More particular in the low frequency region the efficiency values are around 72.4%,

64.3%, and 63.5% for the dual-band PIFA, the hexa-band PIFA, and the coupled monopoles, respectively, whereas in the high frequency region they remain around 54.2%, 53.4%, and 58.4%, respectively. The current distribution of the former radiating structures illustrates the contribution of the antennas to the radiation process as well as the contribution of the ground plane, which becomes more significant in the low frequency region (Fig. 6.8). These current distributions determine the radiation patterns of the structures, which mainly corresponds to that produced by a half wavelength dipole, i.e. they present an omnidirectional behavior in one plane and a null aligned with the long axis of the ground plane.

6.4.2 MIMO Analysis

This section analyzes the performance of the former proposals in a multi-band 2x2 MIMO system. Firstly, two dual-band PIFAs with the same characteristics as those described previously, are placed over a ground plane with dimensions of 100 mm x 40 mm. Each antenna is arranged close to a short side of the ground plane, being its longest dimension substantially parallel to this short side (Fig. 6.9). In this way, the distance between antenna elements is maximized as for allowing low mutual coupling and correlation values. The S-parameters analysis reveals that the antennas maintain their dual-band behavior (GSM900 and GSM1900) (Fig. 6.9). Nevertheless, a significant coupling appears at low frequencies around 900MHz that contribute to degrade their performance by lowering antenna efficiencies up to an average of 40.5% in the low frequency region (880-960MHz), which supposes losses around 2.5dBs with respect to those values obtained when just a single antenna element was considered (Fig. 6.7). The efficiency values in the high frequency region (1850-1990MHz) are not altered, since at these frequencies the transmission coefficient is neglectable as being below -18dBs, thus maintaining the antenna efficiency average value around 56.9% (Fig. 6.10). When a single input/output port is considered, just the reflection coefficient affects the antenna efficiency according to (6.12). Nevertheless, mutual coupling must be carefully considered when regarding a multi-port antenna system such as those required in a MIMO system (6.13).

$$\eta_a = \eta_{rad} \cdot (1 - |S_{11}|^2) \quad (6.12)$$

$$\eta_a = \eta_{rad} \cdot (1 - |S_{11}|^2 - |S_{21}|^2) \quad (6.13)$$

Further to the mutual coupling effects, correlation coefficient should be computed in order to properly characterize the performance of a MIMO system. The correlation values presented along this chapter when referred to simulated results have been computed using the software IE3D based on MoM through radiation patterns (6.9) and in all cases an isotropic propagation model has been considered, i.e. $XPR=1$ and, P_θ and P_ϕ uniform. As previously introduced, envelope correlation could be easily computed through S-parameters (6.10). A comparison is established between both expressions in order to assess the reliability of the latest (Fig. 6.10). As indicated in [6], the higher the radiation efficiency, the better the correlation through S-parameters (6.10) approximates the exact values computed through

radiation patterns (6.9). In those cases where radiation efficiency is not high enough, the S-parameters computation provides an useful qualitative approach, since the curve trend is equivalent to that experimented by the exact expression (Fig. 6.10).

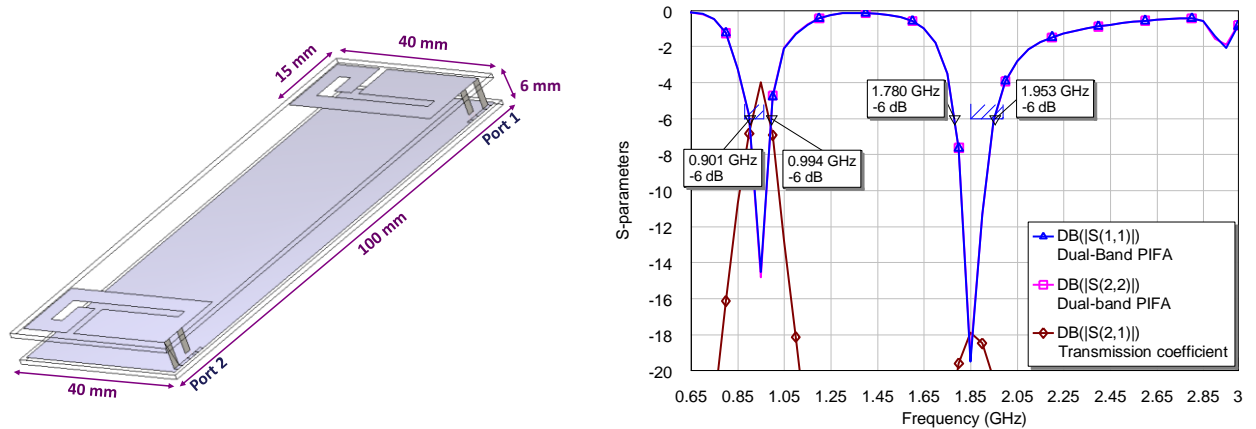


Fig. 6.9 Left) Geometry of the proposed multi-band MIMO system comprising two dual-band PIFA antennas. In this case, the antennas are placed over a 1 mm thick FR4 piece ($\epsilon_r=4.15$, $\tan\delta=0.013$) and the ground plane is also etched over a 1 mm thick FR4 piece ($\epsilon_r=4.15$, $\tan\delta=0.013$); Right) S-parameters. The axis coincide with those illustrated in Fig. 6.4a.

The results reveal that correlation reduces as long as frequency increases. The larger the frequency, the larger the electrical distance between the dual-band PIFAs. This fact contributes to significantly reduce correlation coefficients below 0.10 for frequencies above 1.5GHz. The critical results are found at frequencies below 1GHz where the correlation reaches unacceptable values around 0.90. More particular at a frequency close to 0.9 GHz the radiation patterns are very similar (Fig. 6.11), which leads to a correlation value around 0.79 (Fig. 6.10). Consequently, the challenge that antenna engineers have to face to provide MIMO performance is mainly found at this frequency region where the size of the handset platform is not large enough as to provide the sufficient distance as for ensuring low correlation. Some correlation fadings are appreciated at these low frequencies, appearing the first one close to the theoretical value of 0.5λ [19]-[20]. At the high frequency region, the correlation values remain below 0.10. For this reason the following analysis will be mainly focused on the low frequency region.

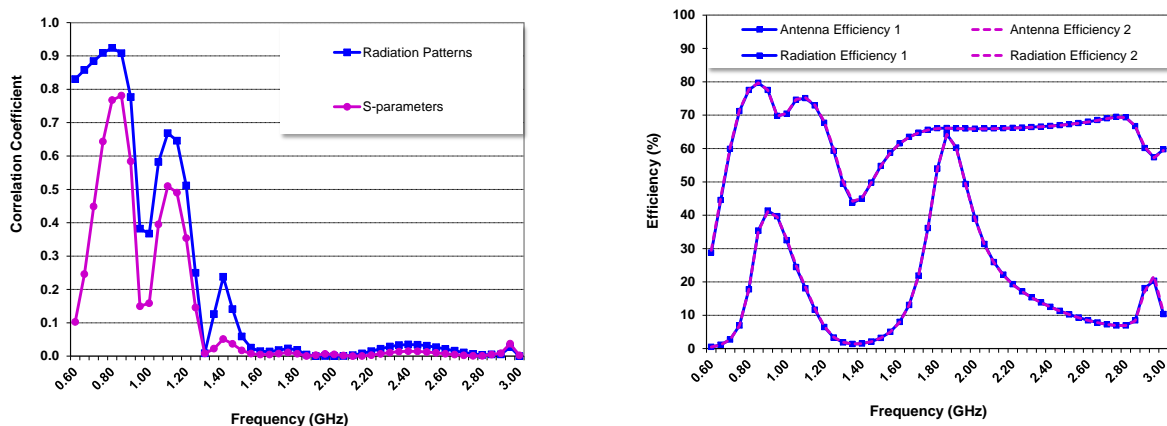


Fig. 6.10 Left) Correlation coefficient computed regarding radiation patterns (6.9) and S-parameters (6.10); Right) Radiation and antenna efficiency for each one of the dual-band PIFAs.

The previous results suggest that a ground plane enlargement could be useful to increase the distance between radiating systems, thus helping to minimize correlation by forcing the first dip

appearance at the center frequency of the low frequency region (824-960MHz). In order to produce this effect without altering the size of the handset platform, the previous dual-band PIFAs are substituted by two hexa-band PIFAs placed over a slotted ground plane capable of increasing the electrical length of the ground plane. In this case a matching network is needed at each antenna port for providing the desired impedance bandwidth (Fig. 6.12).

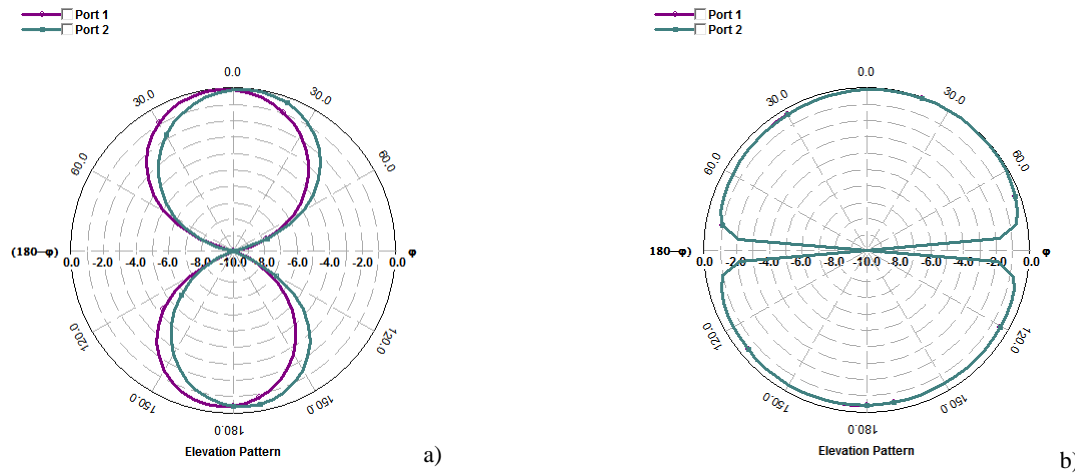


Fig. 6.11 E-total regarding the main cuts of the radiation patterns associated to the radiating systems of Fig. 6.9 at the frequency of 0.9GHz. a) $\phi=0^\circ$; b) $\phi=90^\circ$. Note that the null appearing at $\phi=90^\circ$, $\theta=90^\circ$ is due to infinite FR4 piece considered in the simulation. In practice, when finite dielectrics are regarded, the $\phi=90^\circ$ cut is omnidirectional.

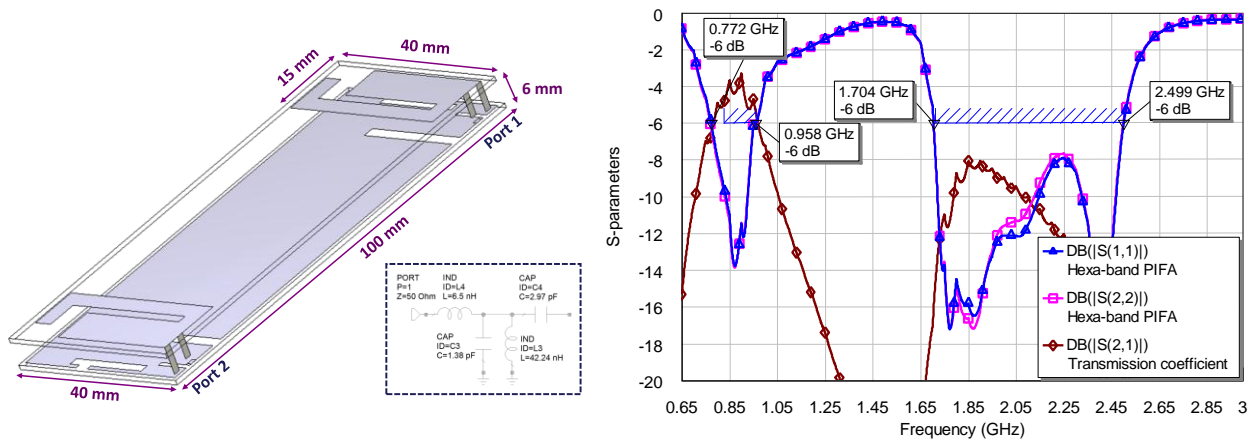


Fig. 6.12 Left) Geometry of the proposed multi-band MIMO system comprising two hexa-band PIFA antennas. In this case, the antennas are placed over a 1 mm thick FR4 piece ($\epsilon_r=4.15$, $\tan\delta=0.013$) and the ground plane is also etched over a 1 mm thick FR4 piece ($\epsilon_r=4.15$, $\tan\delta=0.013$); Right) S-parameters. The axis coincide with those illustrated in Fig. 6.4a.

The impedance bandwidth is maintained with respect to the case where just a single hexa-band antenna was considered (Fig. 6.12). However and owing to the coupling between antenna elements, low isolation appears at both frequency regions (Fig. 6.12), but more significantly at frequencies around 900MHz, fact that contribute to degrade antenna efficiencies (in average 36.3% for the low frequency region (824-960MHz) and 52.3% for the high frequency region (1710-2400MHz) (Fig. 6.13) with respect to the case where just a single antenna element was considered (Fig. 6.7). The correlation coefficient is again computed through radiation patterns (6.9) as well as through S-parameters (6.10) and the matching network effects are taken into account in both cases (Fig. 6.13). In this case, a Matlab code has been developed to compute correlation between radiating systems integrating a matching network. The IE3D computation used in the previous dual-band PIFA analysis only applies in those situations where no

matching network is included, i.e. in those situations where the antenna performance is merely adjusted through its geometry. In other situations, the Matlab code developed in the context of this thesis and based on equation (6.9) is used.

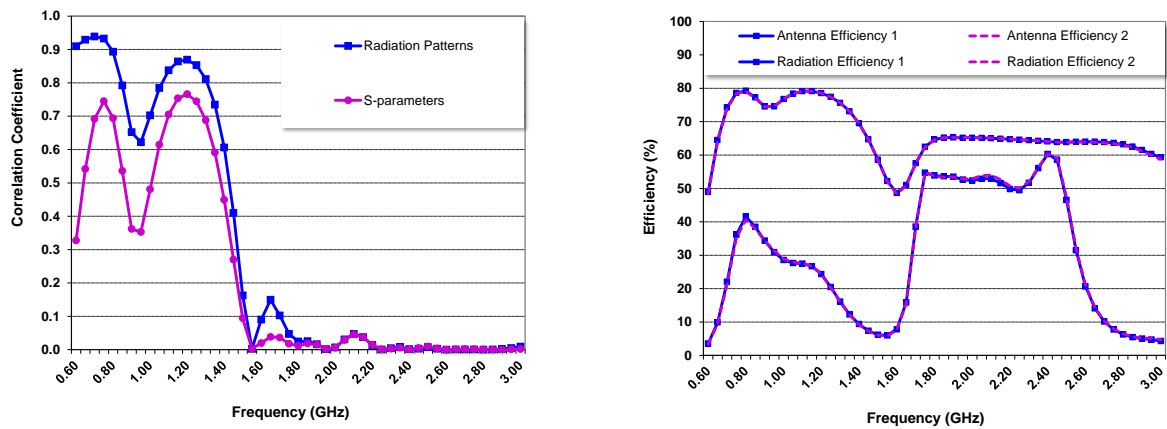


Fig. 6.13 Left) Correlation coefficient computed regarding radiation patterns (6.9) and S-parameters (6.10). The S-parameters computation considers the matching network scheme illustrated in Fig. 6.12 for both ports; Right) Radiation and antenna efficiency for each one of the hexa-band PIFAs. In this case, the matching network is properly considered at each antenna port.

The electrical enlargement of the slotted ground plane slightly shifts the first correlation dip to lower frequencies (in the dual-band PIFA the dip appeared close to 1GHz, whereas in this case it appears close to 0.95GHz). This shifting contributes to reduce the correlation values close to the operating frequencies. In this way, at 900MHz the radiation patterns slightly differ between them (Fig. 6.14) leading to a correlation of 0.65 compared to 0.79 for the dual-band PIFA having more similar radiation patterns (Fig. 6.11). Although this ground plane enlargement advantageously contributes to reduce the correlation values close to the operating frequencies, the values at the first correlation dip (0.40 at 1GHz for the dual-band PIFA and 0.62 at 0.95GHz for the hexa-band PIFA) are larger for the hexa-band PIFA than for the dual-band PIFA. The reason relies on the fact that in this case the ground plane is more excited, thus contributing more significantly to the radiation process. This ground plane excitation increases the similarity between the radiation patterns produced by both radiating systems.

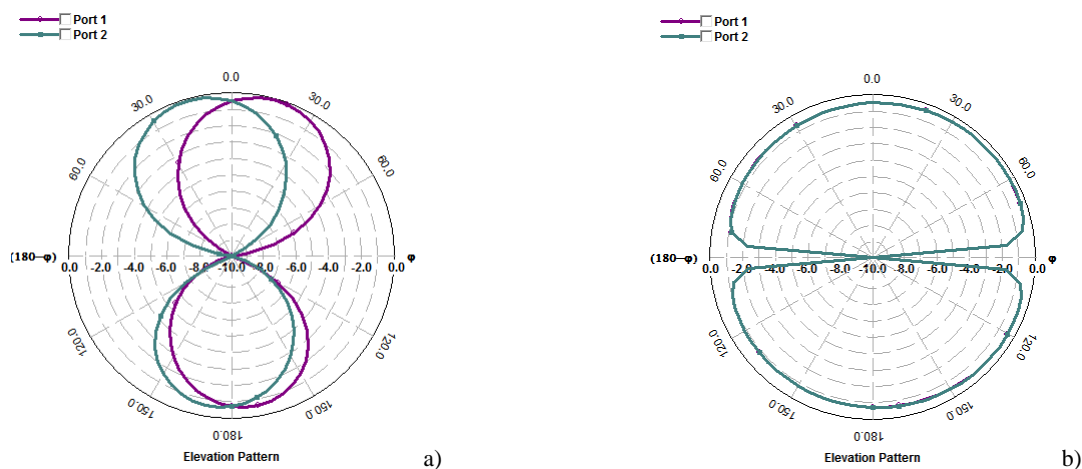


Fig. 6.14 E-total regarding the main cuts of the radiation patterns associated to the radiating systems of Fig. 6.12 at the frequency of 0.9GHz. a) $\phi=0^\circ$; b) $\phi=90^\circ$. Note that the null appearing at $\phi=90^\circ$, $\theta=90^\circ$ is due to infinite FR4 piece considered in the simulation. In practice, when finite dielectrics are regarded, the $\phi=90^\circ$ cut is omnidirectional.

A MIMO system formed by two sets of penta-band coupled monopoles is also considered in the present analysis (Fig. 6.15). This architecture is selected for being a representative sample of low profile elements suitable for being integrated in ultra-slim platforms. In this case, the penta-band behavior is maintained with respect to the case where just a single set of coupled monopoles was considered, but in a similar way as happened with the hexa-band PIFA, low isolation values are attained at both frequency regions (Fig. 6.15), which leads to antenna efficiencies close to 38.6% (in average) in the low frequency region (824-960MHz) and 49.1% (in average) in the high frequency region (1710-2400MHz) (Fig. 6.16).

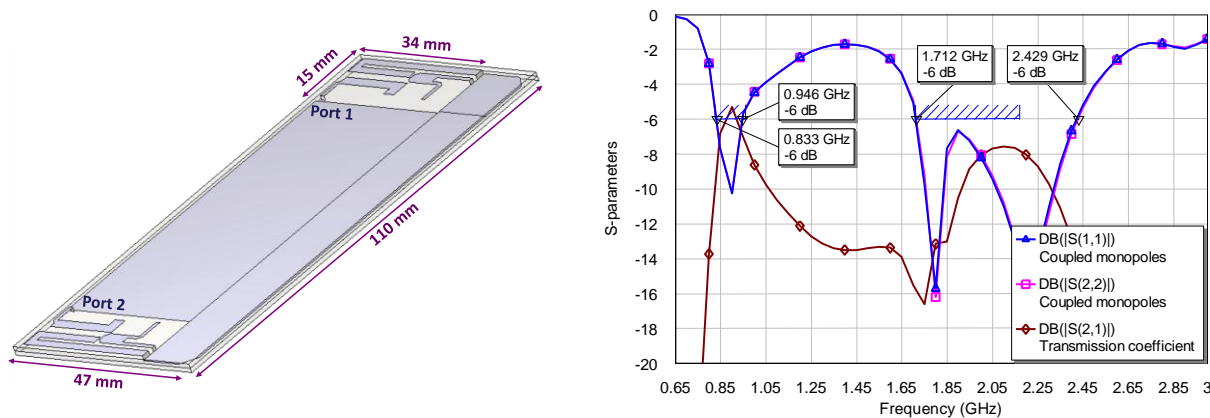


Fig. 6.15 Left) Geometry of the proposed multi-band MIMO system comprising two set of coupled monopoles. The coupled monopoles are etched over a 1 mm thick FR4 piece ($\epsilon_r=4.15$, $\tan\delta=0.013$) and the ground plane is also etched over a 1 mm thick FR4 piece ($\epsilon_r=4.15$, $\tan\delta=0.013$); Right) S-parameters. The axis coincide with those illustrated in Fig. 6.4a.

If a comparison is established between the proposed radiating systems, the MIMO system composed by the two set of coupled monopoles (Fig. 6.15) stands out over those comprising the PIFA antennas, since it attains lower correlation values at the most critical frequencies, i.e. at frequencies below 1GHz (Fig. 6.16). More particular at the center frequency of the low frequency region (0.9GHz) the differences appearing between the radiation patterns of both radiating systems (Fig. 6.17a-b) lead to a correlation value of 0.53, which becomes lower than that offered by the PIFA antennas (Fig. 6.18a). In this case, the ground plane length (110 mm) is larger than in the previous examples (100 mm), thus explaining the improvements in isolation (from approximately 4dBs in the PIFA cases to 6dBs in the coupled monopole case) as well as in correlation.

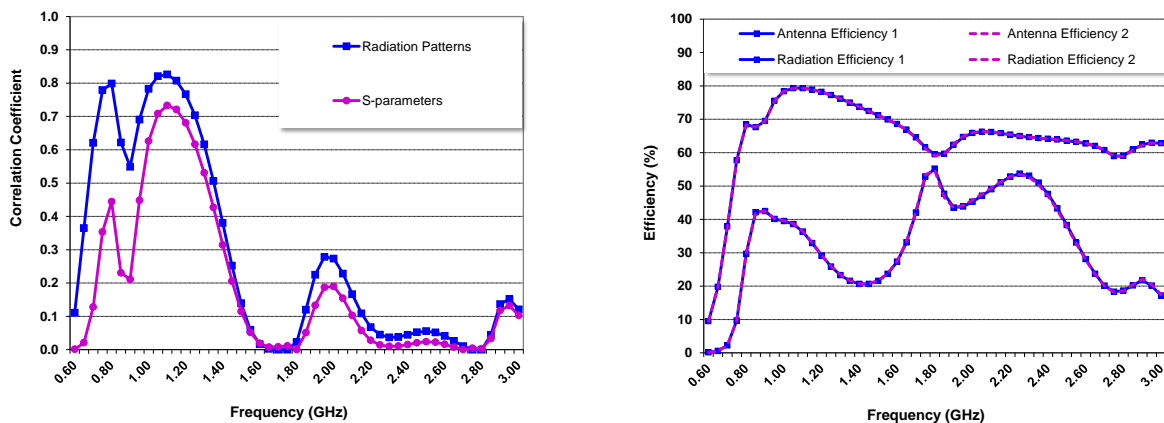


Fig. 6.16 Left) Correlation coefficient computed regarding radiation patterns (6.9) and S-parameters (6.10); Right) Radiation and antenna efficiency for each set of coupled monopoles.

The values for the low frequency region further enhances if the coupled monopoles are fed at opposite edges of the ground plane. In this case, they are close to the acceptable correlation value of 0.5 for the majority of frequencies of the low frequency region (Fig. 6.18b). In particular for the center frequency of 0.9GHz, the correlation values are reduced, from the previous 0.53 value up to 0.34. This effect is clearly appreciated in the main cuts of the radiation patterns, which present larger dissimilarities (Fig. 6.17c-d) with respect to the previous case where the monopoles were fed at the same edge of the ground plane (Fig. 6.17a-b). These differences are even more evident in the radiation pattern cut of $\phi=90^\circ$.

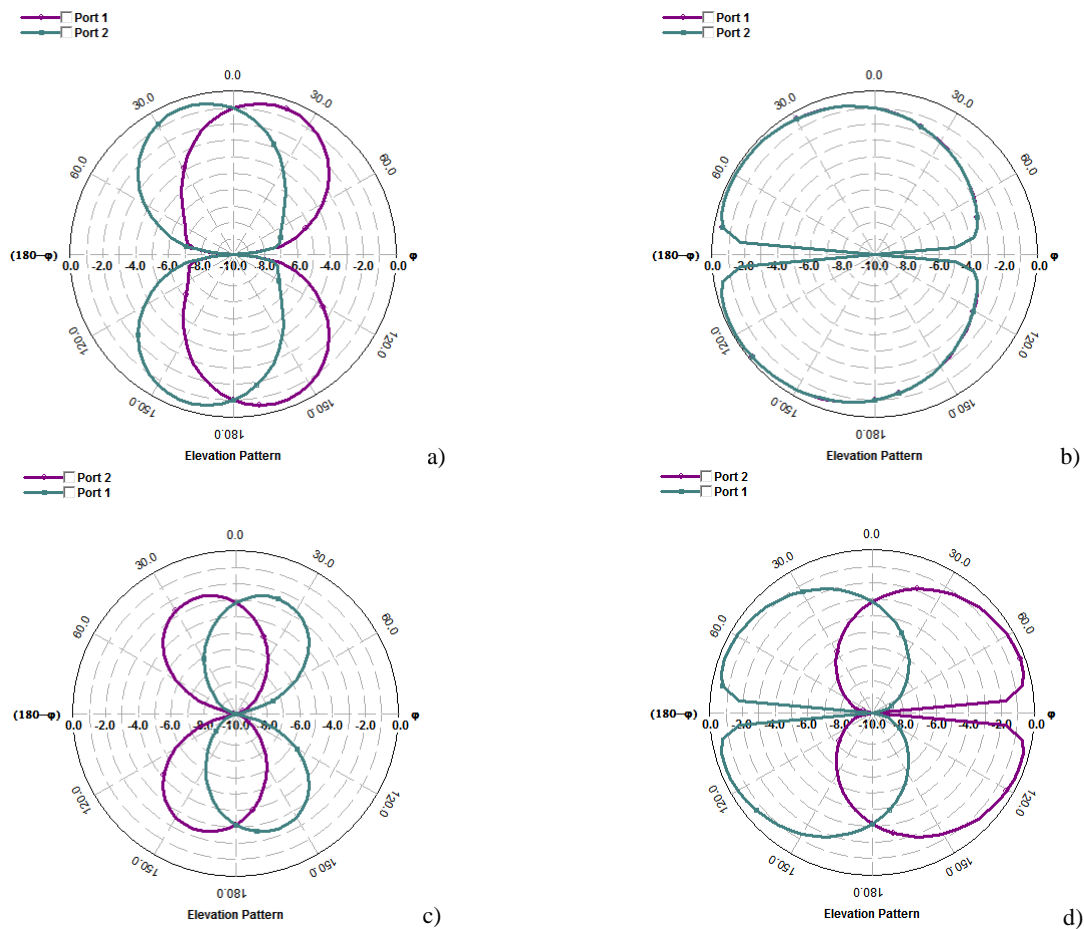


Fig. 6.17 a)-b) E-total regarding the $\phi=0^\circ$ and $\phi=90^\circ$ cuts associated to the radiating systems of Fig. 6.15 at the frequency of 0.9GHz; c)-d) E-total regarding the $\phi=0^\circ$ and $\phi=90^\circ$ cuts associated to the radiating systems of Fig. 6.18e at the frequency of 0.9GHz. Note that the null appearing at $\phi=90^\circ$, $\theta=90^\circ$ is due to the infinite FR4 piece considered in the simulation. In practice, when finite dielectrics are regarded, the $\phi=90^\circ$ cut is omnidirectional.

The previous experiments demonstrate that slotted ground planes are useful to reduce the frequency where the first minimum of correlation appears. In addition, the solution based on coupled monopoles fed at opposite edges of the ground plane stands out as the one that attains the lowest correlation values in the low frequency region. In order to combine the benefits of both proposals, a multi-band MIMO system integrating an hexa-band PIFA and a set of coupled monopoles is proposed (Fig. 6.19). In this case, a matching network is used not only for the hexa-band PIFA but also for the coupled monopoles due to the mutual coupling appearing between both antenna elements, which at the low frequency region remain close to -6dBs.

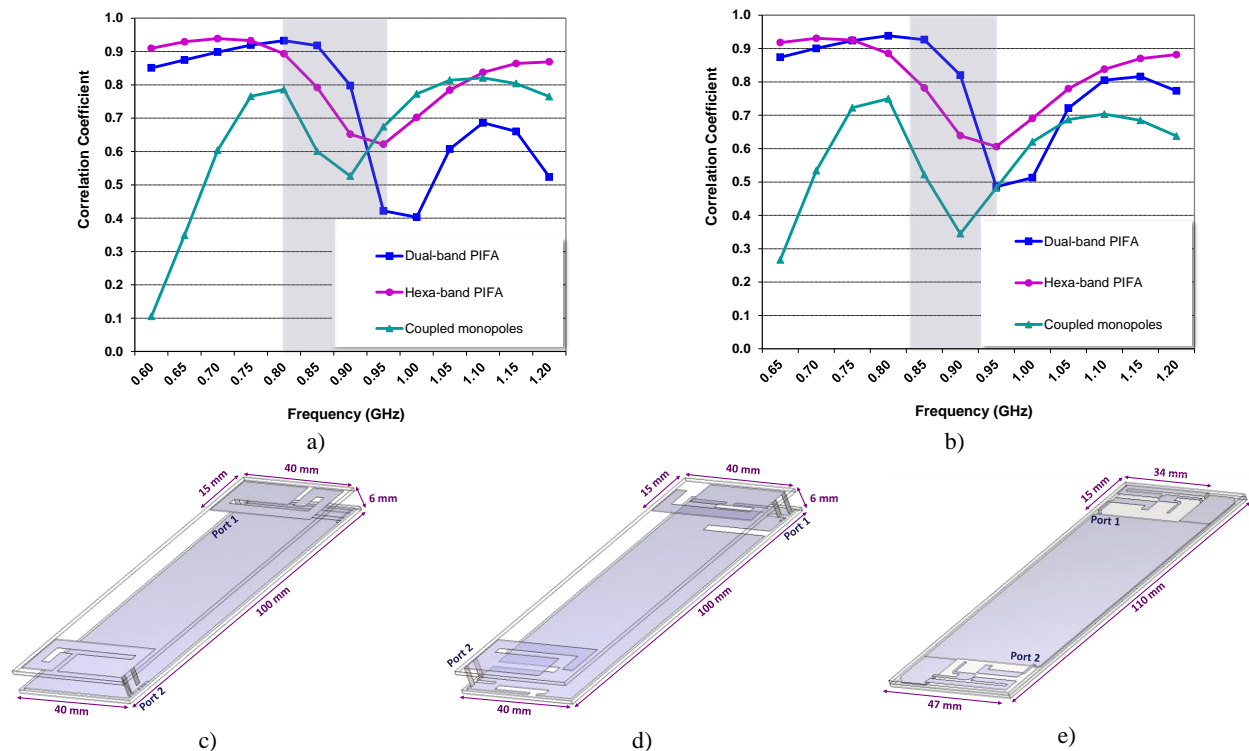


Fig. 6.18 a) Correlation coefficient computed regarding radiation patterns (6.9) when the antenna elements are fed at the same edge of the ground plane; b) Correlation coefficient computed regarding radiation patterns when the antenna elements are fed at opposite edges of the ground plane; Proposed feeding arrangement at opposite edges of the ground plane for c) dual-band PIFA, d) hexa-band PIFA, and e) coupled monopoles. The axis coincide with those illustrated in Fig. 6.4a.

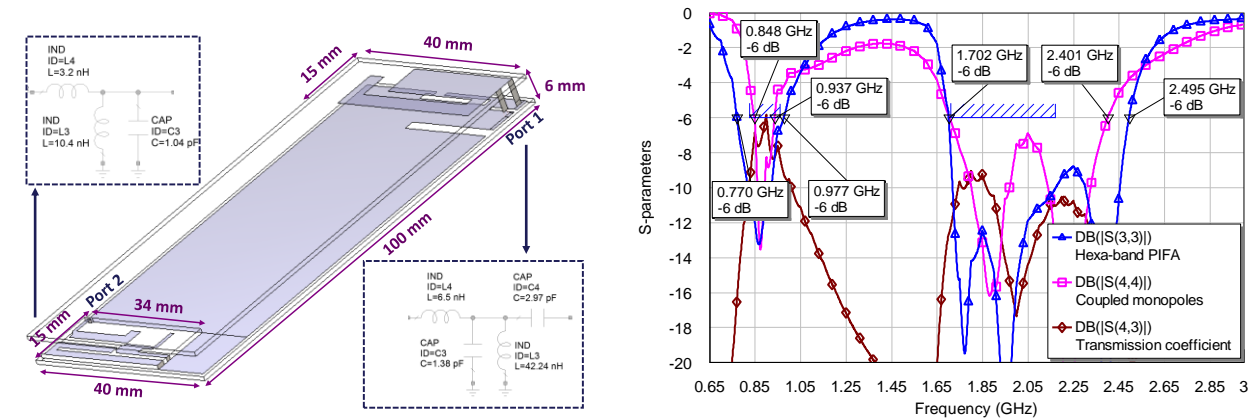


Fig. 6.19 Left) Geometry of the proposed multi-band MIMO system comprising a set of coupled monopoles and an hexa-band PIFA; Right) S-parameters. In this case a matching network is required for the coupled monopoles not only due to the mutual coupling appearing between both structures but also due to the fact that in this case coupled monopoles are etched over a finite piece of FR4 ($\epsilon_r=4.15$, $\tan\delta=0.013$). The axis coincide with those illustrated in Fig. 6.4a.

In a similar manner as happened with the previous proposal, in this case, the correlation also remains at acceptable values close to 0.5 for the majority of frequencies of the low frequency region. This fact is further appreciated in the main cuts of the radiation patterns, computed at the central frequency of the low frequency region (0.9GHz), which clearly present dissimilarities that produce a correlation value of 0.43 (Fig. 6.20 and Fig. 6.21). The current distribution at the center frequency of the low frequency region illustrates that a longitudinal radiation mode is excited in the ground plane, which acts in combination with the radiation modes excited in the antennas (Fig. 6.22a-c). The latest are the responsible of the radiation pattern differences in the low frequency region. In the high frequency region the excited ground plane mode also includes additional transversal components (Fig. 6.22b-d), less significant when

exciting the hexa-band PIFA (Fig. 6.22d). This fact together with the electrical distance experimented at high frequencies make possible to have correlation values below 0.10 along a large frequency range from 1.5GHz up to 3GHz.

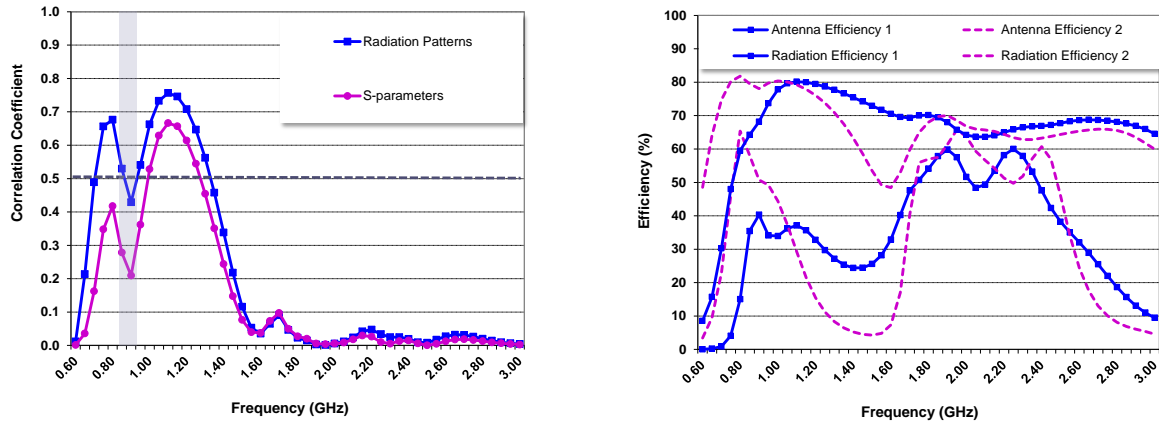


Fig. 6.20 Left) Correlation coefficient computed regarding radiation patterns (6.9) and S-parameters (6.10). In this case the S-parameters computation considers the matching networks illustrated in Fig. 6.19; Right) Radiation and antenna efficiency for each radiating system. Number 1 refers to the coupled monopoles whereas number 2 refers to the hexa-band PIFA.

Accordingly, from the correlation perspective, the current proposal (Fig. 6.19) as well as the previous solution based on two set of coupled monopoles fed at opposite edges of the ground plane (Fig. 6.18e) become the best candidates.

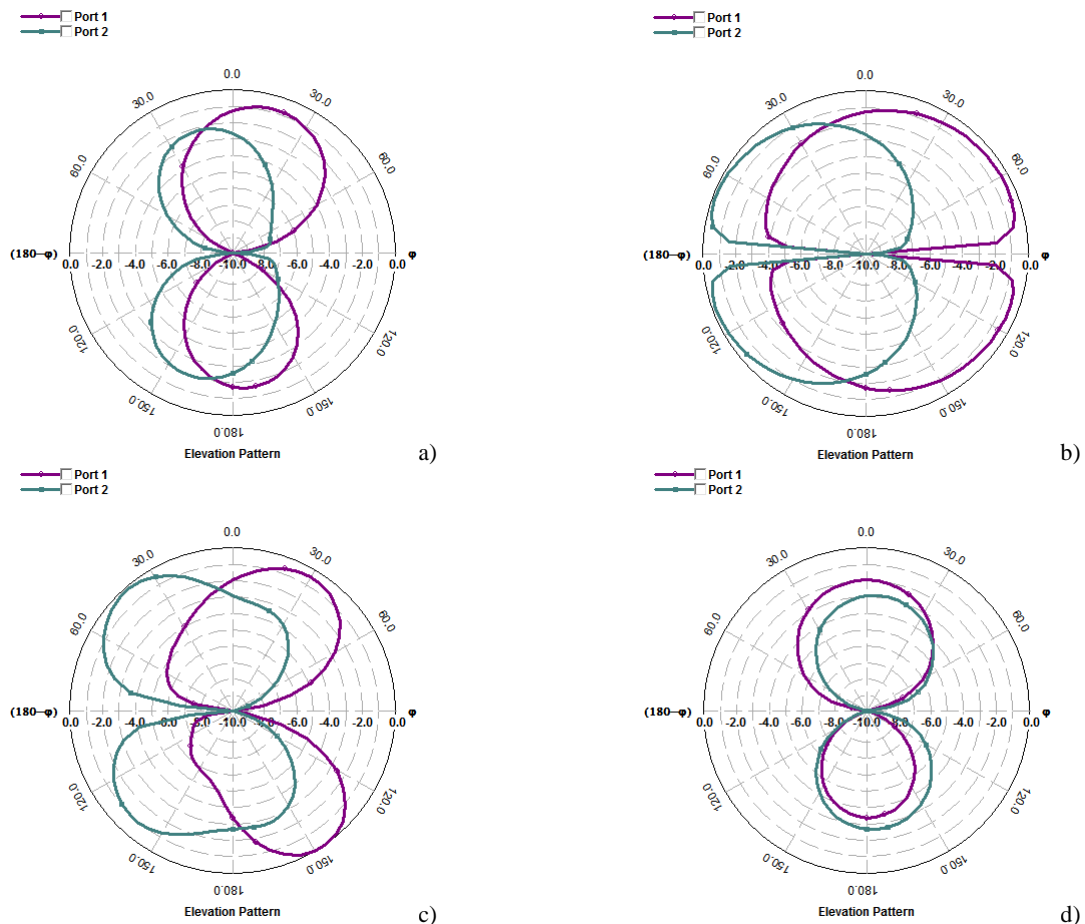


Fig. 6.21 E-total regarding the main cuts of the radiation patterns associated to the radiating systems of Fig. 6.20. a) $\phi=0^\circ$ ($f=900\text{MHz}$); b) $\phi=90^\circ$ ($f=900\text{MHz}$); c) $\phi=0^\circ$ ($f=1900\text{MHz}$); d) $\phi=90^\circ$ ($f=1900\text{MHz}$). Note that the null appearing at $\phi=90^\circ$, $\theta=90^\circ$ is due to the infinite FR4 piece considered in the simulation. In practice, when finite dielectrics are regarded, the $\phi=90^\circ$ cut is omnidirectional.

The current proposal offers higher antenna efficiency values than that attained in the previous experiments. In fact, in this case, the hexa-band PIFA reaches antenna efficiency values close to 55.9% in average for the low frequency region (Fig. 6.20), with respect to the 36.3% offered in the previous proposals (Fig. 6.13). This effect is appreciated in the representation of the current distribution, which shows a higher excitation of the ground plane radiation mode at these frequencies (Fig. 6.22c). The counterpart is the power unbalance produced by the antenna efficiency impairment experimented between both radiating systems.

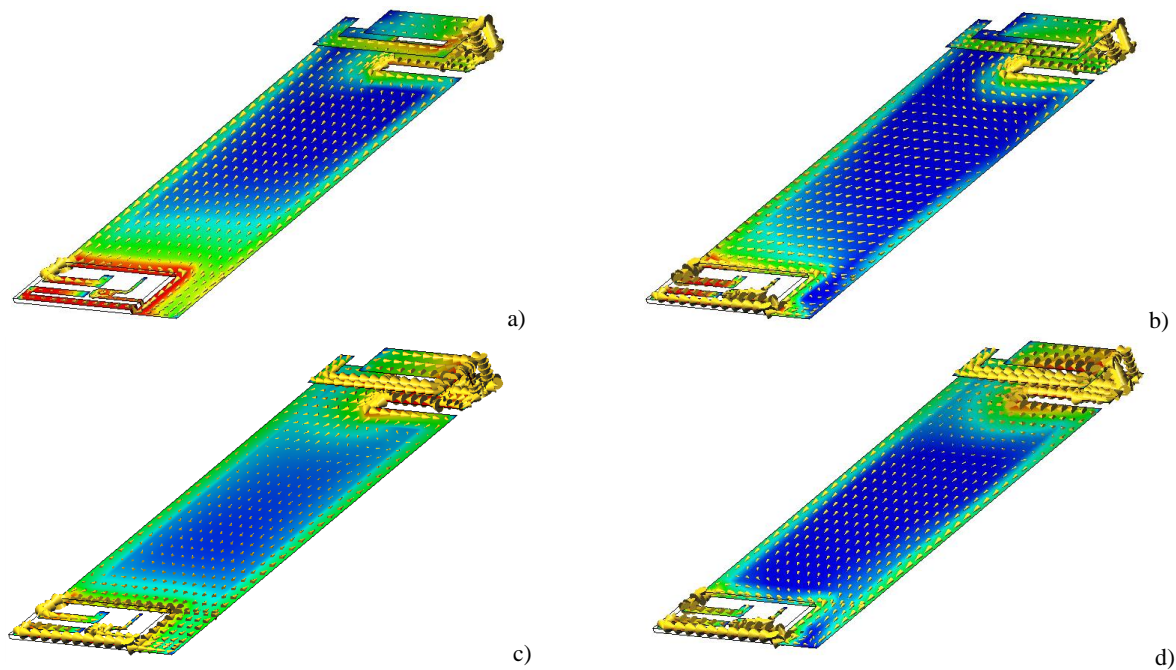


Fig. 6.22 a)-b) Current distribution when the coupled monopoles are excited and the hexa-band PIFA is connected to a 50Ω load for the center frequency of the low (900MHz) and high frequency region (1900MHz), respectively; c)-d) Current distribution when the hexa-band PIFA is excited and the coupled monopoles are connected to a 50Ω load for the center frequency of the low (900MHz) and high frequency region (1900MHz), respectively. Max-E current is 5A/m and the dynamic range is 30dB's. The axis coincide with those illustrated in Fig. 6.4a.

6.5. MIMO Systems combining Resonant Antennas with Boosters

The former section demonstrates that correlation values can be slightly reduced if the distance between the feeding arrangements of the antenna topologies under consideration is maximized. In this sense, some configurations fed at opposite corners of the ground plane are preferred over those fed close to those corners sharing the same edge of the ground plane. In addition, the consideration of different antenna topologies further reduces correlation values due to the asymmetries they produce in the current distribution of the radiating structure, and consequently in the radiation patterns.

Following this spirit, this section combines an antenna system having resonant dimensions, as those illustrated previously, with a radiating system based on ground plane boosters [39].

The section deeply analyzes the effect of the feeding distance over the system performance and proposes isolation techniques capable of enhancing correlation and antenna efficiency, as the most relevant MIMO parameters.

6.5.1 Distance Effect

Firstly the dual-band PIFA is selected for carrying out the study as being a representative sample of widely spread handset antenna technologies. The study will be performed at the low frequency region (frequencies below 1GHz) as being the most critical situation. The ground plane booster operates at GSM850 and GSM900 thanks to the use of a matching network comprising a series inductor, a shunt capacitor and a shunt inductor, whereas the dual band PIFA is tuned to operate at GSM900 and GSM1900 without the need of a matching network. The topology of the matching network remains equal in the three cases under study, whereas its values have been properly adapted according to the ground plane booster arrangement (Fig. 6.23).

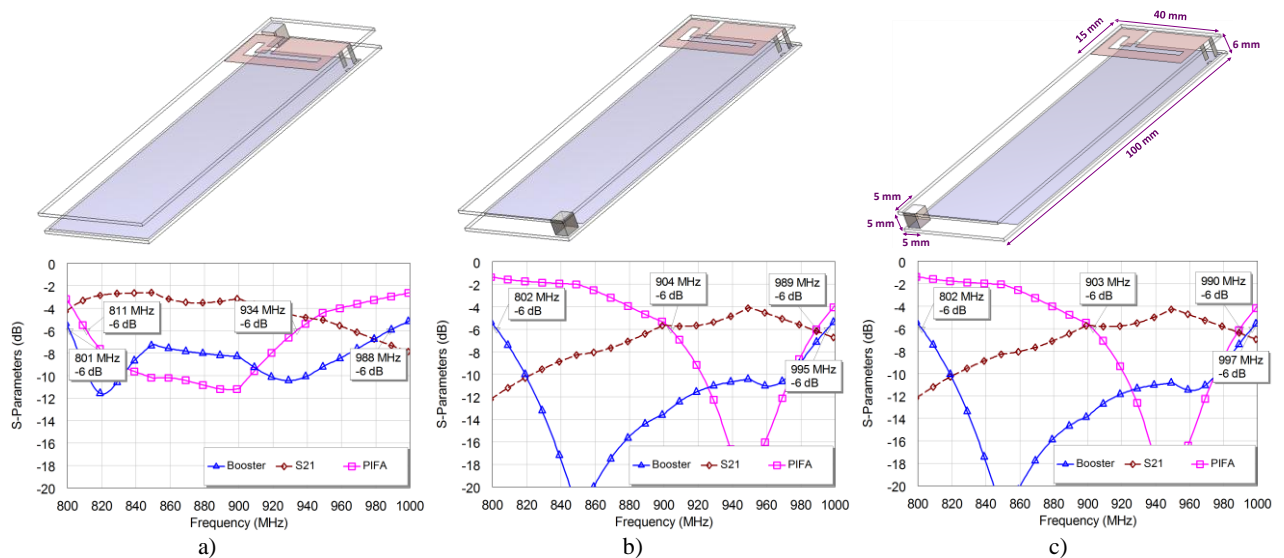


Fig. 6.23 Geometry and S-parameters associated to a multi-band MIMO system comprising a ground plane booster (5 mm x 5 mm x 5 mm) and a dual-band PIFA antenna according to the arrangement of the ground plane booster with respect to the antenna. The ground plane and the PIFA are etched over a 1 mm thick FR4 piece ($\epsilon_r=4.15$, $\tan\delta=0.013$), respectively. The axis coincide with those illustrated in Fig. 6.4a.

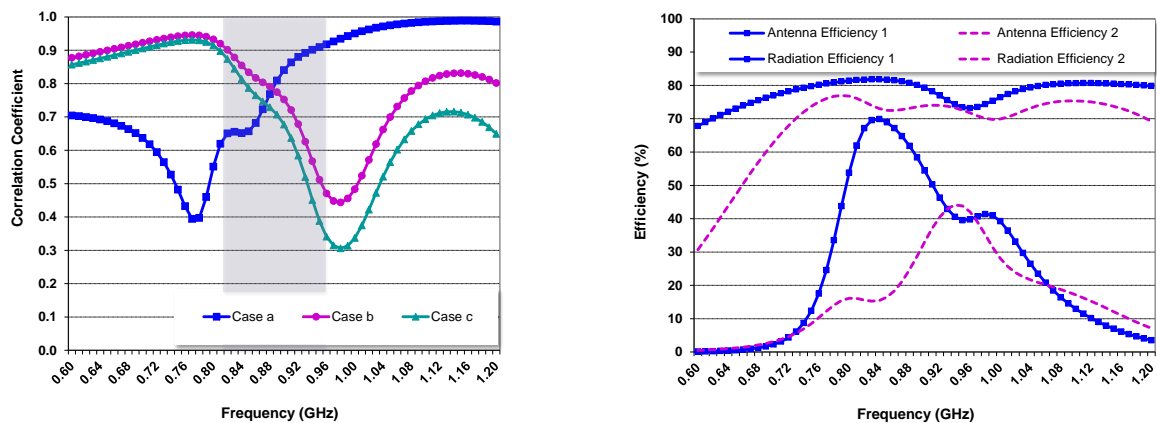


Fig. 6.24 Left) Correlation values computed through radiation patterns (6.9) for each one of the cases illustrated in Fig. 6.23; Right) Antenna and radiation efficiency values regarding case Fig. 6.23c. Number 1 refers to the ground plane booster whereas number 2 refers to the dual-band PIFA.

On one hand, the three cases offer low isolation values in the low frequency region, being worst the one that considers the ground plane booster placed underneath the dual-band PIFA (Fig. 6.23a). In addition, this configuration contributes to undesirably detune the dual-band PIFA to lower frequencies. On the other hand, the configurations that arrange the ground plane booster at the opposite short edge,

offer similar behavior from the S-parameters perspective (Fig. 6.23b-c). Nevertheless, the one that considers a ground plane booster placed at an opposite corner with respect to the feed point of the dual-band PIFA (Fig. 6.23c) becomes preferred when regarding the correlation values (Fig. 6.24). For this reason, this configuration is selected for applying the isolation techniques proposed in the following section and intended for improving not only correlation but also isolation and antenna efficiency with respect to the results attained by this configuration (Fig. 6.24).

6.5.2 Slot in the Ground Plane as Isolation Technique

In order to increase isolation between the radiating systems under study, a slot having a resonant length close to a quarter of a wavelength at the center frequency of the low frequency region (824-960MHz) is proposed. The solution considerably reduces isolation with respect to the case where the slot was not considered (Fig. 6.23c). The worst isolation value is around 9dBs at 880MHz (Fig. 6.25), whereas for the previous case it was located around 4dBs at 950MHz (Fig. 6.23c). In this example, the slot is placed at the middle of a short edge of the ground plane and extends in a direction parallel to the longitudinal edges.

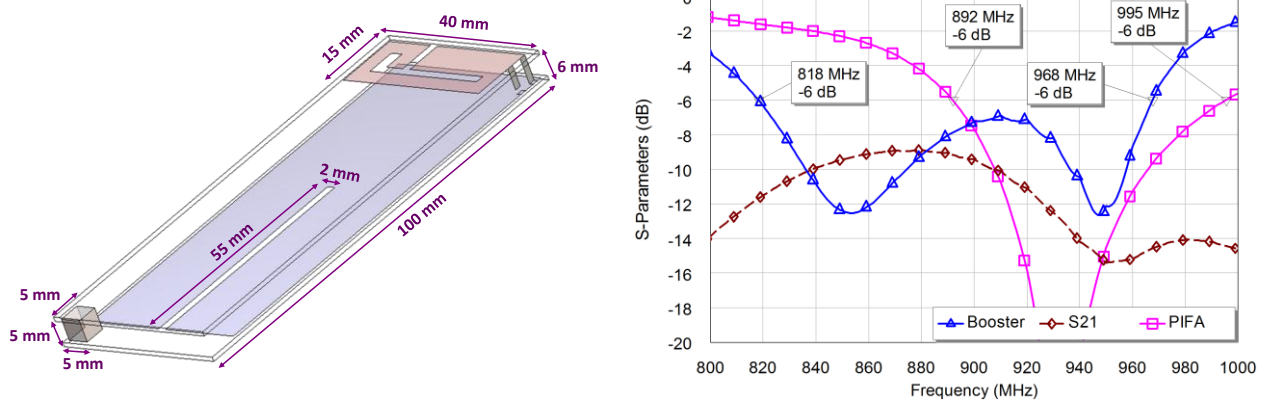


Fig. 6.25 Left) Geometry of the proposed multi-band MIMO system comprising a dual-band PIFA and a booster for the low frequency region. The ground plane and the PIFA are etched over a 1 mm thick FR4 piece ($\epsilon_r=4.15$, $\tan\delta=0.013$); Right) S-parameters. The axis coincide with those illustrated in Fig. 6.4a.

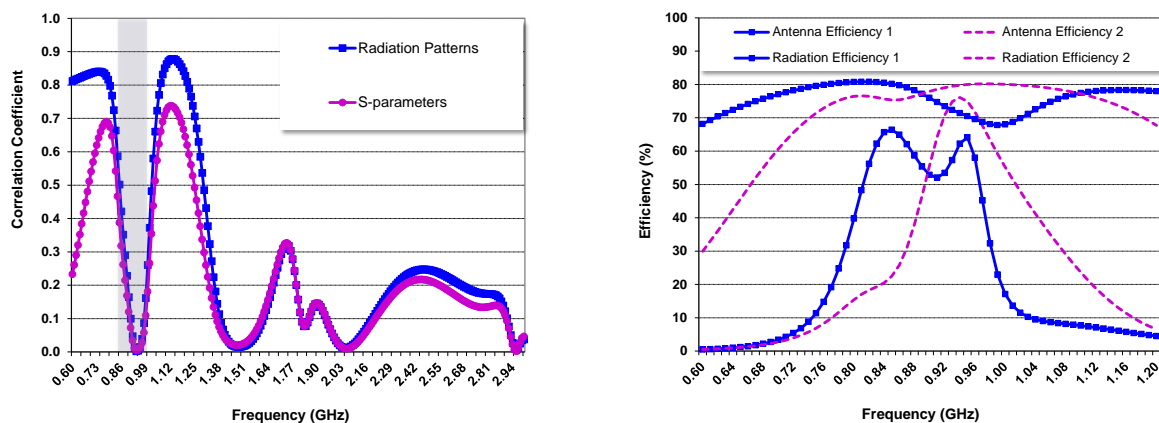


Fig. 6.26 Left) Correlation coefficient computed regarding radiation patterns (6.9) and S-parameters (6.10); Right) Antenna and radiation efficiency values corresponding to the MIMO system illustrated in Fig. 6.25. Number 1 refers to the ground plane booster, whereas number 2 refers to the dual-band PIFA.

The integration of the slot provides a null in the correlation curve close to the center frequency of the low frequency region, i.e. close to 0.9GHz (Fig. 6.26). In addition, the isolation improvements contribute to enhance antenna efficiencies (Fig. 6.26). More particularly, when the slot was not considered, antenna efficiencies were, in average, around 56.1% for the ground plane booster and 37.4% for the dual-band PIFA. The integration of the slot increases antenna efficiency values up to 59.4% and 63.7%, for the ground plane booster and dual-band PIFA, respectively. Thus, this proposal is positioned as a feasible solution to improve isolation, efficiency, and correlation of radiating systems initially coupled and correlated.

6.5.3 MIMO Solution: Coupled Monopoles and Ground Plane Boosters

The previous study is expanded to a multi-band MIMO system not only in the low frequency region (824-960MHz) but also in the high frequency region (1710-2400MHz). The coplanar monopoles, presented along section 6.4.1, are selected to be integrated with a multi-band radiating system based on ground plane boosters not only due to their low-profile properties but also due to its penta-band operation. According to the teachings of the previous section, a slot is etched on the ground plane, whose length has been minimized with respect to the previous proposal. The proposed slot is adjusted for attaining a minimum of the transmission coefficient at the center frequency of the low frequency region through the addition of a capacitor (824-960MHz). The proposal has been simulated and compared with a solution that does not integrate the slot as isolation technique. Finally, a prototype is built and the main MIMO parameters have been measured in order to demonstrate the feasibility of the proposal.

6.5.3.1. Simulated Results

The MIMO proposal consists of integrating a set of coupled monopoles capable of operating the communication standards GSM850, GSM900, GSM1800, GSM1900, UMTS, LTE2100, and LTE2300 with two ground plane boosters, each one intended for covering a particular frequency region.

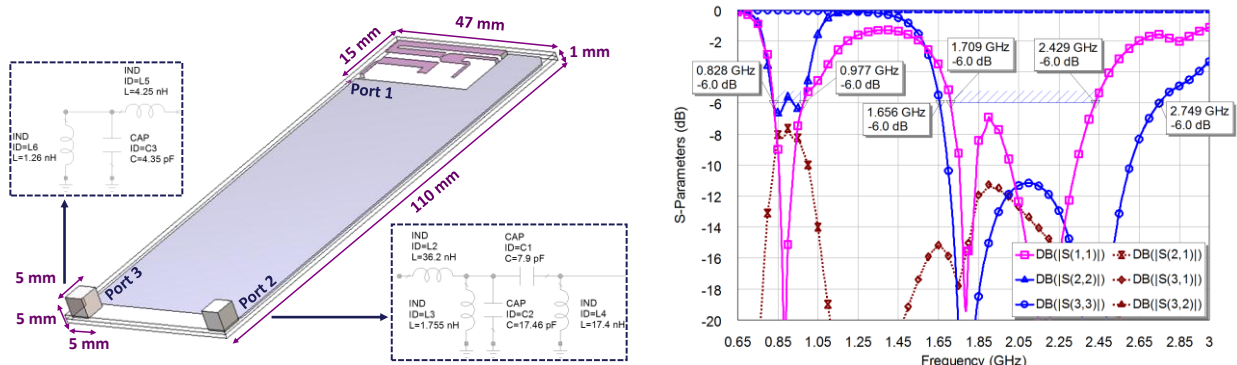


Fig. 6.27 Left) Geometry of the proposed multi-band MIMO system comprising a set of coupled monopoles and two ground plane boosters. The coupled monopoles are etched over a 1 mm thick FR4 piece ($\epsilon_r=4.15$, $\tan\delta=0.013$); Right) S-parameters. The axis coincide with those illustrated in Fig. 6.4a.

The ground plane dimensions are 110 mm x 47 mm and it is etched over a 1 mm thick FR4 piece ($\epsilon_r=4.15$, $\tan\delta=0.013$). On one hand, the ground plane booster intended for the low frequency region (824-960MHz) is connected to port 2 through a matching network including a series inductor, a broadband

matching network, and a fine tuning stage (Fig. 6.27). On the other hand, the ground plane booster intended for the high frequency region (1710-2400MHz) is connected to port 3 through a matching network just including a series inductor and a broadband matching network (Fig. 6.27). The transmission coefficient in the low frequency region remains below -8dBs, whereas in the high frequency region it is approximately below -12dBs (Fig. 6.27).

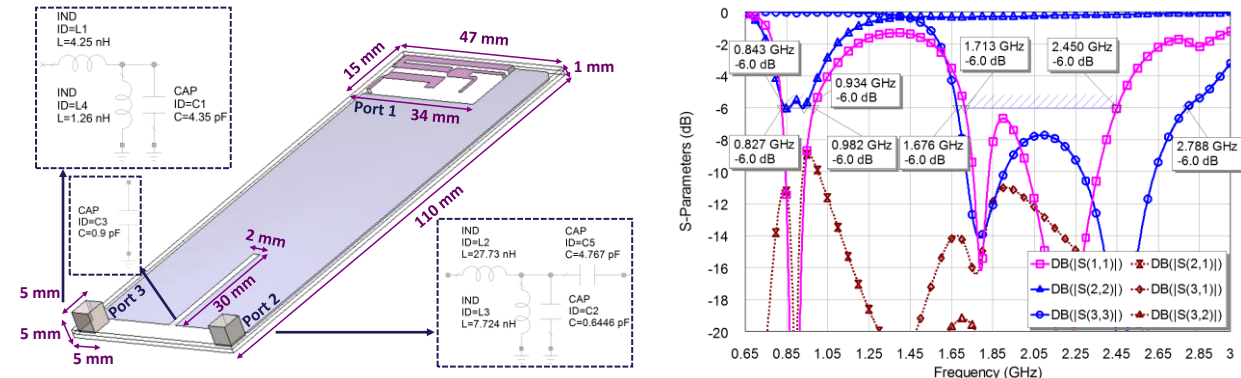


Fig. 6.28 Left) Geometry of the proposed multi-band MIMO system comprising a set of coupled monopoles and two ground plane boosters. The coupled monopoles are etched over a 1 mm thick FR4 piece ($\epsilon_r=4.15$, $\tan\delta=0.013$); Right) S-parameters. The axis coincide with those illustrated in Fig. 6.4a.

A slot is etched in the ground plane with the aim of improving the isolation between the radiating systems, especially in the low frequency region. The previous section demonstrates that an open slot having resonant dimensions at the center frequency of the low frequency region allows reducing isolation and correlation values.

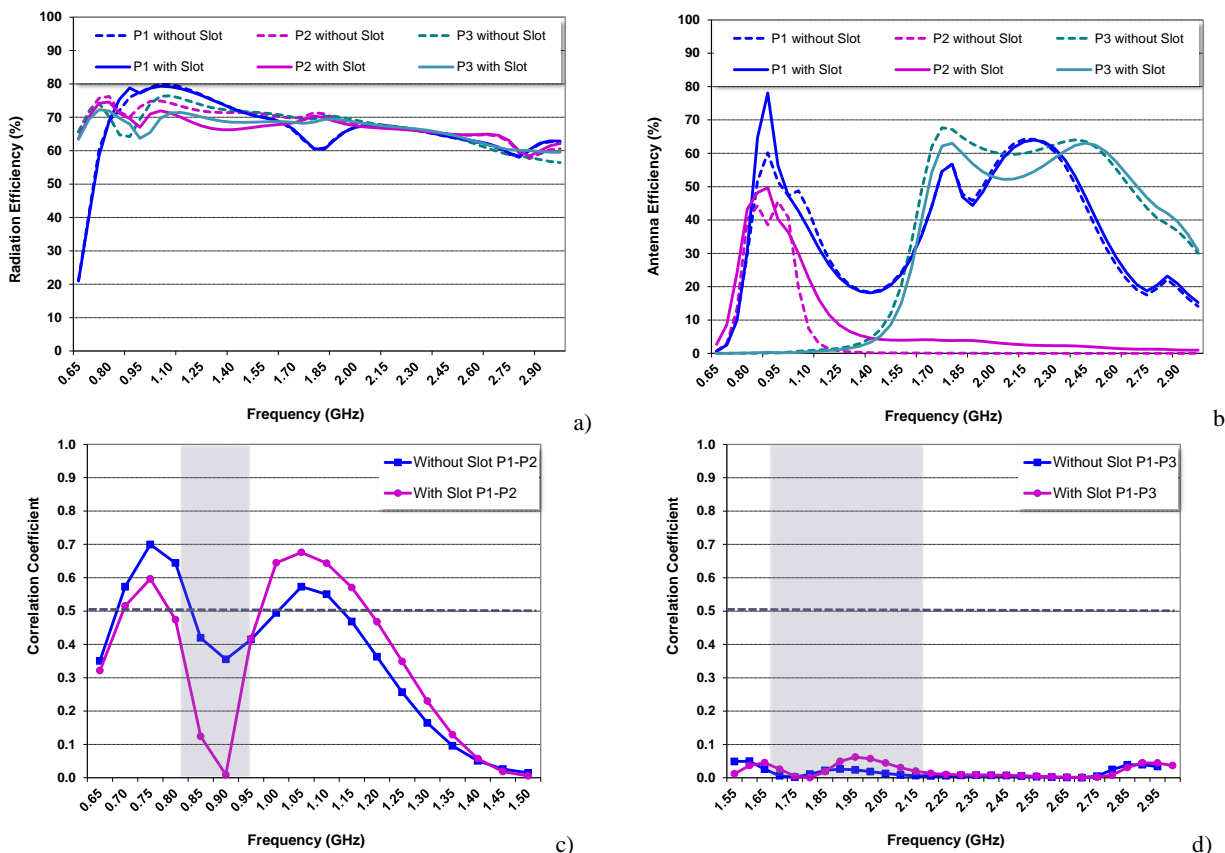


Fig. 6.29 a)-b) Radiation and antenna efficiency for each one of the radiating systems under study for the low and the high frequency region, respectively; c)-d) Correlation coefficient computed regarding radiation patterns (6.9) for the low and high frequency region, respectively.

Nevertheless, unlike the previous proposal, this section proposes the miniaturization of the quarter-wavelength slot through the integration of a capacitor. The analysis reveal that the miniaturization effect of the capacitor is less effective as long as the capacitor approximates the short edge of the slot. For this reason, the capacitor is placed at the open edge of the slot and presents a value of 0.9pF (Fig. 6.28). The addition of the capacitor allows a miniaturization factor around 1.8, since its previous length of 55 mm (Fig. 6.25) is reduced up to 30 mm. A deep null of the transmission coefficient is appreciated at the frequency of 0.9GHz (Fig. 6.25), thus demonstrating the effectiveness of the slot in improving isolation. The radiation efficiencies measured at each one of the three ports under analysis do not suffer significant variations with the integration of slot (Fig. 6.29a). Moreover, antenna efficiencies improve in the low frequency region thanks to the isolation enhancement (Fig. 6.29b).

The correlation coefficient also presents a null at the center frequency of the low frequency region, thus emphasizing the benefits of the slot. The correlation values remain below the accepted threshold of 0.5 along the whole frequency range of the low frequency region (Fig. 6.29c). In the high frequency region, the correlation values are even below 0.10 (Fig. 6.29d).

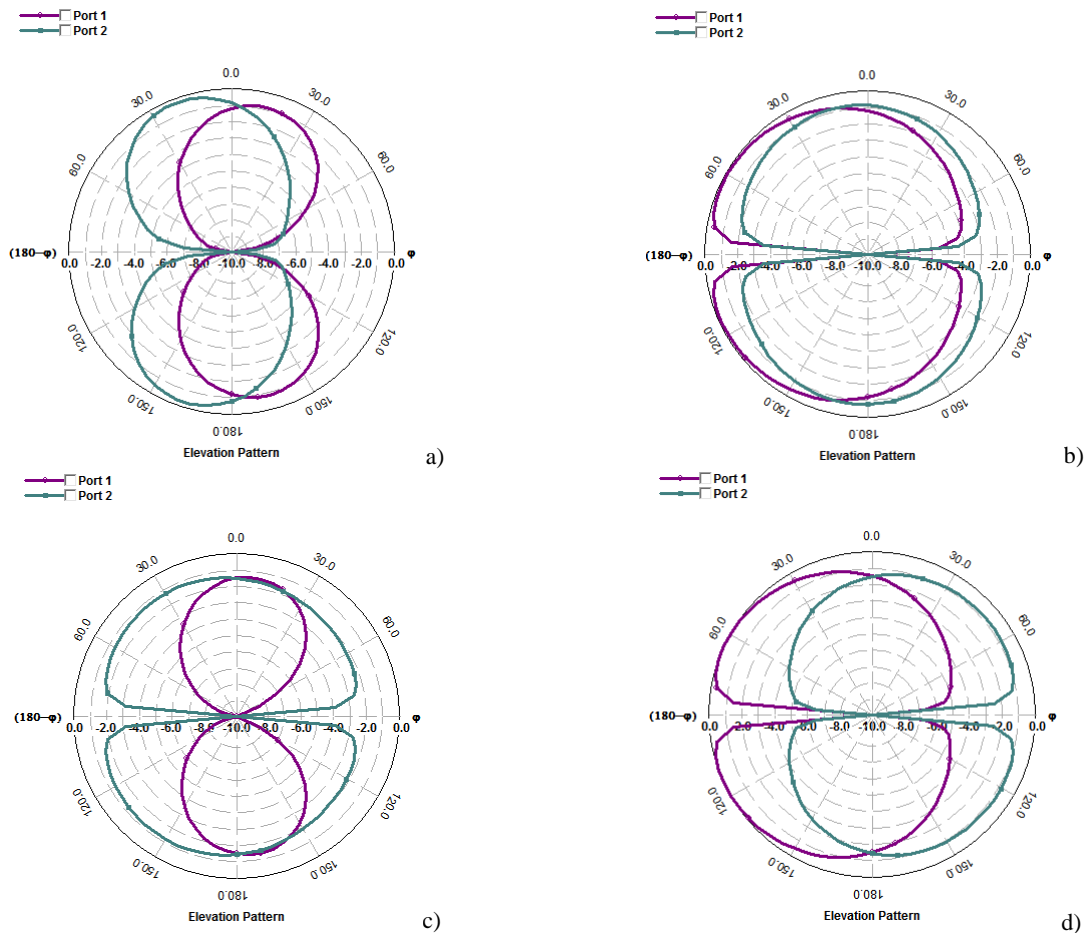


Fig. 6.30 a)-b) E-total regarding the $\phi=0^\circ$ and $\phi=90^\circ$ cuts associated to the radiating systems of Fig. 6.27 at the frequency of 0.9GHz; c)-d) E-total regarding the $\phi=0^\circ$ and $\phi=90^\circ$ cuts associated to the radiating systems of Fig. 6.28 at the frequency of 0.9GHz. Note that the null appearing at $\phi=90^\circ$, $\theta=90^\circ$ is due to the infinite FR4 piece considered in the simulation. In practice, when finite dielectrics are regarded, the $\phi=90^\circ$ cut is omnidirectional.

On one hand, the representation of the main cuts of the radiation patterns (Fig. 6.30) at the central frequency of the low frequency region, where the correlation null appears, also illustrates the advantages

of the miniaturized slot. When the slot is not considered, the correlation at 0.9GHz is around 0.35 and the radiation patterns present some dissimilarities (Fig. 6.30a-b). However, it equals 0 when regarding the slot. This fact, makes more evident the differences between the radiation patterns (Fig. 6.30c-d). On the other hand, the current distribution at this center frequency for both cases also illustrates the improvements in isolation obtained by the slotted ground plane (Fig. 6.31). When the coupled monopoles are excited in the slotted ground plane (Fig. 6.31c), the current appearing close to the feeding point of the ground plane booster operating in the low frequency region (ground plane booster placed at the bottom right) is minimized, and the same happens close to the feeding point of the coupled monopoles when the ground plane booster is excited (Fig. 6.31c). In order to validate the feasibility of the proposal, the following section will present measured results from real prototypes.

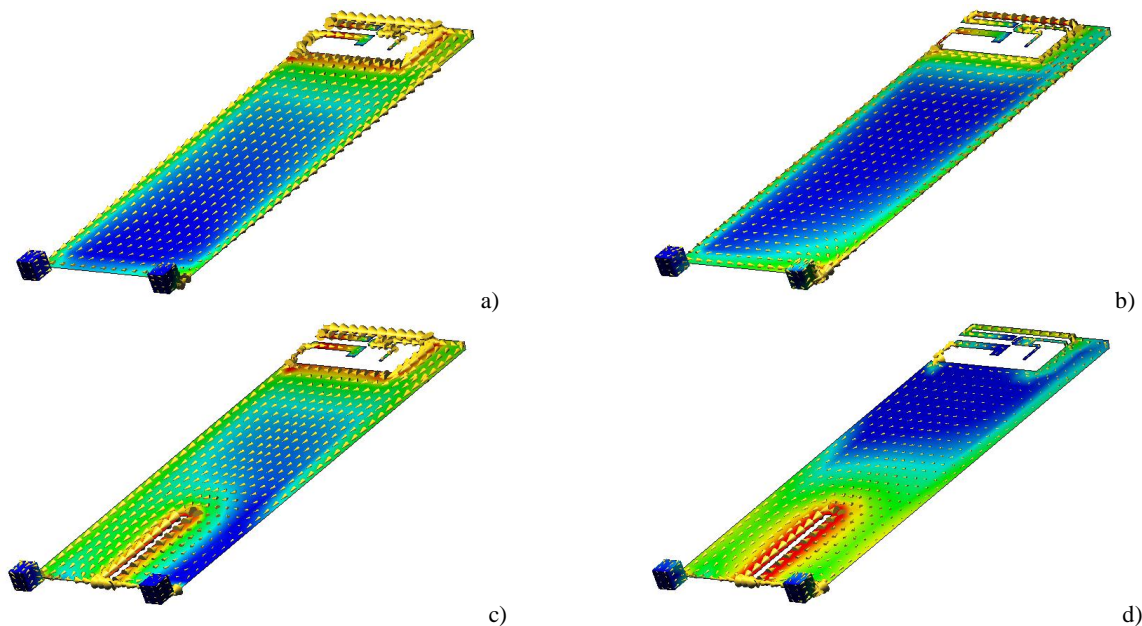


Fig. 6.31 a)-b) Current distribution without the slot when the coupled monopoles and the ground plane booster for the low frequency region are excited, respectively. Port 3 is connected to a 50Ω load; c)-d) Current distribution regarding the slot when the coupled monopoles and the ground plane booster for the low frequency region are excited, respectively. Port 3 is connected to a 50Ω load. Max-E current is 5A/m and the dynamic range is 30dB's. The axis coincide with those illustrated in Fig. 6.4a.

6.5.3.2. Measured Results

The former multi-band MIMO systems have been prototyped with the aim of validating the simulated results. The coupled monopoles are arranged at a short edge of a ground plane having dimensions of 110 mm x 47 mm, and the ground plane boosters, featured by small dimensions of just 5 mm x 5 mm x 5 mm, are placed at the opposite short edge.

As derived from the previous analysis, the distance between the feeding point of the coupled monopoles and the feeding point of the ground plane booster intended for the low frequency region is maximized (Fig. 6.32a). Both radiating systems attain operation in the communication standards GSM850, GSM900, GSM1800, GSM1900, UMTS, and LTE2100. The worst isolation between them is found in the low frequency region. More particularly at 0.9GHz, where the transmission coefficient is around -11dBs (Fig. 6.32b). The matching network topology implemented in the prototyped solution also includes reactance cancellation elements and broadband matching networks for both frequency regions.

The low frequency region further incorporates a fine tuning stage consisting of a series capacitor (Fig. 6.32d). Note that the PCB space occupied by the matching network is minimum, since the pads for interconnecting the lumped elements extend in a direction parallel to the short edge (Fig. 6.32c), thus contributing to the compactness of the MIMO system.

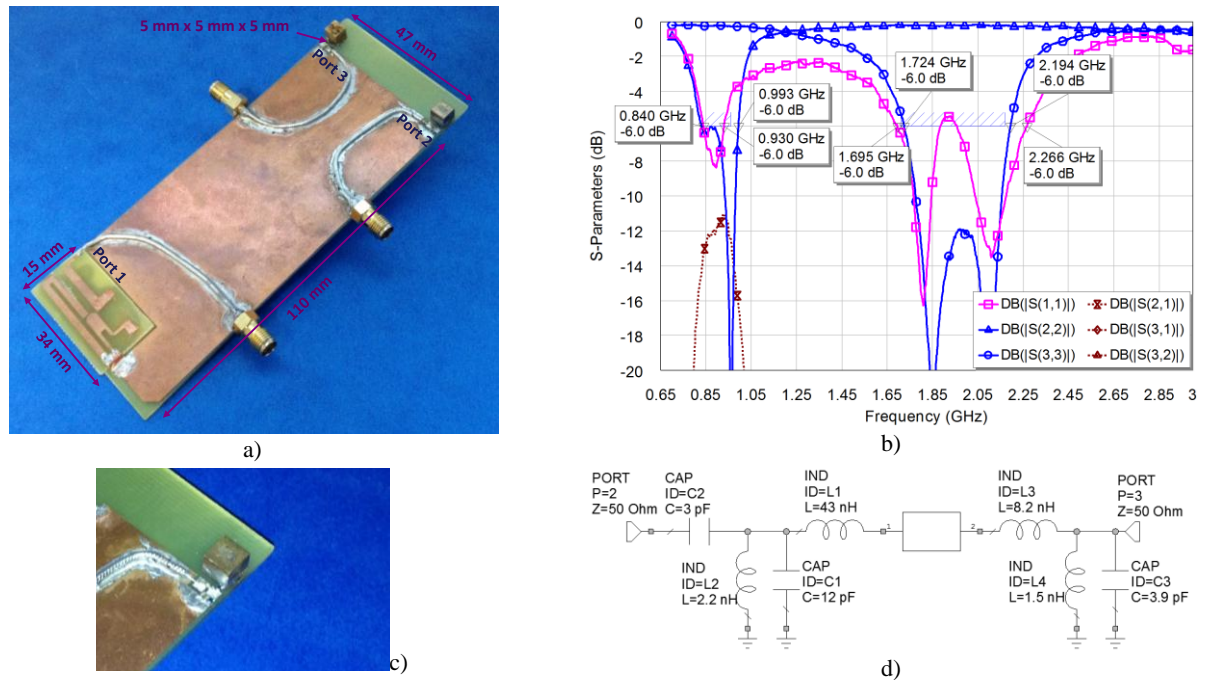


Fig. 6.32 a) Geometry of the proposed multi-band MIMO system. The coupled monopoles and the ground plane are etched over a 1 mm thick FR4 piece ($\epsilon_r=4.15$, $\tan\delta=0.013$), respectively; b) S-parameters. Port 1 refers to the coupled monopoles, whereas port 2 and 3 relate to the ground plane booster intended for the low frequency region and the high frequency region, respectively; c) Detailed view of the ground plane booster and the matching network for the low frequency region d) Schematic representation of the implemented matching networks containing the commercial values of the reactive elements (Murata SMD0402) connected to port 2 and port 3.

In order to demonstrate the effectiveness of the miniaturized slot in reducing isolation as well as correlation, a second prototype including the slotted ground plane is built (Fig. 6.33). The introduction of the slot neither modifies the impedance bandwidth of the coupled monopoles nor the impedance bandwidth of the ground plane booster intended for the high frequency region. Nevertheless, it clearly enhances the impedance bandwidth of the ground plane booster in charge of the low frequency region. Note that in this case, the values and the topology of the matching network remain equal as those illustrated in the previous case where the slot was not considered (Fig. 6.32d).

The experimental results (Fig. 6.34) are in good agreement with the simulated ones (Fig. 6.29), and consequently not only the isolation null appears at the center frequency of the low frequency region (0.9GHz) (Fig. 6.33), but also it is present in the correlation measurements, which are below the accepted threshold of 0.5 along the whole frequency region. In the high frequency region they advantageously remain below 0.10 for a wide range of frequencies (Fig. 6.34). The correlation is computed through a Matlab code developed in the context of this thesis. The code computes the correlation through the radiation patterns of the corresponding prototype, which are measured in the anechoic chamber Satimo Stargate-32. Antenna efficiencies are also measured through the 3D integration of the radiation pattern in

the same anechoic chamber (Fig. 6.34). As expected, it improves with respect to the case where the slot was not regarded.

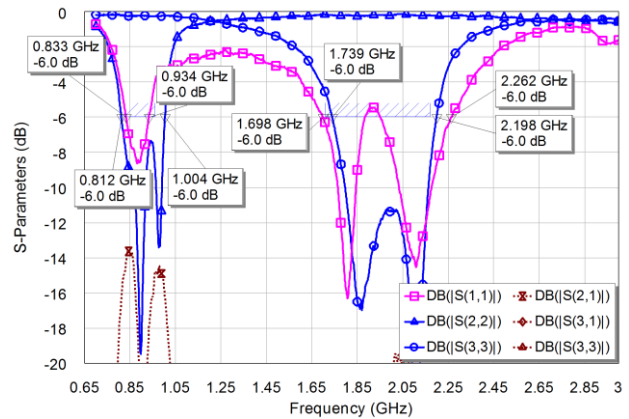
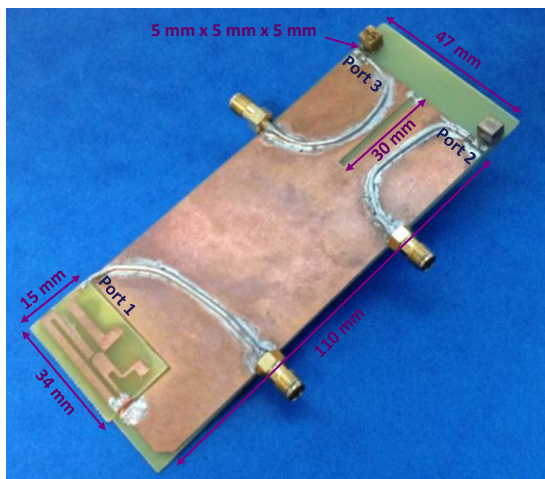
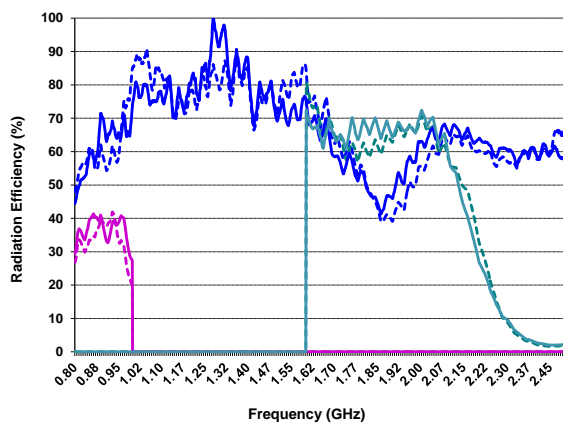
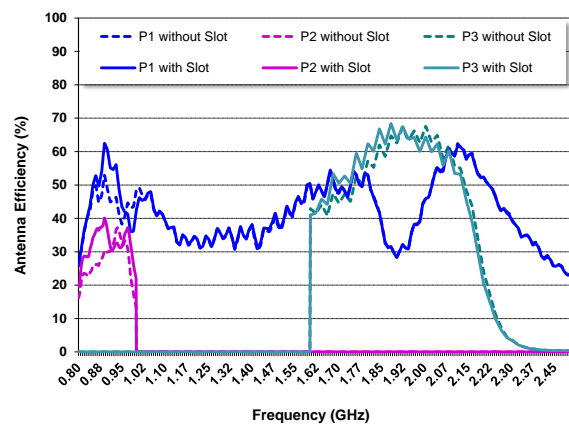


Fig. 6.33 Left) Geometry of the proposed multi-band MIMO system incorporating a miniaturized slot as isolation technique. The coupled monopoles and the ground plane are etched over a 1 mm thick FR4 piece ($\epsilon_r=4.15$, $\tan\delta=0.013$); Right) S-parameters. Port 1 refers to the coupled monopoles, whereas port 2 and 3 relate to the ground plane booster intended for the low frequency region and the high frequency region, respectively.

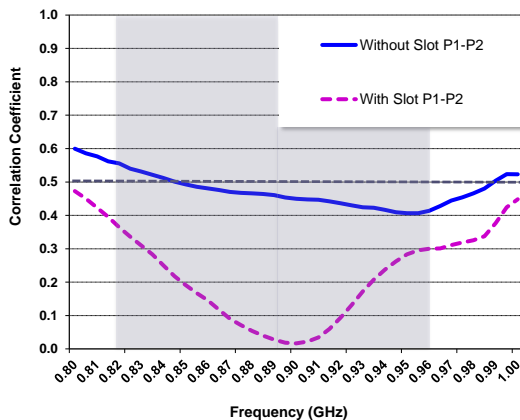
In the low frequency region, the ground plane booster attains antenna efficiency values close to 33.4%, in average, whereas the coupled monopoles reach values close to 49.9%. When the slot was not regarded, the efficiency values were slightly lower, around 29.1% for the booster case and 44.4% for the coupled monopoles.



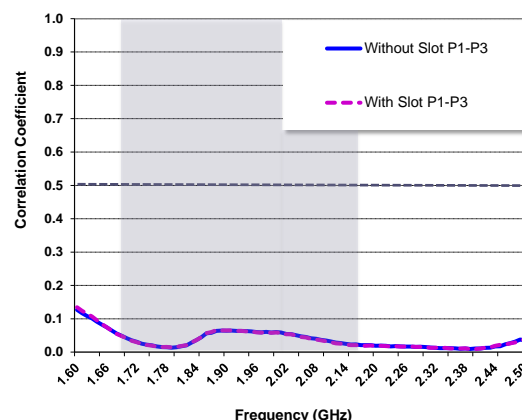
a)



b)



c)



d)

Fig. 6.34 a)-b) Radiation and antenna efficiency for each one of the radiating systems under study regarding the low and the high frequency region, respectively; c)-d) Correlation coefficient computed regarding radiation patterns (6.9) for the low and high frequency region, respectively.

In the high frequency region the average of the efficiency values across the operating frequencies (1710-2170MHz) is around 58.3% for the ground plane booster and 46.9% for the coupled monopoles. The integration of the slot significantly improves the correlation values in the low frequency region. This effect can be further appreciated in the radiation patterns representation. In this case and for the sake of make an easier comparison, the 3D radiation patterns associated to each radiating structure are represented in a 2D plot (Fig. 6.35). The integration of the slot introduces more dissimilarities between the radiation pattern associated to the radiating system including the ground plane booster intended for the low frequency region and that corresponding to the coupled monopoles. In fact, a pronounced null appears in the $\theta=45^\circ$, $\phi=180^\circ$ direction for the coupled monopoles whereas the radiating system associated to the ground plane boosters presents a maximum of radiation at this direction (Fig. 6.35).

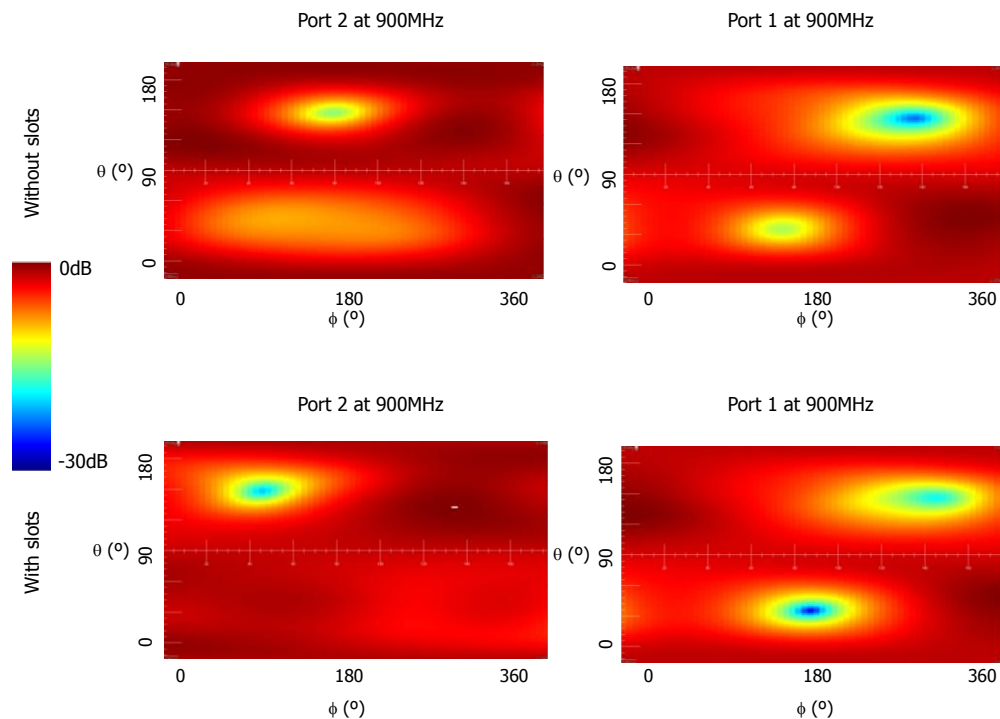


Fig. 6.35 Comparison of the radiation patterns associated to the ground plane booster intended for the low frequency region (port 2) and to the coupled monopoles (port 1) at a frequency where the correlation null appears regarding both configurations, with and without the slot.

6.6. MIMO Systems based on Ground Plane Boosters

The former section demonstrates on one hand, that maximizing the distance between radiating systems operating in the low frequency region by feeding the structures at opposite edges of the ground plane is preferable for reducing correlation values. On the other hand, it demonstrates that the addition of quarter-wavelength resonant slots, which can be minimized with reactive elements, further contributes to reduce correlation and improve isolation as well as antenna efficiency. The analysis concludes with a feasible solution capable of providing 2x2 MIMO operation in the communication standards GSM850, GSM900, GSM1800, GSM1900, UMTS, and LTE2100. The proposal presents a significant low profile that allows the integration of the system in ultra-slim devices. With the aim of improving the compactness of the previous MIMO solutions, the present section substitutes the antennas featuring resonant

dimensions, as considered above, by ground plane boosters. The challenge to accomplish the strict specifications of MIMO systems in terms of isolation, correlation, and efficiency further exacerbates when regarding a full booster-based MIMO solution. In this sense, the present section will be focused on analyzing these challenges and on proposing solutions to provide a compact fully based ground plane booster solution, capable of fulfilling MIMO specifications [39].

6.6.1 Description of the MIMO Solution

The proposed MIMO system comprises four ground plane boosters featuring reduced dimensions of just 5 mm x 5 mm x 5 mm. The four ground plane boosters are placed respectively at the corners of a ground plane having dimensions comparable to that featured by conventional smartphones platforms (120 mm x 50 mm). Two ground plane boosters are intended for the low frequency region (824-960MHz), whereas the other two are in charge of providing operation in the high frequency region (1710-2170MHz). In order to allow operability in the corresponding frequency regions, the four ground plane boosters are connected respectively to a matching network including a series inductor, a broadband matching network, and, if needed, a fine tuning stage. In this way, the MIMO system will comprise two radiating systems operating in the low frequency region and two radiating systems operating in the high frequency region. According to the above teachings, those ground plane boosters operating in the same frequency region are placed at diagonally opposite corners of the ground plane to maximize the distance among them.

The challenge on providing MIMO operation in this case relies on the fact that the radiation in a booster-based system is mainly determined by the ground plane, more significantly when considering the low frequency region. As discussed along this thesis, the ground plane boosters present very poor stand-alone radiation properties at the low frequency region due to their reduced dimensions that lead to high quality factors. In this sense, the differences between the radiation patterns produced by the currents appearing in the resonant antennas, are not present in this case, thus making difficult the achievement of low correlation values. In addition, different radiating modes of the ground plane cannot be excited at these low frequencies, since just the fundamental radiating mode having a longitudinal current distribution appears at the low frequency region (Fig. 2.5). This fact further complicates the achievement of low correlation and isolation values.

With this aim and following the operational principle of the previous proposal, two slots are etched on the ground plane in order to produce enhanced isolation and correlation. In contrast to the previous design, in this case the slots are not only miniaturized through a reactive component but also through their geometry. Accordingly, two miniature slots inspired in the Hilbert fractal are etched in the respective shortest edges of the ground plane. The slots are adjusted to minimize the transmission coefficient in the low frequency region. The proposal has been simulated and compared with a solution that does not integrate the slots as isolation technique. Finally, a prototype is built and the main MIMO parameters have been measured in order to demonstrate the feasibility of the proposal.

6.6.2 Simulated Results

The proposal has been simulated, in the same manner as the previous designs, by means the software IE3D based on Method of Moments (MoM). First of all, the behavior of a MIMO system fully based on ground plane boosters is analyzed. The ground plane boosters are placed at the respective four corners of the ground plane, as being the preferable location of capacitive boosters. Those in charge of the same frequency region are placed in diagonally opposite corners in order to reduce mutual coupling (Fig. 6.36). The simulated results demonstrate that the two ground plane boosters associated to the low frequency region (port 1 and port 3) are able of operating the standards GSM850 and GSM900, whereas those intended for the high frequency region offer a large impedance bandwidth (from 1.69GHz up to beyond 3GHz) ($SWR \leq 3$), hence covering six additional communication standards, GSM1800, GSM1900, UMTS, LTE2100, LTE2300, and LTE2500 (port 2 and port 4). The transmission coefficient for the high frequency region remains below -10dBs, whereas at the low frequency region it reaches peaks of -6dBs (Fig. 6.36).

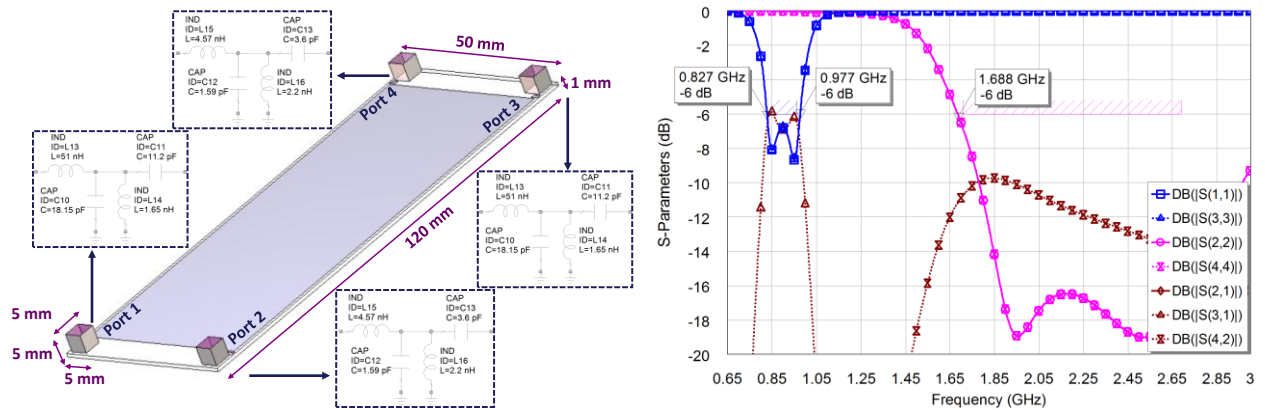


Fig. 6.36 Left) Geometry of the proposed multi-band MIMO system comprising four ground plane boosters placed at the corners of a ground plane (120 mm x 50 mm). The ground plane is etched over a 1 mm thick FR4 piece ($\epsilon_r=4.15$, $\tan\delta=0.013$). The matching network connected to each port contains a series inductor, a broadband matching network, and a series capacitor as a fine tuning stage; Right) S-parameters. The axis coincide with those illustrated in Fig. 6.4a.

The radiation efficiency remains at high values around 85% for a large range of frequencies (0.6-3GHz) (Fig. 6.37a). Nevertheless, the antenna efficiency decreases up to an average of 49% in the low frequency according to (6.13) mainly due to the low isolation values (Fig. 6.37). In the high frequency region, the antenna efficiency remains at high values around 74% (Fig. 6.37b). The average of the antenna efficiency is computed across the operating frequency bands, i.e. across 824-960MHz for the low frequency region and across 1710-2690MHz across the high frequency region.

In order to reduce the coupling appearing between those radiating systems operating in the same frequency region, two slots inspired in the Hilbert fractal are etched in the respective shortest edges of the ground plane. As illustrated in the previous section, the integration of a slot in the ground plane minimizes the coupling, more significantly at the resonant frequency of the slot (Fig. 6.38). In this case and with the aim of enhancing the bandwidth where the transmission coefficient remains below a certain value, two slots are proposed, each one tuned at a particular frequency of the low frequency region (Fig. 6.38). The Hilbert-based geometry has been selected as being a geometry able to pack long operating

wavelengths into a reduced space [40]-[41]. In addition to the miniaturization capabilities provided by the own geometry, the dimensions of the proposed slots inspired in the Hilbert fractal are further minimized thanks to the addition of a reactive element, namely a capacitor placed close to the open edges of the Hilbert slot (Fig. 6.38).

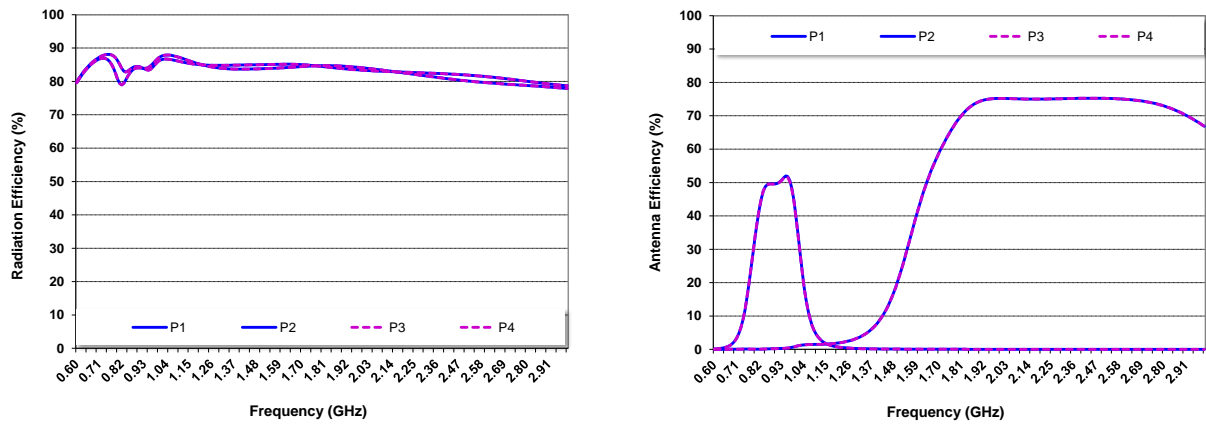


Fig. 6.37 Radiation and antenna efficiency corresponding to the MIMO system illustrated in Fig. 6.36. Port 1 and 3 refer to the ground plane booster intended for the low frequency region, whereas port 2 and 4 relate to those boosters in charge of the high frequency region.

The matching network topologies used in this case are equivalent to those needed in the case where the slots were not considered (Fig. 6.36). Thus, port 1 and port 3 intended for the low frequency region require a series inductor, a broadband matching network, and just a series capacitor as a fine tuning stage. The same topology applies to the high frequency region (port 2 and port 4) (Fig. 6.38). The impedance bandwidth is not altered by the integration of the slots and it continues offering dual-band operation in the low frequency region (824-960MHz (bands 5-8)) and hexa-band operation in the high frequency region (1710-2690MHz) (Table 6.1). Moreover, they significantly contribute to minimize the transmission coefficient, more significantly at the low frequency region where the integration of the slots produces minimums around -12dBs and -14dBs.

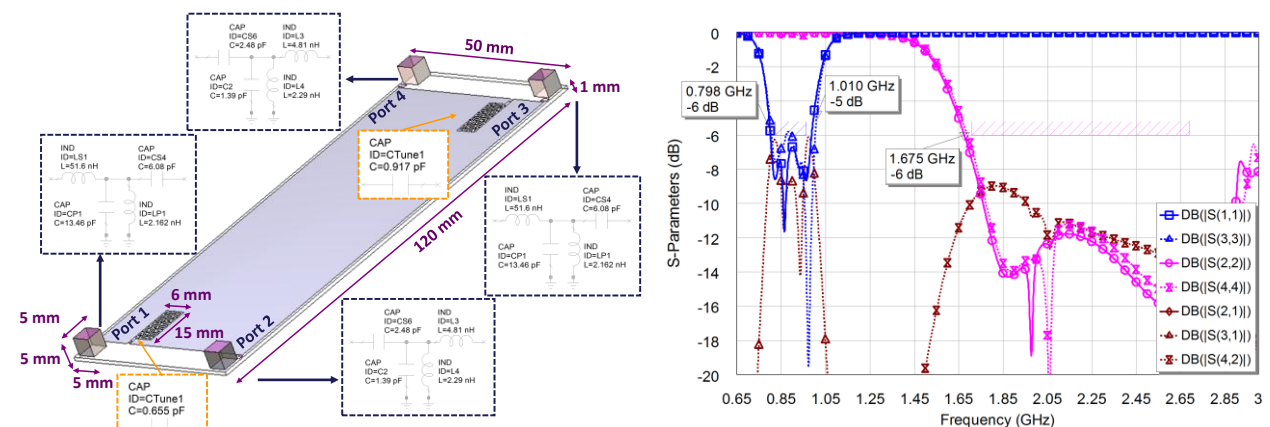


Fig. 6.38 Left) Geometry of the proposed multi-band MIMO system comprising four ground plane boosters and two slots inspired in the Hilbert fractal. The ground plane is etched over a 1 mm thick FR4 piece ($\epsilon_r=4.15$, $\tan\delta=0.013$). The matching network connected to each port contains a series inductor, a broadband, and a series capacitor as a fine tuning stage; Right) S-parameters. The axis coincide with those illustrated in Fig. 6.4a.

The enhancement in isolation introduced by the Hilbert-based slots improves antenna efficiency values at the low frequency region, since peaks of efficiency around 65% appear (Fig. 6.39). The antenna

efficiency in the high frequency region remains at high values. Nevertheless, an undesired dip is appreciated at frequencies around 2GHz. The reasoning behind, relies on the fact, that although the Hilbert-based geometry is suitable to attain miniaturization it could introduce poor radiating or even non-radiating modes at certain frequencies. These modes are featured by opposite currents that tend to reduce the radiation resistance, hence leading to low radiation efficiencies. The simulated radiation efficiency illustrates this fact and shows a periodic efficiency decrement that corresponds to the excitation of these radiating modes having low radiation resistances (Fig. 6.39). These efficiency drops do not affect the low frequency region, since they do not appear in the operating bands. In the high frequency region, the efficiency dip is around 60% and 40% regarding port 2 and port 4, respectively.

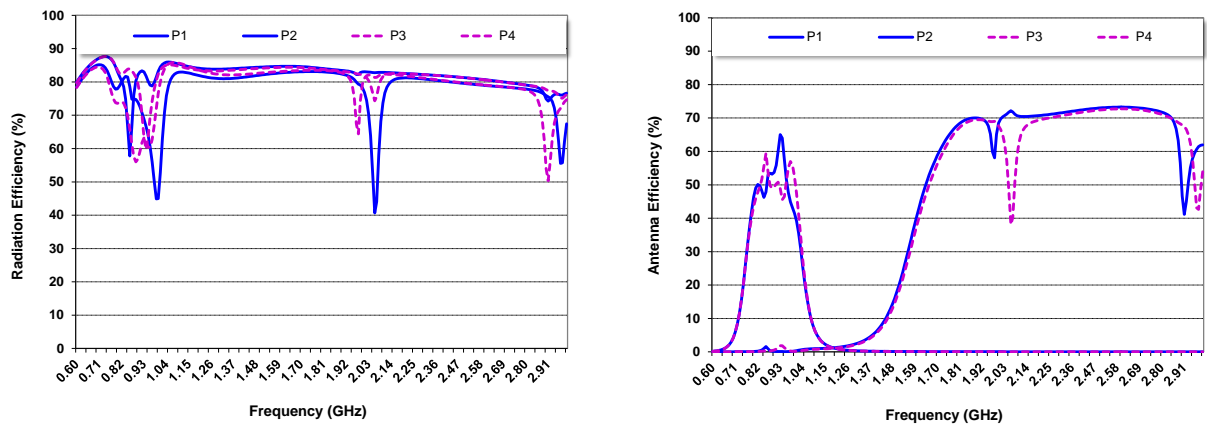


Fig. 6.39 Radiation and antenna efficiency corresponding to the MIMO system illustrated in Fig. 6.38. Port 1 and 3 refer to the ground plane booster intended for the low frequency region, whereas port 2 and 4 relate to those boosters in charge of the high frequency region.

Owing to the correlation, the proposal based on the integration of the two Hilbert-based slots in the ground plane significantly reduces correlation values with respect to the proposal that does not integrate the slots, when regarding the low frequency region.

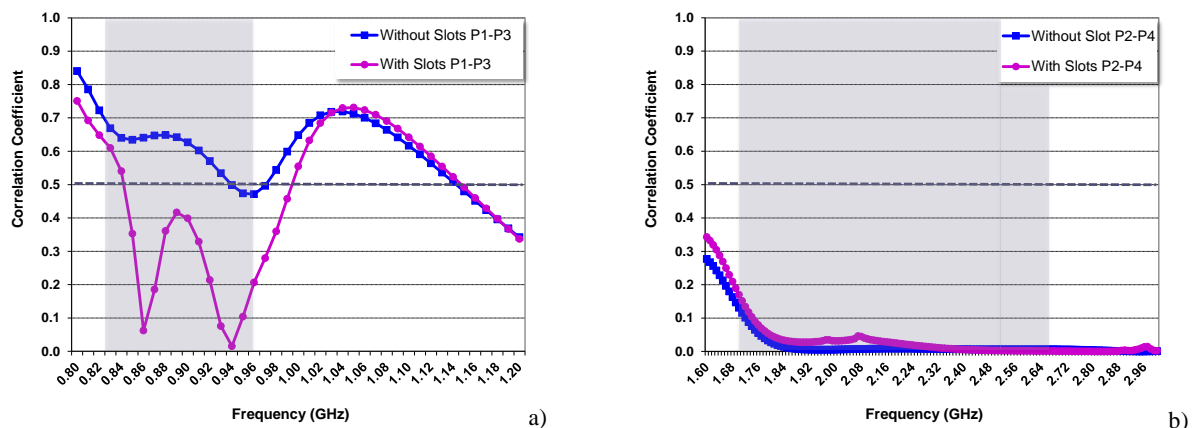


Fig. 6.40 a) Comparison of the correlation coefficient with (Fig. 6.38) and without the Hilbert-based slots (Fig. 6.36) computed through radiation patterns (6.9) for the low and high frequency region.

As discussed in the previous section, the correlation values for the high frequency region are below the required threshold of 0.5 for a large range of frequencies. At these high frequencies, the electrical distance is large enough as for guarantee low correlation coefficients even when having similar or equal radiation patterns, thus avoiding the need of including mechanisms to reduce isolation and correlation.

Nevertheless, at the low frequency region, they are strongly required and even more when regarding radiating system fully based on ground plane boosters. In view of the results, the proposal becomes a feasible solution to reduce not only isolation (Fig. 6.38) but also to minimize correlation (Fig. 6.40) at these low frequencies. In addition, it provides the flexibility to tune the correlation nulls at the desired frequencies, since they can be easily adjusted through the series capacitor connected to the open edges of the Hilbert-based slots. The main cuts of the radiation patterns computed, for instance, at the frequency where the second correlation null appears (0.94GHz), makes evident the differences between them, which lead to this low correlation value (Fig. 6.41).

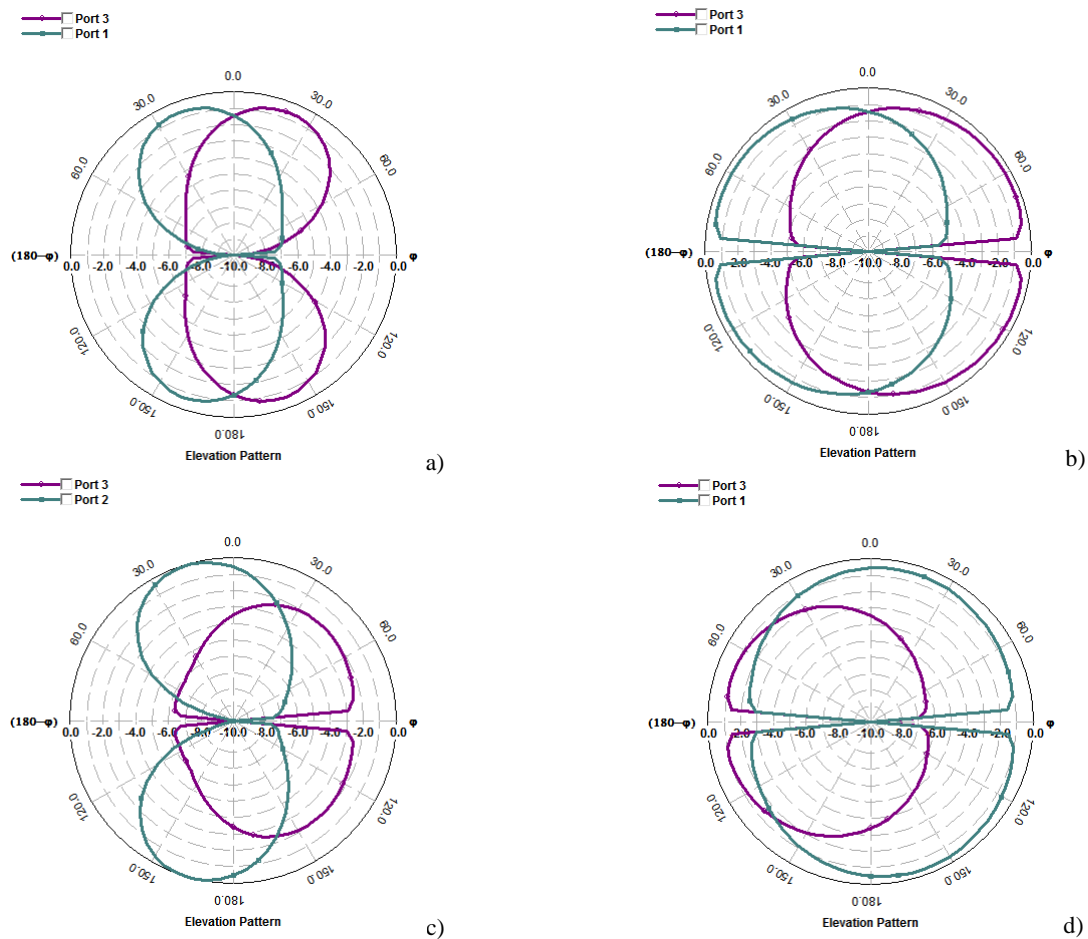


Fig. 6.41 a)-b) E-total regarding the $\phi=0^\circ$ and $\phi=90^\circ$ cuts associated to the radiating systems of Fig. 6.36 at the frequency of 0.94 GHz; c)-d) E-total regarding the $\phi=0^\circ$ and $\phi=90^\circ$ cuts associated to the radiating systems of Fig. 6.38 at the frequency of 0.94 GHz. Note that the null appearing at $\phi=90^\circ$, $\theta=90^\circ$ is due to the infinite FR4 piece considered in the simulation. In practice, when finite dielectrics are regarded, the $\phi=90^\circ$ cut is omnidirectional.

Finally the current distribution analyzed at both MIMO proposals depicts on one hand, how the Hilbert-based slots are excited, more significantly, in the low frequency region, thus explaining their effects over the radiation efficiency of the whole system (Fig. 6.39). On the other hand, it illustrates how the slots contribute to minimize the transmission coefficient between those ports operating in the same frequency region. In this way, the excitation of port 1 induces currents in port 3 when the slots are not present (Fig. 6.42a). Nevertheless, these currents are minimized when the slots are integrated (Fig. 6.42c).

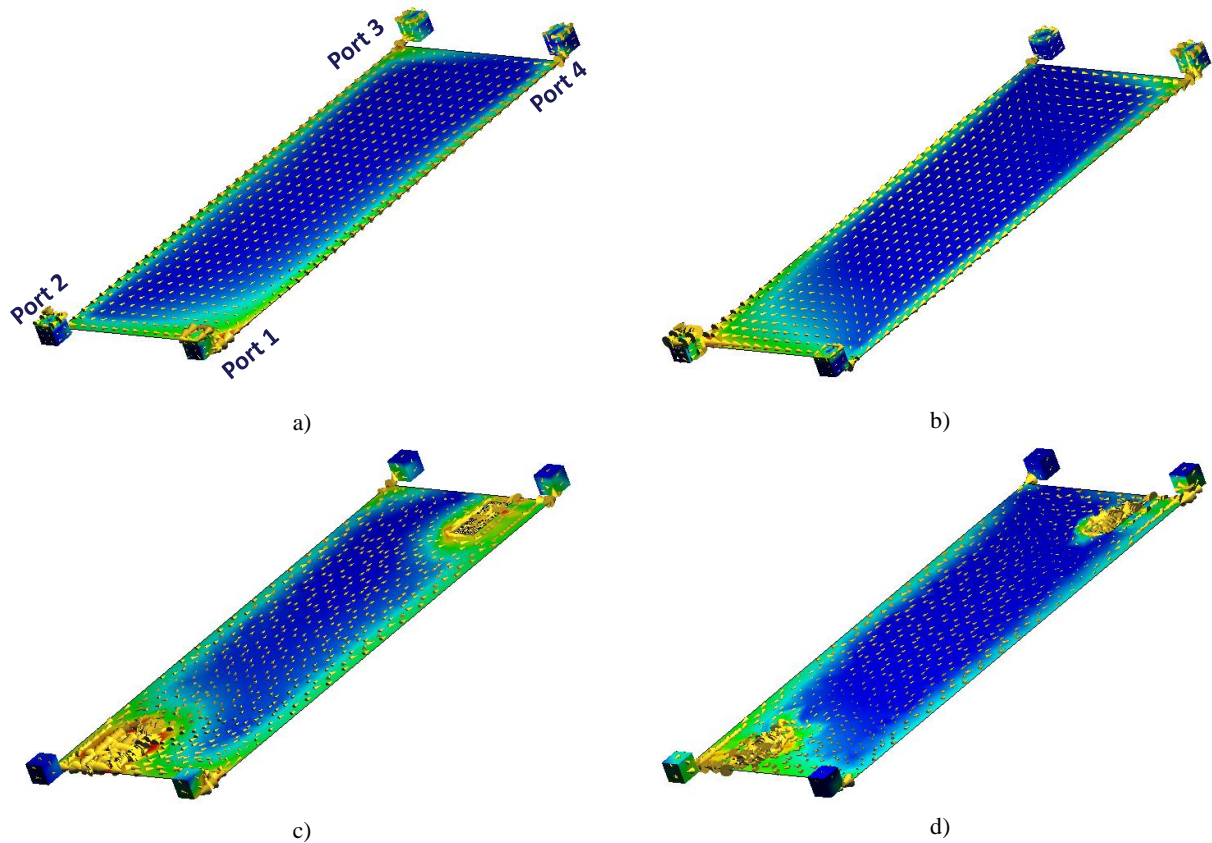


Fig. 6.42 a)-b) Current distribution at 0.9GHz and 1.9GHz without the slot when the ground plane boosters for the low and high frequency region are excited; c)-d) Current distribution regarding the slots inspired in the Hilbert fractal when the ground plane boosters for the low and high frequency region are excited. Port 3 and port 4 are connected to a 50Ω load. Max-E current is 5A/m and the dynamic range is 30dB's. The axis coincide with those illustrated in Fig. 6.4a.

6.6.3 Measured Results

In order to validate the simulated results, two prototypes are built for measuring the MIMO performance of the previous radiating systems. In this sense, four ground plane boosters have been soldered in the respective four corners of a ground plane having typical dimensions of smartphone platforms (120 mm x 50 mm). The ground plane boosters are made of a solid piece of brass and the dimensions of each one are 5 mm x 5 mm x 5 mm (Fig. 6.43a). The measured S-parameters depict that the ground plane boosters intended for the low frequency region (port 1 and port 3) are able of operating the communication standards GSM850 and GSM900 and those in charge of the high frequency region attain a sufficient impedance bandwidth as for covering GSM1800, GSM1900, UMTS, and LTE2100. The detailed view of the prototype illustrates how the proposed matching networks are connected at each port (Fig. 6.43c). The matching network topology illustrated in the simulated results (Fig. 6.36) is maintained in the prototyped solution. Accordingly, each port is connected to a series inductor and to a broadband matching network (Fig. 6.43d). In this case, the fine tuning stage is just used for the low frequency region. The MIMO system under study presents a transmission coefficient that remains below -12 dBs and -18dBs, for the low and high frequency region, respectively (Fig. 6.43b). In order to further improve the transmission coefficient as well as the correlation values in the low frequency range, two slots inspired in the Hilbert geometry are etched at the respective shortest edges of the ground plane. As

explained in the former section, a capacitor is connected to the open edge of each one of the slots with the aim of attaining further miniaturization thereof.

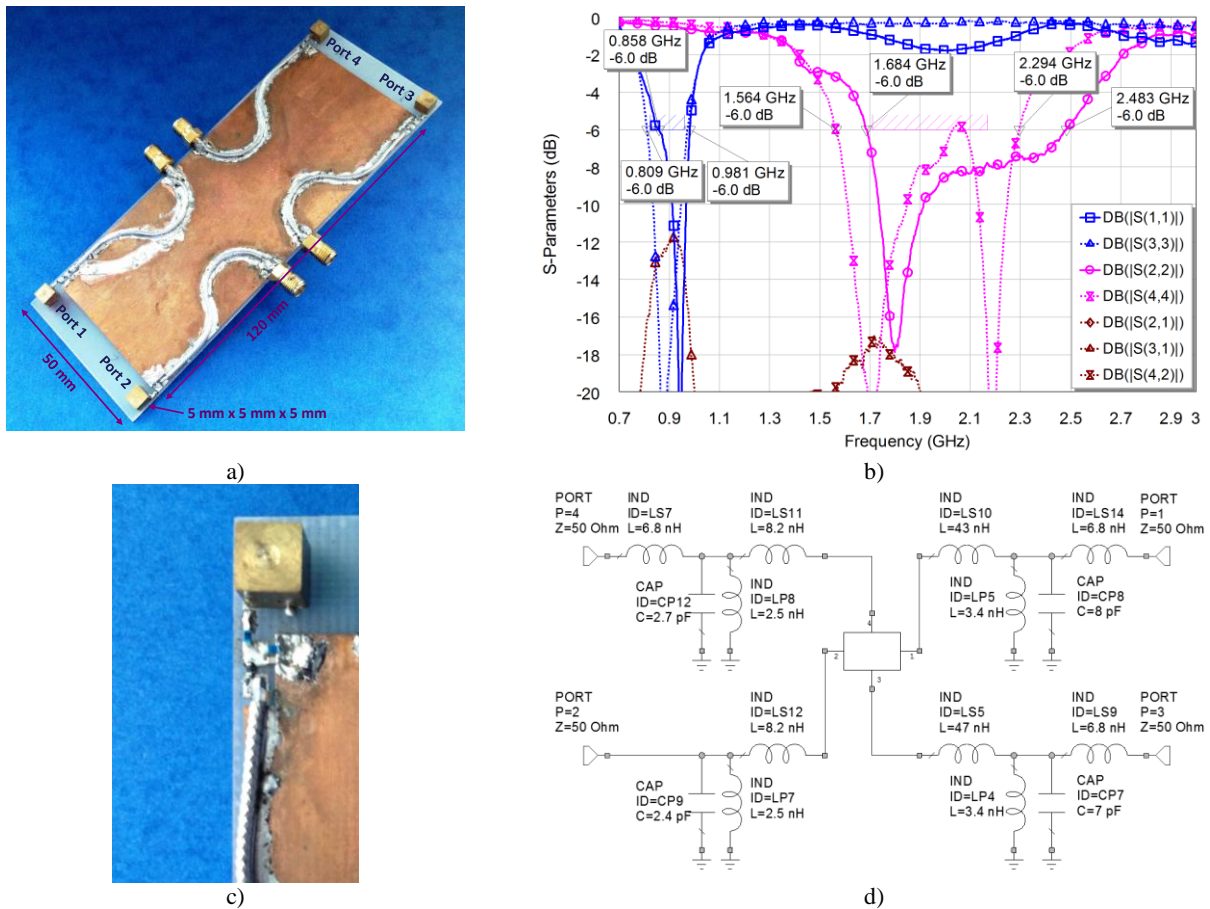


Fig. 6.43 a) Geometry of the proposed multi-band MIMO system comprising four ground plane boosters. The ground plane is etched over a 1 mm thick FR4 piece ($\epsilon_r=4.15$, $\tan\delta=0.013$); b) S-parameters. Port 1 and port 3 relate to the ground plane boosters intended for the low frequency region whereas port 2 and port 4 refers to those in charge of the high frequency range; c) Detailed view; d) Schematic representation of the implemented matching networks containing the commercial values of the reactive elements (Murata 0402).

The measured radiation efficiencies are lower than that obtained by simulation (Fig. 6.37) mainly due to the fact that the simulation considers ideal reactive elements, i.e. infinite Q elements. Nevertheless, in practice, the matching network components are featured by a finite Q , which introduces ohmic losses and degrades radiation efficiency. The radiation efficiencies are, in average, around 43%, in the low frequency region (824-960MHz) and around 75% in the high frequency region (1710-2170MHz). At the same time the antenna efficiencies values are, in average, around 38% and 65% for the low and high frequency region, respectively (Fig. 6.44). In order to increase these values, each one of the two Hilbert slots is etched at each one of the shortest edges of the ground plane with the aim of reducing the mutual coupling, especially appearing in the low frequency region (Fig. 6.45). As expected, the slots reduce the most critical mutual coupling, i.e. that appearing between those ground plane boosters intended for the low frequency region (port 1 and port 3) with respect to the previous situation where the slots were not considered (Fig. 6.43). Unlike the solution presented in section 6.5.3, where the slot was placed at the center of a short edge of the ground plane, in this case, the slots are located closer to those ground plane

boosters in charge of the high frequency region in order to minimize possible impedance mismatch effects over the most critical elements, i.e. those intended for the low frequency region.

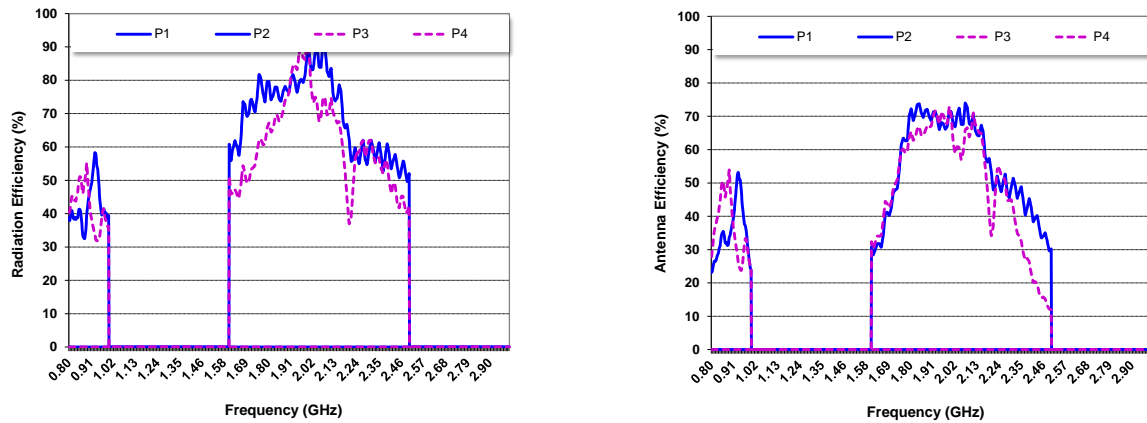
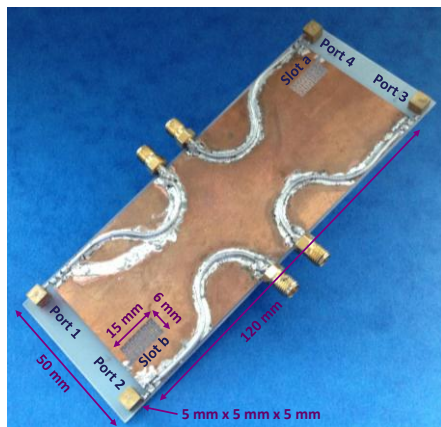
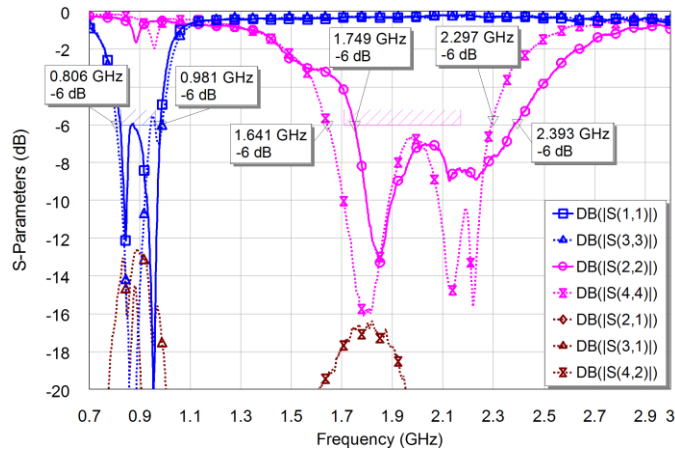


Fig. 6.44 Radiation and antenna efficiency corresponding to the MIMO system illustrated in Fig. 6.43. Port 1 and 3 refer to the ground plane booster intended for the low frequency region, whereas port 2 and 4 relate to those boosters in charge of the high frequency region.

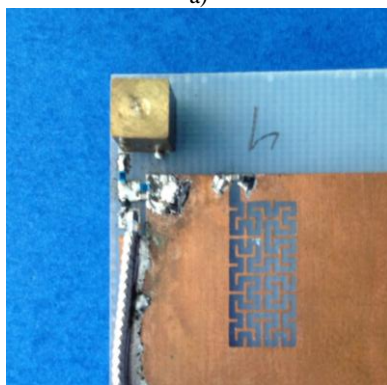
As seen in the simulated results (Fig. 6.38), the slots attain similar impedance bandwidths at both frequency regions with the advantage of providing lower transmission coefficients. Namely, the slots introduce two significant dips in the low frequency region. These drops can be easily adjusted through the capacitors connected to the open edges of the slot. In this way the capacitor of slot *a* produces a drop at 0.95GHz whereas the capacitor at slot *b* produces a drop at 0.85GHz (Fig. 6.45b and Fig. 6.46).



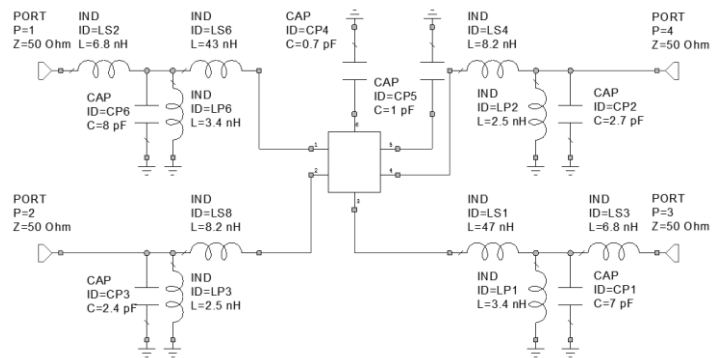
a)



b)



c)



d)

Fig. 6.45 a) Geometry of the proposed multi-band MIMO system comprising the four ground plane boosters and two slots inspired in the Hilbert geometry. The ground plane is etched over a 1 mm thick FR4 piece ($\epsilon_r=4.15$, $\tan\delta=0.013$); b) S-parameters.

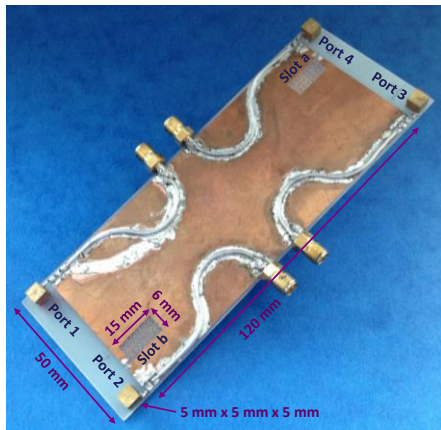
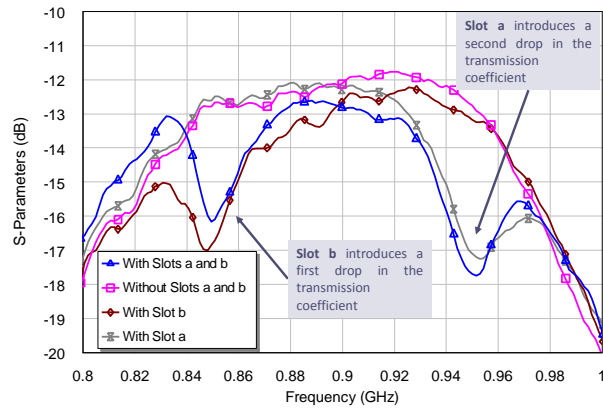


Fig. 6.46 Effect of the Hilbert slots over the transmission coefficient.



The antenna efficiency remains comparable to the case where the slots were not considered (Fig. 6.47). Nevertheless, the correlation values are significantly improved since two correlation dips appear at those frequencies where the slots are tuned. The solution attains correlation values below the threshold of 0.5 across the entire frequency range associated to the low frequency region (824-960MHz) (Fig. 6.48).

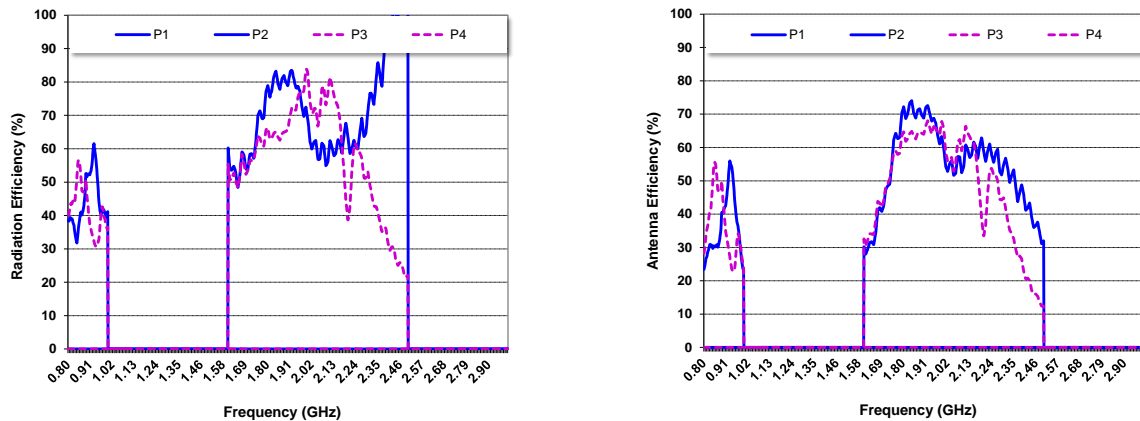


Fig. 6.47 Radiation and antenna efficiency corresponding to the MIMO system illustrated in Fig. 6.45. Port 1 and 3 refer to the ground plane booster intended for the low frequency region, whereas port 2 and 4 relate to those boosters in charge of the high frequency region.

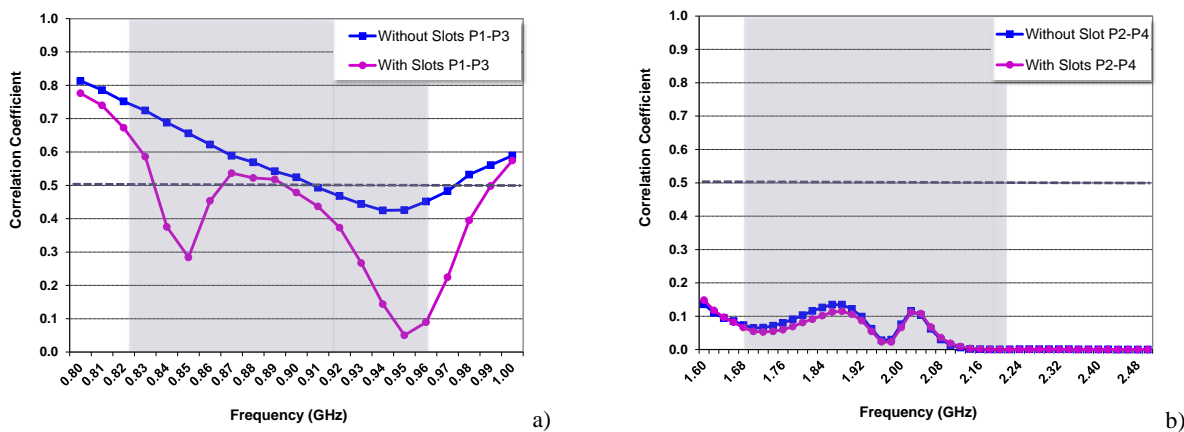


Fig. 6.48 a) Comparison of the correlation coefficient with (Fig. 6.45) and without the Hilbert slots (Fig. 6.43) computed through measured radiation patterns (6.9) for the low and high frequency region.

The comparison between the radiation patterns measured at those ports intended for the low frequency region, namely port 1 and port 3, illustrates the differences that produce the correlation null found at a frequency close to 0.95GHz (Fig. 6.49). In particular, the null found at port 1 when considering

the prototype integrating the slots appears at a direction close to $\phi=180^\circ$, $\theta=150^\circ$. In contrast, this null appears at a direction close to $\phi=100^\circ$, $\theta=40^\circ$, when port 3 is measured, thus illustrating a rotation of the radiation pattern, which is the responsible of the correlation coefficient null close to these frequencies.

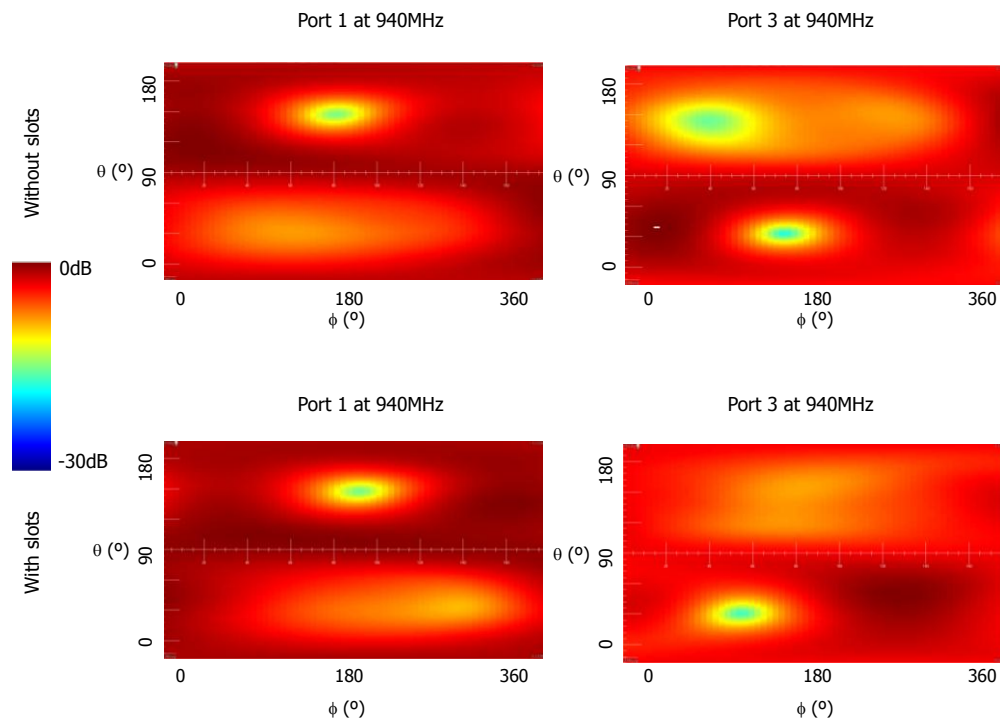


Fig. 6.49 Comparison of the radiation patterns associated to each one of the ports of the low frequency region at a frequency where the correlation null appears regarding both configurations, with and without slots.

6.7. Conclusions

A MIMO system increases the channel capacity by the integration of multiple antennas in transmission and reception. This increment is directly proportional to the number of paired decoupled and uncorrelated antenna elements. Accordingly, the antennas forming a MIMO system must be sufficiently uncorrelated and decoupled as to preserve the benefits of the technology in terms of data rate increments. In this way, a new challenge arises for handset antenna engineers, who not only have to satisfy current requirements focused on providing miniature and multi-band antennas, but also have to face the difficult task of integrating multiple antenna elements operating at the same number of frequency bands in a handset terminal with strict constraints in terms of dimensions, weight, and energy consumption.

The dimensions of current handset platforms hardly limit the integration of multiple antennas, more significantly in the low frequency region (690-960MHz) where some of the new LTE standards, capable of supporting MIMO, are allocated. Sometimes, the electrical distance between antenna elements at these frequencies, mainly fixed by the longest dimensions of the handset platform, is not sufficient for ensuring low coupling and low correlation values. Nevertheless, at frequencies above 1.5GHz, this challenge disappears, since in this case, this electrical distance becomes sufficient as for ensuring high isolation and low correlation. Usually the increment of the electrical length of the ground plane directly translates into an increment of the physical dimensions of the handset platform. This increment is advantageous as long as it does not exceed the specified dimensions of the handset platform, since it allows shifting the

correlation minimums at lower frequencies. In this sense, the coupled monopoles arranged over a ground plane of 110 mm length present a first correlation minimum (0.9GHz) at lower frequencies than those offered by the dual-band (1.0GHz) and the hexa-band PIFA (0.95GHz). Other mechanisms, such as the integration of slots in the ground plane, allow increasing the electrical length of the ground plane, thus reducing the frequency at which the first correlation minimum appears. Nevertheless, this mechanism improves the contribution of the ground plane to the radiation process, thus increasing the similarities between the radiation patterns and consequently the correlation values. Accordingly, the proposed solution based on a set of coupled monopoles in a ground plane having dimensions of 110 mm x 47 mm becomes preferred to maximize isolation while minimizing correlation. These parameters can be further improved if the two set of coupled monopoles are fed at diagonally opposite corners of the ground plane. In this case, the correlation values for the low frequency region (824-960MHz) remain below the required threshold of 0.5. The larger the dissimilarities between the radiating systems, the better the correlation values. Accordingly, the combination of different antenna topologies in a MIMO system becomes preferred, since they introduce dissimilarities in the current distribution of the radiating structure that directly leads to an improvement of the correlation values. In this sense, the proposed MIMO system based on the combination of an hexa-band PIFA with a set of coupled monopoles presents low correlation values below the threshold of 0.5 across the entire frequency range associated to the low frequency region (824-960MHz).

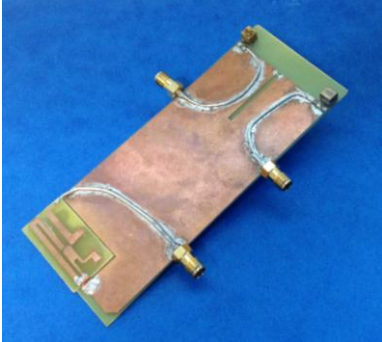
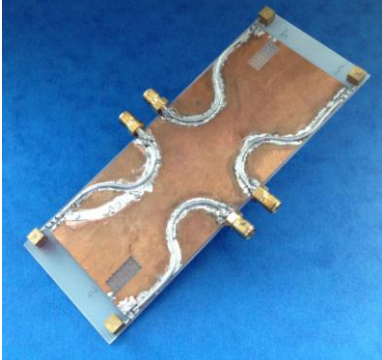
The previous conclusions, extracted from the MIMO analysis of antenna systems having resonant dimensions, remain for the case where these antennas are replaced by non-resonant solutions such as the ground plane boosters proposed along this thesis. Accordingly, the distance between those radiating systems operating in the most critical frequency range, i.e. the low frequency region, should be maximized in order to minimize coupling and correlation. This distance increment is achieved by feeding each radiating structure at diagonally opposite corners of the ground plane.

The integration of a quarter wavelength slot into the ground plane further contributes to improve isolation and correlation. The results illustrate that the isolation between a ground plane booster operating in the low frequency region and the dual-band PIFA improves from 4dBs at 0.95GHz up to approximately 16dBs when a quarter wavelength slot is etched in the ground plane. The reduction of this mutual coupling directly increases antenna efficiencies from the initial average values around 56.1% for the ground plane booster and 37.4% for the dual-band PIFA up to 59.4% and 63.7%, respectively. In addition, the slot introduces a correlation coefficient null at the center frequency of the low frequency region (0.9GHz), thus significantly improving the results with respect to the solution without slot.

The results further demonstrate that the quarter wavelength slot can be miniaturized through reactive elements, namely through the use of a capacitor connected to the open edge of the slot. The proposed multi-band MIMO system formed by the set of coupled monopoles, two ground plane boosters, and a miniaturized slot significantly reduces the correlation coefficient in the low frequency region, attaining values below the threshold of 0.5 across the entire operating frequency range of the low (824-

960MHz) and high frequency region (1710-2170MHz). In fact, at the center frequency of the low frequency region (0.9GHz), the integration of the slot produces a correlation coefficient of 0. Similarly, the slot significantly reduces the mutual coupling in this region by introducing a transmission coefficient dip at this center frequency. This enhancement contributes to improve antenna efficiencies in this low frequency region. The antenna efficiency in the high frequency region remains comparable to the solution without slot since the transmission coefficient does not suffer significant variations at this frequency region. Thus, the proposal provides a 2x2 MIMO system capable of operating in six communication standards, namely GSM850, GSM900, GSM1800, GSM1900, UMTS, and LTE2100.

Table 6.2 Summary of the proposed MIMO solutions based on ground plane boosters.

MIMO Architecture	Features	Performance
	<ul style="list-style-type: none"> • MIMO 2 x 2 at the low and high frequency regions combining ground plane booster antenna technology with a monopole antenna. • Two electric ground plane boosters of 5 mm x 5 mm x 5 mm, one for the low and the other for the high frequency region. One coupled monopole antenna for both frequency regions. • Ground plane: 120 mm x 50 mm. • Slot for decoupling at the low frequency region. Slot is miniaturized with a capacitor. 	<ul style="list-style-type: none"> • First ground plane booster: GSM850 and GSM900 • Second ground plane booster: GSM1800, GSM1900, UMTS, and LTE2100 • Coupled monopoles: GSM850, GSM900, GSM1800, GSM1900, UMTS, and LTE2100
	<ul style="list-style-type: none"> • MIMO 2 x 2 solution comprising only ground plane booster. • Four ground plane boosters, each one of 5 mm x 5 mm x 5 mm. • Ground plane: 120 mm x 50 mm. • Two miniature slots using Hilbert-based geometry and capacitive loading to broadband decoupling at the low frequency region. 	<ul style="list-style-type: none"> • Two ground plane boosters operating at GSM850, GSM900 • Two ground plane boosters operating at GSM1800, GSM1900, UMTS, and LTE2100

The MIMO challenges further increase when a full ground plane booster solution is considered, since in this case the current distribution is mainly determined by the ground plane. The benefits of integrating slots also apply to the proposed full ground plane booster solution. The results demonstrate that the slots not only can be miniaturized through reactive elements but also through its geometry. In this case, two slots are proposed to increase the correlation and isolation bandwidth where correlation and isolation are below the required threshold. The slots are placed at each one of the short edges of the ground plane. In order to minimize some possible impedance mismatch effects over the ground plane boosters intended for the low frequency region, these slots are positioned closer to those ground plane boosters associated to the high frequency region. The full-boosters solution integrating the two miniaturized Hilbert slots significantly reduces correlation values across the entire frequency range

associated to the low frequency region. Not only the correlation values are below the threshold of 0.5 along the whole range but also two correlation nulls appear at those frequencies where the slots are tuned. Similarly, the transmission coefficient is minimized and two significant dips also appear at the frequencies where the slots are tuned. In the high frequency region, the correlation values remain below 0.1 across the entire frequency range and the antenna efficiency remain at high values. In addition, it provides the flexibility to tune the correlation and transmission coefficient nulls at the desired frequencies, since they can be easily adjusted through the series capacitor connected to the open edges of the Hilbert-based slots. Accordingly, this ground plane booster solution positions as a good alternative to provide a compact multi-band MIMO system capable of being integrated in current handset platforms. The solution attains 2x2 MIMO performance in six communication standards (GSM850, GSM900, GSM1800, GSM1900, UMTS, and LTE2100). Table 6.2 summarizes the two proposed architectures for MIMO 2x2, the first one combining the ground plane booster antenna technology with a set of coupled monopoles and the second one only based on ground plane boosters.

6.8. References

- [1] J. P. Arogyaswami, A. G. Dhananjay, U. N. Rohit, and B. Helmut, "An Overview of MIMO Communications – A Key To Gigabit Wireless", *Proceeding of the IEEE*, vol. 92, n°2, February 2004, pp. 198-218.
- [2] S. Chia, T. Gill, L. Ibbetson, D. Lister, A. Pollard, R. Irmer, D. Almodovar, N. Holmes, and. Pike, "3G Evolution", *IEEE Microwave Magazine*, vol. 9, n°4, August 2008, pp. 53-63.
- [3] Multi-Band Antenna Design Guidelines for Mobile Receiver Diversity, Qualcomm, San Diego, CA, June 2009.
- [4] 3rd Generation Partnership Project, Technical Specification Group Radio Access Network, Evolved Universal Terrestrial Radio Access (E-UTRA) Radio Resource Control (RRC), Protocol Specification, 3GPP TS 36.331, v8.4.0, 2008.
- [5] A. Derneryd and G. Kristensson, "Signal Correlation including Antenna Coupling", *IEE Electronics Letters*, vol. 40, n°3, February 2004, pp. 157-159.
- [6] S. Blanch, J. Romeu, and I. Corbella, "Exact Representation of Antenna System Diversity Performance from Input Parameter Description", *IEE Electronics Letters*, vol 39, n°9, May 2003, pp. 705-707.
- [7] T. Taga, "Analysis for Mean Effective Gain of Mobile Antennas in Land Mobile Radio Environments", *IEEE Transactions on Vehicular Technology*, vol. 39, n°2, May 1990, pp. 117-131.
- [8] J. Thaysen and K. B. Jakobsen, "Envelope Correlation in (N, N) MIMO Antenna Array from Scattering Parameters", *Microwave and Optical Technology Letters*, vol. 48, n°5, May 2006, pp. 832-834.

- [9] A. Derneryd, J. Fridén, P. Persson, and A. Stjernman, "Performance of Closely Spaced Multiple Antennas for Terminal Applications", *Proceedings of the Third European Conference on Antennas and Propagation*, EuCAP 2009, Berlin, Germany, March 2009.
- [10] A. A. H. Azremi, M. Kyro, J. Ilvonen, J. Holopainen, S. Ranvier, C. Icheln, and P. Vainikainen, "Five-element Inverted-F Antenna Array for MIMO Communications and Radio-finding on Mobile Terminal", *Loughborough Antennas and Propagation Conference*, Loughborough UK, November 2009, pp. 557-560.
- [11] Z. Li, Z. Du and K. Gong, "Compact Reconfigurable Antenna Array for Adaptive MIMO systems", *IEEE Antennas and Wireless Propagation Letters*, vol. 8, 2009, pp. 1317-1320.
- [12] R. Glogowski, and C. Peixeiro, "Multiple Printed Antennas for Integration into Small Multistandard Handsets", *IEEE Antennas and Wireless Propagation Letters*, vol. 7, 2008, pp. 632-635.
- [13] Y. Gao, X. Chen, Z. Ying, and C. Parini, "Design and Performance Investigation of a Dual-Element PIFA Array at 2.5 GHz for MIMO Terminal", *IEEE Transactions on Antennas and Propagation*, vol. 55, n°12, December 2007, pp. 3433-3441.
- [14] M. Kyrö, M. Mustonen, C. Icheln, and P. Vainikainen, "Dual-Element Antenna for DVB-H Terminal", *Loughborough Antennas and Propagation Conference*, March 2008, Loughborough UK, pp. 265-268.
- [15] S. K. Chaudhury, H.J. Chaloupka, and A. Ziroff, "Novel MIMO Antennas for Mobile Terminals", *Proceedings of the 38th European Microwave Conference*, October 2008, Amsterdam The Netherlands, pp. 1751-1754.
- [16] P. Vainikainen, M. Mustonen, M. Kyrö, T. Laitinen, C. Icheln, and J. Villanen, "Recent Development of MIMO Antennas and their Evaluation for Small Mobile Terminals", *17th International Conference on Microwaves, Radar and Wireless Communications, MIKON 2008*, May 2008, pp. 1-10.
- [17] S. K. Chaudhury, W. L. Schroeder, and H.J. Chaloupka, "Multiple Antenna Concept Based on Characteristic Modes of Mobile Phone Chassis", *Proceedings of the Second European Conference on Antennas and Propagation*, EuCAP 2007, Edinburgh, United Kingdom.
- [18] Q. Rao and G. Wen, "Ultra-Small Cubic Folded Strip Antenna for Handset Devices", *IEEE Antennas and Propagation Society International Symposium, AP-S 2008*, July 2008.
- [19] K-L. Wong, C-H. Chang, B. Chen, and S. Yang, "Three-Antenna MIMO System for WLAN Operation in a PDA Phone", *Microwave and Optical Technology Letters*, vol. 48, n°7, July 2006, pp. 1238-1242.
- [20] D. Manteuffel, "MIMO Antenna Design Challenges", *IEEE Antennas and Propagation Conference*, Loughborough, UK, November 2009, pp. 50-56.

- [21] Q. Rao and D. Wang, "A Compact Dual-Port Diversity Antenna for Long-Term Evolution Handheld Devices", *IEEE Transactions on Vehicular Technology*, vol. 59, n°3, March 2010, pp. 1319-1329.
- [22] S. B. Yeap, X. Chen, J. A. Dupuy, C. C. Chiau, and C. G. Parini, "Integrated Diversity Antenna for Laptop and PDA Terminal in a MIMO System", *IEE Proceedings on Microwave Antennas and Propagation*, vol. 152, n°6, December 2005, pp. 495-504.
- [23] S. Rowson, G. Poilasne, and L. Desclos, "Isolated Magnetic Dipole Antenna: Application to GPS", *Microwave and Optical Technology Letters*, vol. 41, n°6, June 2004, pp. 449-451.
- [24] M. Karaboikis, C. Soras, G. Tsachtsiris, and V. Makios, "Compact Dual-printed Inverted-F Antenna Diversity Systems for Portable Wireless Devices", *IEEE Antennas and Wireless Propagation Letters*, vol. 3, 2004, pp. 9-14.
- [25] J-B. Yan, C.Y. Chiu, and R.D. Murch, "Handset 4-port MIMO antenna using slit separated PIFA and quarter-wave slot antenna pair" *Antennas and Propagation Society International Symposium*, 2008. AP-S 2008.IEEE , 5-11 July 2008, pp.1-4.
- [26] Y. Ding, Z. Du, and Z. Feng, "A Novel Dual-band printed Diversity Antenna for Mobile Terminals", *IEEE Transactions on Antennas and Propagation*, vol. 55, n°7, July 2007, pp. 2088-2096.
- [27] A. S. Andrenko, T. Maniwa, and T. Yamagajo, "Low Correlation Antenna Design for Diversity Handset Applications", *IEEE Microwave Conference*, APMC 2008. Asia-Pacific, December 2008.
- [28] Q. Liu, Z. Du, K. Gong, and Z. Feng, "A Compact Wideband Planar Diversity Antenna for Mobile Handsets", *Microwave and Optical Technology Letters*, vol. 50, n°1, January 2008, pp. 87-91.
- [29] Z. Li, and Y. Rahmat-Samii, "Optimization of PIFA-IFA Combination in Handset Antenna Designs", *IEEE Transactions on Antennas and Propagation*, vol. 53, n°5, May 2005, pp. 1770-1778.
- [30] C. Volmer, J. Weber, R. Stephan, K. Blau, and M. A. Hein, "An Eigen-Analysis of Compact Antenna Arrays and its Application to Port Decoupling", *IEEE Transactions on Antennas and Propagation*, vol. 56, n°2, February 2008, pp. 360-370.
- [31] R. A. Bhatti, S. Yi, and S. Park, "Compact Antenna Array with Port Decoupling for LTE-Standardized Mobile Phones", *IEEE Antennas and Wireless Propagation Letters*, vol. 8, 2009, pp. 1430-1433.
- [32] M. Shanawani, D. L. Paul, S. Dumanli, and C. Railton, "Design of a Novel Antenna Array for MIMO Applications", *3rd International Conference on Information and Communication Technologies: From Theory to Applications*, ICTTA 2008.
- [33] S. Chang, Y. S. Wang, and S. J. Chung, "A Decoupling Technique for Increasing the Port isolation between Strongly Coupled Antennas", *IEEE Transactions on Antennas and Propagation*, vol. 56, n°12, December 2008, pp. 3650-3658.

- [34] B. K. Lau, J. B. Andersen, G. Kristensson, and A. F. Molisch, "Impact of matching network on bandwidth of compact antenna arrays", *IEEE Transactions on Antennas and Propagation*, vol. 54, n°11, November 2006, pp. 3225-3228.
- [35] A. Diallo, C. Luxey, P. Le Thuc, R. Staraj, and G. Kossiavas, "Study and Reduction of the Mutual Coupling between Two mobile Phone PIFAs Operating in the DCS1800 and UMTS Bands", *IEEE Transactions on Antennas and Propagation*, vol. 54, n°11, Part I, November 2006, pp. 3063-3074.
- [36] A. Diallo, C. Luxey, P. Le Thuc, R. Staraj, and G. Kossiavas, "Enhanced Diversity Antennas for UMTS Handsets", *Proceedings of the First European Conference on Antennas and Propagation, EuCAP 2006*, November 2006, Nice, France.
- [37] G. Park, M. Kim, T. Yang, J. Byun, and A. S. Kim, "The Compact Quad-band Mobile Handset Antenna for the LTE700 MIMO Application", *IEEE Antennas and Propagation Society International Symposium, 2009, APSURSI 2009*, June 2009.
- [38] K. Ishimiy, J. Langbacka, Z. Ying, and J. Takada, "A Compact MIMO DRA Antenna", *Proceeding of iWAT2008*, Chiba, Japan, pp. 286-289.
- [39] A. Andújar, J. Anguera, C. Puente, C. Picher, "Wireless Device Capable of Multiband MIMO Operation", *Patent Application WO 2012/017013*, August 3, 2011.
- [40] J. Anguera, C. Puente, E. Martínez, and E. Rozan, "The fractal Hilbert monopole: A two-dimensional wire". *Microwave and Optical Technology Letters*, vol.36, n°2, Jan. 2003, pp.102-104.
- [41] C. Puente, E.Rozan, and J.Anguera, "Space Filling Miniature Antennas", *Patent Application WO 01 54225*, January 19, 2000.

CHAPTER 7 CONCLUSIONS

This thesis demonstrates that the ground plane, inherently present in any wireless device is able of supporting efficient radiating modes at mobile frequencies (from 0.5GHz up to approximately 3GHz). The theory of characteristic modes, developed by Harrington and Mautz in the early 70s, has become a useful tool to compute the wave modes supported by any conducting object just as a function of its shape and size. In the context of this thesis, this theory has been applied to determine the wave modes associated to the typical ground planes of current handset platforms, namely to those supported by a bar phone platform, a smartphone platform, and a clamshell platform. The ground plane modes analysis carried out, not only reveals the modes supported by these conducting structures, but also indicates if these modes are radiating modes or if in contrast they contribute to store electric or magnetic energy. The results demonstrate that efficient radiating modes appear at mobile frequencies. In particular, a ground plane having the typical dimensions of a bar-phone platform (100 mm x 40 mm) presents two efficient radiating modes, which resonate at a frequency around 1.33GHz (fundamental mode) and 2.94GHz, respectively. The advantage of the fundamental radiating mode is that it presents efficient radiation properties from its resonance up to a wide frequency range that includes some of the main communication standards. The study further reveals that the resonance of these radiating modes can be moved to lower frequencies by increasing the longitudinal dimensions of the ground plane. In this sense, a ground plane having the typical dimensions of current smartphone platforms shifts these resonances to 1.08GHz and 2.49GHz, respectively, which become advantageous for those communication standards allocated in low frequency regions, such as GSM850 and GSM900. Similarly, the clamshell platform analyzed further reduces these resonant frequencies due to its larger longitudinal dimensions. In this case, three efficient radiating modes, resonating at 0.63GHz, 1.59GHz, and 2.10GHz, appear, which are advantageous to provide operation in those communication standards allocated at lower frequencies.

Due to the fact that in some cases the computation of these wave modes through the characteristic modes theory could be complicated, this thesis proposes a faster and simpler method to compute the fundamental modes associated to any conducting object, the Radar Cross Section analysis (RCS). It consist in illuminating the conducting object, for instance the ground plane of a wireless device by a plane wave impinging from the normal direction and polarized according to the current distribution of the mode under analysis. Therefore, the method holds as long as the modes to analyze present a polarization aligned with the polarization of the impinging wave. The results of the RCS method are in well agreement with those obtained from the characteristic modes theory, thus validating the proposal. Further to its simplicity, the RCS analysis also has the advantage that it allows considering the effect that dielectric materials as well as techniques to electrically increase the dimensions of the conducting object produce over the resonance of the fundamental modes. The techniques analyzed along the thesis to increase the electrical length of the ground plane mainly consist in the integration of slots in the ground plane and in the addition of metallic strips. The RCS analysis of these methods demonstrates the feasibility thereof, since a

shifting to lower frequencies of the resonant frequency of the fundamental mode is demonstrated in both cases.

The challenge, once the existence of these efficient radiating modes is known, relies on properly exciting them in order to use the ground plane as main radiator. This thesis demonstrates that these efficient radiating modes can be properly excited through the use of non-resonant elements featured by considerably reduced dimensions. In order to arrive to this conclusion, a deep study has been carried out with the aim of determining the role that plays the geometry, the size, and the resonant frequency of the elements, used to excite the ground plane, in the radiation properties thereof. The study concludes that in order to improve the performance of the whole radiating system, the resonance of the element used to excite the fundamental mode of the ground plane, should be equal or above the resonance of the mode. When the resonance of the element coincides with the resonance of the fundamental mode, the geometry of the element affects the performance. Nevertheless, when the elements are small enough as for providing a resonance well above the resonance of the fundamental mode, the geometry loses its relevance. Consequently, non-resonant elements having simple geometries become preferable over resonant elements having more complex geometries, fact that supposes a significant advantage not only in terms of size but also in terms of manufacturing costs.

In order to demonstrate the aforementioned statement, this thesis develops several radiating systems based on the use of small non-resonant elements featured by simple geometries. These elements present very poor radiation properties, since they are featured by high quality factors at the frequency regions of operation. The name ground plane booster is proposed to refer to these electrically small non-resonant elements. The proposals are classified into radiating systems including on one hand electric ground plane boosters, and on the other hand magnetic ground plane boosters. The reasoning behind relies on the fact that not only the size, the geometry, or the resonance of the element used to excite the ground plane modes condition the performance of the system, but also its nature (inductive or capacitive) together with its placement in the ground plane. In this sense, electric ground plane boosters featured by a capacitive input impedance should be placed at the corners of the shortest edges of the ground plane, i.e. where the current distribution of the fundamental ground plane mode is minimized. In contrast, magnetic ground plane boosters should be placed at the center of the longest edges of the ground plane where maximums of current distribution appear. Although these considerations guarantee the proper excitation of the ground plane mode by providing high radiation efficiencies across a wide range of frequencies, they are not sufficient to provide operability in the desired communication standards, since the system is featured by a high reactive input impedance. In order to overcome this shortcoming, this thesis proposes the use of broadband matching networks capable of increasing the impedance bandwidth in a factor around 2.45 (Standing Wave Ratio (SWR) ≤ 3). Since the size of the non-resonant element conditions the performance, this thesis further provides a systematic matching network design, which consists in computing the inherent bandwidth (BW_0) associated to a particular radiating system across the operating frequencies. The knowledge of this BW_0 together with the enhancement factor of the broadband matching

network allows knowing in advance if the radiating system will be able of providing operation in the required communication standards. The systematic design entails significant advantages since it avoids cumbersome matching network processes based on trial and error, which could hide, in some cases, the potential bandwidth of the system. Although most of the proposed solutions rely on a modular design, i.e. a ground plane booster and a radiofrequency system for each frequency region, the thesis further disclose a proposal where at least one ground plane booster is reused at one or more frequency regions. This solution allows simplifying the radiofrequency systems by reducing the number of the required reactive elements with respect to the modular designs. The proposals provide multi-band operation and attain a size reduction around one order of magnitude with respect to other handset antenna solutions, widely spread in the wireless industry (Table 7.1).

The interaction of the human head when, for instance a user holds a handset during a phone call, significantly affects the antenna performance. Nevertheless, not only the human head affects the performance of the antenna, but also the electromagnetic waves radiated by the antenna produce biological effects, such as temperature increments, over the human head. These effects are carefully controlled by standardization organisms which determine safety thresholds (Specific Absorption Rate (SAR) values) intended for ensuring the safe use of the device. Accordingly, the effect of the human interaction over the antenna performance of the proposed radiating systems is analyzed along this thesis from this two main perspectives: functional and biological. The results obtained from the proposed compact radiating systems based on ground plane boosters are compared with those obtained from other handset antenna technologies based on the use of antennas having resonant dimensions, namely to a dual-band Planar Inverted F-Antenna (PIFA), a hexa-band PIFA, and a set of coupled monopoles. In general terms, the effects of the human head over the performance of handset antennas mainly translate into detuning and efficiency decrements. The analyzed radiating systems do not suffer significant detuning effects in the presence of the human head but efficiency decrements. The analysis reveals that the power absorbed by the human head and consequently the effects over the antenna efficiency can be minimized if the distance between the antenna or the ground plane boosters and the human head is maximized. It is accomplished by placing the antennas or the ground plane boosters in the lower part of the Printed Circuit Board (PCB) that is closer to the cheek than to the ear. In this case, the performance of the radiating system based on ground plane booster remains comparable to that offered by the set of coupled monopoles in the low frequency region (824-960MHz) and by the hexa-band PIFA in the high frequency region (1710-2170MHz) but with the advantage of its reduced size. When regarding the biological compatibility in terms of SAR, the compact system based on ground plane booster stands out over the other handset solution, since is the one that considerably reduces SAR values at both frequency regions. In this position the SAR values are below the recommended standards (American standard (ANSI/IEEE): 1.6mW/g (1g) and European standard (ICNIRP) 2mW/g (10g)), even when regarding the touch position, which considers just a distance of 1 mm between the ground plane and the human cheek.

The results conclude that SAR values and power absorption are not directly linked. SAR is defined as the power absorbed by the human head by unity of mass and its dimensions are mW/g. Consequently, it only gives information about the maximum value of absorption and the location where it takes place. On the contrary, the total power absorption is calculated as the integral along all the head volume so it is directly connected with the distribution of the near electrical fields. Therefore, the better solution is the one that maximizes antenna efficiency while minimizes SAR. In order to take into account both parameters when assessing the performance of the solutions under study, a figure of merit, defined as the ratio between antenna efficiency and SAR, is proposed. Further to the advantage of the small dimensions of the compact solution using ground plane boosters (250 mm³), the analysis of the human interaction concludes that the compact radiating system is the one that performs better in the presence of the human head, since it maximizes antenna efficiency while minimizes SAR at both frequency regions.

Further to the human head analysis, hand loading is also an important aspect to consider. When the user holds a phone, the proximity of the hand could also contribute to degrade the antenna performance. In order to minimize detuning effects or efficiency decrements, this thesis further proposes radiating systems robust to hand loading effects. The solutions rely on the redundancy principle and consist in integrating two or more antenna elements operating in the same frequency region into the handset platform. The proposal combines the input impedances of the antenna elements into a single input/output port through a delay means, such as a transmission line, thus attaining a passive antenna array, also called along the thesis as distributed radiating system. The advantage in terms of robustness of the proposed passive antenna array mainly relies on the fact that when the finger of the user obstructs an antenna element, the other elements can still operate properly. The length of this delay means, in a first proposal, is selected to improve the impedance bandwidth with respect to a solution just integrating a single antenna. Thus, the system not only offers greater robustness in front of hand loading, but also improves the performance in free-space with respect to a single element solution. The results demonstrate that the impedance bandwidth can be improved proportionally to the number of antenna elements to be combined. Although performing better than the single element solution, the drawback of this out-of-phase feeding scheme, which is based on the combination of complementary input impedances, relies on the fact that the power is not equally distributed between the elements of the array, hence being the performance dependent on the finger location. In order to overcome this shortcoming, an in-phase feeding mechanism able to equally distribute the input power is proposed. This in-phase feeding scheme does not produce the significant bandwidth enhancement of the previous out-of-phase solution but this inconvenient is solved by the addition of a matching network at the input/output port of the radiating system. After the addition of the matching network, the solution is capable of providing similar impedance bandwidth than the out-of-phase proposal, but with the advantage of removing the dependency of the antenna performance to the finger location. Another benefit of the in-phase solution is that it increases radiation efficiency with respect to that obtained through the out-of-phase mechanism. The reason relies on the fact that the in-phase feeding scheme produces a symmetric excitation of the ground plane whereas the out-of-phase

mechanism could introduce asymmetries in the current distribution, i.e. different amplitudes and phases, which could produce lower efficiency values or even significant efficiency drops at the frequency regions of operation.

The ground plane booster antenna technology has been also applied to the proposed distributed radiating systems in order to minimize as much as possible the volume occupied in the PCB. In this case, the previous out-of-phase proposal based on complementary input impedances has been replaced by an out-of-phase proposal based on conjugated input impedances. This feeding scheme overcomes the previous efficiency shortcomings associated to the out-of-phase mechanism based on complementary input impedances, while preserves the benefits of increasing the impedance bandwidth. In the low frequency region (690-960MHz), the in-phase solution is still preferable not only when the human hand interaction is regarded, but also in free-space conditions. It offers larger efficiencies and impedance bandwidth even when compared with a single element solution having the same volume as that presented by the in-phase proposal. In the high frequency region, the out-of phase scheme based on conjugated input impedances offers greater impedance bandwidth than the in-phase proposal but similar to the single element solution. The advantage in this case is found when the finger loading is regarded, since the distributed solution performs better than the single element case.

The proposed distributed systems do not alter the omnidirectional radiation properties of the radiation pattern, since the half-wavelength and wavelength dipole types radiating modes of the ground plane at the low and high frequency regions, respectively, are preserved. Finally, it is important to underline that the proposed distributed systems are completely passive, being advantageous in terms of simplicity and battery consumption.

In order to be aligned with the market trends, this thesis further proposes handset antenna solutions intended for providing multi-band MIMO (Multiple Input Multiple Output) operation. The challenges of designing multi-band and small handset antennas have been significantly exacerbated with the appearance of the MIMO technology. MIMO systems require the integration of multiple antennas in transmission and reception to provide high speed data rates. In order to preserve the benefits of the technology, these multiple antennas operating in the same number of frequency bands, must be sufficiently uncorrelated and isolated. This fact supposes a significant challenge when regarding the strict constraints otherwise imposed by the handset platforms in terms of size, weight, and energy consumption.

The results reveal that for frequencies above 1.5GHz, the electrical distance between the antennas, usually fixed by the longest dimension of the ground plane, becomes sufficient for providing low correlation and low coupling. The challenge appears when regarding the low frequency region, since in this case the antennas are electrically closer. The analysis carried out along the thesis reveals that the use of different antenna elements fed at diagonally opposite corner of the ground plane significantly reduces correlation. In this way, the proposed MIMO system based on the combination of an hexa-band PIFA with a set of coupled monopoles presents low correlation values below the threshold of 0.5 across the

entire frequency range associated to the low and high frequency region (824-960MHz and 1710-2400MHz).

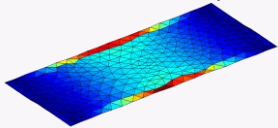
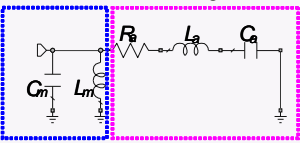



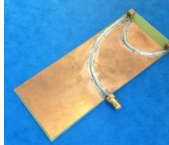



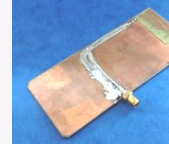


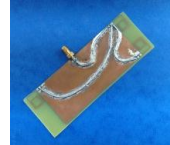



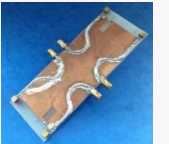
Nevertheless, these solutions are still based on antennas having resonant dimensions which occupy a considerable volume of the PCB. With the aim of minimizing this volume, this thesis expands the MIMO proposal to the use of ground plane boosters. In the previous cases, different current distributions appeared at each antenna according to its geometry, fact that contributed to increase the differences between the radiation patterns thereof. In the ground plane booster-base case, the radiation is mainly provided by the ground plane, thus increasing the difficulty of attaining low correlation values between radiating systems.

The first solution proposes the use of a set of coupled monopoles and two ground plane boosters, each one intended for a particular frequency region. Following the teachings extracted from the MIMO analysis over resonant elements, the ground plane booster intended for the low frequency region is positioned at diagonally opposite corners of the ground plane with respect to the feeding of the set of coupled monopoles. In order to enhance correlation and isolation, this thesis proposes the use of a quarter-wavelength slot placed near the center of a short edge of the ground plane and extending in a direction parallel to the longitudinal edges of the ground plane. The quarter wavelength slot considerably improves isolation and correlation values with respect to a solution without the slot. In particular, it produces a null of transmission coefficient and correlation at that frequency for which the slot is tuned. The thesis further demonstrates that the slot can be miniaturized through reactive elements, namely by connecting a capacitor close to the open edge of the slot. In this case a size reduction of a factor around 1.8 is obtained, while the improvements in correlation and isolation are preserved. The proposal provides a 2x2 MIMO system capable of operating in six communication standards, namely GSM850, GSM900, GSM1800, GSM1900, UMTS, and LTE2100.

Finally, a full-booster multi-band MIMO solutions is proposed. In this case, two slots placed at the short edges of the ground plane are used to further enhance isolation and correlation values. The use of two slots becomes significantly advantageous to produce two pronounced dips of correlation and coupling at the frequency region of operation. The benefit relies on the fact that the bandwidth, where correlation and isolation remain below the required thresholds, can be controlled through the proper adjustment of the resonant frequencies of these slots. In this case, the slots are miniaturized not only through reactive elements but also through their geometry, which has been inspired in the Hilbert fractal. The results further conclude that in order to reduce the effect of the slot over the performance of those boosters intended for the low frequency region, they have to be moved closer to the ground plane boosters in charge of the high frequency region. This solution positions as a good alternative to provide a compact multi-band MIMO system capable of being integrated in current handset platforms. The solution attains 2x2 MIMO performance in six communication standards (GSM850, GSM900, GSM1800, GSM1900, UMTS, and LTE2100).

The feasibility of relying on the ground plane modes of current handset platforms has been deeply analyzed along the thesis. The encouraging results demonstrate that the ground plane booster antenna technology is a promising solution for handset antenna designs to satisfy not only multi-band and miniature requirements for the new wireless handheld devices, but also the specifications imposed by emergent technologies such as MIMO.

Table 7.1 Summary and Conclusions

	Description	Conclusions
<p>Chapter 2 Fundamental Principles</p>	<p>Characteristic mode analysis  Systematic broadband matching network design </p> <p>* GPB: Ground Plane Booster</p>	<p>The efficient radiation modes associated to handset platforms can be effectively excited through GPBs*. However, this excitation does not guarantee the proper performance, since a radiofrequency system capable of matching the input impedance is required. In this sense, the design of radiofrequency systems becomes an essential part of emergent solutions based on GPB. In this regard, a systematic broadbanding mechanism is proposed throughout the thesis based on a LC resonator capable of enhancing the bandwidth 2.45 times at SWR=3.</p>
<p>Chapter 3 Ground Plane Booster Antenna Technology</p>	<p>3D electric GPB  2D electric GPB  Reuse GPB  Magnetic GPB </p>	<p>Volumetric and planar GPB (electric and magnetic) excite ground plane modes to provide operation at several 2G, 3G, and 4G standards. Two kind of architectures have been proposed: the first, where a GPB is in charge of providing operation at a given frequency region; the second, where the different GPBs cooperate. GPB antenna technology provides 1/10 less volume than current state-of-the-art handset antennas.</p>
<p>Chapter 4 Human Head Interaction</p>	<p>Human Head  PIFA  Slotted ground plane  Coupled monopoles  3D electric GPB </p>	<p>Performance of GPB antenna technology has been compared with PIFA, PIFA in slotted ground planes, and monopole antenna concluding that the proposed technology is robust to human head interaction. From the finger loading perspective, GPB antenna technology becomes advantageous because when the finger blocks one GPB, the others can radiate properly.</p>
<p>Chapter 5 Distributed Radiating Systems</p>	<p>Out-of-phase: 2 and 3 monopoles  In-phase monopoles  In-phase GPB  In/Out-of-phase GPB </p>	<p>Distributed antenna technology adds redundancy so as to provide robustness to the finger loading effect. In-phase and out-of-phase architectures provides besides robustness, more bandwidth. Distributed antenna technology combined with GPB antenna technology provides multi-band operation at several standards of 2G, 3G, and 4G while becoming robust to the finger loading effect.</p>
<p>Chapter 6 Ground Plane Boosters in MIMO Systems</p>	<p>Coupled monopoles and GPB  Full GPB </p>	<p>Multi-band 2x2 MIMO solution based on GPB has been positioned as a feasible technology for the new generation of MIMO wireless handheld devices operating at 2G, 3G, and 4G. A first architecture combines a set of multi-band coupled monopoles with two GPBs, one for the low and the other for the high frequency region. Isolation and correlation are improved at the low frequency region by means of a slot capacitively loaded. A second architecture is based on a full GPB solution where two GPBs are used to provide MIMO at the low frequency region and the other two, at the high frequency region. Isolation and correlation are improved at the low frequency region by means of two slots miniaturized thanks to Hilbert-based geometry and capacitively loading.</p>